Vol. 185, July 31, 1986
Complete in one issue

ISSN 0003-2670

ANALYTICA CHIMICA ACTA

International journal devoted to all branches of analytical chemistry

ELSEVIER

ANALYTICA CHIMICA ACTA

International journal devoted to all branches of analytical chemistry
Revue internationale consacrée à tous les domaines de la chimie analytique
Internationale Zeitschrift für alle Gebiete der analytischen Chemie

PUBLICATION SCHEDULE FOR 1986

	J	F	M	A	M	J	J	A	S	O	N	D
Analytica Chimica Acta	179	180	181	182	183	184	185	186	187	188 189	190	191

Scope. *Analytica Chimica Acta* publishes original papers, short communications, and reviews dealing with eve aspect of modern chemical analysis both fundamental and applied.

Submission of Papers. Manuscripts (three copies) should be submitted as designated below for rapid and efficie handling:

Papers from the Americas to: Professor Harry L. Pardue, Department of Chemistry, Purdue University, West Lafayett IN 47907, U.S.A.

Papers from all other countries to: Dr. A. M. G. Macdonald, Department of Chemistry, The University, P.O. Box 36 Birmingham B15 2TT, England. Papers dealing particularly with computer techniques to: Professor J. T. Cler Universität Bern, Pharmazeutisches Institut, Baltzerstrasse 5, CH-3012 Bern, Switzerland.

Submission of an article is understood to imply that the article is original and unpublished and is not being considere for publication elsewhere. Upon acceptance of an article by the journal, authors will be asked to transfer the copyrig of the article to the publisher. This transfer will ensure the widest possible dissemination of information.

Information for Authors. Papers in English, French and German are published. There are no page charge Manuscripts should conform in layout and style to the papers published in this Volume. Authors should consu Vol. 170 for detailed information. Reprints of this information are available from the Editors or from: Elsevier Editori Services Ltd., Mayfield House, 256 Banbury Road, Oxford OX2 7DH (Great Britain).

Reprints. Fifty reprints will be supplied free of charge. Additional reprints (minimum 100) can be ordered. An ord form containing price quotations will be sent to the authors together with the proofs of their article.

Advertisements. Advertisement rates are available from the publisher.

Subscriptions. Subscriptions should be sent to: Elsevier Science Publishers B.V., Journals Department, P.O. Bo 211, 1000 AE Amsterdam, The Netherlands. Tel: 5803 911, Telex: 18582.

Publication. *Analytica Chimica Acta* appears in 13 volumes in 1986. The subscription for 1986 (Vols. 179–191) Dfl. 2730.00 plus Dfl. 312.00 (p.p.h.) (total approx. US $1192.94). All earlier volumes (Vols. 1–178) except Vols. 2 and 28 are available at Dfl. 231.00 (US $90.59), plus Dfl. 15.00 (US $5.88) p.p.h., per volume.

Our p.p.h. (postage, packing and handling) charge includes surface delivery of all issues, except to subscribers in th U.S.A., Canada, Japan, Australia, New Zealand, P.R. China, India, Israel, South Africa, Malaysia, Thailand, Singapor South Korea, Taiwan, Pakistan, Hong Kong, Brazil, Argentina and Mexico, who receive all issues by air delive (S.A.L. — Surface Air Lifted) at no extra cost. For the rest of the world, airmail and S.A.L. charges are available upo request.

Claims for issues not received should be made within three months of publication of the issues. If not they cannot b honoured free of charge.

For further information, or a free sample copy of this or any other Elsevier Science Publishers journal, readers in th U.S.A. and Canada can contact the following address: Elsevier Science Publishing Co. Inc., Journal Informatic Center, 52 Vanderbilt Avenue, New York, NY 10017, U.S.A., Tel: (212) 916-1250.

0003-2670/86/$03.5

Printed in The Netherlands

ANALYTICA CHIMICA ACTA
VOL. 185 (1986)

ANALYTICA CHIMICA ACTA

International journal devoted to all branches of analytical chemistry

ELSEVIER Amsterdam–Oxford–New York–Tokyo

Anal. Chim. Acta, Vol. 185 (1986)

0003-2670/86/$03.

Printed in The Netherlands

Analytica Chimica Acta, 185 (1986) 1—17
Elsevier Science Publishers B.V., Amsterdam — Printed in The Netherlands

PARTIAL LEAST-SQUARES REGRESSION: A TUTORIAL

PAUL GELADI*[a] and BRUCE R. KOWALSKI

Laboratory for Chemometrics and Center for Process Analytical Chemistry, Department of Chemistry, University of Washington, Seattle, WA 98195 (U.S.A.)

(Received 15th July 1985)

SUMMARY

A tutorial on the partial least-squares (PLS) regression method is provided. Weak points in some other regression methods are outlined and PLS is developed as a remedy for those weaknesses. An algorithm for a predictive PLS and some practical hints for its use are given.

The partial least-squares regression method (PLS) is gaining importance in many fields of chemistry; analytical, physical, clinical chemistry and industrial process control can benefit from the use of the method. The pioneering work in PLS was done in the late sixties by H. Wold in the field of econometrics. The use of the PLS method for chemical applications was pioneered by the groups of S. Wold and H. Martens in the late seventies after an initial application by Kowalski et al. [1]. In spite of the large amount of literature that emerged from these groups, most articles describing PLS give algorithms and theory that are incomplete and often difficult to understand. Two recent articles [2, 3] show that PLS is a good alternative to the more classical multiple linear regression and principal component regression methods because it is more robust. Robust means that the model parameters do not change very much when new calibration samples are taken from the total population.

This article is meant as a tutorial. The reader is referred to texts on linear algebra [4, 5] if needed. The two most complete articles on PLS available at present are by S. Wold et al. [4, 6]. The nomenclature used in Kowalski [6] will be used here. Furthermore, all vectors will be column vectors. The corresponding row vectors will be designated as transposed vectors. The notation will be kept as rigorous as possible. Table 1 lists the notation used. The paragraphs on multiple linear regression, principal component analysis and principal component regression are included because they are necessary for a good understanding of PLS. They do not represent a complete treatment of these subjects.

---

[a]Present address: Chemometrics Group, Department of Organic Chemistry, Umeå University, S-901 87 Umeå, Sweden.

0003-2670/86/$03.50

TABLE 1

Symbols

$\| \ \|$	the Fröbenius or Euclidian norm
i	a dummy index for counting samples (objects)
j	a dummy index for counting independent (x) variables
k	a dummy index for counting dependent (y) variables
h	a dummy index for counting components or factors
n	the number of samples in the calibration (training) set
m	the number of independent (x) variables
p	the number of dependent (y) variables
a	the number of factors used ($\leq$ rank of $\mathbf{X}$)
r	the number of samples in a prediction (test) set
$\mathbf{x}$	a column vector of features for the independent variables (size $m \times 1$)
$\mathbf{y}$	a column vector of features for the dependent variables (size $p \times 1$)
$\mathbf{X}$	a matrix of features for the independent variables (size $n \times m$)
$\mathbf{Y}$	a matrix of features for the dependent variables (size $n \times p$)
$\mathbf{b}$	a column vector of sensitivities for the MLR method (size $m \times 1$)
$\mathbf{B}$	a matrix of sensitivities for the MLR method (size $m \times p$)
$\mathbf{t}_h$	a column vector of scores for the $\mathbf{X}$ block, factor h (size $n \times 1$)
$\mathbf{p}'_h$	a row vector of loadings for the $\mathbf{X}$ block, factor h (size $1 \times m$)
$\mathbf{w}'_h$	a row vector of weights for the $\mathbf{X}$ block, factor h (size $1 \times m$)
$\mathbf{T}$	the matrix of $\mathbf{X}$ scores (size $n \times a$)
$\mathbf{P}'$	the matrix of $\mathbf{X}$ loadings (size $a \times m$)
$\mathbf{u}_h$	a column vector of scores for the $\mathbf{Y}$ block, factor h (size $n \times 1$)
$\mathbf{q}'_h$	a row vector of loadings for the $\mathbf{Y}$ block, factor h (size $1 \times p$)
$\mathbf{U}$	the matrix of $\mathbf{Y}$ scores (size $n \times a$)
$\mathbf{Q}'$	the matrix of $\mathbf{Y}$ loadings (size $a \times p$)
$\mathbf{M}_h$	a rank 1 matrix, outer product of $\mathbf{t}_h$ and $\mathbf{p}'_h$ (size $n \times m$)
$\mathbf{E}_h$	the residual of $\mathbf{X}$ after subtraction of h components (size $n \times m$)
$\mathbf{F}_h$	the residual of $\mathbf{Y}$ after subtraction of h components (size $n \times p$)
b_h	the regression coefficient for one PLS component
$\mathbf{I}_n$	the identity matrix of size $n \times n$
$\mathbf{I}_m$	the identity matrix of size $m \times m$

Calibration (training) and prediction (test) steps

Chemical analysis usually consists of two steps. First, the characteristics of a method or instrument are investigated and an attempt is made to find a model for its behavior (a model is a relationship $Y = f(X)$ between two groups of variables, often called dependent Y and independent X). This is the calibration or training step. The data set used for this step is called a calibration or training set. The model parameters are called regression coefficients or sensitivities. The second step is the one in which the independent variables are obtained for one or more samples. These are used together with the sensitivities to predict values for the dependent variables. This is the prediction or test step. The data set used in this step is the prediction or test set.

The terms dependent block and independent block are introduced for the blocks of dependent and independent variables, respectively.

Mean-centering and scaling of variables

Before the model is developed, it is convenient to tailor the data in the calibration set in order to make the calculations easier. For ease of explanation, the values for each variable are used in the mean-centered form. The average value for each variable is calculated from the calibration set and then subtracted from each corresponding variable. In the rest of the text, all variables, both dependent and independent, are assumed to be mean-centered.

There are also different ways of scaling the variables. It should be pointed out that the dependent variables and the independent ones can be scaled differently because the sensitivities absorb the differences in scaling. There are essentially three ways of treating variables. In one, no scaling is needed when all the variables in a block are measured in the same units, as in spectrometry. In the second, variance scaling is used when the variables in a block are measured in different units (e.g., ppm, %, km); scaling is accomplished by dividing all the values for a certain variable by the standard deviation for that variable, so that the variance for every variable is unity. Thirdly, one can decide that certain variables are of less importance and hence should not influence the model very much; so they are given a smaller weight.

An illustration of scaling and mean centering is given in Fig. 1. In the further text, all variables are assumed to have some type of scaling, whichever is considered to be most appropriate.

MULTIPLE LINEAR REGRESSION (MLR)

The multiple linear regression (MLR) problem can be stated as follows. Features are measured for m variables x_j ($j = 1 - m$) and for a variable y with the goal to establish a linear (or first-order) relationship between them. This can be represented mathematically as

$$y = b_1x_1 + b_2x_2 + b_3x_3 + \ldots + b_mx_m + e \qquad (1a)$$

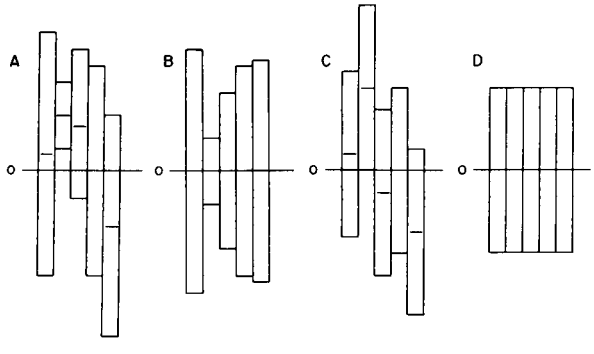

Fig. 1. Data preprocessing. The data for each variable are represented by a variance bar and its center. (A) Most raw data look like this. (B) The result after mean-centering only. (C) The result after variance-scaling only. (D) The result after mean-centering and variance-scaling.

$$y = \sum_{j=1}^{m} b_j x_j + e \tag{1b}$$

$$y = \mathbf{x}'\mathbf{b} + e \tag{1c}$$

In Eqn. 1(a), the x_j are called independent variables and y is the dependent variable, the b_j's are sensitivities and e is the error or residual. In Eqn. 1(c), y is a scalar, **b** is a column vector and $\mathbf{x}'$ is a row vector.

Equation 1 describes multilinear dependencies for only one sample. If one gets n samples, the y_i $(i = 1 - n)$ can be written as a column vector **y**, **b** remains the same and the vectors, $\mathbf{x}_j'$, form the rows of a matrix **X**:

$$\mathbf{y} = \mathbf{X}\mathbf{b} + \mathbf{e} \tag{2}$$

For a better understanding of these matrix equations, they are also given in graphical representation:

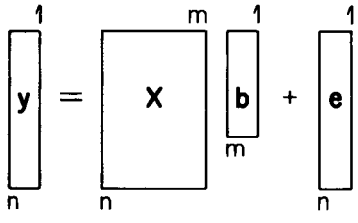

In this case, n is the number of samples and m the number of independent variables.

It is now possible to distinguish among three cases.

(1) $m > n$. There are more variables than samples. In this case, there is an infinite number of solutions for b, which all fit the equation. This is not what is wanted.

(2) $m = n$. The numbers of samples and of variables are equal. This situation may not be encountered often in practical situations. However, it gives a unique solution for **b** provided that **X** has full rank. This allows us to write

$$\mathbf{e} = \mathbf{y} - \mathbf{X}\mathbf{b} = 0 \tag{3}$$

e is called the residual vector. In this case, it is a vector of zeroes: 0.

(3) $m < n$. There are more samples than variables. This does not allow an exact solution for **b**. But one can get a solution by minimizing the length of the residual vector **e** in the following equation:

$$\mathbf{e} = \mathbf{y} - \mathbf{X}\mathbf{b} \tag{4}$$

The most popular method for doing this is called the "least-squares method". The least-squares solution is

$$\mathbf{b} = (\mathbf{X}'\mathbf{X})^{-1}\mathbf{X}'\mathbf{y} \tag{5}$$

(Complete explanations are available elsewhere [5, 7, 8].) Equation 5 gives a hint towards the most frequent problem in MLR: the inverse of $\mathbf{X}'\mathbf{X}$ may

not exist. Collinearity, zero determinant and singularity are all names for the same problem. A good description of this situation is available [9].

At this point, it might appear that there always have to be at least as many samples as variables, but there are other ways to formulate this problem. One of them is to delete some variables in the case $m > n$. Many methods exist for choosing which variables to delete [7, 8].

Multiple linear regression with more than one dependent variable

A popular misconception is that MLR is only possible for one dependent variable. This is the case that is almost always found in textbooks. Also, most software packages run MLR in this way. It is easy to extend MLR for more dependent variables. The example given here is for two variables, but extension to more than two is straightforward.

Suppose there are two dependent variables, $\mathbf{y}_1$ and $\mathbf{y}_2$. In this case, one can simply write two MLR's and find two vectors of sensitivities, $\mathbf{b}_1$ and $\mathbf{b}_2$:

$$\mathbf{y}_1 = \mathbf{X}\mathbf{b}_1 + \mathbf{e}_1; \quad \mathbf{y}_2 = \mathbf{X}\mathbf{b}_2 + \mathbf{e}_2 \tag{6}$$

But one can then put $\mathbf{y}_1$ and $\mathbf{y}_2$ side by side in a $n \times 2$ matrix and do the same for $\mathbf{b}_1$ and $\mathbf{b}_2$ and $\mathbf{e}_1$ and $\mathbf{e}_2$. So one gets

$$\mathbf{Y} = \mathbf{X}\mathbf{B} + \mathbf{E} \tag{7}$$

where $\mathbf{Y} = (\mathbf{y}_1\mathbf{y}_2)$, $\mathbf{B} = (\mathbf{b}_1\mathbf{b}_2)$ and $E = (\mathbf{e}_1\mathbf{e}_2)$. A more graphical representation for $2 - p$ dependent variables is

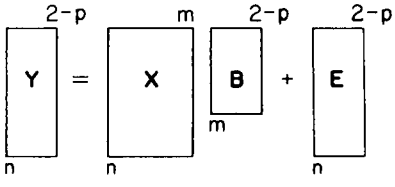

This is the general case that will be referred to in the further text.

Summary: MLR

— For $m > n$, there is no unique solution unless one deletes independent variables.
— For $m = n$, there is one unique solution.
— For $m < n$, a least-squares solution is possible. For $m = n$ and $m < n$, the matrix inversion can cause problems.
— MLR is possible with more than one dependent variable.

PRINCIPAL COMPONENT ANALYSIS (PCA): NIPALS METHOD

Principal component analysis (PCA) is a method of writing a matrix $\mathbf{X}$ of rank r as a sum of r matrices of rank 1:

$$\mathbf{X} = \mathbf{M}_1 + \mathbf{M}_2 + \mathbf{M}_3 + \ldots + \mathbf{M}_r \tag{8}$$

or in graphical representation:

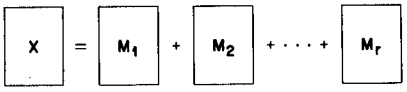

(Rank is a number expressing the true underlying dimensionality of a matrix.) These rank 1 matrices, $\mathbf{M}_h$, can all be written as outer products of two vectors, a score $\mathbf{t}_h$ and a loading $\mathbf{p}_h'$:

$$\mathbf{X} = \mathbf{t}_1\mathbf{p}_1' + \mathbf{t}_2\mathbf{p}_2' + \ldots\ldots\ldots + \mathbf{t}_a\mathbf{p}_a' \qquad (9)$$

or the equivalent $\mathbf{X} = \mathbf{TP}'$ ($\mathbf{P}'$ is made up of the $\mathbf{p}'$ as rows and $\mathbf{T}$ of the $\mathbf{t}$ as columns) or graphically:

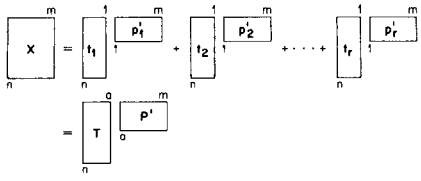

To illustrate what the $\mathbf{t}_h$ and $\mathbf{p}_h'$ mean, an example for two variables, in the two-dimensional plane, is shown in Fig. 2A. Extension to more dimensions is easy but difficult to show on paper. For the example in Fig. 2A, the principal component is the line of best fit for the data points that are shown in Fig. 2B. Best fit means that the sum of squares of x_1 and x_2 residuals is minimized. This is also the average of both regression lines. It goes from $-\infty$ to $+\infty$. The $\mathbf{p}_h'$ is a 1×2 row vector. Its elements, p_1 and p_2, are the direction cosines, or the projections of a unit vector along the principal component on the axes of

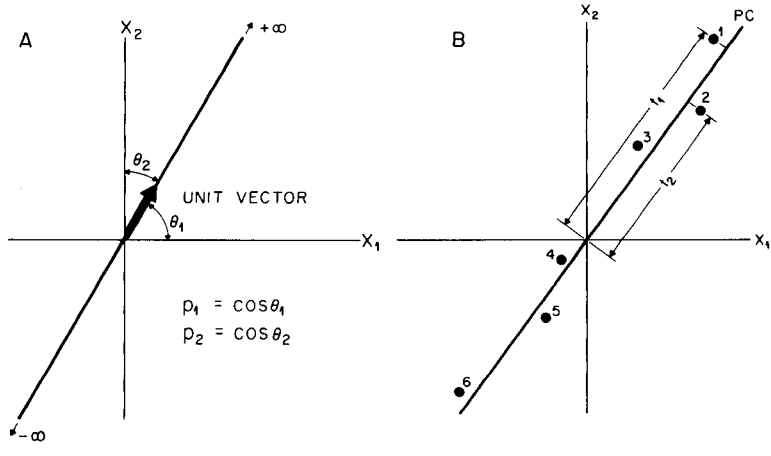

Fig. 2. A principal component in the case of two variables: (A) loadings are the angle cosines of the direction vector; (B) scores are the projections of the sample points (1—6) on the principal component direction. Note that the data are mean-centered.

the plot. The scores vector, t_h, is a $n \times 1$ column vector. Its elements are the coordinates of the respective points on the principal component line (Fig. 2B). For this example, it can easily be understood why one wants the length of the p'_h to be one [$\cos(\theta_1)^2 + \cos(\theta_2)^2 = \cos(\theta_1)^2 + \sin(\theta_1)^2 = 1$]; similar rules exist for more than two dimensions.

Generally, what one wants is an operator that projects the columns of **X** onto a single dimension and an operator that projects the rows of **X** onto a single dimension (see Fig. 3). In the first case, each column of **X** is represented by a scalar; in the second case, each row of **X** is represented by a scalar. In the rest of this section it will be shown that these operators are of a very simple nature.

Nonlinear iterative partial least squares (NIPALS) does not calculate all the principal components at once. It calculates t_1 and p'_1 from the **X** matrix. Then the outer product, $t_1 p'_1$, is subtracted from **X** and the residual E_1 is calculated. This residual can be used to calculate t_2 and p'_2:

$$E_1 = X - t_1 p'_1 \quad E_2 = E_1 - t_2 p'_2 \ldots$$

$$E_h = E_{h-1} - t_h p'_h \ldots \quad E_{\tanh(X)} = 0 = E_{\tanh(X)-1} - t_{\tanh(X)} p'_{\tanh(X)} \tag{10}$$

The NIPALS algorithm is as follows:

(1) take a vector x_j from **X** and call it t_h: $t_h = x_j$ (11)

(2) calculate p'_h: $p'_h = t'_h X / t'_h t_h$ (12)

(3) normalize p'_h to length 1: $p'_{h\,new} = p'_{h\,old} / \| p'_{h\,old} \|$ (13)

(4) calculate t_h: $t_h = X p_h / p'_h p_h$ (14)

(5) compare the t_h used in step 2 with that obtained in step 4. If they are the same, stop (the iteration has converged). If they still differ, go to step 2.

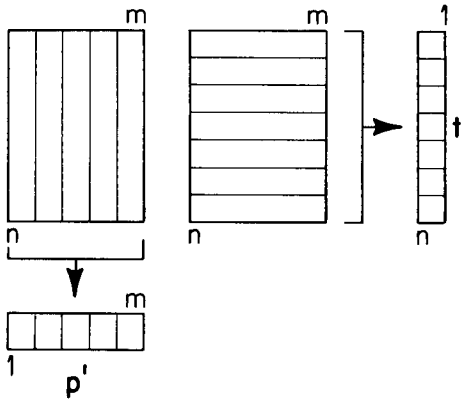

Fig. 3. Scores and loadings are obtained by projecting X into vectors. Loadings: each column of X is projected into an element of the vector p'. Scores: each row of X is projected into an element of the vector t.

(Note that after the first component is calculated, **X** in steps 2 and 4 has to be replaced by its residual.)

An explanation of how NIPALS works can be seen when one realizes that $\mathbf{t}_h'\mathbf{t}_h$ in Eqn. 12, $\|\mathbf{p}_h'\|$ in Eqn. 13 and $\mathbf{p}_h'\mathbf{p}_h$ in Eqn. 14 are scalars. These scalar constants are best combined in one general constant C. Then one can substitute Eqn. 12 into 14: $\mathbf{t}_h = \mathbf{X}\mathbf{p}_h$ and $\mathbf{p}_h' = \mathbf{t}_h'\mathbf{X}$ give $C\mathbf{p}_h' = (\mathbf{X}\mathbf{p}_h)'\mathbf{X}$, or $C\mathbf{p}_h' = \mathbf{p}_h'\mathbf{X}'\mathbf{X}$, or $(C\mathbf{I}_m - \mathbf{X}'\mathbf{X})\mathbf{p}_h = 0$; or one can substitute Eqn. 14 into 12 and get $(C'\mathbf{I}_n - \mathbf{X}\mathbf{X}')\mathbf{t}_h = 0$. These are the eigenvalue/eigenvector equations for $\mathbf{X}'\mathbf{X}$ and $\mathbf{X}\mathbf{X}'$ as used in the classical calculation. ($\mathbf{I}_n$ is the identity matrix of size $n \times n$; $\mathbf{I}_m$ is that of size $m \times m$.) The classical eigenvector and eigenvalue theory is well described by Strang [10].

It has been shown that on convergence, the NIPALS solution is the same as that calculated by the eigenvector formulae. The NIPALS method is convenient for microcomputers; it is also necessary for a good understanding of PLS. Otherwise, it does not matter what method one uses. In practical situations, NIPALS usually converges; in the case of non-convergence, two or more very similar eigenvalues exist. Then it does not matter which combination or rotation of eigenvectors is chosen. The reader is referred to Mardia et al. [5] for a more detailed discussion of PCA.

Summary: PCA

— A data matrix **X** of rank r can be decomposed to a sum of r rank 1 matrices.
— These rank 1 matrices are outer products of vectors called scores and loadings.
— The scores and loadings can be calculated pair-by-pair by an iterative procedure.

PRINCIPAL COMPONENT REGRESSION (PCR)

The results from the section on PCA can be used to explain the principal component transformation of a data matrix **X**. This is a representation of **X** as its scores matrix **T** (where dimensions having small eigenvalues are excluded). The transformation is

$$\mathbf{T} = \mathbf{X}\mathbf{P} \; (= \mathbf{T}\mathbf{P}'\mathbf{P} = \mathbf{T}\mathbf{I}_n) \tag{15}$$

or graphically:

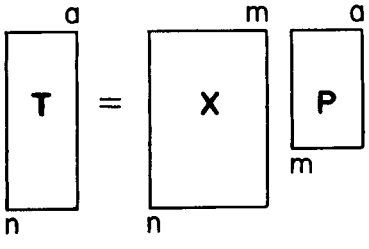

So now the MLR formula can be written as

$$\mathbf{Y} = \mathbf{T}\mathbf{B} + \mathbf{E} \text{ (solution: } \hat{\mathbf{B}} = (\mathbf{T}'\mathbf{T})^{-1}\mathbf{T}'\mathbf{Y}) \tag{16}$$

or graphically:

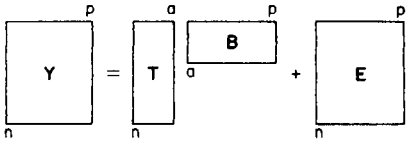

The variables of **X** are replaced by new ones that have better properties (orthogonality) and also span the multidimensional space of **X**. The inversion of $\mathbf{T}'\mathbf{T}$ should give no problem because of the mutual orthogonality of the scores. Score vectors corresponding to small eigenvalues can be left out in order to avoid collinearity problems from influencing the solution [9].

PCR solves the collinearity problem (by guaranteeing an invertible matrix in the calculation of $\hat{\mathbf{B}}$) and the ability to eliminate the lesser principal components allows some noise (random error) reduction. However, PCR is a two-step method and thereby has the risk that useful (predictive) information will end up in discarded principal components and that some noise will remain in the components used for regression.

Detailed information on PCR is given by Mardia et al. [5] and Draper and Smith [7]. Gunst and Mason [8] give a slightly different definition of PCR.

Summary: PCR

— A data matrix can be represented by its score matrix.
— A regression of the score matrix against one or several dependent variables is possible, provided that scores corresponding to small eigenvalues are omitted.
— This regression gives no matrix inversion problems; it is well conditioned.

PARTIAL LEAST-SQUARES REGRESSION

Model building

The PLS model is built on the properties of the NIPALS algorithm. As mentioned in the PCR section, it is possible to let the score matrix represent the data matrix. A simplified model would consist of a regression between the scores for the **X** and **Y** block. The PLS model can be considered as consisting of outer relations (**X** and **Y** block individually) and an inner relation (linking both blocks).

The outer relation for the **X** block (cf. PCA section) is

$$\mathbf{X} = \mathbf{T}\mathbf{P}' + \mathbf{E} = \sum \mathbf{t}_h \mathbf{p}_h' + \mathbf{E} \tag{17}$$

One can build the outer relation for the **Y** block in the same way:

$$\mathbf{Y} = \mathbf{U}\mathbf{Q}' + \mathbf{F}^* = \sum \mathbf{u}_h \mathbf{q}_h' + \mathbf{F}^* \tag{18}$$

Graphically, Eqns. 17 and 18 can be shown as

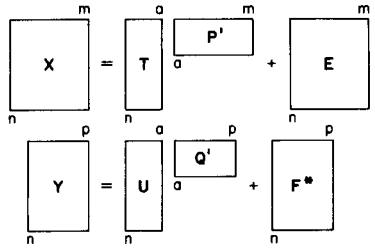

The summations are from 1 to a. One can describe all the components and thus make $\mathbf{E} = \mathbf{F}^* = 0$ or not. How and why this is done is discussed below. It is the intention to describe **Y** as well as is possible and hence to make $\|\mathbf{F}^*\|$ as small as possible and, at the same time, get a useful relation between **X** and **Y**. The inner relation can be made by looking at a graph of the **Y** block score, **u**, against the **X** block score, **t**, for every component (Fig. 4). The simplest model for this relation is a linear one:

$$\hat{\mathbf{u}}_h = b_h \mathbf{t}_h \tag{19}$$

where $b_h = \mathbf{u}_h' \mathbf{t}_h / \mathbf{t}_h' \mathbf{t}_h$. The b_h play the role of the regression coefficients, b, in the MLR and PCR models.

This model, however, is not the best possible. The reason is that the principal components are calculated for both blocks separately so that they have a weak relation to each other. It would be better to give them information about each other so that slightly rotated components result which lie closer to the regression line of Fig. 4.

Over-simplified model: 2x PCA. An over-simplified model can be written in algorithmic form as in the NIPALS section.

For the X block: (1) take $\mathbf{t}_{start}$ = some $\mathbf{x}_j$; (2) $\mathbf{p}' = \mathbf{t}'\mathbf{X}/\mathbf{t}'\mathbf{t}$ (= $\mathbf{u}'\mathbf{X}/\mathbf{u}'\mathbf{u}$); (3) $\mathbf{p}'_{new} = \mathbf{p}'_{old}/\|\mathbf{p}'_{old}\|$; (4) $\mathbf{t} = \mathbf{X}\mathbf{p}/\mathbf{p}'\mathbf{p}$; (5) compare **t** in steps 2 and 4 and if they are equal stop, else go to 2.

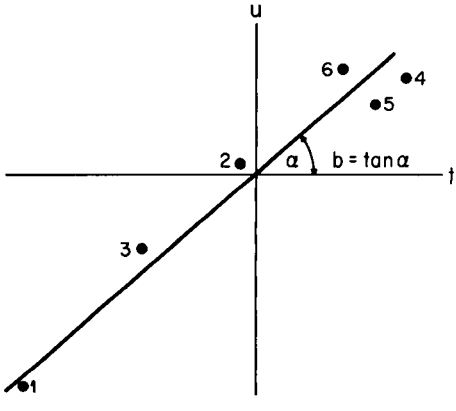

Fig. 4. The inner relation. A linear regression of **u** against **t**. Note that the data are mean-centered.

For the Y block, (1) take $\mathbf{u}_{start}$ = some $\mathbf{y}_j$; (2) $\mathbf{q}' = \mathbf{u}'\mathbf{Y}/\mathbf{u}'\mathbf{u}$ (= $\mathbf{t}'\mathbf{Y}/\mathbf{t}'\mathbf{t}$); (3) $\mathbf{q}'_{new} = \mathbf{q}'_{old}/\|\mathbf{q}'_{old}\|$; (4) $\mathbf{u} = \mathbf{Y}\mathbf{q}/\mathbf{q}'\mathbf{q}$; (5) compare $\mathbf{u}$ in steps 2 and 4 and if they are equal stop, else go to 2.

Improving the inner relation: exchange of scores. The above relations are written as completely separated algorithms. The way each can get information about the other is to let $\mathbf{t}$ and $\mathbf{u}$ change place in step 2. (Note the parts in parentheses in this step.) Thus, the two algorithms can be written in sequence: (1) take $\mathbf{u}_{start}$ = some $\mathbf{y}_j$; (2) $\mathbf{p}' = \mathbf{u}'\mathbf{X}/\mathbf{u}'\mathbf{u}$ ($\mathbf{w}' = \mathbf{u}'\mathbf{X}/\mathbf{u}'\mathbf{u}$); (3) $\mathbf{p}'_{new} = \mathbf{p}'_{old}/\|\mathbf{p}'_{old}\|$ ($\mathbf{w}'_{new} = \mathbf{w}'_{old}/\|\mathbf{w}'_{old}\|$); (4) $\mathbf{t} = \mathbf{X}\mathbf{p}/\mathbf{p}'\mathbf{p}$ ($\mathbf{t} = \mathbf{X}\mathbf{w}/\mathbf{w}'\mathbf{w}$); (5) $\mathbf{q}' = \mathbf{t}'\mathbf{Y}/\mathbf{t}'\mathbf{t}$; (6) $\mathbf{q}'_{new} = \mathbf{q}'_{old}/\|\mathbf{q}'_{old}\|$; (7) $\mathbf{u} = \mathbf{Y}\mathbf{q}/\mathbf{q}'\mathbf{q}$; (8) Compare the $\mathbf{t}$ in step 4 with the one in the preceding iteration step. If they are equal (within a certain rounding error), stop; else go to 2. (In the case for which the Y block has only one variable, steps 5—8 can be omitted by putting $q = 1$.)

This algorithm usually converges very quickly to give rotated components for X and Y block.

Obtaining orthogonal X block scores. There is still a problem; the algorithm does not give orthogonal $\mathbf{t}$ values. The reason is that the order of calculations that was used for the PCA has been changed. Therefore, the $\mathbf{p}'$ are replaced by weights $\mathbf{w}'$ (see formulas in parentheses in previous subsection). An extra loop can be included after convergence to get orthogonal $\mathbf{t}$ values:

$$\mathbf{p}' = \mathbf{t}'\mathbf{X}/\mathbf{t}'\mathbf{t} \tag{20}$$

With $\mathbf{p}'_{new} = \mathbf{p}'_{old}/\|\mathbf{p}'_{old}\|$, it becomes possible to calculate the new $\mathbf{t}$: $\mathbf{t} = \mathbf{X}\mathbf{p}/\mathbf{p}'\mathbf{p}$, but this turns out to be just a scalar multiplication with the norm of the $\mathbf{p}'$ in Eqn. 20: $\mathbf{t}_{new} = \mathbf{t}_{old}\|\mathbf{p}'_{old}\|$. Orthogonal $\mathbf{t}$ values are not absolutely necessary, but they make the comparison with PCR easier. One must give the same rescaling to the weights, $\mathbf{w}'$, if the prediction is to be made without error: $\mathbf{w}'_{new} = \mathbf{w}'_{old}\|\mathbf{p}'_{old}\|$. Then $\mathbf{t}$ can be used for the inner relation as in Eqn. 19, and the residuals can be calculated from $\mathbf{E}_1 = \mathbf{X} - \mathbf{t}_1\mathbf{p}'_1$ and $\mathbf{F}_1^* = \mathbf{Y} - \mathbf{u}_1\mathbf{q}'_1$. In general,

$$\mathbf{E}_h = \mathbf{E}_{h-1} - \mathbf{t}_h\mathbf{p}'_h; \quad \mathbf{X} = \mathbf{E}_0 \tag{21}$$

$$\mathbf{F}_h^* = \mathbf{F}_{h-1}^* - \mathbf{u}_h\mathbf{q}'_h; \quad \mathbf{Y} = \mathbf{F}_0 \tag{22}$$

But in the outer relation for the Y block, $\mathbf{u}_h$ is replaced by its estimator, $\hat{\mathbf{u}}_h = \mathbf{b}_h\mathbf{t}_h$, and a mixed relation is obtained:

$$\mathbf{F}_h = \mathbf{F}_{h-1} - b_h\mathbf{t}_h\mathbf{q}'_h \tag{23}$$

(It is recalled that the aim is to make $\|\mathbf{F}_h\|$ small.) This mixed relation ensures the ability to use the model parameters for predicting from a test set. Furthermore, because the rank of Y is not decreased by 1 for each component, one can go on until the rank of the X block is exhausted. The complete algorithm is given in the Appendix together with an illustration of the matrices and vectors.

Summary: PLS

— There are outer relations of the form $\mathbf{X} = \mathbf{TP}' + \mathbf{E}$ and $\mathbf{Y} = \mathbf{UQ}' + \mathbf{F}^*$.
— There is an inner relation $\hat{\mathbf{u}}_h = b_h \mathbf{t}_h$.
— The mixed relation is $\mathbf{Y} = \mathbf{TBQ}' + \mathbf{F}$ where $\|\mathbf{F}\|$ is to be minimized.
— In the iterative algorithm, the blocks get each other's scores, this gives a better inner relation.
— In order to obtain orthogonal X scores, as in the PCA, it is necessary to introduce weights.

Properties of the PLS factors

For the user of PLS, it is obviously of interest to know what kind of properties to expect from it. The main properties can be summarized as follows.

The quantities $\mathbf{p}_h'$ and $\mathbf{q}_h'$ have unit length for each h: $\|\mathbf{p}_h'\| = \|\mathbf{q}_h'\| = 1$, or $\Sigma p_{hj}^2 = 1$ and $\Sigma q_{hj}^2 = 1$ for $j = 1$ to m.

Both $\mathbf{t}_h$ and $\mathbf{u}_h$ are centered around zero for each h: $\Sigma t_{hi} = 0$ and $\Sigma u_{hi} = 0$ for $i = 1$ to n.

The $\mathbf{w}_h'$ are orthogonal: $\mathbf{w}_i'\mathbf{w}_j = \delta_{ij}\|\mathbf{w}_i'\|^2$ where δ_{ij} is the Kronecker delta.

The $\mathbf{t}_h$ are orthogonal: $\mathbf{t}_i'\mathbf{t}_j = \delta_{ij}\|\mathbf{t}_i\|^2$.

It is useful to check that these properties hold for a number of data sets. These properties are also good indicators for computer rounding errors.

Prediction

The important part of any regression is its use in predicting the dependent block from the independent block. This is done by decomposing the X block and building up the Y block. For this purpose, $\mathbf{p}'$, $\mathbf{q}'$, $\mathbf{w}'$ and b from the calibration part are saved for every PLS factor. It should be noted that the new X block has r samples instead of n.

The independent blocks are decomposed and the dependent block is built up. For the X block, $\mathbf{t}$ is estimated by multiplying X by $\mathbf{w}$ as in the model building part

$$\hat{\mathbf{t}}_h = \mathbf{E}_{h-1}\mathbf{w}_h \tag{24}$$

$$\mathbf{E}_h = \mathbf{E}_{h-1} - \hat{\mathbf{t}}_h\mathbf{p}_h' \tag{25}$$

For the Y block:

$$\mathbf{Y} = \mathbf{F}_h = \sum b_h\hat{\mathbf{t}}_h\mathbf{q}_h' \tag{26}$$

where the summation is over h for all the factors (a) one wants to include and $\mathbf{X} = \mathbf{E}_0$, $\mathbf{Y} = \mathbf{F}_a$.

Number of components

If the underlying model for the relation between X and Y is a linear model, the number of components needed to describe this model is equal to the model dimensionality. Nonlinear models require extra components to describe nonlinearities. The number of components to be used is a very important property of a PLS model.

Although it is possible to calculate as many PLS components as the rank of the X block matrix, not all of them are normally used. The main reasons for this are that the measured data are never noise-free and some of the smaller components will only describe noise, and that, as mentioned in earlier paragraphs, it is common to leave out small components because they carry the problems of collinearity.

This means that there must be one or several methods to decide when to stop. One possible criterion can be found in Eqn. 23, where the norm of $\mathbf{F}_h$ should be small. Figure 5 gives a plot of $\|\mathbf{F}_h\|$ vs. the number of components. It is possible to choose a threshold level and to stop when $\|\mathbf{F}_h\|$ goes below that threshold. Another possibility is to look at the difference between actual and previous $\|\mathbf{F}_h\|$ values and to stop when this becomes small compared to some previously established measurement error. A combination of threshold and difference methods would be preferable.

Sometimes the analysis of variance with F-test on the inner relation can be used to validate the model. In this case, one uses the F-test on the linear regression [7].

The above-mentioned methods are valuable for the model-building stage of PLS. If prediction is desired, another class of methods must be used to establish the number of components needed. These methods are called cross-validation. One can calculate a statistic for lack of prediction accuracy called PRESS (prediction residual sum of squares). Figure 6 gives a sample plot of the PRESS statistic against the number of components. It is obvious that one wants to use the number of components that gives a minimal PRESS. The location of this minimum is not always well defined. The evaluation of the number of components is analogous to the concept of detection limits, i.e., the smallest signal that can be detected in the presence of noise. See [11] for more detail.

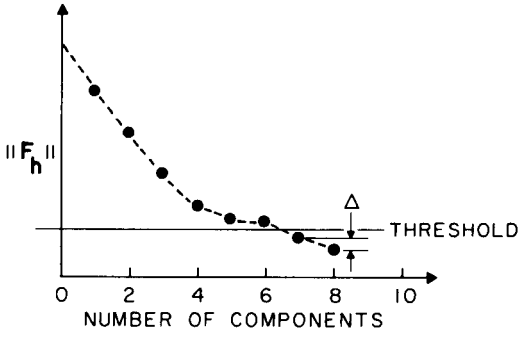

Fig. 5. $\|\mathbf{F}_h\|$ vs. the number of PLS components. A threshold and/or a difference criterion (see Δ in figure) can be used to stop the algorithm.

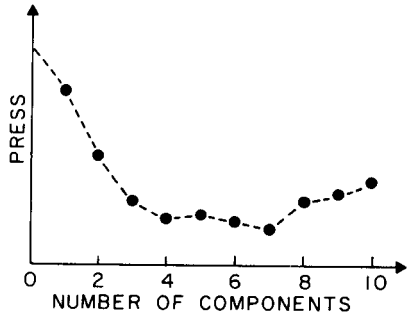

Fig. 6. Plot of PRESS against the number of components. This criterion evaluates the predictive power of the model. The number of components giving a minimum PRESS is the right number for the model that gives optimal prediction. In this example, models with 4—8 components would be acceptable.

Statistics

From the matrices of residuals $\mathbf{E}_h$ and $\mathbf{F}_h$, sums of squares can be calculated as follows: the total sum of squares over a matrix, the sums of squares over rows, and the sums of squares over columns. These sums of squares can be used to construct variance-like estimators. The statistical properties of these estimators have not undergone a rigorous mathematical treatment yet, but some properties can be understood intuitively.

The sum of squares of the $\mathbf{F}_h$ is the indicator of how good the model is (Eqn. 23). The sum of squares of $\mathbf{E}_h$ is an indicator of how much of the **X** block is not used in the model. In some cases, a substantial part of the **X** block does not participate in the model, which means that the independent variables have unexpected properties or large errors.

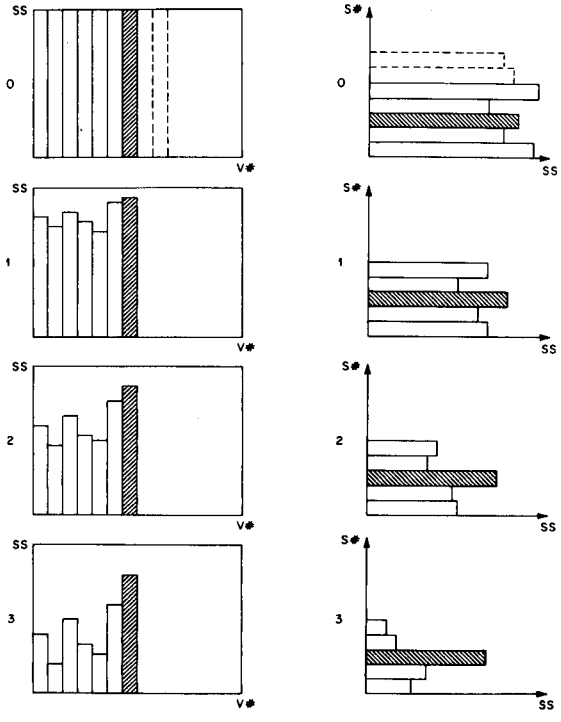

Fig. 7. Statistics for the variables. The data are shown as bars representing the sum of squares per variable (for the model building both X and Y variables; for the prediction only X variables). After 0 PLS components, the data is in mean-centered and variance-scaled form. As the number of PLS components increases, the information in each variable is exhausted. The hatched bar shows the behavior of a "special" variable, one that contributes little to the model.

Fig. 8. Statistics for the objects (samples). The data are shown as bars representing the sum of squares per object. As the number of PLS components increases, the sum of squares for each object decreases. The hatched bar shows the behavior of a "special" object, probably an outlier.

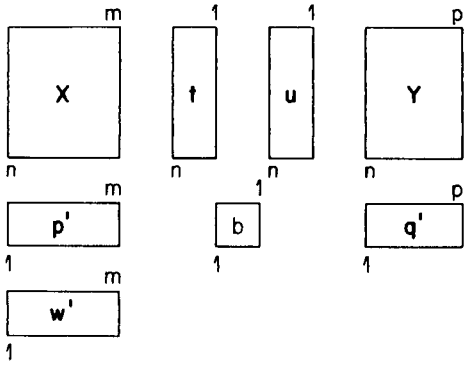

Fig. 9. A graphical representation of the matrices and vectors used in PLS.

Sums of squares over the columns indicate the importance of a variable for a certain component. Sums of squares over the rows indicate how well the objects fit the model. This can be used as an outlier detection criterion. Illustrations are given in Fig. 7 for variable statistics and in Fig. 8 for sample statistics. More on this can be found in the articles by S. Wold et al. as cited elsewhere [4, 6].

An advantage of PLS is that these statistics can be calculated for every component. This is an ideal means of following the model-building process. The evolution of these statistics can be followed (as shown in Figs. 7 and 8) as more and more components are calculated so that an idea of how the different objects and variables fit can be obtained. In combination with a criterion for model dimensionality, the statistics can be used to estimate which objects and variables contribute mainly to the model and which contribute mainly to the residual.

Conclusion

The topic of partial least squares is much larger than the material covered above. Some subjects not discussed at all or not in detail are: outlier detection, treatment of missing data, F and t statistics, classification/pattern recognition, leverage, selection of variables, data transformations, extensions to more blocks and hierarchical models, and lack of fit.

There are also other PLS algorithms. Each may have some advantage in a particular application. The algorithm given here is one of the most complete and elegant ones when prediction is important. An example of its application to simulated data is given in the next paper [11].

The authors thank Svante Wold and Harald Martens for their contributions to the PLS method. This paper results from a number of discussions at the Laboratory for Chemometrics. We thank all colleagues and visitors to the lab and especially Dave Veltkamp for their support and stimulating discussions. The Science Department of the Belgian Ministry of Foreign Affairs provided P. Geladi with a NATO travel grant 10/B/84/BE. Graphics were done by

Louise Rose. This work was supported by a grant from the Center for Process Analytical Chemistry, a National Science Foundation Cooperative Research Center at the University of Washington.

Appendix: The PLS algorithm

It is assumed that X and Y are mean-centered and scaled:

For each component: (1) take $\mathbf{u}_{start}$ = some $\mathbf{y}_j$.

In the X block: (2) $\mathbf{w}' = \mathbf{u}'\mathbf{X}/\mathbf{u}'\mathbf{u}$

(3) $\mathbf{w}'_{new} = \mathbf{w}'_{old}/\|\mathbf{w}'_{old}\|$ (normalization)

(4) $\mathbf{t} = \mathbf{X}\mathbf{w}/\mathbf{w}'\mathbf{w}$

In the Y block: (5) $\mathbf{q}' = \mathbf{t}'\mathbf{Y}/\mathbf{t}'\mathbf{t}$

(6) $\mathbf{q}'_{new} = \mathbf{q}'_{old}/\|\mathbf{q}'_{old}\|$ (normalization)

(7) $\mathbf{u} = \mathbf{Y}\mathbf{q}/\mathbf{q}'\mathbf{q}$

Check convergence: (8) compare the t in step 4 with the one from the preceding iteration. If they are equal (within a certain rounding error) go to step 9, else go to step 2. (If the Y block has only one variable, steps 5—8 can be omitted by putting $q = 1$, and no more iteration is necessary.)

Calculate the X loadings and rescale the scores and weights accordingly:

(9) $\mathbf{p}' = \mathbf{t}'\mathbf{X}/\mathbf{t}'\mathbf{t}$

(10) $\mathbf{p}'_{new} = \mathbf{p}'_{old}/\|\mathbf{p}'_{old}\|$ (normalization)

(11) $\mathbf{t}_{new} = \mathbf{t}_{old}\|\mathbf{p}'_{old}\|$

(12) $\mathbf{w}'_{new} = \mathbf{w}'_{old}\|\mathbf{p}'_{old}\|$

($\mathbf{p}'$, $\mathbf{q}'$ and $\mathbf{w}'$ should be saved for prediction; t and u can be saved for diagnostic and/or classification purposes).

Find the regression coefficient b for the inner relation:

(13) $b = \mathbf{u}'\mathbf{t}/\mathbf{t}'\mathbf{t}$

Calculation of the residuals. The general outer relation for the X block (for component h) is

$\mathbf{E}_h = \mathbf{E}_{h-1} - \mathbf{t}_h\mathbf{p}'_h$; $\mathbf{X} = \mathbf{E}_0$

The mixed relation for the Y block (for component h) is

$\mathbf{F}_h = \mathbf{F}_{h-1} - b_h\mathbf{t}_h\mathbf{q}'_h$; $\mathbf{Y} = \mathbf{F}_0$

From here, one goes to Step 1 to implement the procedure for the next component. (Note: After the first component, X in steps 2, 4 and 9 and Y in steps 5 and 7 are replaced by their corresponding residual matrices $\mathbf{E}_h$ and $\mathbf{F}_h$.)

Matrices and vectors are shown graphically in Fig. 9.

REFERENCES

1 B. Kowalski, R. Gerlach and H. Wold, Chemical Systems under Indirect Observation, in K. Jöreskog and H. Wold (Eds.), Systems under Indirect Observation, North-Holland, Amsterdam, 1982, pp. 191—209.
2 S. Wold, A. Ruhe, H. Wold and W. Dunn, SIAM J. Sci. Stat. Comput., 5 (1984) 735.
3 M. Otto and W. Wegscheider, Anal. Chem., 57 (1985) 63.

4 S. Wold in, H. Martens and H. Russwurm (Eds.), Food Research and Data Analysis, Applied Science Publishers, London, 1983.
5 K. Mardia, J. Kent and J. Bibby, Multivariate Analysis, Academic Press, London, 1980.
6 S. Wold, in B. Kowalski (Ed.), Chemometrics: Mathematics and Statistics in Chemistry, Reidel, Dordrecht, 1984.
7 N. Draper and H. Smith, Applied Regression Analysis, Wiley, New York, 1981.
8 R. Gunst and R. Mason, Regression Analysis and its Applications, M. Dekker, New York, 1980.
9 D. Belsley, E. Kuh and R. Welsch, Regression Diagnostics: Identifying Influential Data and Sources of Collinearity, Wiley, New York, 1980.
10 G. Strang, Linear Algebra and its Applications, Academic Press, New York, 1980.
11 P. Geladi and B. Kowalski, Anal. Chim. Acta, 185 (1986) 19.

Analytica Chimica Acta, 185 (1986) 19—32
Elsevier Science Publishers B.V., Amsterdam — Printed in The Netherlands

AN EXAMPLE OF 2-BLOCK PREDICTIVE PARTIAL LEAST-SQUARES REGRESSION WITH SIMULATED DATA

PAUL GELADI

Chemometrics Group, Department of Organic Chemistry, Umeå University, S 901 87 Umeå (Sweden)

BRUCE R. KOWALSKI

Laboratory for Chemometrics, Department of Chemistry, University of Washington, Seattle, WA 98195 (U.S.A.)

(Received 29th October 1985)

SUMMARY

Practical examples with simulated data are described to illustrate the material described in the preceding tutorial on partial least-squares regression. Starting from the perfect model for two dimensions, noise, nonlinearities and interference are added gradually in order to study their influence. The examples are related to calibration in chemical analysis.

An algorithm for partial least-squares (PLS) regression was described in the preceding paper [1] in which it was explained how PLS emerged from studies of the flaws in multiple linear regression (MLR) and in principal component regression (PCR). The advantages of the PLS method were outlined. Examples of how the PLS method can be used are given here. Simulated data with known properties are used because such data are more suitable for illustrative purposes than practical laboratory data with their unknown sources and extents of vitiating effects. Extensions to real situations can readily be visualized. The focus here is on calibration in chemical analyses. This paper has two purposes: to provide a worked example with all the numerical data for testing computer programs and to study the influence of random noise, nonlinearities and interfering extra components. This last topic is considered in an empirical way with the hope that a more theoretical approach can be developed later. The example is a regression for two chemical components (i.e., two dimensions, tank 2), into which complications including noise, nonlinearities and interferences are gradually introduced.

The PLS method

In the PLS method, an X block of independent variables is related to a Y block of dependent variables by describing outer relations [1]:

$$\mathbf{X} = \mathbf{TP}' + \mathbf{E} = \sum \mathbf{t}_h \mathbf{p}_h' + \mathbf{E} \qquad (1)$$

0003-2670/86/$03.50

$$\mathbf{Y} = \mathbf{UQ}' + \mathbf{F}^* = \sum \mathbf{u}_h \mathbf{q}_h' + \mathbf{F}^* \quad (2)$$

(Symbols are defined in Table 1 [1]). The sums are over the number of dimensions necessary or desired. The regression part of PLS is an inner relation:

$$\hat{\mathbf{u}}_h = b_h \mathbf{t}_h \quad (3)$$

where $b_h = \mathbf{u}_h' \mathbf{t}_h / \mathbf{t}_h' \mathbf{t}_h$; the "hat" indicates that the vector is an estimated one. This leads to the mixed relation [1]

$$\mathbf{Y} = \mathbf{TBQ}' + \mathbf{F} \quad (4)$$

where $\|\mathbf{F}\|$ has to be minimized with the condition that $\|\mathbf{E}\|$ in Eqn. 1 is reduced.

In order to obtain orthogonal scores as in PCR, it is necessary to introduce weighting (**w**); PLS is achieved by using the residuals after each dimension:

$$\mathbf{E}_h = \mathbf{E}_{h-1} - \mathbf{t}_h \mathbf{p}_h'; \quad \mathbf{X} = \mathbf{E}_0 \quad (5)$$

$$\mathbf{F}_h = \mathbf{F}_{h-1} - b_h \mathbf{t}_h \mathbf{q}_h'; \quad \mathbf{Y} = \mathbf{F}_0 \quad (6)$$

Graphic representations of Eqns. 1 and 2 and of the matrices and vectors used in the PLS algorithm for each dimension are in the preceding paper [1]. The PLS dimensions can also be called components or factors. In this paper, the term dimension is used in order to avoid confusion; the symbol **B** indicates the diagonal matrix of the b_h.

It is important to recognize some of the properties of the PLS model: SS_Y, F and $XVAL$. SS_Y is the residual for the Y block after n dimensions. This is usually expressed as the sum of squares for the residual matrix $\mathbf{F}_h$ (Eqn. 4) divided by the number of members of the matrix. For the Y block, this is termed SS_Y. Sometimes, a similar statistic (SS_X) can be useful for the X block.

One way of evaluating the PLS model is to check the inner relation (Eqn. 3). The F-test can be applied to the linear regression in this case (see Draper and Smith [2]). High F values indicate a good inner relation and low F values a poor inner relation; very low F values show that the inner relation is meaningless. The $XVAL$ method [3, 4] describes the predictive quality of a certain PLS dimension by the use of cross-validation and is calculated on the "leave-some-out" basis. The method is described in Appendix A. A value of $XVAL > 1$ means a nonsignificant dimension; $XVAL < 1$ means a significant dimension. The cross-validation for the calculation of $XVAL$ means extra calculations; **F** on the inner relation and SS_Y do not need these.

DATA MATRICES IN CALIBRATION FOR CHEMICAL ANALYSIS

Multivariate calibration means measuring a vector of properties (variables) for calibration standards of known content. This vector may be spectral intensities, current measurements or any relevant collection of data. In this

example, two analytes A and B are used and the responses of the sensors are shown in Fig. 1. Table 1 gives the concentrations of each of these analytes in nine different samples. It is often advantageous to use a factorial design for such an example. Here, a 3^2 design was chosen because of the nonlinearities that will be introduced later. However, it may not always be possible to mix suitable standards (e.g., in food research, geology, environmental samples). In such cases, a collection of samples spanning the maximal expected range in each variable dimension must be chosen. Suitable choice of a design can lead to good results (see below).

In the simple case considered, the data matrix will be the sum of two planes, each consisting of the outer product of the concentration vector and the response vector as in Fig. 2(a). The X-matrix is built from

$$\mathbf{X} = \mathbf{c}_1\mathbf{s}_1' + \mathbf{c}_2\mathbf{s}_2' \tag{7}$$

where $\mathbf{c}_i$ are the concentration vectors from Table 1 and $\mathbf{s}_i'$ are the responses from Fig. 1. In reality, this situation is complicated by the existence of random noise, nonlinearities and interferences, as indicated in Fig. 2(b). The sum matrix in Fig. 2(b) is the independent (X) matrix for the regression of the two vectors of concentrations from Table 1. The following eight cases are possible: linearity with and without random noise for only two components; nonlinearity with and without random noise for two components; linearity with and without random noise for two components and one interfering (background) component, i.e., an extra component not recognized during calibration; and nonlinearity with and without random noise for two components and one interfering component. It is clear here that the last case with random noise, and even more complicated situations, will be encountered in practice, but for illustrative purposes four of the above models will be considered in the following paragraphs. The data will always be used in mean-centered form.

Case 1: Linearity without random noise for two components

In this case (cf. Fig. 9 [1]), it is known in advance that there will only be two components. The criteria for testing the model dimensionality, SS_Y, F and $XVAL$, indicate this. Indeed, for the second PLS dimension, $XVAL$

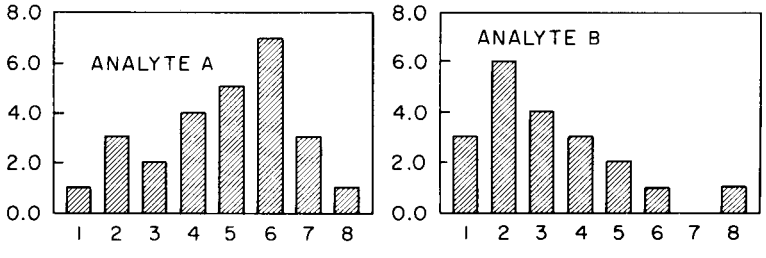

Fig. 1. The responses ("spectra") of an array of eight sensors for analytes A and B. The numbers are arbitrary.

TABLE 1

Concentrations of the analytes A and B used for the PLS calibration

Sample	1	2	3	4	5	6	7	8	9
Concn. (analyte A)	1	3	5	1	3	5	1	3	5
Concn. (analyte B)	1	1	1	3	3	3	5	5	5

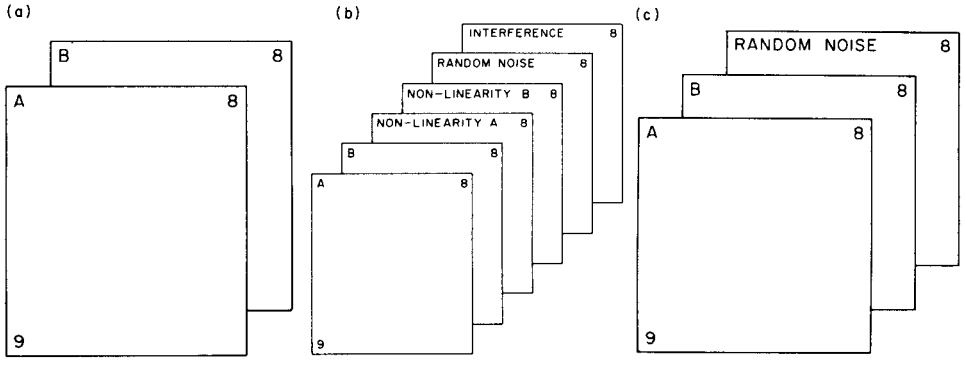

Fig. 2. Composition of the data matrices **X**: (a) for case 1 with two components (analytes A and B) and linearity but without noise and interfering or background components; (b) the most complicated case in which both components have nonlinearities, and both random noise and an interfering (or background) component are present; (c) random noise only added to (a).

becomes zero (the rounding error in most computers) and F becomes infinity (the inverse of the rounding error in most computers). Both SS_X and SS_Y become zero after two components.

It can be shown that the X scores obtained are exactly the same (sometimes with different sign) as those obtained by PCR, i.e., PLS and PCR behave identically in the noise-free case. For PLS, the loadings and weights for the X block are identical. The inner relationships are straight lines, as expected, and so are not shown here. It is of interest to look at the scores plot in Fig. 3. Because of the choice of the concentrations in the experimental design, the plot has the shape of a grid. It should be noted that each dimension describes exactly 50% of the variance in the Y block. This is true both for variance-scaled and non-variance-scaled data. In real cases, noise-free measurements will be very rare. The data for this case are given in Appendix B.

Conclusion. For case 1, SS_X, SS_Y, F and $XVAL$ clearly show that there are two dimensions. The PLS and PCR methods are equivalent in this case, and the PLS loadings and weights are the same. These results are independent of linear scaling of the variables.

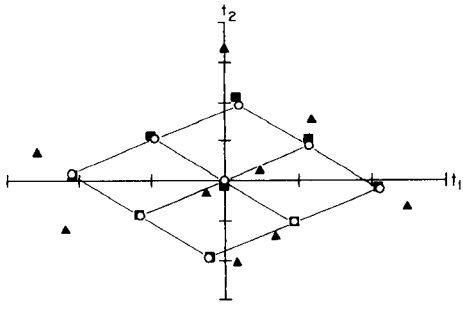

Fig. 3. The scores plot for the data matrix: (○) noise-free data; (■) 10% noise added; (▲) 100% noise added. Because of the choice of the concentrations as a 3^2 design, the points representing the samples fall on a grid for the noise-free data. Large amounts of noise completely destroy the grid structure.

Case 2: Linearity with random noise for two components

The X matrix in this case is shown schematically in Fig. 2(c). The best way to describe the influence of noise is to add increasing amounts of noise to the noise-free data and to see how the PLS models behave. In order to do this, mean-centered noise distributed as $N(0, p)$ (with p = 0.01, 0.02, 0.05, 0.1, 0.2, 0.5 and 1.0) was added to every column of the X matrix after variance-scaling. This way of adding noise ensures that each variable is affected equally; there are many other ways of adding noise to data, so this method simply illustrates a general trend that can be applied to other cases. No noise was added to the Y block; it is assumed that the concentrations of the standards are accurate.

The addition of random noise increases the rank of the X matrix from 2 to the maximum (8 in this case), because the noise is distributed equally in all the dimensions of the variable space. Figure 4 provides a graphic explanation of this phenomenon. This can also be checked by doing a principal component analysis on the noise alone.

As long as the components have a larger variance than the noise in their own dimension, there will be an adequate 2-dimensional model, but the noise may cause slight rotations of the scores. For larger amounts of noise, total confusion of noise and data can be expected. Because the noise will be of different character in real samples, increasing amounts of noise are expected to give increasing prediction errors. It should be noted that random noise is hypothetical. In practice, application of this random noise behaves as a bias. The difference from a real bias is that noise can be averaged out by repeating measurements.

Results are given in Table 2. They are based on only one application of the noise, and so the picture given is only rough. For up to 5% noise added, the first dimension describes almost 50% of the Y block and two dimensions describe almost all the rest. The F-test on the inner relation shows decreasing values with increasing noise, meaning that the inner relation becomes worse.

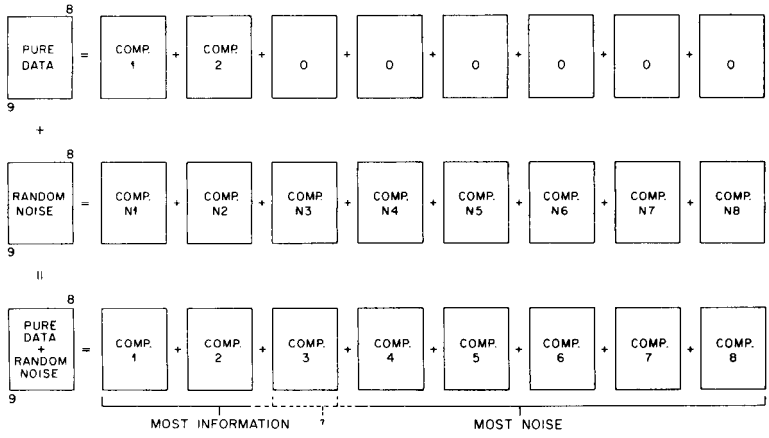

Fig. 4. The influence of noise on the PLS model. For pure analyte data (A and B) the rank of the X block is 2. For only random noise, the rank of the X block is maximal (here 8). For random noise added to the pure analyte data, there will be some disorder: most useful information will end up in the first dimensions and most noise will end up in higher dimensions. PLS can handle small amounts of random noise but higher amounts of noise can prevent the construction of useful models.

TABLE 2

The influence of noise added to the X block on the PLS model[a]

After	Noise added, $N(0, p)$, p =						
	0.01	0.02	0.05	0.1	0.2	0.5	1.0
A: F-test on the inner relation							
Dim. 1	2000000	11800	66000	23000	7300	400	32
Dim. 2	116000	69000	26000	1460	524	59	14
Dim. 3	—	23	5	69	36	3	2.2
Dim. 4	—	—	—	57	21	16	15
B: SS_Y *(%, 100% for no. dimensions calculated)*							
Dim. 1	50	50	50	50.02	50.05	50.9	59
Dim. 2	0.001	0.008	0.019	0.26	0.71	6.2	26
Dim. 3	—	0.005	0.013	0.036	0.15	4.8	22
C: XVAL							
Dim. 1	0.93	0.93	0.93	0.92	0.92	0.91	1.04
Dim. 2	0.009	0.015	0.028	0.076	0.22	0.47	0.87
Dim. 3	1.04	0.99	0.93	0.48	0.57	1.43	1.11
Dim. 4	—	1.08	1.01	0.85	0.75	0.93	0.92

[a]Blank spaces mean that the PLS stopped because residuals were too low.

There is also a steep fall in F after two dimensions. For very noisy data, less significant inner relations are found or the more significant relations appear in later dimensions. *XVAL* shows a 2-dimensional model for up to 5% noise. With 10% or more noise, the models are of higher rank, which confirms the failure to distinguish between data and noise. Figure 3 shows the influence of noise on the scores plot.

Prediction was done by using the 2-dimensional model for noise-free data with test sets with different noise contents. The results are given in Table 3 as the square root of the PRESS (see Appendix A). This statistic behaves like a standard deviation. The results in the table indicate that $(\text{PRESS})^{1/2}$ increases almost linearly with the amount of noise added. The very low result for $p = 0.05$ is due to the nature of the noise applied, as was shown by repeating some calculations.

Conclusion. For case 2, random noise in the X matrix gives it maximum rank. Increasing amounts of random noise shift information towards higher dimensions and make it difficult to decide on the correct number of dimensions. Up to 5% noise gives a precise, quantitative model, but over 5% and up to 100% noise provides a model that only allows qualitative conclusions. Prediction shows that the square root of PRESS increases almost linearly with the random error added.

Case 3: Nonlinearity without random noise for two components

Nonlinearities can be introduced by adding terms that are quadratic in the concentrations:

$$X = \mathbf{c}_1\mathbf{s}_1' + \mathbf{c}_2\mathbf{s}_2' + b_1\mathbf{c}_1^*\mathbf{c}_1\mathbf{s}_1' + b_2\mathbf{c}_2^*\mathbf{c}_2\mathbf{s}_2' \qquad (8)$$

where * indicates the direct vector product and the b_i are constants determining how much nonlinearity is present. A representation with matrices as planes is given in Fig. 5. For linear responses, $b_1 = b_2 = 0$. The Y block contains the linear concentrations so that the nonlinearities will obviously cause

TABLE 3

The result of random error added to a test set on the prediction error, $(\text{PRESS})^{1/2}$ for analytes A and B

Random error $N(0, p)$ p =	$(\text{PRESS})^{1/2}$		$(\text{PRESS})^{1/2}/p$	
	Anal. A	Anal. B	Anal. A	Anal. B
0.01	0.011	0.013	1.1	1.3
0.02	0.016	0.020	0.80	1.0
0.05	0.027	0.024	0.54	0.48
0.1	0.091	0.149	0.91	1.49
0.2	0.194	0.235	0.97	1.18
0.5	0.517	0.530	1.03	1.06
1.0	1.19	1.56	1.19	1.56

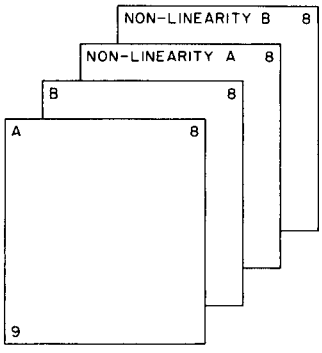

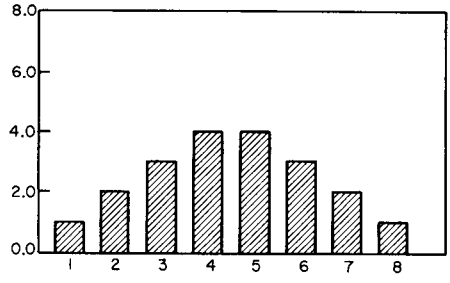

Fig. 5. The data matrix X for two components with nonlinearities. Because of the way that the nonlinearities are defined in Eqns. 8 and 9, each analyte has a set of them.

Fig. 6. The responses (spectrum) of an array of eight sensors for the interfering or background component. The numbers are arbitrary units.

problems. These nonlinearities are not random, but act as a concentration-dependent bias.

The nonlinearities do not increase the rank of the X matrix. This can be seen by writing Eqn. 8 in another way:

$$X = (\mathbf{c}_1 + b_1\mathbf{c}_1^*\mathbf{c}_1)\mathbf{s}_1' + (\mathbf{c}_2 + b_2\mathbf{c}_2^*\mathbf{c}_2)\mathbf{s}_2' \qquad (9)$$

The results for some model calculations with different b_1 and b_2 are listed in Table 4. The data were used in mean-centered and variance-scaled form. These results show that increasing amounts of nonlinearity in a certain component introduce increasing amounts of residual sum of squares for the respective column vector in the Y block. Each analyte behaves independently with respect to the nonlinearity of the other. The F values for the inner relations show that these also become rather curved. The fact that the rank of the X block does not increase, as shown in Eqn. 9, is typical of this mode of adding nonlinearities. The situation changes when cross-terms are added, e.g., if there is mutual interference between the spectra of two analytes as happens frequently in real situations.

Prediction with nonlinear data was tested by using the model parameters for the linear data for prediction with test sets containing nonlinear data. Because of the independent behavior of the two analytes, simplified results are given in Table 5. These results show that higher b_i values cause higher errors and that the higher the concentration the higher the error. Expressing the inaccuracies as percentage shows that they increase linearly with b_i and quadratically with concentration. This is what would be expected from Eqns. 8 and 9.

Conclusion. For case 3, nonlinearities of the type used here do not increase the rank of the X block. Increasing amounts of nonlinearity give larger residuals for the Y block. The results for each analyte are not influenced by the

TABLE 4

Some properties of PLS models for nonlinear data[a]

b_1	b_2	SS_{y1}	SS_{y2}	F_1	F_2
0.01	0	0.006	0	96100	153000
0.1	0	0.26	0	1790	5400
1.0	0	1.32	0	264	10900
0	0.01	0	0.006	137000	103000
0	0.1	0	0.26	2290	3300
0	1.0	0	1.32	276	4100
0.01	0.01	0.006	0.006	59000	59000
0.1	0.1	0.26	0.26	1340	1340
1.0	1.0	1.32	1.32	257	257

[a] b_i and SS_{yi} are for the first and second analyte, respectively, for the complete 2-dimensional model. F_i are for the first and second inner relations.

TABLE 5

Prediction results for nonlinear data

True concn.	Concn. found for b_i =		
	0.01	0.1	1.0
1	1.01 (1%)	1.1 (10%)	2.0 (100%)
3	3.09 (3%)	3.9 (30%)	12 (300%)
5	5.25 (5%)	7.5 (50%)	30 (500%)

nonlinearities for the other analyte. For prediction, the inaccuracies increase linearly with b_i and quadratically with concentration.

Case 4: Linearity without random noise for two components plus one interfering component

There are many possibilities for simulating an interfering or background component. The uncommon case in which the interfering component gives exactly the same analytical response (e.g., spectrum) as one of the required components will not be discussed here, nor will the case in which the concentrations of the interferent are exactly correlated with those of one of the analytes. A trivial situation occurs if the interfering component has the same concentration in all samples; the constant background so obtained is simply removed by mean-centering. The spectrum of the interfering product is given in Fig. 6. A simple pattern of concentrations of interferent is given in Table 6. The amount d can be varied to study its influence on the PLS model. A schematic representation of the X block for this example is the same as that shown in Fig. 2(c); interference simply replaces random noise in the figure. With the interfering component present, the X matrix will have rank 3. The

TABLE 6

Concentrations of analytes A and B and interferent I. The amount d is varied to study its influence on the PLS model

Sample number	Concentrations		
	A	B	I
1	1	1	1d
2	3	1	2d
3	5	1	1d
4	1	3	2d
5	3	3	1d
6	5	3	2d
7	1	5	1d
8	3	5	2d
9	5	5	1d

amount of variation of the Y block explained by the first two components will depend on d and on the correlation of the interferent spectrum with the analyte spectra.

Some results for the PLS model for different d values are shown in Table 7. The F-test clearly shows rapid deterioration of the inner relation as the amount of interferent increases. The SS_Y shows a more than linear increase in the amount of the Y block, which remains unexplained by a 2-dimensional model until a plateau is reached. The $XVAL$ indicates a 2-dimensional model, but it is poor for high values of d. A complicating problem with interferences is that there can be a large variety of spectra to choose from and that the influence on the model depends greatly on the correlation between the analytical responses of the interferents and those of the analytes.

Conclusion. For case 4, the prediction properties were checked for data containing interferent with the model for interference-free data. There is a positive bias which is linearly related to the concentration of the interfering component. Every interfering component increases the rank of the X block by 1. The influence of the interferent on the model is nonlinearly related to the amount of interferent present.

General conclusion

The use of simulated data illustrates that many interesting properties of PLS regression can be found by testing models and prediction. The criteria of dimensionality, SS_Y, F and $XVAL$, each contribute particularly in different situations. In the general case, calculation of all three criteria of dimensionality (and maybe even others) is necessary to obtain a fairly realistic picture of the behavior of a PLS model. Only four of the eight cases mentioned initially were actually tested but it is hoped that these papers will provide a better understanding of the PLS method.

TABLE 7

Some properties of the PLS model as a function of d

	d =						
	0.1	0.2	0.5	1.0	2.0	5.0	10.0
A: F-test on the inner relation							
Dim. 1	18400	4600	740	186	47	8.9	2.7
Dim. 2	172000	19000	7000	1860	570	239	384
B: SS_Y *(%, 100% start situation)*							
Dim. 1	50.02	50.08	50.5	51.8	56.4	72.0	86.0
Dim. 2	0.02	0.08	0.52	0.2	7.1	25.0	40.0
SS_Y/d	0.2	0.4	1.0	2.0	3.5	5.0	4.0
C: XVAL							
Dim. 1	0.93	0.93	0.93	0.94	0.96	1.03	1.07
Dim. 2	0.02	0.05	0.11	0.22	0.40	0.75	0.90

The colleagues in Seattle and Umeå are thanked for their remarks and stimulating discussions. The Science Department of the Belgian Ministry of Foreign Affairs provided P. Geladi with a NATO grant 10/B/84/BE, which is gratefully acknowledged.

Appendix A: Cross-validation in PLS

In building and using a regression model, robust models are needed which will allow prediction with minimal error. The prediction quality can be tested by predicting the independent variables from the dependent ones for some standards of known composition and comparing the results predicted from the model with the known composition. But in many cases, such absolute standards are not available and when they are available it is best to include them in the model. Cross-validation is a method for testing the internal consistency of a regression model while it is being constructed.

Cross-validation can be done for every dimension or for a fixed number of dimensions. The important thing is that a fraction of the calibration standards are omitted in the model building. This fraction can vary from a single object (bootstrapping) to half the objects. This can be written as

$X_m \langle \longrightarrow Y_m$

$X_t \qquad Y_t$

The successive steps are: (1) the model is built between X_m and Y_m; (2) from the model parameters, $\hat{Y}_t$ is predicted from X_t; (3) the sum of squares ss of $(Y_t - \hat{Y}_t)$ is calculated; (4) this sum of squares is added to SS; (5) the fraction that was omitted is reinstated and another fraction of approximately the same size is omitted. Calculations then revert to step 1.

This procedure is repeated until all the objects have been in X_t once. Then SS is the accumulated prediction error sum of squares for all the objects. Finally SS is divided by the size of the Y matrix to give PRESS. (The size of the Y matrix can be replaced by a more fancy number of degrees of freedom.) When this is tested for every dimension, the square root of PRESS is compared with the standard deviation of the Y block of the previous dimension as follows: $XVAL = (\text{PRESS})^{1/2}/s_Y$. If this $XVAL > 1$, the current

TABLE A1

The raw data matrices X and Y for case 1 with mean and standard deviations (SD) and the final data matrices

Object	Variable									
	$x1$	$x2$	$x3$	$x4$	$x5$	$x6$	$x7$	$x8$	$y9$	$y10$
Raw data										
1	4	9	6	7	7	8	3	2	1	1
2	6	15	10	15	17	22	9	4	3	1
3	8	21	14	23	27	36	15	6	5	1
4	10	21	14	13	11	10	3	4	1	3
5	12	27	18	21	21	24	9	6	3	3
6	14	33	22	29	31	38	15	8	5	3
7	16	33	22	19	15	12	3	6	1	5
8	18	39	26	27	25	26	9	8	3	5
9	20	45	30	35	35	40	15	10	5	5
Mean	12	27	18	21	21	24	9	6	3	3
SD	5.4772	11.619	7.7459	8.6603	9.3274	12.247	5.1962	2.4495	1.7321	1.7321
Mean-centered and variance-scaled data matrices										
1	−1.4606	−1.5492	−1.5492	−1.6166	−1.5010	−1.3064	−1.1547	−1.6330	−1.155	−1.155
2	−1.0954	−1.0328	−1.0328	−0.69282	−0.42885	−0.16330	0	−0.81650	0	−1.155
3	−0.73030	−0.51640	−0.51640	0.23094	0.64327	0.97980	1.1547	0	1.155	−1.155
4	−0.36515	−0.51640	−0.51640	−0.92376	−1.0721	−1.1431	−1.1547	−0.81650	−1.155	0
5	0	0	0	0	0	0	0	0	0	0
6	0.36515	0.51640	0.51640	0.92376	1.0721	1.1431	1.1547	0.81650	1.155	0
7	0.73030	0.51640	0.51640	−0.2309	−0.6433	−0.9798	−1.1547	0	−1.155	1.155
8	1.0955	1.0328	1.0328	0.69282	0.42885	0.16330	0	0.81650	0	1.155
9	1.4606	1.5492	1.5492	1.6166	1.5010	1.3064	1.1547	1.6330	1.155	1.155

dimension has no predictive properties. If $XVAL < 1$, the current dimension is useful and the next one should be tested.

An alternative is to collect *SS* for every variable in the Y block instead for over the whole block. This then gives an *XVAL* for each Y variable. Checking these *XVAL*'s is considered a fine-tuning of the cross-validation process and is certainly worthwhile when many Y variables are considered.

Cross-validation can also be done for many dimensions simultaneously. In this case, PRESS is again calculated but for whole models of increasing dimensionality. If this PRESS is plotted against the model dimensionality, it gives a minimum for the model with the best predictive properties. An example is shown in Fig. 6 of the earlier paper.

Appendix B: Example for case 1

This appendix presents a worked example for case 1. The raw data, mean and standard deviations, and the mean-centered, variance-scaled data matrices are shown in Table A1.

Because of the choice of a 3^2 design, interesting patterns show up in both blocks. The center element of the design has zeroes for every variable. The seventh X variable is perfectly correlated to the first Y variable because the second sensor sensitivity is zero here. The columns for the second and third X variables are identical because the ratios for the sensor sensitivities for both are the same. The loadings and scores for two dimensions are shown in Tables A2 and A3. It is very common that the first X-block loading has all-positive elements. Because of the orthogonality requirement, the second X-block loading must have some negative elements. The special property of orthogonality for the Y-block loadings is only valid for this example. The construction of the data matrix as a 3^2 design together with mean-centering and variance-scaling gives symmetrical properties which makes it easier to understand what is happening and to detect erratic behavior.

TABLE A2

Loadings for two dimensions[a]

p	Variable									
	*x*1	*x*2	*x*3	*x*4	*x*5	*x*6	*x*7	*x*8	*y*9	*y*10
1	0.33026	0.35600	0.35600	0.38850	0.37018	0.33148	0.29936	0.38729	0.76965	0.6384
2	−0.4480	−0.3417	−0.3417	0.04154	0.26034	0.44373	0.54149	−0.0787	0.63847	−0.7696

[a]In this case, the loadings and weights for the X block are identical. The Y block has no weights.

TABLE A3

Scores for two dimensions

	Object									
	1	2	3	4	5	6	7	8	9	b[a]
*t*1	−4.180	−1.895	0.3894	−2.285	0	2.285	−0.3894	1.895	4.180	0.3889
*t*2	0.1786	1.048	1.917	−0.8693	0	0.8693	−1.917	−1.048	−0.1786	0.8481
*u*1	−1.626	−0.7372	0.1515	−0.8887	0	0.8887	−0.1515	0.7372	1.626	
*u*2	0.1515	0.8887	1.626	−0.7372	0	0.7372	−1.626	−0.8887	−0.1514	

[a]Regression coefficients for the inner relation.

REFERENCES

1 P. Geladi and B. Kowalski, Anal. Chim. Acta, 185 (1986) 1.
2 N. Draper and H. Smith, Applied Regression Analysis, Wiley, New York, 1981, pp. 33—40.
3 S. Wold, H. Martens and H. Wold, in Ruhe and Kågström (Eds.), Matrix Pencils, Springer, Heidelberg, pp. 286—293.
4 S. Wold, in H. Martens and H. Russwurm (Eds.), Food Research and Data Analysis, Applied Science Publishers, London, 1983, pp. 147—188.

Analytica Chimica Acta, 185 (1986) 33—48
Elsevier Science Publishers B.V., Amsterdam — Printed in The Netherlands

PERFORMANCE OF A GENERAL-PURPOSE ELECTROCHEMICAL INSTRUMENT AIDED BY A STAND-ALONE MICROCOMPUTER SYSTEM IN TRACE ANALYSIS

N. FANELLI, R. FUOCO, D. GUIDARINI and P. PAPOFF*

Istituto di Chimica Analitica Strumentale, C.N.R., c/o Dipartimento di Chimica e Chimica Industriale dell'Università, Via Risorgimento 35, 56100 Pisa (Italy)

(Received 31st December 1985)

SUMMARY

The features of a microprocessor-based data acquisition and control unit, dedicated to electrochemical experiments, are described. The menu-selectable software allows smoothing, baseline drawing and subtraction as well as differentiation, even with signal amplitudes of some tenths of nA at signal/noise ratios lower than one, without forcing the data to follow theoretical models. Concentrations of cadmium ion as low as 2×10^{-7}, 5×10^{-8} and 5×10^{-9} M can be measured, within 10% accuracy and precision, by using sampled d.c. polarography, staircase voltammetry and fast-sweep differential pulse voltammetry, respectively; this is a consistent improvement on literature data. Depending on the electrochemical technique used, the most significant signal parameters, including derivatives, are measured automatically, listed and used in the decision-making process for chemical characterization.

Numerous papers have been published in recent years dealing with computer-aided instruments for polarographic and voltammetric analysis [1—12]. When the final purpose for these instruments is the automatic interpretation of the signal being considered, and very low concentrations of analyte are involved, three steps have to be used consecutively and are decisive in data processing: the steps are smoothing, baseline correction and evaluation of signal parameters. The higher the quality of algorithms used, the higher the accuracy of the measured parameters, and so the easier it will be to identify and quantify the signal.

Generally, smoothing has been done at fairly high concentration levels, e.g., 4×10^{-6} M in differential pulse polarography (d.p.p.) [3], 3×10^{-3} M in sampled d.c.p. [13] and 10^{-3} M in a.c.p. [14], by Savitsky-Golay and Fourier Transform algorithms, and at low concentration levels, e.g., 4×10^{-8} M in d.p.p. [3] and 5×10^{-8} M in square-wave polarography [15], by ensemble averaging. Baseline correction has been done by a linear (tangent fit), quadratic or cubic least-squares fit down to 10^{-6} M in sampled d.c.p. [16], 10^{-7} M in normal pulse polarography (n.p.p.) [16], and 10^{-7} M [17] and 5×10^{-8} M [18] in d.p.p. Experimental procedures have also been proposed for the subtraction of blanks [19—21] and charging currents [22—25]. Evaluation of

signal parameters has been achieved by two different approaches: the use of experimental points only [18, 26, 27] and the use of a cubic least-squares fit to interpolate between experimental points and so gain higher resolution [28]. A study of the literature suggests that no more than two of the above steps have been considered at any one time. This may account for the relatively high concentrations for which signals have been reported. Owing to the characteristics of these signals, the claimed detection limits sometimes appear to be optimistically evaluated.

Based on the above studies, some interesting instruments are now available on the market. However, the existing features of these instruments, even the most advanced ones, are still far from exploiting the full potential of the associated microcomputer systems. It is the aim of this paper to provide a brief illustration of the advantages that can be gained by organizing the computer system in a special way, and to present the latest results obtained in this laboratory. A version of this microcomputer-controlled instrumentation and some significant results (such as shown in Figs. 4 and 7) have already been presented [29].

EXPERIMENTAL

Chemicals and polarographic equipment

Chemicals were of analytical-grade purity. Solutions were thermostated at 25 ± 1°C and deaerated with pure nitrogen before polarographic measurements.

Polarograms were obtained by using a conventional three-electrode configuration. The reference electrode was a saturated calomel electrode (SCE) and the auxiliary electrode was platinum wire. The working electrode was a computer-controlled pulsed-flux mercury electrode [30]. No electrical screening of the cell was found to be necessary.

Computer system

The assembled microcomputer system was of the stand-alone type. It offers the exclusive feature of a software interface which enables FORTRAN-86 language facilities to be used without an operating system. This system is ideal for routine analysis, once all the selected modes of conducting the experiments and of processing the collected data have been tested, and proved to be highly efficient for analytical studies.

Hardware. Digital and analog components were selected for their high quality and were assembled in-house through careful design and build-up of the electric wiring and screening in order to minimize noise pick-up and mutual interaction effects. The hardware consists of a multibus IEEE-796 microcomputer system and the experimental module.

The microcomputer system includes a multibus single-board computer (SBC; PY-8610-CB, Logitech), a multibus expansion EPROM board (B1014-B, 128 kbytes; Central Data Corp), and a multibus user board (developed

in-house) to extend the input/output (I/O) ports. The SBC is based on an Intel 8086 8-MHz CPU and includes an Intel 8087 8-MHz floating point processor, on-board 128 kbytes of random access memory (RAM) as well as 16 kbytes of high-speed erasable programmable read only memory (EPROM).

The experimental module, connected to the SBC via two Intel programmable peripheral interfaces (8255), includes several boards each of which is dedicated to a single device (D/A converter, A/D converter, potentiostat, *i*/V converter, amplifier, mercury drop-fall detector, switch and valve actuator). The mercury drop-fall detector, which is of new design, can distinguish the transient caused by the drop fall from the transient caused by the potential-pulse waveform in the pulsed techniques. The resolution time in the drop-life measure is 0.1 ms. Features of this device will be described in a later paper. For the A/D and D/A converters, in order to couple high resolution with a large dynamic range, a 16-bit 33-kHz Datel DAC-16916B and a 14-bit 20-kHz Datel ADC-149 were used, with 0.15 and 0.61 mV of resolution, respectively.

Software. The software was entirely developed on an Intel MDS 230-III developing system, tested with the Intel ICE-86 emulator and burned on EPROM chips by using an Intel 103 Universal PROM programmer.

The languages used were ASM-86, PLM-86 and FORTRAN-86, depending on the features of the different program parts. ASM-86 was used for the service-interrupt data-acquisition routines that were burned on the EPROM installed on the SBC and are critical in time. In this case, no waiting cycle is added when the processor accesses the EPROM. The data acquisition is done under processor control by a software system based on three different priority levels with interrupts in real time. The highest priority is granted to the mercury drop-fall event, the intermediate priority to the timer service (t_1, t_2, t_3, a_1, a_2 and a_3 time-lags in Fig. 2, with 1 ms in resolution), and the lowest priority to the A/D end-of-conversion event. During the acquisition, for each millisecond, about 200 μs are devoted to the timer service, the most time-consuming event. In the remaining 800 μs, 12 conversions are done (each conversion cycle takes 66 μs, including a 16-μs interrupt latency time). The following operations are done in each ($t_i - a_i$) time-lag: upgrading of the DAC, checking of the progress of potential scan, and calculation of the mean value of the experimental point, after subtraction of the instrumental offset. PLM-86 was used to code the software drivers of the I/O subsystem. The remaining software modules, which represent the main part of the package and include the different modes of experiment handling and data processing, were developed in FORTRAN-86 language and burned, with the PLM-86 modules, on the EPROM installed on the expansion EPROM board.

This program, even in the absence of any operating system, has the same advantages as the FORTRAN-86 high-level I/O support in providing the SBC with a user-friendly means of communication. To achieve this goal, a subroutines library was implemented in-house in PLM-86, and linked to the FORTRAN-86 run-time I/O support. In particular, this library conducted the

WRITE and READ procedures, either formatted or free-field, made by the FORTRAN-86 legal statements for programming external devices for video display, printer plotter and mass memory. These three I/O devices, connected to the microcomputer system, have proved to be essential for the development of interactive working in all steps of an experiment.

The whole program is very appropriate for computer/user interaction and for iteration in data processing by means of a menu-selectable mode. The organization of the program has the following seven features: (a) it provides the electrochemical cell with the required potential waveform selected from the techniques reported in Table 1; (b) it acquires the data; (c) it smooths the data by piecewise polynomial interpolations (PPI), fast Fourier transform (FFT) or ensemble signal averaging; (d) it draws the baseline by PPI and calculates baseline-free curve; (e) it differentiates as required; (f) it computes and lists the most significant signal parameters; and (g) it makes decisions on the chemical characterization of signals.

The main features are shown in Fig. 1 and Table 2. The original raw-data set or that relevant to the data-processing mode last used, which are both automatically stored on the core memory, can be processed iteratively until some specific criteria are satisfied. Thus, any of the data-processing modes can be called up in the forward or backward direction by using the looping facilities. For example, when the derivative information is required without intermediate conditioning of the raw data, the program can take a direct jump to the differentiation step, produce the derivative curve and list the evaluated signal parameters sequentially.

Potential waveform and data sampling modes

Figure 2 shows the potential-waveform and the data-sampling modes that can be accomplished under software control. The potential increment of the staircase ramp ΔE_s and the pulse amplitude ΔE_p can be selected by the operator in the ranges: ±5000 and 0—10 000 or 0 + 10 000 mV. The time-lags t relevant to the potentials applied before (t_1), during (t_2) and after (t_3) the pulse, can be varied in the range 0—32 767 ms, as can the current sampling times a_1, a_2 and a_3. All these time parameters can be selected individually by the operator or invoked in the standard mode.

TABLE 1

List of operating modes

1 D.c. polarography	8 Anodic stripping voltammetry
2 Sampled d.c. polarography	9 Differential-pulse anodic stripping voltammetry
3 Staircase voltammetry	10 Potentiometric stripping analysis
4 Triangular staircase voltammetry	11 i vs. t curve
5 Normal pulse polarography	12 Electrocapillary curve
6 Differential pulse polarography	13 Current measurement at constant potential for kinetic studies
7 Fast-sweep differential pulse voltammetry	

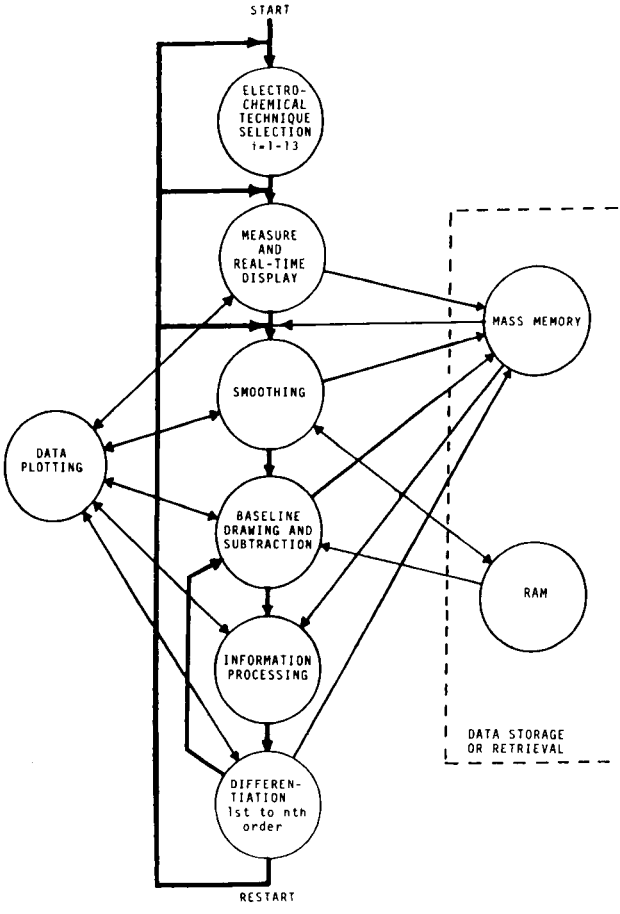

Fig. 1. Flow chart depicting the branching and looping facilities of the software for data and information processing.

TABLE 2

Standard scientific data-processing techniques

Category	Routine
Storage	Data storage. Information retrieval.
Graphics	Digital plotting. CRT display. Printed output.
Correction	Axis unit modification. Offset shift. Offset drift. Scaling of data.
Improvement	Time averaging. Baseline correction. Digital smoothing. Summation of curves. Difference of curves.
Transformation	Derivative curve. Fourier transform.
Calculation	Peak location. Polynomial curve fitting.
Data treatment	Signal-shape analysis. Chemical information.

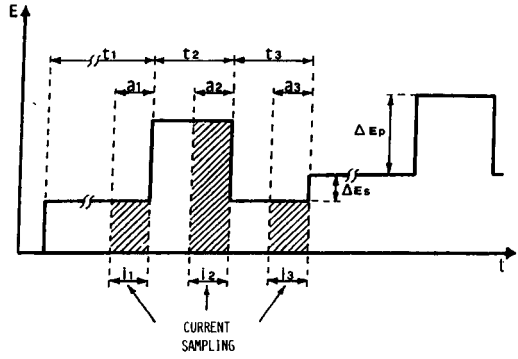

Fig. 2. Potential waveform and data-sampling modes: ΔE_s, potential increment of the staircase ramp; ΔE_p, pulse amplitude. Standard values of the time parameters are as follows. For the polarographic techniques, $t_1 = 0.8\ t_D$; $t_2 = t_3 = 40$ ms and $a_1 = a_2 = a_3 = 20$ ms (t_D, the drop time, is automatically measured at the initial potential). For the voltammetric techniques, $t_1 = t_2 = t_3 = 40$ ms and $a_1 = a_2 = a_3 = 20$ ms.

The i_1, i_2 and i_3 currents, sampled during the relevant time-lags, are accumulated and averaged in real time as 32-bit integer numbers and stored in a reserved RAM buffer. So, once the experiment has been done, data processing can concern i_1, i_2, i_3, $(i_2 - i_1)$, $(i_2 - i_3)$, or $(i_2 + i_3)$ data arrays.

At the sampling rate used, which is the highest consistent with the ADC and interrupt-driven ASM routine overheads, the effect of spiked noise, occasionally mixed with the signal, is decreased. By changing the analog amplification gain, a 30-pA resolution (last significant bit) can be obtained.

Piecewise polynomial interpolation

Smoothing and baseline drawing were done by using iterated interpolation techniques based on piecewise polynomial interpolation algorithms. These are particularly useful in generating a sequence of interpolated points from which the rate of effective convergence can be estimated when, as in the present case, analytical error limits cannot be used. The algorithm uses the well known Newton interpolation formula with divided differences [31]. In this way, each i experimental point is recalculated by a d_i degree polynomial on the basis of the neighbouring points belonging to the interval $\theta_i = d_i + 2$. The d_i degree polynomial interpolation is obtained by linear interpolation over two independent $d_i - 1$ degree polynomials. The $d_i - 1$ degree polynomial interpolation is in turn obtained by linear interpolation over two independent $d_i - 2$ degree polynomials, and so on. The values of d and θ are not defined a priori by the user, being changeable piecewise. The iterative procedure is automatically stopped on the basis of the convergence criteria:

$$(y_i^d - y_i^{d-1}) < (y_i^{d-1} - y_i^{d-2})$$

where y_i^d, y_i^{d-1} and y_i^{d-2} are the sequences of interpolated points for each i point obtained by using, as before, the d, $d-1$ and $d-2$ degree polynomials, respectively.

In the smoothing mode, the PPI algorithm processes the whole set of raw data and the user has only to define the number n_1 of experimental points to be removed for each piece and recalculated, and the number n_2 of iterative smoothing runs to be done sequentially. When the standard smoothing option is invoked, the optimized n_1 and n_2 values are selected automatically. As described in the literature, the data-smoothing procedures are generally based on the least-squares method, and use the piecewise polynomial approximation technique [32]. In this case, both the degree of the polynomial (d) and the number of experimental points (θ), to be used in the best fit procedure, are imposed by the user and are constant throughout the whole set of data.

In the baseline-drawing mode, the PPI algorithm generally processes one selected part of the raw data set at a time. The program selects $n_2 = 1$ and computes n_1 from the selected potential interval, where the faradaic current has to be removed, and the value of ΔE_s. Once the baseline relevant to the first potential interval has been drawn, the program asks for the next one, and so on.

Fast Fourier transform

When the FFT is used in the smoothing mode, the computer utilizes the first 2^m points of the raw data set and sends a message concerning the $n - 2^m$ left-out values (m is the integer part of the $\log_2 n$, where n is the number of raw data). These 2^m points are then multiplied by the Hanning function [33] and processed by FFT. Noise filtering is achieved by multiplication of the Fourier spectrum according to rectangular, triangular or cosine smoothing functions. The cosine smoothing function has a shape similar to the function found by calculating the frequency spectrum of a signal measured with a very high S/N [34]. As for the cut-off frequency selection and the efficiency of the FFT smoothing, one must remember that in the Fourier sense each polarographic or voltammetric signal is interpreted as a summation of various sinusoidal frequencies located in a narrow bandwidth (Δf) near d.c. (0 Hz). Owing to the finiteness of Δf, the cut-off frequency must be higher than the upper limit of Δf to avoid signal distortion and, consequently, any noise (white, flicker or interference in nature) with a frequency lower than the cut-off frequency will remain mixed in the signal after inverse FFT. The best cut-off frequency is decided experimentally for each potential waveform and sampling rate by analysis of the relevant power spectrum obtained at high S/N.

Differentiation

In the differentiation mode, which can be effected before or after baseline subtraction, a five-point approximation derivative formula is used. It was obtained by differentiating the five-point Lagrangian interpolation formula [31]. This approach is similar to the least-squares convolution based on a five-point cubic convolute as proposed by Savitzky and Golay [32].

The decision-making process entrusted to the operator is made easier by

the facility for visualizing the curves after any processing step. For example, in baseline drawing, the different baselines obtained for the different potential ranges invoked are drawn automatically on the same plot. The soundness of the decision in selecting the best baseline can be checked by subsequent visualization of the relevant curves obtained after baseline subtraction and then after differentiation.

The decision-making process entrusted to the computer involves three parts. The first step is to compute and print quickly the potentials of the peak (E_p), half-wave ($E_{1/2}$) or electrocapillary maximum ($E_{e.c.m.}$). The second step is to compute and list, depending on the electrochemical technique used, the most significant signal parameters, such as i_p or i_d, along with E_p or $E_{1/2}$, from the baseline-free curves. In the case of differentiation (only the first derivative is considered for automatic evaluation), E'_p and i'_p are listed for originally sigmoidal signals, and E'_+, E'_-, $E'_{(i'=0)}$, i'_+ and i'_- are listed for originally peak-shape signals, where the apex refers to the differentiation operation and (+) or (−) refer to the positive or negative side of the derivative curve. In peak-potential searching, a higher resolution than that relevant to the experimental width of the potential increment, ΔE_s, of the voltage ramp (Fig. 2) can be obtained by calculating interpolated values of the current by the PPI routine, for each 0.2-mV interval near the peak. The third step required of the operator is to characterize chemically each signal whenever the difference between signal parameters p_s and the reference parameters p_r, loaded in the data base, lies within individually predetermined limits. These limits are automatically computed as three times the standard deviation (S) relevant to the considered parameter. The actual value of S is evaluated by the software at the signal current level i by the $S(i)$ values listed in the data base. If the difference between p_s and p_r does not lie within these limits, no assignment is made. Two different notations are then possible: unknown, when p_s differs by more than $3S$ for all the p_r; or uncertain, when p_s differs by less than $3S$ for more than one p_r.

RESULTS AND DISCUSSION

During optimization of the procedures for smoothing and baseline subtraction, pure solutions with different concentrations of analyte were used. Various parameters such as E_p, $E_{1/2}$, i_p/c and i_d/c, which are independent of concentration, were calculated. Information on the extent of the general validity of the functions used and on the extent of overall distortion caused by the different processing steps was thus obtained. Because the final distortion of the signal also depends on the potential ranges used in baseline interpolation or extrapolation, optimization of these procedures can be quite complex. For this reason, once the best conditions had been defined, it seemed advisable to offer them as standard options but to leave the user to fix the baseline potential range as well as to change the parameters of the smoothing function if necessary.

In the standardization of the smoothing step, the parameters n_1 and n_2 were found to play different roles. In particular, the choice of n_2 is not critical; 5—10 runs were sufficient to obtain good noise filtering, while further runs did not introduce significant distortion of the signal. In contrast, the choice of the best n_1 value is strongly dependent on the number of experimental points which define the signal. Considering a 30—45-point signal, the same PPI standard option was found to operate satisfactorily regardless of the electrochemical technique used, down to very low S/N ratios. From this condition, e.g., a 60-point signal, the new best value of n_1 has to be found.

With the FFT filter, the standard option is confined to the cosine smoothing function, which was shown to be more efficient than the triangular or rectangular functions in restoring the undistorted original signals. This means that when the FFT filter is used, the optimal cut-off frequency and the optimal potential range must be checked throughout a series of measurements.

In baseline subtraction, the effect of varying the potential range was systematically verified using two different electrochemical techniques at very low concentration levels only for PPI, once the relevant n_1 and n_2 filter parameters had been optimized.

Figures 3 and 4 show the original and smoothed curves along with the baseline and baseline-free curves, for staircase voltammetry (3.9×10^{-8} M cadmium ion) and fast-sweep d.p.v. (5×10^{-9} M cadmium ion), respectively. Cadmium in 0.1 M sodium chloride (pH 3) was used for the sake of comparison with the available literature. The different baseline curves refer to a change in the potential range, in which the faradaic current was removed, one point (5 mV) at a time. In Fig. 3, the curve in C is clearly the only one that can be accepted by visual inspection. In Fig. 4B and C, no curve can be disregarded at first sight, even though curve (b) might be preferred because its first derivative has the more regular shape (see Fig. 5B, b). The listing of the significant parameter values and their automatic interpretation yields the following results for the four curves of Fig. 4C: the maximal difference is 5.8 mV in peak potential and 19% in peak current; all of them are assigned to Cd^{2+} because the peak potentials are within the interval 626 ± 6 mV (626 mV is the peak potential of Cd^{2+} stored in the computer library for the 0.1 M NaCl base electrolyte and 6 mV corresponds to three times the standard deviation at a peak current of 0.5 nA); the standard deviation (S) of the peak current, related only to the effect of change in the potential intervals for baseline interpolation, is 0.24 nA. The detection limit expressed in concentration ($3S/\Delta$) is 5×10^{-9} M, where Δ is the slope of the relevant calibration plot. Yet it must be emphasized that the variance of current caused merely by the effects of raw data processing is only part of the overall variance in the determination of the analyte. Another important part is played by the matrix composition of real samples, which affects the form of the baseline. This is why no detection limits are indicated in the present paper.

In Table 3, some figures of merit are reported for the above electrochemi-

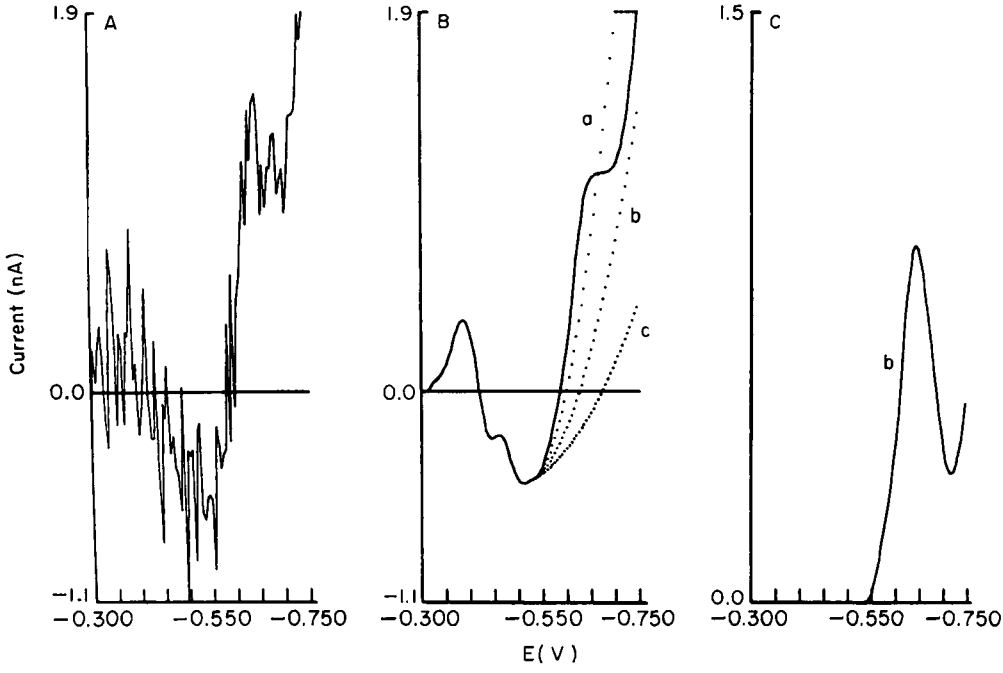

Fig. 3. Staircase voltammogram of 3.9×10^{-8} M Cd^{2+} in 0.1 M NaCl (pH 3); $\Delta E_s = 5$ mV; standard time parameters. A is the original output. B is the smoothed signal along with 3 different baselines for which the extrapolation potential was: (a) —550, —750 mV; (b) —545, —750 mV; (c) —540, —750 mV. C is the signal after subtraction of baseline (b).

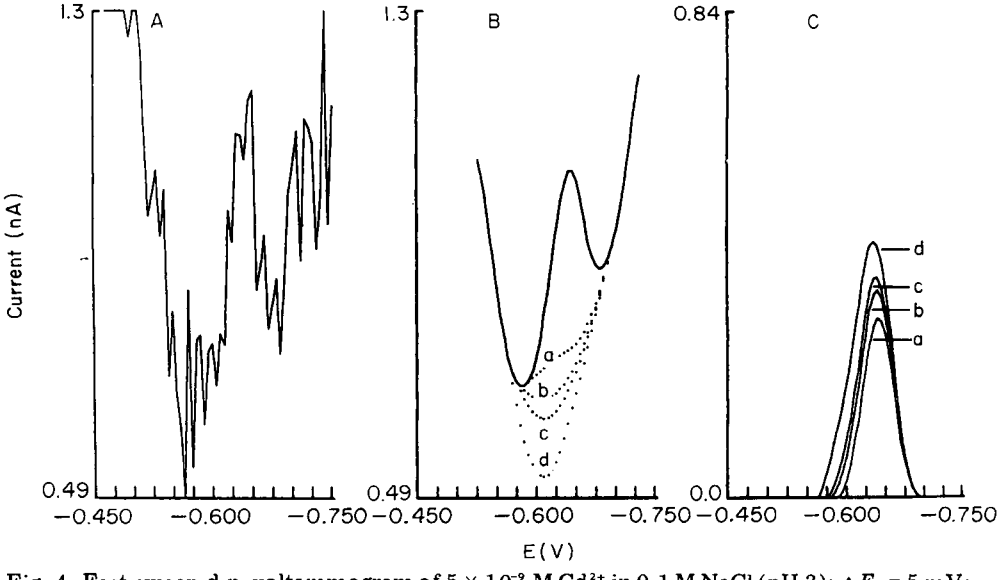

Fig. 4. Fast-sweep d.p. voltammogram of 5×10^{-9} M Cd^{2+} in 0.1 M NaCl (pH 3); $\Delta E_s = 5$ mV; $\Delta E_p = 50$ mV; standard time parameters. A is the voltammogram. B is the smoothed signal along with 4 different baselines for which the potential interpolation intervals were: (a) —590, —690 mV; (b) —585, —690 mV; (c) —580, —690 mV; (d) —570, —690 mV. C shows the smoothed curves after subtraction of these baselines.

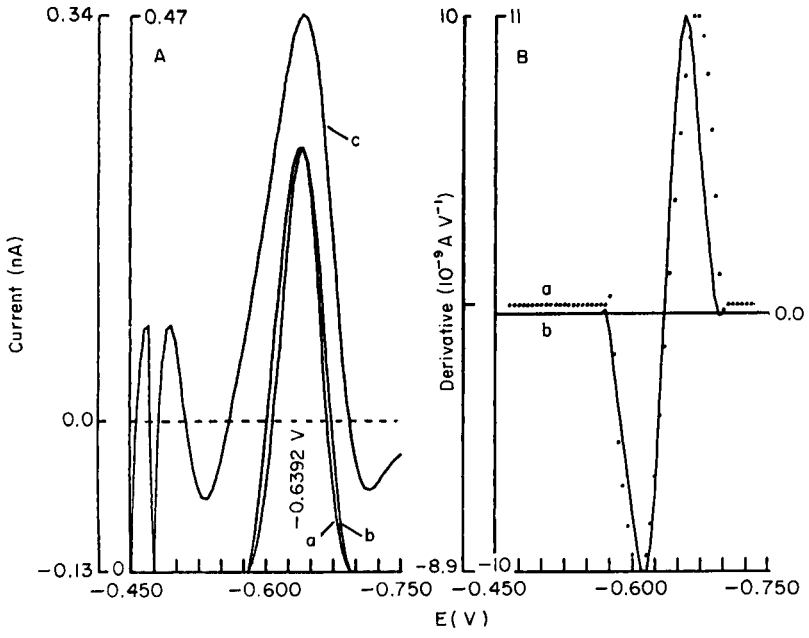

Fig. 5. Effect of different algorithms for smoothing and baseline subtraction on the initial raw data shown in Fig. 4A. Voltammograms: A(a) PPI smoothed minus PPI baseline; A(b) FFT smoothed minus PPI baseline; A(c) PPI smoothed minus cubic best-fit baseline. B shows the derivative curves of (a) (dotted line) and (b) (continuous line).

cal techniques, relevant to a very large cadmium concentration range. From the results obtained by using the PPI algorithm for both smoothing and baseline subtraction, the extent of overall signal distortion caused by digital smoothing, baseline correction and chemical handling, can be estimated for both the techniques. This distortion was 2—3 mV for peak potential and 8—11% for peak current at the lowest concentrations in the case of single curves, and 0.2 mV in potential and 2% in current with a 16-cycle ensemble average. In this way, the possibility of obtaining sound thermodynamic information, even at a very low concentration, about the degree of complexation of the analyte in a real sample becomes available for the first time. Obviously, checks on the validity of the tabulated data are needed. Table 3 also lists some results obtained by using the FFT filter coupled to PPI baseline subtraction, or the PPI filter coupled to a cubic best-fit for baseline subtraction.

With the FFT algorithm, it was found that, at very low S/N levels, the smoothed signals present spurious side lobes and are sensitive to the cut-off frequency selected. These findings have also been proved valid in the other electrochemical techniques. Compared with the PPI algorithm, it was found that the FFT can introduce distortion on the peak current and on the half-peak width ($E'_+ - E'_-$), which does not disappear on ensemble averaging.

TABLE 3

Figures of merit for cadmium ion by staircase voltammetry and fast-sweep differential pulse voltammetry[a]

Algorithm[b]		C (M)	$-E_p$[c] (mV)	i_p/c[c] (A/M)	$E'_+ - E'_-$[c] (mV)	$-i'_+/i'_-$[c]
Sm.	BC					
Staircase voltammetry						
PPI	PPI	5×10^{-8}	640.0(3.0)	0.018(0.002)	70.0(2.0)	1.60(0.20)
PPI[d]	PPI	5×10^{-8}	637.2(0.6)	0.0208(0.0008)	62.2(0.8)	1.70(0.10)
FFT	PPI	5×10^{-8}	648.0(4.0)	0.033(0.004)	85.0(3.0)	1.00(0.20)
FFT[d]	PPI	5×10^{-8}	635.0 —	0.0185 —	66.0 —	1.85 —
PPI	PPI	5×10^{-6}	637.0(0.5)	0.0202(0.0005)	45.4(0.7)	2.83(0.05)
PPI	PPI	5×10^{-4}	637.0(0.2)	0.0202(0.0002)	45.8(0.3)	2.81(0.04)
Fast-sweep d.p.v.						
PPI	PPI	5×10^{-9}	628.0(2.0)	0.062(0.005)	42.0(3.0)	0.90(0.10)
PPI[d]	PPI	5×10^{-9}	625.9(0.5)	0.060(0.002)	52.0(1.0)	0.96(0.07)
FFT	PPI	5×10^{-9}	625.0(2.0)	0.086(0.007)	62.0(3.0)	0.90(0.10)
FFT[d]	PPI	5×10^{-9}	613.0(1.0)	0.064(0.007)	66.0(1.0)	0.95(0.07)
PPI	CUBIC	5×10^{-9}	629.0(4.0)	0.094(0.009)	— —	— —
PPI	PPI	5×10^{-7}	625.8(0.6)	0.058(0.002)	50.0(1.0)	0.98(0.02)
PPI	PPI	5×10^{-5}	625.5(0.2)	0.0593(0.0003)	50.3(0.2)	1.01(0.01)

[a]Experimental conditions: 0.1 M NaCl (pH 3) base electrolyte; for staircase voltammetry, t_1 = 40 ms; a_1 = 20 ms; ΔE_s = 5 mV; for fast-sweep d.p.v., $t_1 = t_2$ = 40 ms, $a_1 = a_2$ = 20 ms, ΔE_s = 5 mV and ΔE_p = 50 mV. [b]Sm., smoothing; BC, baseline correction. [c]Average of five measurements with standard deviation in parentheses. [d]16-cycle ensemble average.

Only in the particular case of i vs. t curves, sampling current at the sub-nA level, does the FFT appear to be more effective for smoothing than PPI.

Cubic best-fitting fails completely in the goal of reproducing the baseline at the lowest concentrations, as shown in Fig. 5 where the curves obtained by using the different algorithms are reported for comparison. The comparison was limited for FFT by selecting the best cut-off frequency and the same potential range as in the PPI treatment, and for cubic best-fitting by selecting the best potential range after PPI smoothing. In Fig. 5A, the curves (a) and (b) are quite similar and well shaped, as confirmed by the relevant first derivative shown in Fig. 5B even though the peak current was only 4×10^{-10} A. Curve (c) in Fig. 5A refers to the cubic best-fit; all the relevant parameters are completely different from the expected ones, as can be inferred more easily from Table 3.

More impressive evidence of the efficiency of the PPI algorithm used in smoothing and background subtraction was achieved in d.p.a.s.v. with which concentrations down to 1.8×10^{-10} M (20 ng l^{-1} cadmium) were measured with standard deviations of 16% in i_p and 6 mV in E_p. Figure 6 shows the smoothed, background-subtracted voltammogram obtained for 20 ng l^{-1}

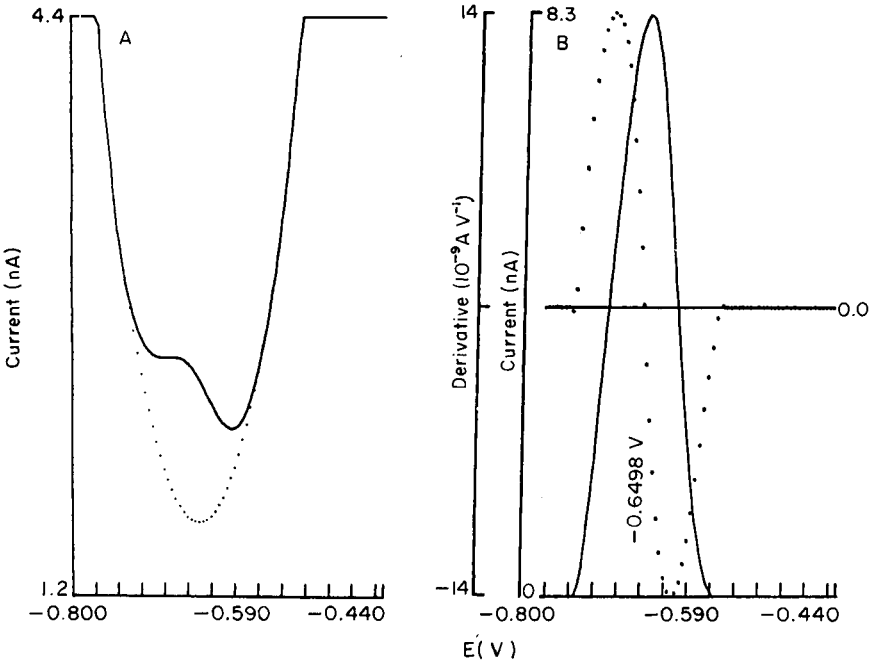

Fig. 6. Differential-pulse anodic stripping voltammogram of 1.8×10^{-10} M Cd^{2+} in 0.5 M NaCl (pH 3); $E_{p_i} = -800$ mV; $\Delta E_s = 5$ mV; $\Delta E_p = 50$ mV; standard time parameters; hanging mercury drop electrode; plating time 4 min; rest time 20 s. Curves: (A) smoothed voltammogram with its calculated baseline; (B) as for A after baseline subtraction (continuous line) and its derivative (dotted line).

cadmium and the relevant first derivative. Again, the voltage interpolation interval was found iteratively until the best i'_+/i'_- was obtained without assuming any particular model. Concentrations at this low level have been measured by Brown and Kowalski [19], who used a rotated disk electrode with a surface area of 0.45 cm^2 instead of the 0.05-cm^2 area of the hanging mercury electrode used in the present work.

Figure 7 shows a multi-element fast-sweep d.p. voltammogram (A) and its derivative (B), after standard PPI smoothing and baseline subtraction over the whole raw-data set. In this case, three potential intervals (−270, −775; −780, −1260; −1390, −1590) were selected wherein the faradaic current had to be removed. In the evaluation list for the peak parameters (Table 4), the third signal was denoted as uncertain, as the relevant peak potential was near to two different species within 3*S*, and the fifth signal was denoted as unknown, because no species were found to have E_p nearer than 3*S*.

Table 5 shows that the list of derivative significant points, in which only the potential and current parameters are reported, makes it possible to obtain quick quantitative information about the effect of signal overlapping by comparison of the amplitude between the left and right sides.

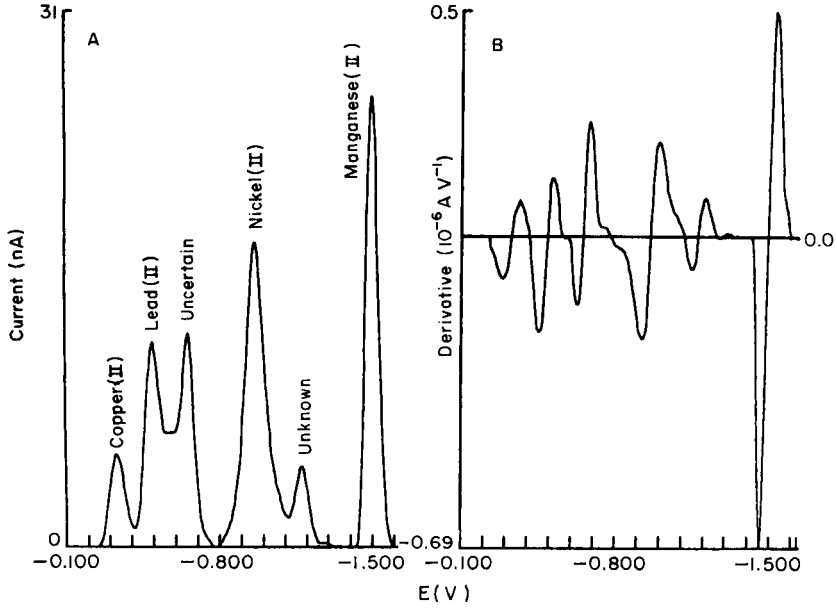

Fig. 7. Multi-element fast-sweep d.p. voltammogram; experimental conditions as in Fig. 4. Curves: (A) after smoothing and baseline subtraction; (B) derivative curve.

In Table 6, data available in the literature for the lowest cadmium concentration measured are compared with the values obtained in the present work, which was extended to sampled d.c. and normal pulse polarography. A consistent improvement seems to have been obtained for all the techniques by using the data-processing procedures described in this paper. The procedures for smoothing and baseline drawing, based on a general purpose algorithm, do not require the raw data to be forced to follow theoretical models.

TABLE 4

Evaluation of peak parameters for the voltammogram shown in Fig. 7A

Element	i_p (nA)	$-E_p$ (V)	E_p TAB (V)	Concentration	
				(10^{-6} M)	($\mu g\ l^{-1}$)
Copper(II)	4.25	0.3310	−0.3310	0.104	6.59
Lead(II)	11.9	0.4960	−0.4970	0.163	33.8
Uncertain	12.4	0.6572	0.0000	0.0	0.0
Nickel(II)	17.6	0.9626	−0.9620	0.332	19.5
Unknown	4.68	1.1762	0.0000	0.0	0.0
Manganese(II)	26.1	1.4970	−1.5000	0.275	15.1

TABLE 5

Evaluation of significant points for the derivative voltammogram shown in Fig. 7B

	Amplitude (10^{-6} A V^{-1})	$-E$ (V)		Amplitude (10^{-6} A V^{-1})	$-E$ (V)
Left side	−0.081	0.2952	Left side	−0.23	0.9280
Central point	0.0	0.3313	Central point	0.0	0.9625
Right side	0.070	0.3666	Right side	0.21	0.9986
Left side	−0.22	0.4594	Left side	−0.072	1.1516
Central point	0.0	0.4962	Central point	0.0	1.1766
Right side	0.125	0.5216	Right side	0.0855	1.2078
Left side	−0.15	0.6322	Left side	−0.69	1.4640
Central point	0.0	0.6571	Central point	0.0	1.4969
Right side	0.26	0.6828	Right side	0.50	1.5216

TABLE 6

Lowest cadmium concentration measured for several electrochemical techniques and comparison with data from the literature

Technique	Lowest concentration measured (M)		
	This work	Literature	Ref.
Sampled d.c. polarography	2×10^{-7}	1×10^{-6}	16[a]
Normal pulse polarography	5×10^{-8}	1×10^{-7}	16[a]
Staircase voltammetry	5×10^{-8}	1×10^{-6}	4
Fast-sweep d.p.v.	5×10^{-9}	5×10^{-8}	15
D.p. anodic stripping voltammetry	2×10^{-10}	2×10^{-10}	19[b]

[a]Signals forced to follow theoretical models. [b]With a 0.45-cm^2 rotated disk electrode.

One of the authors (P. P.) acknowledges financial support from M.P.I. Patents are pending for some parts of the hardware and software described in this paper.

REFERENCES

1 G. Laner, R. Abel and F. C. Anson, Anal. Chem., 39 (1967) 765.
2 S. P. Perone, J. E. Harrar, F. B. Stephens and R. E. Anderson, Anal. Chem., 40 (1968) 899.
3 H. E. Keller and R. A. Osteryoung, Anal. Chem., 43 (1971) 342.
4 S. P. Perone, J. W. Frazer and A. Kray, Anal. Chem., 43 (1971) 1485.
5 S. C. Creason, J. W. Hayes and D. E. Smith, J. Electroanal. Chem., 47 (1973) 9.
6 D. E. Glover and D. E. Smith, Anal. Chem., 45 (1973) 1869.
7 D. E. Smith, Anal. Chem., 48 (1976) 221A, 517A.
8 W. V. Thomas, L. Kryger and S. P. Perone, Anal. Chem., 48 (1976) 761.
9 M. De. Blasi, D. Marino, G. Moramarco and P. Papoff, Automazione e Strumentazione, 11 (1979) 784.

10 T. R. Brumleve, J. J. O'Dea, R. A. Osteryoung and J. Osteryoung, Anal. Chem., 53 (1981) 702.
11 J. E. Anderson and A. M. Bond, Anal. Chem., 53 (1981) 1394.
12 L. Pospisil and M. Stefl, Collect. Czech. Chem. Commun., 48 (1983) 1241.
13 J. W. Hayes, D. E. Glover and D. E. Smith, Anal. Chem., 45 (1973) 277.
14 D. E. Smith, Anal. Chem., 48 (1976) 517A.
15 C. Yarnitzky, R. A. Osteryoung and J. Osteryoung, Anal. Chem., 52 (1980) 1174.
16 A. M. Bond and B. S. Grabaric, Anal. Chim. Acta, 101 (1978) 309.
17 A. M. Bond and B. S. Grabaric, Anal. Chem., 51 (1979) 337.
18 P. He, J. P. Avery and L. R. Faulkner, Anal. Chem., 54 (1982) 1313A.
19 S. D. Brown and B. R. Kowalski, Anal. Chim. Acta, 107 (1979) 13.
20 L. Sipes, S. Kozar, I. Kontusic and M. Branica, J. Electroanal. Chem., 87 (1978) 347.
21 L. Kryger and D. Jagner, Anal. Chim. Acta, 78 (1975) 251.
22 A. Lavy-Feder and C. Yarnitzky, Anal. Chem., 56 (1984) 678.
23 Q. V. Thomas, L. Kryger and S. P. Perone, Anal. Chem., 48 (1976) 761.
24 W. P. Van Bennekom and J. B. Schute, Anal. Chim. Acta, 89 (1977) 71.
25 S. R. Rajagopalan, A. Poojary and S. K. Rangarajan, J. Electroanal. Chem., 75 (1977) 135.
26 X. Andrieu, P. Mericam, A. Astruc and M. Astruc, J. Electroanal. Chem., 138 (1982) 217.
27 T. Wasa, T. Yao, H. Yamamoto and S. Musho, Bunseki Kagaku, 31 (1982) T55.
28 A. M. Bond and I. D. Heritase, Anal. Chem., 57 (1985) 174.
29 N. Fanelli, R. Fuoco, P. Papoff and D. Guidarini, Proceedings of J. Heyrovsky Memorial Congress on Polarography, August, 1980, I (1980) 120.
30 M. L. Foresti and R. Guidelli, J. Electroanal. Chem., 197 (1986) 159.
31 F. B. Hildebrand, Introduction to Numerical Analysis, 2nd edn., TATA McGraw-Hill, New Delhi, 1979, Chap. 2 and p. 111.
32 A. Savitzky and M. Golay, Anal. Chem., 36 (1964) 1627.
33 E. O. Brigham, The Fast Fourier Transform, Prentice-Hall, New Jersey, 1974.
34 G. Horlick, Anal. Chem., 44 (1972) 943.

Analytica Chimica Acta, 185 (1986) 49—55
Elsevier Science Publishers B.V., Amsterdam — Printed in The Netherlands

CYCLIC REGENERATION OF NICOTINAMIDE ADENINE DINUCLEOTIDE WITH IMMOBILIZED ENZYMES
Flow-injection Spectrofluorimetric Determination of Ethanol

M. MASOOM[a] and ALAN TOWNSHEND*
Chemistry Department, University of Hull, Hull HU6 7RX (Great Britain)
(Received 14th November 1985)

SUMMARY

Ethanol (0.05—0.5%) in water is determined by injection of a 20-μl sample into a solution of 1.5×10^{-3} M NAD^+ in pH 8.0 phosphate buffer flowing from a reservoir. The solution passes through a minicolumn of yeast alcohol dehydrogenase immobilized on controlled-pore glass (CPG). The NADH formed is monitored spectrofluorimetrically in the flow system, before reconversion to NAD^+ in a minicolumn of glutamate dehydrogenase immobilized on CPG in the presence of glutarate and ammonium ions, also in the flowing solution. The solution then returns to the reservoir. The regeneration of NAD^+ allows the same coenzyme solution to be used for 50 ethanol determinations daily for 4 days.

Nicotinamide adenine dinucleotide (oxidized form NAD^+, reduced form NADH) is an important coenzyme which functions in many dehydrogenase-catalyzed reactions, such as those used in the determination of ethanol, lactate and amino acids. The analytical procedures based on such reactions normally involve monitoring the formation or consumption of NADH on the basis of its absorbance at 340 nm or fluorescence at 450 nm; NAD^+ does not give a response at these wavelengths.

The advantages of using immobilized enzymes in flow systems for analytical measurements are well known. However, most of the enzymes that have been used in this way are those that do not require coenzymes, such as oxidases or hydrolases, so that the consumption of expensive coenzyme is avoided. Soluble dehydrogenases have been used in flow systems by making use of techniques like merging zones [1] and stopped flow [2] to economize on coenzyme consumption. The high cost of coenzymes justifies attempts to regenerate and reuse them in the system in which they are applied. Immobilization of the coenzyme [3] results in a system of low sensitivity [4]. Electrochemical regeneration of NAD^+ from enzymatically produced NADH, however, has been accomplished in reasonably high yields, especially in flow-through reactor systems [5—9].

---

[a]Present address: Chemistry Department, University of Baluchistan, Quetta, Pakistan.

0003-2670/86/$03.50

Enzyme electrodes for dehydrogenase substrates have been prepared by making use of immobilized enzymes. Blaedel and Engstrom [10] reported reagentless electrodes for ethanol, lactate and malate by constraining the appropriate dehydrogenase and NAD^+ on the surface of a platinum electrode. Malinauskas and Kulys [11] used a soluble dextran—NAD^+ derivative and a dehydrogenase held close to a platinum electrode by a cellulose-based dialysis membrane. Sensors based on this principle were built for ethanol, lactate and glutamate. Yao and Musha [12] reported sensors for ethanol and lactate in which NAD^+ was covalently bonded to a carbon paste electrode. From work done so far with such dehydrogenase sensors, it appears that immobilization of enzyme and coenzyme at the electrode surface suffers from low sensitivity, poor reproducibility and a short lifetime of the analytical sensor.

Closed-loop systems for dehydrogenase reactions have been designed which make repetitive use of soluble enzyme and coenzyme for substrate determination [13, 14]. Limitations arise because of the poor stability of the dissolved enzyme at room temperature.

The major object of the present paper is to describe a flow-injection system based on immobilized dehydrogenases for rapid substrate determination with automatic regeneration and recycling of the coenzyme. The determination of ethanol, which is one of the most frequent analyses in forensic and clinical toxicology laboratories [2], is used to illustrate the principle. The oxidation of ethanol is catalyzed by alcohol dehydrogenase (ADH) in the presence of NAD^+:

$$CH_3CH_2OH + NAD^+ \xrightarrow{ADH} CH_3CHO + NADH + H^+$$

The NADH formed is monitored spectrofluorimetrically, and is a measure of the original ethanol concentration. The oxidation of the NADH formed back to NAD^+ is done with glutamate dehydrogenase (GlDH):

$$NADH + NH_4^+ + \alpha\text{-ketoglutarate} \xrightarrow{GlDH} NAD^+ + \text{glutamate} + H_2O$$

The reactions follow in sequence in a loop:

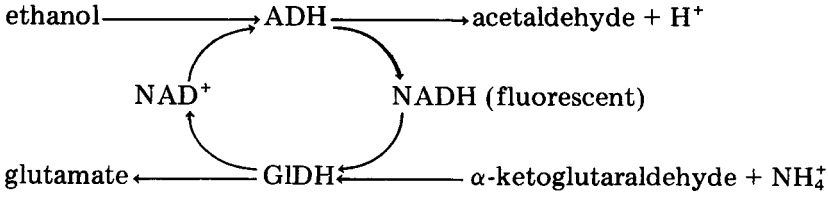

Such a loop is essentially a mechanical analogue of the enzyme cycling procedure pioneered by Lowry et al. [15, 16].

EXPERIMENTAL

The enzymes used were yeast alcohol dehydrogenase (YADH, alcohol:NAD oxidoreductase, EC 1.1.1.1., ex yeast, ca. 300 U mg^{-1}; Boehringer), and glutamate dehydrogenase (GlDH, L-glutamate:NAD oxidoreductase, EC 1.4.1.3., ex bovine liver, ca. 40 U mg^{-1}; Sigma). α-Ketoglutaric acid and NADH (disodium salt, 98%) were obtained from Sigma, and NAD^+ (free acid, 100%) from Boehringer. All other reagents were analytical-reagent grade.

Apparatus and procedures

Measurements were made with a Perkin-Elmer model 3000 fluorescence spectrometer equipped with a flow-through cell (2.00 mm i.d., 25 mm long). The excitation and emission wavelengths used for monitoring NADH were 360 and 460 nm, respectively, with both slits at 10. The injection valve was a Rheodyne RH5020 rotary valve (Anachem) with an injection volume of 20 μl. The manifold and reaction coil tubing was 0.5 mm i.d. teflon. The pump was an Ismatec Minipuls S-820 peristaltic pump (Zurich).

The closed-loop system is shown schematically in Fig. 1. The reservoir, a 60-ml glass bottle, contained 50 ml of solution for circulation. The solution was 0.1 M phosphate buffer (pH 8.0) made 1.5×10^{-3} M in NAD^+, 1×10^{-3} M in α-ketoglutaric acid and 1×10^{-3} M in ammonium acetate. The sample was injected directly into the circulating solution. After mixing with the NAD^+ in the mixing coil, the sample passed through the immobilized YADH column. The NADH produced was monitored spectrofluorimetrically shortly after leaving the column, and the response was fed to a chart recorder. The coil placed after the detector was used to disperse and thus dilute the sample zone to allow more effective oxidation of the NADH as it passed through the immobilized GlDH column. The NAD^+ thus formed was carried back to the reservoir ready for recirculation.

Immobilization of enzymes. The YADH and GlDH were immobilized on controlled-pore glass (CPG-240, 120/240 mesh, 23-nm mean pore diameter; BDH Chemicals) following the procedure described earlier for glucose oxidase [17]. The immobilized enzymes were packed in glass columns (2.5 mm

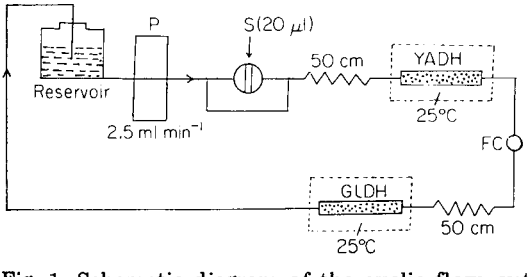

Fig. 1. Schematic diagram of the cyclic flow system for determination of ethanol and regeneration of NAD^+: P, pump; S, sample; FC, flow cell of spectrofluorimeter.

i.d., 50 mm long) maintained at 25°C by water from a thermostat bath flowing around them.

RESULTS AND DISCUSSION

The pH values for maximum activity of the two soluble enzymes are quite different. For YADH it is 8.8 [18], for GlDH it is 7.5 [19]. The pH of the circulating solution, therefore, must be chosen carefully to ensure maximum sensitivity and stability. Also, at pH >9 the destruction of NAD^+ is rapid, whereas NADH is destroyed below pH 6 [16].

The effect of the pH of the circulating solution on the response of the system to ethanol was investigated in the following way. The buffer used in the circulating solution was initially at pH 7.0, and the response to ethanol was measured under these conditions. The pH of the circulating solution was adjusted to 7.5 by adding 0.1 M sodium hydroxide solution to the reservoir, and the ethanol response was measured again. This was repeated at pH 8.0, 8.5 and 9.0. The results are shown in Fig. 2. There was a continuing increase in fluorescence intensity up to at least pH 9.0. However, pH 8.0 was used for subsequent experiments to ensure long-term stability of NAD^+, and because it was closer to the expected pH optimum for GlDH (pH 7.5). The conversion efficiency of GlDH (see below) was the same at pH 7.5 or 8.0.

To investigate the effect of NAD^+ concentration, 0.5 M NAD^+ in pH 8.0 phosphate buffer was added in 10- or 50-μl increments to the solution in the reservoir. The effect on the response of the system to ethanol is shown in Fig. 3. Above 1.5×10^{-3} M NAD^+, the response was essentially independent of NAD^+ concentration. Therefore, this concentration was used for all further experiments.

Calibration

Standard solutions of ethanol (0—0.5% v/v) were prepared from absolute ethanol in pH 8.0 phosphate buffer. Care was taken to avoid evaporation of

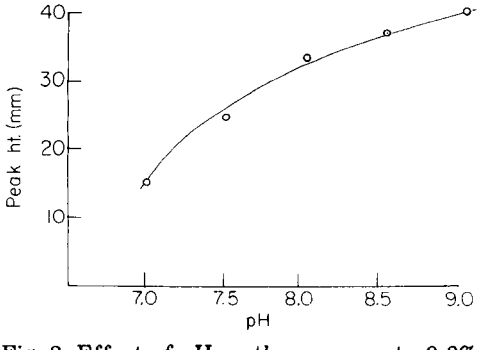

Fig. 2. Effect of pH on the response to 0.3% ethanol.

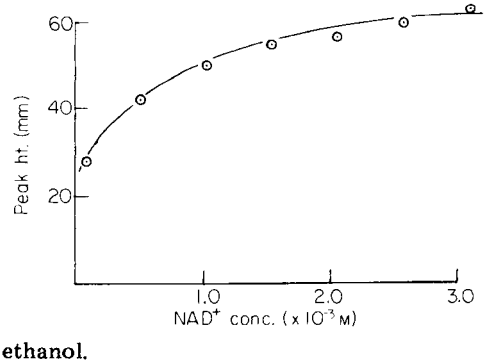

Fig. 3. Effect of NAD^+ concentration on the response to 0.5% ethanol.

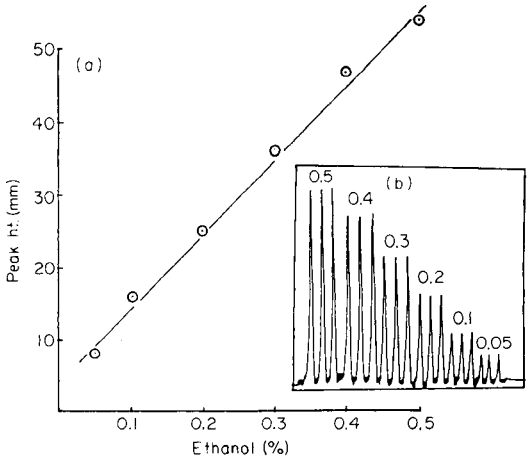

Fig. 4. Calibration graph and (inset) calibration peaks for ethanol (numbers are % alcohol).

the ethanol. The calibration data shown in Fig. 4 were obtained by injecting these solutions into the system shown in Fig. 2. The readout was available after 22 s. The graph is linear over the range investigated (0.05—0.5% ethanol). The relative standard deviation of the peak heights in Fig. 4 was 1.7%.

Immobilized enzyme activity

The immobilized YADH did not show any marked decrease in activity over two months of use. The activity of YADH in the closed loop system was always evident, because it was the NADH formed in the YADH column that was directly monitored. The activity of the immobilized GlDH, however, was not directly monitored by the system and therefore the efficiency of the immobilized enzyme in converting the NADH back to NAD^+ had to be established in other experiments. To do this, a flow injection system with the arrangement shown in Fig. 5 was used. The carrier stream was a 0.1 M phosphate buffer (pH 8.0) containing the same concentration of α-keto acid and ammonium acetate as those in the circulating solution. Freshly prepared solutions (1.0, 0.5 and 0.25 mg ml^{-1} NADH) in the phosphate buffer were

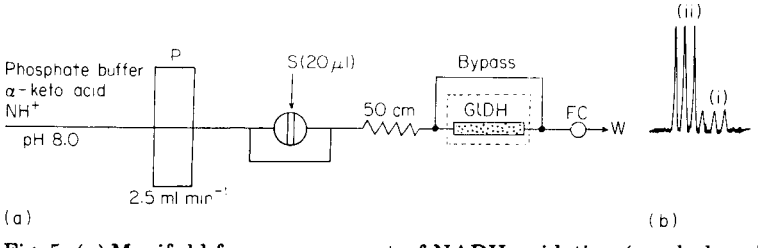

Fig. 5. (a) Manifold for measurement of NADH oxidation (symbols as in Fig. 1). (b) Peaks obtained when 0.25 mg ml^{-1} NADH was passed: (i) through the GlDH column; (ii) around the column via the bypass.

TABLE 1

Extent of conversion of NADH to NAD^+ by GlDH

NADH conc. (mg ml^{-1})	0.25	0.5	1.0
Conversion to NAD (%)[a]	80	71	62

[a]Mean of three readings.

injected into the system. A bypass around the GlDH column controlled by two 3-way switching valves allowed the sample to pass through the column or travel directly to the detector via the bypass. Table 1 shows the efficiency of the GlDH column in converting different concentrations of NADH to NAD^+.

As shown in Table 1, the conversion efficiency increases as the NADH concentration decreases; 80% conversion shows acceptable catalytic activity. No doubt it would be increased by employing a longer GlDH column. However, even if some NADH passes through the GlDH column unoxidized, it is greatly diluted in the reservoir and then is uniformly distributed in the carrier solution, which passes continuously through the GlDH column. This solution, being very dilute in NADH, is continuously converted to NAD^+ during subsequent passage through the GlDH column. In the above experiment the concentrations of α-keto acid and ammonium acetate in the carrier stream was increased in stages from 1 mM to 5 mM each, but there was no appreciable change in activity, therefore 1 mM of each was found to be sufficient in the circulating solution.

Stability of the circulating solution

A typical 50-ml circulating solution was composed of 0.1 M phosphate buffer, 2×10^{-3} M NAD^+, 1.0×10^{-3} M α-ketoglutaric acid and 1.0×10^{-3} M ammonium acetate. The pH of the solution was adjusted to 8.0. When not in use, the reservoir containing the solution was kept stoppered at 4°C. The same circulating solution was used for four consecutive days at room temperture (40—50 injections daily). No significant change in peak height and shape was observed, but on the fifth day very slight turbidity appeared in the solution, which caused baseline fluctuations.

Conclusions

The principle of coenzyme regeneration by recycling in an immobilized enzyme system has been demonstrated. It can probably be applied to the determination of a large number of dehydrogenase substrates [20], many of which (glucose, lactate, malate, pyruvate, etc) are routinely determined in clinical and food laboratories. It undoubtedly greatly decreased the consumption of NAD^+.

REFERENCES

1 J. Růžička and E. H. Hansen, Anal. Chim. Acta, 106 (1979) 207.
2 P. J. Worsfold, J. Růžička and E. H. Hansen, Analyst (London), 106 (1981) 1309.
3 K. Mosbach, P. O. Larsson and C. Lowe, Methods Enzymol., 44 (1976) 859.
4 M. R. Kula, K. H. Korner, H. Hustedt and H. Schutte, Ann. N.Y. Acad. Sci., 369 (1981) 347.
5 R. W. Coughlin, M. Aizawa, B. E. Alexander and M. Charles, Biotechnol. Bioeng., 17 (1975) 515.
6 R. W. Coughlin and B. Alexander, Biotechnol. Bioeng., 17 (1975) 1379.
7 R. M. Kelly and D. J. Kirwan, Biotechnol. Bioeng., 19 (1977) 1215.
8 H. Jaegfeldt, A. Torstensson and G. Johansson, Anal. Chim. Acta, 97 (1978) 221. H. Jaegfeldt, T. Kuwana and G. Johansson, J. Am. Chem. Soc., 105 (1983) 1805. L. Gorton, A. Torstensson, H. Jaegfeldt and G. Johansson, J. Electroanal. Chem., 161 (1984) 103.
9 G. Marko-Varga, R. Appelqvist and L. Gorton, Anal. Chim. Acta, 179 (1986) 371.
10 W. J. Blaedel and R. C. Engstrom, Anal. Chim. Acta, 52 (1980) 1691.
11 A. Malinauskas and J. J. Kulys, Anal. Chim. Acta, 98 (1978) 31.
12 T. Yao and S. Musha, Anal. Chim. Acta, 110 (1979) 203.
13 D. P. Nikolelis, C. C. Painton and H. A. Mottola, Anal. Biochem., 97 (1979) 255.
14 P. Roehrig, C. M. Wolf and J. P. Schwing, Anal. Chim. Acta, 153 (1983) 181.
15 O. H. Lowry and J. V. Passonneau, A Flexible System of Enzymatic Analysis, Academic Press, New York, 1972.
16 O. H. Lowry, J. V. Passonneau and M. K. Rock, J. Biol. Chem., 236 (1961) 2756.
17 M. Masoom and A. Townshend, Anal. Chim. Acta, 166 (1984) 111.
18 J. W. Kuan, S. S. Kuan and G. G. Guilbault, Anal. Chim. Acta, 100 (1978) 229.
19 H. R. Horton, H. E. Swaisgood and K. Mosbach, Biochim. Biophys. Res. Commun., 61 (1974) 1118.
20 P. D. Boyer (Ed.), The Enzymes, Vol. XI, Academic Press, New York, 1975.

Analytica Chimica Acta, 185 (1986) 57—64
Elsevier Science Publishers B.V., Amsterdam — Printed in The Netherlands

INDIVIDUAL AND SIMULTANEOUS ENZYMATIC DETERMINATION OF ETHANOL AND ACETALDEHYDE IN WINES BY FLOW INJECTION ANALYSIS

F. LÁZARO, M. D. LUQUE DE CASTRO and M. VALCÁRCEL*

Department of Analytical Chemistry, Faculty of Sciences, University of Córdoba, Córdoba (Spain)

(Received 12th December 1985)

SUMMARY

The individual and simultaneous enzymatic determination of ethanol and acetaldehyde in wine by flow injection analysis is described. Individual determinations of 0.002—0.016% (v/v) ethanol or 1.0—8.0 $\mu g\ ml^{-1}$ acetaldehyde with r.s.d. 0.7% and 0.5%, respectively, are done with a single-beam spectrophotometer, based on the use of alcohol dehydrogenase and aldehyde dehydrogenase. A diode-array detector and dual reagent injections are used for the simultaneous determination of the two compounds. The errors are <3.5% and <2.0% for ethanol and acetaldehyde, respectively, when the method is applied to wine samples.

As a long-established commercial product of great variety, wine has been studied very thoroughly. Standard methods for the determination of oenological parameters are regulated by national governments [1] and international organizations alike [2]. Official methods of analysis tend to be slow and so uneconomic. Owing to the inherent complexity of wines, separation techniques (distillation, ion-exchange, precipitation, etc.) are usually needed to isolate the analyte [3]. The use of flow injection analysis (f.i.a.) should allow fast determination of oenologic parameters.

Enzymatic methods for the spectrophotometric determination of ethanol or acetaldehyde or both simultaneously, are suggested in this paper. The use of separation techniques prior to the determinations is unnecessary because of the high selectivity of the reactions involved and the high concentrations of these analytes in wine, compared with other alcohols and aldehydes, which necessitates considerable dilution of the samples.

The determination of ethanol is based on its oxidation by NAD^+ in the presence of alcohol dehydrogenase (ADH) at pH 9 [4]. Semicarbazide is used as trapping agent for the acetaldehyde formed in the reaction.

$$CH_3CH_2OH + NAD^+ \overset{ADH}{\rightleftharpoons} CH_3CHO + NADH + H^+$$

Acetaldehyde is determined by oxidation with NAD^+ in the presence of

0003-2670/86/$03.50

aldehyde dehydrogenase, AlDH, at pH 9 [5]:

$$CH_3CHO + NAD^+ + OH^- \overset{AlDH}{\rightleftharpoons} CH_3COO^- + NADH + H^+$$

The NADH is monitored spectrophotometrically in both cases.

The merging-zones mode of f.i.a. and a single-beam spectrophotometer are used for the individual determination of ethanol and acetaldehyde. The problem of the simultaneous determination of both analytes posed by their appreciably different concentrations in the samples is solved by using a diode-array detector [6]. The reversed mode of f.i.a. (in which reagent is injected into a stream of sample) is most suitable in this case.

EXPERIMENTAL

Apparatus and reagents

A Pye-Unicam SP6-500 single-beam spectrophotometer equipped with a Hellma 178.12-QS flow-cell (inner volume 18 μl) was used for the individual determinations. A Hewlett-Packard (HP) 8451A diode-array spectrophotometer furnished with a HP-9121 floppy disc unit, a HP-98155A keyboard and a HP-7470A plotter were used in the simultaneous determinations. Two Ismatec Mini-S-840 peristaltic pumps, a Tecator type-I manifold and a home-made dual variable-volume injection valve were used in both types of determination.

Absolute ethanol standards (purity 99.5%) and distilled acetaldehyde (assayed by iodimetric back-titration [7]) were used. Alcohol dehydrogenase (E.C. 1.1.1.1; ca. 400 U mg^{-1} protein), aldehyde dehydrogenase (E.C. 1.2.1.5; ca. 26.5 U mg^{-1} protein) and the β-nicotinamide adenine dinucleotide (NAD^+) were supplied by Boehringer Mannheim.

The following buffer solutions were prepared. For buffer B1, a mixture of 33.00 g l^{-1} $Na_4P_2O_7$, 1.57 g l^{-1} glycine, 8.76 g l^{-1} NaCl and 8.0 g l^{-1} semicarbazide hydrochloride was adjusted to pH 9.0 with sodium hydroxide. For buffer B2, a mixture of 33.00 g l^{-1} $Na_4P_2O_7$ and 4.9 g l^{-1} KCl was adjusted to pH 9.0 with hydrochloric acid. For buffer B3, a 33.00 g l^{-1} $Na_4P_2O_7$ solution was adjusted to pH 9.0 with hydrochloric acid. Sample solution S1 was wine, diluted as required with buffer B1 (itself diluted 1 + 5) for ethanol and B2 for acetaldehyde determination. Sample solution S2 was wine diluted 200-fold with diluted (1 + 5) buffer B3. Enzyme solution E1 was ADH (130 U ml^{-1}) and NAD^+ (4.0 g l^{-1}) in buffer B1 for the individual determination of ethanol. Enzyme solution E2 was AlDH (8.0 U ml^{-1}) and NAD^+ (4.0 g l^{-1}) buffer in B2.

Configurations

The individual determinations were done with a symmetric merging zones manifold (Fig. 1A) in which the enzyme (E1 or E2) and sample (S1) were injected into pyrophosphate buffer streams (B1 or B2) which later merged, and yielded NADH which was monitored at 340 nm. The reversed flow-

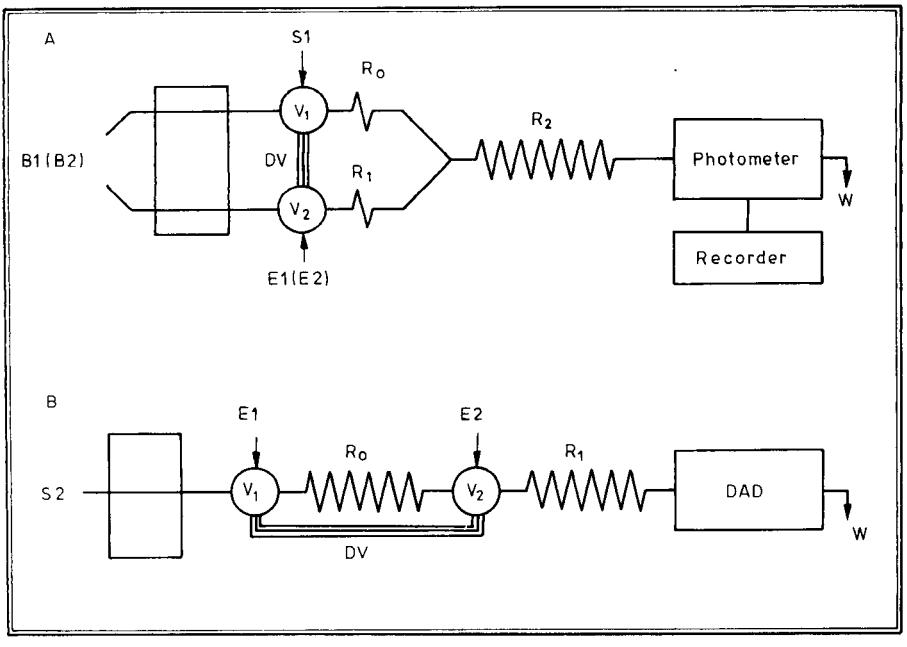

Fig. 1. Configurations used: (A) for the individual determination; (B) for the simultaneous determinations, S1, S2, E1, E2, B1 and B2 are described in the text. DAD and DV denote the diode-array spectrophotometer and dual injection valve (composed of valves V_1 and V_2), respectively. W is waste.

injection scheme for the simultaneous determination of ethanol and acetaldehyde involved two serial injection valves which simultaneously injected separate portions of E1 and E2 into the sample stream (S2) (Fig. 1B). The reactant zones reached the detector at different times.

RESULTS AND DISCUSSIONS

Enzymatic determination of ethanol

The optimization of the flow-injection and chemical variables for greatest sensitivity yielded the values listed in Table 1. The glycine, pyrophosphate and sodium chloride concentrations did not affect the analytical signal; conversely, the semicarbazide concentration exerted a significant influence through its trapping effect. The concentrations of ADH and NAD^+ had the most significant effect on the peak height, which increased with increasing concentration of both until it became almost constant at 130 U ml^{-1} and 4.0 g l^{-1}, respectively.

The sample pH could be varied between wide limits (4.0—9.5) without change in peak height because of the capacity of the buffer added to the enzyme, B1; the pH of the buffer could also range between 7 and 10 without noticeable decrease in the analytical signal. Nevertheless, a pH of 9.0 was

TABLE 1

Optimum values of the variables

Variable	Determination		
	Ethanol[a]	Acetaldehyde[a]	Both analytes simultaneously[b]
ADH (U ml^{-1})	130	—	130
AlDH (U ml^{-1})	—	8.0	8.0
NAD^+ (g l^{-1})	4.0	4.0	4.0
$Na_4P_2O_7$ (g l^{-1})	33.0	33.0	33.0
NaCl (g l^{-1})	8.8	—	8.8
KCl (g l^{-1})	—	14.9	14.9
Glycine (g l^{-1})	1.6	—	1.6
Semicarbazide (g l^{-1})	8.0	—	
Buffer pH	9.0	9.0	9.0
Sample pH	4.0—9.5	3.3—9.5	4.0—9.5
Flow rate (ml min^{-1})	0.78	0.62	1.10
Reactor length R_0 (cm)	6.0	6.0	262
Reactor length R_1 (cm)	6.0	6.0	136
Reactor length R_2 (cm)	193	140	
Loop V_1 volume (μl)	30.0	60.0	30.0
Loop V_2 volume (μl)	60.0	90.0	90.0

[a]Manifold A, Fig. 1. [b]Manifold B, Fig. 1.

chosen for B1 as this was the most suitable for the determination of acetaldehyde (see below). Temperatures of $\leqslant 25°C$ were satisfactory.

The lengths of reactors R_0 and R_1 were the minimum necessary to connect the two injection valves with the manifold. The length of R_2 and the flow rate were chosen so as to obtain the maximum signal. The volume of sample was always smaller than that of the enzyme solution in order to keep the former surrounded by ADH/NAD^+ solution. The sampling frequency achieved for ethanol determinations was 55 h^{-1}.

The determination of ethanol in wine poses a problem deriving from the high concentration of the analyte, and requires much dilution (up to 1:5000). This was implemented by one of three procedures. The manual dilution of the sample prior to introduction into the flow system is the commonest procedure, but is somewhat inaccurate in that it often requires the measurement of a small sample volume. Nevertheless, it allows a wide linear calibration range, and good sensitivity and relative standard deviation (Table 2). The results obtained for ethanol in different types of wine and brandy from Jerez are compared to those obtained by the EEC method [8] in Table 3. The flow dilution technique involves utilizing asymmetric merging zones (chasing zones) in which the "head" of the enzyme sector merges with the tail of the sample. The greater the distance between the heads of the two sectors, the greater the dilution. In this case R_0/R_1 was 8. This procedure afforded a linear calibration range and a precision comparable to that of the manual

TABLE 2

Calibration parameters for the determination of ethanol

Parameter	Dilution method		
	Manual	Flow	Photometric
Linear range (% v/v)	0.004—0.016	0.06—0.26	0.002—0.016
Slope ($\%^{-1}$)	20.207	1.224	14.024
Correlation coefficient[a]	0.9955	0.9988	0.9944
R.s.d. (%)[b]	1.1	1.1	0.7

[a]5 points. [b]11 determinations of 0.008% ethanol (manual and photometric) and 0.16% ethanol (flow).

TABLE 3

Determination of ethanol in wine and brandy

Sample	Ethanol concentration[a] (% v/v)	Errors		
		Manual dilution	Flow dilution	Photometric dilution
Wine 1	14.37	+7.2	+22.6	+14.8
Wine 2	15.17	—4.5	+13.5	+1.7
Wine 3	15.26	+1.0	+13.3	—5.1
Wine 4	15.35	—9.1	+8.3	—3.4
Wine 5	17.45	+4.3	+11.0	+0.7
Wine 6	19.90	—0.5	+19.9	—2.8
Wine 7	20.10	—4.3	—0.1	—0.8
Wine 8	15.46	+2.3	—2.2	+4.4
Brandy 1	39.95	—2.1	—4.4	—1.9
Brandy 2	66.85	—6.7	—6.9	—2.6
Average error		3.9	9.7	3.5

[a]EEC official method.

dilution procedure; however, the errors incurred in its application to real samples were considerably larger (see Table 3). The photometric "dilution" method is based on measuring absorbances at wavelengths away from the absorption maximum [6] and was applied in conjunction with manual dilution to diminish the sensitivity of the method further, thus slightly increasing the linear calibration range (to 0.002—0.016%) and hence decreasing the extent of manual dilution of the sample required. This photometric procedure has the greatest accuracy (average error 3.5%) for the analysis of real samples, and the greatest precision (r.s.d. = 0.7%).

Enzymatic determination of acetaldehyde

The results obtained in the optimization of variables for acetaldehyde also appear in Table 1. As in the ethanol method, the pyrophosphate concentra-

tion did not affect the analytical signal, but the signal did increase with increasing potassium chloride concentration, reaching a maximum at 14.9 g l^{-1}. Increasing the NAD^+ and enzyme concentrations increased the peak height, until it became constant above 4.0 g l^{-1} and 8.0 U ml^{-1}, respectively. Changing the NAD^+ concentration had a less significant effect than changing the AlDH concentration.

The optimum pH range was 8—10, while the sample pH could range between 3.5 and 9.5 without appreciably altering the signal. Acetaldehyde present in wine is found free and bound to sulphur dioxide; therefore, to determine total acetaldehyde, the pH of the carrier solution was adjusted to 9.0 and a 20% (v/v) concentration of this buffer was added to the samples to obtain a final pH of 9.0—9.5, to ensure that all acetaldehyde present was unbound. The other variables (flow injection and temperature) were optimized as for ethanol, except that the sample and enzyme volumes used were somewhat larger so as to increase sensitivity. The sampling frequency attained was 50 h^{-1}.

The calibration graph was linear for 1.0—8.0 $\mu g\ ml^{-1}$ acetaldehyde (correlation coefficient 0.9988, 5 points) with a slope of 0.0335 ml μg^{-1}. The relative standard deviation (11 determinations of 5 $\mu g\ ml^{-1}$) was 0.5%. Owing to its volatility, acetaldehyde was determined in wine by the standard addition method. The values shown in Table 4 were obtained for different sherries. The recovery and mean deviation were 102% and 2.0%, respectively.

Simultaneous determination of ethanol and acetaldehyde

The most serious problem encountered in the simultaneous determination of these compounds is the different dilution required for each (average dilution 1:1500 and 1:80 for ethanol and acetaldehyde, respectively). Attempts were made to bring the determination ranges of both species closer by not using semicarbazide in solution B1, in order to decrease the extent of alcohol oxidation, and by measuring the absorbance at other than the wavelength of maximum absorbance, but the results were unacceptable because the signal from acetaldehyde was too small.

TABLE 4

Determination of acetaldehyde

Wine samples	Concentration found ($\mu g\ ml^{-1}$)	Recovery of standard additions (%)	
		2.0 $\mu g\ ml^{-1}$	5.0 $\mu g\ ml^{-1}$
1	178	98	103
2	131	96	107
3	145	99	103
4	473	112	106
5	362	100	91
6	143	102	103
7	148	106	104
8	334	103	99

TABLE 5

Simultaneous determination of ethanol and acetaldehyde

Sample	Ethanol			Acetaldehyde		
	Found (% v/v)	Recovery (%)		Found ($\mu g\ ml^{-1}$)	Recovery (%)	
		0.04%	0.08%		0.4 $\mu g\ ml^{-1}$	0.8 $\mu g\ ml^{-1}$
1	13.4	105	93	56	90	107
2	12.0	97	100	102	104	99
3	13.3	101	105	135	105	101
4	12.7	101	100	221	104	104
5	13.4	100	94	288	102	98

Finally, a simple flow configuration (Fig. 1B) was chosen in which solutions of different composition (each with a different enzyme) were injected into a stream of diluted (1:200—1:300) sample. The indicator reaction for acetaldehyde developed in reactor R_1, and in R_0 and R_1 for ethanol. The two reacting sectors reached the diode-array spectrophotometer at different times. Absorbance measurements based on the sum of the absorbances in the 336, 338, 340, 342 and 344-nm channels were used for acetaldehyde measurements, which changed the range of the method for acetaldehyde from 1.0—8.0 $\mu g\ ml^{-1}$ to 0.3—2.0 $\mu g\ ml^{-1}$. Semicarbazide was not used in the assay for ethanol and the NADH was monitored at 360 nm, in order to decrease the sensitivity. Also, as the calibration graph for ethanol decreased in sensitivity at higher concentrations, this less sensitive range was used for measurement of the ethanol concentrations in the samples after dilution as described above. Table 5 shows the recoveries obtained on addition to the wine samples of 0.4 and 0.8 $\mu g\ ml^{-1}$ acetaldehyde and 0.04% and 0.08% ethanol. The average recoveries are 101.4% and 98.8%, with absolute average deviations of 4.7% and 3.3% for acetaldehyde and ethanol, respectively.

Conclusions

Comparison of the flow-injection methods with the official EEC methods shows that the flow-injection technique offers a number of advantages. These include lower sample and reagent consumption, less sample manipulation (no prior separation of the analytes is necessary), lower determination limits, high analysis rate (50—55 samples per hour for one analyte), and the simultaneous determination of both analytes.

The CAICyT is thanked for financial support (Grant No. 2012-83). The authors gratefully acknowledge González Byass for providing samples of wine.

REFERENCES

1 France, Ministre de l'Agriculture, Arrêté du 24 juin 1963 relatif aux Méthodes Officielles d'Analyses des Vins et des Moûts, Journal Officiel No. 63-154, 1037 (1963) 4551.
2 Recueil des Méthodes Internationales d'Analyse des Vins, Office International de la Vigne et du Vin, Paris, 1962—1973.
3 J. Ribereau-Gayon, E. Peynaud, P. Sudran and P. Ribereau-Gayon, Traité d'Oenologie. Sciences et Techniques du Vin, Tome I, Dunod, Paris, 1976.
4 E. Bernt and I. Gutmann, in H. U. Bergmeyer (Ed.), Methods of Enzymatic Analysis, 2nd edn., Vol. 3, Verlag Chemie, Weinheim and Academic Press, New York, 1974, p. 1499.
5 F. Lundquist, in H. U. Bergmeyer (Ed.), Methods of Enzymatic Analysis, 2nd edn., Vol. 3, Verlag Chemie, Weinheim, and Academic Press, New York, 1974, p. 1509.
6 F. Lázáro, A. Ríos, M. D. Luque de Castro and M. Valcárcel, Anal. Chim. Acta, 179 (1986) 279.
7 Official Methods of Analysis, 12th edn., Association of Official Analytical Chemists, Washington, DC, 1975, p. 603.
8 Journal Officiel des Communautés Européennes, L. 113, 14 Mai 1982, p. 16.

Analytica Chimica Acta, 185 (1986) 65—73
Elsevier Science Publishers B.V., Amsterdam — Printed in The Netherlands

AN AUTOMATED FLOW-INJECTION SERIAL DYNAMIC DIALYSIS TECHNIQUE FOR DRUG-PROTEIN BINDING STUDIES

P. E. MACHERAS and M. A. KOUPPARIS*

Departments of Pharmacy and Chemistry, University of Athens, 104 Solonos, Athens 106 80 (Greece)

(Received 5th August 1985)

SUMMARY

An automated flow-injection analyzer is interfaced with a dialysis unit to study drug-protein binding interactions. The binding of some sulfonamides to bovine serum albumin is studied by means of the automated system and gives results similar to those obtained by other procedures. A usual time for a complete run is 100 min, including calibration. The dialysable sulfonamides are quantified spectrophotometrically by using a modified Bratton-Marshall method. The system is also used for the calculation of dialysis rate constants.

Studies on drug-protein interaction have become important because of their relevance to pharmacokinetics. Such studies in vitro have been done by various methods including equilibrium dialysis [1—3], dynamic dialysis [4—7], continuous-flow dynamic dialysis [8], fluorescence probe techniques [9, 10] and ultrafiltration [11]. Although the classical equilibrium dialysis technique is still often favoured, it has serious drawbacks and is increasingly replaced by dynamic dialysis methods. These methods offer the advantages of rapidity and the measurement of drug-protein binding over a range of drug concentrations in a single experiment. They are based on the principle that a nondiffusible protein-drug complex reaches rapid equilibrium with free protein and diffusible drug in a protein compartment, which is separated from a sink compartment by a semipermeable membrane. The rate of diffusion across the membrane is directly proportional to the free drug concentration in the protein compartment.

The dialysable drug is sampled by periodic manual removal of a certain volume from the external solution, which is replaced with fresh buffer solution in order to maintain sink conditions. The measurement is done by u.v. spectrophotometry or, when other absorbing species are present, by visible spectrophotometry after derivatization. To avoid invasive sampling, the continuous dynamic dialysis technique [8] was introduced; in this method the absorbance of the dialysable drug is continuously monitored. Although dynamic dialysis techniques have shortened the time needed for an experiment to 4—6 h, any further decrease would be useful.

0003-2670/86/$03.50

The present paper describes an automated method for protein-binding studies based on the principle of dynamic dialysis in conjunction with the versatile techniques of flow injection analysis (f.i.a.). Flow-injection techniques have already been used in drug-protein binding studies with a fluorescence probe [12], but only the percentage displacement of the probe was estimated. In the proposed method, a conventional dialyzer unit, as used in clinical air-segmented analyzers, with two identical compartments of 1.0-ml capacity, is connected to an automated flow-injection analyzer. The receiving compartment becomes the "sample loop" of the analyzer, in which carrier solution is enclosed to receive the dialysable drug of the "protein compartment" through which the protein-drug solution is continuously circulated. Periodically, this "sample zone" is injected into the spectrophotometric manifold and fresh solution is enclosed in the sample loop. The drug concentration in the "protein compartment" is changed by successive manual additions of small volumes of standard drug solution.

The technique described here, which is called hereafter flow-injection serial dynamic dialysis, provides automation of dialysis, sampling and spectrophotometric determination. The features of the method are explored by a binding study of three sulfonamides with bovine serum albumin (BSA). The manifold is based on the classical Marshall-Bratton reaction adapted for f.i.a. [13].

EXPERIMENTAL

Apparatus and reagents

The system, shown in Fig. 1, was developed by interfacing a homemade flow-injection photometric analyzer [14] with a conventional 4-slot dialysis unit (Technicon). This analyzer consists of reagent (RP) and sample (SP) peristaltic pumps, a rotating valve (RV, Rheodyne Type 50) operated with a pneumatic two-position actuator (Rheodyne Model 5001), an appropriate manifold of teflon tubing, a conventional photometer equipped with a flow-

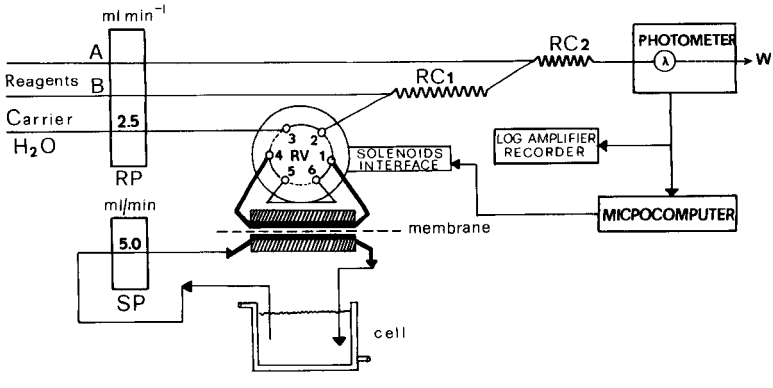

Fig. 1. Schematic diagram of the flow-injection serial dynamic dialysis system: RP, reagent pump; SP, sample pump; RC1 and RC2, reaction coils; W, waste; RV, rotary valve.

cell (Hellma Model 172.12; 18-μl volume), a strip-chart recorder with a logarithmic amplifier, and a Rockwell AIM-65 microcomputer to control the whole system.

The dialyser unit, constructed from plexiglas, has a dialysis surface of 670 mm^2 with two identical chambers of 1.0-ml volume each. The two chambers are separated by a semipermeable membrane (Cuprophan membranes; Technicon) with 20-μm pores, hydrated for a short time before being placed in position. The upper chamber, connected to ports 1 and 4 of the rotary valve (the "sample loop" of the analyzer) serves as the "receiving chamber". The lower chamber is connected to the sample pump which circulates the protein-drug solution from the 50-ml cell thermostatted at 25 ± 0.5°C.

The manifold for the automated determination of sulfonamides is shown in Fig. 2. The reagent pump can be automatically stopped during dialysis to avoid waste of the reagents. All experiments were done at constant temperature, pH, flow rates, stirring, etc.

The sulfonamides used were obtained commercially. Concentrated stock solutions were prepared in 0.05 M sodium hydroxide at concentrations of 0.04 M for sulfamethoxazole and sulfisoxazole, and 0.050 M for sulfamethizole. Bovine serum albumin (fraction V, powder; Sigma) was used to prepare a 5×10^{-4} M working solution in 0.050 M phosphate buffer, pH 7.4. Analytical-grade reagents were used to prepare 0.080 M HCl, 2.0×10^{-4} M sodium nitrite and 0.1% (w/v) *N*-(1-naphthyl)ethylenediamine dihydrochloride (NEDD). Deionized/distilled water was used.

System set-up and operation

The appropriate dialysis program is loaded in the microcomputer memory and the operator is prompted to provide information which includes number of measurements, dialysis, injection and mixing/washing times. Then the reagent pump is started, the appropriate wavelength is set on the photometer (540 nm for sulfonamides) and the 100% transmittance and recorder baseline are calibrated. Buffer or buffered protein solution (50.0 ml) are pipetted into the cell and the sample pump is started. In execution of the program, the rotating valve is turned at the injection position and the operator is

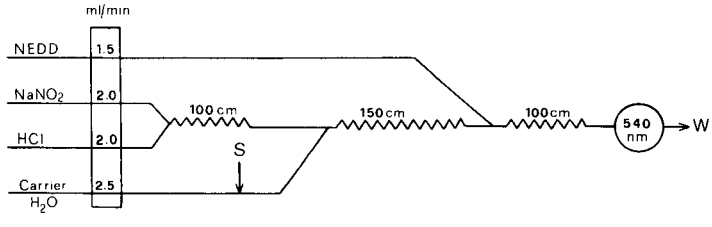

Fig. 2. Manifold for the determination of sulfonamides. NEDD, *N*-(1-naphthyl)ethylenediamine dihydrochloride, 0.10% (w/v); sodium nitrite, 2.0×10^{-4} M; hydrochloric acid, 0.80 M. S represents the dialysate transferred by the carrier into the reagent stream.

prompted to add the first portion of the standard stock solution of the drug under test, using a Hamilton microsyringe. The valve remains in this position, during which time the carrier solution (water) flows through the receiving chamber, for the preset mixing/washing time (1 min) in order to ensure adequate mixing and transference of the protein solution. Then the computer turns the valve to the load position during which time the receiving solution is stopped. When the preset dialysis time is reached, the valve is turned to the injection position and the carrier solution transfers the dialyzate to the spectrophotometric manifold. The absorbance peak, corresponding to the concentration of the dialysed drug, is recorded and its value is read by the microcomputer. After the injection time (30 s) has elapsed, the operator is prompted to add the next portion of the standard stock solution of the drug and the cycle is repeated. The timing diagram of the operation is shown in Fig. 3. During the mixing/washing time the recorder pen is inactivated by the computer to avoid signals from the limited dialysis of the drug, because the valve is in the injection position.

THEORY

In the absence of protein, the passage of small molecules through the dialysis membrane follows first-order diffusion kinetics. The permeation rate can be described by

$$dD_i/dt = k_d (D_t - D_i) \quad (1)$$

where D_i is the instantaneous drug concentration in the receiving compart-

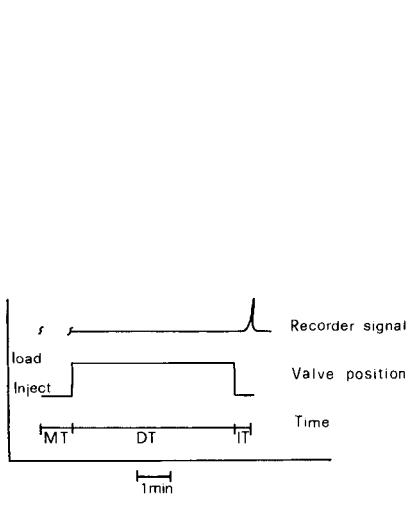

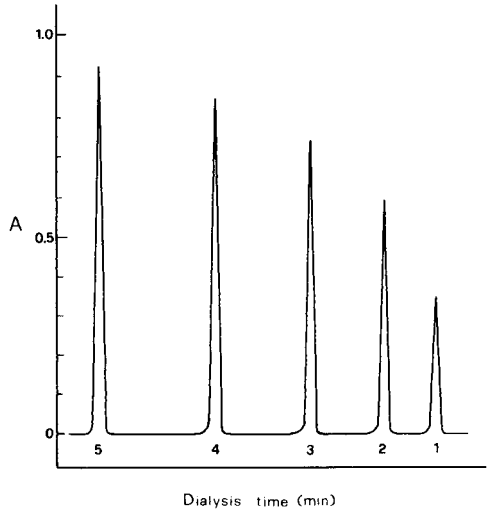

Fig. 3. Timing diagram of operation of the system: MT, mixing time; DT, dialysis time; IT, injection time.

Fig. 4. Typical dialysis profile of sulfamethoxazole (2.5×10^{-4} M) for k_d calculation.

ment, D_t is the concentration in the protein compartment and k_d is the intrinsic dialysis rate constant. When protein is included in the solution undergoing dialysis, small molecules bound to the protein do not diffuse. Therefore, the rate of passage is related not to the total concentration, but to the free or unbound concentration D_f, and the kinetics for each dialysis run is described by $dD_i/dt = k_d(D_f - D_i)$, assuming that the dialysis rate constant is unaffected by the presence of protein. Integration of this equation gives

$$D_i = D_{fo}[1 - \exp(-k_d t)] \quad (2)$$

where D_{fo} is the initial free drug concentration in the protein compartment after equilibrium has been reached and before dialysis is initiated. Equation 2 actually describes the time profile of the dialysate concentration in the receiving compartment during a dialysis run. Because the protein solution has a large volume (50 ml), in comparison with the volume of the receiving solution (1.0 ml), D_f remains practically constant and can be considered as equal to D_{fo}. Clearly, if the experimental conditions and dialysis time remain constant, D_i is linearly related to D_{fo}.

With an appropriate flow-injection manifold, regardless of the type of detector (photometer, fluorimeter, electrochemical detector, etc), the required signal, P_i, is measured as a peak, which is related to D_i in a specified concentration range. Therefore, if an appropriate dialysis time is chosen, the signal measured, P_i, is directly related to D_{fo} over a specified range of concentrations. For the flow-injection analyzer used here with spectrophotometric detection, a calibration graph of absorbance peaks vs. free drug concentration is easily constructed by running a series of drug additions with subsequent dialysis in a buffer solution in the absence of protein. When the procedure is repeated with buffered protein solution and the absorbance peak of each successive drug addition/dialysis is measured, the free drug concentration D_{fo} can be estimated from the calibration graph. Because the total drug concentrations D_t are known from the successive drug additions, the binding parameters can be calculated by the well known Scatchard procedures [15]. In this study a computer program in BASIC based on nonlinear regression was used to obtain these parameters.

The experimental dialysis rate constant can easily be calculated from Eqn. 2. First, several standard solutions of the drug studied are introduced into the receiving compartment through ports 5 and 6 of the rotary valve (Fig. 1). Their absorbance peaks are measured and a calibration graph, absorbance peak vs. D_i, is constructed. Then a buffered solution of the drug is pipetted into the cell and a special program is run which increases the dialysis time in preset steps. Thus, the dialysis/time profile of the drug is obtained. The k_d value can be calculated from

$$\ln[(D_f - D_i)/D_f] = -k_d t \quad (3)$$

which is obtained from Eqn. 2 by rearrangement and logarithmic transformation. In addition, Eqn. 3 can provide the dialysis time required for a specified

percent of dialysis ($\%D_i$), say, 10% for sink conditions: $t = -\ln [1 - (\%D_i/100)/k_d]$. The percent dialysis for a specified dialysis time can then be obtained from

$$\%D_i = 100[1 - \exp(k_d t)] \quad (4)$$

RESULTS AND DISCUSSION

A typical dialysis profile of a sulfonamide obtained by using the proposed system is shown in Fig. 4. Dialysis time was increased stepwise by 1.0 min by the computer program. The calculated dialysis rate constants for sulfisoxazole, sulfamethizole and sulfamethoxazole at pH 7.4 are shown in Table 1, along with statistical data. The excellent linearity of the plots and the precision of the results show the validity of the technique for the rapid evaluation of dialysis rate constants. The time required for a calibration graph of three standards and the dialysis runs (seven points) is only 20 min.

The precision of the system (dialysis and measurement) was studied by running five tests with 2.0×10^{-4} M sulfamethoxazole buffered solutions in the presence and absence of protein. The results are shown in Table 2. The excellent reproducibility results from the precise timing control of the microcomputer and the stability of the flow rates of the pumps. After 30 min of dialysis, the difference in absorbance peaks was negligible, showing that the drug concentration remained practically constant.

TABLE 1

Calculation of dialysis rate constants of sulfonamides at pH 7.4 and 25°C

Drug	Concentration (M)	k_d (±SD) ($n = 5$)	r^a
Sulfamethizole	4×10^{-4}	0.095 ± 0.011	0.997
Sulfamethoxazole	2.5×10^{-4}	0.117 ± 0.011	0.990
Sulfisoxazole	3×10^{-4}	0.138 ± 0.018	0.991

[a]Correlation coefficient of Eqn. 3.

TABLE 2

Precision of the proposed system for five runs with buffered 2×10^{-4} M sulfamethoxazole[a]

	No protein	With protein
Mean peak height	0.814	0.302
Standard deviation	0.011	0.003
RSD (%)	1.4	1.0

[a]Dialysis time 5.0 min, injection time 0.5 min, washing time 1.0 min. Total time of dialyses 32.5 min.

In order to study the effects of ionic strength and viscosity on the dialysis, experiments were done with standard sulfamethoxazole solutions containing various amounts of sodium chloride and sucrose. Sucrose was chosen for studying the effect of viscosity because it is not expected to bind sulfonamides and also, even if it is dialysable, it does not interfere with the analytical procedure. The results shown in Table 3 agree with the conclusions of Meyer and Guttman [5] that increased ionic strength and viscosity do not affect the rate of dialysis.

A typical dialysis experiment for the estimation of the binding parameters of sulfamethizole is shown in Fig. 5. The calibration graph (absorbance peaks vs. D_f) obtained for buffer solution in the absence of protein is shown along with the dialysis runs obtained in the presence of protein (5×10^{-4} M). The statistical data for the calibration graphs are shown in Table 4. The differences in the slopes of the calibration graphs are caused by the differences of k_d and also of the different molar absorptivities of the Bratton-Marshall reaction product for each sulfonamide. The dialysis time chosen for these experiments was 5 min, in order to increase the sensitivity of the measurement. The detection limit of the determinations was then about 5×10^{-6} M (concentration corresponding to an absorbance peak equal to twice the standard deviation of the most dilute standard). The percent dialysis ($\%D_i$) achieved with 5-min dialysis times, ranged from 37.8 to 50% for the three sulfonamides, but the loss of drug from the protein compartment was only 0.8—1.0%. Because the drug concentration is increased before each successive dialysis, the total loss is negligible. In addition the calibration graph serves to correct any loss of this kind. Although sink conditions were not maintained, linear calibration plots were obtained, showing the validity of Eqn. 2.

TABLE 3

Effect of ionic strength (I) and viscosity on dialysis[a]

	Variable	Absorbance peak	Relative change (%)
Effect of ionic strength			
	I (M)		
Buffer[b]	0.11	0.598	—
+1% NaCl	0.28	0.588	−1.7
+10% NaCl	1.82	0.591	−1.2
Effect of viscosity			
	Rel. viscosity		
Buffer[b]	1.000	0.491	—
+1% sucrose	1.026	0.498	+1.4
+10% sucrose	1.333	0.466	−5.0

[a]Dialysis time 3 min. [b]Phosphate 0.050 M, pH 7.4.

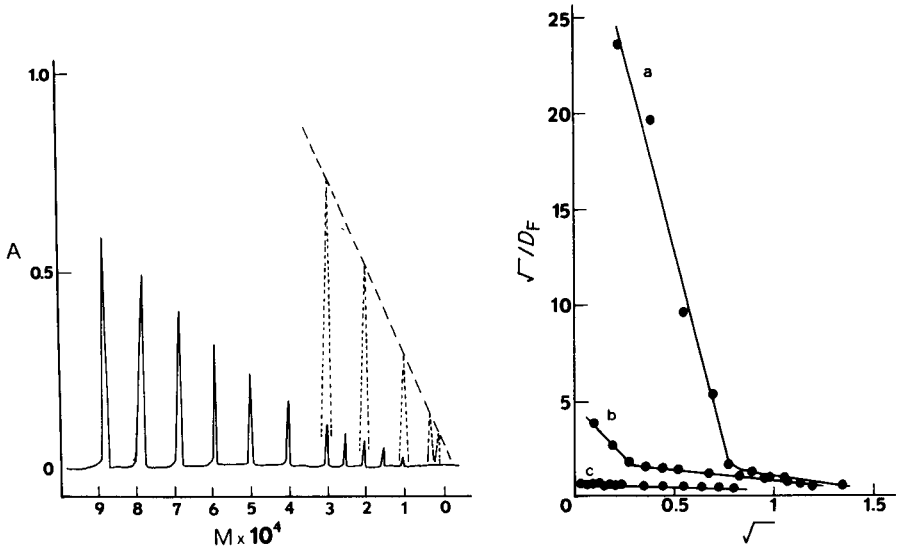

Fig. 5. Typical dialysis experiments for a binding study of sulfamethizole. Peaks for the calibration graph are shown as dashed lines. Protein concentration 5.0 × 10^{-4} M; dialysis time 5 min.

Fig. 6. Typical Scatchard plots for sulfonamide binding studies from data obtained in this study. (a) Sulfisoxazole; (b) sulfamethizole; (c) sulfamethoxazole. Dialysis experiments at pH 7.4, 25°C, with 5 × 10^{-4} M protein. $\sqrt{}$ = concentration of bound drug/total protein concentration.

The binding parameters estimated for each sulfonamide are shown in Table 5. The results are also presented in Fig. 6 in the form of Scatchard plots. Sulfisoxazole and sulfamethizole can be classified as highly bound, with affinities exceeding 5 × 10^3 M^{-1}, while sulfamethoxazole is moderately bound. The parameters found were compared with literature values (Table 5); for sulfamethoxazole, the agreement is good. For sulfamethizole and sulfisoxazole, the present study revealed two groups of binding sites, which have been also reported for other sulfonamides [18]. The estimates for the secon-

TABLE 4

Calibration graphs for dialysis experiments used in sulfonamides binding studies

Drug	Calibration equation	Standard error	r^a	Detection limit (M)
Sulfamethizole	$A = 0.021(\pm 0.012) + 2415(\pm 71)C^b$	0.011	0.999	9.1 × 10^{-6}
Sulfamethoxazole	$A = 0.052(\pm 0.017) + 3858(\pm 143)C$	0.025	0.998	5.7 × 10^{-6}
Sulfisoxazole	$A = 0.016(\pm 0.013) + 4347(120)C$	0.016	0.9992	5.1 × 10^{-6}

[a] Six standards. [b] Drug concentration in mol l^{-1}.

TABLE 5

Binding data for some sulfonamides to bovine serum albumin

Compound	Binding data[a]		Reference
Sulfamethoxazole	$n = 2.0 \pm 0.1$	$K = 2.9 \pm 0.3 \times 10^3\ M^{-1}$	This study
	$n = 2.9$	$K = 1.6 \times 10^3\ M^{-1}$	10
Sulfamethizole	$n_1 = 0.43 \pm 0.06$	$K_1 = 9 \pm 2 \times 10^5\ M^{-1}$	This study
	$n_2 = 2.7 \pm 0.3$	$K_2 = 2.0 \pm 0.5 \times 10^3\ M^{-1}$	This study
	$n = 2.0$	$K = 2.0 \times 10^4\ M^{-1}$	16
	$n = 2.9$	$K = 5.2 \times 10^3\ M^{-1}$	10
Sulfisoxazole	$n_1 = 0.80 \pm 0.02$	$K_1 = 1.3 \pm 0.2 \times 10^6\ M^{-1}$	This study
	$n_2 = 4.1 \pm 1.7$	$K_2 = 5.5 \pm 2.8 \times 10^3\ M^{-1}$	This study
	$n = 2.0$	$K = 1 \times 10^5\ M^{-1}$	16
	$n = 2.5$	$K = 1.47 \times 10^4\ M^{-1}$	17
	$n = 2.9$	$K = 9.6 \times 10^3\ M^{-1}$	10

[a] n, n_1, n_2 are the number of binding sites; K, K_1 and K_2 are the binding constants.

dary binding sites found here are close to the estimates of the single binding sites reported by Hsu et al. [10].

In conclusion, f.i.a. brings to the study of drug-protein binding its usual advantages of flexibility, speed, precise timing control, and automation of the sampling and measurement processes. By developing selective analytical methods (like the one proposed for sulfonamides) competitive binding studies can be done quickly and precisely.

REFERENCES

1 I. M. Klotz, F. M. Walker and R. B. Pivan, J. Am. Chem. Soc., 68 (1946) 1486.
2 M. J. Hunter and S. L. Commerfold, J. Am. Chem. Soc., 77 (1955) 4857.
3 M. T. Bush and J. D. Alvin, Ann. N.Y. Acad. Sci., 276 (1973) 36.
4 M. C. Meyer and E. J. Guttman, J. Pharm. Sci., 57 (1968) 895, 1627.
5 M. C. Meyer and E. J. Guttman, J. Pharm. Sci., 59 (1970) 33, 39.
6 S. P. Colowick and F. C. Womack, J. Biol. Chem., 244 (1969) 774.
7 R. El-Rashidy and S. Niazi, J. Pharm. Sci., 67 (1978) 967.
8 N. A. Sparrow, A. E. Russel and L. Glasser, Anal. Biochem., 123 (1982) 255.
9 L. Brand, J. R. Gohlke and S. Rao, J. Biochem., 6 (1967) 3510.
10 P. L. Hsu, K. H. Ma, H. W. Jun and L. A. Luzzi, J. Pharm. Sci., 63 (1974) 27.
11 I. Feldmann, R. A. Danley and J. F. O'Leary, Anal. Chem., 22 (1950) 837.
12 G. L. Abdullahi, J. N. Miller, H. N. Sturley and J. W. Bridges, Anal. Chim. Acta, 145 (1983) 109.
13 M. A. Koupparis and P. Anagnostopoulou, J. Assoc. Off. Anal. Chem., submitted.
14 M. A. Koupparis and P. Anagnostopoulou, J. Autom. Chem., 6 (1984) 186.
15 G. Scatchard, Ann. N.Y. Acad. Sci., 51 (1949) 660.
16 I. Moriguchi, S. Wada and J. Nishizawa, Chem. Pharm. Bull., 16 (1968) 601.
17 M. Nakagaki, N. Koga and H. Terada, Yakugaku Zasshi, 84 (1964) 516.
18 C. A. Cruze and M. C. Meyer, J. Pharm. Sci., 65 (1976) 33.

Analytica Chimica Acta, 185 (1986) 75—81
Elsevier Science Publishers B.V., Amsterdam — Printed in The Netherlands

FLOW-INJECTION SPECTROPHOTOMETRIC DETERMINATION OF ALUMINIUM IN WATER WITH PYROCATECHOL VIOLET

ODDVAR RØYSET
Norwegian Forest Research Institute, P.O. Box 61, N-1432 Ås-NLH (Norway)
(Received 18th September 1985)

SUMMARY

Optimum conditions for the adaptation of the spectrophotometric pyrocatechol violet method for aluminium to a flow-injection system are described. The detection limit is 3 μg Al l^{-1} and calibration graphs are linear up to 3 or 10 mg l^{-1} (with 200-μl or 10-μl injection loops, respectively). The relative standard deviation is <2% at 0.1 mg Al l^{-1}. Potential interferences of 40 common inorganic ions and of 20 organic substances, including fulvic acid, are reported. With the use of conventional masking agents and predigestion of samples with high organic content, the method is suitable for determining total aluminium in natural waters.

Pyrocatechol violet (PCV) was first proposed by Anton [1] as a chromogenic reagent for the determination of aluminium. The PCV method has been adapted for the determination of aluminium in water [2—4] and for use in AutoAnalyzer systems [5—7]. Pyrocatechol violet was recently compared with aluminon and eriochrome cyanine R, with and without cetyltrimethylammonium bromide, for adaptation to flow injection analysis [8]. Røgeberg and Henriksen [7] and Seip et al. [9] suggested that the PCV method might be applicable for adaptation to speciation procedures [10]. The main purpose of the present work was to optimize a flow-injection method and to study the effect of likely interferences.

EXPERIMENTAL

Flow-injection equipment

The manifold is shown in Fig. 1. A Tecator-Bifok FIA05 flow-injection analyzer was used with an Ismatec MP13 peristaltic pump and a Cecil 292 single-beam spectrophotometer. A Hellma flow-through cell (10-mm light path, 3 mm i.d., 80 μl) was used in all the development and most of the applications of the method. Occasionally a 20-mm light path (3 mm i.d.) Hellma flow-through cell was used for increased sensitivity. The tubings were made of PTFE (0.5 mm i.d.).

0003-2670/86/$03.50

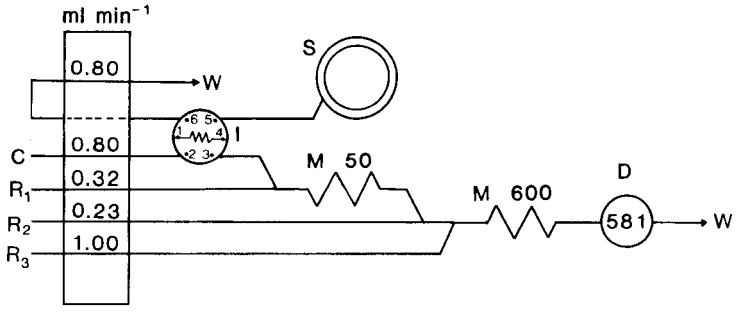

Fig. 1. Flow-injection manifold for the determination of aluminium by pyrocatechol violet: S, autosampler; W, waste; I, injection valve; D, detector (spectrophotometer); M, mixing coil (length in cm); C, carrier; R_1, iron-masking reagent; R_2, PCV reagent; R_3, buffer.

Reagents and samples

The iron-masking reagent (R_1, Fig. 1) is 0.5 M hydroxylammonium chloride with 10 mM 1,10-phenanthroline [2, 3]. The PCV reagent concentration (R_2) is 5 mM. Pyrocatechol violet from Sigma Chemical Company was used; the quality of this reagent from different sources is variable. The buffer (R_3) contains 3.0 M hexamethylenetetramine with 0.20 M hydrochloric acid added to adjust the pH to 6.1—6.2 in the final flow (17 ml 37% w/v HCl to 1 l of buffer). All reagents were stable for at least 4 weeks when stored at room temperature. The carrier solution (C) (and all standards) were prepared in 0.10 M hydrochloric acid. The fulvic acid used was prepared by extraction from a typical podsolic forest soil [11].

The samples were centrifuged (3000 rpm for 30 min), hydrochloric acid was added to a final concentration of 0.10 M and the solutions were digested with peroxodisulphate (1.0 g to 100 ml of sample, heated in Pyrex bottles in an autoclave at 2 atm. for 30 min) before the determination of total aluminium.

RESULTS AND DISCUSSION

Optimization of the flow-injection manifold

Pyrocatechol violet is well known as a chromogenic reagent for aluminium [1—3]. The pH range 6.1—6.2 is optimal to minimize changes in background and sensitivity. Hexamethylenetetramine (hexamine) is the most commonly used buffer [2—8]. The sensitivity for aluminium was unaffected in the range 1.0—3.0 M hexamine and a 3.0 M solution was chosen [8]. Small variations in the acidity of the samples (0.08—0.12 M HCl) then had little effect on the sensitivity [8]. Ethylenediamine had no advantages over hexamine. Under the recommended reaction conditions, calibration graphs were almost linear in the range 0.010—3 mg l^{-1} aluminium when 70- or 200-μl samples were injected; the linear range can be extended to about 10 mg l^{-1} by injecting 10-μl portions. Peak heights were little affected by increasing the length of

the mixing coil from 3 to 12 m, but the baseline noise decreased with longer loops; a 6-m coil was found suitable.

Figure 2 shows calibration graphs at different PCV concentrations. A PCV concentration of 5 mM provides linear response up to about 3 mg Al l^{-1}, and there is little to be gained by using a more concentrated reagent. Figure 3 shows the development of the aluminium/PCV complex with time at different concentrations of PCV; the reaction time is 30 s for the manifold in Fig. 1. As can be seen, the absorbances change rapidly around 30 s for 0.5 and 1 mM PCV but very little for 5 and 10 mM PCV. Obviously, if the lower concentrations were used, the system would become very sensitive to changes in reaction kinetics such as could be caused by interfering species. A high molar excess of PCV over aluminium is also desirable in order to minimize interference from anions which form complexes with aluminium. Figure 4 shows that the interferences from fulvic acid and from citrate are reduced by the use of a stronger PCV reagent. With 10 mM PCV, the interference from up to about 100 mg l^{-1} carbon (from fulvic acid) is almost completely eliminated, and about 5 times more citrate can be tolerated than with 1.0 mM PCV. However, 10 mM PCV produces high background absorption (absorbance ca. 0.6) so that 5 mM PCV provides a suitable compromise between suppression of interference and background absorption.

A much simpler manifold than that described in Fig. 1 would be obtained if all reagents could be mixed into the same solution. A reagent solution containing hydroxylammonium chloride (or ascorbic acid), 1,10-phenanthroline, buffer and PCV in various proportions, pumped at 1.0 ml min^{-1}, was therefore examined; the carrier and sample pump rates were unaltered (0.80 ml min^{-1}).

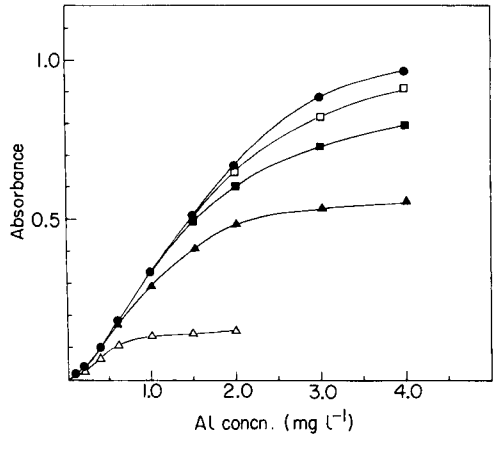

Fig. 2. Calibration graphs for the flow-injection determination of aluminium at different concentrations of the PCV reagent: (●) 10 mM; (□) 5 mM; (■) 1 mM; (▲) 0.5 mM; (△) 0.1 mM.

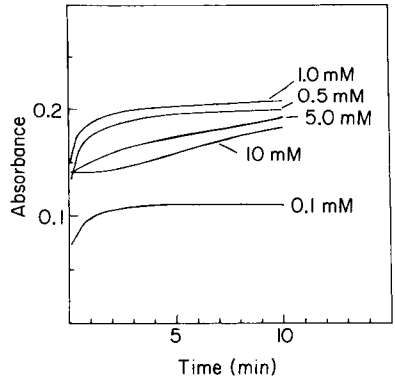

Fig. 3. Development of the aluminium/pyrocatechol violet complex at different concentrations of PCV (in mM). A 0.4 mg Al l^{-1} sample was pumped instead of carrier, and the curves were recorded by stopping the flow.

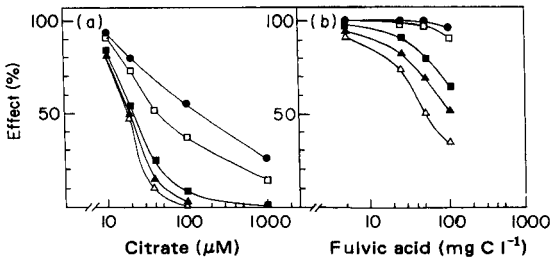

Fig. 4. Interference from citrate and a fulvic acid in the determination of aluminium at different concentrations of PCV reagent: (•) 10 mM; (□) 5 mM; (■) 1 mM; (▲) 0.5 mM; (△) 0.1 mM. The sample contained 1.0 mg Al l^{-1} with increasing amounts of citrate or fulvic acid.

The interfering effect of iron was used as a test case. With the various mixed reagents, least iron interference was found with a reagent containing 0.5 M ascorbic acid and 20 mM 1,10-phenanthroline in the buffer, but none of the mixed reagents were as effective as the three reagents used separately (as in Fig. 1). Importantly, the mixed reagents were unstable (PCV started to decompose after 2 h) and had to be prepared just before use.

Interferences

Main group elements and transition metals. The interference effect of about 40 elements was studied by injection of samples containing only one element at a time. The signal obtained was calculated relative to the signal from aluminium standards, and an interference factor (I_f) was calculated so that the interference effect (E) could be related to the concentration of interferent (C_i): E (mg Al l^{-1}) = $I_f C_i$ (mg l^{-1}). The I_f value thus gives an expression of the selectivity of PCV for aluminium compared to other elements. Table 1 shows that strong interference is caused by 16 of the tested species (I_f values $> 10 \times 10^{-3}$). To avoid significant interference ($E < 0.01$ mg Al l^{-1}), the concentration of elements with $I_f > 10 \times 10^{-3}$ (or $>100 \times 10^{-3}$) must be <1.0 (or <0.1) mg l^{-1}. This is generally the case for ground water and surface water [12], except for iron. Iron interference can be suppressed (by R_1 in Fig. 1) up to about 2 mg Fe l^{-1}, which is sufficient for most natural waters. The iron-masking reagent also suppressed the interference from Zn^{2+}, Ni^{2+}, Cu^{2+}, Pb^{2+} and Co^{2+} (with I_f values from 5×10^{-3} to 20×10^{-3}, giving a tolerable concentration of 0.5—2 mg l^{-1}) up to concentrations of at least 20 mg l^{-1}.

Inorganic anions. Up to 0.5 mg F l^{-1} and 5 mg P l^{-1} (as phosphate) can be tolerated in this method [8]. Sulphide, sulphate, arsenate, tellurate and silicate (which form complexes with aluminium [13]) did not show any interference at 10 mM and 1.0 mg Al l^{-1}.

Organic anions. Humic and fulvic acids in water (dissolved organic carbon, DOC) may bind aluminium and cause interference. In speciation procedures [10], aluminium is also determined in unpretreated samples because pre-

TABLE 1

Interference from elements in the PCV flow-injection determination of aluminium (at pH 6.1, 581 nm). The I_f values are calculated as explained in the text[a]

Interference factors (I_f) ($\times 10^{-3}$)			
0.01—0.1	0.1—1	1—10	>10[b]
Li^+, Na^+, K^+, Rb^+, Mg^{2+}, Ca^{2+}, Sr^{2+}, Ba^{2+}, $H_3SiO_4^-$, NO_3^-, NH_4^+, $H_2PO_4^-$, HS^-, HSO_3^- SO_4^{2-}, $HSeO_3^-$, SeO_4^{2-}, TeO_4^{2-}, Br^-	Sn^{2+}, Cr^{3+}, Mn^{2+}, MnO_4^-	La^{3+}, Bi^{3+}, Co^{3+}	Sb^{3+} (13), Zn^{2+} (13), MoO_4^{2-} (16), Cu^{2+} (17), Ni^{2+} (17), Pb^{2+} (19), H_3BO_3 (36), Ce^{4+} (38), Zr^{4+} (48), VO_3^- (50), In^{3+} (90), Ga^{3+} (160), Ti^{4+} (235), Ge^{4+} (290), Be^{2+} (300), Fe^{3+} (300)

[a]The interferences were studied for chloride and nitrate salts of the cations and alkali metal salts of the anionic species. [b]I_f values given in parentheses. The I_f values were obtained without the iron masking reagent (R_1, Fig. 1).

treatment might dissolve colloidal polymeric aluminium hydroxides/silicates and thereby alter the speciation. For development of speciation procedures, the tolerable concentrations of organic compounds must be known. Some low-molecular-weight aliphatic and aromatic carboxylic and phenolic compounds were investigated to gain information on what types of functional groups might interfere (Table 2). Strong interference is caused by citrate, NTA and EDTA (>1 mg C l^{-1}). Of the aromatic compounds, the strongest interference is caused by 8-quinolinol (>8 mg C l^{-1}) and 2-hydroxybenzenecarboxylic acid (>60 mg C l^{-1}). Additional hydroxyl group in the 3-position increases the interference (>16 mg C l^{-1}). These compounds favour the formation of the stable 5- or 6-membered ring structures with aluminium. Such structures are also predominant in humic compounds [14]. Figure 5 shows that the interference from dissolved humic compounds in bog water occurs at DOC >10—20 mg l^{-1}; Fig. 5 also shows that the humic compounds cause significant background absorption (at 581 nm and pH 6.1) above 10 mg C l^{-1}. The PCV method, as described here, can tolerate DOC <10 mg l^{-1} without risks of serious underestimations of aluminium, and so it might be useful in speciation procedures [10]. However, this aspect requires a better examination of possible reaction kinetic effects (between PCV and different labile monomeric aluminium species) in the very rapid flow-injection system.

Application of the method

Figure 6 shows typical recorder tracings for the method; high reproducibility (<2% r.s.d. at 100 μg l^{-1}), low baseline noise and high sensitivity (detection limit about 3 μg l^{-1}) are evident. The sample throughput is 100 h^{-1} with the manifold in Fig. 1. This flow-injection method has proved to work well in determinations of total aluminium in surface and leachate water con-

TABLE 2

Interference effect of some aromatic and aliphatic organic compounds on the determination of aluminium by the flow-injection PCV method[a]

Interfering species	Tolerable concentration[b]	
	(mM)	(mg C l^{-1})
Benzene-1,2,4,5-tetracarboxylic acid	10	1200
Benzene-1,2,3-tricarboxylic acid	10	1080
Benzene-1,2,4-tricarboxylic acid	10	1080
Benzene-1,2-dicarboxylic acid	10	960
Benzene-3-hydroxycarboxylic acid	10	840
Benzene-4-hydroxycarboxylic acid	10	840
Benzene-2-hydroxycarboxylic acid	0.8	60
Benzene-2,3-dihydroxycarboxylic acid	0.2	16
Benzene-1,2,3-triol	7	420
8-Quinolinol	0.08	8
Citrate	0.01	0.7
EDTA	0.01	1.2
NTA	0.02	1.4
Tartaric acid	1.0	48
Maleic acid	10	480
Oxalic acid	10	240
Pyruvic acid	10	360
Lactic acid	10	360

[a]The f.i.a. manifold was as in Fig. 1 and the reagents as in the experimental section. [b]The interference effect was investigated by preparing samples containing 1.0 mg Al l^{-1} and increasing amounts of interferent until interference was found or up to 10 mM (the highest concentration tested).

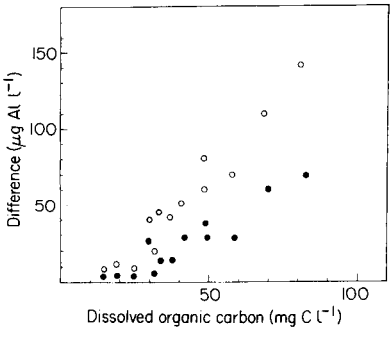

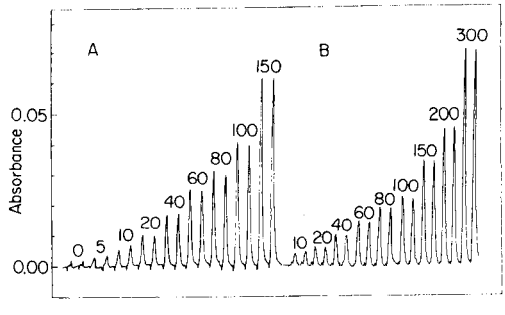

Fig. 5. Interference from humic compounds in bog water by the flow-injection method: (○) the difference between aluminium found in digested and undigested samples; (●) the background absorption from the same humic compounds at 581 nm and pH 6.1, recorded without the PCV reagent in the manifold of Fig. 1.

Fig. 6. Typical recorder tracings for the PCV method for standards from 5 to 300 μg Al l^{-1}. (A) Signals for a flow-through cell with a 20-mm light path; (B) with a 10-mm light path. (200-μl injection loop in both cases.)

taining 0.01—30 mg Al l^{-1}. For routine analyses of total aluminium, all samples are digested with peroxodisulphate to prevent possible interference from organic compounds. The need for digestion for samples containing little DOC (<10 mg l^{-1}) was checked by analyzing 110 samples of leachate water before and after digestion. A regression analysis of the data showed little difference between aluminium found in digested (Y) compared to undigested (X) samples ($Y = 1.024\ X + 0.007$, $s_a = 0.018$, $s_b = 0.007$, $r = 0.997$); indicating that the PCV method can tolerate low concentrations of DOC (<10 mg l^{-1}) as found above.

Conclusions

Pyrocatechol violet is not a very selective chromogenic reagent for aluminium, as strong interferences are caused by several metals. In natural water, however, the concentration of most interfering compounds are below critical levels. The flow-injection method is sensitive, rapid and reproducible. When the possible interferences are taken into account, the method can be used with good confidence for the determination of total aluminium in natural water.

REFERENCES

1 A. Anton, Anal. Chem., 32 (1960) 725.
2 A. D. Wilson and G. A. Sergeant, Analyst (London), 88 (1962) 109.
3 W. K. Dougan and A. L. Wilson, Analyst (London), 99 (1974) 413.
4 Norwegian Bureau of Standards, Water Analysis, NS 4747, Determination of Aluminium, Photometric Method, Oslo, Norway, 1979.
5 A. Henriksen and I. M. Bergmann Paulsen, Vatten, 4 (1975) 339.
6 G. Ogner, A. Haugen, M. Opem, G. Sjøtveit and B. Sørlie, The Chemical Analysis Program at the Norwegian Forest Research Institute, Norw. Forest Res. Inst., N-1432 Ås-NLH, 1984.
7 E. J. S. Røgeberg and A. Henriksen, Vatten, 41 (1985) 48.
8 O. Røyset, Anal. Chim. Acta, 178 (1985) 223.
9 H. M. Seip, L. Myller and A. Naas, Water Air Soil Pollut., 23 (1984) 81.
10 C. T. Driscoll, Int. J. Environ. Anal. Chem., 16 (1984) 267.
11 G. Ogner, Acta Chem. Scand., 27 (1973) 1601.
12 B. Salbu, Doctoral Thesis, University of Oslo, Norway, 1984.
13 L. G. Sillen and A. E. Martell, Stability Constants of Metal-ion Complexes, The Chemical Society, London, 1964.
14 M. Schnitzer, in M. Schnitzer and S. U. Khan (Eds.), Soil Organic Matter, Elsevier, Amsterdam, 1978, p. 9.

Analytica Chimica Acta, 185 (1986) 83—89
Elsevier Science Publishers B.V., Amsterdam — Printed in The Netherlands

KINETIC FLUORIMETRIC DETERMINATION OF HISTIDINE, HISTAMINE AND THEIR MIXTURES

M. C. GUTIERREZ, A. GOMEZ-HENS and M. VALCÁRCEL*

Department of Analytical Chemistry, Faculty of Sciences, University of Córdoba, Córdoba (Spain)

(Received 4th November 1985)

SUMMARY

Kinetic fluorimetric methods for the determination of histidine and histamine, both separately and in mixtures, are described; the methods are based on the accelerating effect of these compounds on the oxidation of 1,1,3-tricyano-2-amino-1-propene by hydrogen peroxide in the presence of copper. A differential rate method is used for resolution of mixtures of these compounds (10^{-5} M level), in which synergic effects are taken into account. The relative standard deviations for histidine and histamine are 1.4% and 2.1%, respectively, for separate determinations but 4.0% and 3.4%, respectively, for determinations of mixtures. Histamine/histidine ratios between 1:1 and 16:1 are satisfactorily resolved.

Histidine and histamine mixtures have usually been determined with the use of separation techniques such as thin-layer [1—4] or paper [5—7] chromatography or electrophoresis [8, 9]. Generally, when these compounds are separated, their detection is accomplished by using *o*-phthalaldehyde [1], ninhydrin [2, 4, 5, 7—9] or fluorescamine [3]. An automated analyzer [10] incorporating an extraction step has been described for the simultaneous assay of histidine and histamine, but this requires two fluorimeters for detection.

Kinetic non-enzymatic methods are not often used for the determination of organic compounds of biochemical interest. Only two kinetic determinations have been described for histidine. In one, histidine was determined through its inhibitory effect on the copper catalysis of the oxidation of luminol by hydrogen peroxide [11]. In the other, histidine activated a mercury(II)-catalyzed reaction [12]. No kinetic determinations have been described for histamine.

This paper describes a simple kinetic fluorimetric method for determination of histidine and histamine, based on the increase in fluorescence intensity of the 1,1,3-tricyano-2-amino-1-propene/hydrogen peroxide/copper(II) system. The tricyano compound has been widely used in several pharmacological studies involving anti-thyroid action [13] or mental diseases [14], as well as in the synthesis of ribonucleic acid [15], but its use as an analytical

0003-2670/86/$03.50

reagent has been very limited. It has been used only in the determination of copper in tissues, urine [16] and serum [17]. This paper describes a differential kinetic method applied to the determination of histidine and histamine. The proposed method is simple, inexpensive, precise and rapid.

EXPERIMENTAL

Apparatus and reagents

All fluorimetric measurements were made on a Perkin-Elmer fluorescence spectrophotometer, Model MPF-43A, fitted with a device for kinetic measurements and 1-cm quartz cells. The cell compartment was thermostatted by circulating water. All measurements were recorded at an instrumental sensitivity of 3, and excitation and emission slits of 6-nm spectral bandpass. A set of fluorescent polymer samples was used daily to adjust the spectrofluorimeter so as to compensate for changes in source intensity.

Stock solutions of L-histidine (1×10^{-2} M) and histamine dihydrochloride (1×10^{-2} M) were prepared in distilled water. Standard solutions of lower concentration were prepared daily by diluting to the appropriate volume with distilled water. A 1,1,3-tricyano-2-amino-1-propene (TRIAP) solution (4×10^{-3} M) was prepared by dissolving 26.4 mg of reagent in 50 ml of distilled water. A copper(II) nitrate solution (10 μg Cu ml^{-1}) and a K_2HPO_4/KH_2PO_4 buffer solution (total concentration 0.1 M, pH 7.5) were also prepared. All solvents and reagents were of analytical-reagent grade.

Procedures

Determination of histidine. To a 10-ml volumetric flask was added an adequate volume of histidine sample to give a final concentration of histidine between 2.0×10^{-5} and 5.5×10^{-5} M. This was subsequently mixed with 0.7 ml of 0.1 M phosphate buffer (pH 7.5), 2 ml of 4×10^{-3} M TRIAP solution, 0.7 ml of 1.25 M hydrogen peroxide and 0.5 ml of a 10 μg ml^{-1} copper(II) solution. The stop-clock was started and the solution was made up to the mark with distilled water. A portion of the reaction mixture was immediately transferred to a thermostatted 1.0-cm cell at 60 ± 0.1°C, starting to record the fluorescence intensity (λ_{ex} = 360, λ_{em} = 425 nm) against time exactly 2 min after preparing the sample. The net fluorescence intensity was obtained by subtracting the measurements obtained for a blank solution prepared in a similar manner but containing no histidine. Calibration graphs were obtained by plotting the initial rate vs. histidine concentration.

Determination of histamine. The sample was prepared as described above, but using the following reagent volumes: 1 ml of 0.1 M phosphate buffer (pH 7.5), 1.5 ml of 4×10^{-3} M TRIAP solution, 0.5 ml of 1.25 M hydrogen peroxide and 1 ml of the 10 μg ml^{-1} copper(II) solution. The range of histamine concentration in the sample must be between 10^{-5} and 1.25×10^{-4} M. The measurements were made as described for histidine.

Determination of mixtures. To a 10-ml volumetric flask was added an appropriate volume of the histidine/histamine sample to give a final concentration between 5×10^{-6} and 2×10^{-5} M histidine, and between 1×10^{-5} and 1×10^{-4} M histamine. Then, 1 ml of phosphate buffer (pH 7.5), 1.5 ml of 4×10^{-3} M TRIAP solution, 1 ml of 1.25 M hydrogen peroxide and 0.5 ml of the 10 μg ml^{-1} copper(II) solution were added, in that order. The solution was diluted to the mark with distilled water and the measurements were completed as described above. Several calibration plots of reaction rate vs. histamine concentration at different fixed amounts of histidine were recorded. The data obtained from these were treated as indicated below.

RESULTS AND DISCUSSION

Fluorescent reaction

The oxidation product of TRIAP shows a fluorescent band at 470—500 nm (λ_{ex} = 370 nm), the greatest fluorescence intensity of which is obtained in an acidic medium. However, the oxidation reaction is faster in a neutral medium. In acidic media, copper(II) acts as a catalyst in the presence of hydrogen peroxide or other oxidants. In neutral media, hydrogen peroxide reduces copper(II) to copper(I), thus concealing its catalytic effect. However, when histidine or histamine is added to this last solution, a transient fluorescence appears at 425 nm (λ_{ex} = 360 nm). This is shown in Fig. 1, and has also been observed when histidine or histamine is replaced by imidazole or one of its derivatives. The figure also shows that the increasing fluorescence intensity cannot be attributed to the individual action of histidine or histamine because it entails the presence of copper. There are two possible

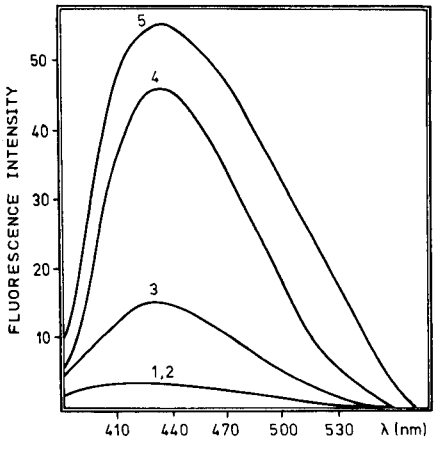

Fig. 1. Emission spectra (λ_{ex} = 360 nm): (1) TRIAP/H_2O_2/Cu^{2+}; (2) histidine/H_2O_2/Cu^{2+}; (3) histamine/H_2O_2/Cu^{2+}; (4) TRIAP/histidine/H_2O_2/Cu^{2+}; (5) TRIAP/histamine/H_2O_2/Cu^{2+}. Conditions: 6×10^{-4} M TRIAP, 6.2×10^{-2} M H_2O_2, 2×10^{-5} M histamine or histidine, 1 mg l^{-1} Cu^{2+}; reaction time 5 min, 60°C.

explanations for this behaviour. First, histidine and histamine could form complexes with copper which might be responsible for the acceleration of the oxidation of TRIAP by hydrogen peroxide; secondly, owing to the reactivity of TRIAP, which has a charge-deficient carbon atom, and to the nitrogen of the imidazole ring, a transient condensation product might be formed between the two compounds, its oxidation by hydrogen peroxide being favoured by the presence of copper. This intermediate product could account for the fluorescence emission at 425 nm.

Effect of variables

The systems were optimized by changing each variable in turn whilst keeping all others constant. The optimum variables taken were those yielding the minimum possible relative standard deviation for the initial rate measurements, under conditions in which the reaction order with respect to the species concerned was zero or near-zero.

The pH dependence of the systems was studied by using sodium hydroxide and hydrochloric acid solutions. The reaction rate was found not to depend on the pH over the range 7.1—7.6 for the histidine system, and over the range 7.4—8.0 for the histamine system, whereas it decreased outside these pH intervals (Fig. 2a). A K_2HPO_4/KH_2PO_4 (pH 7.5) buffer solution was chosen to adjust the pH of the samples, and although the reaction rate generally decreased somewhat for both systems as the concentration of this buffer solution increased, it remained constant for concentrations between 5×10^{-3} and 1.2×10^{-2} M.

The temperature exerted a different influence on each system. The reaction rate in the histidine system was independent of temperature over the

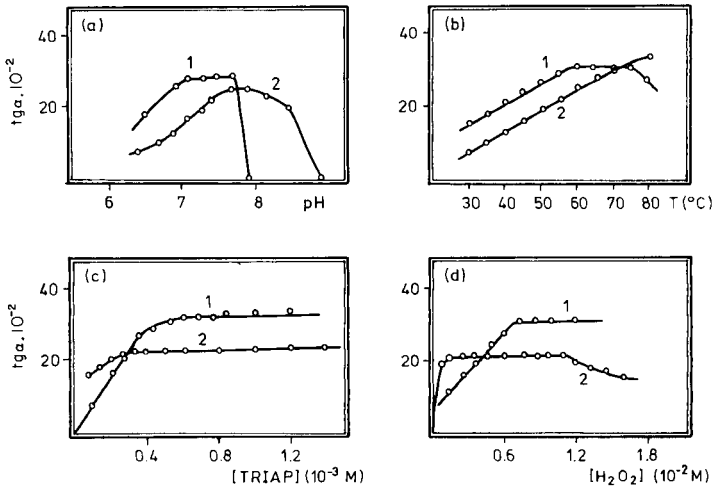

Fig. 2. Effect of variables on reaction rate (tg α): (a) pH; (b) temperature; (c) TRIAP concentration; (d) hydrogen peroxide concentration. Curves: (1) histidine; (2) histamine.

range 55—75°C, whereas there was an almost linear increase in the reaction rate with temperature for the histamine system (Fig. 2b). A decrease in the rate for both compounds was observed if the dielectric constant of the solution was decreased by using organic solvents such as ethanol or dimethylformamide. The best results were obtained in an entirely aqueous medium.

The effect of TRIAP concentration was studied in the range 8×10^{-5}—1.4×10^{-3} M (Fig. 2c). The reaction rate was constant above 6×10^{-4} M TRIAP for the histidine system, and above 3×10^{-4} M for histamine. The variation of the rate with hydrogen peroxide concentration is shown in Fig. 2d, from which optimum concentrations of 8.7×10^{-2} and 6.2×10^{-2} M were chosen for the histidine and histamine systems, respectively. An increase in the copper concentration resulted in a progressive increase in the reaction rate for histamine, whereas it did not affect the histidine system over the range 0.3—0.6 μg ml^{-1}.

The kinetic equations suggested for the recommended procedures for these reactions, based on the results of the above experiments, are as follows:

$$d[TRIAP]_{ox}/dt = k_1[Hd]$$

$$d[TRIAP]_{ox}/dt = k_2[Cu^{2+}]^{2/3}[Hm]$$

where $[TRIAP]_{ox}$ is the concentration of oxidized reagent, [Hd] and [Hm] are the histidine and histamine concentrations, respectively, and k_1 and k_2 are the conditional rate constants.

Determination of histidine and histamine separately and in mixtures

The tangent method (i.e., measurement of the slope of the intensity vs. time plot) was used to calculate the reaction rates, which were plotted as a function of the analyte concentration. The calibration graphs for individual determinations were linear over the ranges 2.0—5.5×10^{-5} M histidine and 1.0—12.0×10^{-5} M histamine. The relative standard deviation ($n = 10$) was 1.4% for histidine and 2.1% for histamine.

Histidine/histamine mixtures cannot be resolved by the usual differential kinetic methods owing to the similar behaviour of both analytes in the TRIAP/hydrogen peroxide/copper(II) system and to the synergic effects encountered. Due to these effects, when a kinetic curve for a sample containing histidine and histamine is recorded, neither the slope nor the maximum fluorescence intensity is the sum of the values obtained when both compounds are studied separately. However, this mixture can be resolved satisfactorily by applying a combined method based on the measurement of the initial rate and the maximum fluorescence intensity [18].

In the calibration graphs obtained for histamine in the presence of different concentrations of histidine (Fig. 3a), the reaction rate shows a linear variation with the histamine concentration, and also depends on the histidine concentration, so that the slopes and intercepts of these calibration graphs are a linear function of the histidine concentration, as shown in Fig. 3(c).

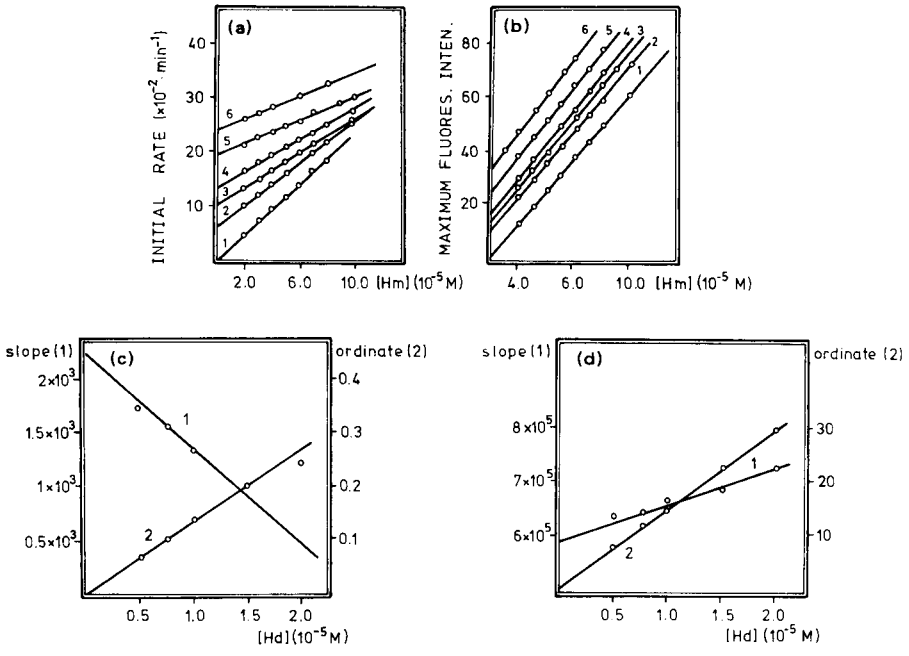

Fig. 3. (a, b) Calibration graphs for histamine (Hm) in the presence of different histidine (Hd) concentrations: (1) 0; (2) 5×10^{-6}; (3) 7.5×10^{-6}; (4) 10^{-5}; (5) 1.5×10^{-5}; (6) 2×10^{-5} M. (c, d) Calibration graphs for histidine obtained from (1) the slopes and (2) the intercepts from (a) and (b), respectively.

Accordingly, the following equation can be established:

initial rate = $v = a'[\mathrm{Hm}] + b'$

where $a' = a[\mathrm{Hd}] + c$, $b' = b[\mathrm{Hd}] + d$ and

$$v = a[\mathrm{Hd}][\mathrm{Hm}] + b[\mathrm{Hd}] + c[\mathrm{Hm}] + d \quad (1)$$

Similar data are obtained from maximum fluorescence intensity data (Fig. 3b, d):

fluorescence intensity = $I_f = m'[\mathrm{Hm}] + n'$

where $m' = m[\mathrm{Hd}] + p$ and $n' = n[\mathrm{Hd}] + q$ and

$$I_f = m[\mathrm{Hd}][\mathrm{Hm}] + n[\mathrm{Hd}] + p[\mathrm{Hm}] + q \quad (2)$$

The terms $a[\mathrm{Hd}][\mathrm{Hm}]$ and $m[\mathrm{Hd}][\mathrm{Hm}]$ from eqns. 1 and 2 represent the synergic effect.

The equations used for the determination of histidine/histamine mixtures incorporated parameters obtained by a previously described method [18] and were as follows (concentration in M, rate in m s^{-1}):

$$v = -8.44 \times 10^7\,[\mathrm{Hd}][\mathrm{Hm}] + 1.34 \times 10^4\,[\mathrm{Hd}] + 2.23\,[\mathrm{Hm}] + 0.00$$

$$I_f = 6.46 \times 10^9\,[\mathrm{Hd}][\mathrm{Hm}] + 1.45 \times 10^6\,[\mathrm{Hd}] + 6.02\,[\mathrm{Hm}] + 1.20$$

TABLE 1

Analysis of histidine/histamine mixtures

Histidine (μmol)		Histamine (μmol)		Histidine (μmol)		Histamine (μmol)	
Taken	Found[a]	Taken	Found[a]	Taken	Found[a]	Taken	Found[a]
20	18.5	20	20.5	10	10.4	60	59
20	18.7	30	32.6	10	9.7	70	70
15	14.6	30	28.6	5	5.1	40	40
20	20.2	60	60	5	4.9	50	59
15	15.1	60	60	5	4.7	60	63
10	11.1	50	44	5	5.0	80	75

[a]Results are the mean of three determinations.

The use of these equations allowed several histidine/histamine mixtures to be analyzed successfully (Table 1). The relative standard deviations (n = 10) for 20 μmol of histidine and 60 μmol of histamine were 4.0% and 3.4%, respectively.

REFERENCES

1 L. Edvinsson, R. Hakanson, A. L. Roennberg and F. Sundler, J. Chromatogr., 67 (1972) 81.
2 S. Lee and S. Yin, J. Chromatogr., 129 (1976) 482.
3 H. Nakamura, J. Chromatogr., 131 (1977) 215.
4 E. R. Lieber and S. L. Taylor, J. Chromatogr., 153 (1978) 143.
5 J. Seto, Jpn. Analyst, 10 (1961) 25.
6 J. E. McNeal, J. Assoc. Off. Anal. Chem., 59 (1976) 570.
7 L. Y. Foo, J. Assoc. Off. Anal. Chem., 60 (1977) 183.
8 K. Fuecker, R. Meyer and H. P. Pietsch, Nahrung, 18 (1974) K1.
9 M. Ferencik, Chem. Listy, 56 (1962) 289.
10 E. S. K. Assem and E. K. S. Chong, Agents Actions, 12 (1982) 26.
11 S. Pantel and H. Weisz, Anal. Chim. Acta, 74 (1975) 275.
12 P. C. Nigam, M. Phull and N. Subbarao, Indian J. Chem., 23A (1984) 105.
13 K. S. Dhinsa, Acta Anat., 106 (1980) 468.
14 J. W. Davenport, Science, 167 (1979) 1007.
15 C. E. Dreiling, Res. Commun. Chem. Pathol. Pharmacol., 19 (1978) 169.
16 K. Ritchie and J. Harris, Anal. Chem., 41 (1969) 163.
17 M. C. Gutiérrez, A. Gómez-Hens and M. Valcárcel, Talanta, in press.
18 A. Rios, M. Silva and M. Valcárcel, Fresenius Z. Anal. Chem., 320 (1985) 762.

Analytica Chimica Acta, 185 (1986) 91—99
Elsevier Science Publishers B.V., Amsterdam — Printed in The Netherlands

INCREASED APPARENT SENSITIVITY BY MEANS OF CONSTANT-ENERGY SYNCHRONOUS SPECTROFLUORIMETRY

J. C. ANDRE*, A. BOUCHY and J. Y. JEZEQUEL
GRAPP, UA 328 CNRS, ENSIC-INPL, 1, rue Grandville 54042 Nancy Cedex (France)
(Received 22nd August 1985)

SUMMARY

Synchronous fluorescence scanning at constant wavenumber (i.e., energy) difference between excitation and emission brings several improvements when compared to the classical spectrofluorimetry or to the method of synchronous wavelength scanning. When quantitative results are required, the constant energy-difference technique should be used whenever the difference between the excitation and emission wavelengths exceeds the difference between the wavelengths of the Rayleigh and Raman peaks. Otherwise, the technique brings only minor advantages in comparison with synchronous wavelength scanning.

In principle, it should be possible to detect decreasingly small concentrations of a fluorescent compound by increasing the intensity of the excitation source, by enlarging the slit widths of the excitation and emission monochromators, or by increasing the amplification ratio of the photodetection system. Nevertheless, below a certain concentration, which depends on the nature of the compound and on the apparatus, many factors limit the sensitivity. In many cases, the emission spectrum of a compound present only at low concentrations can be partly distorted by the Rayleigh and Raman emissions of the solvent. Such an effect can be seen in Fig. 1(a); above 515 nm, the fluorescence signal (continuous line) is distorted by the Raman emission (dashed line) but these two lines do not overlap; below 515 nm they do overlap because of the intense Rayleigh emission.

To eliminate the major effects of Rayleigh scattering at wavelengths adjacent to those of excitation, the synchronous excitation method can be used for the determination of fluorescent compounds [1—3]. This technique was introduced by Lloyd [4] for the detection of aromatic compounds and has since been used by other authors in similar fields (see, e.g. [5]). A typical result of using this technique can be seen in Fig. 1(b). For quantitative measurements, where the fluorescence of a compound is distorted by Rayleigh scatter and by stray reflections at the excitation wavelength, the synchronous excitation method, in which the excitation wavelength (λ_{ex}) and emission wavelength (λ_{em}) are simultaneously scanned with a constant interval between them ($c = \lambda_{em} - \lambda_{ex}$), notably improves the quality of the measurements. When the measurements are hampered by this type of stray light as well as

0003-2670/86/$03.50

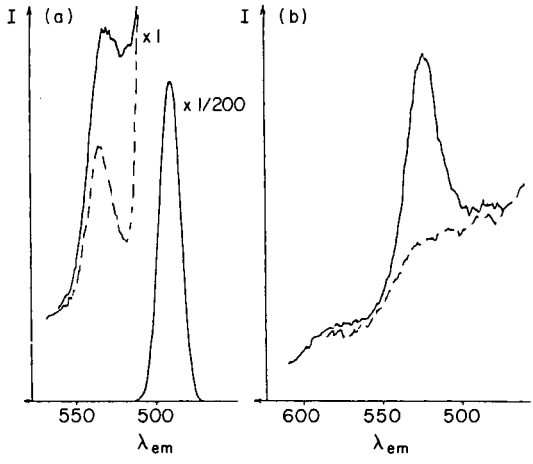

Fig. 1. Comparison between (a) normal fluorescence spectrum and (b) synchronous wavelength spectrum of fluorescein (20 ng l^{-1}) (temperature 20°C, pH 7). The dashed line is the "blank" spectrum obtained prior to each scan.

by Raman scatter, synchronous excitation again improves the quality of the measurements compared to conventional techniques, if appropriate values of c are selected.

Inman and Winefordner [6] proposed a technique of synchronous scanning based on a constant difference between the excitation and emission frequencies. They successfully applied the method to aromatic hydrocarbons. The purpose of the present paper is to show, in agreement with Inman and Winefordner, that the use of this method not only allows spectral information to be preserved when the excitation and emission spectra are resolved but also, mainly from a quantitative point of view, allows the effect of Raman scattering to be removed, thus improving the apparent sensitivity [7].

EXPERIMENTAL

Chemicals and instrumentation

The fluorescence compounds (Fluka puriss.) were used as received. The solvents were of spectroscopic quality (Fluka or Merck). Water was distilled twice from quartz apparatus.

The fluorescence spectra were obtained on a Jobin Yvon JY3 spectrofluorimeter or a Farrand Mk I spectrofluorimeter, to which several units were added as shown in Fig. 2. They were as follows. The stepping motors were 4-phase 11-PMA-005 models (Socitec Co.). Each of the motors was mechanically coupled to a JY3 monochromator via a reduction cogwheel, and to a helipot-type 10-turn potentiometer. A 5-V stabilized potential was applied to this potentiometer and its output voltage was a function of the motor position and consequently of the wavelength. The motor driving cards

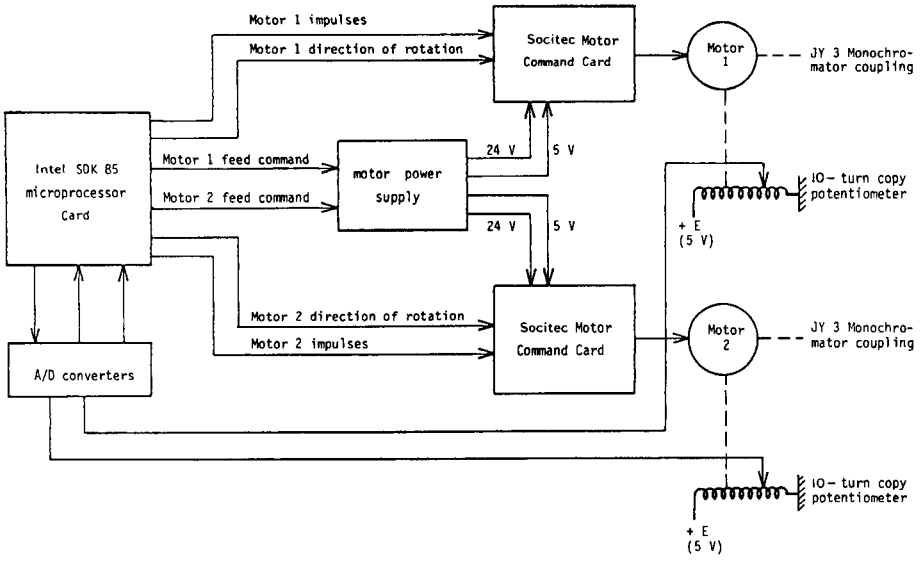

Fig. 2. Schematic diagram of the apparatus.

(SD 41007; Socitec Co.) were used to supply and to commutate the four phases of the motors. They could work by themselves or be driven by an external command-pulse generator; the latter mode was used. An Intel SDK-85 card, with a 8085 microprocessor and two home-made data-acquisition circuits utilizing the user-free space of the card, were used with analog/digital converters (ADC 1210; National Semiconductor) and an Intel 8253 programmable timer. With this unit, the output voltages of the potentiometers were measured and converted into 12-bit data, the wavelengths at which the monochromators were set were computed, the timer which produced the pulses to drive the "excitation" motor was programmed to scan the wavelengths at a chosen speed, and the command pulses driving the "emission" motor were generated and computed to obtain wavelength scanning such that the difference $(\lambda_{ex}^{-1} - \lambda_{em}^{-1})$ was kept constant.

A manual switch was added to provide the following scanning options: "excitation" motor only, "emission" motor only, or both of the motors, in either the wavelength or the wavenumber synchronous excitation modes. To achieve as little interference as possible between the different circuits, separate 5-V power supplies were set up to supply the SDK-85 card, the Socitec motor command cards and the 1210 ADCs. Another card, providing a stabilized 24-V potential was built in an ordinary way to supply the stepping motors with current.

When the operator had chosen the type of excitation, the only information that had to be introduced into the microprocessor via the keyboard was the scanning speed of the stepping motor coupled to the excitation monochromator. This makes this apparatus particularly easy to use.

All the spectra reported are uncorrected from the point of view of instrumental response or source intensity. Correcting the spectra would lead to changes in the relative intensities of the spectral peaks, but in no way would this affect the conclusions. The exact relative peak intensities and Raman intensity do not affect the principles discussed here.

RESULTS AND DISCUSSION

Qualitative analysis

Anthracene is an excellent experimental example to illustrate the use of synchronous wavenumber excitation in qualitative analysis. In agreement with Inman and Winefordner [6], it is possible to retain the essential form of the conventional spectrum of this compound if a suitable initial difference between λ_{ex} and λ_{em} is taken, and selectivity is preserved, or even improved, because there is better resolution of peaks in the spectrum (Fig. 3). However, when wrong conditions are selected, there may be a loss in selectivity because of appreciable loss of maxima, as shown for pyrene in Fig. 4.

Increase of apparent sensitivity

The difference between the excitation and Raman wavenumbers is independent of frequency; it depends only on the solvent. Because the monochromators used were not linear in wavenumbers, the first step was to conduct a computer simulation of the wavelength constant-step spectra of cyclohexane as a function of the step size, based on the performance characteristics of the Farrand Mk I spectrofluorimeter, i.e., lamp intensity, mono-

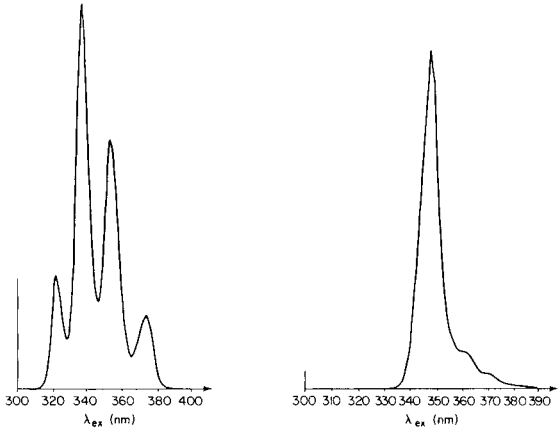

Fig. 3. Synchronous wavenumber spectrum of anthracene (10 ng l^{-1}) in heptane. (Initial excitation at 300 nm; initially c = 50 nm; wavenumber interval ($\Delta\nu$) = 4762 cm^{-1}; 4-nm slit widths.)

Fig. 4. Synchronous wavenumber spectrum of pyrene (10 ng l^{-1}) in heptane. (Initial excitation at 300 nm; initially, c = 17.5 nm; $\Delta\nu$ = 1837 cm^{-1}; 4-nm slit widths.)

chromator transmission and photomultiplier tube (PMT) response, which are functions of the wavelength (or frequency).

The computed variations of the Raman emission signal at the output of the PMT are shown in Fig. 5 for the case of a common solvent (cyclohexane) when the wavelength synchronous excitation method is used, for several wavelength intervals. In Fig. 5, as well as in the experimental spectrum (Fig. 6), it can be seen that the synchronous wavelength technique leads to a "broad" Raman spectrum. This widening depends on the selected interval c and on the widths of the slits [3]. In contrast, Fig. 7 shows the simulated variations in the signal at the output of the PMT when wavenumber synchronous excitation is used under the same experimental conditions as in Fig. 5; the recorded signal is particularly widened. This phenomenon is most noticeable when the energy difference between the excitation (ν_{ex}) and emission (ν_{em}) frequencies is exactly equal to the energy of one of the vibrational levels of the solvent, ν_R. When ν_R is different from $\nu_{ex} - \nu_{em}$, the signal intensity remains important but is much lower than when $\nu_{ex} - \nu_{em} = \nu_R$. This can be seen in Fig. 7 when spectrum 4 is compared to the other spectra.

In any case, for given excitation and emission wavelengths, the intensity of the radiation (I) at the entrance of the PMT is the sum of the intensities of the fluorescence emission (I_F) and the scattered radiation (I_s). At low concentrations, it becomes necessary to subtract I_s from the observed intensity I. The scattered radiation can be measured by interpolation or by recording a "blank" spectrum with a solution free from the added fluorescent com-

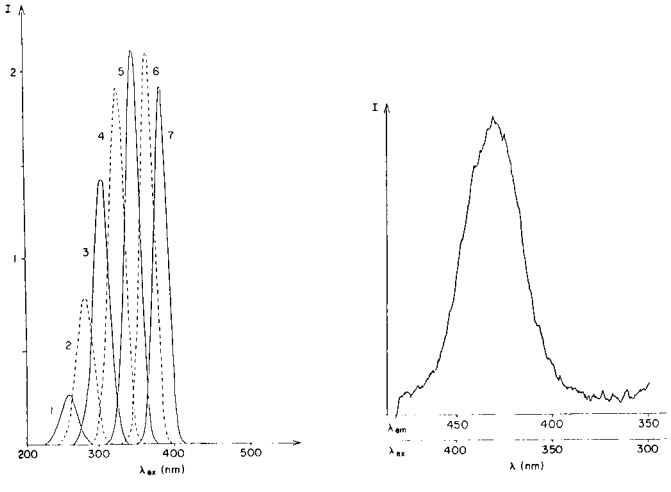

Fig. 5. Wavelength constant-step simulated spectra of cyclohexane for different values of interval c: (1) 20; (2) 25; (3) 30; (4) 35; (5) 40; (6) 45; (7) 50 nm. Intensity is in arbitrary units.

Fig. 6. Experimental wavelength constant-step spectrum of cyclohexane. (Initial excitation at 300 nm; c = 50 nm; 5-nm slit widths.)

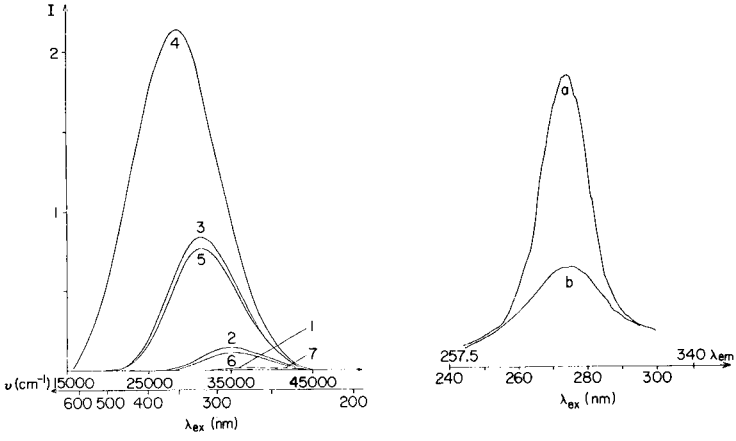

Fig. 7. Wavenumber constant-step simulated spectra of cyclohexane for different values of the wavenumber interval, $\Delta\nu$: (1) 2250; (2) 2500; (3) 2750; (4) 3000; (5) 3250; (6) 3500; (7) 4000. Intensity is in arbitrary units.

Fig. 8. Synchronous wavenumber spectrum: (a) phenol in water (22 ng ml^{-1}); (b) "pure" water. (Initial excitation at 240 nm; initial interval c = 17.5 nm; $\Delta\nu$ = 2832 cm^{-1}; 10-nm slit widths.)

pound. The curvature and the slope of the "scattering" band lead to appreciable error when the background is assessed by a simple interpolation procedure. However, when the wavenumber synchronous excitation method is used, the scattered radiation intensity remains almost constant within the fluorescence range, which allows reliable interpolation.

From an experimental point of view, it is especially unreliable to attempt to measure the concentration of a product with great precision when its maximum emission wavelength lies between the excitation and the Raman emission wavelengths. In classical emission spectrometry, it is possible to get rid of part of the dispersing effect by using crossed polarizers. This increases the I_F/I_s ratio but decreases the intensity of the signal at the entrance of the PMT by a factor greater than four. It is therefore better to use synchronous excitation techniques than classical spectrofluorimetry, especially if I_s and I_F have the same order of magnitude because the electronic noise cannot usually then be neglected (cf. Figs. 1 or 6, for example).

Measurement of phenol concentration

It has already been shown [3] that use of the synchronous wavelength technique lowered the detection limit for phenol although the Raman and Rayleigh emissions interfered with its fluorescence. To increase the sensitivity of the synchronous techniques (i.e., to maximize $I_F/(I_s + I_E)$, in which I_E is the intensity corresponding to the electronic noise), it can be necessary to set λ_{em} away from the maximum emission wavelength, λ°_{em}, for phenol. In

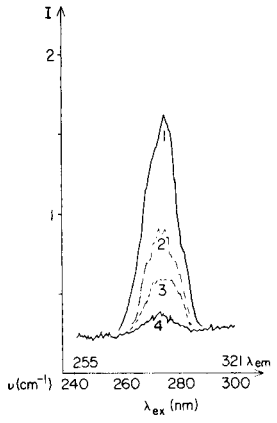

Fig. 9. Synchronous wavenumber spectra of aqueous phenol solutions of different concentrations: (1) 17; (2) 6.5; (3) 3; (4) 0 ng ml^{-1}. (Initial excitation at 240 nm; initial interval c = 15 nm; $\Delta\nu$ = 2451 cm^{-1}; slit widths l = 4 nm with 2 $l < c$.)

that case, the Raman emission intensity, I_s, can be lowered by a factor much greater than the $I_F(\lambda_{em})/I_F(\lambda^{\circ}_{em})$ ratio. The use of synchronous wavenumber excitation can further increase this sensitivity because, as described above, the baseline drift is smaller and, more importantly, it is almost linear. A comparison of Figs. 8 and 9 clearly illustrates this. In Fig. 8, the maximum signal intensity was sought. This was obtained with $\Delta\nu$ = 2832 cm^{-1} (curve a) but at the same time the Raman emission (curve b) was such that interpolation was made difficult. In Fig. 9, $\Delta\nu$ was set smaller (2451 cm^{-1}) which resulted in a much weaker and almost constant baseline drift, although the electronic noise was much more prominent. This was due to the use of narrower monochromator slits. These experimental conditions not only allowed easier interpolation but also somewhat increased the sensitivity. It is sufficient to compare $I_F/(I_F + I_s)$ in Fig. 8 for 22 ng ml^{-1} phenol and in Fig. 9 (curve 3) for 3 ng ml^{-1}.

If an initial interval is chosen such that c is greater than the difference between the Raman and Rayleigh emission wavelengths, then in principle there is no longer any major limitation on the choise of slit widths. However, as can be seen in Fig. 10, there are distorting emissions [8], even in the case of recently distilled water. Their occurrence implies that the fluorescence signal is not purely that of the analyte. The method is no longer limited by the Raman emission but by solvent impurities. Under these conditions, the quality of the measurement is poorer than the one obtained when the step chosen is smaller than the difference between the wavelengths of the Raman and Rayleigh emissions.

In the experiments in which aqueous phenol solutions were used, it was found [3] that the minimum measurable concentration was a few ng ml^{-1}. In Fig. 9, it can be seen that the use of the synchronous wavenumber technique

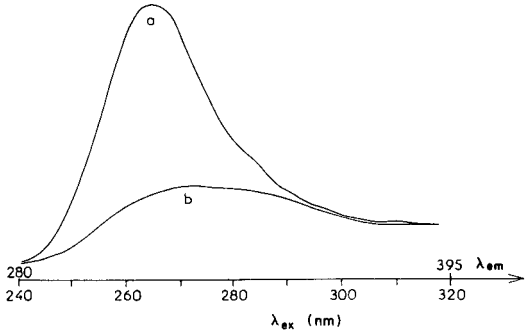

Fig. 10. Synchronous wavenumber spectrum: (a) phenol in water (22 ng l^{-1}); (b) "pure" water. (Initial excitation at 240 nm; initial interval c = 40 nm; $\Delta\nu$ = 5952 cm^{-1}; slit widths l = 10 nm with 2 $l < c$.)

allows concentrations of the same order of magnitude to be measured. However, it is worth noting that the "blank" spectrum is somewhat flatter than when the synchronous wavelength method is used.

Conclusions

The different techniques are compared in Table 1.

The use of synchronous scanning techniques for quantitative purposes is interesting, not only because of the possibility of obtaining narrower spectra but also because they allow the effects of Rayleigh scatter to be removed almost completely. If the synchronous wavelength scanning technique is limited in its use when distorting effects are caused by Raman scattering [3], the synchronous wavenumber scanning technique presented here can improve the quality of the measurements. This method should be used whenever the difference between the excitation and emission wavelengths exceeds the difference between the Raman and Rayleigh emission wavelengths. In

TABLE 1

Comparison of the different fluorescence techniques for quantitative purposes

Technique	Rayleigh scatter	Raman scatter with $c > (\lambda_{Raman} - \lambda_{Rayleigh})$	Raman scatter with $c < (\lambda_{Raman} - \lambda_{Rayleigh})$
Classical spectrum	Important	Possible subtraction of the Raman spectrum	Measurement limited by Rayleigh scatter
Synchronous wavelength excitation	Much less important	Effects partly suppresed	Raman and Rayleigh effects suppressed[b]
Synchronous wavenumber excitation	Much less important	Effects totally suppressed[a]	Raman and Rayleigh effects are suppressed[b]

[a]In principle. [b]Monochromator slit widths (l) selected so that $c > 2\ l$.

other cases, when the synchronous wavelength scanning signal is not distorted, the method presented here only brings minor advantages.

The authors are grateful to the engineer in computer science, L. M. Vincent, the senior electronic engineer, S. Joly, and the mechanic P. Pommier for their help when setting up the apparatus.

REFERENCES

1 J. C. Andre, M. Bouchy, P. Baudot and M. Niclause, Anal. Chim. Acta, 92 (1977) 369.
2 J. C. Andre, P. Baudot and M. Niclause, Clin. Chim. Acta, 76 (1977) 55.
3 J. C. Andre, M. Bouchy and M. L. Viriot, Anal. Chim. Acta, 105 (1979) 297.
4 J. B. F. Lloyd, Nature (London) Phys. Sci., 231 (1971) 64; J. Forensic Sci. Soc., 2 (1971) 83, 153, 235.
5 T. Vo-Dinh, in E. L. Wehry (Ed.), Modern Fluorescence Spectroscopy, Vol. 4, Plenum Press, New York, 1981, p. 167, and references therein.
6 E. L. Inman and J. D. Winefordner, Anal. Chem., 54 (1982) 2018.
7 E. L. Inman and J. D. Winefordner, Anal. Chim. Acta, 138 (1982) 245.
8 C. A. Parker, in P. W. Shallis (Ed.), Proc. of SAC Conference Nottingham, Heffer, Cambridge, 1965, p. 127; Photoluminescence of Solutions, Elsevier, Amsterdam, 1968, p. 421.

Analytica Chimica Acta, 185 (1986) 101—107
Elsevier Science Publishers B.V., Amsterdam — Printed in The Netherlands

CHARACTERIZATION OF ETHYLENE OXIDE/TERT-OCTYLPHENOL CONDENSATES BY ULTRAVIOLET AND INFRARED SPECTROMETRY

JUAN LUIS CARRION, SALVADOR SAGRADO and MIGUEL DE LA GUARDIA*

Department of Analytical Chemistry, Faculty of Chemistry, University of Valencia, Dr. Moliner 50, Burjasot, Valencia (Spain)

(Received 8th October 1985)

SUMMARY

The average degree of condensation of ethylene oxide/tert-octylphenol condensate surfactants can be estimated rapidly by u.v. and i.r. spectrometry. The u.v. method is based on evaluating the specific absorptivity, a, at 275 nm in aqueous ethanol (60:40 v/v), and inserting this value in equations obtained from previously characterized samples, relating a to the average properties to be determined. Infrared spectrometry is applied similarly; the average properties to be determined are related to the ratio between the band heights at 960 and 840 cm^{-1}. The relative standard deviations (n = 10) obtained for a sample of Triton X-100 were 2% by u.v. spectrometry, and 3% by i.r. spectrometry. The accuracy was similar to that obtained by n.m.r.

Surfactants are extensively used in numerous industrial processes because of their emulsifying, solubilizing, moistening and detergent properties [1, 2]. These compounds have also been used in analytical chemistry in order to maintain relatively insoluble species in aqueous solution, to form stable emulsions and to modify the microenvironment of chemical systems. In addition, they can improve the sensitivity, selectivity or detection limit in atomic absorption spectrometry [3], u.v./visible spectrophotometry or spectrofluorimetry [4]; they are also used in electroanalytical and separation techniques [4].

The influence that the nature and degree of condensation of the surfactants used have on chemical processes can differ among compounds with the same commercial denomination from different origins, or even among different batches of the same product from the same manufacturer. Therefore, in order to recommend the use of a given surfactant in an analytical procedure, it is necessary to specify some of its properties so that the results can be reproduced.

The methods proposed in the literature are mainly focussed on the determination of surfactants by chromatographic, spectrometric and electroanalytical techniques [5]. The use of n.m.r. spectrometry has been proposed for the characterization of non-ionic surfactants, by the absolute integration of the different types of protons in the molecule [6] and by use of an empirical equation involving the relative integrations of lipophilic and hydrophilic

0003-2670/86/$03.50

protons and the hydrophilic/lipophilic balance (HLB) values [7]. It has been verified [8] that direct treatment of the n.m.r. data provides a rapid and precise method which can be generalized to compounds of the same type from different manufacturers, in contrast to the method based on the use of empirical equations. Mass spectrometry has also been used [9]. These methods require expensive instrumentation. The availability of methods of characterization which are rapid and require relatively cheap instrumentation is desirable.

Ultraviolet/visible spectrophotometry has been used [10] to determine the average properties of ethylene oxide/nonylphenol condensates by measuring the specific absorptivity a ($l\ g^{-1}\ cm^{-1}$) and inserting this experimental value into equations relating a to the average properties to be determined. Infrared spectrometry [11] has been used similarly, based on the relationship between the average properties to be determined and the ratio between the band heights at 960 and 840 cm^{-1}.

The aim of the present paper is to characterize ethylene oxide/tert-octylphenyl condensate non-ionic surfactants by u.v. and i.r. spectrometry and to compare the results with those obtained by n.m.r.

EXPERIMENTAL

Apparatus and reagents

The spectrometers used were as follows: a Perkin-Elmer R-12 n.m.r. spectrometer, with a magnetic field intensity of 14 092 gauss and a resolution of 0.35 Hz, equipped with a double resonance accessory; a Shimadzu 240 u.v. spectrophotometer equipped with a graphic printer PR-1, with 1-cm quartz cells; and a Pye-Unicam SP-2000 i.r. spectrometer, with sodium chloride cells. The associated glassware was of standard manufacture [12].

A 3.5% (w/v) solution of tetramethylsilane (TMS) was prepared in distilled carbon tetrachloride. Samples of ethylene oxide/tert-octylphenol condensates from the Triton X series (X-114 and X-100) were obtained from Serva, Panreac, Merck and Fluka.

Analysis by n.m.r.

Surfactant (500 ± 1 mg) was dissolved in an equivalent amount (ca. 8 ml) of TMS solution and the spectrum of a portion was recorded between 0 and 10 ppm vs. TMS. The spectrum shows three groups of peaks, one at δ values of ca. 7 ppm (aromatic moiety), another between 3 and 4 ppm (ethylene oxide protons) and the third between 0.5 and 2 ppm (tert-octyl protons). The absolute integration of the aromatic protons was used as an internal reference to estimate the number of protons corresponding to the other peaks.

Analysis by u.v. spectrophotometry

Surfactants (0.1—0.2 g) were analysed as described previously [10].

Analysis by i.r. spectrometry

A drop of the surfactant was placed between two sodium chloride windows and its i.r. spectrum recorded. The ratio between the heights of the bands at 960 and 840 cm^{-1} (h_2/h_1) was calculated, and this value was inserted in the equations relating this parameter to $\bar{M}$, $\bar{x}$ or *HLB* obtained from samples previously analysed by n.m.r.

Reference method

In order to evaluate the accuracy of the methods proposed, the UNE 55-518-75 method [12] was used for the iodimetric titration of ethylene oxide groups as described previously [10].

RESULTS AND DISCUSSION

Characterization by n.m.r. spectrometry

Table 1 shows the values and precisions obtained for the average molecular weight ($\bar{M}$), average degree of condensation ($\bar{x}$) and *HLB* of the surfactants studied by the recommended n.m.r. procedure. The percentages of ethylene oxide (EO) calculated from $\bar{x}$ and $\bar{M}$, as given by $\%EO = 100 \times 44.052\ \bar{x}/\bar{M}$, are also listed. These values were used to estimate the accuracy of the method by comparison with the UNE Norme values.

Characterization by u.v. spectrophotometry

Figure 1 shows u.v. spectra of an ethylene oxide/tert-octylphenol condensate of a Triton X-100 type. The band at 275 nm corresponding to the aromatic group was chosen as a working wavelength because it allows a wider surfactant concentration range to be dealt with, because of its relatively low intensity.

TABLE 1

Average properties of ethylene oxide/tert-octylphenol condensates obtained by n.m.r. spectroscopy[a]

Sample	N.m.r.				UNE Norme
	$\bar{M}$	$\bar{x}$	*HLB*	*EO*(%)	*EO*(%)
Triton X-114(1)[b], Serva	580(2.7)	8.3(2.6)	13.2(0.6)	63.3(0.55)	62.6(1.3)
Triton X-114(2)[b], Serva	550(0.6)	8.0(1.4)	13.3(0.8)	63.6(0.81)	— —
Triton X-114, Fluka	550(0.7)	7.9(0.7)	13.1(0.9)	62.6(0.94)	— —
Triton X-100, Serva	660(0.5)	10.3(2.0)	14.1(0.1)	67.9(0.08)	68.6(0.8)
Triton X-100, Fluka	660(3.9)	10.3(4.2)	14.1(1.1)	67.9(1.11)	— —
Triton X-100, Panreac	710(3.0)	11.3(4.0)	14.5(1.0)	70.2(1.19)	— —
Triton X-100, Merck	660(1.5)	10.2(1.3)	14.3(0.3)	68.7(0.32)	— —

[a]Relative standard deviations (%) are given in parentheses (n = 3). [b]Different batches of the same product.

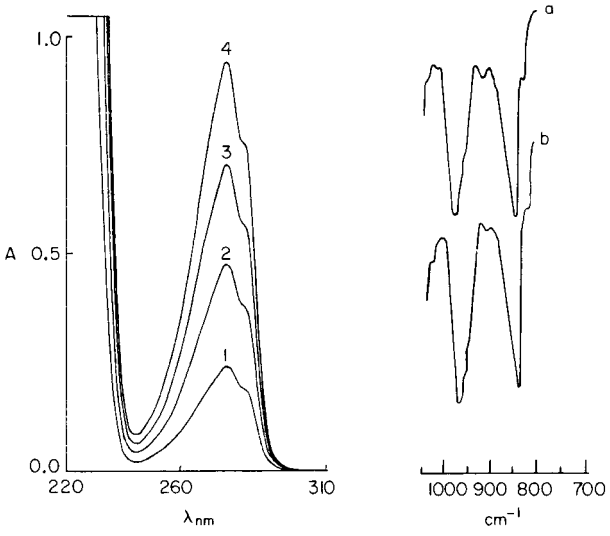

Fig. 1. Ultraviolet absorption spectra of Triton X-100 at different concentrations: (1) 0.10; (2) 0.2; (3) 0.3; (4) 0.4 g l^{-1}.

Fig. 2. Infrared spectra: (a) Triton X-114; (b) Triton X-100.

The number of aromatic groups in one surfactant molecule does not change as the number of ethylene oxide molecules condensing per tert-octylphenol molecule increases, whereas the weight of surfactant that has to be dissolved in order to have one mole in solution increases in proportion to the number of ethylene oxide residues. This allows the molecular weight of the surfactant to be evaluated from the absorbance (A) at the working wavelength and from the mass of surfactant dissolved, if the value of the molar absorptivity (ϵ) is known, because $M = \epsilon bc/A$, where b is the path length and c is the concentration in g l^{-1}. The value of the molar absorptivity can be determined for this type of compound from pairs of A/c values, where c is again measured in g l^{-1}, for solutions of samples of known molecular weight. It was found that the experimental values corresponding to each assay, for each compound and for different degrees of dilution, provide an average value of 1520 ± 40, which is statistically similar to that found for the ethylene oxide/nonylphenol condensates (1600 ± 60) [10].

The determination of other properties, such as the degree of condensation or *HLB*, would require a study of the variation of the specific absorptivity of these surfactants with their average properties.

From the absorbance values found for each sample at the different dilution levels and from the concentration values in g l^{-1}, it is possible to obtain a calibration, differing from one compound to another in the value of the slope (specific absorptivity). The values decrease with increasing molecular weight. Table 2 shows the values of the specific absorptivity (a) for seven surfactant samples of the Triton X series, as well as the standard deviations

TABLE 2

Average properties of ethylene oxide/tert-octylphenol condensates obtained by u.v. spectrophotometry[a]

Sample	Ultraviolet method						UNE Norme
	a	$\bar{M}^b$	$\bar{M}^c$	$\bar{x}^c$	HLB^c	$EO(\%)^c$	$EO(\%)$
Triton X-114(1)[d], Serva	2.66(0.02)	570(3)	560(3)	8.1(0.1)	13.2(0.04)	63.8(0.2)	62.6(0.8)
Triton X-114(2)[d], Serva	2.66(0.03)	570(6)	560(7)	8.1(0.1)	13.2(0.07)	63.6(0.3)	— —
Triton X-114, Fluka	2.68(0.03)	570(5)	550(6)	7.9(0.1)	13.2(0.07)	63.3(0.3)	— —
Triton X-100, Serva	2.25(0.02)	680(9)	670(9)	10.6(0.2)	14.2(0.07)	69.2(0.4)	68.6(0.6)
Triton X-100, Fluka	2.31(0.01)	660(2)	650(2)	10.2(0.1)	14.1(0.02)	68.4(0.1)	— —
Triton X-100, Panreac	2.19(0.01)	690(4)	690(4)	11.0(0.1)	14.4(0.03)	70.2(0.2)	— —
Triton X-100, Merck	2.25(0.01)	670(3)	670(3)	10.6(0.1)	14.2(0.03)	69.2(0.2)	— —

[a]Standard deviations (n = 3) are given in parentheses. [b]Values obtained from the molar absorptivity (ϵ). [c]Values obtained from the empirical equations involving the specific absorptivity (a). [d]Different batches of the same product.

corresponding to three independent assays for each compound. Least-squares regression between a and the values obtained by n.m.r. for $\bar{M}$, $\bar{x}$ and HLB provided the following relationships:

$$\log a = 2.92 - 0.907 \log \bar{M} \qquad (r^2 = 0.96, \text{ seven points})$$

$$\log a = 0.990 - 0.623 \log \bar{x} \qquad (r^2 = 0.96, \text{ seven points})$$

$$a = 7.85 - 0.393\, HLB \qquad (r^2 = 0.98, \text{ seven points})$$

Comparison of the regression equations for ethylene oxide/tert-octylphenol condensates with those obtained for ethylene oxide/nonylphenol condensates shows they are the same for molecular weight and analogous for degree of condensation. However, as would be expected, those for the HLB are clearly different, because of the presence of different lipophilic groups.

The values of the average molecular weight, average degree of condensation and HLB were obtained by insertion of the specific absorptivity values in the above equations. The percentage of ethylene oxide was determined from these data. The values found are shown in Table 2.

TABLE 3

Average properties of ethylene oxide/tert-octylphenol condensates obtained by i.r. spectrometry

Sample	h_2/h_1	$\bar{M}$	$\bar{x}$	HLB	$EO(\%)$
Triton X-114(1)[a], Serva	0.91(0.07)	550(8)	7.9(0.2)	13.0(0.1)	63.1(0.4)
Triton X-114(2)[a], Serva	0.90(0.04)	570(30)	8.3(0.6)	13.3(0.3)	64.0(1.0)
Triton X-114, Fluka	0.85(0.02)	540(9)	7.7(0.2)	13.0(0.1)	62.7(0.4)
Triton X-100, Fluka	1.01(0.03)	650(21)	10.0(0.5)	14.0(0.2)	67.7(0.9)
Triton X-100, Panreac	1.10(0.04)	750(15)	12.1(0.4)	14.8(0.1)	71.6(0.7)
Triton X-100, Merck	1.01(0.00)	650(2)	10.0(0.1)	14.0(0.0)	67.6(0.1)

[a]Standard deviations (n = 3) are given in parentheses. [b]Different lots of the same product.

Characterization by i.r. spectrometry

Figure 2 shows a region of the i.r. spectrum of ethylene oxide/tert-octylphenol condensates corresponding to Triton X-100 and Triton X-114. For these compounds, an increase in the degree of condensation produces an increase in the ratio of the band height at ca. 900 cm^{-1} (h_1) to that at 800 cm^{-1} (h_2). This ratio was obtained from three spectra recorded for each surfactant studied. Table 3 summarizes these values as well as their standard deviations.

The equations obtained for h_2/h_1 as a function of the average molecular weight, degree of condensation and *HLB* were:

$$\log h_2/h_1 = -2.41 + 0.858 \log \bar{M} \qquad (r^2 = 0.95, \text{six points})$$

$$\log h_2/h_1 = -0.604 + 0.608 \log \bar{x} \qquad (r^2 = 0.96, \text{six points})$$

$$\log h_2/h_1 = -2.43 + 2.123 \log HLB \qquad (r^2 = 0.95, \text{six points})$$

These equations were obtained from the values of the average properties determined by n.m.r. (Table 1).

The insertion of the experimental values of the h_2/h_1 parameter, for each of the compounds studied, in the corresponding empirical equations, allows the values of $\bar{M}$, $\bar{x}$ and *HLB* to be obtained. Table 3 summarizes the results found.

Comparison of the characterization methods

The different methods suggested above can be compared on the basis of precision and accuracy, and on the time and instrumentation required. For n.m.r. spectrometry, the relative standard deviations for three independent analyses of a given sample were in the ranges 0.5—3% for $\bar{M}$, 0.7—4% for $\bar{x}$, 0.1—1% for *HLB*, and 0.08—1.2% for *%EO*. The values found for *%EO* are very similar to those obtained by using the UNE Norme, the difference being only 1% relative. The relative standard deviations for ten independent analyses of a given sample by u.v. spectrophotometry were 1.3% for $\bar{M}$, 2% for $\bar{x}$ and 0.5% for *HLB*. The accuracy, evaluated by comparison with results obtained by the UNE Norme, was <2% relative. Ten analyses by i.r. spectrometry gave relative standard deviations of 2% for $\bar{M}$, 3% for $\bar{x}$ and 0.7% for *HLB*. The accuracy, estimated by comparison with the UNE Norme, was 1% relative. These results indicate that all the methods used have similar accuracy and precision, though i.r. spectrometry is slightly less precise.

In order to confirm the accuracy of the u.v. and i.r. results, the correlation between these results and those obtained by n.m.r. was studied statistically [13]. Table 4 summarizes the regression equations for the 21 values obtained by u.v. and n.m.r. for the *%EO* $\bar{M}$, $\bar{x}$ and *HLB* for the different compounds assayed, and also for the 18 values obtained by i.r. Also included are the values of Student's t, defined by $t = (\bar{M} - \bar{M}_0)/s_M$ in which M is the slope or intercept of the corresponding equation, $M_0 = 1$ for the slope test and 0 for the intercept test, and s_M is the standard deviation. These t values confirm that the intercepts are statistically zero and the slopes are equal to one,

TABLE 4

Comparison between the values obtained by the u.v. and i.r. methods with those obtained by n.m.r.

Technique	Parameter	Regression equation[a] $y = a + bx$	r^2	t_1	t_2
U.v.	$EO(\%)$	$y = 2.054 + 0.978x$	0.90	0.130	0.092
	$\bar{M}$	$y = 18.68 + 0.962x$	0.88	0.328	0.417
	$\bar{x}$	$y = -0.219 + 1.034x$	0.94	0.375	0.552
	HLB	$y = 0.279 + 0.98x$	0.90	0.265	0.262
I.r	$EO(\%)$	$y = 0.995 + 0.99x$	0.73	0.111	0.077
	$\bar{M}$	$y = -59.26 + 1.101x$	0.73	0.575	0.608
	$\bar{x}$	$y = -0.866 + 1.108x$	0.74	0.567	0.662
	HLB	$y = -1.171 + 1.084x$	0.73	0.518	0.512

[a] y are values obtained by u.v. or i.r.; x are values obtained by n.m.r. t_1 are the Student's t experimental values for the intercept and t_2 for the slope; the theoretical values are 2.086 for the u.v. data and 2.11 for the i.r. data.

because the experimental t values are less than the theoretical values. Thus the u.v. and i.r. data require no blank correction and do not have constant relative errors with respect to the values found by n.m.r.

The i.r. and u.v. methods, in contrast to the n.m.r. and UNE 55-518-75 Norme methods, require previously analysed samples as standards in order to characterize other samples. They have the advantages of being equally accurate and rapid and of not requiring expensive instrumentation.

REFERENCES

1 M. J. Rosen, Surfactants and Interfacial Phenomena, Wiley, New York, 1978.
2 C. H. Tanford, The Hydrophobic Effect. Formation of Micelles and Biological Membranes, 2nd edn., Wiley, New York, 1980.
3 M. de la Guardia, El Emples de las Emulsiones en el Analisis por Espectroscopia Atomila, Universidad de Valencia, 1982.
4 K. L. Mittal, Solution Chemistry of Surfactants, Vol. 1, Plenum, New York, 1979.
5 R. A. Llenado and R. A. Jamieson, Anal. Chem., 53 (1981) 174R.
6 H. J. Crutchfield, R. R. Irani and J. T. Yoder, J. Am. Oil. Chem. Soc., 41 (1964) 129.
7 J. R. Bergueiro, M. Bao and J. J. Casares, An. Quim., 74 (1979) 529.
8 J. L. Carrión, M. de la Guardia and J. Medina, Quim. Anal., 2(4) (1983) 271.
9 H. J. Danes and A. M. Casanovas, Tenside Deterg., 16 (1979) 317.
10 M. de la Guardia, J. L. Carrión and J. Medina, Anal. Chim. Acta, 155 (1983) 113.
11 M. de la Guardia, J. L. Carrión and J. Medina, Analyst (London), 109 (1984) 457.
12 UNE 55-518-75, Instituto Nacional de Racionalización y Normalización, Madrid, 1975.
13 M. de la Guardia, A. Salvador and V. Berenguer, An. Quim., 77B (1981) 125; 79B (1983) 446.

Analytica Chimica Acta, 185 (1986) 109—117
Elsevier Science Publishers B.V., Amsterdam — Printed in The Netherlands

DETERMINATION OF TRACE METALS IN SEDIMENT STANDARD REFERENCE MATERIALS BY GRAPHITE-FURNACE ATOMIC ABSORPTION SPECTROMETRY WITH A STABILIZED TEMPERATURE PLATFORM

M. BETTINELLI*, N. PASTORELLI and U. BARONI
ENEL DCO Central Laboratory, 29100 Piacenza (Italy)
(Received 19th November 1985)

SUMMARY

Trace elements (As, Be, Cd, Co, Cr, Cu, Mn, Mo, Ni, Pb, V, Zn) in NBS 1645 (river sediment), NBS 1646 (estuarine sediment), MESS-1 and BCSS-1 (marine sediments), IAEA SL-1 (Lake Sediment) and IAEA Soil-5, are determined by graphite furnace atomic absorption spectrometry with the L'vov platform. The samples (ca. 0.25 g) are dissolved in a mixture of nitric, perchloric and hydrofluoric acids in a PTFE bomb. Results based on direct calibration with simple aqueous solutions are in good agreement with those obtained by the method of standard additions and with recommended values. The relative standard deviations are generally 5—10%. Chromium determinations are also evaluated by inductively-coupled plasma/atomic emission spectrometry.

The concentration of metals in aquatic sediments is of particular importance and interest in environmental chemistry. It is generally recognized that sediments, both suspended and bottom, constitute a potential source of many dissolved chemical species in waters. Because near-shore marine sediments are usually composed primarily of clay minerals derived from continental weathering, along with minor amounts of other minerals, procedures developed for dissolution of silicate rocks are often appropriate for sediments, although consideration must be given to the sometimes appreciable organic content of near-shore sediments.

The dissolution of geological materials can be accomplished by numerous techniques which fall into two general categories: fusion and acid dissolution. Previous studies [1—4] involving trace element determinations in sediments by atomic absorption spectrometry (a.a.s.) have favored acid digestion procedures, although some problems of incomplete recovery have been encountered [5]. All these techniques are very effective in dissolving siliceous material but they do not destroy the large quantities of organic matter present in some silt and clay lake sediments. Several authors [6—8] have discussed the incorporation of soluble organic matter into sediments, and its association with trace elements. The correlation between organic matter and trace element content of sediments is well known for several elements,

0003-2670/86/$03.50

therefore, in the preparation of sediment samples, the important step of destruction of organic matter must be very rigorous. Because the chemical composition of lake and river sediments is somewhat different from inorganic siliceous rocks, but not so different from coal fly ash, a digestion method previously found satisfactory for fly ash was used for the present study.

Two approaches were used to evaluate the accuracy and precision of the results obtained: a standard additions method, with injection of sample solution directly into the furnace, and a direct comparison of the integrated signals from sediment solutions with those from a calibration graph prepared from standards in acidified deionized water (1% nitric acid).

EXPERIMENTAL

Apparatus

A Perkin-Elmer model 5000 atomic absorption spectrometer, with deuterium-arc background correction, a HGA-500 graphite furnace and an AS-40 autosampler were used. Electrodeless discharge lamps operated from an external power supply were used for arsenic, cadmium and lead. Conventional hollow-cathode lamps were used for all other elements determined. Pyrolytically-coated graphite tubes with solid pyrolytic graphite platforms were used. Zinc in all standard materials and chromium in NBS 1645 were determined with the same atomic absorption spectrometer, fitted with an air/acetylene burner. The instrumental conditions conformed to those given in the instrument manual and are summarized in Tables 1 and 2. A Perkin-Elmer Autoclave-3, heated in a drying oven with temperature control, was used for all pressure decompositions.

Reagents

Standard solutions were prepared from 1000 mg l^{-1} standards for a.a.s. (BDH Chemicals) by dilution with deionized water. Sulfuric acid (96% w/v), perchloric acid (70% w/v), nitric acid (65% w/v) and hydrofluoric acid (40% w/v) were Suprapur reagents (Merck). The nickel matrix-modifier solution was prepared from the BDH atomic absorption standard solution. Magnesium nitrate hexahydrate was of Suprapur grade (Merck); ammonium dihydrogenphosphate used as the matrix modifier solution for lead determinations was an Ultrex reagent (J. T. Baker).

Procedures

Acid dissolution. About 0.25 g of sample, 4.0 ml of 65% nitric acid, 2.0 ml of 70% perchloric acid and 4.0 ml of 40% hydrofluoric acid were placed in the PTFE beaker of the Autoclave-3. The bomb was heated for 3—5 h at 130°C in a drying oven. After being cooled to room temperature, the contents of the beaker were evaporated slowly to dryness on an aluminum block at 200°C. After addition of 1 ml of nitric acid and 10 ml of water, the solution was transferred to a polypropylene flask and diluted to 100 ml with

TABLE 1

Instrumental operating conditions for a.a.s.

Model 5000 spectrometer			
Calibration mode			Peak area
Integration time			6 s
Background corrector			Deuterium arc
HGA-500 graphite furnace			
Step no.	*Temp. (°C)*	*Ramp time (s)*	*Hold time (s)*
1	80	1	4
2	120	10	10
3	—[a]	30	15
4	—[a]	1	5
5	—[a]	0[c]	6
6	—[b]	1	3
7	20	1	10
Purge gas			Argon, interrupted
Sample volume			20 μl
Alternative volume			20 μl

[a]Charring and atomization temperatures for each element as in Table 2; the temperature was the same in steps 3 and 4. [b]100°C higher than the temperature in step 5. [c]Maximum power heating mode; "read" activated at —2 s.

TABLE 2

Experimental conditions

Element	λ (nm)	Slit (nm)	Power or current	Modifier[a]	Temp. (°C)		m_0[b]	
					Char	Atomize	Direct method	Standard addition
As	193.7	0.7	8 W	3	1300	2300	16 ± 1	17 ± 2
	197.2	0.7	8 W	3	1300	2300	32 ± 3	33 ± 3
Be	234.9	0.7	30 mA	1	1500	2500	1.2 ± 0.13	1.3 ± 0.2
Cd	228.8	0.7	5 W	2	1000	1500	0.41 ± 0.06	0.48 ± 0.09
Co	240.7	0.2	35 mA	1	1400	2400	8.5 ± 1	9.1 ± 2
Cr	357.9	0.7	20 mA	1	1600	2500	3.5 ± 0.3	4.0 ± 0.5
Cu	324.7	0.7	20 mA	—	1200	2300	3.8 ± 0.2	4.1 ± 0.2
Mn	279.5	0.2	20 mA	1	1400	2200	2.3 ± 0.1	2.4 ± 0.2
Mo[c]	313.3	0.7	35 mA	—	1800	2700	9.5 ± 1	9.9 ± 1
Ni	232.0	0.2	30 mA	1	1400	2700	12 ± 2	12 ± 2
Pb	283.3	0.7	9 W	2	750	2000	11 ± 1	12 ± 2
V[c]	318.4	0.7	20 mA	—	1500	2700	27 ± 2	27 ± 3

[a]Modifiers were: (1) 50 μg $Mg(NO_3)_2$; (2) 200 μg PO_4^{3-} + 10 μg $Mg(NO_3)_2$; (3) 20 μg $Ni(NO_3)_2$. [b]"Characteristic mass": pg of element that produces an integrated absorbance signal equivalent to 0.0044 absorbance × seconds; values are mean ±95% confidence limits (n = 15). [c]Atomization from tube wall.

deionized water. Blank decompositions with the same reagents, but without a sample, were run with each set of sample decompositions. The matrix-modifier solution was added by the AS-40 autosampler, in 10-μl portions, on top of the sample aliquot on the platform.

When the method of standard additions was used, the standards were added directly to the sample on the platform, and finally the matrix modifier was dispensed onto the platform. All analyses involved dilutions in water of the original sample solutions that varied up to 100-fold to keep the integrated absorbance ($A \times s$) signals in the linear calibration range. The temperature conditions and modifiers were similar to those reported by Slavin et al. [9] and are summarized in Table 2. Before nickel determinations, the contact rings and surrounding areas were cleaned to remove accumulated salts [10].

Fusion procedure. About 0.25 g of sample and 0.5 g of lithium tetraborate were placed in a 50-ml platinum crucible and thoroughly mixed. The sample/flux mixture was fused in a muffle furnace at 1000 ± 30°C for 45 min. When fusion was complete, the cooled crucible was placed in a 100-ml beaker, a small teflon-coated stirrer was inserted and 25 ml of 5% nitric acid was added. The solution was heated for 15—20 min at 50—60°C, and transferred to a 100-ml polypropylene flask. The dissolution procedure was repeated with a second aliquot of nitric acid and this solution was added to the flask, after which the contents of the flask were adjusted to volume with deionized water.

RESULTS AND DISCUSSION

Sample dissolution

The bomb digestion method used here is similar to that previously described [11] for organic and silica-rich sediments. Although perchloric acid was used and the digestion temperature was increased to 150°C (the manufacturer's suggested upper limit), a carbonaceous residue was observed with some samples. A possible explanation is that when the bomb method is used below 200°C (the normal boiling point of the 78% perchloric acid azeotrope), the perchloric acid does not achieve its maximum oxidizing ability. In order to ensure complete oxidation of resistant organic matter and also to remove perchloric and hydrofluoric acid completely from the solution, the sample was evaporated slowly to dryness. This was preferred to addition of boric acid [3, 11] because it resulted in solutions with much lower concentrations of dissolved solids and because perchloric acid has been shown to be responsible for many interference effects in graphite-furnace a.a.s. [12, 13].

Matrix interferences

The L'vov platform seems to be capable of significantly decreasing matrix interferences in graphite-furnace a.a.s. [12—16], and provides a definite advantage over atomization from the tube wall in that use of the method of standard additions is no longer necessary. In this work with sediment solutions, the performance characteristics of the L'vov platform were verified by

direct comparison of the standard additions method with direct calibration. The "characteristic mass" (m_0) [15] was calculated for both procedures. The values obtained are given in Table 2. The values for arsenic are reported at two different wavelengths (193.7 and 197.2 nm) because at the former, aluminum produces significant non-specific absorption which is not eliminated by using continuum-source background correction of matrix modifiers. As reported previously [17], at 197.2 nm there was no spectral interference, although at this wavelength the sensitivity is halved.

Standard samples

Table 3 lists the results obtained for the determination of As, Be, Cd, Co, Cr, Cu, Mn, Mo, Ni, Pb, V and Zn in the NBS 1645, NBS 1646, MESS-1, BCSS-1, IAEA SL-1 and IAEA Soil-5a standards. The results of blank measurements, based on direct injection of the solution, against a calibration graph prepared from aqueous standards, are negligible for all these elements. The mean values (±95% confidence limits) obtained for five separate blank determinations were: 0.21 ± 0.09 $\mu g\ g^{-1}$ As; 0.028 ± 0.009 $\mu g\ g^{-1}$ Be; 0.012 ± 0.004 $\mu g\ g^{-1}$ Cd; 0.10 ± 0.03 $\mu g\ g^{-1}$ Co; 0.20 ± 0.08 $\mu g\ g^{-1}$ Cr; 0.76 ± 0.09 $\mu g\ g^{-1}$ Cu; 0.37 ± 0.10 $\mu g\ g^{-1}$ Mn; 0.04 ± 0.01 $\mu g\ g^{-1}$ Mo; 0.37 ± 0.11 $\mu g\ g^{-1}$ Ni; 0.64 ± 0.17 $\mu g\ g^{-1}$ Pb; 0.53 ± 0.15 $\mu g\ g^{-1}$ V.

The data reported in Table 3 reveal good agreement (except for lead in MESS-1 and BCSS-1) between the results obtained by the two graphite-furnace a.a.s. procedures (direct injection and standard additions) and the certified values, at the 95% confidence level. The data obtained for lead in MESS-1 and BCSS-1 are systematically lower than the certified values. The results are more consistent, for the MESS-1 standard, with those reported by Sturgeon et al. [19].

Contrary to the report of Sturgeon et al. [19], no background-correction problems were encountered in chromium determinations and therefore chromium was determined by using platform atomization. Sinex et al. [20] reported excellent chromium recoveries for SRM-1645, probably because this sediment contains chromium in a relatively labile form [21]. This material is from a highly polluted industrial river and is unusually high in iron, chromium and organic material. Apparently, therefore, methods which dissolve most of the trace metals in SRM-1645 do not necessarily achieve similar levels of dissolution with normal estuarine sediments. For example, McLaren et al. [22] reported low chromium results for BCSS-1 and MESS-1 and indicated that incomplete dissolution was responsible. They concluded that certain chromium-containing minerals (e.g., chromite) are not dissolved by nitric/perchloric/hydrofluoric acid mixtures.

In order to verify this point, three portions of standard sediments were treated by the procedure described in this paper and by a fusion method with lithium tetraborate [23] which had been used successfully for fly ashes. In the solution deriving from the mixed acid digestion procedure, the chromium content was determined by graphite-furnace a.a.s. and by inductively-coupled

TABLE 3

Comparison of results by graphite-furnace a.a.s. and the L'vov platform with certified values for six standard sediments

Element	Element content[a] ($\mu g\ g^{-1}$)		Certified value[b]	Element content[a] ($\mu g\ g^{-1}$)		Certified value[b]
	Direct injection	Standard additions		Direct injection	Standard additions	
NBS 1645 River Sediment[c]				*NBS 1646 Estuarine Sediment*		
As	59 ± 8	63 ± 7	(66)	11 ± 2	12 ± 3	11.6 ± 1.3
Be	0.78 ± 0.12	0.92 ± 0.04	—	1.4 ± 0.2	1.4 ± 0.2	(1.5)
Cd	9.1 ± 0.3	10.0 ± 0.3	10.2 ± 1.5	0.33 ± 0.06	0.35 ± 0.07	0.36 ± 0.07
Co	7.5 ± 0.3	8.6 ± 0.4	(8)	11.9 ± 0.8	12.0 ± 1.0	10.5 ± 1.3
Cr	3.1 ± 0.4	—	2.96 ± 0.28	72 ± 5	77 ± 6	76 ± 3
Cu	107 ± 9	115 ± 14	109 ± 19	17 ± 3	20 ± 5	18 ± 3
Mn	828 ± 44	802 ± 39	785 ± 97	356 ± 13	367 ± 10	375 ± 20
Mo	22.6 ± 1.4	21.2 ± 1.3	—	2.1 ± 0.1	2.1 ± 0.1	(2.0)
Ni	49.9 ± 2.3	48.2 ± 4.0	45.8 ± 2.9	33 ± 7	34 ± 4	32 ± 3
Pb	737 ± 15	731 ± 16	714 ± 28	31.3 ± 2.1	32.7 ± 2.6	28.2 ± 1.8
V	22.8 ± 7.6	21.8 ± 7.7	23.5 ± 6.9	95 ± 10	95 ± 5	94 ± 1
Zn	1685 ± 45	—	1720 ± 169	132 ± 7	—	138 ± 6
BCSS-1 Marine Sediment				*MESS-1 Marine Sediment*		
As	9.8 ± 0.7	10.5 ± 0.8	11.1 ± 1.4	9.1 ± 0.8	10.1 ± 1.0	10.6 ± 1.2
Be	1.3 ± 0.06	1.5 ± 0.05	1.3 ± 0.3	1.8 ± 0.1	2.1 ± 0.2	1.9 ± 0.2
Cd	0.22 ± 0.03	0.25 ± 0.03	0.25 ± 0.04	0.48 ± 0.02	0.50 ± 0.01	0.59 ± 0.10
Co	10.0 ± 0.7	10.8 ± 0.7	11.4 ± 2.1	8.9 ± 2.1	9.6 ± 2.2	10.8 ± 1.9
Cr	118 ± 7	120 ± 7	123 ± 14	66 ± 2	67 ± 2	71 ± 11
Cu	17.2 ± 1.3	20.9 ± 1.4	18.5 ± 2.7	20.9 ± 1.4	26.1 ± 0.6	25.1 ± 3.8
Mn	214 ± 9	210 ± 12	229 ± 15	480 ± 28	488 ± 23	513 ± 25
Mo	2.6 ± 0.3	2.2 ± 0.2	(1.9)	2.7 ± 0.3	2.2 ± 0.3	(2.2)
Ni	56.8 ± 2.8	57.9 ± 3.1	55.3 ± 3.6	30.5 ± 3.4	31.6 ± 3.8	29.5 ± 2.7
Pb	15.7 ± 0.7	18.0 ± 0.6	22.7 ± 3.4	23.5 ± 2.3	27.1 ± 2.9	34.0 ± 6.1
V	92.0 ± 1.5	95.1 ± 1.8	93.4 ± 4.9	73.3 ± 3.0	75.6 ± 2.8	72.4 ± 5.3
Zn	108 ± 7	—	119 ± 12	182 ± 10	—	191 ± 17

IAEA SL-1 Lake Sediment				*IAEA Soil-5a*		
As	32.5 ± 5	32.0 ± 5	27.5 ± 2.9	101 ± 3	100 ± 3	93.9 ± 7.5
Be	2.1 ± 0.5	2.2 ± 0.4	—	1.5 ± 0.4	1.6 ± 0.7	(1.8)
Cd	0.31 ± 0.06	0.31 ± 0.08	0.26 ± 0.05	1.2 ± 0.05	1.4 ± 0.05	(1.5)
Co	15.6 ± 0.7	17.6 ± 0.7	19.8 ± 1.5	12.8 ± 2.0	14.6 ± 2.2	14.8 ± 0.76
Cr	99 ± 10	96 ± 11	104 ± 9	29.8 ± 2.4	30.0 ± 3.1	28.9 ± 2.8
Cu	32.7 ± 5.9	33.7 ± 7.5	30.0 ± 5.6	73.5 ± 6.1	78.0 ± 6.5	77.1 ± 4.7
Mn	0.353 ± 0.036	—	0.346 ± 0.016	865 ± 21	868 ± 25	852 ± 37
Mo	1.3 ± 0.4	1.6 ± 0.3	(1.3)	1.5 ± 1.0	1.8 ± 0.7	(1.7)
Ni	42.5 ± 3.8	47.5 ± 4.1	44.9 ± 8.0	13.4 ± 2.2	15.3 ± 2.8	(13)
Pb	38.3 ± 4.4	38.7 ± 5.1	37.7 ± 7.4	122 ± 12	127 ± 15	129 ± 26
V	174 ± 12	172 ± 11	170 ± 15	160 ± 5.3	157 ± 6.3	(151)
Zn	221 ± 12	—	223 ± 10	372 ± 12	—	368 ± 8.2

[a]Mean of 3 results with 95% tolerance limit. [b]Values given in parentheses are reported but not certified by NBS [18] or IAEA. The certified values for the BCSS and MESS sediments are from Sturgeon et al. [19]. [c]Literature values for this sample include 67 ± 3 $\mu g\ g^{-1}$ arsenic, 1.0 $\mu g\ g^{-1}$ beryllium, 9.2 ± 1.3 $\mu g\ g^{-1}$ cobalt and 25 $\mu g\ g^{-1}$ molybdenum [18].

TABLE 4

Operating conditions for chromium determination by i.c.p./a.e.s.

Spectrometer	Perkin-Elmer ICP/6000
Wavelength	267.716 nm
Background intervals	−0.125 nm, +0.097 nm
Incident RF power	1250 W
Reflected RF power	5 W
Plasma gas flow rate	15 l min^{-1}
Auxiliary gas flow rate	0.8 l min^{-1}
Nebulizer gas pressure	26 psig
Viewing height	14 mm above load coil

TABLE 5

Determination of chromium ($\mu g\ g^{-1}$) in sediment standard reference materials using different decomposition procedures and measurement techniques

Standard	Acid procedure[a]		Fusion procedure[a]	Certified value
	A.a.s.	I.c.p.	I.c.p.	
NBS 1645	3.08 ± 0.42	3.09 ± 0.26	3.10 ± 0.21	2.96 ± 0.28
NBS 1646	72 ± 5	76 ± 6	77 ± 7	76 ± 3
BCSS-1	118 ± 7	121 ± 10	130 ± 9	123 ± 14
MESS-1	66 ± 2	69 ± 4	73 ± 2	71 ± 11
IAEA SL-1	99 ± 10	102 ± 5	105 ± 6	104 ± 9

[a]Results are mean ±95% confidence limits ($n = 3$).

plasma/atomic emission spectrometry (i.c.p./a.e.s.). In the solution deriving from the fusion procedure, only the plasma technique was used. The conditions for the latter measurements are summarized in Table 4. The results, reported in Table 5, reveal good agreement between the chromium recoveries obtained by the two measurement techniques and also between the acid dissolution and fusion procedures. Quantitative dissolution and recovery of chromium in all the sediments analyzed is evident, indicating that complete dissolution of chromium-bearing minerals was achieved.

Conclusions

The results obtained for the standard samples after acid digestion are in good agreement with the certified values and have good precision. The technique is simple and reliable. Direct calibration can be used, so that the method of standard additions is unnecessary.

REFERENCES

1 R. T. T. Rantala and D. H. Loring, At. Absorpt. Newsl., 14 (1975) 117.
2 R. T. T. Rantala and D. H. Loring, At. Absorpt. Newsl., 12 (1973) 97.

3 H. Agemian and A. S. Y. Chau, Anal. Chim. Acta, 80 (1975) 61.
4 M. Sakata and O. Shimota, Water Res., 16 (1982) 231.
5 S. A. Sinex, A. Y. Cantillo and G. R. Helz, Anal. Chem., 116 (1980) 433.
6 C. D. Curtis, in G. D. Hobson and M. C. Louis (Eds.), Advances in Organic Geochemistry, Pergamon, Oxford, 1966.
7 R. I. Thomas, Can. J. Earth Sci., 9 (1972) 636.
8 E. S. Pilkington and L. J. Warren, Environ. Sci. Technol., 13 (1979) 295.
9 W. Slavin, G. R. Carnrick, D. C. Manning and E. Pruszkowska, At. Spectrosc., 4 (1983) 69.
10 B. E. Manning, At. Spectrosc., 4 (1983) 159.
11 C. Hsu and D. C. Locke, Anal. Chim. Acta, 153 (1983) 313.
12 C. W. Fuller, Anal. Chim. Acta, 81 (1976) 199.
13 S. R. Koirtyohann, E. D. Glass and F. E. Lichte, Appl. Spectrosc., 35 (1981) 22.
14 V. B. L'vov, Spectrochim. Acta, Part B: 33 (1978) 153.
15 W. Slavin and D. C. Manning, Spectrochim. Acta, Part B: 35 (1980) 701.
16 D. C. Gregoire and C. L. Chakrabarti, Anal. Chem., 49 (1977) 2018.
17 K. W. Riley, At. Spectrosc., 3 (1982) 120.
18 E. S. Gladney, C. E. Burns, D. R. Perrin, I. Roelants and T. E. Gills, 1982 Compilation of Elemental Concentration Data for NBS Biological, Geological and Environmental Standard Reference Materials, NBS Special Publication 260-88, Washington, DC, March 1984.
19 R. E. Sturgeon, J. A. H. Desaulniers, S. S. Berman and D. S. Russell, Anal. Chim. Acta, 134 (1982) 283.
20 A. Sinex, A. Y. Cantillo and G. R. Helz, Anal. Chem., 52 (1980) 2342.
21 M. Soma, H. Seyama and K. Okamoto, Talanta, 32 (1985) 177.
22 J. W. McLaren, S. S. Berman, V. J. Boyko and D. S. Russell, Anal. Chem., 53 (1981) 1802.
23 M. Bettinelli, Anal. Chim. Acta, 148 (1983) 193.

Analytica Chimica Acta, 185 (1986) 119—126
Elsevier Science Publishers B.V., Amsterdam — Printed in The Netherlands

DIRECT NON-DESTRUCTIVE DETERMINATION OF MANGANESE(II) IN CADMIUM SELENIDE BY ELECTRON SPIN RESONANCE SPECTROMETRY

V. Yu. NAGY* and S. S. GRAZHULENE

Institute of Problems of Microelectronics Technology and Superpure Materials, U.S.S.R. Academy of Sciences, 142432 Chernogolovka, Moscow District (U.S.S.R.)

O. M. PETRUKHIN, Ya. L. KHARIF, V. Yu. BREZHNEV and P. V. KOVTUNENKO

Mendeleev Institute of Chemical Technology, 125820 Moscow (U.S.S.R.)

(Received 15th August 1985)

SUMMARY

A rapid (1—2 min) non-destructive method based on electron spin resonance is described for the determination of manganese in cadmium selenide powders suitable for semiconductors. Measurements of the amplitude of the first-derivative curves provide linear calibration over a wide range. Neither a low-temperature facility nor single-crystal samples are needed. The method is useful for determining 10^{-4}—10^{-1}% manganese with a relative standard deviation of about 0.03. The detection limit is 5×10^{-6}%. The dependence of the e.s.r. signal of manganese(II) on experimental variables is discussed.

Electron spin resonance (e.s.r.) spectrometry is noted for a rare combination of two advantages which are of particular importance for determining impurities in solids. On the one hand, e.s.r. signals depend on the chemical state of the impurities to be determined to a greater extent than those produced by other methods; the parameters of the e.s.r. spectrum are fully governed by the oxidation state of the element and the nature of its coordination environment. On the other hand, e.s.r. spectrometry often enables a component in solids to be determined nondestructively, thus ensuring the maintenance of the real chemical form of the impurity up to the moment of measuring the signal. Owing to these distinctive characteristics, e.s.r. spectrometry can be used extensively and reliably for direct selective determinations of specific impurity forms in solids.

The e.s.r. method can, of course, be used to determine concentrations of paramagnetic states only, but extensive data reported recently indicate that there are many such states in real solids [1—3]. Practically all the transition metals exhibit paramagnetic properties in one of their valency states (and sometimes in more). Quite unusually (from the point of view of "wet chemistry"), paramagnetic oxidation states are often stabilized in solids. Some non-metals are paramagnetic in a number of solid matrixes. The few papers in which e.s.r. spectra of solids were utilized for direct determinations of impurity concentrations have been reviewed [4].

The advantages of e.s.r. spectrometry mentioned above, combined with the speed of such determinations, make it a potentially beneficial method for the analysis and testing of semiconductor materials. There is information [5] on its use for the determination of different oxidation states of chromium in gallium arsenide. The present paper reports the e.s.r. spectrometry determination of manganese(II) in cadmium selenide which is a widely used semiconductor material in optoelectronics. Manganese(II) is one of the impurities which are difficult to extract from this material. And, in certain instances, manganese is artificially introduced into II—VI semiconductors as a dopant. The e.s.r. method appears to be a convenient non-destructive method for the rapid determination of manganese(II) content in cadmium selenide.

EXPERIMENTAL

Equipment

A Soviet-made RE-1306 X-band spectrometer with a magnetic field modulation frequency of 100 kHz was used with a TE_{011} cavity and quartz cylindrical ampoules of various diameters (wall thickness ca. 0.15 mm). For low-temperature investigations, the thermal system was based on a gaseous nitrogen stream. The *g* factors were evaluated with respect to 2,2-diphenyl-1-picrylhydrazyl (DPPH), the resonance field strength being measured with a Sh1-1 instrument and a GZ-4 frequency meter. The magnetic field scan was measured with a Mn^{2+}/MgO standard which had a hyperfine structure constant of 86.8 Oe (Oersted).

The atomic absorption spectrometric determinations were done with an AAS-1 flame spectrometer (Zeiss, G.D.R.).

Preparation of standard samples

Samples of cadmium selenide and selenium were of high-purity grade and those of manganese metal were of reagent purity. Samples with different manganese(II) contents were prepared by using manganese(II) diselenide.

The manganese(II) diselenide was synthesized by heating a mixture of manganese and selenium with a 50% excess of the latter in a graphitized vacuum-sealed ampoule. The mixture was heated with an oxygen burner. Heating was stopped when the exothermal reaction started and then the ampoule with the sample was annealed for 20 h at 770 K. The product was powdered and annealed again for 3 h in a vacuum quartz ampoule at the same temperature. By this operation, the excessive selenium was distilled off into the other part of the ampoule kept at 300 K. The manganese(II) diselenide obtained was identified by x-ray diffraction.

A stock sample of cadmium selenide containing 1% manganese(II) was prepared by grinding the cadmium selenide and manganese(II) diselenide mixture in a mortar and then annealing in a vacuum quartz ampoule for 10 h at 1270 K. This sample was used to prepare those with lower manganese

contents down to 10^{-4}% by successive dilutions with cadmium selenide with homogenization under the same conditions. The manganese content in the powdered samples obtained was determined by flame atomic absorption spectrometry after dissolution of the samples.

RESULTS AND DISCUSSION

Spectrum characteristics

In cadmium selenide single crystals which did not undergo additional saturation with elemental selenium vapour, manganese is found in the divalent state replacing cadmium(II) ions in the cubic crystal lattice [6]. The manganese(II) ion has a 3 d^5 configuration and a ground electron state $^6S_{5/2}$, which is paramagnetic. The e.s.r. spectrum manganese(II) in cadmium selenide single crystals at liquid nitrogen temperature is composed of numerous lines owing to hyperfine splitting on the ^{55}Mn nuclei (I = 5/2; 100%); six of these lines are particularly intense [7, 8].

By virtue of the isotropy of the g factor and the negligible value of the zero-field splitting parameter, the above six-line pattern corresponding to the $|-1/2> \leftrightarrow |1/2>$ transition displays a very weak angular dependence and is easily observed both in single crystals and in powder spectra where other line systems are smoothed over (Fig. 1). The g factor is equal to 2.003 ± 0.001; the hyperfine splitting constant reflecting the strength of the manganese(II/VI) semiconductor anion bond [8, 9] is 65.9 Oe (61.6 × 10^{-4} cm^{-1}), as the present data indicate. The narrowness of the manganese(II) spectral

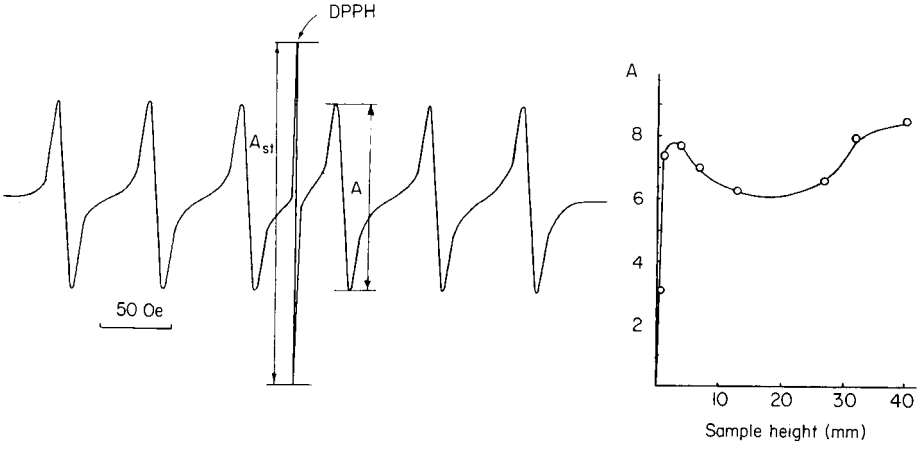

Fig. 1. The e.s.r. spectrum of manganese(II) in the II—VI semiconductor powder at room temperature.

Fig. 2. Dependence of the first-derivative amplitude of the manganese(II) spectrum on the sample height in a 2-mm i.d. tube. The size of the powder particles is ⩾0.2 mm. The middle of the sample coincides with that of the cavity vertical axis. Microwave power 1 mW.

lines in powdered samples (ΔH_{pp} = 9 Oe) provides simple, highly sensitive determinations of the ion concentration.

Optimization of the conditions for determinations

Preliminary investigations of the influence of various experimental factors on the required signal and the selection of optimal conditions are required to achieve high accuracy and precision as well as low detection limits in e.s.r. determinations.

Sample state and size. The weak anisotropy of the manganese(II) spectrum, which provides low detection limits even for powdered samples, makes it unnecessary to keep the size of the powder particles within a narrow range. Once a cadmium selenide sample placed into the cavity of an e.s.r. spectrometer consists of more than 10—15 single crystals orientated in a random way, the e.s.r. spectrum exhibits lines which do not differ in width from the spectral lines of much finer powders.

The considerable influence of cadmium selenide samples on the Q factor of the cavity makes it expedient to go over from conventional 3-mm sample tubes to 2-mm tubes. Further reduction of the diameter providing even greater sensitivity cannot be recommended in all cases, because it sets limits on the maximum size of the powder particles and causes difficulties for changing samples in sample tubes.

The dependence of the signal on the height of the powdered sample in a 2-mm sample tube (Fig. 2) is rather complicated because of large dielectric losses of the sample. Of the two ranges of heights providing the largest (and approximately equal) spectrum amplitudes, the first (h = 4—5 mm) is the better for analysis because overloading the cavity with large samples containing paramagnetic centres in high concentrations may affect the accuracy of results [10, 11]. A 0.1 g sample accepted as a standard portion provides a sample height of 4—6 mm in the sample tube.

The measurable influence of cadmium selenide samples on the Q factor of the cavity requires accurate fixing of the sample tube position in the cavity. The best signal reproducibility was achieved when the same sample tube with a rigidly fixed collar was utilized for all samples. The collar provided fixed orientation of the tube in the cavity with respect to both the height and the vertical axis. The procedure used to standardize the weight, form and position of the sample made it possible to achieve the signal reproducibility within 3%.

The manganese(II) spectrum in a cadmium selenide sample recorded at 120 K is only almost doubled compared to the spectrum at room temperature. Such an insignificant effect of reducing the temperature does not justify the complication of the analytical procedure caused by the use of a low-temperature facility. Room temperature was accepted as optimal for analysis.

Adjacent standard. The dependence of the signal on both the ion content and the dielectric losses of the sample appeared to be an important problem

in the e.s.r. spectrometric determination of manganese(II) in cadmium selenide (the term "dielectric" is used conditionally, meaning all SHF power losses brought about by the interaction of the sample and the electric component of the electromagnetic field). The effect of the fluctuations in the sample conductivity on the results of e.s.r. spectrometry is so great that the hypothesis of a linear correlation of the e.s.r. signal with the manganese-(II) content in the sample was not verified by a statistical check based on the r_{xy} criterion.

A small crystal of diphenylpicrylhydrazyl (DPPH) glued to the bottom of the sample tube was used as an adjacent standard to take account of the conductivity effect. The amplitude of the DPPH spectral line which is suitably interposed on the manganese(II) spectrum (Fig. 1) is affected by the cavity Q factor as much as the amplitude of the ion to be determined. The ratio of the amplitudes does not depend on the dielectric losses of the sample and can be accepted as a measure of the manganese(II) concentration.

Thus, the adjacent standard was used only to check the Q factor and not as a reference material with a known content of paramagnetic centres. Evaluation of the data available in the literature shows that correct determination of the number of paramagnetic centres by comparison with standards of different nature has several prerequisites that are difficult to fulfil. The relative error for such an approach is rarely less than 20—30%. The availability of cadmium selenide samples with known manganese(II) content made it possible to avoid the use of other standards. The DPPH signal was used only in the relative expression regardless of the absolute number of paramagnetic molecules in the DPPH sample.

The procedure for the determination included preliminary recording of the e.s.r. spectra of some cadmium selenide reference samples with known manganese(II) content in the same sample tube (with an adjacent standard); the manganese(II) content of samples of unknown composition was determined by using the same ampoule tube with the adjacent standard, on the basis of the plotted calibration line. In this respect, the use of DPPH as a standard is justified despite the fact that it is not identical with the analyzed samples in several characteristics, e.g., the Curie temperature [12].

Instrumental variables. Under the conditions of a varying Q factor, the ratio of the line amplitudes of manganese(II) and DPPH can be a valid measure of the signal only if both amplitudes equally correspond to the SHF power changes. As shown in Fig. 3, this condition is met over the 0—1 mW range of incident radiation power, the upper limit of which is the optimal value of this variable for determinations. When manganese(II) is determined close to the detection limit (for which higher sensitivity is essential and the requirements for accuracy are less stringent), it may prove feasible to increase the power to 6—7 mW; this will approximately double the signal while any error resulting from the non-uniform saturation of the sample and standard will still not exceed 30% (Fig. 3).

The modulation amplitude of the magnetic field in modern e.s.r. spec-

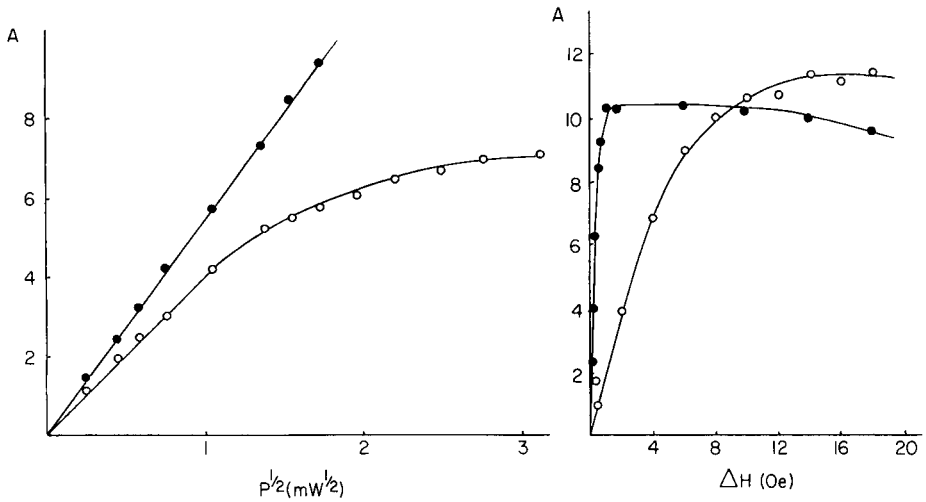

Fig. 3. Dependences of the first-derivative amplitudes of the spectra on the microwave power (P): (○) manganese(II); (●) DPPH. Manganese content 1×10^{-3}%.

Fig. 4. Dependence of the first-derivative amplitudes of the spectra on the magnetic field modulation amplitude (ΔH): (○) manganese(II); (●) DPPH. Manganese content 1×10^{-3}%; microwave power 1 mW.

trometers exhibits uncontrolled variations during operation to a lesser extent than the SHF power in the sample; there is little information in the analytical literature on the instability of modulation amplitudes [13]. Therefore, work on the relation of linear dependence of manganese(II) and DPPH amplitudes on this factor was not considered necessary.

In contrast, when the saturation region of both curves (e.g., to $\Delta H = 14$ Oe) is reached, as shown in Fig. 4, a 10—100-fold decrease in the detection limit can be achieved without any appreciable increase of error in the results from the possible small uncontrolled variations of the amplitude modulation. When the adjacent standard procedure is used outside the linear region of the curve (Fig. 4), the value of the modulation amplitude, once established, must not be altered without special preliminary investigations, because the conventional rules of signal normalization [13] are not valid in this case.

The optimal values of the SHF radiation power, modulation phase, time and field scanning rate constants were maintained constant throughout the whole period of operation with only the precalibrated amplification of the receiver being varied. When the same sample tube with a fixed adjacent standard was used to record the spectra from samples with significantly different manganese(II) contents, it was sometimes necessary to change the amplification in the spectrum scanning between the DPPH and manganese lines. In doing so, great care was taken that the time between the amplification change and the beginning of recording of the manganese line was not less than ten time constants.

TABLE 1

Precision (standard deviation, s_r, for n determinations) of the e.s.r. determination of manganese(II) in cadmium selenide

Mn content (%)	1×10^{-4}	5×10^{-4}	1×10^{-3}	3×10^{-3}	7×10^{-3}	1×10^{-1}
s_r	0.051	0.024	0.025	0.048	0.018	0.005
n	6	5	3	6	6	5

TABLE 2

Results of the e.s.r. and flame atomic-absorption determination of manganese in cadmium selenide samples ($P = 0.95$)

Sample no.	E.s.r.			A.a.s.		
	Mn content ($\times 10^{-3}$%)	n^a	m^b	Mn content ($\times 10^{-3}$%)	n^a	m^b
1	1.23 ± 0.17	2	13	1.24 ± 0.05	6	48
2	2.81 ± 0.14	3	12	2.83 ± 0.10	6	48
3	7.75 ± 0.45	2	13	7.51 ± 0.10	6	48

[a]Number of replicate measurements of the signal of a sample. [b]Number of points on the calibration plot.

Analytical characteristics of the method

In the concentration range of 10^{-4}—0.1% manganese(II), the width of the spectral lines is invariable, and the calibration plot constructed from spectrum amplitudes of samples with known composition is linear. Among the samples of high-purity cadmium selenide available, none had a manganese(II) content of less than 1×10^{-4}%, but the signal/noise ratio for a sample with this minimum content indicated that, with the use of the RE-1306 e.s.r. spectrometer, the detection limit for manganese(II) is about 5×10^{-6}%.

The precision for determinations of different manganese(II) contents is given in Table 1.

To check the accuracy of the method, a few cadmium selenide samples with unknown manganese content were analyzed simultaneously by the atomic absorption and e.s.r. spectrometric methods. For e.s.r. spectrometry, a calibration chart was constructed on the basis of signals from samples with known metal contents. Both the reference and test samples were synthesized under conditions that eliminated the possibility of oxidation of manganese(II) to higher oxidation states. There is a good agreement between the results of the analyses by the two methods (Table 2); the larger confidence limits for the e.s.r. data result from fewer reference samples and, consequently, from fewer points used to construct the calibration plot.

Conclusions

The determination of manganese(II) in cadmium selenide is methodologically simple. It is not necessary to use a low-temperature installation or single-crystal samples. Over a wide concentration range, it is possible to use the simplest measure of signal intensity, i.e., the amplitude of the first-derivative curve. The method exhibits high sensitivity; even with a rather insensitive e.s.r. spectrometer, the detection limit is about 5×10^{-6}%, which is 1.5 orders of magnitude lower than the limit provided by flame atomic-absorption spectrometry. The e.s.r. technique allows highly sensitive determinations of manganese even in very pure samples. Unlike most other techniques, e.s.r. does not require dissolution of the sample which often results in the release of toxic selenium-containing gases. The absence of the dissolution stage makes the procedure rapid (1—2 min) and saves the sample. In some cases, the capacity of the e.s.r. technique to determine only manganese(II) appears to be beneficial. It tends to be assumed that when cadmium selenide is saturated with elemental selenium vapour, the manganese present in the semiconductor may be converted to higher oxidation states. The e.s.r. technique could serve as a reliable method of determining the degree of oxidation.

Preliminary investigations have shown that manganese(II) can also be determined by a very similar procedure in zinc selenide and cadmium sulfide.

The authors are grateful to G. F. Telegin for the atomic absorption analyses of the samples.

REFERENCES

1 H. A. Buckmaster, Magn. Reson. Rev., 8 (1983) 283.
2 T. A. Kennedy, Magn. Reson. Rev., 7 (1981) 41.
3 A. L. Porte, Electron Spin Reson., 7 (1982) 69.
4 I. B. Goldberg, Electron Spin Reson., 6 (1981) 1.
5 G. H. Stauss, J. J. Krebs, S. H. Lee and E. M. Swiggard, J. Appl. Phys., 50 (1979) 6251.
6 R. S. Title, in M. Alen and J. S. Prener (Eds.), Physics and Chemistry of II—VI Compounds, North-Holland, Amsterdam, 1967, p. 265.
7 J. E. Wertz and J. R. Bolton, Electron Spin Resonance, Elementary Theory and Applications, McGraw-Hill, New York, 1972, p. 303.
8 R. S. Title, Phys. Rev., 130 (1963) 17.
9 O. Matumura, J. Phys. Soc. Jpn., 14 (1959) 108.
10 B. Vigouroux, J. C. Gourdon, P. Lopez and J. Pescia, J. Phys. E: 6 (1973) 557.
11 I. B. Goldberg and H. R. Crowe, Anal. Chem., 49 (1977) 1353.
12 Yu. N. Molin, V. M. Chibrikin, V. A. Shabalkin and V. F. Shuvalov, Zavodsk. Lab., 32 (1966) 933.
13 W. G. Bryson, D. P. Hubbard, B. M. Peake and J. Simpson, Anal. Chim. Acta, 77 (1975) 107.

Analytica Chimica Acta, 185 (1986) 127—136
Elsevier Science Publishers B.V., Amsterdam — Printed in The Netherlands

THE FLUORIDE ION-SELECTIVE ELECTRODE IN FLOW INJECTION ANALYSIS
Part 1. General Methodology

WOLFGANG FRENZEL* and PETER BRÄTTER

Hahn-Meitner-Institut für Kernforschung, Arbeitsgruppe Spurenelementforschung in der Biomedizin, Glienicker Str. 100, D-1000 Berlin-West 39 (Federal Republic of Germany)

(Received 20th December 1985)

SUMMARY

A simple flow-injection system for determination of traces of fluoride by means of the fluoride-selective electrode is presented. A comparison of several flow-cell arrangements confirmed the advantages of a wall-jet design. Systematic investigations of the parameters affecting response times (i.e., polishing procedure, flow rate, carrier composition) established the optimal experimental conditions for measurements down to 1 $\mu g\ l^{-1}$ fluoride. Calibration plots in the lower $\mu g\ l^{-1}$ range were neither Nernstian nor linear, but good precision (0.5—5%) was obtained even when the potential differences for concentration steps of one decade were as small as 3 mV.

Since the introduction of the solid-state fluoride-selective electrode by Frant and Ross in 1966 [1], numerous papers have borne witness to its wide applications. The outstanding features of this electrode include high selectivity, stability and wide working range. The detection limit in batch procedures is about 10^{-6} mol l^{-1}, although the electrode responds down to 10^{-9} mol l^{-1} [2, 3] when ion buffers are used. However, determinations at fluoride concentrations below 10^{-5} mol l^{-1} are tedious and often suffer from poor reproducibility.

The incorporation of the fluoride-selective electrode in continuous flow [4—6] and flow injection systems [7—9] has immense benefits when compared with stationary measurements. Manipulations are no longer prone to subjective errors of the operator and interferences caused by displacement of the electrode are avoided [10, 11]. High sampling rates have been obtained [8] and remarkable detection limits have been reported [7]. In the present study, the performance characteristics of the fluoride electrode in flow injection analysis (f.i.a.) were systematically examined with respect to various parameters which affect the response time. General guidelines are given for the layout of the flow system to match required concentration ranges, with special emphasis on trace determinations (below 100 $\mu g\ l^{-1}$ fluoride) and high sample throughput. Investigations on interference problems and the feasibility of application to environmental and biological studies will be presented in later papers.

0003-2670/86/$03.50

EXPERIMENTAL

Apparatus

All measurements were made with Orion 96-09 combination fluoride electrodes (Orion Research, Cambridge, MA). A Knick 645 pH meter (Knick, Berlin, F.R.G.) connected to a strip-chart recorder was used to record the electrode potential with respect to time. A variable d.c. source was connected in parallel with the recorder input to provide an offset of up to 1.0 V and thus allow for maximum recorder sensitivity.

The flow-injection system was built around a manual injection valve with variable loop length. The carrier solution was propelled either by gravity flow or by means of a peristaltic pump (Gilson Minipuls). Various flow-cell designs (Fig. 1) were constructed and tested. The wall-jet cell (Fig. 1a) was made from a piece of teflon in which holes were drilled to insert the fluoride combination electrode, the inlet screw and stainless steel outlet capillary. The distance between inlet nozzle and electrode surface can be changed by turning the screw. The open cells (Fig. 1b—d) were simply made by fixing the electrode and the end of the tubing with ordinary laboratory clamps.

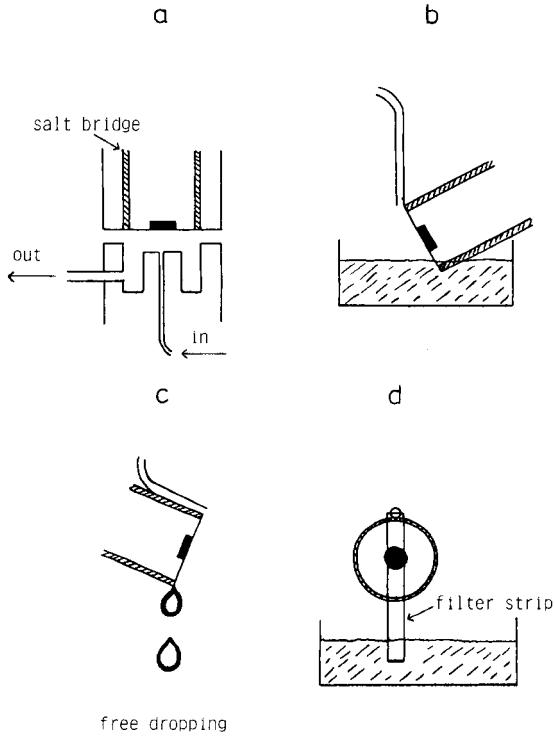

Fig. 1. Different flow-cell arrangements for flow-injection potentiometry: (a) wall-jet detector with variable distance between inlet nozzle and sensing membrane; (b) cascade-type detector; (c, d) parallel flow without and with filter strip to maintain continuous liquid stream.

The idea of using a small filter strip to maintain a continuous liquid stream along the sensing crystal was taken from recent work on electrochemical stripping analysis [12] and flow-injection potentiometry [13]. Teflon tubing (0.5 mm i.d.) was used for interconnections.

Chemicals and solutions

Fluoride standard solutions were prepared by appropriate dilution of a 1 g l^{-1} stock solution (Merck Titrisol) with deionized/twice-distilled water. Unless otherwise stated, TISAB-III (Orion) was added to standards and samples to give a 1:10 dilution as recommended by the manufacturer. Aluminium and iron standards (1 g l^{-1}, respectively) were also prepared from Merck Titrisol solutions. The carrier solutions were (1 + 9) diluted TISAB-III, containing varying amounts of fluoride and were deaerated before measurements by use of a water vacuum pump. This prevents the accumulation of air bubbles at the electrode surface when the wall-jet cell is used.

Procedure

The flow rate was adjusted to the required value by changing the height of the reservoir (gravity flow) or by selecting the appropriate pump speed and pumping tube (peristaltic pump). The electrode potential was recorded until a stable baseline was obtained. For carrier fluoride concentrations in the 0.01—10 mg l^{-1} range, this usually took less than 5 min. Further electrode drift was found to be due to the liquid junction. Therefore, as required, the electrode was removed and the conical diaphragm was cleaned and rinsed with some milliliters of the electrolyte solution. At carrier fluoride concentrations below 10 μg l^{-1}, continuous drift and baseline fluctuations were sometimes observed, which could not be overcome by cleaning the liquid junction.

To calibrate the electrodes under steady-state conditions, the standard fluoride solutions were used as a carrier. The potentials were read when a stable potential was achieved. For flow-injection measurements, the standard solutions were injected and the transient potential change was recorded. Subsequent injections were made after return to the baseline. Carry-over is thus avoided (or controlled) provided that the injection loop is free from seepage and the previous sample is washed out carefully. Generally, the loop was rinsed with a fivefold loop volume of twice-distilled water and a threefold sample volume. This was particularly necessary when very low concentrations were measured at high carrier fluoride concentrations and when samples with large concentration differences were analyzed.

RESULTS AND DISCUSSION

Steady-state conditions

Prior to flow-injection measurements all electrodes were calibrated in batch and continuous-flow mode under steady-state conditions. Figure 2A shows the results for four different electrodes. The responses are nearly

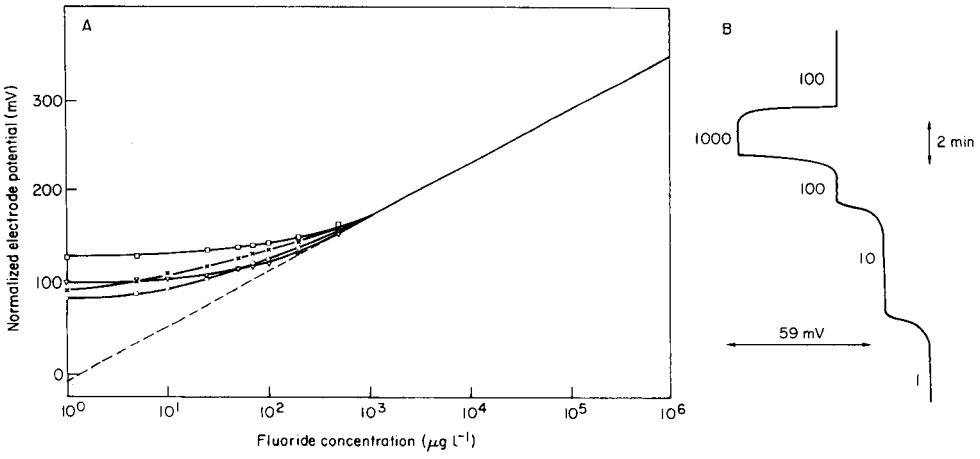

Fig. 2. (A) Calibration plots for four different fluoride-selective electrodes in the 0.001—1000 mg l^{-1} range under steady-state conditions in continuous flow. (B) Recorder trace for steady-state calibration in a flow system in the 0.001—1 mg l^{-1} range; the numbers on the trace refer to μg l^{-1} fluoride.

identical in the 1—1000 mg l^{-1} range with slopes between 57.2 and 59.0 mV. Below 1 mg l^{-1}, all responses deviate from linearity in varying degrees. The original recorder trace for a steady-state calibration under flow conditions in the 0.001—1 mg l^{-1} range is shown in Fig. 2B. Electrode drift was usually less than 1 mV h^{-1}. In batch calibration procedures, however, the electrode potential for the same solution measured before and after exposure of the sensing membrane to air was sometimes found to change by more than ±2 mV. This indicates the increased precision of flow systems compared with batch procedures [10].

Transient conditions

In flow-injection potentiometry, limited dispersion [14] is advisable because the original composition of the sample should be measured. When comparatively large sample volumes are injected and the distance between the point of injection and the electrode is short, the centre of the sample zone is not dispersed and a steady state can be reached, at least briefly, if the response time (the time necessary to reach equilibrium potential) is shorter than the time required for the sample zone to pass the electrode. However, the response time of a particular electrode depends on several parameters. In flow systems with high or medium dispersion, the response profile of the electrode is the result of the superimposition of the concentration change and the response-time characteristics of the electrode.

Parameters affecting response time

Generally, the response time of ion-selective electrodes is affected by the surface condition of the membrane, the boundary layer thickness, the height

of the concentration jump, the direction of concentration change, the sample composition and, in flow systems, by the composition of the carrier solution.

Cell geometry. Numerous flow-through systems for potentiometry have been described, e.g., for industrial on-line monitoring [15, 16] and continuous flow measurements (AutoAnalyzer principle) [17, 18]. Detector cells of different construction have been reported, e.g., thin-layer, tubular and flow-through caps [16, 19]. In flow-injection potentiometry, the question of the cell design is of special importance because small dead volumes and well-defined hydrodynamic conditions are required. The transient signals are much more sensitive to fluctuations in flow and irregularities in dispersion. Růžička et al. [20] proposed a cascade-type detector which has been used in several other investigations. However, amperometric and voltammetric studies [21] have shown that a wall-jet design is favorable; the solution is spread uniformly over the entire membrane and carry-over is minimal. The effective cell volume depends on flow rate and distance between inlet nozzle and electrode surface. It can be as small as 1 μl under normal experimental conditions.

A comparison of the four cell configurations shown in Fig. 1 with respect to response time and carry-over confirmed these findings. The baseline stability is excellent for the wall-jet and filter strip covered thin-layer cell. The other two designs lack stability, probably because of irregular flow conditions at the membrane and the diaphragm. The rest of this work was done with the wall-jet cell.

Surface condition. The europium-doped lanthanum fluoride sensing crystal is sensitive to adsorption and contamination. Only clean and scratch-free surfaces provide fast response and reproducible signals. Polishing of the membrane was proposed by van Oort and van Eerd [22] to achieve faster response. Their procedure was used and proved to be beneficial, although only minimal improvement was obtained for some electrodes. Baseline drift and bad signal reproducibility during the first 10—30 min was, however, observed when alumina powder was used for polishing. This is probably due to aluminium contamination of the surface, which is only slowly removed. The use of 0.3-μm diamond paste is therefore recommended. The decreased response time after electrode polishing remains for many working hours and in some cases for several weeks without significant change, depending on the sample solutions used. Therefore, the polishing procedure was only repeated when unusually small signals were obtained.

Carrier composition. The composition of the carrier (ionic strength, pH, viscosity) should be as similar as possible to that of the samples. Therefore, TISAB III was used as recommended. To prevent the electrode being in a "vacuum" when no sample is injected, appropriate fluoride concentrations were added to the carrier solution. This is advantageous for baseline stability, response time and wash characteristics [5] and has been used by other workers [7, 22]. In Table 1, the peak height (mV) is given for the injection of fluoride solutions in the 1 μg l^{-1} to 1 mg l^{-1} range into a carrier containing

TABLE 1

Influence of fluoride concentration in the carrier on response[a]

Fluoride injected ($\mu g\ l^{-1}$)	Peak height (mV) with 1—1000 $\mu g\ l^{-1}$ F^- in carrier			
	1	10	100	1000
1	—	3.7	10.3	21.5
10	5.2	—	6.5	19.4
100	11.1	7.2	—	16.2
1000	39.0	35.1	34.7	—

[a]Flow rate 1.3 ml min^{-1}, injection volume 125 μl.

different amounts of fluoride. It is obvious that injections of samples with concentrations above the carrier content give higher signals for the same concentration step compared to the reverse case. This is in agreement with earlier findings [23]. In Fig. 3, this is demonstrated for the step between 0.1 and 1 mg l^{-1} and vice versa. Table 2 lists the potential differences obtained for three decadal changes in concentration depending on the carrier fluoride concentration. These data clearly demonstrate that the highest signals are obtained when the carrier concentration is at the low end of the required working range.

Injection volume. The higher the injection volume, the longer the residence time of the sample, and so the greater the likelihood of attaining the steady-state potential [14]. Attainment of a steady state is, of course, unnecessary in flow-injection potentiometry and is achieved at the cost of sample through-

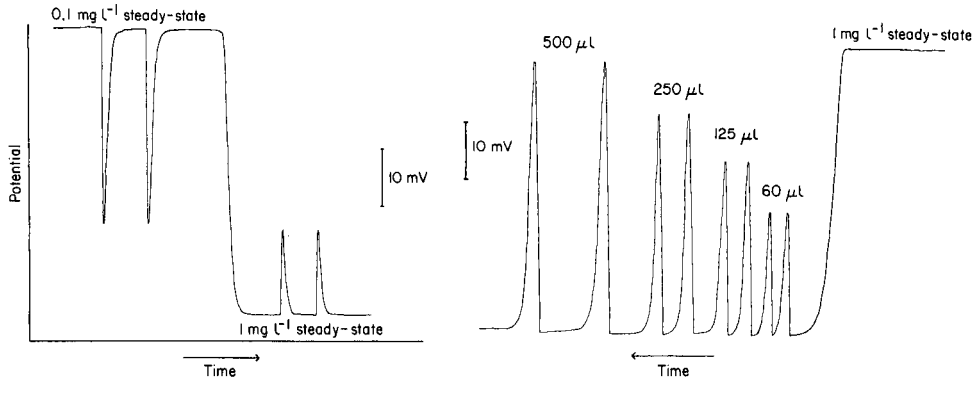

Fig. 3. Effect of direction of concentration change on the electrode response. Injection of a 1 mg l^{-1} fluoride standard into a carrier containing 0.1 mg l^{-1} fluoride leads to about 75% of the steady-state signal, whereas in the reverse case only 25% is obtained.

Fig. 4. Influence of injection volume on signal height. Flow rate 0.5 ml min^{-1}, carrier fluoride concentration 0.1 mg l^{-1}, sample concentration 1 mg l^{-1}. For comparison, the steady-state signal for 1 mg l^{-1} fluoride is shown on the right.

TABLE 2

Potential difference (p.d.) for decadal concentration steps[a]

Concentration step ($\mu g\ l^{-1}$)	P.d. (mV) with 1—1000 $\mu g\ l^{-1}$ F^- in carrier			
	1	10	100	1000
1—10	5.2	3.7	3.8	2.1
10—100	5.9	7.2	6.5	3.2
100—1000	27.9	27.9	34.7	16.2

[a]Flow rate 1.3 ml min^{-1}, injection volume 125 μl.

put and higher consumption of sample and reagent volumes. Figure 4 shows a typical recorder trace for consecutive injections of the same sample at increasing volume. A 500-μl sample gives about 95% of the maximum value. The data cannot be generalized because the situation is response time-dependent. At low concentrations, even a 5-ml sample may not produce the steady-state potential, whereas at concentrations above 1 mg l^{-1} this is usually attained with 100—200 μl of sample volumes.

Effect of flow rate. With a constant injection volume, the residence time of the sample is inversely proportional to the flow rate. Therefore, low flow rates would seem most likely to produce a steady-state signal, but of course lower flow rates also lead to increased response times (thicker boundary layers). Again, the situation is also dependent on all the factors influencing the response time (e.g., carrier fluoride concentration, concentration step direction and height). In Fig. 5 this is demonstrated for two different electrodes under different experimental conditions. In Fig. 5A, gravity flow was

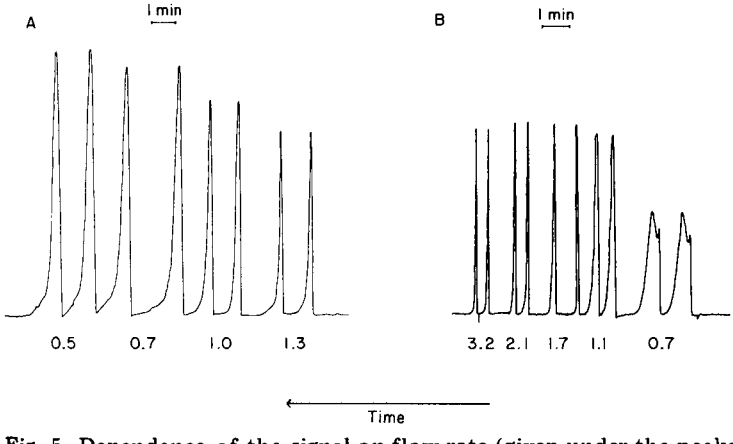

Fig. 5. Dependence of the signal on flow rate (given under the peaks in ml min^{-1}) for two electrodes under different experimental conditions: (A) gravity flow, 1 mg l^{-1} fluoride sample, 0.1 mg l^{-1} fluoride carrier, injection volume 125 μl; (B) peristaltic pump 1 mg l^{-1} fluoride sample, 0.25 mg l^{-1} fluoride carrier, injection volume 125 μl. The double peak in B at 0.7 ml min^{-1} is due to back-diffusion of the sample, caused by pump pulsation.

used and 125-μl samples containing 1 mg l^{-1} fluoride were injected. The carrier fluoride concentration was 0.1 mg l^{-1}. A steady decrease is observed with increasing flow rate largely because the response time of the electrode is not fast enough to follow the concentration change. In Fig. 5B, the signal increases gradually up to 2.1 ml min^{-1}, which suggests that the decrease in response time caused by a thinner boundary layer has more effect than the shorter residence time of the sample. It can be concluded that several processes influence the responses and their overall magnitude is a characteristic of the particular electrode. The peak width decreases with increasing flow rate (Fig. 5), which will be of advantage when high sample throughput is required; this has to be weighed against the slightly worse sensitivity.

Calibration

Trojanowicz and Matuszewski [24] have discussed the limitation of linear response in flow-injection potentiometry. Their assumptions and results are, however, only applicable in the concentration range where the electrode behaves in Nernstian fashion. In the non-Nernstian concentration range (below about 1 mg l^{-1} for the fluoride electrode in the flow system), the calibration plots are neither Nernstian nor linear but in practice there is no serious problem with curve-fitting.

All parameters influencing the response time of the electrode cause a change in the shape of the calibration plot and can be optimized to match the required working range. As stated above, the carrier fluoride concentration should be at the low end of the calibration curve. This requires knowledge of the sample concentration. It is, however, possible to calibrate the electrode below and above the fluoride concentration of the carrier. Figure 6A shows a recorder trace for a calibration in the 1—1000 μg l^{-1} range and Fig. 6B shows the corresponding calibration plot.

The reproducibility of triple injections of the same standard is better than 1% for concentrations above 100 μg l^{-1} and 2—5% for lower concentrations. The reliability of the calibration was established by successive re-injection of

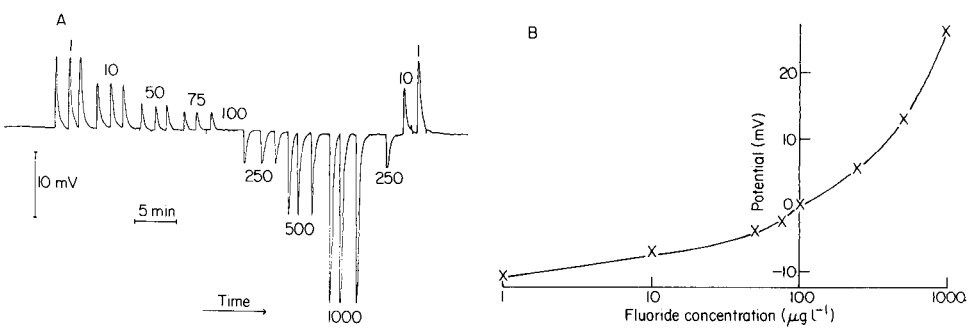

Fig. 6. Typical recorder trace (A) and calibration plot (B) for fluoride concentrations in the 1—1000 μg l^{-1} range. Carrier fluoride concentration 100 μg l^{-1}, flow rate 1.0 ml min^{-1} (gravity flow), injection volume 125 μl. The numbers on the peaks refer to μg l^{-1} fluoride.

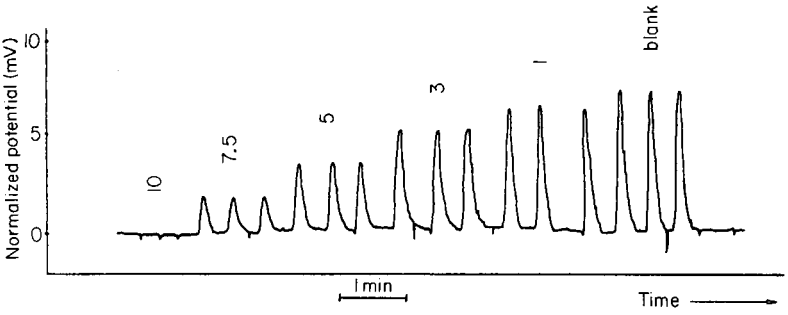

Fig. 7. Triplicate injections of standards with low fluoride content (10—1 $\mu g\ l^{-1}$ as indicated on the peaks). Carrier fluoride concentration 10 $\mu g\ l^{-1}$, flow rate 1.2 ml min^{-1}, injection volume 125 μl.

standard solutions during a period of 3 h; the deviation was found to be insignificant. Excellent stability of the baseline (usually the fluctuations were below the resolution of the pH meter, i.e., 0.1 mV) suggests that better precision would be achieved with better instrumentation.

Figure 7 shows the signals for injections of a blank solution and 1, 3, 5, 7.5 and 10 $\mu g\ l^{-1}$ fluoride standards, respectively. The good reproducibility enables precise measurements to be obtained even at very low levels. Even concentrations below the $\mu g\ l^{-1}$ range appear to be accessible. A critical evaluation of fluoride determinations at ng l^{-1} levels and detection limits in flow-injection potentiometry in general will be reported later.

Conclusions

Earlier findings about the application of the fluoride electrode in flow injection analysis [7, 8, 22] are generally confirmed in this work. A simple inexpensive system with outstanding features is described. Small samples (10—250 μl) are sufficient to determine fluoride. With 125-μl samples, down to 1 $\mu g\ l^{-1}$ fluoride can be quantified according to absolute detection limits in the picogram range. The residence time of the sample is usually below 10 s and baseline return is obtained within 20—60 s, which enables sampling rates of 60—180 h^{-1} depending on the concentration. The flow-injection system is very flexible for dealing with different concentration ranges under slightly varied experimental conditions. The wall-jet flow-cell arrangement seems to be particularly suitable for flow-injection potentiometry; fast response time, minimum carry-over and good surface cleaning properties are observed. Calibration plots are neither linear nor Nernstian at the low concentration range because of the transient responses in f.i.a.

The authors express their gratitude to Jolanta Oleksy for her assistance in the initial stage of this work and to Frank Chisela and Dieter Gawlik for critical comments.

REFERENCES

1 M. S. Frant and J. P. Ross, Science, 154 (1966) 1553.
2 E. W. Baumann, Anal. Chim. Acta, 54 (1971) 189.
3 J. Buffle, N. Parthasarathy and W. Haerdi, Anal. Chim. Acta, 68 (1974) 257.
4 D. E. Erdmann, Environ. Sci. Technol., 9 (1975) 252.
5 D. C. Cowell, Anal. Chem. Biochem., 14 (1977) 269.
6 J.-C. Landry, F. Cupelin and C. Michal, Analyst, 106 (1981) 1275.
7 J. Slanina, W. A. Lingerak and F. Bakker, Anal. Chim. Acta, 117 (1980) 91.
8 P. van den Winkel, G. de Backer, M. Vandeputte, N. Mertens, L. Dyron and D. L. Massart, Anal. Chim. Acta, 145 (1983) 207.
9 T. Greatorex and P. B. Smith, J. Inst. Water Eng. Sci., 39 (1985) 81.
10 E. Pungor, Z. Fehér, G. Nagy and K. Tóth, Crit. Rev. Anal. Chem., 14 (1983) 175.
11 K. Tóth, G. Nagy, Z. Fehér, G. Horvai and E. Pungor, Anal. Chim. Acta, 114 (1980) 45.
12 W. Frenzel and G. Schulze, Analyst, in press.
13 L. Ilcheva and K. Camann, Fresenius Z. Anal. Chem., 322 (1985) 323.
14 J. Růžička and E. H. Hansen, Anal. Chim. Acta, 114 (1980) 19.
15 O. Rochefort, J. Gleyvod and D. Petrilli, Analusis, 12 (1984) 331.
16 D. Eicken, Gewässerschutz, Wasser, Abwasser, 39 (1979) 181.
17 M. Trojanowicz, Anal. Chem. Symp. Ser., 18, Part A, Electrochemical Detection in Flow Analysis, Matrafüred, Elsevier, Amsterdam, 1982, p. 189.
18 M. Vandeputte, L. Dyron and D. L. Massart, Anal. Chim. Acta, 91 (1977) 113.
19 E. Pungor, Z. Fehér, G. Nagy, K. Tóth, G. Horvai and M. Gratzl, Anal. Chim. Acta, 109 (1979) 1.
20 J. Růžička, E. H. Hansen and E. A. Zagatto, Anal. Chim. Acta, 88 (1977) 1.
21 B. Fleet and C. J. Little, J. Chromatogr. Sci., 12 (1974) 747.
22 W. J. van Oort, E. J. J. M. van Eerd, Anal. Chim. Acta, 155 (1983) 21.
23 J. Mertens, P. van den Winkel, D. L. Massart, Anal. Chem., 48 (1976) 272.
24 M. Trojanowicz, W. Matuszewski, Anal. Chim. Acta, 138 (1982) 71.

Analytica Chimica Acta, 185 (1986) 137—158
Elsevier Science Publishers B.V., Amsterdam — Printed in The Netherlands

COPPER ION-SELECTIVE CHALCOGENIDE GLASS ELECTRODES
Analytical Characteristics and Sensing Mechanism

YU. G. VLASOV*, E. A. BYCHKOV and A. M. MEDVEDEV
Department of Chemistry, Leningrad University, Leningrad 199164 (U.S.S.R.)
(Received 12th April 1985)

SUMMARY

New copper ion-selective electrodes based on chalcogenide glasses, $Cu_xAg_{25-x}As_{37.5}Se_{37.5}$, display high copper(II) ion sensitivity with Nernstian response in the range pCu 1—6, short response time, high selectivity, potential stability and reproducibility. These electrodes are 10—30 times more sensitive in strongly acidic media than crystalline copper ion-selective sensors and are superior to the copper(I) selenide electrode in selectivity and resistance to acids and oxidation. A model is proposed to explain the ion sensitivity of these chalcogenide glass sensors. The sensitivity depends on direct exchange of copper(II) ions between solution and the modified surface layer of the glass. The modified surface layer is formed as a result of partial destruction of the glass network on soaking in solution; its atomic density is 2.0—2.5 times less than that of the original glass. The structural defects and hollows make fast copper(II) ion migration within the modified surface layer possible. Exchange sites in this layer can be formed by both disproportionation and oxidation of copper(I) in the glass network, as well as by diffusion of copper(II) ion from solution in the case of glasses with low copper content. Experimental confirmation of this model is provided by x-ray, photo-electron and scanning Auger electron spectroscopy.

Chalcogenide glasses are promising membrane materials for solid-state ion-selective electrodes. Trachtenberg and co-workers [1, 2] were the first to show that Fe-doped $Ge_{28}Sb_{12}Se_{60}$ vitreous alloys are sensitive to iron(III) ions. Vlasov and Bychkov [3] studied the electronic properties and local environment of iron in these glasses and established that the potential-generating process at the chalcogenide glass/solution interface was electronic exchange between Fe^{2+} (d^6) deep donor centers on the membrane surface and electron acceptors in solution. It was pointed out by Owen [4] that reversible solid-state contact to semiconducting chalcogenide glass membranes is easy to obtain. Lead ion-selective electrodes based on silver ion-conducting glasses, 0.6 $AgAsS_2$/0.4 PbI_2, were investigated by Bohnke et al. [5, 6]. Vlasov et al. [7—10] showed that chalcogenide glass sensors have several advantages compared to the corresponding crystalline ones; for example, silver ion-selective electrodes based on Ag-As-S or Ag-As-Se glasses make it possible to conduct direct potentiometric determinations of silver ions in 6 M nitric acid [7]. Chalcogenide glasses doped with lead iodide or sulfide are 5—20 times more selective to cadmium ions and 10—100 times more

stable to treatment with active oxidizing agents [8, 9]. Greater stability in strongly acidic media and higher selectivity to alkali cations, thallium, barium, nickel and iron(III) ions are the advantages of cadmium ion-selective sensors based on chalcogenide glasses [10].

Copper(II) ion-sensitive chalcogenide glass electrodes were described by several authors. Jasinski et al. [11] found high sensitivity and selectivity for glassy/crystalline $Cu_x(As_2S_3)_{1-x}$ materials. Owen [4] and Tohge et al. [12] studied the electrode response of copper-arsenic-selenium glasses.

The aim of the study reported here was to investigate the analytical characteristics of new copper ion-selective electrodes based on Cu-Ag-As-Se glasses, as well as the processes which govern the ionic sensitivity of chalcogenide glass sensors. Depending on copper content, $Cu_xAg_{25-x}As_{37.5}Se_{37.5}$ vitreous alloys can be either narrow band non-crystalline p-type semiconductors or amorphous solid electrolytes with high silver-ion conductivity [13]. Thus, investigations of the electrode response of these membranes, as well as of glasses with or without silver, could elucidate the role of transport characteristics in the bulk of the membrane and the role of silver in the behaviour of the sensors.

EXPERIMENTAL

Glass synthesis and electrode preparation

$Cu_xAg_{25-x}As_{37.5}Se_{37.5}$ alloys containing 0, 0.05, 0.1, 0.2, 0.5, 1.0, 2.0, 5.0, 10.0, 12.5, 15.0, 20, 23, 24 and 25 atom% copper were prepared. Evacuated (0.1—0.01 Pa) quartz ampoules containing the high-purity elements, with a total mass of 3 g, were heated in a furnace for 8—12 h at a maximum temperature of 1200 K. Ampoules were air-quenched, with an average cooling rate of 5—6 K s^{-1}. The amorphous state and uniformity of the alloys were confirmed by x-ray diffraction, infrared and scanning electron microscopy. The glass composition was checked with an electron microprobe.

To prepare electrode membranes, discs (1—3 mm thick and 6—10 mm in diameter) were cut from the melts. All membranes were thoroughly polished with very fine diamond paste and sealed with epoxy resin into PVC tubes. The inner solution was 0.05 M $Cu(NO_3)_2$/0.05 M $AgNO_3$/0.1 M KNO_3, and a silver wire was the inner reference electrode.

To prepare the all-solid-state electrode, the membrane was polished on the outer side only and a silver layer was obtained by vacuum evaporation on the inner side. A wire lead was attached to the latter with silver microadhesive. Then the inner side was coated with epoxy resin and the membrane was sealed into a PVC tube.

Fifty-two electrodes were prepared for electrochemical measurements. Several (4—6) electrodes of each composition were studied, except for sensors with low copper contents (0.05—2.0 atom% Cu). To compare the electrode properties of different membrane materials, all electrochemical measurements were taken with chalcogenide glass sensors and crystalline electrodes of two

types: (i) the copper ion-selective electrode (Crytur 29-17) with $Cu_{1.8}Se$ single-crystal membrane, and (ii) the polycrystalline CuS/Ag_2S sensor prepared as described earlier [14].

Methods

Potentiometric measurements. The potentiometric measurements were made with the following electrochemical cells:

$$\text{Ag, AgCl} \left| \begin{matrix}\text{KCl}\\ \text{sat.}\end{matrix} \right| \text{KNO}_3 \left| \begin{matrix}\text{test}\\ \text{solution}\end{matrix} \right| \text{glass} \left| \begin{matrix}\text{Cu(NO}_3)_2\\ \text{AgNO}_3\end{matrix} \right| \text{Ag} \qquad \text{(I)}$$

$$\text{Ag, AgCl} \left| \begin{matrix}\text{KCl}\\ \text{sat.}\end{matrix} \right| \text{KNO}_3 \left| \begin{matrix}\text{test}\\ \text{solution}\end{matrix} \right| \text{glass} \left| \text{Ag} \right. \qquad \text{(II)}$$

Test solutions in the concentration range 10^{-8}—10^{-1} M were prepared by successive tenfold dilutions of 1 M copper(II) nitrate stock solution. Solutions with low copper concentration (10^{-5}—10^{-8} M) were prepared, just before the measurements, in a teflon cell by addition of known quantities of concentrated copper(II) nitrate solutions to a standard volume of distilled water or supporting electrolyte.

Selectivity coefficients were measured by the mixed solution method. Known volumes of copper(II) nitrate test solutions were added to 100 ml of a 1 M solution of interfering ion salt (usually nitrate). The selectivity coefficient was calculated from the equation

$$K^{\text{pot}}_{\text{Cu}^{2+},\text{M}^{z+}} = c_{\text{Cu}^{2+}}/(c_{\text{M}^{z+}})^{2/z}$$

where $c_{\text{Cu}^{2+}}$ is the copper(II) ion concentration corresponding to the intersection of the interfering ion response and the response to copper(II) ion. Concentrations not activities were used in these calculations because all measurements were taken in solutions having constant ionic strength. Selectivity coefficients for lead and cadmium ions were measured in 0.1 and 1.0 M solutions of interfering ion. $K^{\text{pot}}_{\text{Cu}^{2+},\text{Fe}^{3+}}$ was measured at pH 1; the concentration of iron(III) (as nitrate) was 10^{-5}, 10^{-4} or 10^{-3} M. The selectivity coefficient $K^{\text{pot}}_{\text{Cu}^{2+},\text{Ag}^{+}}$ was determined by the separate solutions method.

The pH range of the electrodes was studied in solutions with constant copper(II) nitrate concentrations and the pH was adjusted by addition of nitric acid or potassium hydroxide. Experiments in strongly acidic media were done with copper(II) nitrate solutions in 1 and 3 M nitric acid.

For measurements of response times, known volumes of copper(II) nitrate test solution were added to a rapidly stirred solution in which the electrode was dipped.

All measurements were made at room temperature. A magnetic stirrer was used to stir solutions. The e.m.f. of the cells I and II was measured with a digital voltmeter. A high input-impedance recorder was used for response-time measurements.

Investigation of the copper valence state. E.s.r. spectra were taken in the X-band (9.5 GHz) at room temperature and at the temperature of liquid

nitrogen. Magnetic susceptibility was measured by Faraday's method in the temperature range 4.2—300 K with the help of a Setaram MGD3-12FG instrument.

Study of membrane surface. Surfaces were investigated on just-prepared glass specimens both before and after soaking in various aqueous solutions. The dynamics of alterations in surface composition was studied in 0.01 and 1.0 M copper(II) nitrate, and in 0.01 M copper(II) chloride. The specimens were dipped in the copper(II) ion solutions for different periods of time, washed with distilled water, blotted dry with filter paper, and put in the spectrometer chamber. A Hewlett-Packard 5950A ESCA instrument was used to record photoelectron spectra. X-ray Al-$K_{\alpha 1}$ radiation (monochromator) was used for photoelectron emission. Electron binding energies, E_b, were evaluated with respect to the carbon 1*s* line (E_b = 284.4 eV). Atomic ratios were calculated by the method of Wagner [15]. Collision cross-sections were taken from Scofield [16]. For quantitative comparison, the atomic ratios were calculated from the most intense peak of the elements involved.

Depth profiles of the components were studied with a Riber ASC 2000 scanning Auger microprobe. Argon ions with energy 2.5 keV were used for ion sputtering, the ion-current density being 75 μA cm^{-2}.

RESULTS

Glass-forming ability

Under the above conditions of synthesis and cooling, all alloys appeared to be amorphous and uniform. According to the electron microprobe study, the glass composition corresponded to original mixture composition. Sometimes, after intensive mechanical grinding and polishing, crystallites 5—20 μm in size were found in a few samples containing 2 and 5 atom% copper. Quantitative analysis of these crystallites with the electron microprobe showed that they contained 80—100 atom% arsenic. Probably this is connected with an inadequate period of synthesis, which could lead to spontaneous arsenic crystallization because of local heating of the glass surface during intensive mechanical treatment. The data obtained on these specimens are not discussed in the present paper.

Electrical properties

It was shown earlier [13] that alloys containing up to 2 atom% copper are solid electrolytes with a silver transference number of about unity. For the glass $Cu_5Ag_{20}As_{37.5}Se_{37.5}$, the ionic σ_i and hole σ_p conductivities at room temperature are comparable. Alloys containing $\geqslant$10 atom% copper are non-crystalline p-type semiconductors. The dependence of the glass conductivity at 298 K on composition is shown in Fig. 1. Small quantities of copper hinder silver ion transport in glass and slightly increase σ_p. This phenomenon resembles the mixed-alkali effect in oxide glasses and other ion conductors [17, 18], but it is likely to be due to increase in density of the glass structure

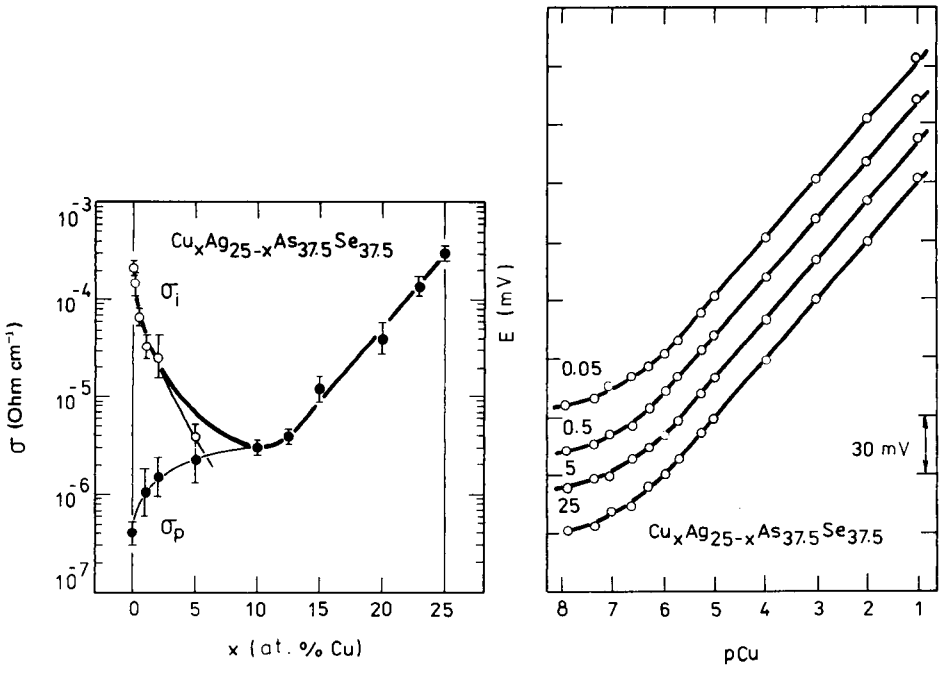

Fig. 1. Room-temperature (298 K) conductivity of $Cu_xAg_{25-x}As_{37.5}Se_{37.5}$ glasses: (○) ionic conductivity σ_i; (●) hole conductivity σ_p; the heavy line indicates total conductivity σ_t.

Fig. 2. Response of some $Cu_xAg_{25-x}As_{37.5}Se_{37.5}$ glass electrodes to copper(II) nitrate in 0.3 M KNO_3. Values of x (atom%) are shown on the calibration curves.

after addition of the first copper portions and corresponding decrease of silver ion mobility. The linear dependence of log $\sigma_{298\,K}$ on copper concentration x, when $x \geqslant 12.5$ atom% copper, is stipulated by the alteration of the top of the valence band of semiconducting glasses. Valence-band photoelectron spectra of the glasses [13] showed that the top of the valence band was formed by Cu 3*d* states, which determined the energy gap width of the glasses containing considerable quantities of copper, and consequently their electronic properties.

Copper valence state in glasses

Magnetic susceptibility measurements showed that $Cu_xAg_{25-x}As_{37.5}Se_{37.5}$ glasses are diamagnetic. In the low temperature range ($T < 40$ K), some decrease of diamagnetic susceptibility was observed which was connected with the presence of a small quantity of paramagnetic impurities (10^{-3}—10^{-4} atom%) in the glasses. These results show that in the glasses studied copper is present in the monovalent state Cu^+ (d^{10}), its 3*d*-level being filled up. According to e.s.r. data, the copper(II) concentration in the glass is not more than 10^{16} atoms cm^{-3}. This means that only one copper atom per million can be divalent.

The results of these investigations of copper valence states are in good agreement with those of Matias [19] and Taylor et al. [20], who also consider that copper in chalcogenide glasses is in the lower valence state.

Copper(II) ion response

The electrode responses of some chalcogenide glass sensors in copper(II) nitrate solutions with constant ionic strength (I = 0.3) are shown in Fig. 2. Electrodes with membranes of all compositions reveal high sensitivity to copper(II) ions. The Nernstian range of the electrode response is 10^{-1}—10^{-6} M copper(II) nitrate, and the detection limit is about 10^{-7} M. The slope S of the electrode responses of these sensors is about 30 mV/pCu, essentially the same as the theoretical value from the Nernst equation $E = E_0 + RT/2F \ln a_{Cu^{2+}}$. The slopes of the calibration curves of electrodes with low copper content ($x < 5$ atom% copper) were also Nernstian, but considerable drift of the standard potential E_0 (up to 50 mV) was observed during successive calibration measurements. The electrode with the $Ag_{25}As_{37.5}Se_{37.5}$ membrane appeared to be copper(II)-sensitive as well; its S value varied from 33 to 50 mV/pCu.

An unusual form of calibration curve with super-Nernstian slope in the low concentration range was observed in solutions with high ionic strength, $I > 1.0$, for sensors containing less than 10 atom% copper in their membranes (Fig. 3). The phenomenon will be discussed in detail below.

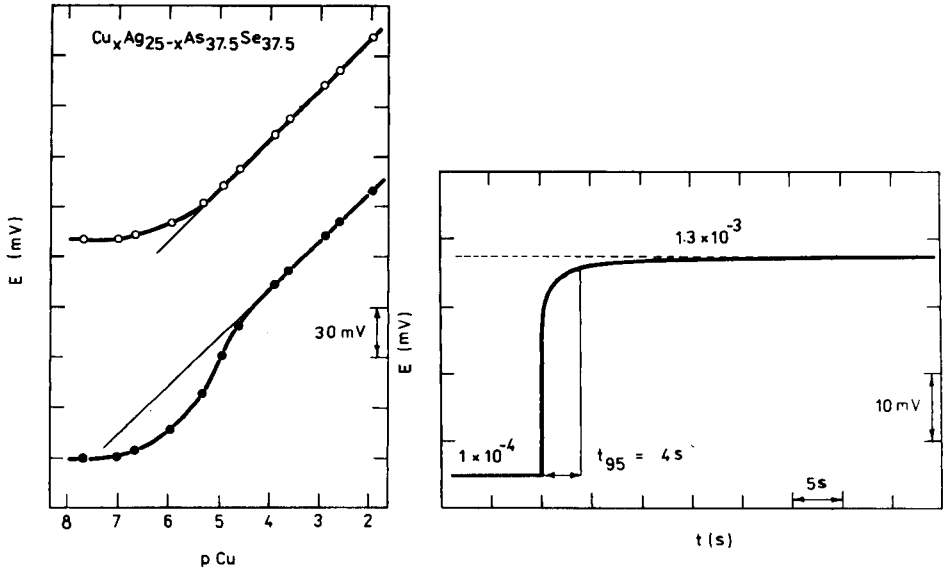

Fig. 3. Response of chalcogenide glass electrodes with different copper contents in solutions with high ionic strength, I = 3.0. Copper content: (○) 12.5—25.0 atom% Cu; (●) 0.05—10.0 atom% Cu.

Fig. 4. Typical response curve of a chalcogenide glass sensor (x = 12.5) for a change from 1 × 10^{-4} M to 1.3 × 10^{-3} M Cu(II).

The potential stability of the all-solid-state electrodes was slightly better than that of the sensors with internal solution. Sensitivity and Nernstian range of the electrodes of both types differed very little.

Chalcogenide glass sensors with copper content $x > 10$ atom% displayed stable and reproducible responses for 3—15 months. The potential stability of an electrode during a day was ±0.02 mV h^{-1}. The average E_0 drift during a year was ±6 mV. The standard potentials of electrodes with the same membrane composition differed by not more than ±5 mV. The standard deviation of E_0 did not exceed ±20 mV for sensors with different membrane composition.

Analytical response times, t_{95}, were about 10—15 s in diluted, and 3—4 s in concentrated, copper(II) solutions. Typical response dynamics are shown in Fig. 4. It should be noted that the t_{95} values observed characterize not only the electrode response itself, but also the diffusion kinetics of copper(II) ions in the solution and stagnant layer. This means that the t_{95} values mentioned depend on hydrodynamic conditions.

The sensitivity, response time and potential stability of crystalline copper ion-selective electrodes are quite similar to those of chalcogenide glass sensors.

Selectivity

A typical plot for the evaluation of selectivity coefficients is shown in Fig. 5. Selectivity coefficients, $K^{pot}_{Cu^{2+},M^{z+}}$, of chalcogenide glass electrodes (with x = 12.5—25 atom% copper) and crystalline copper(II) sulfide/silver sulfide and copper(I) selenide sensors, are summarized in Table 1. It can be seen that 10^5—10^6-fold amounts of alkali and alkali-earth cations, and 10^4—10^5-fold amounts of manganese(II), cobalt(II), nickel(II), zinc(II), lead(II) and cadmium(II) ions do not influence the chalcogenide glass electrode potential. The $K^{pot}_{Cu^{2+},Ag^+}$ value is 10^9—10^{10}, therefore silver ions must not be present during potentiometric determination of copper(II) ions. Considerable interference of iron(III) ions was also observed. The $K^{pot}_{Cu^{2+},M^{z+}}$ values in Table 1 are average selectivity coefficients for chalcogenide glass sensors containing 12.5—25 atom% copper in the membranes.

The selectivity of the polycrystalline CuS/Ag_2S membrane electrode was similar to that of the chalcogenide glass sensors. The single-crystal $Cu_{1.8}Se$ membrane electrode displayed worse selectivity for copper(II) ions. The difference in selectivity coefficients is the most striking for calcium(II), zinc(II), manganese(II) and iron(III) ions. The selectivity of the crystalline electrodes is in satisfactory agreement with earlier data [21].

The inadequate selectivity of the copper(I) selenide electrode to iron(III) and manganese(II) ions is probably connected with the high sensitivity of single-crystal membranes to oxidants in solution. Permanganate can be present in manganese(II) nitrate solutions, and manganese(II) ion can catalyze oxidizing reactions [22]. Vesely [23] pointed out earlier that Crytur copper ion-selective electrodes in very dilute copper(II) ion solution are sensitive to dissolved oxygen. Considerable sensitivity to oxidation is a

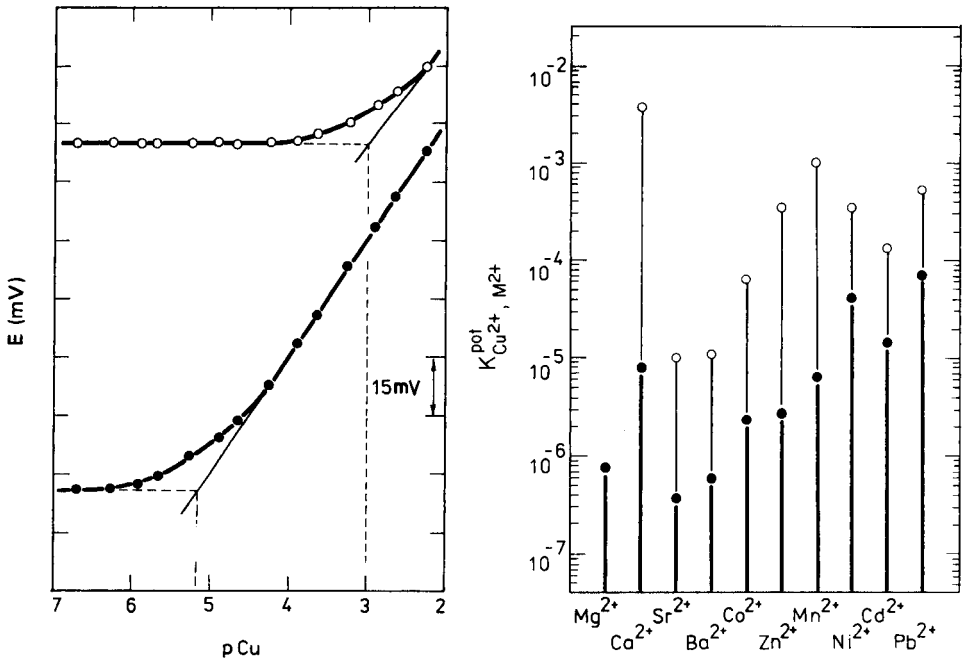

Fig. 5. Selectivity of the copper(I) selenide membrane electrode (○) and the $Cu_{25}As_{37.5}Se_{37.5}$ glass sensor (●) in 1 M manganese(II) nitrate. The selectivity coefficients obtained are 1.0×10^{-3} and 6.6×10^{-6}, respectively.

Fig. 6. Graphic comparison of the selectivity to some divalent cations of different electrodes: (○) $Cu_{1.8}Se$; (●) $Cu_{25}As_{37.5}Se_{37.5}$.

consequence of the high hole conductivity σ_p in single-crystal $Cu_{1.8}Se$. Other binary copper chalcogenides are also practically metallic conductors ($\sigma_p = 10^2$—10^4 ohm^{-1} cm^{-1} [24]). This means that potentiometric sensors based on crystalline binary copper chalcogenides will have the same deficiencies as single-crystal selenide electrodes. Low sensitivity to active oxidizing agents is, however, typical of silver-free chalcogenide glasses. The electrode characteristics of sensors with $Cu_{25}As_{37.5}Se_{37.5}$ and $Cu_{12.5}Ag_{12.5}As_{37.5}Se_{37.5}$ membranes are similar despite the 70-fold increase in σ_p at room temperature as the copper concentration increases from 12.5 to 25 atom% (Fig. 1). A graphic comparison of selectivity coefficients for two copper selenide sensors (single-crystal and vitreous) is shown in Fig. 6.

Viable pH ranges

The influence of pH on electrode response in solutions with constant ionic strength ($I = 1.0$) is shown in Fig. 7. Typical dependences are shown for chalcogenide glass, CuS/Ag_2S, and $Cu_{1.8}Se$ electrodes. It can be seen (Fig. 7A) that the potential of the chalcogenide glass electrode does not depend on pH

TABLE 1

Selectivity coefficients of chalcogenide glass electrodes (with x = 12.5—25% Cu) and crystalline sensors

Interfering ion	Concentration of interfering ion (M)	log $K^{pot}_{Cu^{2+},M^{z+}}$		
		Cu-Ag-As-Se	$CuS-Ag_2S$	$Cu_{1.8}Se$
Li^+	1.0	−6.0	—	—
Na^+	1.0	−5.4	—	—
K^+	1.0	−6.7	—	—
NH_4^+	1.0	−5.6	—	—
Mg^{2+}	1.0	−6.1	—	—
Ca^{2+}	1.0	−5.1	−5.1	−2.4
Sr^{2+}	1.0	−6.3	−6.1	−5.0
Ba^{2+}	0.3	−6.2	−6.2	−5.0
Mn^{2+}	1.0	−5.2	−5.1	−3.0
Co^{2+}	1.0	−5.6	−5.5	−4.2
Ni^{2+}	1.0	−4.5	−4.6	−3.5
Zn^{2+}	1.0	−5.6	−5.4	−3.5
Pb^{2+}	0.1	−4.5	−4.1	−3.0
	1.0	−4.1	−4.2	−3.6
Cd^{2+}	0.1	−4.7	−4.3	−3.7
	1.0	−5.0	−4.9	−4.0
Fe^{3+}	10^{-5}	1.0	1.2	3.3
at pH 1	10^{-4}	0.6	0.4	2.2
	10^{-3}	0.6	0.5	1.1

at pH $\geqslant$ 1. Increased acidity causes a monotonous decrease of electrode potentials. A similar phenomenon was observed earlier for silver ion-selective chalcogenide glass sensors [7] and may be related to changes in the liquid-junction potential at the salt bridge electrolyte/test solution boundary as a result of the excess of highly mobile hydrogen ions. As will be shown below, this potential decrease in acid solutions does not affect the sensitivity of the chalcogenide glass electrode in strongly acidic media. The potential decrease in the alkaline range can be explained by the precipitation of copper(II) hydroxides.

Chalcogenide glass electrodes are more stable to acids than the crystalline copper ion-selective electrodes. The increase in potential with increased acidity for both the crystalline electrodes (Fig. 7B and C) is probably caused by insufficient selectivity of these sensors against hydrogen ions and by partial dissolution of the membrane.

Typical responses to copper(II) ion of chalcogenide glass and copper(II) sulfide/silver sulfide electrodes in 1 M nitric acid are shown in Fig. 8. It can be seen that the sensitivity of chalcogenide glass sensors in strongly acidic media is 10—30 times greater than that of the crystalline copper ion-selective electrodes.

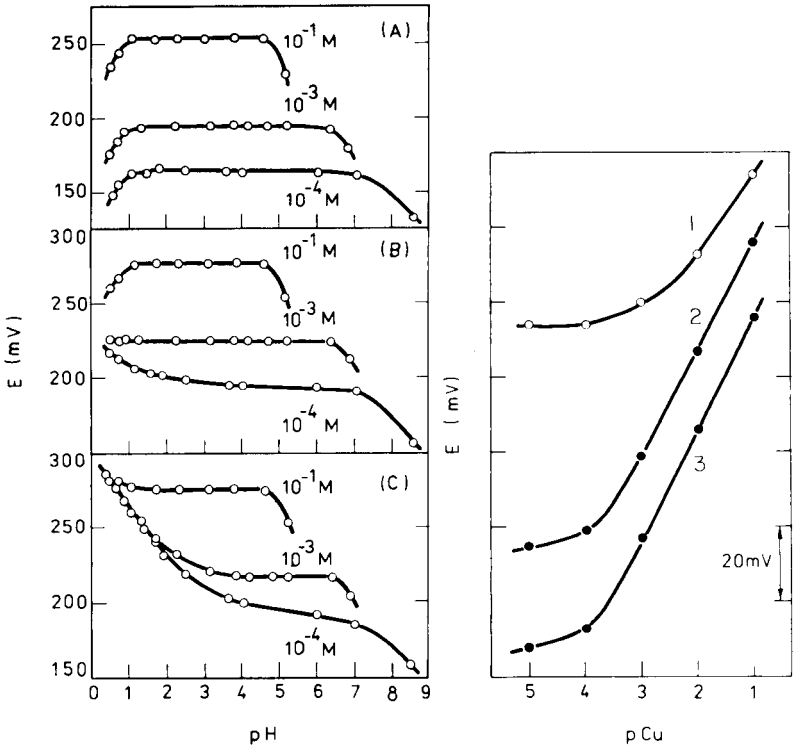

Fig. 7. Viable pH ranges for different types of electrode at copper concentrations of 10^{-1}—10^{-3} M: (A) chalcogenide glass electrodes; (B) copper(II) sulfide/silver sulfide membrane electrode; (C) copper(I) selenide single-crystal electrode.

Fig. 8. Response to copper(II) in 1 M nitric acid of different electrodes: (1) copper(II) sulfide/silver sulfide membrane electrode; (2) $Cu_{25}As_{37.5}Se_{37.5}$ glass sensor; (3) $Cu_{12.5}Ag_{12.5}As_{37.5}Se_{37.5}$ glass sensor.

Electrode response in redox media

The redox responses of the chalcogenide glass and crystalline sensors were studied in solutions of potassium hexacyanoferrate(III)/(II) at pH 5 and iron(III)/(II) sulfate in 0.1 M sulfuric acid. The responses were compared with the behavior of a platinum electrode. The platinum electrode behaved in the expected manner, whereas unstable potentials and sluggish responses were observed with the membrane sensors, revealing small exchange currents at the membrane/redox solution interface. Typical responses of platinum and chalcogenide glass electrodes in hexacyanoferrate mixtures are shown in Fig. 9. In the low redox potential range and at high total concentrations of the redox couple (0.1 M), the potential of the membrane sensor was close to that of the platinum electrode. The potentials of chalcogenide glass and crystalline electrodes were much lower than those of the platinum electrode in solutions with higher redox potential and in solutions with only 10^{-2}—10^{-3} M

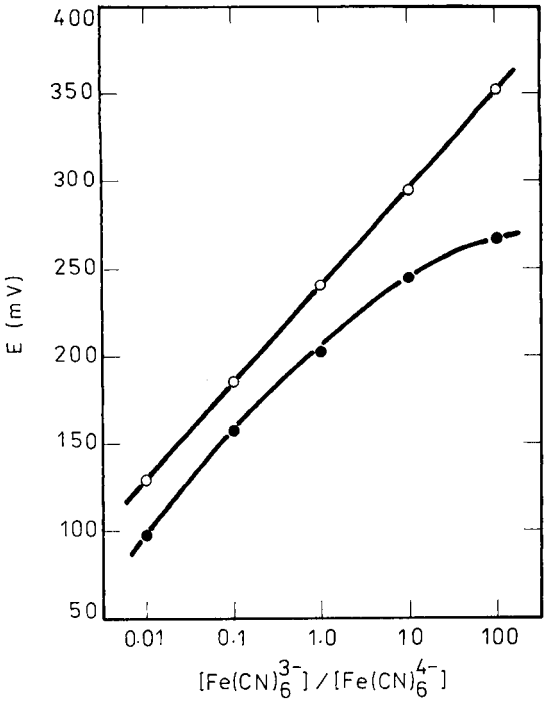

Fig. 9. Typical responses to potassium hexacyanoferrate(II)/(III) solutions at a total concentration of 0.1 M: (○) platinum electrode; (●) $Cu_5Ag_{20}As_{37.5}Se_{37.5}$ electrode.

total concentrations of the redox couple. Particularly, in iron(III)/iron(II) solutions, the potentials of all electrodes were lower by 200—300 mV than the equilibrium redox potential.

DISCUSSION

Characteristics of the ionic sensitivity

The principal characteristics of the behaviour of chalcogenide glass electrodes are as follows. First, glasses of all compositions display a response to copper(II) ion, though there were both semiconductors and silver ion conductors among them. Secondly, the standard potentials of electrodes of all compositions are quite close to each other, whether or not silver is present in the membrane. Thirdly, the slope S of the electrode response is usually about 30 mV/pCu. Finally, from the e.s.r. and magnetic susceptibility data, only one copper ion per million can be divalent in $Cu_xAg_{25-x}As_{37.5}Se_{37.5}$ glasses, which have had no contact with solution.

Possible mechanisms of copper(II) ion response

At present, there are several points of view on the sensing mechanism of solid-state ion-selective electrodes (see, e.g., [25—28] and references therein).

According to the most widely used model, the response of the copper(II) ion-selective electrode is connected with the following equilibria near the membrane surface:

$$CuS \rightleftharpoons Cu^{2+} + S^{2-}; Ag_2S \rightleftharpoons 2\ Ag^+ + S^{2-}$$

Exchange of silver ion between the membrane and the adhering layer of solution is considered to be a potential-generating process. Silver ion activity in the adhering layer, a_{Ag^+}, is determined in this case by the copper(II) ion activity in solution, $a_{Cu^{2+}}$, and the solubility products of copper sulfide, $K_{so}(CuS)$, and silver sulfide, $K_{so}(Ag_2S)$:

$$a_{Ag^+} = [K_{so}(Ag_2S)a_{Cu^{2+}}/K_{so}(CuS)]^{1/2}$$

Thus, the copper(II) sulfide/silver sulfide membrane electrode is sensitive to copper(II) ion.

However, it is impossible to explain the copper(II) ion response of a copper selenide membrane or the lead ion response of a single-crystal PbS electrode from this point of view. Silver ion exchange on the glass/solution interface cannot be a potential-generating process in the case of copper(II) ion-selective chalcogenide glass electrodes, because their electrochemical characteristics, including standard potentials, differ very little for all membrane compositions, whether they contain silver or are silver-free.

Hulanicki and Lewenstam [29] suggested a diffusion-layer model to explain the copper(II) ion sensitivity of a chalcocite (Cu_2S) membrane electrode. According to this model, the electrode potential depends on the copper(I) ion activity, $a^0_{Cu^+}$, in the adhering layer:

$$E = E_0 + RT/F \ln a^0_{Cu^+}$$

Hulanicki and Lewenstam [29] took into account three contributions to the total activity of potential-generating copper(I) ions: the activity of the analytical copper(I) ions in solution near the electrode surface $a_{Cu^+}(A)$, the activity of copper(I) ions caused by finite membrane dissolution $a_{Cu^+}(L)$, and the activity of copper(I) ions generated by an exchange-type reaction with interfering ions $a_{Cu^+}(E)$:

$$a^0_{Cu^+} = a^0_{Cu^+}(A) + a^0_{Cu^+}(L) + a^0_{Cu^+}(E)$$

Superscript 0 means that the copper(I) ion activity in the diffusion layer is under consideration. The copper(II) ion response of the chalcocite electrode is connected with the exchange reaction, $Cu_2S + Cu^{2+} \rightleftharpoons CuS + 2\ Cu^+$, when the principal contribution to chalcocite electrode potential is due to $a_{Cu^+}(E)$ activity.

The application of the diffusion-layer model to chalcogenide glass electrodes is hindered for two reasons. First, the stability of copper(I) ions in nitrate media is highly debatable, even if copper(I) ions were generated by the exchange reaction near the electrode surface. Secondly, this model fails to explain the copper(II) ion response of the $Ag_{25}As_{37.5}Se_{37.5}$ sensor.

Jasinski et al. [11] and Owen [4] put forward multi-step adsorption models to explain the copper(II) ion sensitivity of chalcogenide glass electrodes. Preliminary soaking and electrode surface oxidation in concentrated copper(II) ion solutions are essential components of these models. However, according to our results and the study of Tohge et al. [12], chalcogenide glass electrodes with polished membranes do not need any special surface treatment, which is important in the adsorption models mentioned above. The effect of soaking will be explained below within the framework of a modified surface-layer model. Finally, Tohge et al. [12] suggested that the copper(II) ion response of copper-arsenic-selenium glasses derives from the potential-generating reaction, $Cu^{2+} + 2\ e^- \rightleftharpoons Cu^0$, which produces metallic copper in the surface layer of the glass. In other words, the sensing mechanism of chalcogenide glass electrodes is identical to that of a classical electrode of the first kind [Cu^{2+}(aq)/Cu^0(metal)]. The principal argument in favour of this reaction is that the slope of the electrode response is about 30 mV/pCu.

However, the unstable potentials and sluggish responses of chalcogenide glass electrodes in redox media (Fig. 9) provide evidence of the small exchange currents of electrons (holes) at the glass/redox couple solution interface. Thus, the stable electrode response to copper(II) ions even at micromolar concentrations makes it doubtful that electron exchange is a potential-generating process for copper(II) ion-selective chalcogenide glass electrodes.

Modified surface-layer model

It seems possible to explain the ionic sensitivity of chalcogenide glass electrodes within the framework of the following model: (1) a modified surface layer is formed at the surface of the chalcogenide glass membrane after contact with solution, and the potential-generating processes, which can be electronic or ionic exchange, proceed in this layer; (2) the most probable potential-generating process is direct copper(II) ion-exchange between solution and modified surface layer. The ion-sensing mechanism on the basis of such principles can be presented as follows.

A modified surface layer is formed on the chalcogenide glass membrane surface as a result of interaction with solution and partial destruction of the glass network. A considerable copper(II) ion concentration exists in the surface layer, and copper(II) ion migration is also easier in this layer. A potential-generating process is direct copper(II) ion-exchange between solution and modified surface layer:

Cu^{2+}(solution) $\rightleftharpoons$ Cu^{2+}(modified surface layer)

Reversibility at the modified surface layer/glass bulk interface is achieved by

Cu^{2+}(modified surface layer) $\rightleftharpoons$ Cu^{+}(bulk) + h^{+}

where h^+ is a positive charge hole. Copper(II) ions in the surface layer are generated as a result of two processes: (1) disproportionation of copper(I)

ions, $2\,Cu^{+} \rightarrow Cu^{2+} + Cu^{0}$, and subsequent copper metal oxidation; (2) diffusion of copper(II) ions from solution. The latter is more probable for glasses with low copper content.

Experimental data obtained in the present investigation and also the characteristics of the ionic sensitivity of lead [8, 9] and cadmium [10] ion-selective chalcogenide glass sensors (response times in solutions with high ionic strength, the mode of dependence of selectivity coefficients on ionic radii of alkali and alkali-earth cations) support the proposed model.

If the potential-generating process is copper(II) ion-exchange between the solution and modified surface layer of the glass, then the structure, composition and transport properties of the surface layer will be of prime importance in the description of electrode properties. This is why chalcogenide glasses with different bulk composition and different types of conductivity display similar electrode properties. Certainly, the electrode response depends on the copper bulk concentration in the glass, but on the whole, this dependence is connected with exchange-current density at the membrane/solution interface. The differences in exchange-current density affect the potential stability and reproducibility as well as the electrode response in solutions with high ionic strength (Fig. 3) and also affect the first calibration measurements taken from freshly prepared electrodes (Fig. 10). These phenomena are easy to explain by the modified layer model.

In a concentrated solution of supporting electrolyte, the modified surface layer is filled up by cations of this electrolyte. The equilibrium potential on the surface layer/solution interface corresponds to this state. After the first addition of copper(II) ions to the test solution, these ions migrate to the exchange sites in the glass. Because of the retarded diffusion kinetics of the copper(II) ions and insufficient exchange-current density of sensors with low copper concentration in the membrane, non-equilibrium instead of equilib-

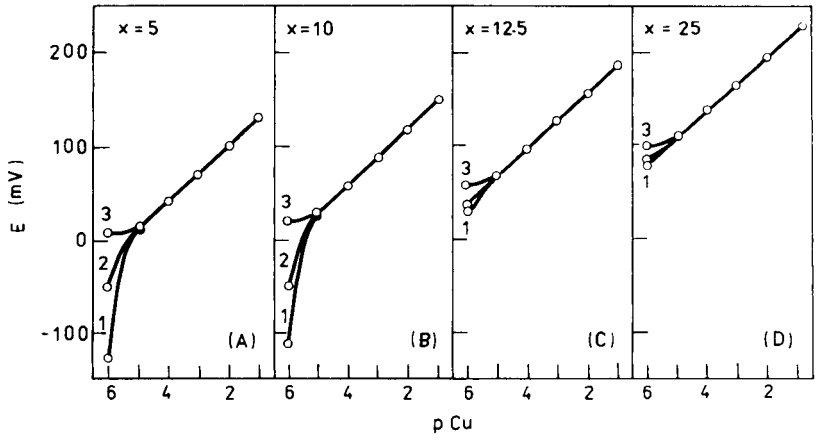

Fig. 10. First calibration curves of just-prepared chalcogenide glass electrodes. Copper content in membranes: (A) 5; (B) 10; (C) 12.5; (D) 25 atom% Cu. Curves: (1) first calibration; (2) second calibration; (3) third calibration.

rium potentials can be measured. The difference between equilibrium and non-equilibrium potentials results in a super-Nernstian slope. The kinetic character of the above phenomena is confirmed by the instability and drift of the potential of electrodes with low copper content in this concentration range. Further increases in the copper(II) ion concentration in solution cause increased exchange current density, and the electrode response then attains its usual form. It should be noted that no anomalous behaviour is observed in solutions without constant ionic strength and in solutions with $I < 1.0$.

The difference in the dynamics of the modified layer formation affects the first calibration measurements with freshly prepared sensors (Fig. 10). Jasinski et al. [11] also noted super-Nernstian slopes during the first calibration measurements. We consider that the super-Nernstian response of electrodes with low copper contents (Fig. 10A and B) is related primarily to copper(II) ion diffusion in a membrane surface layer which contains an inadequate quantity of copper, and to disproportionation and oxidation of copper(I) ions in the surface layer of the glass. The final formation of the modified surface layer which governs the electrode properties is due to these processes.

For sensors with high copper contents ($x > 10$ atom% copper), formation of the modified surface layer is quite rapid, therefore the first and subsequent calibration curves differ very little (Fig. 10C and D). For sensors with low copper contents, formation of the modified surface layer is slower. Probably, the response of an electrode with the $Ag_{25}As_{37.5}Se_{37.5}$ membrane is unstable because of the surface layer; its slope was 33—50 mV/pCu.

To confirm the proposed model, some extra experiments were conducted.

Spectroscopic evidence for the proposed model

The formation of surface layers on oxide glasses has been investigated by many authors (see, e.g., [30—33] and references therein). Chalcogenide glasses have not been studied from this point of view. Only Voigt and Wolf [34] showed that a modified surface layer did appear after contact of GeS_2 chalcogenide glasses with atmospheric moisture. Using i.r. spectroscopy, they found that the glass surface became hydrated, which caused deterioration of the optical properties.

Different spectroscopic methods were used here to verify the proposed model of ionic sensitivity of chalcogenide glasses. The examination of the model included two aspects. First, copper(II) ions should appear at the glass surface after contact with the solution. Secondly, after soaking of the glass, the original surface composition should undergo considerable changes connected with the formation of the surface layer.

Pungor et al. [35] were the first to use x-ray photo-electron spectroscopy (x.p.s.) for investigations of the oxidation of copper(II) sulfide/silver sulfide electrodes. It was found by x.p.s. that sulfur on the membrane surface is present both as sulfide and as sulfate but no change in the copper valence state was observed.

In the present study, x.p.s. was used to establish the copper valence state on the glass surface after soaking in various aqueous solutions and also to investigate the membrane surface composition.

Copper $2p_{3/2}$ photo-electron spectra of the glass $Cu_{20}Ag_5As_{37.5}Se_{37.5}$ are shown in Fig. 11. It can be seen that the spectra are single peaks with full width at half maximum (FWHM) of 1.3 ± 0.1 eV. Electron-binding energies E_b (Table 2) are typical of copper-containing selenide glasses [36, 37] and crystalline copper selenides [38]. Unfortunately, the copper valence state cannot be determined from E_b values because the chemical shifts of the Cu $2p_{3/2}$ lines in copper(I) and copper(II) chalcogenides have almost the same values [38, 39]. Romand et al. [38] and Ueno and Odajima [37] used the Auger parameter α to determine the copper valence state in crystalline and glassy chalcogenides, but it was impossible to obtain suitable x-ray-induced Auger electron high-resolution spectra in the present work.

The data about the copper valence state were obtained from the spectra of glasses containing oxygen impurities in the form of As_2O_3 (Fig. 12). In dry $Cu_{24}Ag_1As_{37.5}Se_{37.5}$ glass containing oxygen, the photo-electron spectrum shows a single peak. The E_b value of this peak (Table 2) coincides with the binding energies of the Cu $2p_{3/2}$ lines in glasses without oxygen impurities.

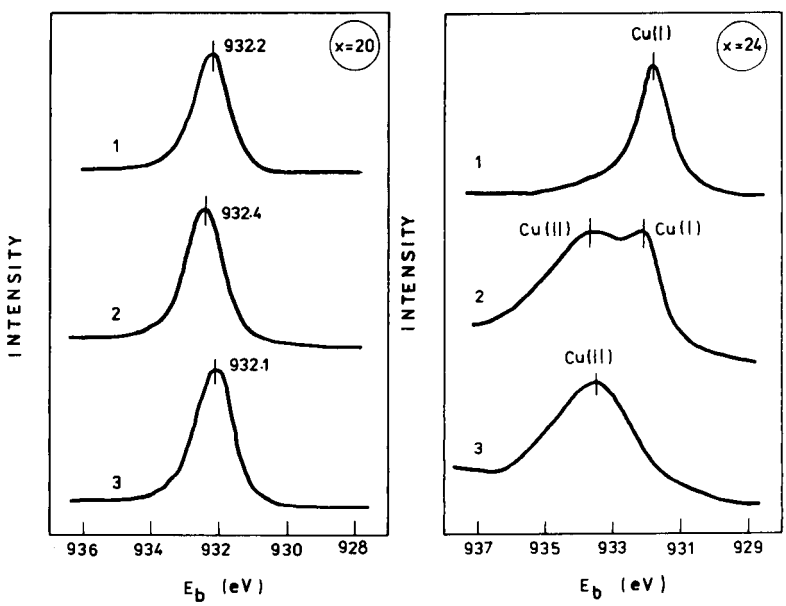

Fig. 11. The Cu $2p_{3/2}$ photo-electron spectra of $Cu_{20}Ag_5As_{37.5}Se_{37.5}$ glasses: (1) dry glass; (2) the glass after soaking in water; (3) the glass after soaking in 0.1 M copper(II) nitrate solution.

Fig. 12. The Cu $2p_{3/2}$ photo-electron spectra of $Cu_{24}Ag_1As_{37.5}Se_{37.5}$ glass containing As_2O_3 impurities: (1) dry glass; (2) the glass after soaking in water; (3) the glass after soaking in potassium permanganate solution.

TABLE 2

Binding energies E_b and full width at half maximum (FWHM) values of Cu $2p_{3/2}$ photoelectron peaks of copper-silver-arsenic-selenium glasses

Glass surface treatment	E_b (eV)	FWHM (eV)
$Cu_{12.5}Ag_{12.5}As_{37.5}Se_{37.5}$		
Dry	931.9	1.3
Soaked in water	932.6	1.3
Soaked in 0.01 M copper(II) nitrate	932.2	1.4
$Cu_{20}Ag_5As_{37.5}Se_{37.5}$		
Dry	932.2	1.2
Soaked in water	932.4	1.4
Soaked in 0.1 M copper(II) nitrate	932.1	1.3
$Cu_{24}Ag_1As_{37.5}Se_{37.5}:As_2O_3$		
Dry	931.8	1.3
Soaked in water	932.1	1.5
	933.7	2.5
Soaked in 0.01 M potassium permanganate	933.5	2.8

After soaking of this glass in water, the second peak shifted to a higher E_b region (Fig. 12, curve 2). The significant width of the second line (2.5 eV) and its E_b value (Table 2) allow the conclusion that copper(II) ions appear at the glass surface after soaking in water. Actually, in copper oxides and ferrite oxides, the E_b values of copper(II) ions are greater than that of copper(I) ions by 1.1–2.7 eV [39, 40]. The widths of the x.p.s. peaks for copper(II) ions are broader than those for copper(I) ions, because of multiplet splitting of the paramagnetic ions [39, 40]. All copper ions on the surface of the glass oxidized by permanganate solution (Fig. 12, curve 3) are copper(II) ions.

The alteration of the surface composition of chalcogenide glass membranes after soaking in various aqueous solutions was confirmed by x.p.s. The dynamics of changes in composition of a $Cu_{12.5}Ag_{12.5}As_{37.5}Se_{37.5}$ glass surface after soaking in 0.01 M copper(II) nitrate is shown in Fig. 13. Even short treatment (a few minutes) in copper(II) nitrate solution leads to a considerable increase in the silver concentration at the membrane surface and to a sharp fall in the arsenic content. The copper concentration within the 2–10-nm thick surface layer (such is the usual free path of photo-electrons in solids) decreased to half its initial value after the glass had been soaked in copper(II) nitrate for a day. The selenium surface concentration changed least of all. Glasses treated with 1.0 M copper(II) nitrate and 0.01 M copper(II) chloride displayed similar behaviour. The formation of the modified surface layer in water is considerably slower.

Perceptible alteration of the surface composition is not followed by

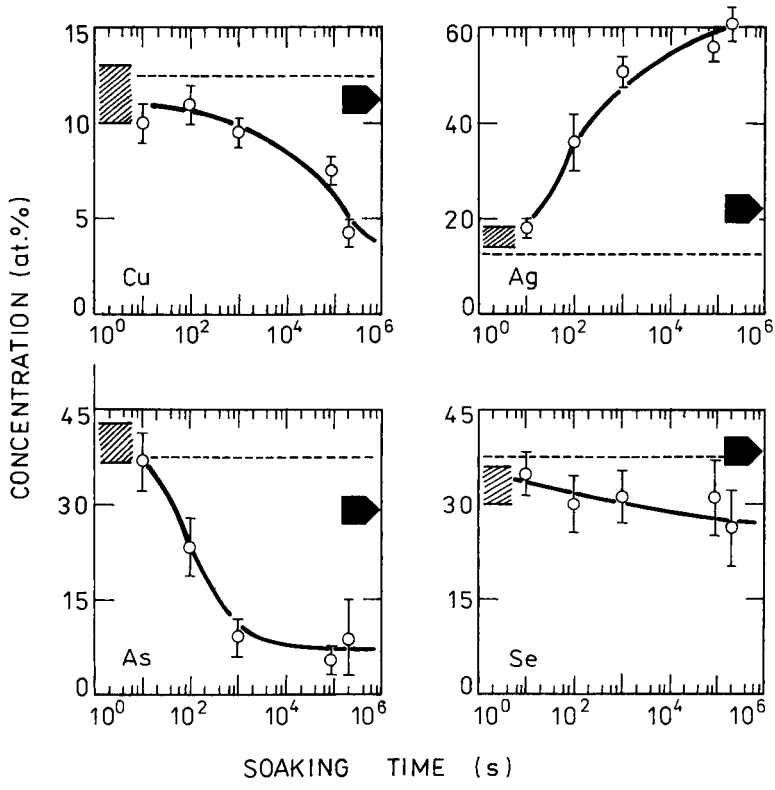

Fig. 13. Surface composition of $Cu_{12.5}Ag_{12.5}As_{37.5}Se_{37.5}$ glass after soaking for different times in 0.01 M copper(II) nitrate. The shaded areas correspond to the original glass surface composition and the dashed lines correspond to bulk concentration. Arrows indicate the surface composition of the glass after soaking in water for a week.

changes in the chemical state of glass components (copper valence state was discussed above). The binding energies E_b of As 3*d* and Se 3*d* photoelectron lines, which were measured for $Cu_{12.5}Ag_{12.5}As_{37.5}Se_{37.5}$ glass after soaking in copper(II) nitrate and copper(II) chloride solutions, are given in Table 3. These E_b values are characteristic of crystalline and vitreous copper and arsenic selenides [36—38] and remain constant during the soaking.

The depths of the modified surface layer and the profiles of glass components are of significant interest. Preliminary information of this kind was obtained by scanning Auger-electron spectroscopy. Depth profiles of components in the original glass $Cu_{12.5}Ag_{12.5}As_{37.5}Se_{37.5}$, and in the same glass after soaking in 0.01 M copper(II) nitrate solution for two days, are shown in Fig. 14. The concentrations of components at the dry glass surface are practically independent of sputtering time by argon ions. The silver and arsenic concentrations at the surface of the glass after soaking approach those in the bulk only after 40—60 min of ion sputtering. The most significant

TABLE 3

Binding energies E_b and FWHM values of the As 3*d* and Se 3*d* photo-electron peaks of a $Cu_{12.5}Ag_{12.5}As_{37.5}Se_{37.5}$ glass after soaking in copper(II) nitrate and chloride

Soaking time (s)	As 3*d*		Se 3*d*	
	E_b (eV)	FWHM (eV)	E_b (eV)	FWHM (eV)
0.01 M copper(II) nitrate				
10	41.7	1.8	53.9	2.0
1.0×10^2	41.8	1.5	53.6	1.7
1.0×10^3	41.9	1.5	53.7	1.8
8.8×10^4			53.9	2.0
1.0 M copper(II) nitrate				
3.0×10^2	41.6	2.0	53.9	2.0
1.8×10^3	41.7	1.6	53.8	1.8
1.3×10^4	41.8	1.7	53.9	1.9
0.01 M copper(II) chloride				
1.6×10^2	41.8	1.7	53.9	1.9
7.6×10^2	41.8	1.8	53.8	2.0
6.6×10^3	41.6	1.7	53.6	1.9

changes in concentration occur during the first 5—10 min of the depth profile analysis. A compilation of data obtained for silicon, silicon dioxide, boron nitride, aluminium and some other solids [41] made it possible to estimate the depth of the modified surface layer for the glasses in question. It appears that the greatest alterations in glass composition take place in the surface layer 100—200 nm thick.

To understand the copper(II) ion sensitivity within the framework of this modified surface-layer model, one must take into account the essential nature of the mechanism of the direct copper(II) ion-exchange between the solution and the modified surface layer of the glass. This problem is closely connected

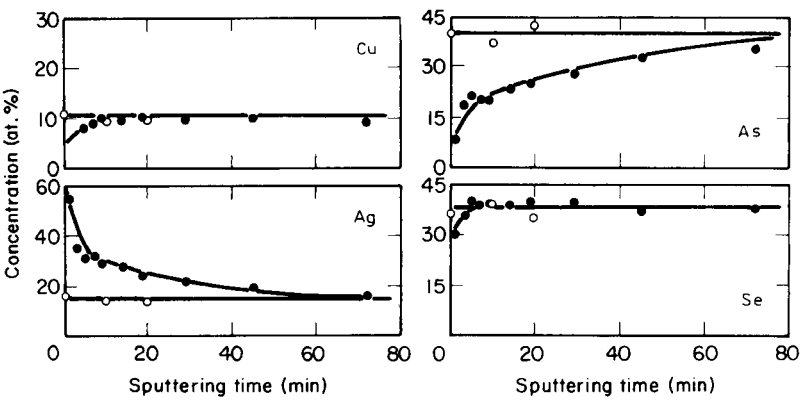

Fig. 14. Depth profiles of components: (○) in original glass $Cu_{12.5}Ag_{12.5}As_{37.5}Se_{37.5}$; (●) in the same glass after soaking for 2 days in 0.01 M copper(II) nitrate.

with copper(II) ion migration in the surface layer. Different solid electrolytes with high copper(I) ion conductivity are well known in solid-state ionic studies, whereas the diffusion coefficients for copper(II) ion in solids are significant only at high temperatures [42]. If on admits the existence of a large number of vacancies, hollows and other structural defects and imperfections, however, copper(II) ion migration is possible at room temperature. In considering the likelihood of such migration in the modified surface layer of the glasses studied, it should be recalled that the concentration changes discussed above are relative concentration changes. This means that the increase in the concentration of silver atoms on the surface (i.e., the number of Ag atoms per 100 atoms of the surface) can be caused by an actual increase in the number of silver ions on the surface, by a decrease in the other kinds of atoms on the surface, or by both effects simultaneously. However, during the depth profile analysis of the glass, the specimen geometry, time, counting efficiency of Auger electrons, energy and current density of the primary beam of monoenergetic electrons, ruster sizes, etc., were fixed. In such a case, the ratio of the intensities of Auger signals of an element is proportional to the ratio of atomic densities of this element (i.e., the number of atoms in unit volume) [43]. Our evaluation of Auger signal intensities showed that the density of the modified surface layer was 2.0—2.5 times less than the atomic density of the original glass (this difference is shown schematically in Fig. 15). The presence of such structural defects and hollows must certainly lead to high copper(II) ion diffusion coefficients in the modified surface layer of the glass.

Applicability to crystalline sensors

The modified surface-layer model can be applied to crystalline ion-selective electrodes. Siemroth and Hennig [44] found that after contact of a single-crystal copper(I) selenide membrane with aqueous solutions, copper selenide

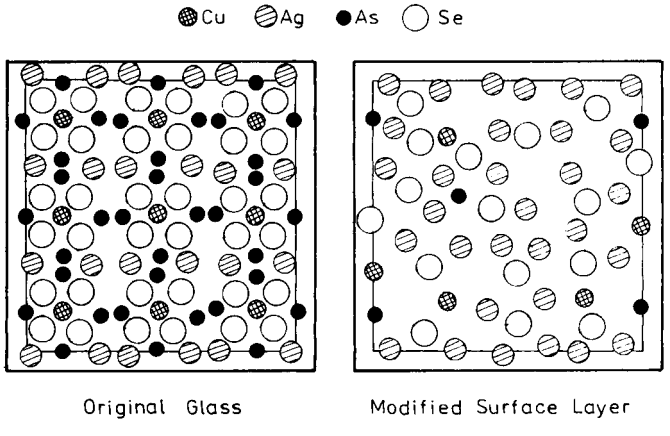

Fig. 15. Diagram of the original glass surface composition and the modified surface layer on the same glass after treatment with copper(II) nitrate solution.

of another stoichiometry is formed. Lindner et al. [45] and Harsanyi et al. [46] noted the essential role of adsorption and direct exchange of the primary ion on the membrane surface during investigations of the response time and detection limit of solid-state ion-selective electrodes. Chaudhari and Cheng [47] showed, with the help of the radioisotope ^{210}Pb, that adsorption and/or exchange of lead ions occurred on the surface of a lead sulfide/silver sulfide membrane. Later, Cheng and co-workers [48, 49] used x.p.s. to study the surface of such electrodes. Alterations of the chemical state of components on the membrane surface after soaking in various aqueous solutions as well as changes in the surface composition of the membrane were observed. Vlasov et al. [50] studied bromide ion-exchange between the solution and surface layer of a single-crystal silver bromide membrane with the help of ^{82}Br isotope; no bromide exchange was observed for silver bromide/silver sulfide/arsenic sulfide glasses, which did not display bromide response.

The above data confirm the existence of modified surface layers for crystalline membranes and of the direct exchange of the primary ion between solution and the modified surface layer.

The authors thank Dr. Yu. P. Kostikov and V. S. Strykanov for the x.p.s. measurements. Dr. M. A. Kvantov for the magnetic susceptibility measurements, Dr. E. A. Zhilinskaya for the e.s.r. measurements, Dr. V. S. Ivanov for the scanning a.e.s. measurements and Dr. Yu. E. Ermolenko for the copper(II) sulfide/silver sulfide preparation.

REFERENCES

1 C. T. Baker and I. Trachtenberg, J. Electrochem. Soc., 118 (1971) 571.
2 R. Jasinski and I. Trachtenberg, J. Electrochem. Soc., 120 (1973) 1169.
3 Yu. G. Vlasov and E. A. Bychkov, Hung. Sci. Instrum., 53 (1982) 35.
4 A. E. Owen, J. Non-Cryst. Solids, 35/36 (1980) 999.
5 C. Bohnke, A. Saida and G. Robert, C. R. Acad. Sci. Paris, C290 (1980) 97.
6 C. Bohnke, J. P. Malugani, A. Saida and G. Robert, Electrochim. Acta, 26 (1981) 1137.
7 Yu. G. Vlasov, E. A. Bychkov, E. A. Kazakova and Z. U. Borisova, Zh. Anal. Khim., 39 (1984) 452.
8 Yu. G. Vlasov, E. A. Bychkov and A. V. Legin, in Ionoselektivnye elektrody i ionnyi transport (Ion-Selective Electrodes and Ion Transport), Nauka, Leningrad, 1982, p. 113.
9 Yu. G. Vlasov, E. A. Bychkov and A. V. Legin, paper presented at Fourth Scientific Session on Ion-Selective Electrodes, Matrafured, Hungary, October 1984.
10 Yu. G. Vlasov, E. A. Bychkov, A. D. Safarov, P. P. Antonov and M. M. Miloshova, Zh. Anal. Khim., 40 (1985), in press.
11 R. Jasinski, I. Trachtenberg and G. Rice, J. Electrochem. Soc., 121 (1974) 363.
12 N. Tohge, T. Minami and M. Tanaka, Yogyo-Kyokai-Shi, 91 (1983) 32.
13 Yu. G. Vlasov and E. A. Bychkov, Solid State Ionics, 14 (1984), in press.
14 Yu. G. Vlasov, S. B. Kocheregin and Yu. E. Ermolenko, Zh. Anal. Khim., 32 (1977) 1843.
15 C. D. Wagner, Anal. Chem., 49 (1977) 1282.
16 J. H. Scofield, J. Electron Spectrosc. Relat. Phenom., 8 (1976) 129.

17 C. T. Moynihan and A. V. Lesikar, J. Am. Ceram. Soc., 64 (1981) 40.
18 M. D. Ingram and C. T. Moynihan, Solid State Ionics, 6 (1982) 303.
19 M. Matias, in Amorphous Semiconductors '74, Reinhardsbrunn, G.D.R., 1974, p. 69.
20 P. C. Taylor, E. J. Friebele and S. G. Bishop, in B. L. H. Wilson (Ed.), Physics of Semiconductors, 1978, Institute of Physics, Bristol, 1979, p. 1305.
21 E. Pungor, K. Toth and A. Hrabeczy-Pall, Pure Appl. Chem., 51 (1979) 1913.
22 H. Remy, Lehrbuch der Anorganischen Chemie, Band 2, Akademische Verlagsges, Gees and Portig K.-G., Leipzig, 1961.
23 J. Vesely, Collect. Czech. Chem. Commun., 36 (1971) 3364.
24 K. Okamoto, S. Kawai and R. Kiriyama, Jpn. J. Appl. Phys., 8 (1969) 718.
25 J. Koryta, Anal. Chim. Acta, 61 (1972) 329; 91 (1977) 1; 111 (1979) 1; 139 (1982) 1; 159 (1984) 1.
26 E. Pungor and I. Buzas (Eds.), Ion-Selective Electrodes, Akademiai Kiado, Budapest, 1973; 1978; 1981; 1985.
27 R. P. Buck, in H. Freiser (Ed.), Ion-Selective Electrodes in Analytical Chemistry, Vol. 1, Plenum Press, New York, 1978, p. 1.
28 W. E. Morf, The Principles of Ion-Selective Electrodes and of Membrane Transport, Akademiai Kiado, Budapest, 1981.
29 A. Hulanicki and A. Lewenstam, Talanta, 23 (1976) 661.
30 G. Eisenman (Ed.), Glass Electrodes for Hydrogen and Other Cations, Dekker, New York, 1967.
31 A. A. Belijustin, Fiz. Khim. Stekla, 7 (1981) 257.
32 V. Gottardi (Ed.), The Chemical Durability of Glass. A Bibliographic Review of the Literature, International Commission on Glass, Institut du Verre, Paris, 1965; 1973.
33 D. E. Clark and E. L. Yen-Bower, Surf. Sci., 100 (1980) 53.
34 B. Voigt and M. Wolf, J. Non-Cryst. Solids, 51 (1982) 317.
35 E. Pungor, K. Toth, M. K. Papay, L. Polos, H. Malissa, M. Grasserbauer, E. Hoke, M. F. Ebel and K. Persy, Anal. Chim. Acta, 109 (1979) 279.
36 K. S. Liang, A. Bienenstock and C. W. Bates, Phys. Rev., B: 10 (1974) 1528.
37 T. Ueno and A. Odajima, Jpn. J. Appl. Phys., 21 (1982) 230.
38 M. Romand, M. Roubin and J. Deloume, J. Electron Spectrosc., 13 (1978) 229.
39 P. E. Larson, J. Electron Spectrosc., 4 (1974) 213.
40 A. D'Huysser, B. Lerebours-Hannoyer, M. Lenglet and J. P. Bonnelle, J. Solid State Chem., 38 (1981) 246.
41 V. S. Ivanov, private communication.
42 G. C. Farrington and B. Dunn, Solid State Ionics, 7 (1982) 267.
43 R. Shimizu, Jpn. J. Appl. Phys., 22 (1983) 1631.
44 J. Siemroth and I. Hennig, in E. Pungor and I. Buzas (Eds.), Ion-Selective Electrodes, 3, Akademiai Kiado, Budapest, 1981, p. 339.
45 E. Lindner, K. Toth and E. Pungor, Anal. Chem., 54 (1982) 202.
46 E. G. Harsanyi, K. Toth and E. Pungor, Anal. Chim. Acta, 152 (1983) 163.
47 S. N. K. Chaudhari and K. L. Cheng, Mikrochim. Acta, II (1980) 159.
48 S. N. K. Chaudhari, F. C. Chang, K. L. Cheng and V. Y. Young, Anal. Chem., 53 (1981) 2048.
49 V. Y. Young, S. N. K. Chaudhari and K. L. Cheng, Surf. Interface Anal., 3 (1981) 176.
50 Yu. G. Vlasov, E. A. Bychkov and D. V. Golikov, Elektrokhimiya, 21 (1985) in press.

Analytica Chimica Acta, 185 (1986) 159—169
Elsevier Science Publishers B.V., Amsterdam — Printed in The Netherlands

THE DETERMINATION OF FREE AMMONIA IN AMBIENT AIR WITH DIFFUSION/DENUDER TUBES

N. A. DIMMOCK and G. B. MARSHALL*

Central Electricity Generating Board, Central Electricity Research Laboratories, Kelvin Avenue, Leatherhead, Surrey KT22 7SE (Great Britain)

(Received 30th December 1985)

SUMMARY

Ammonia is important in atmospheric chemistry because it neutralises acidic species and increases the pH of cloud droplets. Data on the concentration of free ammonia in the atmosphere are sparse because it is difficult to separate free ammonia from particulate ammonium salt aerosol. A manual method for the determination of free ammonia in air is described based on diffusion/denuder tube separation of ammonia from ammonium salt aerosol. When air is drawn through a tube coated with a selective absorbent (here oxalic acid) separation is achieved because the gaseous species diffuses much more rapidly to the tube wall than the particles. After the sampling period (usually 1—4 h, depending on the free ammonia concentration expected), the sorbed ammonia is washed from the tube and measured potentiometrically with an ammonia probe. The method is tested theoretically and experimentally. The absorption efficiency of the coated tubes is ca. 90%. In samples of room air containing 12—28 $\mu g\ m^{-3}$, the standard deviation is estimated as 1.0 $\mu g\ m^{-3}$. In field use, ammonia contents were in the range 0.53—5.9 $\mu g\ m^{-3}$.

Ammonia is the most important naturally-occurring alkaline species present in the atmosphere and is therefore of great importance in atmospheric chemistry. Because of its alkalinity, it neutralises acidic species in the atmosphere, e.g., sulphuric acid and nitric acid. It dissolves readily in cloud water, increasing the pH of cloud droplets, facilitating the uptake of sulphur dioxide and nitrogen oxides, and thereby influencing the conversion of these gaseous species to sulphate and nitrate aerosols. Sources of ammonia in the atmosphere are biological in origin and result from the natural decomposition of organic materials, e.g., urine from animals.

It is important that the procedure for the determination of free ammonia be able to distinguish it from the particulate ammonium salt aerosol also present. This has been attempted previously by pre-filtration of the air sample to remove ammonium salt aerosol with subsequent determination of free ammonia downstream of the filter [1, 2]. Alternatively, diffusion/denuder tubes have been used [3, 4]; these are based on the principle that when air is drawn through a tube coated with a selective absorbent, separation is achieved because of the much more rapid diffusion of gaseous species to the tube walls compared with that of the particles. Free ammonia diffuses rapidly to

0003-2670/86/$03.50

the walls of the diffusion/denuder tube and is retained, whereas ammonium salt particles pass through unabsorbed. Filter methods do not really give an accurate separation of free ammonia from ammonium aerosols because of interactions on the filter [5—7]. There are three particular interaction mechanisms: (i) ammonia can be retained on the filter because of reaction with or adsorption on particles on the filter; (ii) ammonium aerosol retained on the filter may dissociate and volatilise to release free ammonia because of departures from the equilibria these particles previously held with free ammonia in air; and (iii) ammonium salt particles can react with alkaline sea salt particles on the filter to release free ammonia.

This paper describes a manual procedure for the determination of free ammonia in air based on separation on a diffusion/denuder tube from ammonium salt aerosol. The sampling time is kept to a minimum by rigid control of conditions. The effectiveness of the method in separating free ammonia from ammonium aerosol is tested with a laboratory-constructed aerosol generator.

THEORY

Air is passed through a cylindrical tube coated with a selective absorbent (here oxalic acid) and the molecules of reactive ammonia gas diffuse to the walls according to the mathematical model first developed by Gormley and Kennedy [8]. It is assumed that the wall collisions are inelastic. In this model

$$C/C_0 = 0.819 \exp(-14.6272\pi DL/4F) \quad (1)$$

where C is the mean concentration of ammonia in the air leaving the tube, C_0 is the concentration of ammonia in the incoming air, D is the diffusion coefficient of ammonia in air, L is the length of coated tube and F is the flow rate.

Errors from concomitant ammonium salt aerosols may arise from two mechanisms [3]. In the first, free ammonia can be released from the ammonium salt aerosol passing through the tube because of the departure from the previous equilibrium of free ammonia and aerosol in ambient air, i.e., the partial pressure of ammonia in the diffusion denuder tube will be lower than the ambient partial pressure of ammonia because of diffusion of ammonia in the tube to the wall. This favours decomposition of ammonium aerosol particles to release further free ammonia. With the experimental conditions used in this work (air flow of 2 l min^{-1} and coated tube length of 35 cm), the residence time of a particle within the tube is as little as 0.07 s and so contributions from particulate dissociation are assumed to be negligibly small.

The second mechanism involves direct deposition of particles as they pass through the tube. For deposition to be avoided, the flow of air through the coated part of the tube should be laminar and this is so if the Reynolds number (Re) is <2000. Laminar flow throughout the coated region of the tube is ensured if there is an uncoated length of tubing (L') upstream of the coated

tube. Prandtl and Tietjens [9] have defined its length as $L' > 0.05 \times d \times Re$, where d is the tube diameter and $Re = \bar{v}d\rho/\eta$, $\bar{v}$ being the mean velocity of the air, ρ its density and η its dynamic viscosity. If the volumetric flow rate $F = \bar{v}\pi(d/2)^2$, then $Re = 4F\rho/\pi d\eta$. For the experimental conditions used in this work (an air flow of 2 l min^{-1} and a tube diameter of 3 mm), this equation gives $Re = 988$. Therefore, from the definition of Prandtl and Tietjens, the length of the uncoated tubing should be $L' \geqslant 15$ cm.

Particles can be deposited by gravitation and this becomes significant for particles of >1—10 μm [3], but the problem can be overcome by placing the tubes in a vertical position. Particles can also diffuse to the tube walls because of Brownian motion. Fuchs [10] has quoted an expression

$$n/n_0 = 2.56\mu^{2/3} - 1.2\mu - 0.177\mu^{4/3} \quad (2)$$

where $\mu = \pi DL/F$, n is the number of particles per unit volume of air deposited on the tube wall, and n_0 is the number of particles per unit volume of air entering the tube.

EXPERIMENTAL

Equipment

The diffusion/denuder tubes were made of glass (50 cm long, 3-mm i.d.). An etch mark was made 15 cm from the end open to the atmosphere. The remaining 35 cm was coated with the selective absorbent (see below). Before first use, the tubes were soaked overnight in a chromic acid cleaning solution, washed with deionized/distilled water and stored completely submerged in deionized water in a 500-ml measuring cylinder.

The air-sampling apparatus is shown in Fig. 1. Air was drawn through the diffusion/denuder tube by a diaphragm pump (Capex 2D; Charles Austen, Byfleet) and the volume was measured by a gas meter (Model G4; UGI Meters, London). The flow of air was controlled by a rotameter valve.

Ammonia measurements were made on the aqueous extracts from the diffusion/denuder tube with a potentiometric ammonia probe (Philips IS561) housed in a temperature-controlled cabinet at 35 ± 1°C. The operation of the ammonia probe has been adequately described by Midgley and Torrance

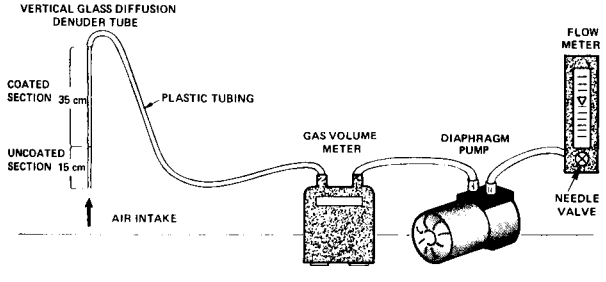

Fig. 1. Apparatus for sampling free ammonia in ambient air with a diffusion/denuder tube.

[11] and by the manufacturer. The e.m.f. was measured with a pH meter (Beckman model 4500) attached to a chart recorder.

All chemicals were obtained from BDH Chemicals.

Procedures

The oxalic acid coating solution was prepared daily. Oxalic acid (AristaR grade) was recrystallised from water; 0.15 g of this oxalic acid was dissolved in 10 ml of ethanol (Spectrosol grade) and kept in a sealed container.

Before being coated, the diffusion/denuder tube was washed successively with deionized/distilled water, methanol (AnalaR), and ethanol (Spectrosol). The open end of the 35-cm section of the tube was placed in the 1.5% (w/v) oxalic acid solution and, with the aid of a pipette filler, the tube was filled to the etch mark and then allowed to drain back into the oxalic acid container. This operation was repeated five times. The coated tube was left to drain for 20 s and then dried by pumping dry air through it for 20 s with a diaphragm pump. Both ends of the tube were then immediately sealed with Parafilm if the tube was to be stored. The unsealed diffusion/denuder tube was placed in position in the sampling apparatus (Fig. 1) and sampling was commenced at about 2 l min^{-1}. At the end of the sampling period the tube was removed and sealed at both ends with Parafilm if it was to be stored, and the volume of air sampled was recorded.

The open end of the coated section of the exposed and unsealed tube was placed in 5 ml of deionized/distilled water in a small sample vial and, with a pipette filler, the water was drawn into the tube to the etch mark and then allowed to drain out. This operation was repeated five times. All ammonia measurements were made at 35°C in the temperature-controlled cabinet. After addition of 0.5 ml of 1 mol l^{-1} sodium hydroxide (maintained at 35°C by storage in the cabinet) to the 5 ml of oxalic acid and ammonia washings, the e.m.f. of the stirred solution was read after equilibrium had been attained. The e.m.f. was compared with a previously prepared calibration curve for ammonia standard solutions within the range 10—1000 $\mu g\ l^{-1}$. In all cases, measurements were made by approaching from a solution of lower concentration; for low levels of ammonia ($<100\ \mu g\ l^{-1}$), this should be deionized/distilled water.

The concentration of free ammonia in air (assuming 100% absorption efficiency) is given by $C_0\ (\mu g\ m^{-3}) = a \times 5/v$, where a is the concentration ($\mu g\ l^{-1}$) of ammonia in the 5 ml of washing solution and v is the volume (l) of air sampled.

RESULTS

Method development

Electrode response time. At room temperature, the ammonia probe responds very slowly to concentration changes of ammonium ion below about 200 $\mu g\ l^{-1}$ and this limits the usefulness of the electrode even though there is

sufficient sensitivity in this region for measurements to be possible. The electrode assembly was therefore housed in a temperature-controlled cabinet at 35°C and all measurements were made at this temperature. Table 1 shows the electrode response times at 20°C and 35°C. Operation at 35°C allows the electrode to be used conveniently at levels of ammonium ion as low as 10 $\mu g\ l^{-1}$, presumably because of accelerated transport of ammonia across the membrane.

Effect of air flow rate on absorption efficiency. Theoretical percentage absorption efficiencies ($C/C_0 \times 100$) can be calculated from Eqn. 1 in the theory section. In all work, the coating length, L, was 35 cm. Table 2 shows the effect of varying sample flow rates on the theoretical absorption efficiency of a coated diffusion/denuder tube; the diffusion coefficient of ammonia in air was taken as $2.36 \times 10^{-5}\ m^2\ s^{-1}$ [12]. From these results, air flows of 2 l min^{-1} were appropriate for further work.

The experimental absorption efficiency for ammonia was then evaluated at different flow rates. Two tubes were connected in series and examined separately after 50 l of room air had been sampled at various flow rates. Absorption efficiency was calculated from (lower tube concentration × 100/ lower tube + upper tube concentration). Table 2 shows that variations in sample air flow did not affect the experimental absorption efficiency (mean value 90.5%) significantly.

Ammonia measurements in the presence of ammonium salt particles

Particulate ammonium salt aerosol can diffuse to the diffusion/denuder tube walls by Brownian diffusion and the theoretical absorption efficiency can be calculated from Eqn. 2. Under the experimental conditions used here, the second and third terms of Eqn. 2 can be ignored because their effect is insignificant. Table 3 shows the absorption efficiencies for particles of various sizes. Diffusion coefficients are taken from Fuchs [10]. The mass of airborne particles tends to be in the range 0.01—4 μm and so it can be concluded that there is insignificant deposition of these particles by Brownian diffusion under the present experimental conditions.

TABLE 1

Response times[a] of the ammonia probe at room temperature (20°C) and at 35°C

Concentration change ($\mu g\ l^{-1}$)[b]	Response time (min)	
	at 20°C	at 35°C
0 → 10	—	12
0 → 20	>40	10
0 → 50	—	8
0 → 100	—	4

[a]Response time is defined here as the time for the electrode to attain a steady response to the concentration changes shown. [b]0 $\mu g\ l^{-1}$ refers to deionized water alone.

TABLE 2

Effect of sample flow rate on the theoretical and experimental absorption efficiency of a 35-cm coated diffusion/denuder tube

Flow rate ($l\ min^{-1}$)	Ammonia found ($\mu g\ m^{-3}$)		Absorption efficiency (%)	
	Upper tube	Lower tube	Found	Theor.
0.26	1.55	16.4	91.4	—
0.34	1.98	16.1	89.0	—
1.00	—	—	—	99.7
1.26	1.92	21.0	91.6	—
1.42	1.54	16.4	91.4	—
1.63	2.85	22.2	88.6	—
2.00	1.92	19.2	90.9	95.4
2.50	—	—	—	91.6
3.00	—	—	—	87.7
4.00	—	—	—	80.3

TABLE 3

Effect of particle size on particulate deposition on the diffusion/denuder tube wall by Brownian diffusion[a]

Particle size (μm)	Diffusion coefficient ($m^2\ s^{-1}$)	n/n_0
0.01	1.35×10^{-8}	1.50×10^{-2}
0.1	2.21×10^{-10}	9.69×10^{-4}
1.0	1.27×10^{-11}	1.44×10^{-4}

[a]Air flow 2 $l\ min^{-1}$; coated length 35 cm.

To ascertain experimentally whether the presence of ammonium salt aerosol particles interfered with the procedure for free ammonia, aerosol particles were artificially generated from a laboratory-constructed aerosol generator, which was a modification of that used by Slanina et al. [5]. It is shown, with its dimensions, in Fig. 2. The concentration of ammonium particles in the air stream was calculated from the solution and air flow rates. Ammonium sulphate was chosen because it is the predominant ammonium salt in the atmosphere. Ammonium sulphate solution (1 $\mu g\ ml^{-1}$ NH_4^+) was passed to the nebulizer at a flow rate of 0.144 ml min^{-1}, and dispersed into an air stream at 20 l min^{-1}. The concentration of ammonium sulphate particles in the air stream was therefore 7.2 $\mu g\ m^{-3}$. The particle size of the aerosol was measured by sampling at the open outlet of the generator into a particle size analyser (Royco 225). The results of seven runs of 1-min duration showed that 95% of the particles counted had a diameter <0.5 μm, with a negligible number of particles of diameter <1 μm; no counts were obtained in the 1.4—5.0 μm range. Ambient ammonium salt particles are of similar

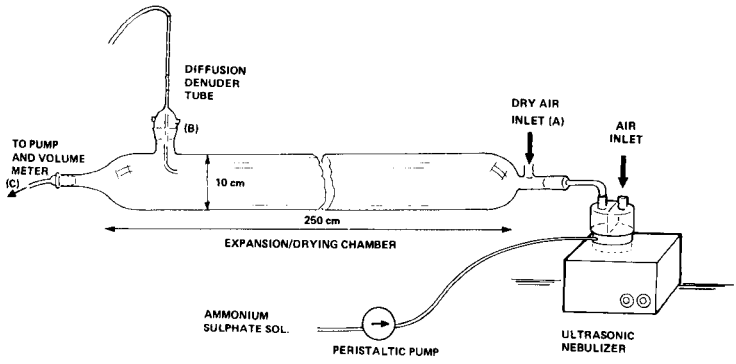

Fig. 2. Aerosol generator. Aerosol from the ultrasonic nebulizer (Engstrom NB108) is directed down a long glass tube where it is dried by an auxiliary flow of air from inlet A. The air and particles are sampled at position B, where a diffusion/denuder tube is attached. A solution of ammonium sulphate is fed to the nebulizer at a controlled rate by a peristaltic pump (Watson-Marlow). The volume of air into which the aerosol is dispersed is measured by a volume meter (UGI model G4).

diameter and so the ammonium aerosol generated can be taken to be representative of aerosol present in the atmosphere.

The determination of free ammonia in the presence of ammonium particles was then checked experimentally. All apparatus was thoroughly cleaned before these experiments were begun. Air was drawn and not pumped through the ultrasonic nebulizer and generator tube, to avoid contamination from the components of the pump. A diaphragm pump capable of sampling at 20 l min^{-1} was placed at position C (Fig. 2). A volume meter was also placed in the line at this point. A solution of ammonium sulphate (1 μg ml^{-1} ammonium ion) was pumped to the ultrasonic nebulizer at 0.05 ml min^{-1} and air was drawn through the nebulizer at 15—20 l min^{-1}. Coated diffusion/denuder tubes were set up in the region of the air intake point (A) and the aerosol generator outlet sampling point (B). For a set period of time, free ammonia in room air was compared with the free ammonia determined in the presence of ammonium particles. The concentration of ammonium sulphate particles in the air was calculated as outlined above, and was typical of that found in ambient air. The results (Table 4) show that the presence of particles has a negligible effect on the determination of free ammonia in air.

Storage of the diffusion tubes

Tests were conducted to ascertain how long coated diffusion/denuder tubes could be stored both before use and after exposure prior to determining ammonia.

It quickly became apparent that coated tubes very readily absorbed ammonia when left to stand in room air without their ends being sealed. The mechanism of absorption is not known but the effect could be quite large. For instance, a noticeable effect was found after standing for only 10 min;

TABLE 4

Free ammonia determination in the presence of ammonium particles

Ammonia found ($\mu g\ m^{-3}$)		Particulate concn. ($\mu g\ m^{-3}\ NH_4^+$)
Without particles	With particles	
22.25	22.45	2.89
19.61	19.45	3.92
19.94	20.15	3.31

when a tube was left for 2.5 h, its blank value (the ammonium concentration in the 5 ml of washing solution) increased to 80 $\mu g\ l^{-1}$ compared with the usual level of $\ll 10\ \mu g\ l^{-1}$ found when ammonia was measured immediately after coating. This effect was overcome by sealing the ends of the tube with Parafilm; when this was done, sealed tubes could be left unexposed for at least 4 days.

Exposed tubes, if left to stand before ammonia was determined, were found to give increased free ammonia concentrations even when sealed at both ends with Parafilm, compared with tubes processed immediately. Table 5 gives a selection of results obtained when exposed tubes were sealed with Parafilm or with a rubber bung and left for varying times; for comparison, a duplicate tube was processed immediately after exposure. The calculated free ammonia concentration was found to increase by as much as 20% in some instances, but there was no correlation between the time of storage and the percentage increase in free ammonia concentration.

Performance characteristics

The performance characteristics of the proposed method were assessed. In all cases the method as described in the procedure was followed.

A typical calibration graph for the ammonia probe electrode is shown in Fig. 3. For best results, a fresh calibration was prepared with each batch of samples. Between batches, the electrode was left to stand (submerged in water) in the temperature-controlled cabinet at 35°C, where it proved to be stable for periods up to at least 2 months. After this time, the internal filling solution was replaced.

To estimate the absorption efficiency of the diffusion/denuder tubes, the percentage of ammonia absorbed on coated tubes was measured by connecting two tubes in series and determining ammonia in each tube separately. Different volumes of room air were analysed on separate occasions. The results are given in Table 6. An acceptable absorption efficiency of 88—91% was obtained in the lower tube.

The precision of the method was estimated by sampling room air through two tubes in parallel on 18 separate occasions. The free ammonia contents of the air samples ranged from 12 to 28 $\mu g\ m^{-3}$ and the standard deviation was estimated as 0.99 $\mu g\ m^{-3}$.

TABLE 5

Effect of storage on exposed tubes when sealed with Parafilm or a rubber bung

	Ammonia found ($\mu g\ m^{-3}$) after different storage times[a]				
Seal	2 h	4 h	8 h	16 h	24 h
Parafilm	13.8/15.7(13.8%)	13.4/14.9(11.2%)	—	16.9/18.7(10.7%)	15.1/17.5(15.9%)
Rubber bung	15.6/18.6(19.2%)	14.4/15.9(10.4%)	14.2/14.5(2.1%)	17.8/20.3(14.0%)	14.0/16.8(20.0%)

[a]The first result in each pair (e.g., 13.8/15.7) relates to the tube processed immediately and the second result to the stored tube. The % increase in ammonia content on storage is given in parentheses.

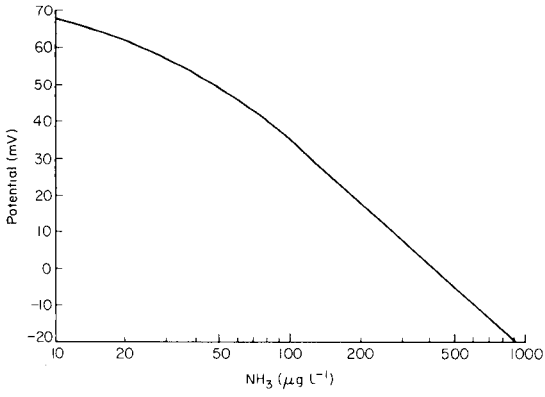

Fig. 3. Ammonia probe calibration line.

Tube blank. It is important that blank diffusion/denuder tubes are included in any series of measurements, by coating, sealing, and processing in exactly the same way as sample tubes. In most cases, the level of ammonia found in the 5 ml of deionized/distilled water after dissolution of the coating was $\leqslant 10\ \mu g\ l^{-1}$ but on occasions the levels were $>10\ \mu g\ l^{-1}$. Ion-chromatography of 1.5% (w/v) oxalic acid solution showed ammonia contents of about $0.02\ \mu g\ ml^{-1}$ (or $1.3\ \mu g\ g^{-1}$ ammonia in the solid oxalic acid). Because no more than 0.1 ml of the oxalic acid solution was expected to be deposited on each tube, the contribution of ammonia from oxalic acid is no more than $0.4\ \mu g\ l^{-1}$ in the 5 ml of water used to dissolve the coating and accordingly does not contribute significantly to the blank. If high blanks ($>10\ \mu g\ l^{-1}$ in the 5 ml of water) are encountered, contamination is likely to be the source. This most probably arises by diffusion of atmospheric ammonia into solution in uncovered sample containers and, as mentioned previously, by diffusion into the coated tubes. The determination of tube blanks serves as a means of checking the cleanliness of working. If tube blanks prove difficult to keep below $10\ \mu g\ l^{-1}$ in the 5 ml of water, the air sampling time should be increased so that at least $100\ \mu g\ l^{-1}$ levels of ammonia are examined in the sample. This

TABLE 6

Absorption efficiency of ammonia diffusion/denuder tubes

Volume sampled (l)	Ammonia found ($\mu g\ m^{-3}$)		Absorption efficiency (%)
	Upper tube	Lower tube	
216	1.3	9.5	88.0
206	1.7	13.1	88.5
50	1.9	19.2	90.9

means that for an ammonia concentration of 1 $\mu g\ m^{-3}$ in air, a sampling time of approximately 4 h is required.

Measurements of free ammonia in air

Measurements of free ammonia in air were made in the field at four different sites. The sampling apparatus was mounted onto a frame and powered from a 12-V car battery. Sampling was done for approximately 1 h at each site on a day when the weather was overcast and it had recently been raining. Duplicate blank tubes were prepared and determined at the same time as the samples and gave negligible ammonia concentrations. On a previous occasion, air was sampled at CERL, both in the morning and afternoon when the weather was warm (27°C) and sunny. Results are given in Table 7.

DISCUSSION

The technique described, in which free ammonia is separated from particulate ammonium salts in a diffusion/denuder tube, allows free ammonia to be determined in the atmosphere at the levels expected to be encountered, i.e., 0.2—10 $\mu g\ m^{-3}$. The lowest level of ammonia that can sensibly be determined potentiometrically in the 5 ml of water used to extract ammonia from the coated tube is about 10 $\mu g\ l^{-1}$. Although the electrode has sufficient sensitivity, its very sluggish response precludes its use below this level. For the determination of very low levels of ammonia ($<1\ \mu g\ m^{-3}$), it is recommended that air be sampled for at least 4 h. If the levels are $>1\ \mu g\ m^{-3}$, a 1-h sampling time will probably be adequate.

It is very important that contamination be avoided because errors can be quite large, especially for low ammonia concentrations and short sampling times. If results of the highest precision are required, sampling times should be increased accordingly.

The method was examined both theoretically and experimentally. The experimentally derived absorption efficiencies of the diffusion/denuder tubes were approximately 90% and this agrees well with the 95% calculated from the mathematical model. The mathematical model also indicated that

TABLE 7

Free ammonia concentration in air at five separate sites

Site		Free ammonia found ($\mu g\ m^{-3}$)	Site		Free ammonia found ($\mu g\ m^{-3}$)
Chessington	TQ177614[a]	0.85	CERL Leatherhead[b]	a.m.	3.98
Morden	TQ253676[a]	0.94	CERL Leatherhead[b]	p.m.	3.80
Sutton	TQ255650[a]	1.05	CERL Leatherhead[b]	p.m.	5.89
Ranmore Common	TQ141504[a]	0.53			

[a]Sampled on 29:11:84. The Ordnance Survey reference is given. [b]Sampled on 18:6:1984.

interference from particulate ammonium salts should be negligible and this was confirmed experimentally.

It is important that coated tubes are sealed with Parafilm before use. For the best results, it is recommended that the analysis be conducted immediately.

The work was done at the Central Electricity Research Laboratories and this paper is published by permission of the Central Electricity Generating Board.

REFERENCES

1 A. D. Shendrikar and J. P. Lodge, Atmos. Environ., 9 (1975) 431.
2 R. Abbas and R. L. Tanner, Atmos. Environ., 15 (1981) 277.
3 M. Ferm, Atmos. Environ., 13 (1979) 1385.
4 R. S. Braman, T. J. Shelley and W. A. McClenny, Anal. Chem., 54 (1982) 358.
5 J. Slanina, L. Lamoen-Doornebal, W. A. Lingerak, W. Meilof, D. Klockow and R. Niessner, Int. J. Environ. Anal. Chem., 9 (1981) 59.
6 M. Possanzini, A. Febo and A. Liberti, Atmos. Environ., 17 (1983) 2605.
7 J. L. Gras, Tellus, 36B (1984) 38.
8 P. G. Gormley and M. Kennedy, Proc. R. Ir. Acad., Sect. A: 52 (1949) 163.
9 L. Prandtl and O. Tietjens, Hydro- und Aero-mechanik, Vol. 2, Springer-Verlag, Berlin, 1931, p. 28.
10 N. A. Fuchs, The Mechanisms of Aerosols, Pergamon, Oxford, 1964, p. 205.
11 D. Midgley and K. Torrance, Potentiometric Water Analysis, Wiley, New York, 1978, p. 34.
12 J. M. Coulson and J. F. Richardson, Chemical Engineering, Vol. 1, Pergamon, Oxford, 1954, p. 239.

Analytica Chimica Acta, 185 (1986) 171—178
Elsevier Science Publishers B.V., Amsterdam — Printed in The Netherlands

USE OF ION-SELECTIVE ELECTRODES IN INDUSTRIAL FLOW ANALYSIS

PETR PETÁK

Ore Research Institute, Modřanská 23, 140 00 Prague 4 (Czechoslovakia)

KAREL ŠTULÍK*

Department of Analytical Chemistry, Charles University, Albertov 2030, 128 40 Prague 2 (Czechoslovakia)

(Received 9th August 1985)

SUMMARY

Two cells with ion-selective electrodes are described for industrial flow analysis, involving the flow-injection technique and continuous monitoring. The dependence of the electrode signal on the experimental parameters is discussed using the determination of cyanide as a model. It is shown that sensitive and reproducible measurements are possible even if the industrial application requires that the measuring cell be large, provided that the flow rate of the carrier liquid is sufficiently high. Large cell volumes are advantageous in continuous monitoring, as the signal approaches that obtained under steady-state conditions. Experiments with a calcium ion-selective electrode and with an ammonia gas probe show that the slow response of the sensor severely limits its applicability in flow analysis.

Ore treatment plants, especially those involving hydrometallurgical processes, as well as many other industrial enterprises, are at present extensively automated and thus require automatic analytical control. Chemical analyzers must work reliably under extreme conditions of dirty production lines and must therefore be simple, robust and easy to operate. Some electrochemical measurements are well suited for this purpose because they yield easily treated signals (e.g., electrical conductance, voltage or current) that permit instantaneous monitoring of a process, and feed-back control.

Ion-selective electrodes (ISEs) have been applied extensively for flow measurements (see, e.g. [1—3]), both for continuous monitoring and for flow-injection analysis (f.i.a.) [4]. However, greater attention has been paid to laboratory analyses than to industrial measurements; the latter have been reviewed [5].

The performance of a detector in a flowing liquid depends on the properties of the sensor itself, on the geometry of the measuring cell and on the dispersion of the test substance in the connecting pathways in the apparatus. To date, cell construction, the sensor properties and solute dispersion in tubes have mostly been studied in connection with h.p.l.c. detection [6] and f.i.a. [4]. Several models have been developed to describe dispersion

0003-2670/86/$03.50

phenomena quantitatively; useful surveys are available [7, 8]. In these studies, the systems were optimized to match the models.

This paper describes an investigation of the performance of detectors with ISEs that have been constructed for industrial applications. Therefore, the cells and connecting tubing are larger to prevent blocking and to accommodate large electrodes; they consequently deviate from the conditions required by the theoretical models. In order to provide some criteria for the construction of cells which cannot be optimized from the point of view of solute zone dispersion and cell geometry, the dependencies of the detector signal on the measuring conditions are studied here by using continuous monitoring and a flow-injection system for the determination of cyanide. The results from these model systems are applied in the construction of an automatic on-line analyzer for waste waters from industrial cyanide extraction of gold. To compare the results obtained with ISEs with various response rates, measurements were also made with a calcium-selective electrode and an ammonia gas probe.

EXPERIMENTAL

The measurements were made with the apparatus outlined in Fig. 1 which consisted of a peristaltic pump (Zalimp 304, Poland), a mixing coil, a rotary sampling valve and a potentiometric detector containing a cyanide ion-selective electrode (Crytur, Czechoslovakia) and a saturated calomel reference electrode (Radelkis, Hungary). Silicone rubber connecting tubing (1 mm i.d.) was used.

The rotary sampling valve (Fig. 2) is analogous to one described earlier [9]. It consists of two PVC stators, between which an exchangeable PTFE rotor can be turned by 180°. The diameter of the rotor channel determines the sample volume, from tens to hundreds of microlitres. Silicone rubber seals are placed between the rotor and the stators. The test solution flows through one tube, the carrier liquid through the other, and the sample is injected by rapidly turning the rotor by 180°. The increase in the pressure in the system during turning of the rotor is compensated by the elastic stretch-

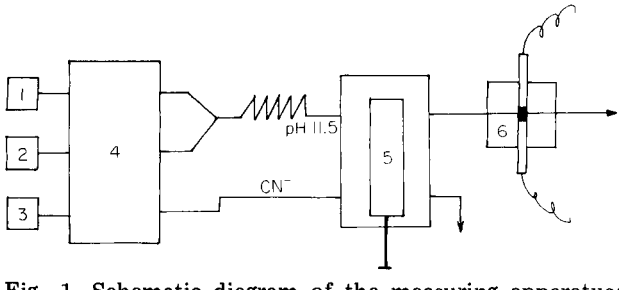

Fig. 1. Schematic diagram of the measuring apparatus: (1) NaOH reservoir; (2) water reservoir; (3) cyanide inlet; (4) peristaltic pump; (5) sampling valve; (6) potentiometric detector.

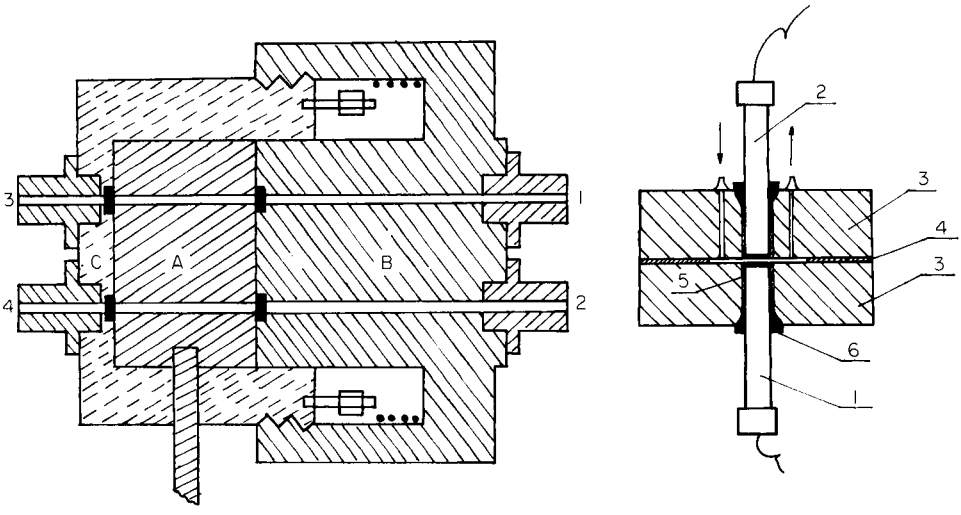

Fig. 2. The sampling valve: (A) PTFE rotor (3.8 cm tall, 6.0 cm o.d.) with channels of known volume; (B, C) stators; (1) carrier solution inlet; (2) sample inlet; (3) outlet to the detector; (4) outlet to waste. Inlets and outlets are 1 mm i.d.

Fig. 3. The two-electrode measuring cell: (1) ISE; (2) reference electrode; (3) cell body; (4) spacer; (5) rubber seal; (6) fixing screws. The inlet and outlet channels are of 1 mm diameter.

ing of the walls of the silicone rubber tubes up to flow rates of ca. 5 ml min^{-1}; at higher flow rates, a pinhole in the inlet tube for the carrier solution suffices to relieve the pressure.

Two detector cells were used. One cell (Fig. 3) consists of two polymethylmethacrylate blocks with holes for an ISE and a reference electrode. The polished faces are separated by a PTFE or silicone rubber spacer which defines the working space, varying from a few tens to over 1000 microlitres, depending on the spacer thickness. The other polymethylmethacrylate cell (Fig. 4) contains three electrodes (two ISE's and a reference electrode) in the channel through which the test solution flows. The seals surrounding the electrodes contain small holes through which air bubbles that may be formed during the measurement can escape. The cell permits simultaneous measurement of two quantities (e.g., the cyanide content and the pH) and has an internal volume of 0.5 ml.

Measurements were made at laboratory temperature (20 ± 2°C) in the following way. Solutions of sodium hydroxide, water and potassium cyanide were pumped through the apparatus. The sodium hydroxide solution and water were mixed in the coil (usually 90 cm long) to adjust the pH to 11.5, and the mixture was fed through the sampling valve into the detector as the carrier liquid. The potassium cyanide solutions were pumped through the other tube and 70-μl samples with cyanide concentrations of 5—50 mg l^{-1}

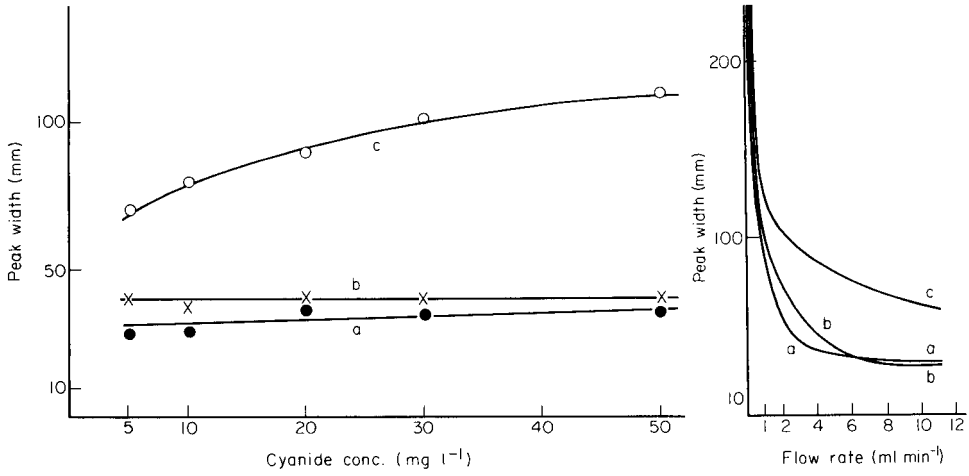

Fig. 4. The calibration graphs obtained for cyanide: (a) by the flow-injection system; (b) by continuous monitoring.

Fig. 5. Dependence of the peak height (A) and the peak half-width (B) on the liquid flow rate for different cell volumes: (a) 25; (b) 100; (c) 1500.

were introduced into the carrier stream. The cell volumes studied were 25, 100 and 1500 μl. For some measurements, a calcium ion-selective electrode (Crytur, Czechoslovakia) and an ammonia gas probe (Radelkis, Hungary) were also used. For the preparation of the solutions used, p.a. chemicals (Lachema, Czechoslovakia) were used as received.

RESULTS AND DISCUSSION

Solute zone dispersion and response rate

In contrast to the photometric detectors which are most often used in checking the validity of the Taylor [10] and the tanks-in-series [4] models or the validity of the criteria formulated by Vanderslice et al. [11], where laminar flow can be assumed to exist from the injection port to the sensor, the present detectors clearly involve turbulence in the relatively large cell, and thus are more similar to the model of Pungor et al. [12] for the system with a mixing chamber placed close to the detector cell or in the detection space. In the connecting tubing, laminar flow can be assumed at the flow rates and tubing diameters considered here. Therefore, convection is the predominant factor controlling the solute zone dispersion in the cell, producing detector signal peaks with pronounced tailing (cf. Fig. 3 [8]). As would be expected, the importance of convective dispersion increases with increasing volume of the cell (Fig. 5). The experimental baseline-to-baseline times are larger than the values calculated from the equation derived by Vanderslice et

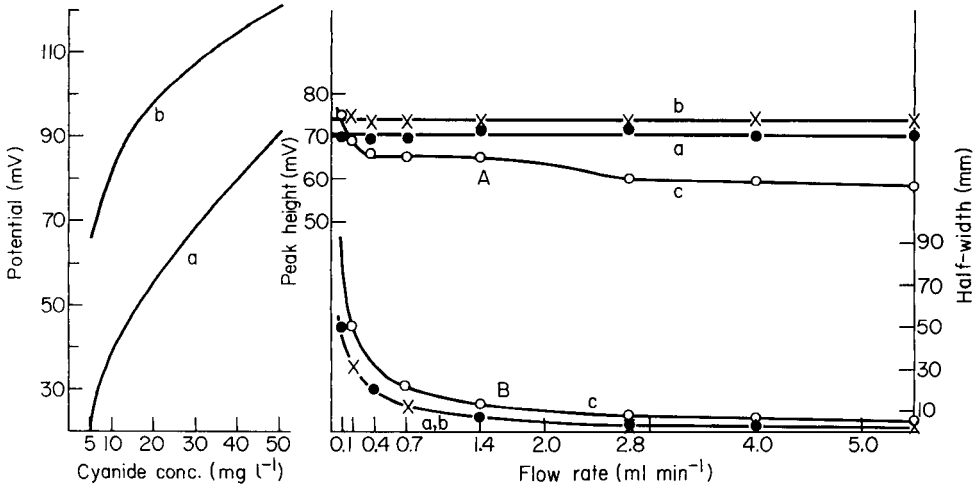

Fig. 6. Dependence of the baseline-to-baseline peak width on the sample concentration for different cell volumes: (•) 25; (X) 100; (○) 1500 μl.

Fig. 7. Dependence of the baseline-to-baseline peak width on the carrier flow rate for different cell volumes: (a) 25; (b) 100; (c) 1500 μl.

al. [11] for convective-diffusional dispersion and laminar flow. However, the increasing significance of diffusional dispersion with decreasing volume of the cell is demonstrated by the dependence of the baseline-to-baseline peak width on the sample concentration (Fig. 6). While this peak width is independent of the sample concentration for cell volumes of up to 100 μl, there is a pronounced increase with increasing concentration for a cell volume of 1500 μl.

The tailing of the peaks increases greatly when the flow rate decreases below a certain value for all the detector volumes. As can be seen in Fig. 7, this increase begins at a flow rate of ca. 3 ml min^{-1} for a detector cell volume of 25 μl, at ca. 6 ml min^{-1} for a volume of 100 μl, and at a flow rate greater than 12 ml min^{-1} for a volume of 1500 μl.

The response rate can be expressed in terms of the time constant, defined as the time required for the signal to attain 63.2% of its maximum value [13]. The response volume values are then calculated by multiplying the time constants by the volume flow rate. The time constants and the response volumes obtained here in relation to the liquid flow rate are summarized in Table 1. It can be seen that, at low flow rates, the response time of detector cells with volumes of up to 100 μl is similar, while the cell with a volume of 1500 μl exhibits a substantially slower response. However, with increasing flow rate, the response times of all the cells gradually become more similar. The response volumes of the smaller cells (25 and 100 μl) are larger than the geometric volumes, indicating that diffusion plays a role in signal control.

TABLE 1

Time constants (k_t) and response volumes (V_r) in relation to the carrier flow rate for different volumes of the detector cell

Flow rate (μl s^{-1})	Detector cell volume					
	1500 μl		100 μl		25 μl	
	k_t (s)	V_r (μl)	k_t (s)	V_r (μl)	k_t (s)	V_r (μl)
1.5	135.0	200	75.0	110	75.0	110
3.0	75.0	225	50.0	150	47.5	140
6.0	40.0	240	25.0	150	25.0	150
12.0	21.6	260	15.0	180	15.0	180
22.0	12.5	275	7.5	165	6.0	130
47.0	9.0	420	5.0	235	2.5	120
92.0	5.0	460	4.0	360	2.0	180
180.0	4.0	720	2.5	450	1.5	270

However, the response volume of the 1500-μl cell is substantially smaller than the geometric volume; this demonstrates that the effective volume of the cell is smaller than the geometric volume, i.e., that only part of the test substance reaches the sensor during the residence time in the cell. The response volumes increase with increasing flow rate from a certain value for each detector volume; these values are ca. 1.5, 3.0 and 6.0 ml min^{-1} for detector volumes of 1500, 100 and 25 μl, respectively. This increase reflects not only the increasing importance of diffusion in the detector signal control with increasing flow rate, but probably also the effect of the limited response rate of the sensor itself. On the whole, it can be concluded that higher flow rates should be used when the detector cell volume must be large.

Calibration graphs, reproducibility and the response dependence on flow rate

The magnitude of the detector signal is affected to a certain extent by the length of the inlet tubing. With 30 cm of tubing (1 mm i.d.) between the sampling valve and the detector cell, the calibration plots differ for different cell volumes because of an unstabilized concentration profile in the liquid stream. When the length of the inlet tubing is increased to 100 cm with the same internal diameter, the same signal is obtained for all the detector cell volumes. The calibration graphs for the flow-injection procedure and the continuous monitoring of cyanide are given in Fig. 8. For continuous monitoring, the length of the inlet tubing is unimportant but the cell geometry is decisive; large volume cells are advantageous here, as the detector response approaches that obtained under steady-state conditions.

The detection limit, calculated as twice the standard deviation of the noise, is 0.08 mg l^{-1} cyanide under optimal conditions. The long-term reproducibility was tested by continuous passage of the carrier liquid for several days, with periodic injections of cyanide; the relative standard deviation (n = 50)

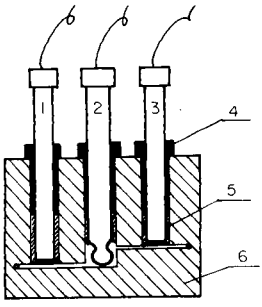

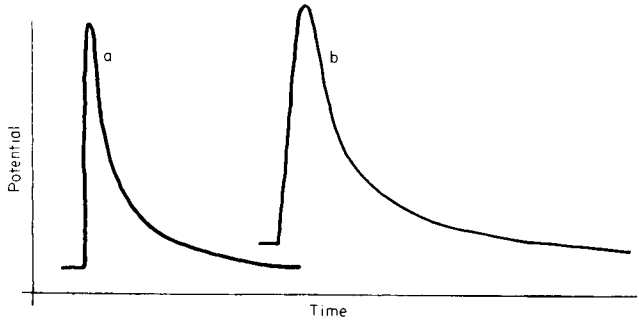

Fig. 8. The three-electrode measuring cell: (1) reference electrode; (2) glass electrode; (3) another sensing electrode; (4) fixing screws; (5) silicone rubber seal; (6) cell body.

Fig. 9. Typical signal shapes in f.i.a. for different cell volumes: (a) 25 μl; (b) 1500 μl. Conditions: 20 mg l^{-1} cyanide, flow rate 3 ml min^{-1}, chart speed 50 s cm^{-1}, potential scale 5 mV cm^{-1}.

was 2.5% for 10^{-3} M cyanide. The cyanide-selective electrode permitted continuous measurement for three weeks without electrode regeneration. Some authors [14, 15] have recommended that a small concentration of the test substance be added to the carrier liquid to stabilize the baseline; however, this addition leads to a substantial decrease in the potential change in the determination of small concentrations of cyanide and limits the measuring sensitivity. It seems that more frequent calibration, connected with automated zeroing, is preferable.

The dependence of the peak height and half-width on the carrier flow rate is depicted in Fig. 9. The peak half-width decreases with increasing flow rate as expected. The peak height is virtually independent of the flow rate for small cell volumes, whereas it increases with decreasing flow rate for the large cell. However, this increase is not large enough to outweigh the advantage of rapid response time at high flow rates.

The effect of the sensor response rate

Slow response rates of sensors can severely limit their applicability in flow measurements. For this reason, flow measurements were also tested with a calcium ion-selective electrode and with an ammonia gas probe, both of which have substantially slower responses than the cyanide-selective electrode. It was found that the sensitivity of the flow-injection system was very poor with these electrodes and that the response in continuous monitoring was very sluggish, especially with the gas probe. Moreover, in the determination of calcium in the presence of magnesium [16], the electrode becomes unresponsive because of adsorption of the organic compounds used for masking magnesium and has to be mechanically cleaned every 30—60 min.

Conclusion

In the construction of industrial flow detectors with ISEs it is possible to use large cells with results comparable to those obtained with low-volume

laboratory detectors, provided that the liquid flow rate is sufficiently high. A large cell volume is advantageous in continuous monitoring, as the detector response approaches that obtained under steady-state conditions. The electrodes used must have fast response times if satisfactory measuring sensitivity and reproducibility are to be attained.

REFERENCES

1 J. Veselý, D. Weiss and K. Štulík, Analysis with Ion-Selective Electrodes, Horwood, Chichester, 1978.
2 J. Koryta and K. Štulík, Ion-Selective Electrodes, Cambridge University Press, Cambridge, 1983.
3 K. Tóth, G. Nagy, Zs. Fehér, G. Horvai and E. Pungor, Anal. Chim. Acta, 114 (1980) 45.
4 J. Růžička and E. H. Hansen, Flow Injection Analysis, Wiley, New York, 1981.
5 P. L. Bailey, Ion-Sel. Electrode Rev., 1 (1979) 81.
6 K. Štulík and V. Pacáková, CRC Crit. Rev. Anal. Chem., 14 (1984) 297.
7 D. Betteridge, Anal. Chem., 50 (1978) 832A.
8 C. C. Painton and H. A. Mottola, Anal. Chim. Acta, 154 (1983) 1.
9 J Růžička and E. H. Hansen, Anal. Chim. Acta, 114 (1980) 19.
10 G. Taylor, Proc. R. Soc. London, Ser. A: 219 (1953) 186.
11 J. T. Vanderslice, K. K. Stewart, A. G. Rosenfeld and D. J. Higgs, Talanta, 28 (1981) 11.
12 E. Pungor, Zs. Fehér, G. Nagy, K. Tóth, G. Horvai and M. Gratzl, Anal. Chim. Acta, 109 (1979) 1.
13 G. K. C. Low and P. R. Haddad, J. Chromatogr., 198 (1980) 235.
14 Zs. Fehér, G. Nagy, K. Tóth and E. Pungor, Anal. Chim. Acta, 98 (1978) 193.
15 W. E. van der Linden and R. Oostervink, Anal. Chim. Acta, 101 (1978) 419.
16 A. Hulanicki and M. Trojanowicz, Anal. Chim. Acta, 68 (1974) 155.

Analytica Chimica Acta, 185 (1986) 179—185
Elsevier Science Publishers B.V., Amsterdam — Printed in The Netherlands

NEUTRAL LIPID ENZYME ELECTRODE BASED ON ION-SENSITIVE FIELD EFFECT TRANSISTORS

MAMIKO NAKAKO*, YOSHIO HANAZATO, MITSUO MAEDA and SATORU SHIONO
Central Research Laboratory, Mitsubishi Electric Corporation, 1-1 Tsukaguchi-Honmachi 8-Chome, Amagasaki, Hyogo 661 (Japan)

(Received 3rd December 1985)

SUMMARY

An enzyme electrode for neutral lipid determination based on hydrogen ion-sensitive field effect transistors (pH-FET's) is described. The electrode is composed of two pH-FET's with an immobilized lipase membrane on one pH-FET, and a platinum wire. Triglycerides are solubilized with 10% (v/v) Triton X-100. The electrode is used to determine triglycerides over wide concentration ranges with response times of ca. 2 min. Relations between signal and the logarithm of the concentration are linear over the ranges 100—400 mM triacetin, 3—50 mM tributylin and 0.6—3 mM triolein. In the case of triolein, the detection limit is 9 μg ml^{-1} (signal/noise = 3:1). The effect of Triton X-100 on the electrode response is discussed.

Much work has been done on the development of bioelectrodes which enable organic compounds to be determined simply and rapidly for clinical, industrial and environmental purposes. Recently, ion-sensitive field effect transistors (ISFET's) have received more attention as electrochemical transducers for such bioelectrodes, since Caras and Janata [1] reported a penicillin-sensitive ISFET electrode. Several enzyme or microbial ISFET electrodes have been reported [2—6]. The present authors have reported a multi-enzyme ISFET system for glucose and urea, and showed that an inert metal can be used as a pseudo-reference electrode instead of a liquid-containing reference electrode such as the Ag/AgCl electrode [4, 7]. The advantages of ISFET's as electrochemical transducers for such electrodes have been discussed [7].

The determination of neutral lipids, triglycerides, is of clinical and industrial importance. Some enzyme electrodes for neutral lipids have been reported: a pH electrode-based enzyme electrode with an immobilized lipase reactor [8, 9], a lipase thermistor [10] and an oxygen electrode-based enzyme electrode by simultaneous use of lipase, glycerol dehydrogenase and peroxidase [11]. In the study reported here, an ISFET-based enzyme electrode was constructed for the determination of neutral lipids by combining a membrane holding immobilized lipase with pH-sensitive FET's (pH-FET's). The system is composed of two pH-FET's with an immobilized lipase membrane on one of them and a platinum wire used as a pseudo-reference electrode. The thin immobilized lipase membrane is formed directly on the gate

0003-2670/86/$03.50

area of the pH-FET by a water-soluble cross-linkable polymer. The enzyme electrode is shown to be useful for the determination of neutral lipids.

EXPERIMENTAL

Materials

Lipase (triacylglycerol acylhydrolase, E.C. 3.1.1.3, from *Candida cylindracea*) was obtained from Sigma Chemical Co. (595 Sigma U mg^{-1}) and also from Boehringer Mannheim (500 IU mg^{-1}). These are designated as lipase A and lipase B, respectively. Bovine serum albumin (BSA) was obtained from Sigma Chemical Co. Other chemicals used were glutaraldehyde (25% solution in water; Ishizu Pharmaceutical Co., Osaka), polyvinylpyrrolidone (PVP, K-90, average molecular weight 360,000; Nakarai Chemicals, Kyoto) 4,4′-diazidostilbene-2,2′-disulfonic acid, sodium salt (Kanto Chemicals, Tokyo), and polyvinyl alcohol (PVA; Kuraray, Kurashiki, Japan). Triolein and tributylin (both from Wako Chemicals, Osaka) and triacetin (Nakarai Chemicals) were used without further purification.

Other reagents were of analytical-reagent grade. Distilled-deionized water was used.

Electrode construction and apparatus

The method of electrode fabrication and the apparatus used for the measurements were the same as in the previous paper [4]. Figure 1 shows the structure of the pH-FET-based enzyme electrode for neutral lipids.

Immobilized-enzyme membrane. A polymer solution suitable for cross-linking under radiation was prepared by dissolving 0.1 g of 4,4′-diazidostilbene-2,2′-disulfonic acid (sodium salt) in 100 ml of an aqueous 10% (w/v) PVP solution. Unless otherwise stated, 15 mg of lipase and 10 mg of BSA were added to 200 μl of this polymer solution. The immobilized enzyme membrane formed on the pH-FET (see Fig. 1) was prepared in a way similar to that described previously [7]. Briefly, a small amount of lipase/BSA/photopolymer solution was placed on one of the two pH-FET's and the electrode was spun at 3000 rpm for 2 min to make a thin membrane containing lipase over the gate. After drying at room temperature, the membrane was treated with u.v. radiation (Hoya UV filter, 350-W mercury lamp) for 5 min, then with glutaraldehyde solution for 15 min at 4°C and finally with 0.1 M glycine at 4°C. After being washed with water, the electrode was stored in buffer solution at 4°C.

Procedure

The lipase electrode was placed in the electrode cell [4] thermostated at 30°C. Tris-maleate buffer, 10 mM or 1 mM, was used. Buffer solutions (pH 7.0) with and without triglycerides were alternately pumped into the electrode cell through the water jacket [4] at certain time intervals by a peristaltic

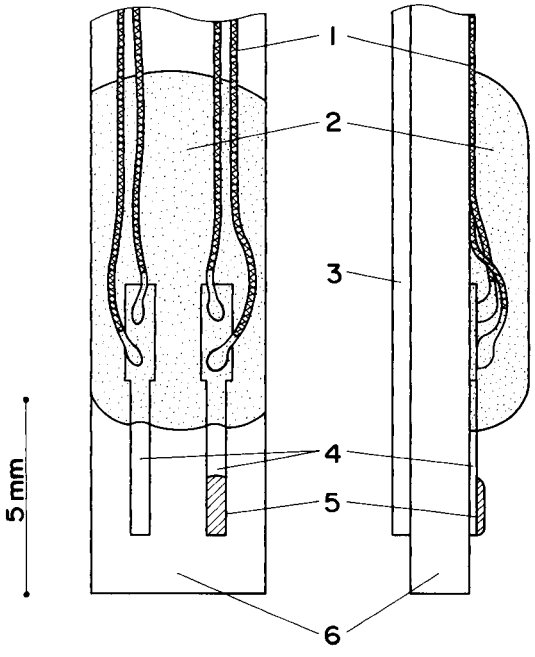

Fig. 1. Structure of enzyme electrode: (1) connecting; (2) epoxy resin; (3) platinum wire; (4) pH-FET; (5) immobilized lipase membrane; (6) epoxy laminate.

pump. The water jacket was also thermostated at 30°C. The flow rate was about 6 ml min^{-1}. Sample solutions containing triglycerides in Tris-maleate buffer were prepared according to one of the following procedures: (1) direct dissolution of triglycerides in the buffer, (2) emulsification of triglycerides in the presence of 2% PVA by brief ultrasonic treatment (100 W, for 30 s twice) [12], and (3) dissolution with 10% (v/v) Triton X-100 [10].

RESULTS AND DISCUSSION

Response of the enzyme electrode

Three triglycerides, namely triacetin, tributylin and triolein, were selected as representative triglycerides. The solubilities of these triglycerides decrease in the order given, being 300 mM for triacetin and 0.5 mM for tributylin, whereas triolein is practically insoluble. The enzyme electrode for neutral lipids was made with lipase A. Figure 2A shows a typical response curve of the lipase electrode to 100 mM triacetin in 10 mM Tris-maleate buffer. The baseline represents the output potential obtained for the same buffer solution without triacetin. When a triacetin-containing sample solution is pumped into the electrode cell, the potential begins to increase and reaches a steady-state value within ca. 2 min. The steady-state value depends on the triacetin

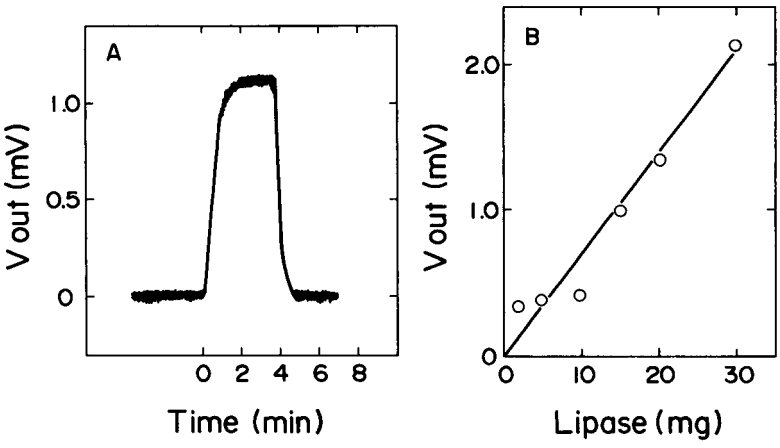

Fig. 2. (A) Typical response curve of the lipase electrode for 100 mM triacetin. Conditions: 10 mM Tris-maleate buffer, pH 7.0, 30°C. (B) Relationship between the output potential of the electrode for 100 mM triacetin and the lipase content in the photopolymer mixture (200 μl) containing BSA (10 mg). Conditions: 10 mM Tris-maleate buffer, pH 7.0, 30°C.

concentration. When the buffer is pumped again, the potential returns to its initial level.

Figure 2B shows the influence of the amount of lipase A, added with a constant amount of BSA to the photopolymer solution, on the magnitude of the electrode response. The higher the lipase content, the bigger the output potential of the electrode. However, the immobilized lipase membrane became mechanically weak with increasing lipase content. A lipase membrane made from a lipase/BSA/polymer solution containing more than 20 mg of lipase per 200 μl of photopolymer solution was impractical because of its poor mechanical strength. Therefore, in this study, the immobilized lipase membrane was prepared with a mixture of 15 mg of lipase, 10 mg of BSA and 200 μl of photopolymer solution.

Solubilization of triglycerides

When sample solutions were prepared by direct dissolution of triglycerides in 10 mM Tris-maleate buffer, the electrode responded to triacetin or tributylin solutions. It gave responses dependent on triacetin concentration up to 350 mM, or tributylin concentration up to 0.5 mM, both of which are in close agreement with the respective solubilities of the triglycerides. However, in the case of triolein the electrode gave no response even when 1 mM Tris-maleate buffer was used instead of 10 mM buffer. The direct dissolution of triglycerides for sample preparation was clearly inadequate. Emulsification of the triglycerides in the presence of PVA by sonication, which is commonly used to measure lipase activity [12], was therefore tested for the preparation of triglyceride sample solutions. But this was also found not to

be practical, because there was no response to triolein. The electrode responses to emulsified triacetin and tributylin solutions were almost the same as those obtained for directly dissolved solutions. Presumably, immobilized lipase can catalyze the decomposition reaction only when the triglyceride molecules are actually dissolved in water.

Solubilization of triglycerides with Triton X-100 was used successfully in the study on the neutral lipid enzyme thermistor [10]. When 1 mM Tris-maleate buffer was used, the electrode responded to triolein in solutions prepared by the dissolution of triolein in the presence of Triton X-100. The effect of the Triton X-100 concentration on the electrode response is shown in Fig. 3. For 0.4 mM tributylin, which is soluble in water without detergent, there was a drastic decrease in the electrode response with increasing detergent concentration. In contrast, for 0.4 mM and 2 mM triolein, which are insoluble without detergent, the electrode responses increased from zero, reached a maximum value and then decreased gradually. Figure 3 shows that the sensitivity of the enzyme electrode for 2 mM triolein is about 10 times higher with 10% Triton X-100 than with 0.5% detergent and is about doubled for 0.4 mM triolein with 10% detergent compared to 0.5% detergent. And the higher detergent concentration allowed a wider concentration range of triolein to be determined by the enzyme electrode. Actually, a 0.4 mM triolein solution becomes clear with more than 1% Triton X-100 and a 2 mM triolein solution is transparent with more than 6% detergent. (Although in the paper on the enzyme thermistor [10] it was reported that 0.5% Triton X-100 could solubilize up to 5 mM triolein, we could not obtain clear solutions containing more than 0.4 mM triolein with 0.5% Triton X-100). Therefore, 10% Triton X-100 was used in this study.

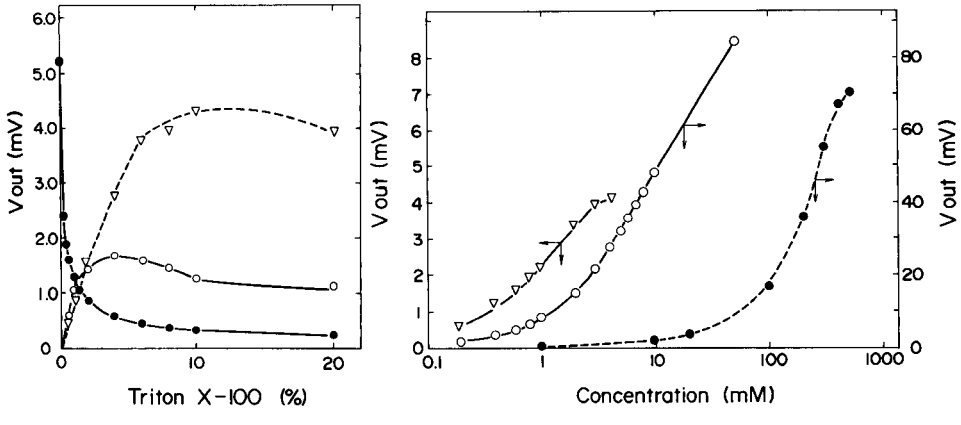

Fig. 3. Effect of Triton X-100 concentration on output potential: (•) 0.4 mM tributylin in 10 mM Tris-maleate buffer; (○) 0.4 mM triolein in 1 mM Tris-maleate buffer; (▽) 2 mM triolein in the 1 mM buffer. Conditions: pH 7.0, 30°C.

Fig. 4. Calibration curves: (•) triacetin; (○) tributylin; (▽) triolein. Conditions: 1 mM Tris-maleate buffer, 10% (v/v) Triton X-100, pH 7.0, 30°C.

Because of the low critical micelle concentration of Triton X-100 (0.015%), almost all detergent molecules form micelles over the detergent concentration ranges used here to evaluate the performance of the lipase electrode. The increase in the electrode response to triolein with increasing Triton X-100 concentration can be explained as follows: triolein molecules in detergent micelles can be hydrolyzed by lipase whereas molecules undissolved in water can not (see above); and the ratio of the former to the latter in water increases with increasing detergent concentration. The decrease in the electrode response to tributylin over the full concentration range of Triton X-100 and to triolein over the higher detergent concentration range might be explained as follows: (1) competitive and/or uncompetitive inhibition of lipase by the detergent molecules; (2) higher reactivity of free triglyceride molecules in water compared to triglyceride molecules in micelles (in the case of 0.4 mM tributylin); and (3) the decreasing diffusion coefficient of micelles with increasing detergent concentration.

Figure 4 shows the calibration curves of the electrode for the three triglycerides. In the case of triacetin and tributylin, the magnitude of the electrode response is much less than that without Triton X-100 (data not shown, see Fig. 3), but the concentration ranges that can be determined are much extended in comparison with the direct dissolution method. Linear relationships were obtained between the output potential and the logarithm of the concentrations of triglycerides for 100—400 mM triacetin, 3—50 mM tributylin and 0.6—3 mM triolein.

Electrode with immobilized lipase of higher activity

In order to increase the magnitude of the electrode response to triolein, the enzyme electrode was prepared by immobilizing lipase B, which had about 50 times greater activity per milligram than lipase A. The same composition of lipase/BSA/photopolymer solution (15 mg/10 mg/200 μl) was used. The calibration curves for this electrode are shown in Fig. 5; the sensitivity of the electrode is improved 4—5 times compared with the electrode made from lipase A. A linear relationship is obtained between the output potential and the concentration of triolein over the range 0.05—0.6 mM, and between the output potential and logarithm of the triolein concentration over the range 0.6—4 mM. The detection limit for triolein was 0.05 mM (9 μg ml^{-1}, signal/noise = 3:1). Figure 6 shows the long-term stability of the enzyme electrode, which was checked with 3 mM triolein. Except during measurements, the electrode was stored at 4°C in 1 mM Tris-maleate buffer. Figure 6 shows that the output potential decreases gradually but that the electrode response gives 88% of the initial value after 44 days.

Optimization of the composition of the reaction mixture for the immobilized lipase membrane was done, but little improvement in the electrode sensitivity was obtained (data not shown).

In conclusion, the pH-FET-based enzyme electrode for neutral lipid determination has been shown to be feasible for clinical and industrial applications.

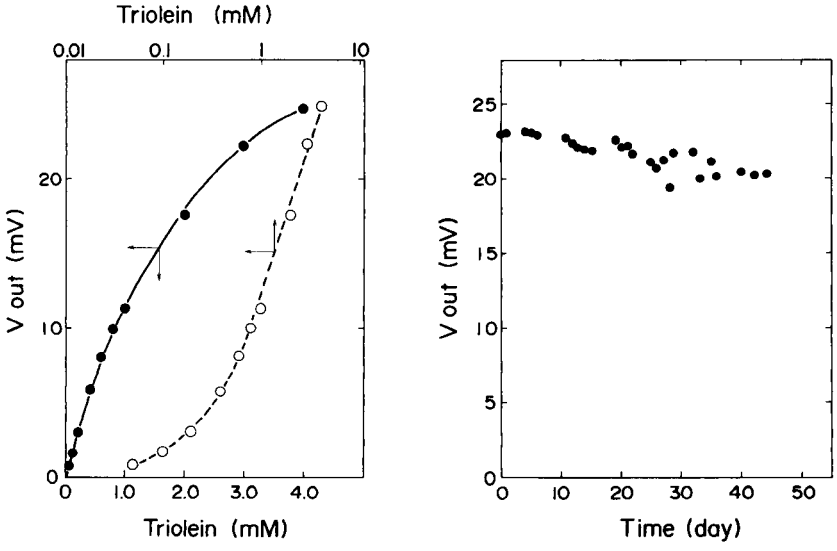

Fig. 5. Calibration curves of an electrode with lipase B: (•) linear scale; (○) logarithmic scale. Conditions: 1 mM Tris-maleate buffer, 10% Triton X-100, pH 7.0, 30°C.

Fig. 6. Long-term stability of enzyme electrode. Conditions: 3 mM triolein, 1 mM Tris-maleate buffer, 10% Triton X-100, pH 7.0, 30°C.

By using Triton X-100, triglycerides with slight solubility can be determined over a wide concentration range within about 2 min. The enzyme electrode with extensively purified lipase shows higher sensitivity.

REFERENCES

1 S. Caras and J. Janata, Anal. Chem., 52 (1980) 1935.
2 Y. Miyahara, S. Shiokawa, T. Moriizumi, H. Matsuoka, I. Karube and S. Suzuki, Proc. 2nd Sensor Symp., Tsukuba, (1982) 91.
3 Y. Miyahara, F. Matsu, T. Moriizumi, H. Matsuoka, I. Karube and S. Suzuki, Proc. Int. Meet. Chem. Sens., Fukuoka, (1983) 501.
4 Y. Hanazato and S. Shiono, Proc. Int. Meet. Chem. Sens., Fukuoka, (1983) 513.
5 T. Kuriyama, J. Kimura and Y. Kawana, 16th Int. Conf. Solid State Devices Mater., Kobe, Late News Abstr., (1984) LC-12-3.
6 J. Kimura, T. Kuriyama and Y. Kawana, Proc. Int. Conf. Solid State Sens. Actuators, (1985) 152.
7 Y. Hanazato, M. Nakako and S. Shiono, IEEE Trans. Electron Devices, ED-33 (1986) 47.
8 I. Satoh, I. Karube and S. Suzuki, J. Solid-Phase Biochem., 2 (1977) 1.
9 I. Satoh, I. Karube, S. Suzuki and K. Aikawa, Anal. Chim. Acta, 106 (1979) 369.
10 I. Satoh, B. Danielsson and K. Mosbach, Anal. Chim. Acta, 131 (1981) 255.
11 T. A. Kelly and G. D. Christian, Analyst (London), 109 (1984) 453.
12 N. Tomizuka, Y. Ota and K. Yamada, Agric. Biol. Chem., 30 (1966) 576.

Analytica Chimica Acta, 185 (1986) 187—193
Elsevier Science Publishers B.V., Amsterdam — Printed in The Netherlands

PLANT TISSUE-BASED MEMBRANE BIOSENSOR FOR L-ASCORBIC ACID

L. MACHOLÁN* and B. CHMELÍKOVÁ

Department of Biochemistry, Faculty of Science, J. E. Purkyně University, 611 37 Brno (Czechoslovakia)

(Received 19th September 1985)

SUMMARY

Coupling of a slice of the mesocarp of squash (*Cucurbita pepo*) or cucumber (*Cucumis sativus*) to a Clark-type oxygen electrode allows 0.02—0.57 mmol l^{-1} L-ascorbic acid to be determined amperometrically. The method is based on monitoring the decrease in the current of oxygen at an applied potential of —650 mV vs. Ag/AgCl; oxygen is consumed in the analyte oxidation catalyzed by ascorbate oxidase in the plant tissue. One tissue slice serves for 50—80 measurements at 30°C and pH 6. Spare slices can be stored for at least a year in aqueous 50% glycerol without substantial loss of enzyme activity. The biosensor is highly selective towards ascorbic acid with a response time of 70—90 s, the relative standard deviation being about 3%. Satisfactory results were obtained in the analysis of some fruit juices and vitamin tablets.

Enzyme electrodes for the determination of important bio-organic substances in coloured and/or turbid samples have become of increasing interest. The first bioselective electrode for ascorbic acid, consisting of a bipolar oxygen electrode and squash ascorbate oxidase cross-linked on polyamide netting with albumin and glutaraldehyde, proved efficient in analyzing different kinds of fruit [1]. On the same principle of the measurement of oxygen uptake in the biocatalytic layer, two modified sensors were developed with cross-linked enzyme from cucumber [2] or with rat liver microsomes [3]. Isolated ascorbate oxidase was also covalently attached to a nylon net support coupled with a pO_2 electrode [4] or directly on the surface of a carbon cathode impregnated with an epoxy resin [5].

All sensors based on immobilized ascorbate oxidase require highly purified (and expensive) enzyme to function reliably. The microsomal sensor lacks sensitivity and long-term stability [3]. The advantages of replacing another copper-containing enzyme, mushroom polyphenol oxidase, by tissue slices for determining phenols [6] stimulated the idea of designing an analogous tissue-based amperometric detector for ascorbic acid which would be easily accessible to workers without experience in enzymology. Squash tissue slices have been used in a glutamate sensor based on a potentiometric carbon dioxide probe [7]; the tissue contained adequate amounts of glutamate decarboxylase. Here it is shown that similar tissues also contain a high activity of

0003-2670/86/$03.50

ascorbate oxidase and operate as a reaction layer with naturally immobilized enzyme. Optimum conditions are described for achieving fast response as well as linearity and maximum slope of the steady-state current vs. concentration plots. Useful applications of the new biosensor are also reported.

EXPERIMENTAL

Materials

All chemicals were of analytical grade. L-Ascorbic acid was purchased from Pharmakon (C.S.S.R.); calibration solutions containing 10 mg ml^{-1} (57 mM) ascorbic acid in 0.5 mM EDTA were prepared daily. All solutions were prepared with distilled, deionized water.

Yellow and green autumn squash (*Cucurbita pepo*) and cucumbers (*Cucumis sativus*) were obtained from commercial sources. Longitudinal tissue slices, 0.3-mm thick, were cut with a sledge microtome (Reichert, Austria) from the mesocarp layer occurring in the pericarp to a depth of 2—3 mm (Fig. 1); cutting by means of razor blade is recommended for routine work. Slices were stored in aqueous 50% (v/v) glycerol at 4°C.

Apparatus and procedures

For construction of the biosensor, an oxygen electrode (Radiometer E-5047) was inverted and a plant tissue slice (5 × 5 mm) was placed on its 12-μm teflon membrane towards the cathode without air bubbles; the slice was held in place by polyamide net (25 mesh mm^{-2}, fibre thickness 60 μm) fixed by an O-ring. The biosensor was connected through a pO_2 analyzer (Model DOX-81, University Olomouc) to a TZ-4100 line recorder (Laboratorní přístoje, Praha; scale width 250 mm, chart speed 15 mm min^{-1}).

The measurements were made at 30 ± 0.1°C in a thermostatted water-jacketed cylindrical vessel filled with 3 ml of 0.1 M sodium/potassium phosphate buffer, pH 6.0, containing 0.5 mM EDTA; the buffer was equilibrated with atmospheric oxygen for 3 min. The biosensor was placed in the vessel, polarized to −650 mV vs. Ag/AgCl and constant magnetic stirring was started (300 rpm); when the output current had stabilized, 2—50-μl aliquots of the ascorbic acid standard solution and the sample solutions were successively

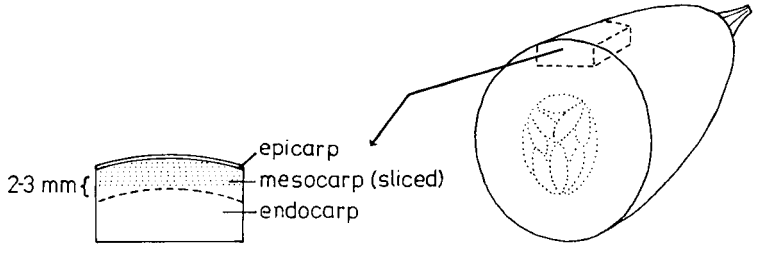

Fig. 1. Cross-section of squash (or cucumber) showing the origin of the biocatalytic layer.

injected into the buffer at 2—3 min intervals from a Hamilton repeating dispenser. The amount of ascorbic acid present in the samples was calculated from a calibration graph of the decrease in steady-state current vs. ascorbic acid concentration. In the analysis of fruit juices stored under nitrogen gas, correction must be made for the drop in oxygen level after injection of the same volume of oxygen-free water.

For comparison, differential pulse polarography of ascorbic acid in fruit juices was used. Samples were added to 10 ml of 0.1 M phosphate buffer, pH 7.0, saturated with nitrogen. The instrumental conditions were: potential scan at 2 mV s^{-1} from −250 mV to 0 mV, pulse amplitude +50 mV, sensitivity 5 nA cm^{-1}, and mercury drop time 2 s.

RESULTS AND DISCUSSION

Location of ascorbate oxidase

The peel of squash or cucumber is known to be a good source of ascorbate oxidase. To examine the maximum occurrence of the enzyme, the electrode response to ascorbic acid was measured after longitudinal peel slices had been fixed to the Clark oxygen cell. It was confirmed that ascorbate oxidase occurred mostly in the mesocarp layer to a depth of about 2 mm (Fig. 2).

For the ascorbate oxidase electrode, the most suitable thickness of slice, from either source, was 0.3 mm; thinner slices were very variable in activity, whereas thicker slices caused longer response times. Slices from a young cucumber (30-mm diameter) were 1.3 times more active than those from fully grown fruits (50-mm diameter) and twice as active as slices from old, yellowing fruits.

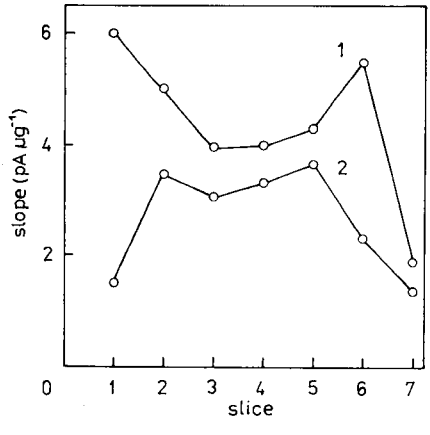

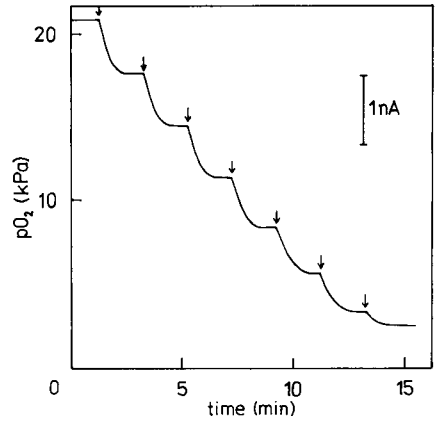

Fig. 2. Variation of the slope of the calibration graph with different mesocarp slices of green squash (1) or cucumber (2); on the *x*-axis, the sequence relates to 0.3-mm slices down from the cuticle.

Fig. 3. Response of the biosensor based on squash tissue to stepwise additions of 100 µg of ascorbic acid which increased the concentration in the measuring cell by 0.19 µmol l^{-1} in each step.

Response of biosensor to ascorbic acid

A typical recording of the decrease in the cathodic oxygen current after addition of ascorbic acid to the pH 6 reaction medium is shown in Fig. 3. Sensors assembled with a 0.3-mm slice of the most active mesocarp layer of half-matured cucumber or squash exhibited a response time of 70—90 s. Potassium cyanide (10 mM) caused a complete and irreversible loss of electrode sensitivity, which proves the enzymatic character of ascorbate oxidation in the tissue slice. The action of the copper chelating agents, sodium diethyldithiocarbamate (1 mM) and 8-quinolinol (5 mM), was the same.

In the phosphate buffer, the electrode response to constant amounts of ascorbic acid changed by only 15% within the pH range 5—8, whether the tissue slice came from a squash or a small cucumber (Fig. 4). In this work, the reaction medium was kept at pH 6.0 in order to prevent interference from the non-enzymatic oxidation of polyphenol substances [1]; if citric acid is present in the sample, the concentration of the inhibiting monoanion is negligible.

Calibration, accuracy and reproducibility

For calibration, increments of standard 57 mM L-ascorbic acid were added to the working buffer. The calibration curves were linear for just over one concentration order; the lower limit of detection was 0.02 mM (signal/noise = 5). The upper limit was 0.57 mM; with respect to the reaction stoichiometry [8], this concentration corresponds to the concentration of dissolved oxygen in the air-saturated buffer medium.

The relative standard deviation for ten successive measurements of 0.1 mg of ascorbic acid with one squash slice was 2.7%; for one cucumber slice, it

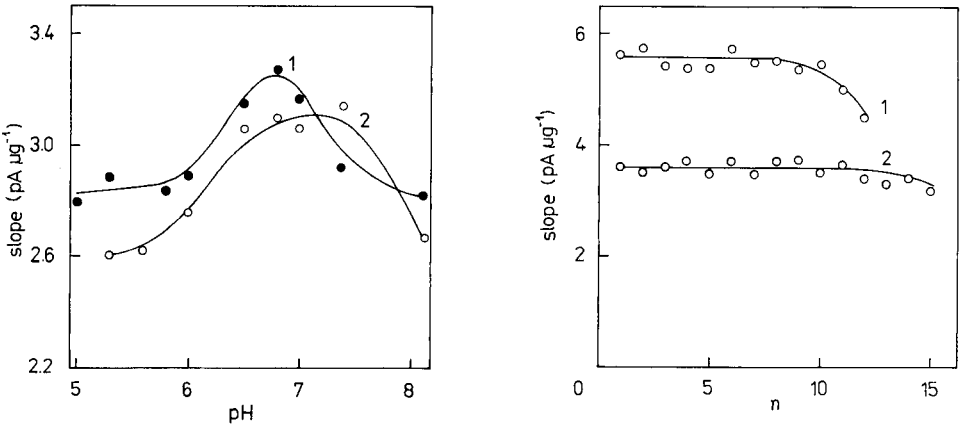

Fig. 4. Effect of pH on the slope of the calibration graph for ascorbic acid at 30°C. One 0.3-mm mesocarp slice of gherkin (1) or yellow squash (2) was used.

Fig. 5. Operation stability of a single tissue slice at 30°C and pH 6: (1) young cucumber; (2) yellow squash. The number of repeated successive calibrations (n) each represents 7—8 additions of ascorbic acid standard solution.

was 3.1%. The average current change was 0.362 and 0.551 nA, respectively. Different slices from the most active layer of the same fruit can, however, differ very significantly in their activity (Fig. 2). When slices are changed, a new calibration is always essential. The way in which the slice is placed on the sensitive part of the pO_2 electrode can also influence the sensitivity of the biosensor. In the course of placing the same squash slice ten times, the relative standard deviation of the slopes of the calibration graphs was 8.7%.

Selectivity and operational stability

When an amperometric oxygen cell is used, the squash tissue provides a biosensor which is highly selective for L-ascorbic acid. At pH 6 it is quite insensitive to different organic acids, mono- and poly-phenols, amino acids, glucose, *p*-phenylenediamine, glutathione, the B vitamins, etc. Synthetic D-isoascorbic acid and triose-reductone, though not tested, would interfere, as in immobilized enzyme electrodes [2, 5].

The pO_2 electrode with a slice of cucumber or squash gave constant response during 50 or 80 successive measurements (Fig. 5). Between measurements, the sensor was stored in the working buffer at room temperature. The lifetime of the squash tissue was confirmed to be longer by an experiment in which the slices were incubated 7 h at 20°C with excess of ascorbic acid in 67 mM phosphate buffer, pH 6, with continual bubbling of air. With slices of green and yellow squash, the ratios of the slopes of the calibration graphs at the beginning and end of the experiment were 1.1 and 1.7, respectively, but with slices from gherkin and salad cucumber, the measured ratios were 2.5 and 2.7, respectively.

For long-term storage of slices, the best preservative proved to be glycerol or the antiseptic Merthiolate. Slices of yellow squash kept at 4°C in aqueous 50% (v/v) glycerol gave constant responses on a pO_2 electrode for at least a year; in 0.1% Merthiolate, the activity of the slices decreased by 14% after 5 months, but at −24°C it was fully preserved. Squash slices were again more stable than cucumber slices. In isotonic sodium chloride solution, the slices quickly lost their enzyme activity.

Determination of L-ascorbic acid in actual samples

The content of ascorbic acid in pharmaceutical preparations was determined by dissolving the tablets in a known volume of water and injecting a small amount of the solution into 3 ml of the buffer, into which the biosensor had been immersed. On achieving stabilized current, a calibration solution of ascorbic acid was added to the same buffer medium. The amount of vitamin C in the sample was calculated from comparison of the current changes and from the standard concentration. The obtained values were in acceptable agreement with the content declared (Table 1).

Fruit juices pressed from ripe fruits were also analyzed. Nitrogen was bubbled through the juices to prevent the loss of ascorbic acid. The dependence of the decrease in steady-state current on standard ascorbic acid con-

TABLE 1

Analysis of drugs containing vitamin C by means of the biosensor based on a squash-tissue slice

Preparation	Ascorbic acid content (mg/tablet)	
	Found	Nominal
Spofavit (multivitamin)	53.3	50
Celaskon	93.0	100
Celaskon effervescens	503.9	500

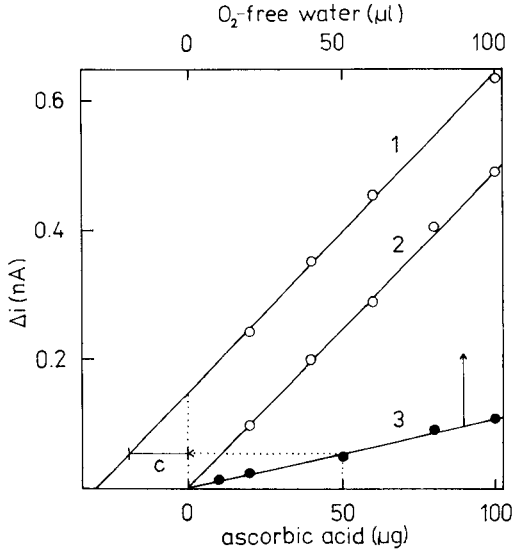

Fig. 6. Determination of ascorbic acid in fruit juice. Calibration plots: (1) with additions of 50 µl of orange juice stored under nitrogen, (2) without addition of juice, (3) the decrease in current on addition of O_2-free water. (c) The corrected content of ascorbic acid in the juice sample.

TABLE 2

Assay of ascorbic acid in fruit juices

Source	Ascorbic acid content (mg l^{-1})		Literature values [9]
	Found		
	Biosensor	D.p.p.	
Orange	523	525	300—500
Lemon	443	478	200—500
Grapefruit	476	—	240—400
Apple	58	—	18—64
Pear	40	39	33—40
Tomato	73	—	80—150
Lemon peel	573	—	520

centration with and without the addition of a constant amount of juice is shown in Fig. 6. The addition of a larger volume of juice kept under nitrogen caused a drop in the oxygen concentration in the reaction medium; it was therefore necessary to correct the measured change in current by the value produced by the addition of an equal volume of water saturated with nitrogen, as indicated in Fig. 6. The corrected values of ascorbic acid were in good agreement with the values from differential pulse polarography (d.p.p.) as well as with literature data (Table 2).

The authors are indebted to Dr. J. Turánek for the assays of ascorbic acid in fruits by differential pulse polarography. This paper was presented at the 10th Congress of the Czechoslovak Biochemical Society, Martin, September, 1984.

REFERENCES

1 P. Posádka and L. Macholán, Collect. Czech. Chem. Commun., 44 (1979) 3395.
2 K. Matsumoto, K. Yamada and Y. Osajima, Anal. Chem., 53 (1981) 1974.
3 F. Schubert, F. Scheller and D. Kirstein, Anal. Chim. Acta, 141 (1982) 15.
4 M. Mascini, M. Iannello and G. Palleschi, Anal. Chim. Acta, 146 (1983) 135.
5 T. Wasa, K. Akimoto, K. Ueda and T. Yao, Bunseki Kagaku, 33 (1984) 472.
6 L. Macholán and L. Schánĕl, Biológia (Bratislava), 39 (1984) 1191.
7 S. Kariyama and G. A. Rechnitz, Anal. Chim. Acta, 131 (1981) 91.
8 B. G. Malmström, L. E. Andréasson and B. Reinhammar, in P. D. Boyer (Ed.), The Enzymes, Vol. 12/B, Academic Press, New York, 1975, p. 507.
9 V. Šanda, in J. Frágner (Ed.), Vitaminy, jejich chemie a biochemie, Vol. 2, Academia, Prague, 1961, p. 724.

Analytica Chimica Acta, 185 (1986) 195—200
Elsevier Science Publishers B.V., Amsterdam — Printed in The Netherlands

A MICROSENSOR FOR UREA BASED ON AN ION-SELECTIVE FIELD EFFECT TRANSISTOR

ISAO KARBUE*, EIICHI TAMIYA and JONATHAN M. DICKS

Research Laboratory of Resources Utilization, Tokyo Institute of Technology, Nagatsuta, Midori-ku, Yokohama 227 (Japan)

MASAO GOTOH

Research Department, NOK Corporation, 4-3-1 Tsujidoshinmachi, Fujisawa 251 (Japan)

(Received 10th December 1985)

SUMMARY

The pH response of a pH-sensitive field-effect transistor (FET) is not affected by a ca. 1-μm thick membrane formed from γ-aminopropyltriethoxysilane and glutaraldehyde over the gate insulator by a vapor deposition method. The response between pH 5.5 and 8.5 is ca. 61 mV pH^{-1} at 37°C in 5 mM Tris-HCl buffer. When urease is immobilized on the membrane, the sensor gives a linear relationship between the initial rate of the output gate voltage change and the logarithmic value of urea concentration between 16.7 and 167 mM. Determination of urea is possible within 30 s. The optimum pH is 6.0—6.5, at 37°C. The system can be used for 20 days with only slight loss of enzymatic activity.

The determination of urea in serum and other biological fluids is important for diagnostic clinical purposes. Conventional methods for urea determination are mostly based either on a direct color reaction [1, 2] or on the spectrophotometric measurement of ammonia produced by the hydrolysis of urea by urease [3]. These methods, however, involve complicated and delicate procedures and the assay times are rather long because of the several reactions involved. The spectrophotometric methods cannot be applied directly to colored samples or biological fluids. Alternative systems based on electrochemical sensors have been developed for urea [4, 5]. These methods mainly involve electrochemical detection of ammonia produced in the presence of urease. Typically, a urea enzyme sensor consists of immobilized urease and an electrochemical device such as an ion-selective electrode [6—10]. The development of simple inexpensive assays is of importance for the determination of urea in clinical work and miniaturization of the enzyme sensors is particularly important. Caras and Janata [11] reported the development of an enzyme field-effect transistor (FET), using an ion-selective FET as the electrochemical detector. Since then, several studies on the application of ISFETs to enzymatic analysis have been reported. Miyahara et al. [12] reported a pre-

[a]Present address: Cranfield Biotechnology Centre, Cranfield Institute of Technology, Cranfield, Bedford MK43 0AL, Gt. Britain.

0003-2670/86/$03.50

liminary study of an immobilized enzyme FET for urea. In this sensor, urease was immobilized onto a cellulose triacetate membrane by reaction with glutaraldehyde and triamine 1,8-diamino-4-aminomethyloctane. The characteristics of the sensor were, however, strongly dependent on the immobilized enzyme membrane and especially on the membrane thickness, which affected the response time because of its effect on diffusion. In this paper, a thin organic membrane formed by vapor deposition is used for immobilization of urease on an ISFET surface. The characteristics of this urea microsensor are discussed.

EXPERIMENTAL

Materials

The main materials used were urease (E.C. 3.5.1.5, from jack beans, 3.9 U mg^{-1}; Sigma Chemical Company), γ-aminopropyltriethoxysilane (γ-APTES) and glutaraldehyde (both from Tokyo Kasei Industries), cellulose triacetate (Eastman Kodak), dichloromethane (Kanto Chemical Company), urea (Shudzui Hikotaro Shoten Company), and 1.8-diamino-4-aminomethyloctane which was a gift from Asahi Kasei Industries. All other chemicals used were of analytical grade. All solutions were prepared with distilled water.

Construction of the sensor

The ISFET device. The procedure for making the ISFET was reported by Matsuo and Esashi [13]. After wire-bonding, the chip was fixed with epoxy resin onto the end of a glass tube. The gate insulator of the ISFET is composed of two layers; the lower is thermally grown silicon dioxide, and the upper is silicon nitride, which is sensitive to hydrogen ions and also has a barrier effect on ion penetration. The thickness of the silicon dioxide or nitride layer is ca. 0.1 μm.

Formation of the organic membrane over the gate insulator of the ISFET. Before enzyme immobilization, the organic membrane was formed over the surface of the silicon nitride by vapor deposition or by dipping. The vapor deposition system is shown in Fig. 1. The ISFET was fixed inside a bell-jar

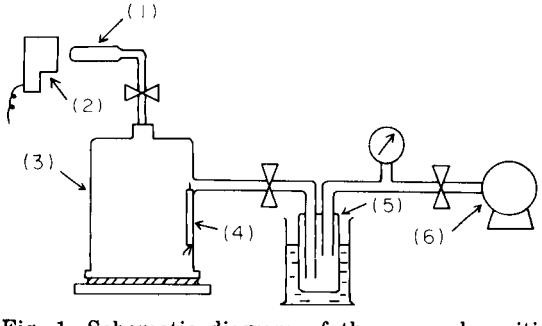

Fig. 1. Schematic diagram of the vapor deposition system for forming the thin organic membrane: (1) tube containing monomer; (2) heater; (3) bell-jar; (4) ISFET fixed inside the bell-jar; (5) trap; (6) vacuum pump.

and 100 μl of γ-APTES was vaporized at 80°C, 0.5 Torr for 30 min, followed by 100 μl of aqueous 50% (w/v) glutaraldehyde solution vaporized under the same conditions. The ISFET thus chemically modified was stored at room temperature for ca. 24 h to complete the reaction. In the dipping method, 250 mg of cellulose triacetate was dissolved in 10 ml of dichloromethane; 200 μl of aqueous 50% (w/v) glutaraldehyde solution and 1 ml of 1,8-diamino-4-aminomethyloctane were added, and the mixture was stirred for 30 min. The tip of the ISFET was dipped into this mixture. The device was stored at room temperature for about 24 h to achieve cross-linking.

Immobilization of the enzyme onto the organic membrane. The tip of the ISFET, where the organic membrane had been formed over the gate insulator by vapor deposition or dipping, was immersed in 20 mg ml^{-1} urease solution at 4°C for 24 h. In this way, urease was immobilized on the surface of the organic membrane, producing an enzyme FET.

Procedure for urea determination

The circuit diagram for measuring the gate voltage (V_g) is shown in Fig. 2. The Ag/AgCl reference electrode was placed in the same solution as the enzyme FET. A gate voltage, V_g, was applied across the reference electrode and the source of the enzyme FET. The surface potential on the silicon nitride insulator of the FET is affected by solution pH, with a concomitant change in the gate voltage proportional to the change in surface potential. Therefore, the surface potential change on the silicon nitride insulator of the enzyme FET, caused by variation in pH, can be measured as a change in the gate voltage. In this case, the initial voltage applied across the source and drain was constant at 1.0 V, with a constant current of 150 μA. The gate voltage obtained was displayed on a recorder (TOA Electronics, Model EPR-100A). The total volume of buffer in the cell was 4.4 ml of 5 mM Tris-HCl. The enzyme FET and reference electrode were allowed to stand in this solution at 37°C for 10—20 min. After the gate voltage had reached a steady value, 100-μl aliquots of urea solution were injected into the cell and the change in V_g was recorded. All solutions were thermostated at 37 ± 1°C.

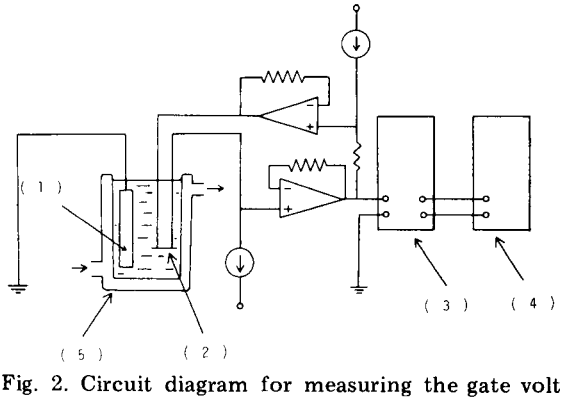

Fig. 2. Circuit diagram for measuring the gate voltage, V_g: (1) Ag/AgCl reference electrode; (2) treated FET; (3) electrometer; (4) recorder; (5) electrochemical cell.

RESULTS AND DISCUSSION

The response of the ISFET to 100-μl additions of 0.2 M hydrochloric acid to the cell shown in Fig. 2 is given in Fig. 3. The response times of the ISFET to pH change are very rapid, being less than 10 ms by oscillosope observation.

Figure 4 shows the effect of the organic membrane, formed by vapor deposition over the gate insulator, on the pH response of the ISFET. The linear V_g—pH characteristics of the ISFET with and without the membrane are essentially the same over the pH range 5.5—8.5. The pH sensitivity was about 61 mV pH^{-1} at 37°C, which is substantially in agreement with Nernstian behavior.

Characteristics of the enzyme FET

Figure 5 shows the effect of pH on the initial rate of change of the gate voltage, 30 s after injection of urea to give a final concentration of 167 mM. The optimum pH for free urease is 6.5—7.5, but for immobilized urease the greatest activity was at pH 6. This may be attributed to an alkaline microenvironment around the immobilized urease resulting from localization of ammonium ions. Subsequent experiments were done at 37°C and pH 6.5.

Figure 6 shows a comparison of the response curves to 167 mM urea for

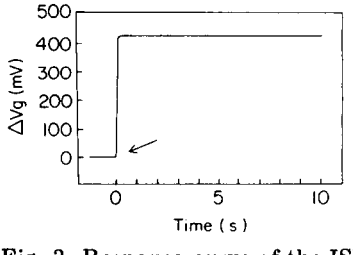

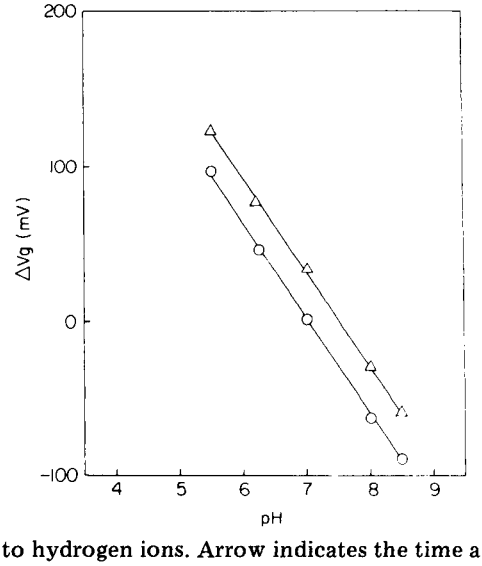

Fig. 3. Response curve of the ISFET to hydrogen ions. Arrow indicates the time at which 100 μl of 0.2 M HCl was injected into 4.4 ml of distilled water at 37°C. ΔV_g is the difference between the initial and response gate voltages.

Fig. 4. Effect of the thin organic membrane on the pH response of the ISFET at 37°C; (○) ISFET without membrane; (△) ISFET with organic membrane. ΔV_g is the difference between the gate voltage of the ISFET without the membrane at pH 7.0 and the gate voltage measured at other pH values.

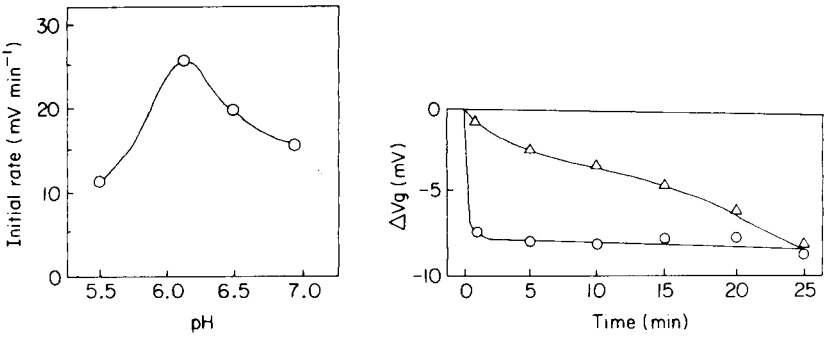

Fig. 5. Effect of pH on the initial rate of change of the gate voltage of the enzyme FET in 167 mM urea solution. The initial rates were measured 30 s after injection of the urea solution, at 37°C.

Fig. 6. Comparison of response curves for thin and thick organic membranes, for urea injected into pH 6.5 buffer solution at 37°C, to give a final concentration of 167 mM: (○) thin membrane; (△) thick membrane.

sensors with organic membranes formed by vapor deposition (giving a thin membrane) and by dipping (giving a thick membrane). The response time with the thin membrane was very rapid; that with the thick membrane was very long (many minutes). It was expected that the thickness of the membrane would affect the response time of the enzyme FET. The thin membrane was estimated to be ca. 0.1 μm thick and the thick membrane 100 μm. The time responses of the thin-membrane FET to urea addition were 30 s to achieve 85% of the steady-state value, and 1 min to achieve 95%.

The initial rate of the gate voltage change 30 s after injection was plotted against the logarithmic value of urea concentration. The calibration graph for urea was linear over the range 16.7—167 mM, the initial rate being 2 mV min^{-1} at the lower extreme and 13 mV min^{-1} at the higher limit. At <16.7 mM urea, the response could not be distinguished from that for the buffer alone. Likewise, the responses to >167 mM urea were almost the same as that for 167 mM urea. The results indicate the possibility of determination of urea within 30 s.

When the urea sensor was tested over a period of three weeks for 167 mM urea, the reproducibility of measurements was within ±1.5 mV min^{-1}. Between measurements, the enzyme FET was stored at 4°C. Over this period, the sensitivity decreased by about 10%.

REFERENCES

1 H. L. Rosenthal, Anal. Chem., 27 (1955) 1980.
2 R. L. LeMar and D. Bootzin, Anal. Chem., 29 (1957) 1233.
3 J. K. Fawcett and J. E. Scott, J. Clin. Pathol., 13 (1960) 156.

4 R. A. Llenado and G. A. Rechnitz, Anal. Chem., 46 (1974) 1109.
5 J. Růžička, E. H. Hansen, A. K. Ghose and H. A. Mottola, Anal. Chem., 51 (1979) 199.
6 G. G. Guilbault and J. G. Montalvo, J. Am. Chem. Soc., 91 (1969) 2164.
7 G. G. Guilbault and J. G. Montalvo, J. Am. Chem. Soc., 92 (1970) 2533.
8 H. Nilsson, A. Akerlund and K. Mosbach, Biochim. Biophys. Acta, 320 (1973) 529.
9 G. G. Guilbault and M. Tarp, Anal. Chim. Acta, 73 (1974) 355.
10 M. Mascini and G. G. Guilbault, Anal. Chem., 49 (1977) 795.
11 S. Caras and J. Janata, Anal. Chem., 52 (1980) 1985.
12 Y. Miyahara, F. Matsu, T. Moriizumi, H. Matsuoka, I. Karube and S. Suzuki, Proceedings of an International Meeting on Chemical Sensors, Fukuoka, September 1983, Elsevier, Amsterdam, 1983, p. 513.
13 T. Matsuo and M. Esashi, Sens. Actuators, 1 (1981) 77.

Analytica Chimica Acta, 185 (1986) 201—208
Elsevier Science Publishers B.V., Amsterdam — Printed in The Netherlands

CATALYTIC DETERMINATION OF VANADIUM WITH THE BROMATE/IODIDE/ASCORBIC ACID LANDOLT REACTION AND CONDUCTOMETRIC MONITORING

J. A. AMBERSON and G. SVEHLA*
Department of Analytical Chemistry, The Queen's University, Belfast (Great Britain)
(Received 3rd December 1985)

SUMMARY

Vanadium (0—1 mg l^{-1}) is determined in solutions by a catalytic procedure with conductometric detection. Reaction times of the bromate/iodide/ascorbic acid Landolt reaction are evaluated from conductance vs. time traces, obtained with an instrument with compensation facilities. Results are evaluated by means of calibration graphs, where the $t(0)/t(c)$ ratios are plotted against the concentration of vanadium. Kinetics and mechanism of the reactions are discussed and values for the rate coefficients as well as entropies and enthalpies of activation are presented.

Vanadium can be determined catalytically by means of the bromate/iodide/ascorbic acid Landolt reaction [1]. The time elapsed between the mixing of the reagents and the appearance of the colour of iodine was determined by visual monitoring and then related, through a calibration graph, to the concentration of vanadium, which catalyses the reaction between bromate and iodide. The visual end-point determination, though simple, is tedious, requires constant attention and, should it be missed, a new attempt. It is not suitable for automation and cannot be adapted for flow-injection systems. Observation of the end-point of such kinetic runs can be made easier by introducing electrometric techniques. In this paper the application of conductometry is described.

The advantages and disadvantages associated with conductometric monitoring have been discussed [2]. It was pointed out that even when modern conductometric apparatus is used, which allows not only direct reading and recording of conductivity but also compensation of the signal, the direct monitoring of reaction rates is still impractical. However, when the reactions applied involve an abrupt change in the conductivity after a predetermined amount of reactant has been consumed (e.g., Landolt reactions), such monitoring becomes feasible. When the method was optimized for conductometric monitoring, it was found that a sharper end-point was obtained by reducing the concentration of iodide in the reaction mixture. Otherwise, the procedure is quite similar to that described for visual monitoring.

0003-2670/86/$03.50

EXPERIMENTAL

Reagents

Analytical-grade reagents were used whenever possible. Water twice-distilled from a glass still was used in all solution preparation.

A vanadium stock solution (1000 mg l^{-1} vanadium) was prepared by dissolving 2.2963 g of ammonium metavanadate in water and diluting to 1 l. A 10 mg l^{-1} stock solution was obtained by appropriate dilution and working standards (0.2—1.0 mg l^{-1} vanadium) were obtained by appropriate dilution of this solution.

Solution A (oxidizing) contained 0.06667 mol (11.1339 g) of potassium bromate and 1.20 mol (252 g) of citric acid monohydrate per litre. Solution B (reducing) contained 0.0125 mol (2.075 g) of potassium iodide, 0.0376 mol (11.06 g) of trisodium citrate dihydrate and 0.00667 mol (1.1748 g) of ascorbic acid per litre.

Apparatus

The conductometer used must have facilities for compensation of conductivity and linkage to a chart recorder. A Metrohm E-518 conductometer was used with a Metrohm E-586 Labograph. A standard Metrohm EA-880 universal titration vessel (with thermostatted jacket) was used with two Metrohm EA-211 platinized platinum sheet electrodes; these did not have protecting glass umbrellas around them, thus allowing free circulation of the liquid. Solutions were stirred magnetically during the kinetic runs. The cell constant for this arrangement was 2.6 mS cm^{-1}. Daily, the cell was calibrated with 0.01 mol l^{-1} potassium chloride solution (with a specific conductivity of 1.4087 mS cm^{-1} at 25°C); all signals were then measured as specific conductivities. In a typical run, the initial conductivity of 10 ml of solution A with 10 ml of water was 7.2×10^{-3} S cm^{-1}; on addition of 10 ml of solution B, the conductivity increased initially by about 4×10^{-4} S cm^{-1}, then fell back near to the original level and, after a trough with a well-defined peak, began to rise when iodine started to appear. Most of the initial conductivity was then compensated with the appropriate control on the instrument; with a full-scale sensitivity of 1 mS cm^{-1} on the conductometer and a 1000-mV full scale sensitivity on the Labograph, readings remained on-scale until the end-point was reached. A chart speed of 50 or 100 mm min^{-1} was usually suitable.

All solutions and the reacting mixture were thermostatted in a water bath held at 25 ± 1°C with a BTL Circon heater-circulator unit.

Procedure

The vanadium standards and the sample solution should contain 0—1 mg l^{-1} vanadium. Place 10.00 ml of sample or standard into the cell, add 10.00 ml of solution A and start recording the conductivity. When the reading becomes nearly constant, add 10.00 ml of solution B. The conductivity rises abruptly, then falls back to near its original level. Finally, it decreases further, and

after reaching a minimum begins to rise quickly; simultaneously, the colour of iodine becomes visible in the cell, marking the end of the reaction time. Monitoring is then stopped and reaction times, $t(c)$, are evaluated from the recorded trace as indicated in Fig. 1. Measure a blank reaction time, $t(0)$, by placing 10.00 ml of water in the cell. After each run, rinse the cell and electrodes carefully with water, and remove all the liquid from the cell and electrodes with a suction tube attached to a water pump. For very accurate work, the vessel and electrodes should be dried before each run, but this is impractical for routine work. The results given here were obtained by emptying the vessel by suction.

To draw the calibration graph, calculate the $t(0)/t(c)$ ratios and plot these against the concentration of vanadium. A straight line is obtained with an intercept of 1 on the $t(0)/t(c)$ axis.

RESULTS AND DISCUSSION

Analytical study

The shape of the conductometric trace (Fig. 1) can be explained from the chemical reactions occurring during the operation. The initial changes in the measured signal are obviously a consequence of the finite rate of mixing and offer a very sharp reference point for the later evaluation. The decrease in conductivity near the end-point marks the removal of conducting ions and the appearance of iodine; this is followed by a sharp increase of conductivity because of the release of hydronium ions. The local minimum of the conductance signal serves to mark the end of the period to be measured.

The calibration plot for the range 0—1.0 mg l^{-1} vanadium, with $t(c)$ in the range 3.66—1.29 min and $t(0)/t(c)$ in the range 1—2.85, had a slope of 1.886 l mg^{-1}, with intercept 1.007 and a correlation coefficient of 0.9988. The lowest determinable concentration [3] was 0.07 mg l^{-1}. The advantage of using the $t(0)/t(c)$ ratio (instead of the reciprocal reaction time) for evaluation is that the ratios are easily reproducible whereas the reproducibilities of the

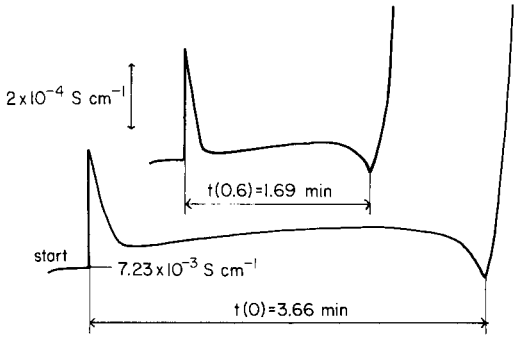

Fig. 1. Conductometric traces and their evaluation.

individual $t(0)$ and $t(c)$ values are worse. The repeatability of time measurements (with the same solutions) was better than 3 s.

An earlier detailed study of interferences [1] showed that, with the citrate buffer used, none of the 19 common metal ions studied interfered. In the absence of citrate (acetate buffer), molybdenum (1 mg ml^{-1}), as well as copper, iron and titanium (10 mg l^{-1}) interfered seriously.

Kinetic study

For the proper understanding of a catalytic method of analysis, and in particular to establish which parameters will affect the measured signal, it is important to know the overall reaction stoichiometry, the mechanism, rate coefficients and activation parameters of the uncatalysed and catalysed reactions. The reaction between bromate and iodide has been studied extensively in the past 100 years; the earliest observations were made by Ostwald [4]. Barton and Wright [5] gave a full historic account. The rate law for the bromate/iodide reaction [5] takes the form

$$v = -d[BrO_3^-]/dt = (k_0 + k_b[BA^-])[H^+]^2[BrO_3^-][I^-] \quad (1)$$

where BA^- is the buffer anion. The value of k_0 was found to be around 50 l^3 mol^{-3} s^{-1}, while the value of k_b, depending on the nature of the buffer, was in the range 0.25×10^4—5.4×10^4 l^4 mol^{-4} s^{-1}. For the vanadium-catalysed reaction, no reliable kinetic data seem to be available. As the experimental circumstances of the Landolt reaction are quite different from those quoted in the literature, a brief kinetic study was undertaken, limited to the experimental parameters used in the quantitative procedure.

The rate coefficients. Initially, the uncatalysed reaction (i.e., in the absence of vanadium) was investigated. If the reaction mechanism suggested by Barton and Wright [5] with constant concentrations of hydrogen and buffer ions is accepted, then the rate law can be simplified to

$$v_{un} = (-d[BrO_3^-]/dt)_{un} = k_{un}[BrO_3^-][I^-] \quad (2)$$

An attempt was made to evaluate k_{un} (and to prove that its value is really constant). For this, the rate equation had to be integrated under the boundary conditions defined by the present experiment. When the notation $B = [BrO_3^-]_0/([BrO_3^-]_0 - [Asc]_0)$ is introduced from the integrated equation, the uncatalysed rate coefficient can be expressed as

$$k_{un} = \ln B/[t(0)C(I^-)] \quad (3)$$

The concentrations marked 0 are the initial concentrations of bromate and ascorbic acid, respectively; $C(I^-)$ is the analytical concentration of the iodide (which remains constant during the period of observation because of the presence of ascorbic acid), and $t(0)$ is the measured reaction time. Results of experiments conducted with different initial concentrations of bromate, iodide and ascorbic acid are shown in Table 1. The results confirm the simplified rate law defined by Eqn. 2. These results can be compared with those of

TABLE 1

Kinetic study of the uncatalysed reaction

$[BrO_3^-]_0$ (10^{-2} mol l^{-1})	$[Asc]_0$ (10^{-3} mol l^{-1})	$C(I^-)$ (10^{-3} mol l^{-1})	$t(0)$ (s)	k_{un} (10^{-2} l mol^{-1} s^{-1})
2.223	2.223	4.167	250.8	3.244
1.905	1.905	3.571	340.2	2.791
1.667	1.667	3.125	464.4	2.336
1.482	1.482	2.778	601.8	2.028
1.334	1.334	2.500	773.7	1.750
		Mean		2.43
		Standard deviation		0.75

Barton and Wright [5]. From Eqns. 1 and 2, k_{un} can be expressed as

$$k_{un} = (k_0 + k_b[BA^-])[H^+]^2 \quad (4)$$

The (mean) pH of the solution during the observed period was 2.3, i.e., $[H^+] = 5.012 \times 10^{-3}$ mol l^{-1}, and the concentration of the buffer anion $[BA^-]$ was 0.4 mol l^{-1}. With $k_0 = 50$ and $k_b = 2500$ (a value which is valid for an acid strength nearest to citric acid), Eqn. 3 gives the value 2.64×10^{-2} for the uncatalysed rate constant, which is in very good agreement with the present experimental value (2.43×10^{-2}).

The catalytic action of vanadium(V), present predominantly as the dioxovanadium(V) ion, can be explained through the following mechanism:

$$BrO_3^- + VO_2^+ \underset{k_{-1}}{\overset{k_1}{\rightleftharpoons}} BrVO_5$$

$$BrVO_5 + I^- \xrightarrow{k_2} BrO_2^- + IO^- + VO_2^+$$

These rate-determining steps are then followed by fast steps, with a mechanism identical to the fast steps in the uncatalysed reaction (see Barton and Wright [5]). The rate of the catalysed reaction can be expressed as

$$v_{cat} = -(d[BrO_3^-]/dt)_{cat} = k_2[BrVO_5][I^-] \quad (5)$$

The concentration of $BrVO_5$ is not known; but it can be estimated considering that it is low and, except at the beginning and end of the period under investigation, constant (steady-state approximation). From the steady-state condition,

$$d[BrVO_5]/dt = k_1[BrO_3^-][VO_2^+] - k_{-1}[BrVO_5] - k_2[BrVO_5][I^-] = 0,$$

the concentration of $BrVO_5$ can be expressed as

$$[BrVO_5] = k_1[BrO_3^-][VO_2^+]/(k_{-1} + k_2[I^-])$$

Because of the steady-state condition, $[VO_2^+] = C(V)$, which is the analytical concentration of vanadium, and $k_2[I^-] \gg k_{-1}$. Thus if the notation k_1 is denoted as k_{cat}, the rate of the catalysed reaction can be expressed as

$$-(d[BrO_3^-]/dt)_{cat} = k_{cat}[BrO_3^-]C(V) \quad (6)$$

The catalysed reaction cannot be examined experimentally alone, because when vanadium is present, the uncatalysed and catalysed reactions run simultaneously. The overall rate has to be examined; it can be expressed as the sum of Eqns. 2 and 6:

$$-d[BrO_3^-]/dt = k_{un}[BrO_3^-]C(I^-) + k_{cat}[BrO_3^-]C(V) \quad (7)$$

This rate equation can be integrated with similar boundary conditions as applied with the uncatalysed reaction. From the integrated rate equation, the rate coefficient of the catalysed reaction can be expressed as

$$k_{cat} = \{[1/t(c)] \ln B - k_{un}C(I^-)\}/C(V) \quad (8)$$

where $t(c)$ is the measured reaction time in the presence of the catalyst. To test the validity of this mechanism and kinetics, experiments were done with different initial reactant concentrations. From the results, k_{cat} values were calculated through Eqn. 8 and are listed in Table 2. These values indicate that the proposed mechanism and the corresponding kinetics are valid; within the concentration ranges involved, the catalysed rate coefficient seems to be more constant than the rate coefficient of the uncatalysed reaction, especially if the first of the results in Table 2 is ignored. No comparisons can be made as this rate coefficient does not seem to have been reported previously.

The activation parameters. In investigations of the temperature dependence of reaction rates, it is best to determine the activation parameters for both the uncatalysed and catalysed processes. These are defined through the Eyring equation [6], which takes the form

TABLE 2

Kinetic study of the catalysed reaction

$[BrO_3^-]_0$ (10^{-2} mol l^{-1})	$[Asc]_0$ (10^{-3} mol l^{-1})	$C(I^-)$ (10^{-3} mol l^{-1})	$C(V)$ (10^{-7} mol l^{-1})	$t(c)$ (s)	k_{cat} (10^{-1} l mol^{-1} s^{-1})
2.223	2.223	4.167	0.654	87.0	4.432
1.905	1.905	3.571	0.841	81.9	3.891
1.667	1.667	3.125	0.982	75.6	3.798
1.482	1.482	2.778	1.091	71.4	3.734
1.334	1.334	2.500	1.178	66.6	3.806
		Mean[a]			3.807
		Standard deviation[a]			0.064

[a]Excluding the first result.

$$k = (kT/h) \exp (\Delta S^{\ddagger}/R) \exp (-\Delta H^{\ddagger}/RT) \quad (9)$$

Here $\Delta S^{\ddagger}$ is the entropy and $\Delta H^{\ddagger}$ the enthalpy of activation. These can be defined for the uncatalysed and the catalysed reactions separately. In their dimension, the mol^{-1} refers to 1 mol of the activated complex.

To evaluate these activation parameters, kinetic runs were conducted at different temperatures, with all the initial concentrations of the reactants kept constant. From the results, $F(T)$ temperature functions were calculated, which are related to the activation parameters through the equation

$$F(T) = \Delta S^{\ddagger} - \Delta H^{\ddagger}/T \quad (10)$$

The same temperature function for the uncatalysed reaction can be written (by combining Eqns. 3, 9 and 10) in the form

$$F(T)_{un} = R \ln \{[h/t(0)/C(I^-)/k/T] \ln B\} \quad (11)$$

The combination of Eqns. 8—10, with the definition of B, gives the temperature function for the catalysed reaction:

$$F(T)_{cat} = R \ln \{h/C(V)/k/T[(1/T) \ln B - C(I^-)k_{un}]\} \quad (12)$$

where the values of the k_{un} rate constant have to be calculated from

$$k_{un} = (kT/h) \exp (\Delta S^{\ddagger}_{un}/R) \exp (-\Delta H^{\ddagger}_{un}/RT) \quad (13)$$

By plotting these $F(T)$ functions against $1/T$, straight lines are obtained, with the intercept equalling $\Delta S^{\ddagger}$ and the slope $\Delta H^{\ddagger}$.

Results from the present experiments are shown in Table 3. The values of the parameters were calculated through linear regression; the correlation coefficients (r) are shown in the last line and the ranges are given at the 95%

TABLE 3

Determination of the activation parameters
($h = 6.626 \times 10^{-34}$ J s; $k = 1.381 \times 10^{-23}$ J K^{-1}; $R = 8.314$ J K^{-1} mol^{-1}; $[Asc]_0 = 2.223 \times 10^{-3}$ mol l^{-1}; $[BrO_3^-]_0 = 2.223 \times 10^{-2}$ mol l^{-1}; $C(I^-) = 4.167 \times 10^{-3}$ mol l^{-1}; $C(V) = 6.543 \times 10^{-6}$ mol l^{-1})

Temperature		$t(0)$ (s)	$t(c)$ (s)	$F(T)_{un}$ (J K^{-1} mol^{-1})	$F(T)_{cat}$ (J K^{-1} mol^{-1})
(°C)	(K)				
15.5	288.7	662.4	238.8	−281.2	−222.6
20.0	293.2	502.8	177.6	−279.1	−220.4
25.5	298.7	353.4	119.4	−276.3	−217.2
30.5	303.7	243.0	80.4	−273.3	−213.8
33.5	306.7	178.2	—	−270.8	—
34.5	307.7	—	58.8	—	−211.1

$\Delta H^{\ddagger}_{un} = 48.4 \pm 6.3$ kJ mol^{-1}; $\Delta H^{\ddagger}_{cat} = 55 \pm 11$ kJ mol^{-1}
$\Delta S^{\ddagger}_{un} = -113 \pm 21$ J K^{-1} mol^{-1}; $\Delta S^{\ddagger}_{cat} = -29 \pm 39$ J K^{-1} mol^{-1}
$r_{un} = 0.997$; $r_{cat} = 0.993$

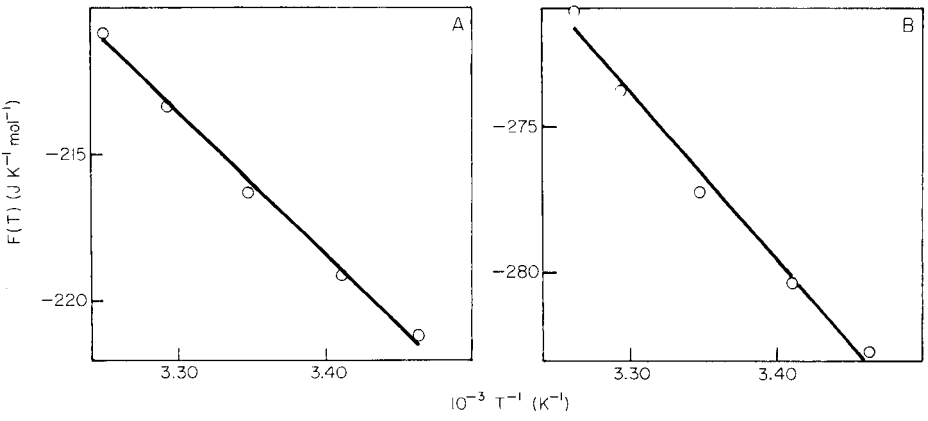

Fig. 2. Temperature functions: (A) the uncatalysed reaction; (B) the catalysed reaction.

level of significance. The temperature functions, plotted against reciprocal absolute temperature, are shown in Fig. 2.

It is noteworthy to mention that the enthalpy of activation of the catalysed process is actually higher than that of the uncatalysed one; the catalysed reaction becomes faster because of the higher (less negative) entropy of activation (or the pre-exponential factor). This is of course expected when the rate-determining step in the uncatalysed process is the encounter of two negatively-charged species (bromate and iodide), while in the catalysed reaction a positively- and a negatively-charged species (dioxovanadium(V) and bromate) are involved. The fairly high scatter in the values of the catalysed parameters are due to the propagation of errors, which is considerable with the complicated $F(T)$ functions each containing two logarithms.

REFERENCES

1 H. Thompson and G. Svehla, Microchem. J., 13 (1968) 576.
2 J. A. Amberson and G. Svehla, Anal. Chim. Acta, 178 (1985) 255.
3 K. Doerffel, Statistik in der Analytischen Chemie, VEB Deutscher Verlag für Grundstoffindustrie, Leipzig, 1966, p. 177.
4 W. Ostwald, Z. Phys. Chem., 2 (1888) 127.
5 A. F. M. Barton and G. A. Wright, J. Chem. Soc. A: (1968) 1747.
6 W. F. K. Wynne-Jones and H. Eyring, J. Chem. Phys., 3 (1935) 492.

Analytica Chimica Acta, 185 (1986) 209—218
Elsevier Science Publishers B.V., Amsterdam — Printed in The Netherlands

APPLICATION OF A COPPER-BASED MERCURY FILM ELECTRODE IN CATHODIC STRIPPING VOLTAMMETRY

MIKOŁAJ DONTEN and ZENON KUBLIK*
Department of Chemistry, University of Warsaw, ul. Pasteura 1, Warsaw 02093 (Poland)
(Received 9th September 1985)

SUMMARY

The utility of a copper-based mercury film electrode (MFE) in cathodic stripping voltammetry (c.s.v.) is tested by comparing the cyclic and stripping voltammograms obtained with this electrode for thiocyanate, tryptophane, cysteine and benzotriazole against those obtained with the hanging copper-amalgam drop electrode (HCADE) and the HMDE. The cathodic stripping peaks obtained at the copper-based MFE and the HCADE are usually narrower and higher and are located at more negative potentials than the peaks obtained at the HMDE. Lower detection limits and better separations of adjacent peaks are thus achieved, and useful peaks can be separated from the mercury waves obtained with the conventional HMDE. The advantage of the copper-based MFE over the HCADE is its simplicity of preparation and maintenance. Thiocyanate, tryptophane, cysteine and benzotriazole can be determined at the copper-based MFE by c.s.v. with detection limits of 1×10^{-8}, 1×10^{-8}, 5×10^{-9} and 2×10^{-8} mol dm^{-3}, respectively.

Cathodic stripping voltammetry (c.s.v.) which exploits the anodic accumulation of sparingly soluble mercury(I) or mercury(II) compounds on a mercury electrode surface is well known in trace analysis [1, 2]. Some recent results indicate, however, that the accumulation of copper(I) compounds on the electrode surface may be more advantageous in some cases than accumulation of the mercury compounds. This variation of the conventional analysis has been used for traces of penicillamine [3], cysteine and cystine [4], penicillin [5] and thiocyanate [6]. In these methods, the appropriate copper(I) deposits were formed by the reduction of Cu(II) ions added to the bulk solution. Such a procedure has several disadvantages. First, the stripping peak occurs on the Cu(II) reduction current and this current decreases in accordance with the Cottrell equation. This effect can make it difficult to measure the stripping peak height precisely. Secondly, the addition of Cu(II) ions to the bulk solution may produce some unfavourable side-reactions. In order to eliminate these disadvantages, Bilewicz and Kublik [6, 7] proposed that Cu(I) should be generated anodically from the hanging copper amalgam drop electrode (HCADE). The HCADE was also used by Tanaka and Yoshida [8] to determine cysteine by anodic stripping voltammetry.

The aim of the present work was to check whether a copper-based mercury film electrode (MFE) could find wider uses in c.s.v. Such an electrode should

0003-2670/86/$03.50

be easier to work with than other kinds of copper amalgam electrodes. Copper-based MFE's have been used previously [9—12]. The characteristics of such electrodes have recently been examined in detail [13].

EXPERIMENTAL

The voltammetric curves were recorded with a three-electrode arrangement and a Radelkis OH-105 polarograph. A saturated calomel reference electrode (SCE) was used; all the potentials given here are referred to this electrode. The salt bridge was filled with sodium nitrate solution. The auxiliary electrode was a platinum foil with a surface area of ca. 1 cm^3. The indicating electrode was usually the copper-based MFE. The electrode was prepared as described previously [13] and was stored in a small volume of mercury. After storage, excess of mercury was removed by wiping with a copper foil. This procedure usually gives a film 3—4 μm thick [13], but for practical work the thickness need not be measured. Prior to use and after prolonged use, the electrode was conditioned [13]. For comparison, a conventional HMDE [14] and a HCADE were used. Because the copper amalgam is not stable [15], the concentrations of copper in the amalgam were calculated on the basis of the Sevčik-Randles equation from the height of the dissolution peak of copper. The value of the diffusion coefficient of copper in mercury was taken as 1.06×10^{-5} cm^2 s^{-1} [16]. In stripping experiments, the solutions were stirred magnetically.

Thrice-distilled water was used to prepare solutions. The supporting electrolyte and acetate, phosphate and borate buffer solutions were prepared from reagent-grade chemicals. In most cases, 0.5 mol dm^{-3} sodium perchlorate was used as supporting electrolyte. This solution was adjusted to the required pH with dilute perchloric acid or sodium hydroxide solution, or with the appropriate buffer. Solutions of benzotriazole, cysteine (both from Reanal, Budapest) and tryptophane (Sigma Chemical Co.) were prepared daily and small samples of these solutions were added by a microsyringe to the deaerated supporting electrolyte. Argon was used for deaeration. All experiments were done at 25 ± 1°C.

RESULTS

Investigations with thiocyanate

Thiocyanate does not give a peak under c.s.v. conditions at the HMDE [17] but traces of thiocyanate can be determined at the HCADE [6]. Figure 1A illustrates the behaviour of thiocyanate at the HMDE and at the copper-based MFE. On both curves, the anodic peaks are nearly the same in height whereas the cathodic branches differ markedly. The shape of the cathodic peak obtained with the HMDE shows that this peak is diffusion-controlled. In contrast, the peak obtained with the copper-based MFE corresponds to electroreduction of the species accumulated on the electrode

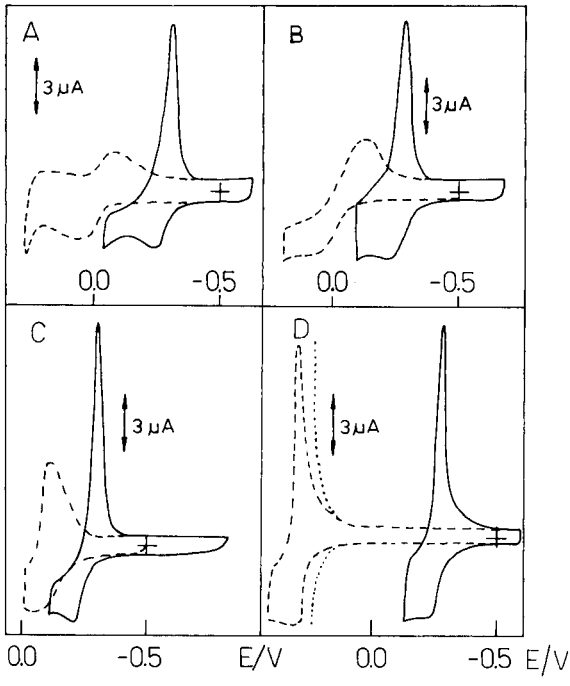

Fig. 1. Cyclic voltammetric curves obtained for 1×10^{-5} mol dm^{-3} solutions: (A) thiocyanate; (B) tryptophane; (C) cysteine; (D) benzotriazole. Electrode: (---) HMDE; (—) copper-based MFE. Supporting electrolyte 0.5 mol dm^{-3} $NaClO_4$. pH: (ACD) 2; (B) 5. Dotted lines were obtained in the presence of 1×10^{-3} mol dm^{-3} chloride. Voltage scan rate 1 V min^{-1}.

surface during the anodic scan. Thus, the copper-based MFE can be exploited to determine traces of thiocyanate by c.s.v. The voltammograms obtained for thiocyanate at the copper-based MFE and at the HCADE showed peaks with nearly the same shape and height.

Figure 2 shows c.s. voltammograms for $1—5 \times 10^{-8}$ mol dm^{-3} thiocyanate. Essential data characterizing the stripping process are presented in Table 1. Each curve shows a single, well-defined cathodic stripping peak. The calibration plot (Fig. 2) is linear up to 3×10^{-7} M thiocyanate with very good correlation. The plateau region at higher thiocyanate concentrations corresponds to coverage of the electrode surface by a monolayer of copper(I) thiocyanate [18]. Marked prolongation of the deposition time does not improve the detection limit but decreases the linear range of the calibration plot. A decrease in the deposition time increases the upper limit of the linear range.

The stripping peak of the copper(I) thiocyanate obtained at the copper-based MFE is not affected by the addition of 0.1 mol dm^{-3} sodium nitrate or sulphate or 0.01 mol dm^{-3} sodium chloride, i.e., such solutions can also serve as supporting electrolyte. The peak height was also independent of variations in pH within the range 1—9, regardless of the mode of pH adjust-

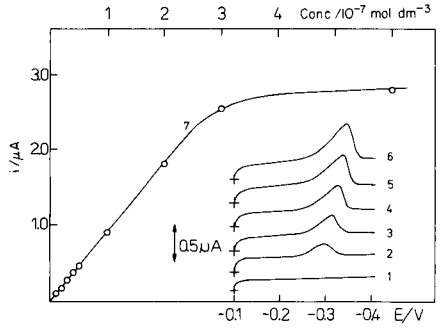

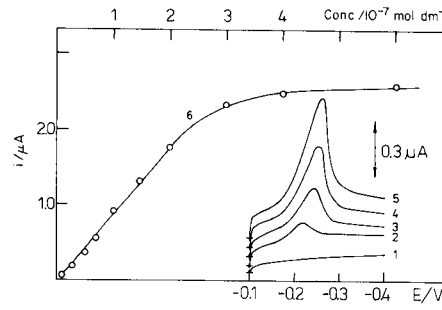

Fig. 2. (1—6) Cathodic stripping curves with the copper-based MFE in 0.5 mol dm^{-3} $NaClO_4$ (pH 2) for thiocyanate: (1) 0; (2) 1; (3) 2; (4) 3; (5) 4; (6) 5×10^{-8} mol dm^{-3}. (7) Calibration plot. Conditions: 3 min accumulation at —0.1 V with stirring; voltage scan rate 1 V min^{-1}; electrode surface area 19.6 mm^2.

Fig. 3. (1—5) Cathodic stripping curves with the copper-based MFE in 0.5 mol dm^{-3} $NaClO_4$ (pH 5) for tryptophane: (1) 0; (2) 1; (3) 3; (4) 5; (5) 7×10^{-8} mol dm^{-3}. (6) Calibration plot. Conditions as for Fig. 2.

TABLE 1

Characteristics of the cathodic stripping peaks obtained at the copper-based MFE for the substances studied

Substance	Optimum range of deposition		Peak width at $i_p/2$ (mV)	Linear range of calibration (mol dm^{-3})	Correl. coeff.	Charge needed for monolayer formation ($\mu C\ cm^{-2}$)
	pH	V[a]				
Thiocyanate	1—9	—0.05— —0.20	46	1×10^{-8}—3×10^{-7}	0.997	60
Tryptophane	4.5—8	—0.05— —0.20	52	1×10^{-8}—3×10^{-7}	0.992	48
Cysteine	1—10	—0.04— —0.15	40	5×10^{-9}—8×10^{-7}	0.998	50
Benzotriazole	1—3 and 5—12	—0.05— —0.20	40	2×10^{-8}—2×10^{-6}	0.9995	50

[a]In acidic solution.

ment (addition of acid, base or the appropriate buffer). It should be noted that Lundquist and Cox [19] determined phosphate by c.s.v. at a polycrystalline copper electrode, thus phosphate buffer seemed likely to interfere. However, under the present experimental conditions, the use of phosphate buffer (pH 6—8) did not produce any additional stripping peaks. In the presence of 0.1 mol dm^{-3} chloride, the stripping peak for thiocyanate decreased slightly but traces of thiocyanates could still be determined. Interference by

iodide, even at equimolar concentrations, was severe because of significant overlap of the stripping peaks of iodide and thiocyanate. The copper(I) thiocyanate peak is quite close to the reduction peak of lead(II) ions, but lead(II) interfered significantly only at concentrations exceeding 5×10^{-5} mol dm^{-3}.

Investigations with tryptophane

Tryptophane is neither reduced nor oxidized at mercury electrodes in aqueous solutions [20]. The interactions between tryptophane and Cu(II) ions have been studied polarographically by Quintin and Foglizzo [21]. Tomaszewski [22] showed that tryptophane reacts anodically with mercury and copper amalgam electrodes giving a deposit on the electrode surface.

Figure 1B illustrates the cyclic behaviour of tryptophane at the HMDE and at the copper-based MFE. The shape of the cathodic peaks obtained at both electrodes suggests that the products formed during the anodic scan accumulate on the electrode surface, i.e., both electrodes can be used for determination of tryptophane by c.s.v. However, the cathodic peak obtained at the copper-based MFE is significantly thinner and higher, and so more useful analytically. Copper(II) ions added to the bulk solution did not give any precipitate with tryptophane; the deposit on the electrode surface probably corresponds to copper(I) tryptophane. The cathodic peak obtained at the copper-based MFE is slightly thinner and higher than the peak obtained at the HCADE.

Figure 3 presents c.s. voltammograms for increasing concentrations of tryptophane and a calibration curve. The stripping peak is well defined. As in the case of thiocyanate, a plateau is reached at concentrations exceeding 3×10^{-7} M. Characteristic data for tryptophane peak are shown in Table 1. The charge needed for the formation of a monolayer of deposit is similar to the charge needed for the deposition of a monolayer of copper(I) thiocyanate; this supports the above suggestion that the anodic deposit is formed by copper(I) not copper(II) tryptophanate. As for thiocyanate, very long accumulation times decrease the linear calibration range; decreased deposition times increase the upper determination limit but also the detection limit.

As in the case of thiocyanate, the stripping peak of tryptophane at the copper-based MFE is not affected by addition of 0.1 mol dm^{-3} sodium nitrate or sulphate. Chloride (0.1 mol dm^{-3}) affected the peaks obtained at the copper-based MFE slightly; under the same conditions, the peak obtained at the HMDE was masked completely by the mercury dissolution current. Variations in pH over the range 4.5—8 did not affect the stripping peak height; below pH 4.5 the peak height decreased and below pH 3 the peak disappeared completely. The stripping peak of the copper(I)-tryptophane complex was severely distorted by the presence of thiocyanate and iodide. The influence of lead(II) ions was similar to that described above for thiocyanate.

Investigations with cysteine

Cysteine is not reduced under polarographic conditions but reacts with the mercury electrode to form a sparingly soluble deposit [23]. The properties of this deposit were studied thoroughly by Stankowich and Bard [24], who showed that the film consists of the mercury(II)-cysteine complex. Cysteine was determined by c.s.v. at the HMDE by Berge and Jeroschewski [25]. According to Florence [2], the reproducibility of the c.s.v. results for cysteine at mercury electrodes is poor. The accumulation of the copper(I)-cysteine complex on the HMDE was exploited for the determination of cysteine by Forsman [4]. Tanaka and Yoshida [8] proposed a determination of cysteine by anodic stripping voltammetry at the HCADE.

Figure 1C shows a comparison of the cyclic voltammetric curves for cysteine at the HMDE and the copper-based MFE. It is evident that the latter electrode offers better conditions for the determination of cysteine by c.s.v.; however, cyclic voltammograms for cysteine at this electrode and at the HCADE had, in practice, the same shape.

Figure 4 shows cathodic stripping curves obtained at the copper-based MFE for increasing cysteine concentrations, as well as calibration plots for cysteine for the copper-based MFE and the HMDE. Data characterizing the stripping peak of the copper(I)-cysteine complex are presented in Table 1. At half-height, the stripping peaks obtained for the copper(I)-cysteine

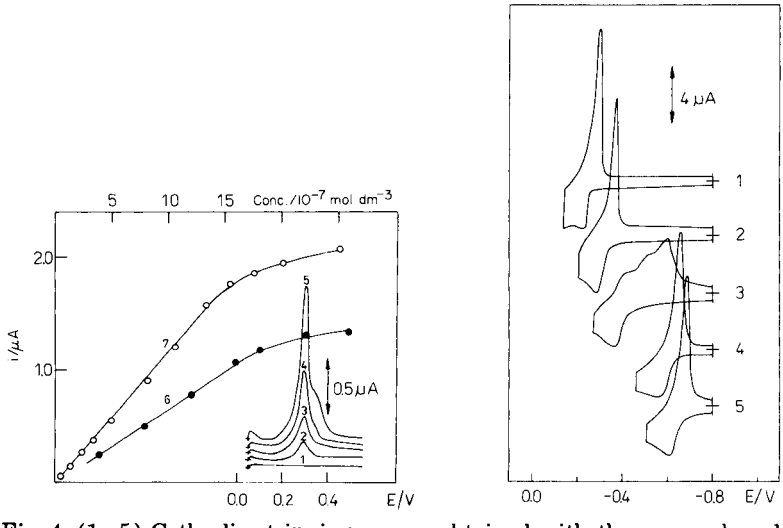

Fig. 4. (1—5) Cathodic stripping curves obtained with the copper-based MFE in 0.5 mol dm^{-3} $NaClO_4$ (pH 2) for cysteine: (1) 0; (2) 0.67; (3) 1.3; (4) 2.7; (5) 6.3 × 10^{-7} mol dm^{-3}. Calibration plots: (•) HMDE; (○) copper-based MFE. Conditions as for Fig. 2.

Fig. 5. Cyclic voltammetric curves obtained with the copper-based MFE for 1 × 10^{-5} mol dm^{-3} benzotriazole at different pH: (1) 1; (2) 3; (3) 5; (4) 6.5; (5) 12. Supporting electrolyte 0.5 mol dm^{-3} $NaClO_4$; voltage scan rate 1 V min^{-1}.

complex are narrower than those obtained under the same conditions for thiocyanate and tryptophane, and also narrower and higher than the stripping peak for the mercury(II)-cysteine complex. Because of this, the slopes of the calibration plots in Fig. 4 are different. In contrast to the plots shown in Fig. 2 and 3, the plot obtained for cysteine is slightly more complex, i.e., there was no strictly horizontal segment of the plot. Probably, in the case of the copper(I) cysteine complex the potentials for formation of the first and the second monolayers are quite close so that the observed peak may contain a contribution from the formation of the second monolayer. The quantity of electricity passed at the point where the slope of the plot changes is markedly smaller than the value (80 μC cm^{-2}) found by Stankowich and Bard [24] for the mercury(II)-cysteine complex. This supports the conclusion that the copper(I)- and not copper(II)-cysteine complex is formed at the copper-based MFE.

In principle, the copper(I)-cysteine film accumulated at the electrode could be stripped either cathodically or anodically. Tanaka and Yoshida [8], working with the HCADE (probably filled with dilute copper amalgam), observed the anodic stripping peak but ascribed it not to the oxidation of the copper(I)-cysteine complex but to the conversion of the copper(II)-cysteine complex to the mercury(II)-cysteine complex. In the present experiments with the copper-based MFE, such a peak was not observed, probably because it was masked by the copper dissolution current.

The cathodic stripping peak of the copper(I)-cysteine complex was not affected by sodium nitrate, sulphate or chloride (0.1 mol dm^{-3}) so that any of these could serve as the supporting electrolyte in cysteine determinations. Variations in pH over the range 1—10 (Table 1) had no essential effect on the stripping peak height; the pH could be adjusted with acid or base or an appropriate buffer. Thiocyanate, iodide, and tryptophane obviously interfered severely. The harmful action of tryptophane could be eliminated by decreasing the pH (Table 1). Cystine gives a stripping peak at nearly the same potential as cysteine. This peak is markedly pH-dependent; the interference of cystine is less significant in acidic than in alkaline solution.

Investigation of benzotriazole

Benzotriazole has not been determined by c.s.v. either at the HMDE or at the copper amalgam electrodes though it forms sparingly soluble compounds with copper(I) [26] and copper(II) [26, 27] ions. Studying the Cu(II)/Cu(I)/Cu(Hg) system in the presence of benzotriazole by polarographic and chronocoulometric methods, Pergola et al. [28] found that the slightly soluble copper(I)-benzotriazole complex is easily deposited on the surface of a dropping copper amalgam electrode.

Figure 1D shows a comparison of the cyclic voltammetric curves obtained for benzotriazole at the HMDE and at the copper-based MFE. The curves obtained at the two electrodes are similar in shape but differ markedly in their position on the potential axis. The results obtained at the HCADE were very

similar to those obtained at the copper-based MFE. A significant advantage of using either of these electrodes rather than the HMDE occurs in solutions containing small amounts of chloride. As the dotted lines in Fig. 1D show, even a little chloride (1×10^{-3} mol dm^{-3}) shifts the mercury dissolution current sufficiently to mask the anodic peak corresponding to the insoluble mercury-benzotriazole complex.

Figure 5 shows the influence of variations in pH on the shape and position of the cyclic voltammetric curves of benzotriazole. Over the pH range 1—3, the simple anodic/cathodic system of peaks is obtained with the cathodic peak being significantly higher. Above pH 3, the cathodic branch becomes complex but at pH 5.2—12 the simple system reappears. Figure 6 shows cathodic stripping voltammograms obtained for increasing concentrations of benzotriazole and the related calibration plot. The characteristics of the stripping peak of the copper(I)-benzotriazole complex are shown in Table 1. The influence of pH is complex; but over the two ranges of pH given, the height of the stripping peak is constant, whether the pH is adjusted with acid or base or the appropriate buffer.

The stripping peak of the copper(I)-benzotriazole complex is unaffected by neutral salts, and affected by interferences, as described above for cysteine which, of course, interferes.

DISCUSSION

The most widely used type of c.s.v. exploits the anodic accumulation of the species being determined as a deposit with the electrode material. Most such determinations have been done with mercury electrodes, primarily

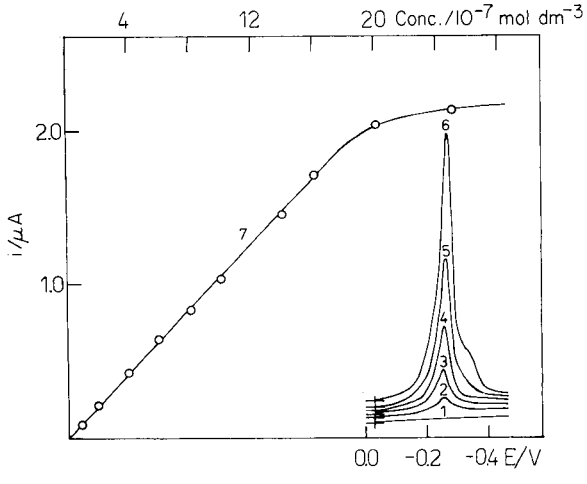

Fig. 6. (1—6) Cathodic stripping curves obtained with the copper-based MFE in 0.5 mol dm^{-3} $NaClO_4$ (pH 2) for benzotriazole: (1) 0; (2) 1; (3) 2; (4) 4; (5) 8; (6) 16×10^{-7} mol dm^{-3}. Conditions as for Fig. 2.

because the voltammograms obtained with the solid polycrystalline materials are usually complex, which means that reproducibility is poor and detection limits are high. For example, Parubotchaya et al. [29] determined thiocyanate by c.s.v. at a silver electrode and attained a detection limit of about 1×10^{-6} mol dm^{-3} whereas the use of the copper-based MFE offers a detection limit as low as 1×10^{-8} mol dm^{-3}. Lundquist and Cox [19], using c.s.v. with a plain copper electrode determined phosphate with a detection limit of about 1×10^{-7} mol dm^{-3}.

The use of amalgam electrodes offers new possibilities for widening the scope of c.s.v. An amalgam electrode maintains its fluid homogeneous surface and so the stripping peaks obtained are quite simple in shape. Moreover, when the amalgam-forming metal is less noble than mercury, the stripping peaks occur at more negative potentials than the peaks observed at pure mercury electrodes. As yet, this approach has been little used and the work that has been done has been based mainly on copper amalgam electrodes. Such electrodes can be prepared in situ by adding Cu(II) ions to the solution under study, or by preliminary electrolytic formation of an amalgam, or by covering a copper substrate with a mercury film.

At first sight, the first manner of preparing the copper amalgam electrode, and consequently the deposition of a copper(I) compound on the electrode surface, seems to be the simplest. However, under such conditions, it is necessary to take into account the possibility of the occurrence of interfering side-reactions, e.g., precipitation of the copper(II)-benzotriazole complex in the bulk solution, which according to Curtis [27] is complete over the pH range 7—8.5. In the case of cysteine, interference is caused by the reaction $2Cu(II) + 4RS^- = 2RSCu(I) + RSSR$ (where RS^- and RSSR are cysteine anion and cystine, respectively); this was studied in detail by Kolthoff and Stricks [30]. At high Cu(II) ion concentration, the copper(I)-cysteine deposit is oxidized to cystine according to the reaction $2RSCu(I) + 2Cu(II) = RSSR + 4Cu(I)$. According to Forsman [4], cystine reacts with the copper amalgam electrode regenerating cysteine, and this process may eliminate the influence of the reactions mentioned above. However, the c.s.v. activity of cystine is strongly pH-dependent and in acidic solutions the side-reactions described above may lead to a decreased cysteine stripping peaks. In the case of thiocyanate, interference may be caused by metathesis reactions between mercury and copper thiocyanates [31], which proceed easily at open circuit.

The use of the HCADE or the copper-based MFE eliminates the harmful side-reactions discussed above. However, these electrodes introduce their own problems. The disadvantage of the HCADE lies in the fact that the stripping peak heights depend not only on the concentration of the substance being determined but also on the copper concentration in the amalgam. The preparation of an amalgam with a strictly known concentration is not easy because the amalgam is not stable with time [15]; the copper concentration in the amalgam must be checked frequently. The concentration of copper in the amalgam covering a copper substrate in the copper-based MFE

is constant but the surfaces of all kinds of mercury film electrodes require regular renewal. The conditioning procedure needed for the copper-based electrode has been described [13].

This work was done as part of the Project MR-I-32 (CPBP 01.17).

REFERENCES

1 Kh. Z. Brainina, Inversionnaya Voltammetria Twierdykh Phaz, Khimiya, Moskow, 1972.
2 T. M. Florence, J. Electroanal. Chem., 97 (1979) 219.
3 U. Forsman, J. Electroanal. Chem., 111 (1980) 325.
4 U. Forsman, J. Electroanal. Chem., 122 (1981) 215.
5 U. Forsman, Anal. Chim. Acta, 146 (1983) 71.
6 R. Bilewicz and Z. Kublik, Anal. Chim. Acta, 123 (1981) 201.
7 R. Bilewicz and Z. Kublik, Anal. Chim. Acta, 171 (1985) 205.
8 S. Tanaka and H. Yoshida, J. Electroanal. Chem., 149 (1983) 213.
9 L. Palecek, Z. Anal. Chem., 162 (1958) 1.
10 N. A. Kotova, O. N. Guranova, W. A. Igolinski and W. I. Tyablikova, Zavods. Lab., 40 (1974) 1449.
11 H. J. Landaez-Machado, A. Darchen and C. Moinet, Electrochim. Acta, 25 (1980) 1321; 25 (1980) 1519.
12 P. W. Alexander and U. Akapongkul, Anal. Chim. Acta, 148 (1983) 103.
13 M. Donten and Z. Kublik, J. Electroanal. Chem., 196 (1985) 275.
14 W. Kemula and Z. Kublik, Anal. Chim. Acta, 18 (1958) 104.
15 S. Głodowski and Z. Kublik, Anal. Chim. Acta, 149 (1983) 137.
16 Z. Galus, CRC Crit. Rev. Anal. Chem., (1975) 401.
17 F. Vydra, K. Stulik and E. Julakova, Electrochemical Stripping Analysis, Horwood, Chichester, 1976, p. 219.
18 R. Bilewicz and Z. Kublik, J. Electroanal. Chem., 195 (1985) 137.
19 L. Lundquist and J. A. Cox, Anal. Chem., 46 (1974) 360.
20 M. F. Larouche, D. Buffaigeis and R. Jensen, Bull. Soc. Pharm. Bordeaux, 111 (1972) 14; Electroanal. Abstr., 12 (1974) 1200.
21 M. Quintin and M. R. Foglizzo, C. R. Acad. Sci., Ser. C: 262 (1966) 1500.
22 W. Tomaszewski, M. S. Thesis, University of Warsaw, 1985.
23 I. M. Kolthoff and C. Barnum, J. Am. Chem. Soc., 62 (1940) 3061.
24 M. T. Stankowich and A. J. Bard, J. Electroanal. Chem., 75 (1977) 487.
25 H. Berge and P. Jeroschewski, Fresenius Z. Anal. Chem., 212 (1965) 278.
26 J. B. Cotton and I. R. Scholes, Brit. Corros. J., 2 (1967) 1.
27 J. A. Curtis, Ind. Eng. Chem., Anal. Ed., 13 (1941) 349.
28 F. Pergola, M. R. Moncelli and R. Guidelli, J. Electroanal. Chem., 107 (1980) 295, 307.
29 K. S. Parubotchaya, V. V. Pnev and M. S. Zakharov, Zh. Anal. Khim., 33 (1978) 1800.
30 I. M. Kolthoff and W. Stricks, J. Am. Chem. Soc., 73 (1951) 1728.
31 R. Bilewicz and Z. Kublik, Anal. Chim. Acta, 152 (1983) 203.

Analytica Chimica Acta, 185 (1986) 219—228
Elsevier Science Publishers B.V., Amsterdam — Printed in The Netherlands

A CRITICAL STUDY ON THE DETERMINATION OF SELENIUM IN GALLIUM ARSENIDE BY POLAROGRAPHIC TECHNIQUES

P. LANZA* and S. ZAPPOLI

Istituto di Tecnologie Chimiche Speciali, University of Bologna, Viale Risorgimento 4, 40136 Bologna (Italy)

(Received 14th October 1985)

SUMMARY

A simple voltammetric method is described for the determination of traces of selenium in gallium arsenide. Differential-pulse cathodic stripping voltammetry permits a direct determination of selenium without preliminary enrichment or separation processes. Selenium can be determined down to levels of 1—2 $\mu g\ g^{-1}$, with relative standard deviations of about 10%, in $\leqslant$100-mg samples of gallium arsenide. Results for gallium arsenide doped with 7—75 $\mu g\ g^{-1}$ selenium agree in most cases with those obtained by spectrophotometry based on 4-chloro-*o*-phenylenediamine.

Extensive studies in recent years have provided sufficient evidence that selenium has important effects on human, animal and vegetal metabolism. The concentration range between selenium as an essential nutrient and a toxic substance is, however, rather narrow. Uncontrolled introduction of selenium into the environment may therefore represent a noteworthy pollution source or even a health hazard. The constantly increasing demand for selenium by various branches of industry (e.g., for the production of particular alloys, semiconductors, thermo- and photo-elements, electronic devices, catalysts, and additives in many industrial products) shows the need for sensitive and reliable procedures for determining selenium in various and often very complex matrices. An excellent survey on the relevance of selenium in the environment with an extensive review of its determination has been published recently by Raptis et al. [1].

Although the number of papers dealing with the determination of selenium in very varied matrices has increased rapidly in recent years, applications of voltammetric methods to this problem are rather few. Yet, voltammetry is suitable for determining traces of selenium by various methods including a.c. polarography [2], anodic stripping voltammetry (a.s.v.) with solid electrodes such as a tubular gold electrode [3] or a rotating gold disk electrode [4], and cathodic stripping voltammetry (c.s.v.). Differential-pulse cathodic stripping voltammetry (d.p.c.s.v.) appears to be the most sensitive and has been extensively applied [3—9]. Few papers, however, have been concerned with the determination of selenium in gallium arsenide by these electrochemical techniques.

0003-2670/86/$03.50

An early contribution to the application of polarography to this problem was a paper by Bush and Cornish [10], who succeeded in determining selenium down to concentrations of about 0.005 $\mu g\ g^{-1}$ by linear-sweep polarography, using 2-g samples of gallium arsenide. These authors also first pointed out the catalytic effect of As(V) on the polarographic reduction of Se(IV). More recently, Kaplin and Portnyagina [11] used stripping voltammetry at a graphite electrode for analyzing films of Se-doped gallium arsenide; the heights of the cathodic peaks were found to be linearly related to the Se(IV) concentration in the range 0.05—2 μM.

Stripping voltammetry at the hanging mercury drop electrode (HMDE) does not seem to have been applied to this determination in spite of the encouraging results obtained with this technique by many authors in the determination of selenium in plant materials [12], soils [5], biological materials, rocks and soils [13], potable water [14], etc. The main purpose of the present research is to investigate the practical possibilities and advantages of differential-pulse voltammetry (d.p.v.) and differential-pulse cathodic stripping voltammetry at the HMDE in the determination of selenium in selenium-doped gallium arsenide for electronic purposes.

The polarography of selenium was first studied many years ago by Schwaer and Suchy [15], later by Lingane and Niedrach [16] and, more recently, by Christian et al. [17]. The polarographic reduction of selenium(IV) proceeds by a rather complex mechanism. Several waves can appear; their shape and potential depend on many parameters such as pH, solution composition and selenium concentration [16]. In dilute hydrochloric acid two main waves develop. The usually accepted mechanism can be summarized by the following electrode reactions. For the first wave at 0—0.05 V (SCE),

$$SeO_3^{2-} + 6e^- + 8H^+ \rightarrow H_2Se + 3H_2O$$

$$H_2Se + Hg \rightarrow HgSe + 2H^+ + 2e^-$$

with the net reaction

$$SeO_3^{2-} + 4e^- + 6H^+ + Hg \rightarrow HgSe + 3H_2O \qquad (1)$$

and for the second wave at —0.54 V (SCE),

$$HgSe + 2H^+ + 2e^- \rightarrow H_2Se + Hg \qquad (2)$$

During the first process, a deposit of the sparingly soluble HgSe accumulates on the electrode surface. This intermediate product can be removed by cathodic stripping. The peak heights observed in this way are proportional to the Se(IV) concentration and can be used for quantitative purposes. The polarographic behaviour of selenium appears, even now, to be somewhat complex and often the observations and some conclusions of different authors disagree. Several papers have appeared dealing with fundamental studies and applications of the cathodic stripping of selenium [6, 7, 14, 18]. Even though some features of the electrochemical process are not yet fully

explained, the general pattern of the electrode mechanism seems to have been accepted.

In order to establish a practical procedure allowing a sufficiently straightforward determination, and possibly avoiding separation and enrichment processes, a careful preliminary investigation into the interference sources from the matrix and, more generally, into the characteristics of the polarographic signal as a function of the main experimental conditions, was undertaken.

EXPERIMENTAL

Apparatus and reagents

A multipurpose polarograph (Model 471; AMEL, Milan, Italy) was used. For d.p.c.s.v., a Metrohm Model E410 HMDE or a slowly dropping (40—60 s) conventional capillary was used. A suitable design of polarographic cell made it possible to run the d.p.p. or d.p.c.s.v. measurements without mercury accumulating at the bottom of the cell and so without any reaction with the Se(IV) present in the tested solution.

For sample processing, PTFE test tubes (30 × 130 mm) were used; these tubes were fitted with T29/32 adapters with inlet and outlet tubes for air circulation over the processed solution. Air filtered through a Millipore membrane (GSWP, 0.22-μm pore size) helped to accelerate the drying process.

Measurements were made at room temperature (23 ± 0.5° C). Twice-distilled water was used for all solution preparations.

A selenium stock solution was prepared by dissolving 0.1405 g of selenium dioxide (99%; C. Erba) in water and diluting to 100 ml (1.00 mg Se ml^{-1}). The solution was stored in a Pyrex bottle and remained stable for at least six months. For calibrations, working solutions with selenium contents of 1—10 $\mu g\ ml^{-1}$ were prepared daily.

The stock solution of copper was a standard solution for atomic absorption (C. Erba). The stock solution (0.5% w/v) of 4-chloro-1,2-phenylenediamine (4-Cl-PDA; Aldrich Chemical Co.) was prepared in aqueous ethanol (1 + 1). Citrate buffer was 0.07 M sodium citrate/0.33 M sodium hydroxide.

All glassware and PTFE containers were washed with warm nitric acid/hydrochloric acid (1 + 3) and then rinsed with hot distilled water for at least two days. The PTFE ware was stored in twice-distilled water.

Preliminary study

Choice of supporting electrolyte. Selenium was studied in various supporting electrolytes. Polarographic reduction of Se(IV) occurs in a wide pH range [16, 17] and consequently various solutions have been used as the supporting electrolyte [18, 19]. Hydrochloric acid in a fairly extended concentration range appears to be the most used electrolyte. It permits good sensitivity and provides a valuable resolution of the selenium peaks. However, any procedure which will allow samples of gallium arsenide to be analyzed with the minimum

of chemical treatments and without matrix elimination, will obviously limit the choice of supporting electrolyte.

Procedures for dissolving gallium arsenide usually involve the use of oxidizing acidic mixtures such as hydrochloric acid/nitric acid. In such a mixture, gallium arsenide forms gallium arsenate [20] almost quantitatively:

$$3GaAs + 8HNO_3 \rightarrow 3GaAsO_4 + 8NO + 4H_2O$$

This gallium compound is soluble only in very acidic or very basic solutions, with minimum solubility at about pH 3 [21]. Hydrochloric acid easily dissolves gallium arsenate and appears to be a suitable reagent for dissolving the residue and for the subsequent polarographic determination.

The effect of the hydrochloric acid concentration on the polarographic behaviour of Se(IV) was examined. Calibration curves were prepared by adding suitable quantities of selenous acid to the hydrochloric acid solutions. The results and the experimental conditions are shown in Fig. 1. One can observe that the higher acid concentrations lessen the sensitivity but extend the linear range towards higher concentrations of selenium. Most of the preliminary experiments were done with 4 M hydrochloric acid.

There are considerable discrepancies in the available literature as regards the range of proportionality of the peak current with the selenium concentration. The distortions or splitting of the peaks probably cause the loss of linearity of the calibration graphs. It is not easy to elucidate the mechanism which generates this serious difficulty. Many factors such as the concentrations

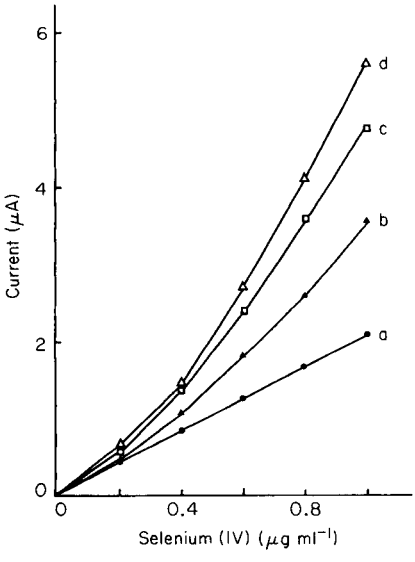

Fig. 1. Influence of hydrochloric acid concentration on the peak current of Se(IV) by d.p.p.: (a) 4 M; (b) 2 M; (c) 1 M; (d) 0.1 M. Pulse amplitude —50 mV, scan rate 2 mV s^{-1}, drop time 2 s.

of selenium and of supporting electrolyte, deposition potential, electrolysis time, interfering substances, are undoubtedly responsible for this effect, which is not readily reproducible [18].

Interferences from the matrix. Arsenic, which constitutes 51.8% of gallium arsenide, is potentially an important interferent and, in some conditions, can disturb or even completely mask the Se(IV) peak. It is well known that only As(III) displays a polarographic activity; indeed, arsenic(V) can be reduced at the DME only in an exceedingly acidic medium. In the dissolution of gallium arsenide, arsenic is oxidized to As(V), but some As(III) can form owing to the reaction with concentrated hydrochloric acid:

$$H_3AsO_4 + 5HCl \rightarrow AsCl_3 + Cl_2 + 4H_2O$$

The d.c. and d.p.p. polarograms of As(III) and Se(IV) in hydrochloric solutions are very similar (Fig. 2) and this can explain the interferences. Because of the slowness of the reduction of As(V) to As(III), the formation of As(III) can be greatly reduced by avoiding prolonged heating with an excess of too concentrated hydrochloric acid. Arsenic(V) at a concentration of 10^{-3} M, added as KH_2AsO_4 to 4 M hydrochloric acid, does not initially affect the background current of the differential pulse polarogram. After about 2 h, however, this solution shows noticeable changes because of formation of As(III), which can develop peaks at −0.24 V and −0.60 V.

Gallium arsenate dissolved in 4 M hydrochloric acid does not greatly influence the residual d.p.p. baseline in the narrow potential range within

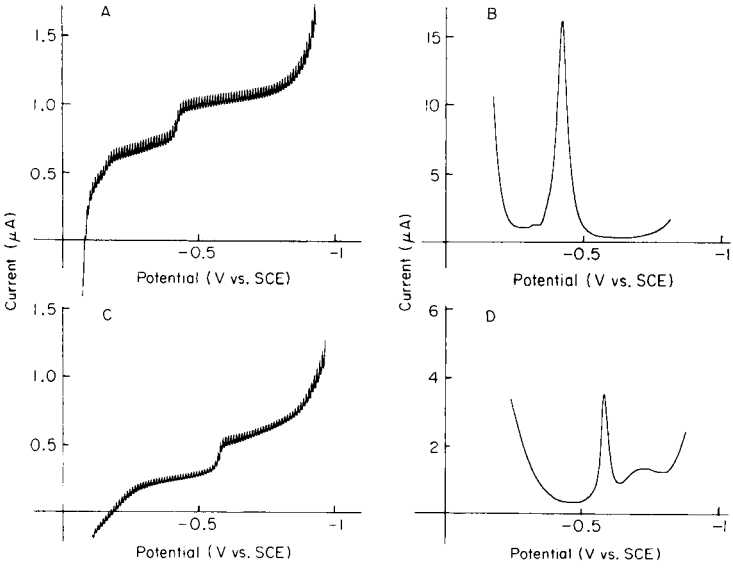

Fig. 2. Direct current and differential pulse polarograms for 6×10^{-5} M Se(IV) and 5×10^{-5} M As(III) in 4 M HCl. (A, B) Selenium; (C, D) arsenic. Technique: (A, C) d.c. polarography; (B, D) d.p.p. Instrumental parameters for d.p.p. as in Fig. 1.

which the Se(IV) peak develops but the shape of the background voltammogram becomes a narrower parabola, leaving less space for the development of the selenium peak. The gallium arsenate concentration has a serious effect on the peak height for selenium, however. Figure 3 shows this effect. The presence of gallium arsenate also causes a positive shift of the baseline. All these effects obviously restrict the effectiveness and accuracy of the correction of the background current in practical analytical work.

In d.p.c.s.v., some different interference effects were observed. The presence of gallium arsenate does not substantially change the baseline obtained with pure dilute hydrochloric acid solution except for an increase in the slope. This causes some difficulties in exact measurement of the peaks for small selenium concentrations. When the gallium arsenate concentration is increased, the stripping peak decreases (Fig. 4), showing just the opposite behaviour from that obtained with d.p.p.

Differential-pulse cathodic stripping voltammetry. This technique was used to re-examine some important experimental parameters and, especially, to investigate the nature of possible interferences, in order to achieve a practical procedure for determining traces of selenium in gallium arsenide.

Experiments were conducted with the HMDE and with slowly dropping capillaries. Hydrochloric acid was chosen as the electrolyte. Its concentration

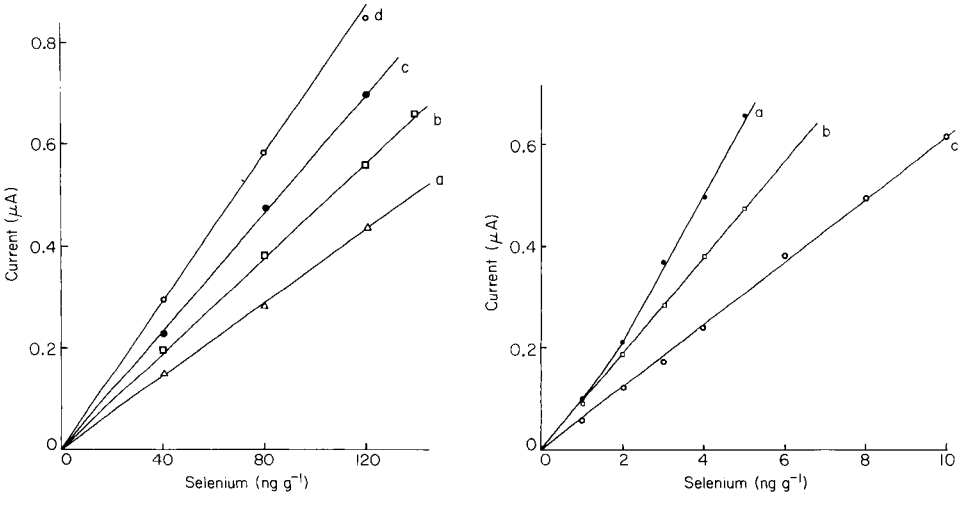

Fig. 3. Influence of the concentration of gallium arsenate on the slopes of the calibration plots for Se(IV) in 4 M HCl. Gallium arsenate concentration (mM): (a) 15.4; (b) 28.8; (c) 43.4; (d) 55.5. Instrumental parameters for d.p.p. as in Fig. 1.

Fig. 4. Influence of the concentration of gallium arsenate on the heights of the cathodic stripping peaks of Se(IV) in 0.15 M HCl with 5 μg ml^{-1} Cu(II). Gallium arsenate concentration (mM): (a) 7.7; (b) 13.6; (c) 22.6. Instrumental parameters: deposition time 40 s, scan rate 10 mV s^{-1}, pulse amplitude 25 mV.

does not appear to be a very critical parameter, but the optimum concentration was found to be in the range 0.1—1 M.

The deposition time is an important factor in stripping analysis because the detection limit can be enhanced by protracting the electrolysis. In cathodic stripping of selenium, however, the peak current is proportional to the deposition time only over a limited range, depending on the selenium concentration. This fact, first pointed out by Adeloju et al. [22], was confirmed under the present experimental conditions. For selenium concentrations within the range 0—20 $\mu g\, l^{-1}$, deposition times of 40—60 s were adequate for obtaining linear calibration graphs.

The height, potential and shape of the stripping peak of selenium can be strongly influenced by the presence of copper, and other metals such as bismuth, silver and gold [7, 23]. Some authors, considering the effects of these metals as interferences, have proposed suitable treatments for their elimination [5, 6, 22]. Others, however, have pointed out that a small copper(II) concentration aids in the development of the selenium peak [7, 13] and have prescribed additions of 1—5 $\mu g\ ml^{-1}$ copper(II) to the sample solution [9, 19, 22, 24]. It was found here that addition of copper(II) is in fact advisable; therefore, 5 $\mu g\ ml^{-1}$ copper(II) was always added to the final solution before proceeding with the deposition of selenium(IV).

It is well known that the peak potential in acidic solutions is somewhat dependent on the selenium concentration. This causes splitting of the peak and failure of the proportionality with the concentration. This happens even in the presence of copper. A rather high scan rate (e.g., 10—20 $mV\, s^{-1}$) reduces the splitting of the peaks. This can probably be attributed to the somewhat high time constants in the sampling circuitry of the AMEL Model 472 apparatus used in this work. Anyhow, at higher scan rates, the linear range and the sensitivity improved considerably.

Prolonged contact of mercury with the solution during the procedure caused a gradual lowering of the peak as a result of the reduction of Se(IV), probably according to the reaction

$$H_2SeO_3 + 4Hg + 4HCl \rightarrow Se + 2Hg_2Cl_2 + 3H_2O$$

The action of mercury on Se(IV) can be proved easily by stirring a little mercury with the solution. In order to minimize this effect, a suitable polarographic cell was designed, with a draining tube, to remove the dropped mercury from the cell.

Procedures

Sample treatment. To PTFE vessels containing 10—100 mg of finely ground gallium arsenide, add 2 ml of hydrochloric acid (37.5%) and 0.5 ml of nitric acid (65%). Evaporate the mixture to dryness in a hot aluminium block, under a flow of filtered air. Dissolve the white residue at room temperature, in the same vessel, with 2 ml of 2 M hydrochloric acid.

Determination of selenium by d.p.c.s.v. Add 25 ml of twice-distilled water containing 5 μg ml^{-1} Cu(II) (as copper chloride) to the sample solution, in the same PTFE vessel (the base electrolyte is thus about 0.15 M in hydrochloric acid). Transfer an aliquot (20 ml) of the solution to the polarographic cell and deaerate with nitrogen for 10 min. Electrolyse for 40 s at —0.380 V (vs. SCE) while stirring, at a slowly dropping mercury electrode (the drop time at open circuit in the same solution was 62 s). Record the cathodic stripping voltammogram from —0.380 to —0.700 V at a scan rate of 20 mV s^{-1} and a pulse amplitude of —50 mV.

Add to the cell three successive 0.1-ml aliquots of 1.00 μg ml^{-1} Se(IV) standard solution. After every addition, the voltammogram is automatically recorded four times, by the repeat mode provided in the Model 472 polarograph. The mean of the four measured peak heights is used to calculate the selenium content by the standard addition method.

Spectrophotometric determination of selenium in gallium arsenide. In order to check the accuracy of the stripping method an independent spectrophotometric procedure was used. Selenium reacts with the adjacent amine groups of *o*-phenylenediamine and its 4-methyl, 4-chloro and 4-nitro derivatives in acidic medium to form benzo-2,1,3-selenodiazoles [25]. The method was modified for analyzing gallium arsenide, in order to avoid precipitation of gallium arsenate.

Dissolve 50—100 mg of finely ground gallium arsenide with the mixed acids, as described above, and evaporate to dryness. Add to the residue 2 ml of 1 M hydrochloric acid and, when dissolution is complete, add 25 ml of twice-distilled water followed by 2 ml of 0.5% (w/v) 4-chloro-*o*-phenylenediamine solution in aqueous ethanol (1 + 1). Let stand for 50—60 min. Adjust the pH to 6—7 by adding 8 ml of citrate/sodium hydroxide buffer. Add exactly 3 ml of toluene, extract the complex and measure the absorbance at 341 nm against toluene. Prepare calibration graphs by adding suitable quantities of selenium to solutions obtained from selenium-free gallium arsenide, taken through the same procedure.

RESULTS AND DISCUSSION

The described procedures were used for determining selenium in samples of selenium-doped gallium arsenide supplied by the Istituto Materiali Speciali (MASPEC, C.N.R., Parma, Italy). Table 1 shows good agreement with the results obtained independently by spectrophotometry for samples 14/4, 14/5 and 14/6. It was not possible to obtain reliable results for spectrophotometry for samples 14/2 and 14/3 because of lack of sensitivity; the adopted procedure avoided any enrichment process. Analysis based on the Hall effect gave apparently lower contents for most of the samples. This can be attributed to the fact that only a fraction of the selenium present as dopant can contribute to the electrical conductivity [26].

TABLE 1

Analysis of real samples of gallium arsenide by different methods[a]

Sample no.	D.p.c.s.v.			Spectrophotometry			Hall effect[b] Se found ($\mu g\ g^{-1}$)
	Se found ($\mu g\ g^{-1}$) S.d.	n	R.s.d. (%)	Se found ($\mu g\ g^{-1}$) S.d.	n	R.s.d. (%)	
14/3	7.4 ± 0.7	6	10.0	—	—	—	0.97
14/2	7.9 ± 0.5	8	6.5	—	—	—	6.1
14/5	25 ± 1	8	4.0	28 ± 2	7	6.0	6.1
14/4	9.9 ± 0.4	5	4.0	9 ± 1	4	10.0	9.7
14/6	74 ± 6	10	8.0	69 ± 6	12	8	9—12

[a]Mean results with standard and relative standard deviations and number of determinations. [b]Results supplied by MASPEC C.N.R., Parma.

Selenium can be determined by d.p.c.s.v. in samples of gallium arsenide not greater than 100 mg, at levels as low as 1—2 $\mu g\ g^{-1}$ with a relative standard deviation of about 10%. (We had no real samples with lower Se content.) Lower concentrations would require an enrichment process, which, of course, would make the method less useful for practical routine monitoring.

The sensitivity and the determination limits are essentially established by the rather high baseline current at the high matrix concentration, and particularly by the difficulty of obtaining precise measurements for small peaks on a baseline which is not very reproducible. This fundamental problem in stripping voltammetry has been discussed by many authors [27] but no effective solutions have so far been discovered. The d.p.p. technique does not offer advantages over d.p.c.s.v., owing to lack of sensitivity, if enrichment processes are to be avoided.

This work was supported by the Consiglio Nazionale delle Ricerche, under a contract related to the Progetto Finalizzato per la Chimica Fine e Secondaria.

REFERENCES

1 S. E. Raptis, G. Kaiser and G. Tölg, Fresenius Z. Anal. Chem., 316 (1983) 105.
2 A. M. Shafiqul Alam, O. Vittori and M. Porthault, Anal. Chim. Acta, 87 (1983) 437.
3 R. W. Andrews and D. C. Johnson, Anal. Chem., 48 (1976) 1056.
4 R. W. Andrews and D. C. Johnson, Anal. Chem., 47 (1976) 294.
5 S. Forbes, G. P. Bounds and T. S. West, Talanta, 26 (1979) 473.
6 B. L. Dennis, J. L. Moyers and G. S. Wilson, Anal. Chem., 48 (1976) 1611.
7 G. Henze, P. Monks and G. Tölg, Fresenius Z. Anal. Chem., 295 (1979) 1.
8 G. Henze, Mikrochim. Acta, II (3-4) (1981) 343.
9 K. B. Ebhardt and F. Umland, Fresenius Z. Anal. Chem., 310 (1982) 406.
10 E. L. Bush and E. H. Cornish, in M. S. Brook and J. K. Kennedy (Eds.), Ultrapurification of Semiconductor Materials, Macmillan, London, 1961, p. 454.
11 A. A. Kaplin and E. O. Portnyagina, Zh. Anal. Khim., 36 (1981) 1965.

12 J. Paul and R. C. Daniel. Mitt. Geb. Lebensmittelunters. Hyg., 72 (1981) 78.
13 Heng-Bin Han, G. Kaiser and G. Tölg, Anal. Chim. Acta, 128 (1981) 9.
14 C. Arlt and R. Naumann, Fresenius Z. Anal. Chem., 282 (1976) 463.
15 L. Schwaer and K. Suchy, Collect. Czech. Chem. Commun., 7 (1935) 25.
16 J. J. Lingane and L. W. Niedrach, J. Am. Chem. Soc., 71 (1949) 196.
17 G. D. Christian, E. C. Knobloch and W. C. Purdy, Anal. Chem., 35 (1963) 1128.
18 G. Jarzabek and Z. Kublik, Anal. Chim. Acta, 143 (1982) 121.
19 P. Deldime and J. P. Hartman, Anal. Lett., 13(B2) (1980) 105.
20 P. Lanza and M. Taddia, Anal. Chim, Acta, 157 (1984) 37.
21 P. Pascal, in Masson (Ed.), Nouveau Traité de Chimie Mineral, Tome V, Paris, 1961, p. 768.
22 S. B. Adeloju, A. M. Bond, M. H. Briggs and H. C. Hughes, Anal. Chem., 55 (1983) 2076.
23 S. B. Adeloju and A. M. Bond, Anal. Chem., 57 (1985) 1728.
24 S. B. Adeloju, A. M. Bond and H. C. Hughes, Anal. Chim. Acta, 148 (1983) 59.
25 F. D. Snell, Photometric and Fluorimetric Methods of Analysis, Vol. 3 (Non-metals), Wiley, New York, 1981, p. 514.
26 H. Kressel and H. Nelson, in G. Hass (Ed.), Physics of Thin Films, Vol. 7, Academic Press, New York, 1973, p. 147.
27 See, e.g., J. Wang and B. Greene, Anal. Chim. Acta, 144 (1982) 137 (and references therein).

Analytica Chimica Acta, 185 (1986) 229—238
Elsevier Science Publishers B.V., Amsterdam — Printed in The Netherlands

DETERMINATION OF TRACES OF GALLIUM BASED ON STRIPPING VOLTAMMETRY WITH ADSORPTIVE ACCUMULATION

J. WANG* and J. M. ZADEII
Department of Chemistry, New Mexico State University, Las Cruces, NM 88003 (U.S.A.)
(Received 23rd December 1985)

SUMMARY

Trace levels of gallium can be quantified by linear-sweep voltammetry after absorptive preconcentration of the gallium/solochrome violet RS chelate on the hanging mercury-drop electrode. The interfacial and redox behaviors are evaluated by cyclic voltammetry. The adsorbed chelate yields two distinct reduction peaks that can be utilized to quantify gallium. The effects of preconcentration time and potential, dye concentration, bulk concentration of gallium, and other variables on the chelate peaks are investigated. For a 2-min preconcentration time, the detection limit is 0.08 $\mu g\ l^{-1}$. With preconcentration for 60 s, calibration plots are linear for the range 0—16 $\mu g\ ml^{-1}$ gallium. Possible interferences by other trace metals and surface-active organic materials are investigated. Gallium added to samples of sea and rain water was quantified readily.

Few analytical techniques possess the sensitivity required for trace and ultratrace quantitation of gallium [1, 2]. The utility of neutron activation methods, which permit measurements down to the sub-$\mu g\ l^{-1}$ level, is restricted by instrumentation cost, long exposure times or matrix interference [1, 2]. With spectrometric techniques, such as atomic or molecular absorption or fluorescence, detection limits are substantially higher [2].

The conventional electroanalytical technique for trace quantitation of gallium is anodic stripping voltammetry (a.s.v.) [3]. The solubility of gallium in mercury and its reversible reduction process make a.s.v. a potentially attractive approach for trace quantitation of this metal. However, while the technique offers the desired sensitivity it suffers from various difficulties as far as gallium is concerned. First, because of the negative peak potential of gallium, its stripping response is masked by the hydrogen evolution current when acidic solutions are used. Secondly, the accuracy of the measurement is adversely affected by the formation of intermetallic compounds between gallium and copper, zinc, or nickel. Indeed, the addition of gallium, as a third element, is commonly used to alleviate Cu-Zn or Ni-Zn intermetallic problems [4]. Thirdly, the similarity of the gallium and zinc peak potentials results in a resolution problem between these two adjacent stripping peaks.

The aim of this research was to develop an alternative stripping approach for ultratrace quantitation of gallium. It has been shown recently that trace

0003-2670/86/$03.50

and ultratrace quantities of various metals can be determined by means of adsorptive stripping voltammetry [5]. This approach is based on the formation of a suitable surface-active metal chelate, its adsorptive preconcentration onto the surface of the working electrode, and the voltammetric measurement of the surface-bound species. Thus, low concentrations of nickel [6], cobalt [7], vanadium [8], aluminum [9], lanthanides [10, 11], iron [12], copper [13], zinc [14], manganese [15], and molybdenum [16], can be determined following complexation with dimethylglyoxime [6, 7], catechol [8, 12—14], 8-quinolinol [16], cresolphthalexon [10], or various dihydroxyazo dyes [9, 11, 15]. Clearly, the interfacial accumulation can extend the scope of applications of stripping voltammetry toward many metals that cannot be determined by conventional stripping measurements. Improvements in the response for metals, e.g., copper or zinc, traditionally determined by conventional stripping voltammetry, have also been reported [13, 14]. In the present work, the interfacial accumulation of chelates of gallium with different dihydroxyazo dyes is exploited for the trace determination of gallium. Several dihydroxyazo dyes form discrete polarographic reduction waves in the presence of gallium [17, 18]. The distinct reduction waves of these chelates at the dropping mercury electrode, coupled with their surface-active properties, allowed polarographic quantitation of gallium down to $\mu g\ ml^{-1}$ levels. It is shown that the use of the hanging mercury drop electrode permits full exploitation of the signal enhancement associated with the adsorption of these chelates. The adsorptive approach offers certain advantages over conventional a.s.v. measurements of gallium. The results of a detailed investigation on the adsorptive stripping of gallium in the presence of dihydroxyazo dyes are reported below.

EXPERIMENTAL

Apparatus and reagents

The equipment used to obtain the voltammograms, a PAR 264A voltammetric analyzer with a PAR 303 static mercury drop electrode, was described in detail previously [9, 10]. All solutions were prepared from double-distilled water. The gallium stock solution (1000 mg l^{-1}) was obtained from Aldrich. Solochrome violet RS (SVRS) and other dyes were purchased from Aldrich; a stock solution of the dye, 1×10^{-4} M, was prepared daily. Supporting electrolyte was acetate buffer (pH 4.8). Sea water was unfiltered surface water collected at San Diego, CA, and stored frozen. Rain samples were filtered by passing through a glass filter (10—15-μm porosity).

Procedure

Supporting electrolyte solution (10 ml), containing 2×10^{-6} M of SVRS, was pipetted into the cell, and deoxygenated with nitrogen for 8 min. The preconcentration potential (usually —0.40 V) was applied to a fresh mercury drop while the solution was stirred (400 rpm). After the preconcentration

period, the stirring was stopped and after 15 s the voltammogram was recorded by applying a negative linear potential scan. The scan was terminated at −1.30 V. After background stripping voltammograms had been obtained, aliquots of the gallium standards were introduced. Throughout this operation, nitrogen was passed over the solution surface. Conventional a.s.v. was preceded (in the absence of chelating dye) by deposition at a potential negative of the reduction potential followed by a positive-going scan. All data were obtained at room temperature.

RESULTS AND DISCUSSION

Adsorption and redox behaviors

Figure 1 shows repetitive cyclic voltammograms for 25 $\mu g\ l^{-1}$ gallium in an acetate buffer (pH 4.8) solution containing 2×10^{-6} M SVRS. Stirring the solution for 60 s prior to the scan (A, scan 1) results in three cathodic peaks associated with the reduction of the adsorbed chelate (at −0.51 V and −1.05 V) and of the adsorbed dye (at −0.41 V). Small, and irreproducible, peaks are observed in the anodic branch. Subsequent repetitive scans yield significantly smaller cathodic peaks, indicating rapid desorption of the chelate and free dye from the surface. While most metal chelates of dihydroxyazo dyes yield a single reduction step [17], two defined cathodic peaks were observed for the gallium/SVRS chelate. This unusual behavior is in agreement with that reported in polarographic studies [17, 18]. When the same experiment was repeated after preconcentration at −0.40 V (B, scan 1), only two cathodic peaks, caused by the reduction of the adsorbed chelate, were observed at −0.51 V and −1.05 V. These peaks are substantially larger than those observed after preconcentration at −0.20 V. This indicates that competition by the free dye on the surface sites is minimized at −0.40 V (as dis-

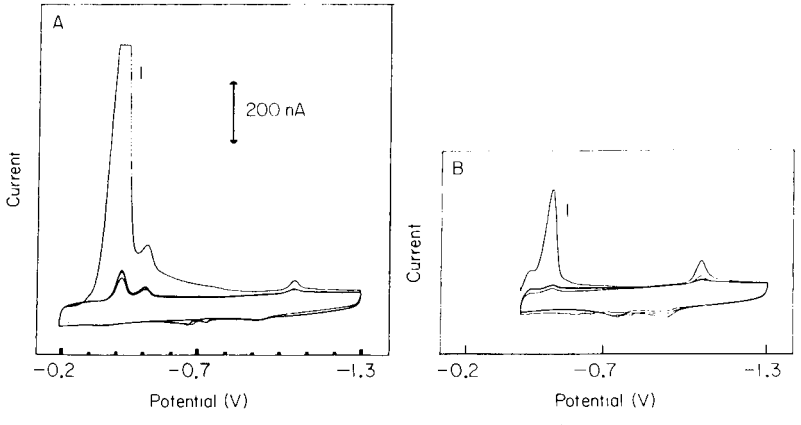

Fig. 1. Repetitive cyclic voltammograms for 25 $\mu g\ l^{-1}$ gallium in an acetate buffer (pH 4.8) solution, containing 2×10^{-6} M SVRS, after stirring for 60 s at −0.20 V(A) and −0.40 V(B). Scan rate 50 mV s^{-1}. See text for detail.

cussed below). Maximum adsorption density of the gallium/SVRS chelate was observed after stirring for 180 s (other conditions, as in Fig. 1B). Division of the number of coulombs transferred under these conditions, 0.41 μC, by the conversion factor (nFA) yields a surface coverage of 7.1×10^{-11} mol cm^{-2} (n = 4). The effect of potential scan rate (v) on the peak current and potential was evaluated after the electrode had been coated with the maximum amount of the Ga/SVRS chelate. The magnitude of the first (more positive) chelate peak increased linearly with the scan rate over the 10—200 mV s^{-1} range tested. A log i_p vs. log v plot yielded a slope of 1.05 and correlation coefficient of 0.994. A slope of 1.0 is expected for an ideal redox couple immobilized on an electrode surface. A negative shift in peak potential, from —0.46 to —0.54 V, was observed when the scan rate was increased from 10 to 200 mV s^{-1}. The resulting plot of E_p vs. log v was linear, with a correlation coefficient of 0.999.

Several other dihydroxyazo dyes were tested and yielded distinct reduction peaks in the presence of trace levels of gallium. These include eriochrome blue black B (mordant black 3) and mordant blue 9 (in acetate buffer, pH 4.8) and eriochrome black T (in both acetate and ammonia/ammonium chloride pH 9.4 buffers). No response for gallium was observed in the presence of mordant brown 6, acid blue 161, or mordant black 17. Best results, with respect to the shape and size of the chelate reduction peaks, were obtained by using SVRS in an acetate buffer (pH 4.8) solution. Such conditions were used throughout this study.

The adsorption of the Ga/SVRS chelate can be used as an effective preconcentration step, prior to the voltammetric measurement. Figure 2 shows linear scan voltammograms for 4 μg l^{-1} (5.7×10^{-8} M) gallium, in the presence of SVRS, after different preconcentration times. Both chelate peaks rapidly increase with increasing preconcentration time, indicating enhanced adsorption of the chelate. For example, a 60-s preconcentration period yielded a 6.5-fold enhancement of the first peak, compared to the response without preconcentration (Fig. 2, inset). As expected for an adsorptive preconcentration step, curvature in the response was observed (at times longer than 90 s). Convenient quantitation of gallium at μg l^{-1} concentrations is feasible with short preconcentration times. Both chelate peaks can be used to obtain the required analytical information; each can offer advantages in certain situations. While the second peak is smaller than the more positive one, it is less prone to interferences (see below).

Other experimental conditions affecting the gallium/SVRS reduction currents include the SVRS concentration and preconcentration potential (Fig. 3). The magnitude of the second (negative) chelate peak increased rapidly with the SVRS concentration, up to about 1.2×10^{-6} M, and then started to level off (Fig. 3, curve a). The first chelate peak exhibited a similar dependence (not shown). A SVRS concentration of 2×10^{-6} M was used in the stripping measurements reported here. The effect of the preconcentration potential on the height of the second chelate peak was examined over the

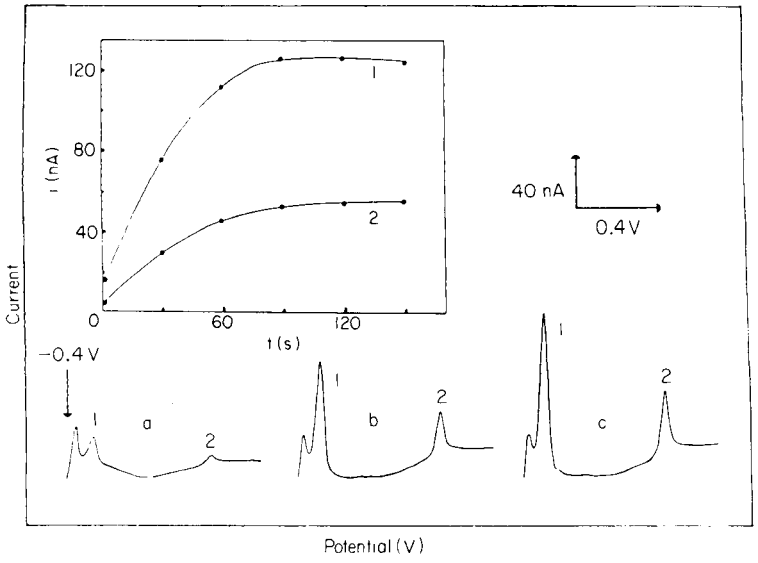

Fig. 2. Linear scan voltammograms for 4 $\mu g\ l^{-1}$ gallium after different preconcentration periods: (a) 0; (b) 30; (c) 60 s. Preconcentration at −0.40 V; other conditions as in Fig. 1. The inset shows the increase of peaks 1 and 2 with preconcentration time.

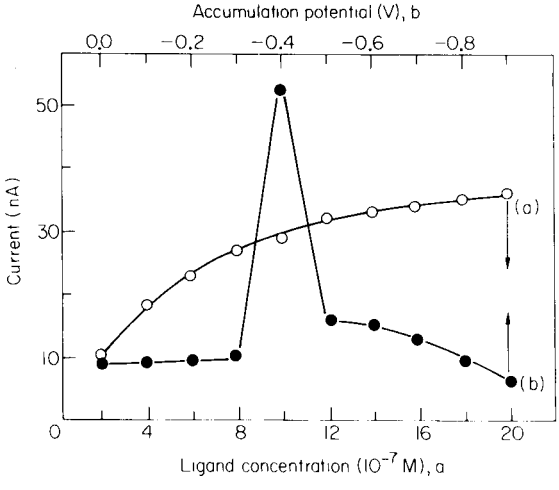

Fig. 3. Effect of SVRS concentration (a) and preconcentration potential (b) on the gallium peak current (at −1.05 V). Gallium concentration: (a) 5; (b) 6 $\mu g\ l^{-1}$. Other conditions as in Fig. 1B.

range 0.0 to −0.9 V. The peak current remained essentially the same over the 0.0 to −0.3 V region, but increased substantially with preconcentration at −0.4 V and then decreased (Fig. 3, curve b). This profile is attributed to a competition by the free dye on the surface sites, that occurs at potentials

more positive than —0.4 V (as supported by cyclic voltammetry data), and to weak adsorption of the chelate at more negative potentials (—0.5 to —0.9 V). Careful choice of the preconcentration potential is essential also to minimize an overlapping response associated with the preceding reduction peak of the free dye. A potential of —0.4 V was used for preconcentration in all subsequent work.

Quantitative utility

Figure 4 shows the response for successive standard additions of 2 μg l^{-1} gallium with 60-s preconcentration. Both chelate peaks exhibit a well-defined concentration dependence. Thus, μg l^{-1} levels can be quantified even with short preconcentration times. These three measurements were part of a series of eight successive concentration increments, the results of which are also shown in Fig. 4. The response is linear over the 0—16 μg l^{-1} range tested; slopes are 19.3 and 6.4 nA l μg^{-1} for the first and second chelate peaks, respectively (correlation coefficients, 0.999 and 0.998). These data indicate low surface coverage, i.e., conditions of a linear adsorption isotherm. Deviations from linearity are expected at longer preconcentration periods, or at higher concentrations as full surface coverage is approached. Measurements of 1 μg l^{-1} (1.43×10^{-8} M) gallium were used to evaluate the detection limit of the method; under the conditions given for Fig. 1B with a preconcentration time of 120 s, a detection limit of 0.08 μg l^{-1} (1.1×10^{-9} M) was estimated, based on a signal-to-noise ratio of 3.

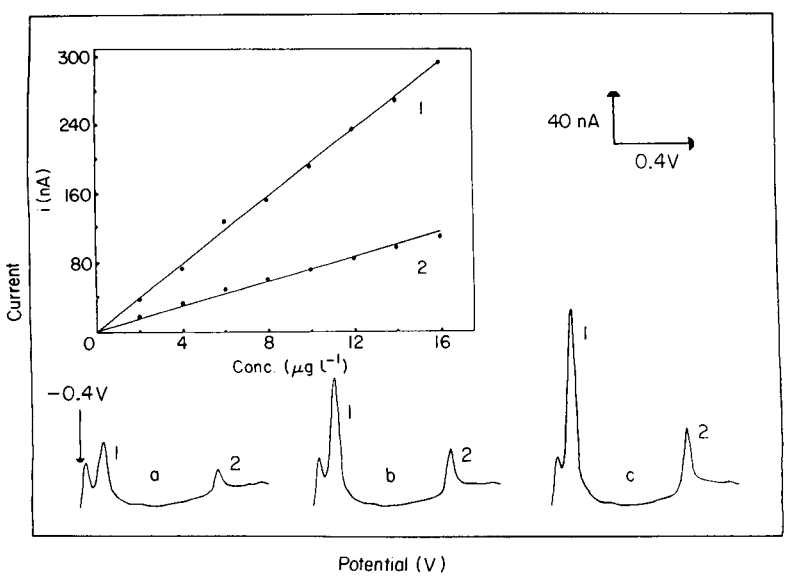

Fig. 4. Stripping voltammograms obtained for solutions of increasing gallium concentration: (a) 2; (b) 4; (c) 6 μg l^{-1}. Also shown are the resulting calibration plots for the first (1) and second (2) chelate peaks over the 2—16 μg l^{-1} range. Conditions as in Fig. 1B.

As a result of its inherent sensitivity, the adsorptive approach compares favorably with conventional a.s.v. for gallium. For example, Fig. 5 compares voltammograms for 5 $\mu g\ l^{-1}$ gallium, obtained at the hanging mercury drop electrode after adsorptive and electrolytic preconcentrations for 60 s. While both schemes permit convenient quantitation at this level, the improved sensitivity offered by the adsorptive approach is clear. Other advantages of the adsorptive approach are associated with interferences (see below). The high sensitivity is accompanied by good precision, which was estimated from a series of ten successive measurements of 5 $\mu g\ l^{-1}$ gallium (conditions as in Fig. 1B). For the first and second chelate peaks, the mean currents were 79.9 and 28.8 nA, respectively, with ranges of 77 to 82 nA and 27 to 31 nA, and relative standard deviations of 1.6 and 4.8%.

Co-existing metal ions can interfere with the determination of gallium if they form reducible and/or adsorbable chelates with SVRS. Ions tested at the 25 $\mu g\ l^{-1}$ level and found not to interfere in the determination of 5 $\mu g\ l^{-1}$ gallium were Bi(III), Al(III), Cu(II), Sn(IV), Pb(II), Mn(II), Ni(II), Ca(II), Ba(II), and Mg(II). Additions of 25 $\mu g\ l^{-1}$ iron(III) resulted in 31% and 21% depressions of the first and second peaks, respectively, from 5 $\mu g\ l^{-1}$ gallium

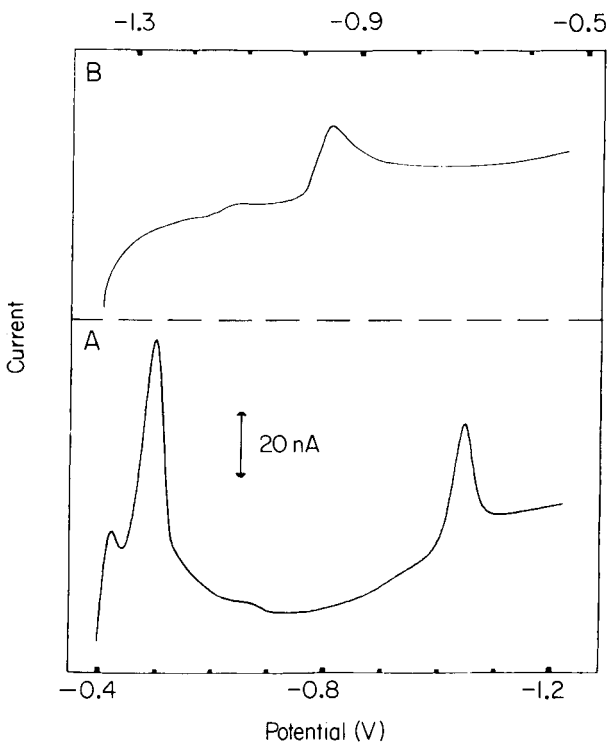

Fig. 5. Voltammograms for 5 $\mu g\ l^{-1}$ gallium: (A) by the adsorptive approach; (B) by conventional a.s.v. Conditions: (A) as in Fig. 1B; (B) as in (A) except that preconcentration at −1.35 V was followed by an anodic scan, in absence of SVRS.

and a Fe(III)/SVRS peak appeared at −0.70 V. Depressions (14% and 10% of the first and second gallium peaks, respectively) were observed in the presence of 25 $\mu g\ l^{-1}$ cadmium. Additions of 25 $\mu g\ l^{-1}$ mercury(II) resulted in 13% depression of the second gallium peak. Substantial (21% and 300%) enhancements of the first gallium peak were observed after additions of 25 $\mu g\ l^{-1}$ indium and titanium, respectively. The unaffected second gallium peak permits quantitation in the presence of these metals. The large Ti/SVRS response is currently being studied for adsorptive stripping voltammetry of titanium. Of particular significance are the effects of Cu(II), Zn(II), and Ni(II). These ions interfere with the gallium peaks in conventional a.s.v., via the formation of intermetallic compounds. In contrast, a ten-fold excess of these ions had only negligible effects on the adsorptive stripping response for 5 $\mu g\ l^{-1}$ gallium. In addition to the problem of intermetallic compounds, conventional a.s.v. measurements of gallium may be subject to resolution problems in the presence of metal ions, e.g., Zn(II), Ni(II), with similar redox potentials. For example, a 5-fold excess of zinc did not permit quantitative measurement of 5 $\mu g\ l^{-1}$ gallium (under the conditions given for Fig. 5B, except that the preconcentration potential was −1.45 V). No such zinc interference was observed in the adsorptive approach. Additions of nickel to the gallium solution resulted in the appearance of a new peak (at −0.68 V) associated with the reduction of the Ni/SVRS chelate. The size of this peak increased linearly with the nickel concentration (up to the 50 $\mu g\ l^{-1}$ level tested). As the gallium response is not affected by increasing nickel concentration, simultaneous measurements of these ions are feasible.

Surface-active organic materials could interfere by competitive adsorption on the mercury surface. Addition of gelatin (4 and 8 mg l^{-1}) to a 5 $\mu g\ l^{-1}$ gallium solution (conditions as in Fig. 1B) caused 16% and 31% depressions of the first Ga/SVRS peak, respectively. The second Ga/SVRS peak decreased rapidly as the gelatin concentration increased, and disappeared at the 5 mg l^{-1} gelatin level. Conventional a.s.v. measurements are also subject to surfactant interference [3]. Organic interferences in adsorptive stripping measurements are commonly eliminated by u.v. irradiation [8], but this is not essential when various real samples are concerned. For example, Fig. 6 illustrates voltammograms for an untreated coastal sea water spiked with gallium. The response for the original sample indicates the absence of interferences around the second Ga/SVRS peak; the absence of a gallium response is expected from the short (30 s) preconcentration time used, and the level (0.2 $\mu g\ l^{-1}$) of gallium in sea water [19]. A small peak, possibly from the reduction of the Ti/SVRS chelate, was observed at a potential similar to that of the first Ga/SVRS peak (not shown). The standard additions give well-defined peaks, similar to those found in pure solutions. The resulting calibration plot (Fig. 6) is linear with a slope of 4.7 nA l μg^{-1} and a correlation coefficient of 0.999. In a separate experiment under the same conditions, four successive standard additions of 2 $\mu g\ l^{-1}$ gallium to an untreated rain water yielded well-defined chelate peaks; again no interference was observed around the second chelate

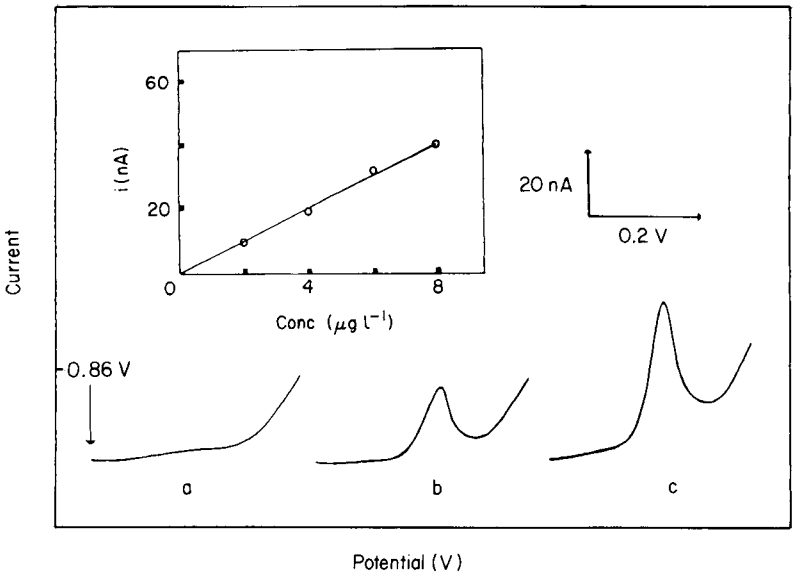

Fig. 6. Standard additions of gallium to sea water (8 ml of sea water, 2 ml of acetate buffer and 2×10^{-6} M SVRS). (a) Voltammogram for the sample after 30-s preconcentration at −0.40 V; (b) as (a) after addition of 4 μg l^{-1} gallium; (c) as (b) after addition of 4 μg l^{-1} gallium. Other conditions as in Fig. 1B. Inset is the standard addition plot for the 2—8 μg l^{-1} range.

peak, which increased linearly with concentration giving a slope of 6.4 nA l μg^{-1} and a correlation coefficient of 0.996.

In conclusion, the present study describes an effective means for the determination of trace levels of gallium. Quantitation at the μg l^{-1} level is feasible with short preconcentration times. The adsorptive approach offers a useful alternative to conventional a.s.v. While most metal chelates of dihydroxyazo dyes yield one reduction peak, two peaks are observed for the Ga/SVRS chelate (each may have advantages over the other under certain conditions). Work is continuing toward the development of new absorptive voltammetric schemes for other metals.

This work was supported in part by the National Institutes of Health under Grant No. GM 30913-02.

REFERENCES

1 J. C. Yu and C. M. Wai, Anal. Chem., 56 (1984) 1689.
2 E. D. Moorhead and P. H. Davis, Anal. Chem., 47 (1975) 622.
3 J. Wang, Stripping Analysis: Principles, Instrumentation and Applications, VCH Publishers, Deerfield Beach, FL, 1985.

4 M. I. Abdullah, B. Reusch Berg and R. Klimek, Anal. Chim. Acta, 84 (1976) 307.
5 See, e.g., J. Wang, Am. Lab., 17(5) (1985) 41.
6 B. Pihlar, P. Valenta and H. W. Nürnberg, Z. Anal. Chem., 307 (1981) 337.
7 A. Meyer and R. Neeb, Z. Anal. Chem., 315 (1983) 118.
8 C. M. G. van den Berg and Z. Q. Huang, Anal. Chem., 56 (1984) 2383.
9 J. Wang, P. A. M. Farias and J. S. Mahmoud, Anal. Chim. Acta, 172 (1985) 57.
10 J. Wang, P. A. M. Farias and J. S. Mahmoud, Anal. Chim. Acta, 171 (1985) 215.
11 J. Wang and J. M. Zadeii, Talanta, 33 (1986) 321.
12 C. M. G. van den Berg and Z. Q. Huang, J. Electroanal. Chem., 177 (1984) 269.
13 C. M. G. van den Berg, Anal. Chim. Acta, 164 (1984) 195.
14 C. M. G. van den Berg, Talanta, 31 (1984) 1069.
15 J. Wang and J. S. Mahmoud, Anal. Chim. Acta, 182 (1986) 147.
16 C. M. G. van den Berg, Anal. Chem., 57 (1985) 1532.
17 G. W. Latimer, Talanta, 15 (1968) 1.
18 B. A. Cooney and J. H. Saylor, Anal. Chim. Acta, 21 (1959) 276.
19 J. P. Riley, in J. P. Riley and G. Skirrow (Eds.), Chemical Oceanography, Vol. 3, 2nd edn., Academic Press, London, 1975, Chap. 19.

Analytica Chimica Acta, 185 (1986) 239—248
Elsevier Science Publishers B.V., Amsterdam — Printed in The Netherlands

LIQUID-LIQUID EXTRACTION BEHAVIOR OF ARSENIC(III), ARSENIC(V), METHYLARSONATE AND DIMETHYLARSINATE IN VARIOUS SYSTEMS

NOBUO SUZUKI*, KIYOKI SATOH, HIDETOSHI SHOJI and HISANORI IMURA
Department of Chemistry, Faculty of Science, Tohoku University, Sendai 980 (Japan)
(Received 26th November 1985)

SUMMARY

The liquid-liquid extraction of inorganic arsenite and arsenate and of methylarsonate and dimethylarsinate is investigated by using the corresponding arsenic species labeled with arsenic-74. The extraction systems tested are halides (chloride, bromide and iodide), diethylammonium diethyldithiocarbamate, didodecyltin dichloride, and pyrogallol/tetraphenylarsonium chloride. All the arsenic species were quantitatively extracted in the iodide system; from the log D values obtained in extraction and back-extraction, they are probably extracted as the corresponding tervalent species because of reduction with iodide. Appropriate conditions for selective extraction of As(III), As(V) and methylarsonate are described.

Arsenic occurs in nature mainly as inorganic species, including arsenite and arsenate, and as methylated species, including methylarsonate [MeAs(V)] and dimethylarsinate [$Me_2As(V)$]. To understand the behavior of these arsenic species in nature, accurate methods for their separation and determination are necessary. The separation of inorganic and methylated arsenic species has been investigated by using ion-exchange chromatography [1—5] and gas chromatography [6—12] but little has been done on liquid-liquid extraction methods.

Among such extraction systems most attention has been focused on the inorganic species, As(III) and As(V). Arsenic(III) can be extracted with halides or diethyldithiocarbamate, while As(V) can be extracted as the heteropoly molybdoarsenic acid [13]. Recently, As(V) has been extracted by using new reagents such as dialkyltin salts [14] and pyrogallol/tetraphenylarsonium chloride [15].

In the present paper, the liquid-liquid extraction of As(III), As(V), MeAs(V), and $Me_2As(V)$ is examined with various reagents including halides, diethyldithiocarbamate, didodecyltin(IV), and pyrogallol/tetraphenylarsonium chloride.

0003-2670/86/$03.50

EXPERIMENTAL

Preparation of radioactive arsenic species

For ^{74}As(III), about 100 mg of high-purity arsenic(III) trioxide (available for the semiconductor industry) was irradiated with 30—50-MeV bremsstrahlung from an electron linear accelerator at Tohoku University and dissolved in a little 1 M sodium hydroxide. The solution was adjusted to 10 M hydrochloric acid and shaken with benzene to extract As(III), then As(III) was back-extracted from benzene to 0.1 M sulfuric acid and the solution was diluted to the required concentration of As(III) with 0.1 M sulfuric acid.

For ^{74}As(V), irradiated arsenic(III) trioxide was dissolved in a little 1 M sodium hydroxide. After dilution with water, As(III) was oxidized to As(V) with a large excess of 30% hydrogen peroxide by heating for 1 h, and the solution was completely evaporated to dryness. The residue was dissolved in water and diluted to the required concentration of As(V).

For methylarsonate labeled with ^{74}As, methylarsonate was prepared by the Meyer reaction [16] from the irradiated arsenic(III) trioxide and methyl iodide, and then purified by ion-exchange chromatography [2]. To 90 mg of irradiated arsenic(III) trioxide were added 0.3 ml of 10 M sodium hydroxide and 0.15 ml of methyl iodide and the contents were stirred overnight. The sodium salt of MeAs(V) was crystallized from the reaction mixture by adding a little ethanol and dissolved in a small amount of an acidic aqueous solution. The solution was passed into a cation-exchange column (Bio-Rad AG50W-X8, 100—200 mesh, 2.5-cm inner diameter, and 45 cm height), and eluted with water at a flow rate of 1 ml min^{-1}, and fractions were collected. The MeAs(V) fraction having high radioactivity was collected and diluted to the required concentration of MeAs(V) (calculated from the radioactivity) with water.

For dimethylarsinate labeled with ^{74}As, dimethylarsinate was also prepared by the Meyer reaction from MeAs(III) and methyl iodide [16]. The starting material, MeAs(III), was prepared by reducing MeAs(V) with iodide and extracting with benzene. An aqueous solution of the radioactive MeAs(V) comprising 18 ml of 5 M sodium iodide, 18 ml of 1 M sodium hydrogensulfite, and 36 ml of 5 M sulfuric acid was shaken with 10 ml of benzene. The benzene phase was shaken with 2 ml of 5 M sodium hydroxide to back-extract MeAs(III). Immediately the aqueous phase was added to 0.2 ml of methyl iodide and stirred overnight. The reaction mixture was adjusted to pH 2—3 with hydrochloric acid and passed into a cation-exchange column similar to that used above for MeAs(V). After elution of by-products such as As(III), As(V), and MeAs(V) with water, the main product of $Me_2As(V)$ was eluted with aqueous 1.5 M ammonia. Further, to isolate $Me_2As(V)$ with high purity from the relatively large amounts of reaction products and the starting chemicals, the $Me_2As(V)$ fraction obtained was again fed into a small cation-exchange column (0.8-cm inner

diameter, 10 cm height) and eluted with water. The $Me_2As(V)$ solution so obtained was diluted to the required concentration of $Me_2As(V)$ with water.

Identification of labeled compounds

The labeled methyl compounds purified by ion-exchange chromatography were further identified by paper chromatography; the developing solvent was acetic acid/ethyl acetate/water (3:3:1). Sodium methylarsonate, used as the reference, was synthesized in the same manner as the labeled compound. The elemental composition of MeAs(V) purified by recrystallization was found to be $Na_2CH_3AsO_3 \cdot 5H_2O$ by elemental analysis and measurement of water content (found 4.6% C, 5.0% H, 33% H_2O; calculated 4.4% C, 4.78% H, 32.9% H_2O. Sodium dimethylarsinate ($Na(CH_3)_2AsO_2 \cdot 3H_2O$) used as a reference for $Me_2As(V)$ was of guaranteed reagent grade. Each species on the chromatographed paper could be detected by spraying 1 M sodium iodide and 2 M sulfuric acid followed by heating, or by the γ-activity measurement of the chromatographed paper in the case of the labeled compounds. The R_F value for each species was 0.27 ± 0.04 for As(III), 0.51 ± 0.04 for As(V), 0.79 ± 0.03 for MeAs(V), and 0.92 ± 0.03 for $Me_2As(V)$. The R_F values of the labeled MeAs(V) and $Me_2As(V)$ were consistent with those of reference compounds.

Extractants

Didodecyltin dichloride was purified as follows. To didodecyltin dichloride solution in ethanol was added 1 M sodium hydroxide with stirring. The white precipitate formed was filtered, thoroughly washed with ethanol and water, and placed in a separatory funnel containing hexane and 11 M hydrochloric acid. On shaking, didodecyltin dichloride was extracted. Then it was crystallized from the hexane solution by removing most of the solvent. Diethylammonium diethyldithiocarbamate, sodium halides, pyrogallol, and tetraphenylarsonium chloride were of guaranteed reagent grade.

Organic solvents such as benzene, carbon tetrachloride, chloroform, and methyl isobutyl ketone were purified in the usual manner. Other reagents were of guaranteed grade or super-high-purity grade.

Extraction procedures

An aqueous solution which was 5×10^{-5} M in the radioactive arsenic species was shaken with an equal volume of an organic solvent in the presence of an appropriate amount of an extractant for 2—60 min. Aqueous conditions tested were 0.1—9 M sulfuric acid, 0.1—5 M perchloric acid, and 0.1 M sodium perchlorate at pH 2—11. After centrifugation, an aliquot was pipetted from each phase and the γ-activity was measured with an NaI(Tl) scintillation counter. The distribution ratio (D) of the arsenic species was calculated from the γ-activity of the two phases. If necessary, the equilibrium pH was measured with a glass electrode just after the phase separation. In the back-extraction procedure, the organic solution containing the extracted arsenic species was shaken with a fresh aqueous solution.

RESULTS AND DISCUSSION

Halide system

The extractability of As(III), As(V), MeAs(V), and $Me_2As(V)$ into benzene from 1.0 M chloride, bromide, and iodide solution as a function of sulfuric acid concentration is shown in Fig. 1. In all the halide systems, the extraction increases with increasing acidity. This trend is similar to that

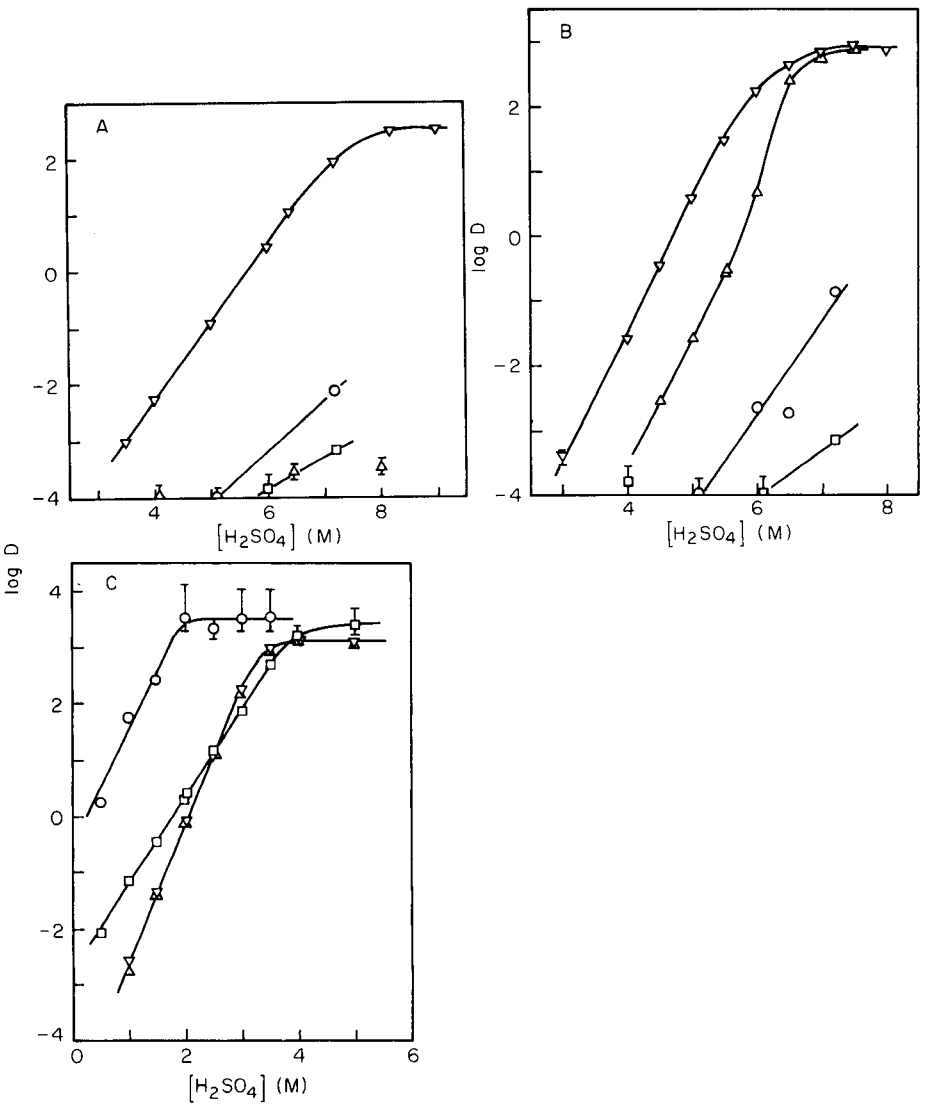

Fig. 1. Extraction of arsenic species into benzene from sulfuric acid solutions containing 1.0 M sodium halide: (A) chloride; (B) bromide; (C) iodide. Species: (▽) As(III); (△) As(V); (○) MeAs(V); (□) $Me_2As(V)$. Shaking time, 2 min.

observed in the iodide extraction of other elements such as germanium(IV), antimony(III), and tin(IV) [17]. In the chloride system (Fig. 1A), the extractability of the arsenic species increases in the order of As(V) ≈ $Me_2As(V)$ < MeAs(V) ≪ As(III). Only As(III) is quantitatively extracted from 8–9 M sulfuric acid containing 1.0 M chloride, where log D reaches 2.50. It has been reported that As(III) is extracted from 10—12 M hydrochloric acid with a maximum value of log D of 1.26 [18]. More complete extraction of As(III) can be attained by the addition of sulfuric acid. In the bromide system (Fig. 1B), the extractability of the arsenic species increases in the order of $Me_2As(V)$ < MeAs(V) < As(V) < As(III). The inorganic arsenic species, As(III) and As(V), are quantitatively extracted from 7—8 M sulfuric acid containing 1.0 M bromide.

In the iodide system (Fig. 1C), the extraction behavior is rather different from that in the other halide systems. The extractability increases in the order of As(III) = As(V) ≈ $Me_2As(V)$ < MeAs(V); the log D values of As(III) are completely consistent with those of As(V). To study the extraction with iodide in detail, the effect of iodide concentration on the extraction from 4.0 M sulfuric acid was examined. The results are shown in Fig. 2. The log D

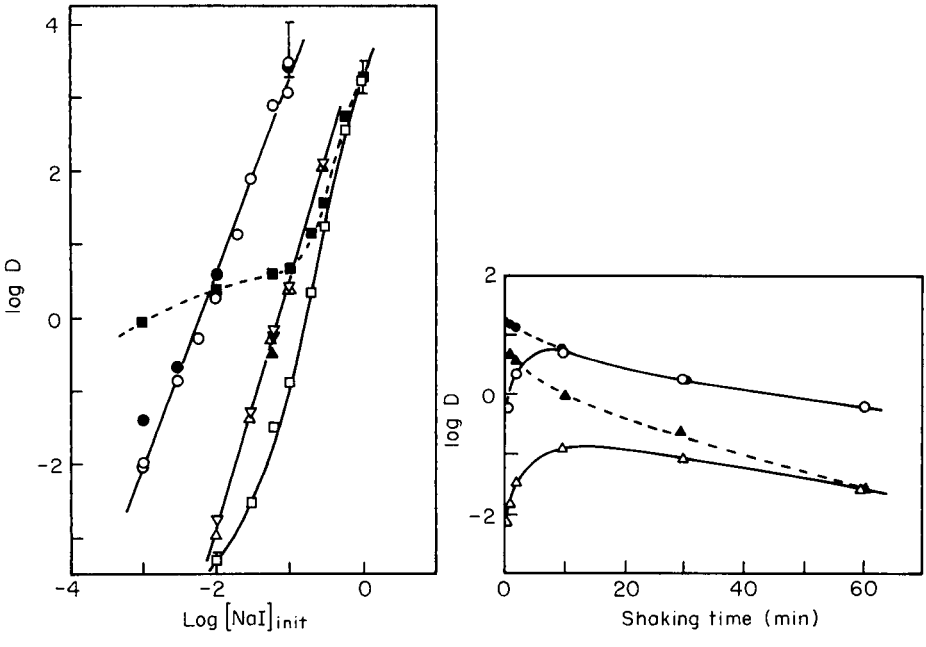

Fig. 2. Effect of iodide concentration on the extraction and back-extraction of arsenic species in the 4.0 M sulfuric acid/benzene system: (▽▼) As(III); (△▲) As(V); (○●) MeAs(V); (□■) $Me_2As(V)$. Solid symbols denote the back-extraction. Shaking time, 2 min.

Fig. 3. Effect of shaking time on the extraction and back-extraction of $Me_2As(V)$ in iodide systems with a 4 M sulfuric acid aqueous phase: (○●) 0.20 M NaI; (△▲) 0.060 M NaI. Solid symbols denote the back-extraction.

values for As(III), As(V), and MeAs(V) increase linearly with increasing iodide concentration, and log D obtained from the back-extraction is in agreement with that from the forward extraction. This means that the extraction equilibrium for these species is attained rapidly within the shaking time of 2 min. The identical nature of the extraction behavior of As(III) and As(V) found in Figs. 1C and 2 can be ascribed to the reduction of As(V) to As(III) with iodide in the aqueous phase; probably both these species are extracted as arsenic(III) triiodide. Also MeAs(V) may be reduced to MeAs(III) with iodide and extracted as $MeAsI_2$. This compound can be synthesized by treatment of a solution of MeAs(V) and potassium iodide with hydrochloric acid and sulfur dioxide and is known to be soluble in organic solvents such as diethyl ether and carbon disulfide [19]. The formation of MeAs(III) is also supported by the following experimental results. The methylarsenic species, presumed to be MeAs(III), extracted from iodide solution into benzene was back-extracted into 5 M sulfuric acid. Then this MeAs(III) solution was subjected to the halide extraction and the results were compared with those in Fig. 1, in which the extraction was done with the MeAs(V) solution. In the iodide system, the log D values were the same as in Fig. 1C but in the chloride and bromide systems, the values were significantly different from those in Fig. 1A and B, respectively; the log D values for MeAs(III) at 5 M sulfuric acid containing 1.0 M chloride and bromide increased by -1.30 and -1.05, respectively. However, these differences in log D were diminished measurably when an aged aqueous solution of back-extracted MeAs(III) was used. This may be ascribed to the gradual oxidation of MeAs(III) to MeAs(V) on standing in contact with air. In contrast, the log D value for $Me_2As(V)$ obtained from the forward extraction was markedly different from that obtained from the back-extraction when the concentration of iodide was less than 0.1 M. This shows that extraction equilibrium was not attained with low concentrations of iodide within the shaking time of 2 min. Hence the effect of the shaking time on the extraction and the back-extraction of $Me_2As(V)$ was investigated. The results are shown in Fig. 3. The log D values reach a maximum at about 10 min and then decrease gradually, whereas the log D values in the back-extraction decrease monotonously. This decrease seems to be related to the decreased iodide concentration in the aqueous phase; during the shaking, iodide is oxidized gradually to iodine which is extracted into benzene. Nevertheless, the log D values obtained from the extraction and the back-extraction agree at prolonged shaking times, so that it appears that extraction equilibrium can be reached under these conditions. From these phenomena, $Me_2As(V)$ seems to be rather slowly reduced to $Me_2As(III)$ with iodide and extracted as the iodide (Me_2AsI). The formation of this compound has been confirmed by gas chromatography in a similar extraction system [6], where hydroiodic acid was used.

Diethyldithiocarbamate system

Figure 4 shows the extraction curves of the arsenic species with 1.0×10^{-2} M diethylammonium diethyldithiocarbamate (DDC) in carbon tetrachloride. Only As(III) is quantitatively extracted in the pH region. The other three species are partly extracted in the acidic region and log D increases with increasing acid concentration. The extraction of As(III) shows the reverse trend and is similar to that generally observed in the extraction of other metal ions with DDC [20]. Because the back-extraction curve of As(V) against the acid concentration was almost the same as that of As(III), As(V) was considered to be extracted as As(III) by reduction with the extractant [21]. The extraction behavior of the methyl species, MeAs(V) and Me_2As-(V), is quite similar to that of As(V); these species may also be reduced to the respective arsenic(III) species and extracted as diethyldithiocarbamate complexes. These complexes have been synthesized by the reaction of $MeAsI_2$ and Me_2AsI with DDC and are sufficiently stable for use in gas chromatography [7].

Didodecyltin system

Dialkyltin compounds such as dioctyltin dinitrate and dinonyltin dinitrate have been tested for the extraction of inorganic acids such as phosphate and arsenate [14]. In this work, didodecyltin dichloride (DDDT) was used as the extractant for the present series of arsenic species. When a benzene solution of DDDT was shaken with water, the insoluble hydroxide was readily formed, but this was avoided by using a mixture of benzene and methyl isobutyl ketone (1:1). Figure 5 shows the extraction curves for

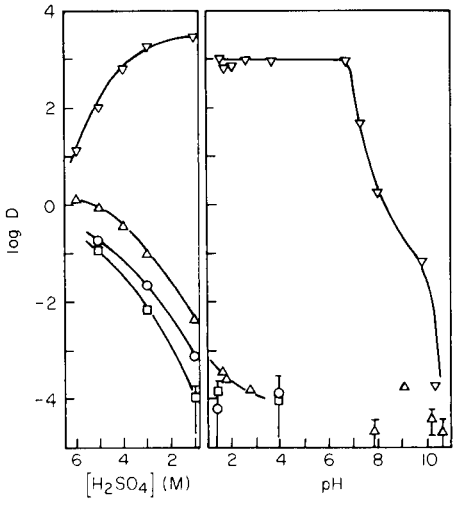

Fig. 4. Extraction of arsenic species with 1.0×10^{-2} M diethylammonium diethyldithiocarbamate in carbon tetrachloride from aqueous solutions of various acidity. Species: (▽) As(III); (△) As(V); (○) MeAs(V); (□) Me_2As(V). Shaking time, 5 min.

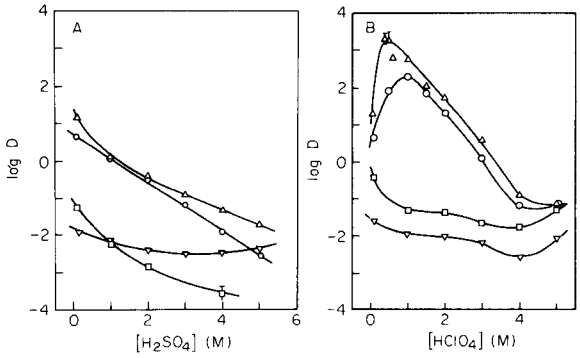

Fig. 5. Extraction of arsenic species with 1.0×10^{-3} M didodecyltin(IV) dichloride in 1:1 benzene/methyl isobutyl ketone from acid solutions: (A) sulfuric acid; (B) perchloric acid. Shaking time, 60 min. Symbols as in Fig. 4.

the four arsenic species with 1.0×10^{-3} M DDDT in benzene/methyl isobutyl ketone solution from sulfuric acid and perchloric acid solutions. In the sulfuric acid system (Fig. 5A), the log D values of the arsenic species other than As(III) decreased gradually as the acidity increased, but quantitative extraction is not achieved under the present experimental conditions. In the perchloric acid system (Fig. 5B), the log D values of arsenic species other than As(III) were much higher than those in the sulfuric acid system. Particularly, log D for As(V) and MeAs(V) reached 3.2 at 0.5 M perchloric acid and 2.3 at 1 M perchloric acid, respectively, hence these species can be extracted quantitatively. In the sulfuric acid system, the arsenic acid, methylarsonic acid, and dimethylarsinic acid may compete with sulfuric acid for complexation with didodecyltin(IV), whereas in the perchloric acid system, there would be virtually no competition. The order of extractability of the arsenic species is in agreement with the order of their first acidity constants [22], i.e., As(III), $10^{-9.61} < Me_2As(V)$, $10^{-6.2} <$ MeAs(V), $10^{-3.6} <$ As(V), $10^{-2.24}$. This suggests that the dissociated anion of these arsenic species reacts with the organotin(IV).

Pyrogallol/tetraphenylarsonium system

Extraction of the arsenic species, As(III), As(V), MeAs(V), and Me_2As-(V) was tested from a sulfuric acid solution containing 0.20 M pyrogallol into chloroform containing 5.0×10^{-4} M tetraphenylarsonium (TPA) chloride. As shown in Fig. 6, only As(V) was quantitatively extracted and readily separated from other species. None of the species was extracted without TPA. Although the extracted species was not identified in the previous investigations on the extraction of As(V) with pyrogallol [15] and catechol [23], it is probable that As(V) forms an anionic complex with the di- or tri-hydroxybenzene and is then extracted as an ion-pair with TPA.

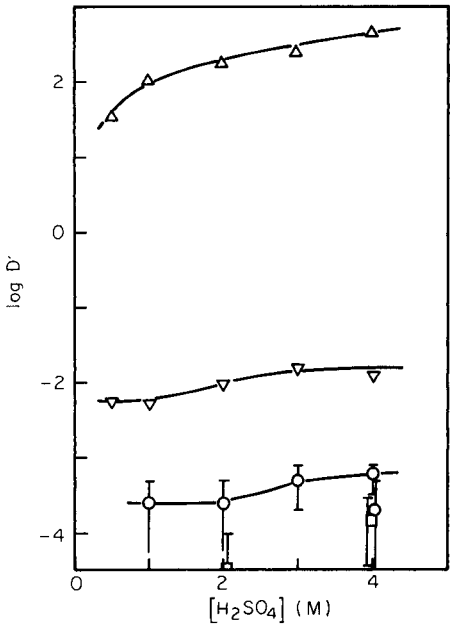

Fig. 6. Extraction of arsenic species with 0.20 M pyrogallol/5.0 × 10^{-4} M tetraphenylarsonium chloride from sulfuric acid solutions to chloroform. Shaking time, 30 min. Symbols as in Fig. 4.

Selective extraction

In the halide and DDC systems, arsenic(III) species were selectively extracted as complexes having arsenic(III) as the central element. In the DDDT system, only arsenic(V) species were extracted. Table 1 summarizes the extraction conditions useful for the separation of each arsenic species. For example, As(III) can be separated quantitatively from other species both in the chloride system and in the DDC system; As(V) is separated in the

TABLE 1

Summary of extraction conditions for the separation of arsenic species (log D)

Extractant	Conditions	As(III)	As(V)	MeAs(V)	$Me_2As(V)$
NaCl[a]	7.5 M H_2SO_4	2.1	<−3.0	−2.0	<−3.0
NaBr[a]	6.5 M H_2SO_4	2.6	2.4	−2.7	<−3.0
NaI[a]	1.2 M H_2SO_4	−2.0	−2.0	2.0	−0.9
NaI[b]	4.0 M H_2SO_4	−0.5	−0.5	2.4	−2.0
DDC[c]	pH 1.5–6.7	3.0	<−3.5	<−3.5	<−3.5
DDDT[d]	1.0 M $HClO_4$	−2.0	2.8	2.3	−1.3
PG[e]/TPA[f]	2.0 M H_2SO_4	−2.0	2.3	<−3.0	<−3.0

[a]1.0 M. [b]0.05 M. [c]0.01 M. [d]0.001 M. [e]0.2 M pyrogallol. [f]5 × 10^{-4} M.

pyrogallol/TPA system, and MeAs(V) is separated in the iodide system. Therefore, the four arsenic species can be mutually separated by combining these extraction systems.

The authors express their appreciation to Kyodo Yakuhin Co. Ltd. for the kind supply of organotin compounds.

REFERENCES

1 M. Yamamoto, Soil Sci. Soc. Am. Proc., 39 (1975) 859.
2 E. A. Dietz, Jr. and M. E. Perez, Anal. Chem., 48 (1976) 1088.
3 F. T. Henry and T. M. Thorpe, Anal. Chem., 52 (1980) 80.
4 G. R. Ricci, L. S. Shepard, G. Colovos and N. E. Hester, Anal. Chem., 53 (1981) 610.
5 W. A. Maher, Anal. Chim. Acta, 126 (1981) 157.
6 C. J. Soderquist, D. G. Crosby and J. B. Bowers, Anal. Chem., 46 (1974) 155.
7 E. H. Daughtrey, Jr., A. W. Fitchett and P. Mushak, Anal. Chim. Acta, 79 (1975) 199.
8 S. Fukui, T. Hirayama, M. Nohara and Y. Sakagami, Talanta, 28 (1981) 402.
9 S. Fukui, T. Hirayama, M. Nohara and Y. Sakagami, Talanta, 30 (1983) 89.
10 B. Beckermann, Anal. Chim. Acta, 135 (1982) 77.
11 Y. Talmi and D. T. Bostick, Anal. Chem., 47 (1975) 2145.
12 Y. Odanaka, N. Tsuchiya, O. Matano and S. Goto, Anal. Chem., 55 (1983) 929.
13 A. K. De, S. M. Khopkar and R. A. Chalmers, Solvent Extraction of Metals, Van Nostrand-Reinhold, New York, 1970.
14 V. M. Shkinev, B. Ya. Spivakov, G. A. Borob'eva and Yu. A. Zolotov, Anal. Chim. Acta, 167 (1985) 145.
15 K. Kratzer and J. Stary, Radiochem. Radioanal. Lett., 40 (1979) 61.
16 A. J. Quick and R. Adams, J. Am. Chem. Soc., 44 (1922) 805.
17 A. R. Byrne and D. Gorenc, Anal. Chim. Acta, 59 (1972) 81.
18 G. O. Brink, P. Kafalas, R. A. Sharp, E. L. Weiss and J. W. Irvine, Jr., J. Am. Chem. Soc., 79 (1957) 1303.
19 I. T. Millar, H. Heaney, D. M. Heinekey and W. C. Fernelius, in E. G. Rochow (Ed.), Inorganic Syntheses, McGraw-Hill, New York, 1960, Vol. 6, p. 113.
20 T. Honjo and H. Imura, Bull. Chem. Soc. Jpn., 53 (1980) 1753.
21 H. Imura, M.Sc. Thesis, Kanazawa University, 1977.
22 C. F. Baes, Jr. and R. E. Mesmer, The Hydrolysis of Cations, Wiley, New York, 1976, p. 366.
23 J. Rais, P. Selucky and S. Drazanova, J. Inorg. Nucl. Chem., 33 (1971) 3087.

Analytica Chimica Acta, 185 (1986) 249—258
Elsevier Science Publishers B.V., Amsterdam — Printed in The Netherlands

DETERMINATION OF ORGANIC AND INORGANIC MERCURY COMPOUNDS BY REVERSE-PHASE HIGH-PERFORMANCE LIQUID CHROMATOGRAPHY AFTER EXTRACTION OF THE COMPOUNDS AS THEIR DITHIZONATES

WENCHE LANGSETH

Department of Chemistry, The University of Oslo, P.O. Box 1033, Blindern, 0315 Oslo 3 (Norway)

(Received 13th December 1985)

SUMMARY

A sensitive and selective method is described for the simultaneous determination of inorganic and organic mercury compounds. The mercury compounds are extracted into toluene or chloroform with dithizone, and the dithizonates are separated by liquid chromatography on an ODS column. Complete resolution was obtained between methyl-, ethyl-, phenyl- and inorganic mercury with a mobile phase of THF/methanol (2:1) with 0.05 M acetate buffer pH 4 (62 + 38), containing 50 μM EDTA. The mercury chelates were detected spectrophotometrically at 475 nm. The detection limits were at the sub-nanogram level. The method is applicable to human urine, tap water and tomatoes.

The toxicity and the general chemistry of mercury are known to be highly dependent on the groups attached to the metal atom [1]. Westöö [2] developed a method for organomercury speciation based on gas chromatography (g.c.), and several variations have later been described [3, 4]. However, long clean-up procedures are necessary, and several organomercury compounds are thermally unstable or are strongly retained on most g.c. columns [5—7].

High-performance liquid chromatography (h.p.l.c.) has proved to be a powerful instrumental method for the trace determination of involatile and thermally unstable compounds. The use of h.p.l.c. for metal compounds, especially in the form of chelates, has increased rapidly [8, 9]. Inorganic and organic mercury compounds have been separated on ODS columns as alkyldithiocarbamates [10—12]. They were detected by an u.v. spectrophotometer at 254 nm. Lack of selectivity is a disadvantage of this method. Many organic compounds absorb at the same wavelength, and some of the commoner metals interfere. Some workers have solved the selectivity problem by using an element-specific detector, e.g., an atomic absorption [13—15] or microwave-induced plasma spectrometer [16]. These approaches, however, need expensive equipment and are often far too complicated.

The aim of this work was to find a relatively selective method, capable of trace determinations of inorganic and organic mercury compounds, using

0003-2670/86/$03.50

only a combination of ordinary h.p.l.c. equipment. Fairly good selectivity can often be obtained for compounds detectable in the visible region or by fluorescence.

Dithizone (3-mercapto-1,5-diphenylformazan; H_2Dz) is known to form stable chelates with both inorganic and most alkyl-, alkoxyalkyl- and arylmercury compounds [17—19]. Inorganic mercury forms an orange-yellow 1:2 chelate of the form $Hg(HDz)_2$, with an absorbance maximum at about 490 nm and a molar absorptivity (ϵ) of 7.0×10^4 l mol^{-1} cm^{-1}, when extracted from acidic or mildly alkaline solution with excess of dithizone. Yellow 1:1 chelates of the form RHg(HDz) are formed by the mono-organomercury compounds, under similar conditions. The wavelength of maximum absorbance is about 475 nm and the molar absorptivity is about 3.3×10^4 l mol^{-1} cm^{-1}. The formation of chelates with dithizone has been used for post-column detection in the h.p.l.c. [20], g.c. and t.l.c. [21—24] of mercury compounds. The t.l.c. separations were done on silica gel plates, but hardly any resolution was obtained between methyl- and ethylmercury.

In this paper, separation of inorganic and organomercury chelates of dithizone by reverse-phase h.p.l.c. is described and the application of the method to real samples is reported.

EXPERIMENTAL

Reagents

All reagents were of analytical-reagent grade, obtained from commercial sources. The standard inorganic and organic mercury solutions were made from the chloride salts. The mercury(II) chloride solution was prepared in 0.5 M nitric acid, and the organic mercury chlorides in methanol. They were stored in a refrigerator as 1.0 g l^{-1} solutions. (All concentrations of mercury compounds given in this paper refer to the mercury content of the compound.) The purities of the mercury chlorides were checked by the given h.p.l.c. method.

Dithizone (Merck) was either dissolved directly in toluene without any further purification and stored as a 0.01 M solution in a refrigerator or purified by the following procedure. It was first recrystallized from chloroform as described by Sandell and Onishi [17]; it was then chromatographed on a glass column packed with silica gel 60 (0.040—0.063 mm; Merck) and toluene as eluent. The concentration of the isolated fraction was determined spectrophotometrically.

The stock ethylenediaminetetraacetic acid solution (5 mM) was made from the disodium salt.

The chromatographic solvents were of h.p.l.c. grade (Fisons). The tetrahydrofuran (THF) and the toluene used for sample preparation were purified on a glass column filled with aluminium oxide (basic, activity grade 1, Woelm B). Quartz-distilled/deionized water was used. All aqueous solutions used in the mobile phase were filtered through 0.45-μm Millipore filters. Helium was used for deaerating the mobile phase.

Apparatus

The h.p.l.c. equipment consisted of a Perkin-Elmer dual-pump module (Series 2) with a Rheodyne injector (Model 7105). The detector was usually a Perkin-Elmer LC-75 spectrophotometer but occasionally a Waters 440 filter photometer. All area calculations were done with a Milton-Roy CI-10 integrator.

Three prepacked reverse-phase columns were used in this study: (1) RP-18 Spheri-5, 5-μm MPLC cartridge (Brownlee Labs.), 100 × 4.6 mm i.d.; (2) Spherisorb ODS-2, 3-μm column (Phase Separation), 150 × 4.6 mm i.d.; (3) Nova-pak C_{18}, 4-μm column (Waters), 150 × 3.9 mm i.d. The 50-mm guard column was dry-packed with LC-18 40 μm pellicular packing (Supelco). All columns were of stainless steel.

Procedure

The following procedure was used for preparation of test samples.

A portion (5 ml) of 0.5 M acetate buffer, pH 4.0, was added to a centrifuge tube. An appropriate aliquot of standard mercury solution was transferred to the tube and 4 ml of toluene and 1 ml of 0.01 M dithizone solution were added. The mixture was shaken on a Whirlimixer (Fison) for 3 min and centrifuged. Usually, 2 ml of the organic phase was transferred to a sample vessel and evaporated to dryness with a gentle stream of nitrogen. The residue was dissolved in 2 ml of methanol. An aliquot (usually 5 μl) of this methanol solution was injected into the chromatograph. A mixture of THF/methanol (2:1) with 0.05 M acetate buffer, pH 4.0 (62 + 38), containing 50 μM EDTA was normally used as the mobile phase. The wavelength control of the spectrophotometer was set at 475 nm. The flow rate was 1.0 ml min^{-1} for the Spheri-5 and Nova-pak columns, and 0.8 ml min^{-1} for the Spherisorb column.

The peak heights were normally measured.

RESULTS AND DISCUSSION

Sample preparation

Inorganic and most of the organomercury compounds that form chelates with dithizone can be extracted quantitatively in the pH range 1—8 [18]. In contrast to the use of diethyldithiocarbamate as extraction reagent, no decomposition of the organomercury compounds examined was observed with acidic solution. A 0.5 M acetate buffer of pH 4.0 was found to give good reproducibility. When the method was applied to real samples a lower pH was often used because protein-bound organomercury compounds are released more easily in hydrochloric acid solutions [25].

Manganese(II), Fe(II), Fe(III), Co(II) and Ni(II) remained in the aqueous phase after extraction at pH 4; Ag(I), Cu(II), Zn(II), Cd(II) and Pb(II) were at least partly extracted into the organic phase. This is in agreement with the results given by Sandell and Onishi [17]. However, as long as excess of dithizone was present, they had no influence on the extraction of the mercury

compounds. No peak corresponding to $Cu(HDz)_2$ or the other metal chelates could be observed within the retention volumes of the mercury compounds.

Both chloroform and toluene can be used as the extraction medium. For most purposes, toluene was chosen because of its lower toxicity. Only small amounts of chloroform extract could be injected directly into the chromatograph before asymmetric peaks were observed. The volume could be increased somewhat with the use of toluene, but the limit of tolerance varied in both cases from one column to another. With the Nova-pak column, the sample had to be injected in methanol. Almost no change in peak shapes were seen with methanol for injection volumes less than 25 μl.

Dithizone is known to be very sensitive to oxidants present in the solution [17]. Several products can be formed. There was also a slow decomposition in the mobile phase. A peak appearing between phenyl mercury and inorganic mercury belonged to a decomposition product, which was also not stable. Another compound was formed, which seemed to be 1,5-diphenylformazan from mass spectrometric data. It was eluted just after dithizone (see Fig. 2). Further examination of these products was not made. Purification of dithizone prior to use is normally recommended for spectrophotometric measurements [17]. The decomposition products mentioned were, however, not affected by purification procedures. Hardly any difference was observed between the purified and unpurified reagent when not more than 10 nmol of dithizone was injected, which is equal to the amount given in the above procedure. With the injection of larger amounts, which is often necessary for the trace determination of mercury compounds in real samples, small interfering peaks appeared at maximum sensitivity. Purification of the dithizone is therefore recommended for trace determinations of mercury compounds.

Excess of dithizone could be removed from the sample by back-extraction with 2% (w/v) ammoniacal solution. Many of the oxidation products will, however, remain in the organic phase, and neither dithizone itself nor the main decomposition products interfered with the mercury separation. Better reproducibility was obtained when dithizone was left in the organic phase.

The dithizonate extracts of the mercury compounds could be stored at $-18°C$ for at least 24 h without noticeable changes, but prolonged storage caused decomposition of the chelates.

Conditions for h.p.l.c.

While metal alkyldithiocarbamates have been separated mostly by reverse-phase elution on apolar columns [26], silica columns have been used for dithizonates [27—29]. Methyl-, phenyl- and inorganic mercury chelates were separated successfully by thin-layer chromatography on silica [21, 23]. Normal-phase elution of these chelates by h.p.l.c. showed broad peaks, however, and more than one peak could often be observed for each compound. Both unmodified and cyanopropyl-bonded silica columns were tried.

Reverse-phase elution of the mercury dithizonates on an ODS column proved to be more successful. The aqueous part of the mobile phase had to

be buffered, otherwise decomposition of the chelates was observed. Different buffers could be used. Formic acid (pH 1.9), acetic acid (pH 2.9) and acetate buffers of pH 4.0 and 4.7 all gave successful results. No difference was seen between 0.05 and 0.1 M acetate buffers. A 0.05 M acetate buffer of pH 4.0 was chosen as the aqueous part of the eluent.

Good separation between all four mercury dithizonates was obtained with a mobile phase prepared from THF, methanol and acetate buffer (Figs. 1 and 2). Exclusion of THF spoiled the separation between ethyl- and phenylmercury. The best conditions were obtained with 2:1 THF/methanol; with higher THF contents, one of the decomposition products of dithizone interfered. The retention volumes increased with increasing buffer content of the mobile phase. Sufficient separation for most purposes was obtained with 35—40% (v/v) buffer.

All types of exchange and reduction reactions, including those which have been suggested to occur between the metal parts of the chromatographic equipment and the metal chelates [26, 30, 31], seemed to be avoided by the addition of a little EDTA to the mobile phase. A concentration of 50 μM EDTA was chosen in this study. It is, however, recommended to use quartz-distilled water in the mobile phase.

The shapes of the peaks, and so the separation, depended on the amount injected as well as on the column used. Linear calibration graphs were obtained for the organomercury dithizonates with the Nova-pak column when the peak height was plotted versus the quantity injected. In the case of inorganic mercury, linearity was observed only up to about 10 ng and beyond 20 ng. A small bend was seen between these two points, giving a convex curve. This irregularity in the graph of $Hg(HDz)_2$ could be eliminated by co-extraction of some copper(II) ion together with the mercury compounds (Fig. 3). The concentration of copper should be about a quarter that of dithizone; $Cu(HDz)_2$ probably acts as a dithizone source during the elution, as a consequence of the great difference in the formation constants [32]. The detection could then not be made at wavelengths less than 475 nm, because the general level of absorption was too high in that range.

Linear calibration graphs were not obtainable with the Spheri-5 and Spherisorb ODS-2 columns for low concentrations when the peak heights were measured. Nonlinearity was observed up to about 30 ng. The tail of the peak seemed to increase with decreasing amounts injected. Because the deviation from linearity was found to increase with increasing silanol activity of the column, adsorption of the chelates to the residual silanol groups is believed to occur. To examine whether or not this adsorption was followed by decomposition, peak height and area measurements were compared. Calibration graphs, prepared with respect to both peak heights and areas, were produced for the Spherisorb column, with samples containing 40—200 ng each of methylmercury and inorganic mercury. Excess of dithizone was back-extracted from the sample solution. The intercept with the x-axis was calculated in each case. The intercept value of the graphs with respect to

peak areas was 6.9 ng for methylmercury and 15.1 ng for inorganic mercury. These results indicate that both of the chelates decomposed somewhat during the elution, but to a greater extent for inorganic mercury. The intercepts of the graphs with respect to peak heights indicated little difference in the degree of adsorption between the two compounds; 20.0 ng was found for methylmercury and 19.3 ng for inorganic mercury. The standard deviation was found to be about 3.2 ng for these calculations [33]. These results suggest that the mercury atom of organomercury chelates can interact to a greater degree with free silanol groups without decomposition. Adsorption of inorganic mercury chelates are more often followed by decomposition.

In many procedures applied for h.p.l.c. separation of metal chelates, addition of a little free ligand to the eluent is recommended to suppress adsorption of the chelates, but free dithizone was not stable in the mobile phase, so that this could not be done in the present work. A small but significant decrease of the adsorption of the mercury chelates was observed when the excess of dithizone was not removed from the extract to be injected. Better reproducibility was also obtained.

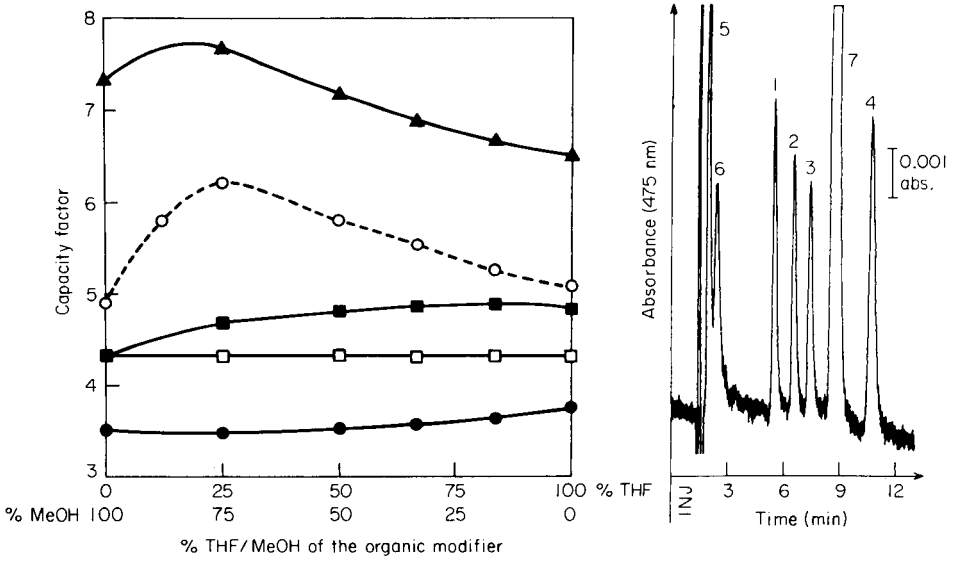

Fig. 1. Effect of the THF/methanol ratio in the mobile phase on the separation of the mercury dithizonates: (•) MeHg(HDz); (□) EtHg(HDz); (■) PhHg(HDz); (▲) $Hg(HDz)_2$; (○) decomposition product of dithizone. The buffer content was regulated to give a constant capacity factor of ethylmercury. Conditions: Nova-pak C_{18} column (4 μm, 150 × 3.9 mm i.d.) with guard column; THF/methanol/0.05 M acetate buffer pH 4.0/50 μM EDTA as mobile phase (see text).

Fig. 2. Chromatogram of the different mercury dithizonates. Peaks: (1) MeHg(HDz); (2) EtHg(HDz); (3) PhHg(HDz); (4) $Hg(HDz)_2$; (5) dithizone; (6) decomposition product of dithizone, probably 1,5-diphenylformazan; (7) decomposition product of dithizone. Conditions: column as for Fig. 1; eluent THF/methanol (2:1) with 0.05 M acetate buffer pH 4.0 (62 + 38) and 50 μM EDTA; flow rate 1.0 ml min^{-1}; 10 ng of each mercury compound injected.

The correlation coefficients of the calibration graphs were found to be >0.998 in all cases. Best precision was obtained with the peak-height measurements without the use of an integrator. The detection limits are often taken as twice the noise level of the baseline but the noise will depend on the equipment used and especially on the detector. The following detection limits were obtained with a Perkin-Elmer LC-75 spectrophotometer at 475 nm: 0.3 ng MeHg, 0.4 ng EtHg, 0.5 ng PhHg and 0.4 ng Hg. When a Waters 440 filter photometer (436 nm) was used, the detection limits were about half these amounts.

Application to real samples

The proposed method was applied to human urine, tap-water and tomatoes in order to test its suitability.

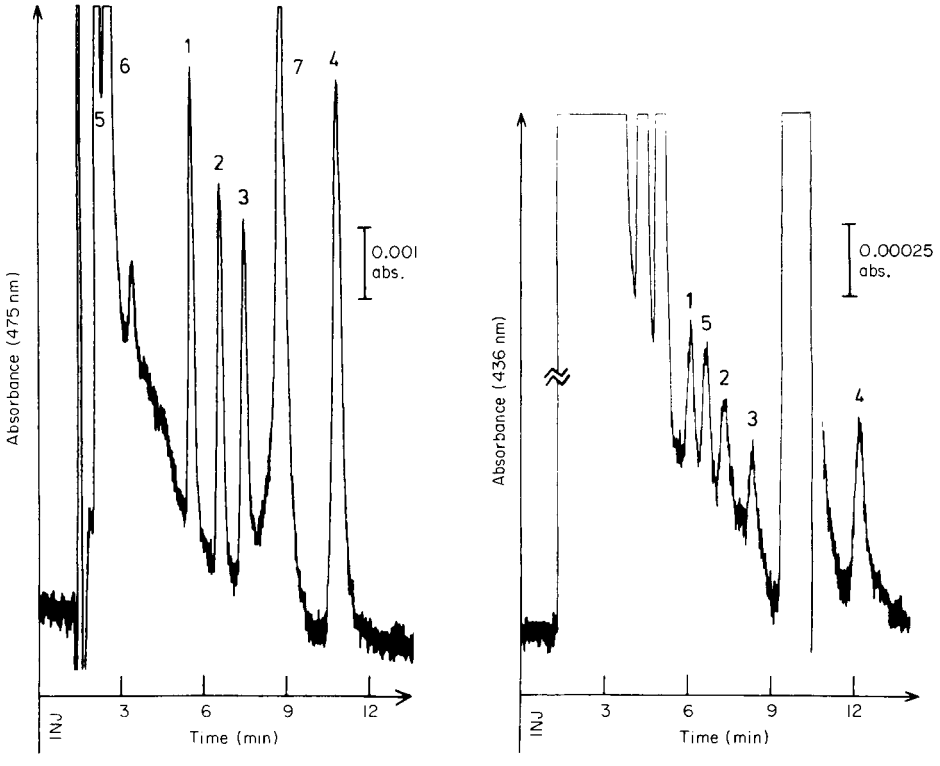

Fig. 3. Chromatogram of the different mercury dithizonates when some copper was co-extracted with the mercury compounds. See text for further information. Chromatographic conditions and peaks as for Fig. 2.

Fig. 4. Chromatogram of an extract of human urine spiked with the mercury compounds (4.0 $\mu g\ l^{-1}$ each). Peaks: (1) MeHg(HDz); (2) EtHg(HDz); (3) PhHg(HDz); (4) $Hg(HDz)_2$; (5) decomposition product of dithizone (this peak is hardly seen at 475 nm). The urine sample was found to contain 2.1 $\mu g\ l^{-1}$ methylmercury and 9.2 $\mu g\ l^{-1}$ inorganic mercury. Chromatographic conditions as for Fig. 2.

Human urine. The sample preparation procedure given by Bruno et al. [23] was used, but with some variations. Aliquots (0—100 μl) of a standard mercury solution containing 1.00 μg ml^{-1} each of methyl-, ethyl-, phenyl- and inorganic mercury, were added to different centrifuge tubes, each containing 5 ml of urine. Each sample was then adjusted to about pH 1.0 by addition of 250 μl of 2 M hydrochloric acid. After addition of 2 ml of chloroform and 1 ml of toluene containing about 0.30 μmol of dithizone, the samples were shaken vigorously for at least 10 min to obtain maximum extraction efficiency, and then centrifuged at 4000 rpm. The organic phases were placed in sample vessels and evaporated to dryness with a gentle stream of nitrogen. Each residue was dissolved in 250 μl of methanol and 20 μl was injected into the chromatograph. The same chromatographic conditions as for test samples were used. In this case, a filter photometer equipped with a filter for around 436 nm was used as detector. Better signal-to-noise ratios were obtained with the filter photometer.

Only one extraction was normally made because the total recovery with only one extraction was more than 80%. A second extraction gave only 5—10% higher recovery. Recoveries were found to be highest for phenylmercury and lowest for methylmercury. Better precision was obtained with only one extraction step, probably because less dithizone was injected into the chromatograph. A combination of chloroform and toluene was found to give better separation between the two phases than toluene alone.

A urine sample from the author, who had obviously been exposed to these mercury compounds during work, was examined more closely (Fig. 4). The sample was found, by the standard addition method given above, to contain 2.1 μg l^{-1} methylmercury and 9.2 μg l^{-1} inorganic mercury. The ethyl- and phenyl-mercury contents were below the detection limit, which was established as 1.5 μg l^{-1}. The total mercury content of this urine sample was found to be 10.8 μg l^{-1} by the cold-vapour atomic absorption technique.

Tap water. The samples were prepared in the same way as for urine, but only toluene was used as extraction medium. For water with a high copper concentration, the dithizone content had to be increased because both copper and the mercury compounds are extracted at pH 1. The detection then had to be made at 475 nm, because of the high background absorption.

Tomatoes. The possibility of extracting the mercury compounds directly into toluene with dithizone, in the same way as for urine, was studied. A simplified variation of the sample preparation procedure given by Tatton and Wagstaffe [21] was used. Thus, 3 ml of propan-2-ol, 3 ml of water and 250 μl of 2 M hydrochloric acid were added to 1 g of homogenized tomatoes, and the mixture was extracted with 3 ml of toluene containing 0.50 μmol of dithizone. No interfering peaks appeared in the chromatogram at 475 nm. About the same recovery as for urine was obtained for the organomercury compounds. The calibration graphs were found to be linear for the range 0—10 μg g^{-1} mercury in the organomercury compounds. The recovery of

inorganic mercury was poor. For tomatoes, this extraction procedure is therefore only suitable for the determination of organomercury compounds.

Conclusion

Reverse-phase separation of organic and inorganic mercury compounds as their dithizonates appears to have considerable potential for the examination of mercury compounds. No special apparatus is required except ordinary h.p.l.c. equipment. Clean-up procedures can usually be kept to a minimum because of the selectivity offered by this method. A simultaneous determination of both organic and inorganic mercury is often possible, in contrast to various procedures described earlier. Of the arylmercury compounds, only phenylmercury was incorporated in this study, but there is no reason to believe that the proposed method is restricted to this compound. It should be applicable to most alkyl-, aryl- and alkoxyalkyl-mercury compounds.

REFERENCES

1 L. Friberg and J. Vostal, Mercury in the Environment, CRC Press, Cleveland, 1972.
2 G. Westöö, Acta Chem. Scand., 20 (1966) 2131.
3 Analytical Methods Committee, Analyst (London), 102 (1977) 769.
4 C. J. Cappon and J. C. Smith, Anal. Chem., 49 (1977) 365.
5 R. C. Dressman, J. Chromatogr. Sci., 10 (1972) 468.
6 V. Luckow and H. A. Rüssel, J. Chromatogr., 138 (1977) 381.
7 G. L. Baughman, M. H. Carter, N. L. Wolf and R. G. Zepp, J. Chromatogr., 76 (1973) 471.
8 H. Veening and B. R. Willeford, Adv. Chromatogr., 22 (1983) 117.
9 A. R. Timerbaev, O. M. Petrukhin and Yu. A. Zolotov, Zh. Anal. Khim., 36 (1981) 811.
10 S. Inoue, S. Hoshi and M. Sasaki, Bunseki Kagaku, 31 (1982) E243.
11 S. Inoue, S. Hoshi and M. Mathubara, Talanta, 32 (1985) 44.
12 L. Lajunen, E. Eijärvi and P. Niemi, Finn. Chem. Lett., (1984) 146.
13 F. E. Brinckman, W. R. Blair, K. L. Jewett and W. P. Iverson, J. Chromatogr. Sci., 15 (1977) 493.
14 J. W. Robinson and E. D. Boothe, Spectrosc. Lett., 17 (1984) 673.
15 W. Holak, J. Liq. Chromatogr., 8 (1985) 563.
16 D. Kollotzek, D. Oechsle, G. Kaiser, P. Tschöpel and G. Tölg, Fresenius Z. Anal. Chem., 318 (1984) 485.
17 E. B. Sandell and H. Onishi, Photometric Determination of Traces of Metals, General Aspects, 4th edn., Wiley, New York, 1978, p. 579.
18 H. Irving and A. M. Kiwan, Anal. Chim. Acta, 45 (1969) 243, 255, 447.
19 A. T. Hutton, H. Irving, L. R. Nassimbeni and G. Gafner, Acta Crystallogr., Sect. B: 36 (1984) 2064.
20 C. H. Gast and J. C. Kraak, Int. J. Environ. Anal. Chem., 6 (1979) 297.
21 J. O'G. Tatton and P. J. Wagstaffe, J. Chromatogr., 44 (1969) 284.
22 K. Teramoto, M. Kitabatake, M. Tanabe and J. Noguchi, J. Chem. Soc., Jpn., Ind., Chem. Sect., 70 (1967) 1601.
23 P. Bruno, M. Caselli and A. Traini, J. High Resolut. Chromatogr., Chromatogr. Commun., 8 (1985) 135.
24 L. Gagliardi, A. Amato, G. Ricciardi and S. Chiavarelli, Farmaco, Ed. Prat., 32 (1977) 306.

25 J. O. Watts, K. W. Boyer, A. Cortez and E. R. Elkins, J. Assoc. Off. Anal. Chem., 59 (1976) 1226.
26 S. R. Hutchins, P. R. Haddad and S. Dilli, J. Chromatogr., 252 (1982) 185.
27 D. E. Henderson, R. Chaffee and F. P. Novak, J. Chromatogr. Sci., 19 (1981) 79.
28 J. W. O'Laughlin and T. P. O'Brien, Anal. Lett., A11 (1978) 829.
29 M. Lohmüller, P. Heizmann and K. Ballschmiter, J. Chromatogr., 137 (1977) 165.
30 Y. T. Shih and P. W. Carr, Talanta, 28 (1981) 411.
31 N. Haering and K. Ballschmiter, Talanta, 27 (1980) 873.
32 K. Ueno, K. Shiraishi, T. Togo, T. Yana, I. Yoshida and H. Kobayashi, Anal. Chim. Acta, 105 (1979) 289.
33 K. Eckschlager, Errors, Measurement and Results in Chemical Analysis, Van Nostrand-Reinhold, New York, 1972, p. 111.

Analytica Chimica Acta, 185 (1986) 259—269
Elsevier Science Publishers B.V., Amsterdam — Printed in The Netherlands

FLOW-INJECTION EXTRACTION WITH A MICROVOLUME MODULE BASED ON INTEGRATED CONDUITS

YLVA SAHLESTRÖM

Department of Analytical Chemistry, Royal Institute of Technology, S-100 44 Stockholm (Sweden)

BO KARLBERG*

Bifok AB, Box 124, S-191 22 Sollentuna (Sweden)

(Received 20th January 1986)

SUMMARY

A self-contained module for liquid—liquid extractions is described. The module contains engraved conduits for mixing of sample and reagent, an engraved segmentor, a detachable extraction coil, a membrane separator, and a rinsing system for the flow cell. The membrane in the separator is supported by a teflon-coated steel grid and can be replaced rapidly. The segmented stream enters at the centre of the circular membrane and travels through an engraved, coiled channel in contact with the membrane before leaving the membrane area at the periphery. The volume of the receptor chamber for the organic phase is 10 μl. For a detector flow-cell volume of 8 μl, an aqueous flow rate of 2.0 ml min^{-1} and an organic flow rate of 1.2 ml min^{-1}, the "loss factors" caused by analyte dispersion are 3.2 and 1.5 for caffeine sample volumes of 40 μl and 100 μl, respectively, compared with batch extraction. The system is also tested for extraction of anionic surfactants as their ion-pairs with methylene blue.

There are several reasons why the overall volumes involved in an extraction procedure should be reduced to a few millilitres or less: organic solvents are expensive, there are disposal problems, there are exposure risks for the technicians, and the sample supply is often limited. Manual extractions of such small volumes are not practicable. Consequently, interest has been focussed on mechanized extractions of small sample volumes based on the flow-injection extraction principle first described in 1977 [1, 2]. The application was to the extraction of aqueous caffeine samples by chloroform and subsequent measurement of the absorbance of caffeine in the organic phase at 275 nm. Refinements of this system have been made since then with respect to almost every detail but the essential parts and the performance of present systems are very similar to the system first reported. Despite the larger number of papers reporting technical improvements, there have been very few attempts to find an overall design that would meet basic practical demands such as short start-up time, low maintenance level, reproducible behaviour over several days, and inherently small sample dilution characteristics. Most

0003-2670/86/$03.50

early designs for flow-injection extraction suffer from the fact that they are susceptible to mechanical variations. Very often, both segmentation and separation characteristics change when a part in the system is moved or turned. The secondary flow in a coiled tube is disrupted when its coiling radius or its position are changed and as a consequence the mechanical forces on sample dispersion will be altered. The complex flow pattern of flow-injection systems for extraction, "the spaghetti syndrome", has definitely frightened many potential users. With the introduction of microconduits for classical one-phase applications of flow-injection analysis (f.i.a.) [3], a simple technique has become still simpler. The microconduits are tailormade for different given applications and their dimensions are comparable with those of a credit card. One aim of this work was to see if the microconduit concept would be applicable in the development of an extraction manifold so that many of the current technical difficulties could be overcome. A second aim was to develop a reliable device with minimum sample dilution characteristics which would allow extraction of microlitre sample volumes with minimal loss of sensitivity compared with the batch extraction approach.

EXPERIMENTAL

Description of the extraction module

Figure 1 shows the flow diagram of a typical extraction system based on f.i.a. The extraction module, framed by the broken line in Fig. 1, comprises carrier and reagent inlets, a carrier and reagent mixing coil, an organic solvent inlet, a segmentor, an extraction coil, a separator and a joint waste outlet. All conduits, except for the extraction coil and the separator, are engraved in a poly(vinyl difluoride) (PVDF) plate, 12 × 9 × 2 cm^3. The PVDF plate is attached by six screws to a steel plate sandwiching a gasket of inert rubber to prevent leakage. A dense synthetic rubber material was selected, to avoid plugging of, or swelling into, the engraved channels. The cross-section of a conduit is thus semicircular or slightly crescent-shaped. Figure 2 is a schematic diagram of the extraction module. Inlet and outlet tubes were of PTFE, and their ends were flanged and provided with inert rubber washers and polypropylene standard connectors. The injector and the detector are connected

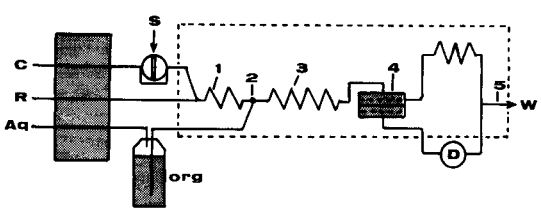

Fig. 1. Flow scheme of a typical extraction system in f.i.a.: C, carrier; R, reagent; Aq, aqueous stream to displacement bottle containing organic solvent (org); D, detector; W, waste; S, sample; 1, mixing coil; 2, segmentor; 3, extraction coil; 4, separator; 5, joint waste outlet. The extraction module is framed by the broken line.

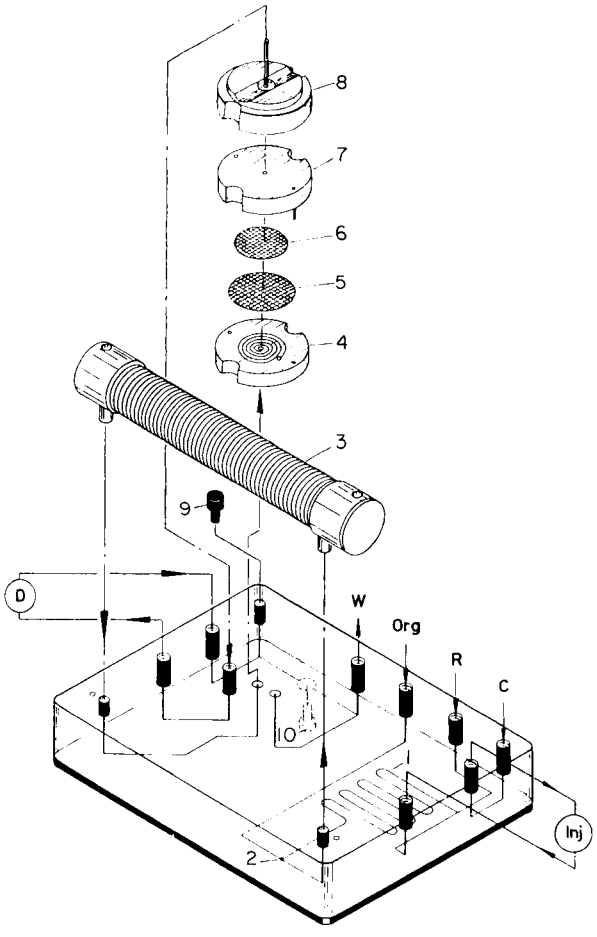

Fig. 2. Exploded view of the extraction module: C, carrier; R, reagent; Org, organic phase; W, waste; Inj, injector; D, detector; 1, mixing conduit, aqueous phase; 2, segmentor; 3, extraction coil; 4, separator, "donor" half; 5, membrane; 6, grid; 7, separator, "acceptor" half; 8, organic phase outlet; 9, stopper, rinse system; 10, shut-off valve, rinse system.

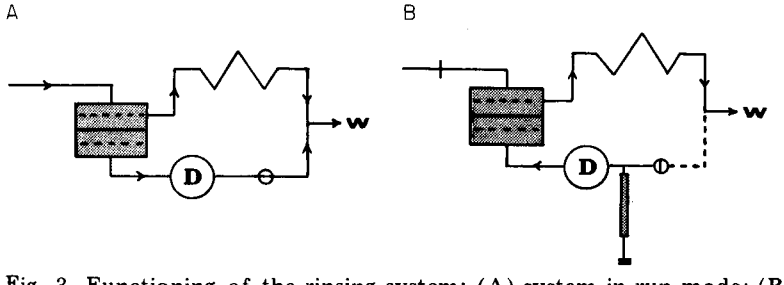

Fig. 3. Functioning of the rinsing system: (A) system in run mode; (B) system in rinse mode. The detector flow cell and the separator are rinsed with ethanol provided from a syringe.

to the carrier stream as shown in Fig. 2. The carrier and the reagent streams are merged and mixed in a 25-cm conduit, the internal volume being about 100 μl. The organic stream is supplied by a displacement bottle arrangement (Tecator, Sweden). The geometry of the segmentation point was found to be critical; both the size of the mixing cavity and its proximity to "turbulent points" (i.e., points at which the flow direction changes drastically) had to be optimized so that segments of uniform size resulted.

The extraction tubing is of teflon (0.5-mm i.d., 2 m long). It is wound round a helically coiled groove on a plastic rod. The ends of the extraction coil are flanged and provided with spacers and rubber washers.

The separator unit and the extraction coil are situated on the top of the PVDF body. The segmented stream enters the separator unit from below via an engraved channel in the bottom surface of the PVDF body and further via a perpendicularly drilled hole. Figure 2 shows an exploded view of the separator unit. The contact area between the membrane and the segmented donor stream is a coiled groove (4). A teflon-coated steel grid (6) prevents the membrane (5) from expanding into the acceptor chamber for the organic phase. The volume of the acceptor chamber is about 10 μl, with a coiled groove similar to that shown for the donor stream. The separated organic stream is led to a spectrophotometric flow cell and thereafter rejoins the aqueous stream to a common waste outlet. This arrangement is necessary in order to balance the pressure and so to diminish the risk of solvent evaporation in the separator.

For convenience, a rinsing system is integrated into the module. The functioning of this rinsing system is illustrated in Fig. 3. No disconnection of tubing is necessary in order to rinse the flow cell and the membrane.

Procedure

When the system is started up, a flow of organic solvent is provided to the system from the displacement bottle. One of the two pumps of the FIAstar 5020 unit (Tecator, Sweden) is reserved for propelling the organic flow, whereas the other pump, propelling the carrier and the reagent, is started when the organic flow has already entered the system. When needed, ethanol is injected into the rinsing system to clean the flow cell from water droplets and the membrane from impurities. The membranes used here were Fluoropore 0.2—1.0 μm. An 8-μl flow cell was used.

Normally, a steady baseline is obtained after a few minutes. The flow rates of C, R and Org in Fig. 2 were typically 1.2, 0.8 and 1.2 ml min^{-1}, respectively. Samples are injected into the carrier. Evaluations of peak heights are calculated automatically and the results are displayed on the FIAstar 5020-unit display.

For measurements of pressure drop over the membrane and flow rate through the detector, the extraction module was replaced by two detached separator and segmentor units of similar design. An on-line pressure sensor was connected at different sites both before and after the separator unit. The

pressure drop values were output to a strip-chart recorder. Also, when the dispersion characteristics of different types of separator and segmentor were investigated, detached units had to be used. Flow rates were measured by using a stopwatch and a measuring cylinder.

Chemicals

Caffeine, iodine and anionic surfactants were used as test compounds. The stock iodine solution was prepared by dissolving 0.5 g of potassium iodate and 4 g of potassium iodide in 250 ml of distilled water; 2 ml of concentrated hydrochloric acid was added to lower the pH. The anionic surfactants were sodium dodecyl sulphate (m.w. 288; Merck), sodium dioctyl sulphosuccinate (m.w. 444; Rohm and Haas), sodium decyl sulphate (m.w. 260; Merck), sodium octyl sulphate (m.w. 232; Merck), sodium tetradecyl sulphate (m.w. 316; Eastman-Kodak) and sodium dodecyl benzosulphonate (m.w. 348; Fluka). Aqueous stock solutions, 1 mM, were prepared and stored for a maximum of one week. All other test solutions were prepared daily.

For the determination of the anionic surfactants, a methylene blue reagent solution was prepared as follows: 0.05 g of methylene blue was dissolved in about 200 ml of a pH 7 phosphate buffer in a 1-l volumetric flask; 400 ml of methanol was added and the solution was diluted to volume with distilled water. This solution could be stored at room temperature and used for at least two weeks, but it was always filtered before use. The carrier was degassed distilled water.

For those experiments in which no reagent was needed, distilled water replaced the reagent solution. Chloroform, freon (1,1,2-trichloro-1,2,2-trifluoroethane), 1,2-dichloroethane, 4-methylpentan-2-one (MIBK), toluene, 1-pentanol and iso-octane were shaken to equilibrium with distilled water before use. All reagents and solvents were of analytical grade.

RESULTS AND DISCUSSION

Optimization of the microvolume extraction system

A fundamental question is to what extent the microvolume sample is "diluted" during the course of an extraction in the flow-injection system. Table 1 shows the absorbance at the peak maximum as a function of injected sample volume for simple caffeine extractions. The batch value was obtained by shaking conveniently large volumes of the chloroform phase and the aqueous sample phase in proportions corresponding to the flow rates in the flow-injection system (1.2 ml min^{-1} organic phase and 2.0 ml min^{-1} total aqueous phase). The batch value was set to represent an extraction efficiency of 100%. As expected, dilution of the sample occurs even for volumes of 200 μl, but the "dilution loss factor" is only 1.5 for a sample volume of 100 μl. Batch extractions of such small volumes are difficult, especially if a phase volume ratio of about 1:1 is to be preserved; the risk of significant volume reduction by evaporation is obvious. As can be seen in Table 1, it is

TABLE 1

Flow-injection extraction of different volumes of 0.05 M caffeine into chloroform compared with batch extraction

Sample volume (μl)	Absorbance at peak maximum	Dilution loss factor	Yield (%)
40	0.126	3.2	31
100	0.272	1.5	67
200	0.369	1.1	90
300	0.410	1.0	100
Batch	0.408	—	100[a]

[a]Defined as 100%.

possible to achieve the same degree of extraction efficiency in the flow system as in the batch system provided that such "large" volumes as 300 μl are used. However, the overall performance of an extraction system based on the flow-injection principle with respect to sample dispersion (or dilution) is best estimated if small volumes, i.e., volumes less than 100 μl, are used. The dispersion process acting on sample material in the aqueous part of the system is easily controllable [4] and will not be discussed further, even though the principle of using engraved conduits seems to be beneficial [3].

In Table 2, two segmentors are compared, the original T-piece type [2] and the engraved type described above; anionic surfactants served as test substances. Separator 1 (see Fig. 2) was used in both cases. As mentioned previously, the construction of the segmentor is crucial but its contribution to the

TABLE 2

Extraction of a 0.08 mM anionic surfactant solution with different types of separators and segmentors
(Chloroform as solvent; joint waste outlet.)

Separator no.	Separator inlet chamber	Segmentor	Absorbance at peak maximum	Peak width[a] (s)
1	Coiled groove (centred inlet)	T-piece	0.491	21
1	Coiled groove (centred inlet)	Engraved	0.541	19
2	Glass T-tube	Engraved	0.165	42
3	Straight groove	Engraved	0.550	19
4[b]	Conical chamber (peripheral inlet)	Engraved	0.296	30

[a]Peak width at 0.01 absorbance. [b]A restrictor (50 cm, 0.5 i.d.) was inserted between the separator waste outlet and the merging point of outlet streams.

total dispersion process is small. The internal volumes of the "aqueous sections" of the two systems were equal; despite this, the engraved design was found to contribute less to the overall sample dispersion process. Table 2 also includes results showing that the construction of the separator is the most critical part of the system with respect to dispersion. Separator 1 is compared with some earlier types of separators. Separator 2 is the glass T-separator, into which a teflon tape is inserted to attract organic phase; its separation ability derives from the different densities and wetting properties of the two phases [5]. Separator 3 is a groove-type membrane separator. It consists of two PVDF halves, of which the lower half has a straight groove of $2 \times 40 \times 0.8$ mm^3 filled with a porous polyethylene material [6]; the upper half also has a straight groove, $2 \times 40 \times 0.4$ mm, which is unfilled. Separator 4 is the phase separator developed by Bäckström et al. [7]; it consists of two chambers, the lower one being cylindrical with a volume of about 10 μl and the upper one conical with a volume of about 50 μl.

Once again, it was confirmed that membrane phase separators are superior to separators based on the affinity/density principle. However, a more interesting conclusion is that the groove inlet configuration seems to be preferable to the chamber inlet configuration. Separator 1 has a peripherical waste outlet. When the segmentor stream was run in the reverse direction (i.e., by reversing the inlet and outlet ports), a peak height decrease of about 25% was obtained. This observation could explain, at least to some extent, the relatively low peak heights observed for separator 4. However, this last separator required a restrictor directly after the separator waste outlet in order to maximize the separation efficiency. A complete separation between chloroform and water/methanol was difficult to obtain and this may also account for the low peak heights. The coiled groove and the straight groove separators had similar properties with respect to sample dispersion. The disadvantage of the straight groove separator (no. 3) is that it is inconvenient to operate; circular membranes are more easily applied that oblong membranes.

Separation efficiency of different organic solvents

Several organic solvents were tested in the extraction module with aqueous iodine as the test substance. The results are given in Table 3. An efficiency of more than 85% was obtained for all solvents, which must be regarded as quite satisfactory. For best sensitivity, the desirable separation efficiency is close to 100%. When the two waste streams were kept separate, the separation efficiency could easily be estimated by measuring the individual ingoing and outgoing flow rates. For obvious reasons, the outgoing individual flow rates could not be measured when the two waste streams were joined. The separation efficiency should be directly proportional to the peak height for constant ingoing flow rates and for a constant injection volume [5]. Thus, the separation efficiencies given in Table 3 were estimated by relating the two peak absorbances for each solvent; the first value obtained when the two waste streams were detached, and the second one when they were joined.

TABLE 3

Flow-injection extraction of iodine into different organic solvents with measurements at 510 nm

Solvent	Organic flow rate (ml min^{-1})		Waste streams	Absorbance at peak max.	Separation efficiency (%)
	Inlet	From flow cell			
Freon	1.06	1.01	Detached	0.379	
	1.06	—	Joint	0.400	100
1,2-Dichloroethane	1.06	0.95	Detached	0.370	
	1.06	—	Joint	0.368	90
Iso-octane	1.06	1.00	Detached	0.458	
	1.06	—	Joint	0.420	87
Toluene	1.06	1.03	Detached	0.432	
	1.06	—	Joint	0.408	92
Chloroform[a]	1.03	1.03	Detached	0.243	
Chloroform[a]	1.03	—	Joint	0.244	100

[a]Extraction of caffeine with measurements at 275 nm.

4-Methylpentan-2-one cannot be used in the module because of swelling problems of the rubber material and 1-pentanol gave problems with the separation because water droplets penetrated the membrane.

Pressure drop measurements

According to the Hagen-Poiseuille equation, $\Delta P/L = \text{const.}\ \eta u/d^2$, i.e., the pressure drop (ΔP) over the length (L) of a tube with uniform inner diameter (d), should depend only on flow rate (u) and viscosity (η). In a simple test, the pressure drop was measured at constant tube length (145 cm) and diameter (0.5 mm) at different flow rates of distilled water, chloroform, and a segmented flow of these liquids (1:1, segment length 4 mm). The results are shown in Fig. 4. The difference in slope between the aqueous and the chloroform phases is due to viscosity: the pressure drop ratio at a flow rate of 2 ml min^{-1}, for instance, was 1.70 which agrees excellently with the corresponding viscosity ratio 1.72 at 20°C. As can be seen in Fig. 4, the pressure drop with the segmented flow resembles that with the aqueous flow. Intuitively, one would expect the aqueous segments to slide on the organic film shown to exist in a segmented flow [8], but a lot of energy is undoubtedly required for the film formation and for the intrasegment dynamics. This may account for the pressure drop characteristics of the segmented flow. It is interesting to note that the linear relationship between pressure drop and flow rate, as predicted by the Hagen-Poiseuille equation, seems to hold also for the segmented stream. Furthermore, the apparent viscosity of the segmented stream was at least 1 centipoise. This is of great importance for explaining the fact that the counter pressure in the aqueous waste stream from the separator unit remains almost unchanged even when the separation efficiency decreases. In

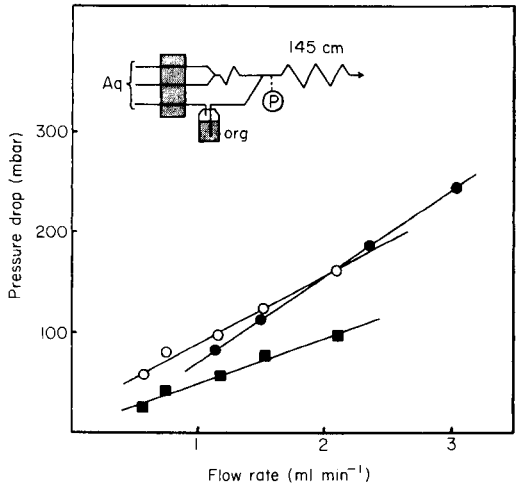

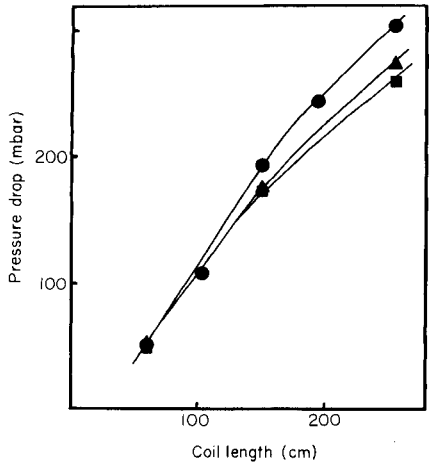

Fig. 4. Pressure drop over a PTFE coil (145 cm long, 0.5 mm i.d.) as a function of flow rate: (▪) 100% chloroform; (○) 100% water; (●) 1:1 chloroform/water. The inset shows the set-up used for 1:1 chloroform/water; pressure drop measured at point P.

Fig. 5. Pressure drop as a function of a coil length at constant flow rate: (●) 40% (v/v) chloroform/44% water/16% methanol; (▲) 100% chloroform; (▪) 40% chloroform/60% water.

a subsequent test, the pressure drop was measured for different coil lengths by pumping pure distilled water, water/chloroform and water/chloroform/methanol (Fig. 5). As observed previously, water and water/chloroform behave similarly. However, addition of methanol produced an even larger counter pressure or, equivalently, a larger apparent viscosity. Solvating and dissolving effects have been observed when methanol is introduced in a chloroform/water extraction system [9]. These effects would require some energy and so would increase the counter pressure.

A slight deviation from the linear behaviour predicted by the Hagen-Poiseuille equation can be observed for tube lengths above 200 cm; this might be due to nonlinearity of the sensor used for pressures above 250 mbar. The pressure was also measured before and after the separator, and the pressure drop was calculated for three different membranes with different pore sizes (0.2, 0.5 and 1.0 μm). The pressure drop was about 60 mbar in all cases; obviously, the membrane pore size was of little importance for the pressure drop over the separator unit.

Extraction of anionic surfactants

The determination of anionic surfactants was selected to investigate the practical applicability of the extraction module. Distilled water was used as carrier (C, Fig. 1) into which 0.01—0.10 mM surfactant samples were injected. The methylene blue reagent contained 40% methanol and chloroform served as the organic solvent; absorbances were measured at 660 nm [9].

Table 4 shows the results for sodium dodecyl sulphate (SDS), which was used as the main reference substance. The decreased yield obtained for SDS compared with caffeine (Table 1) can be explained by the decreased separation efficiency caused by the third component, methanol. The separation efficiency was estimated to be about 60% by comparing measurements with separate waste streams and measurements with joint waste streams. The use of separate waste streams did not change the separation efficiency significantly but irregular behaviour was frequently observed because of evaporation of the organic phase.

In Table 5, comparative results are given for the six anionic surfactants tested. An injection volume of 40 μl was used throughout. Sodium dodecyl sulphate served as the reference substance. The absorbance at the peak maximum obtained for SDS was defined at 100, as was the absorbance obtained by batch extraction in which analogous phase-volume proportions were used. The dilution loss factor was calculated as 6.5, which means that the flow-injection procedure with only 40 μl of the sample was a factor of 6.5 less

TABLE 4

Comparison between flow-injection and batch extractions of SDS and the effect of different injected volumes

Injected volume (μl)	Peak height (absorbance)		Dilution loss factor	Yield (%)
	0.01 mM	0.02 mM		
40	0.071	0.138	6.5	15.4
100	0.153	0.298	3.0	33.3
200	0.244	0.480	1.9	52.9
300	0.282	0.552	1.6	61.0
Batch	0.462	0.906	1.0	100[a]

[a]Defined as 100%.

TABLE 5

Comparison between flow-injection and batch extractions of 0.02—0.1 mM anionic surfactant samples with SDS as standard

Sample[a]	Normalized absorbance		
	Flow	Batch	Flow/batch
Dodecyl sulphate	100[b]	100[b]	1.0
Dioctyl sulphosuccinate	79	93	0.85
Decyl sulphate	105	102	1.03
Octyl sulphate	73	76	0.96
Tetradecyl sulphate	95	94	1.01
Dodecyl benzosulphonate	82	83	0.99

[a]All as sodium salts. [b]Defined as 100; see text.

sensitive than the batch procedure. If it is assumed that this factor is constant for all anionic surfactants tested, then SDS can be taken as a common standard for the flow-injection method, provided that the different extractabilities observed in the batch experiment are accounted for. As can be seen in Table 5, this is true for all the surfactants tested except sodium dioctyl sulphosuccinate. This surfactant has a branched structure and two sulphonic groups instead of one; the lower yield obtained is probably due to incomplete extraction during the short residence time in the system.

Conclusions

The new extraction module with integrated conduits is capable of meeting the high demands of routine use. The start-up time was typically of the order of 3—5 min and the relative standard deviation was less than 1% for iodine extractions. Its reliability was tested over 14 days, by running a daily test cycle comprising start-up, extraction of twenty iodine samples, and closing down. No change of membrane was required and no malfunction occurred during this test period.

The separation efficiency was at least 85% for various solvents used in single combination with water. When a third liquid (e.g., methanol) was introduced, the separation efficiency dropped to about 60% and the counter pressure in the system increased considerably. When the separated organic phase rejoined the aqueous phase after the detector flow cell before passing to waste, the performance of the extraction system was greatly improved. The detection limit for chloroform extractions of anionic surfactants was found to be 0.1 μM, using methylene blue as ion pair forming species and methanol in the reagent solution to improve the extractability. Compared with batch extraction, there is some loss of sensitivity with the flow module; the loss factor is 1.5—7, depending to a great extent on the sample volume injected. A range of routine extraction methods based on ion-pair formation and subsequent detection of the chromophore in the organic phase is currently being adapted to the extraction module.

The authors are indebted to Prof. F. Ingman and Dr. L. Nord for valuable discussions.

REFERENCES

1 Swedish Patent No. 7711016-1 (1977).
2 B. Karlberg and S. Thelander, Anal. Chim. Acta, 98 (1978) 1.
3 J. Růžička and E. H. Hansen, Anal. Chim. Acta, 161 (1984) 1.
4 J. Růžička, E. H. Hansen and H. Mosbaek, Anal. Chim. Acta, 92 (1977) 235.
5 L. Nord and B. Karlberg, Anal. Chim. Acta, 118 (1980) 285.
6 Y. Sahlestrom and B. Karlberg, Anal. Chim. Acta, 179 (1986) 315.
7 K. Bäckström, L.-G. Danielsson and L. Nord, Anal. Chim. Acta, 169 (1985) 43.
8 L. Nord and B. Karlberg, Anal. Chim. Acta, 164 (1984) 233.
9 J. Kawase, A. Nakae and M. Yamanake, Anal. Chem., 51 (1979) 1640.

Analytica Chimica Acta, 185 (1986) 271—277
Elsevier Science Publishers B.V., Amsterdam — Printed in The Netherlands

THE EFFICIENCY OF CELLEX-P FOR THE PRECONCENTRATION OF LEAD AND OTHER TRACE METALS FROM WATERS

KRYSTYNA BRAJTER* and KRYSTYNA SŁONAWSKA
Department of Chemistry, University of Warsaw, Pasteura 1, 02-093 Warsaw (Poland)
(Received 24th October 1985)

SUMMARY

The chelating ion-exchanger Cellex-P, a cellulose phosphate ester, is shown to be effective for the preconcentration of Cu, Ni, Mn, Cd, Zn and Pb from water. The pH of the sample is not critical within the approximate range 5—8. The collected ions can be eluted efficiently in 10—25 ml of 1 M nitric acid from 2—16.5-cm columns of resin. Common salts present in natural waters do not interfere. Cellex-P is used for the preconcentration and determination of the metal ions in potable water by graphite-furnace atomic absorption spectrometry.

The detection limits of the most frequently used instrumental methods are inadequate for determining various trace transition elements simultaneously in natural waters and particularly in potable waters. The preconcentration of metals from waters is therefore important. Co-precipitation, liquid-liquid extraction, sorption and chelating ion-exchange are the most frequently used preconcentration methods [1—4]. Preconcentration of trace metals on a chelating ion-exchanger is normally done with Chelex-100, an iminodiacetic chelating resin, although Ca-Chelex-100 is unsuitable for the preconcentration of lead from tap waters [2].

In recent investigations in this laboratory on the behaviour of different ion-exchange resins, it was found that the commercial chelating ion-exchanger Cellex-P, a dibasic phosphate ester of cellulose, is very suitable for the preconcentration of trace metal ions. Its properties include great selectivity for metal ions and excellent kinetics of the ion-exchange processes which allows rapid preconcentration from large volumes of water samples. In this paper, it is shown that Cellex-P is efficient for the preconcentration of not only lead but also Cu, Ni, Zn, Cd and Mn from water. Very high preconcentration factors were possible at high flow rates. Atomic absorption spectrometry (a.a.s.) with electrothermal atomization was used to quantify the metals after elution.

EXPERIMENTAL

Reagents and apparatus

Metal stock standard solutions (1000 mg l^{-1}, for atomic absorption; Merck) were diluted as required. All other chemicals were analytical-grade reagents. Twice-distilled water was used. All laboratory glassware and polyethylene bottles were thoroughly cleaned by soaking in (1 + 9) nitric acid and then rinsing with twice-distilled water.

Cellex-P was used in the hydrogen form (BioRad Laboratories). It was equilibrated and regenerated as recommended by BioRad. The exchange capacity found was 0.94 meq g^{-1}.

A Beckman model 1272 atomic absorption spectrometer was used with a Pye-Unicam GRM-1268 graphite furnace. The conditions used for the various elements were those recommended by the manufacturers. The pH of solutions was measured with an Elpo model N-517 pH meter and a combined glass/calomel electrode (Radiometer). The glass exchange columns (20 cm high, 0.8 cm inner diameter) had a Rotaflo tap at the bottom. In all the preliminary column experiments, the bed heights were 2 cm, corresponding to 0.20 g of dry Cellex-P; larger columns were used for applied work. The flow rate was regulated with a peristaltic pump.

Procedures

Retention of metal ions as a function of pH. Aqueous solutions (1.0 l), containing the metal ion under study (0.1 mg l^{-1}) and adjusted to the required pH, were passed at a flow rate of 7—8 ml min^{-1} through the column. Retained metal ions were eluted with 25 ml of 1 M nitric acid and quantified by a.a.s. The percentage recoveries are shown in Fig. 1; they are similar to those found by batch methods [5].

Determination of breakthrough capacity. A 0.5 mg l^{-1} solution of lead(II) at pH 3.1 or a 0.1 mg l^{-1} solution of copper(II) at pH 4.4 was passed through the column. The flow rate was 13.6 ml min^{-1} for lead and 7.6 ml min^{-1} for copper. The breakthrough point is taken as the position at which $c/c_o = 0.1$ where c_o is the concentration added and c is the concentration found in the eluate (Fig. 2).

Analysis of tap water. Tap water of pH 7.1 (2.0 l) was passed through a column containing 2.0 g of Cellex-P (bed height 16.5 cm, column diameter 10 mm) at a flow rate of 8 ml min^{-1}. The concentrated metal ions were eluted with 25 ml of 1 M nitric acid and quantified by a.a.s.

RESULTS AND DISCUSSION

The above experiments confirmed the great efficiency of Cellex-P for the preconcentration of Pb, Zn, Mn, Cu, Cd and Ni ions. These metal ions are the most frequently determined in all kinds of waters. A column of resin only 2 cm high (0.20 g of resin) sufficed for quantitative recovery of these

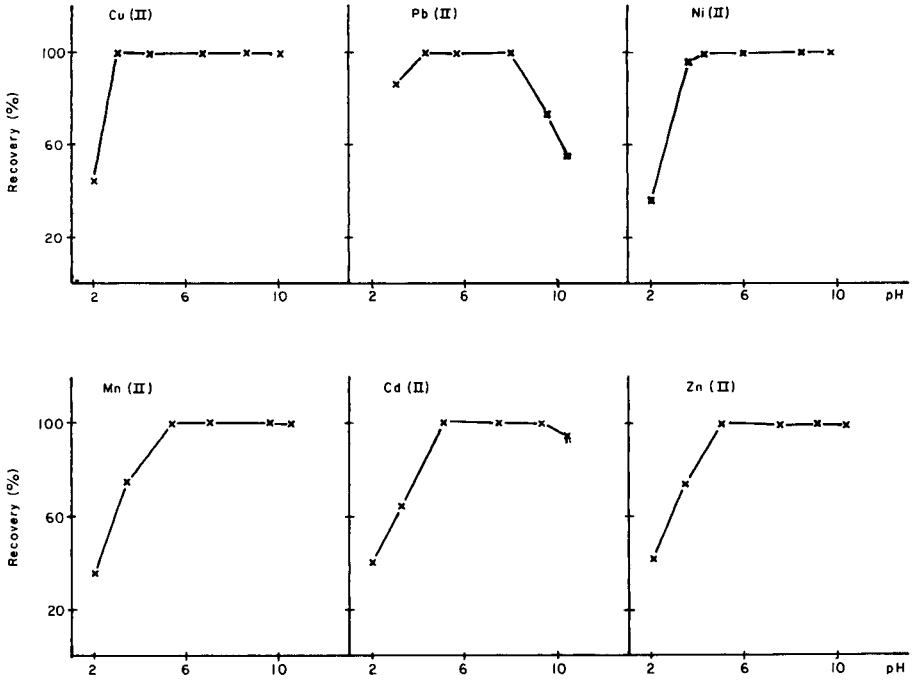

Fig. 1. Effect of pH on the retention of metal ions on the Cellex-P ion-exchanger.

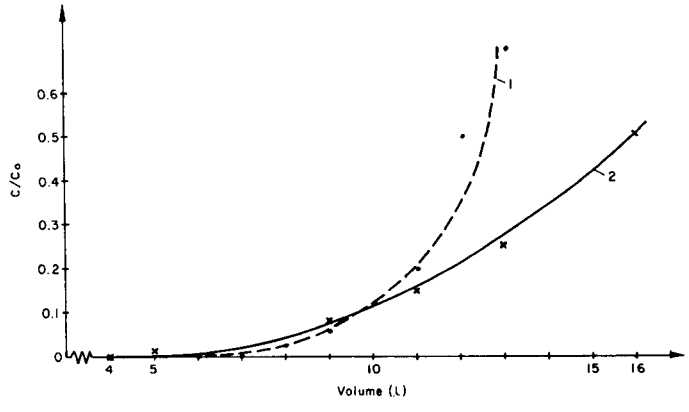

Fig. 2. Breakthrough curves: (1) lead; (2) copper. See text for details.

metal ions at the 0.1 mg l^{-1} level from 1 l of solution. The amount of Cellex-P and the diameter of the column were examined in order to provide quantitative recovery of all these metal ions at the highest possible flow rate. The maximum flow rate giving quantitative recovery was 15.5 ml min^{-1}. The preconcentration factor obtained for these metal ions was 100. Higher factors can be obtained if the volume of the aqueous sample is larger.

The breakthrough capacity under the given operating conditions was evaluated for lead and copper (Fig. 2). The breakthrough curve for lead is quite sharp, which indicates that the rate of the exchange process is favourable under such operating conditions. At the breakthrough point (c/c_0 = 0.1), 10 l of aqueous lead solution had passed through the column. The breakthrough curve for copper is less sharp (even at the lower flow rate of 7.6 ml min^{-1}) but the efficiency of the resin bed is still good. The shapes of the two curves confirm the earlier conclusion that Cellex-P is efficient for preconcentration of metal ions [5].

The influence of pH in the range 2—10 on the retention of metal ions was examined for column operation. The results (Fig. 1) showed that the recovery was almost 100% over a wide pH range so all the cations studied could be preconcentrated effectively at the normal pH of natural waters. Table 1 shows the retention of different mixtures of metal ions at various pH values. The results confirm the high efficiency of Cellex-P for the recovery of metal ions. After collection of metal ions on Cellex-P, the elution characteristics were examined. The percentage elutions with different volumes of 1 M and 2 M nitric acid are listed in Table 2. The optimum amount was 15 ml of 1 M nitric acid. These conditions guarantee high preconcentration factors. The application of higher acidities is not desirable for a.a.s.

Before the Cellex-P resin was tested for the preconcentration of metal ions in natural waters, the influence of substances which might be present in large amounts was investigated. Table 3 lists the retention of Cu, Mn, Zn, Pb, Cd and Ni as a function of the concentration of seven common salts. Lead was affected by high concentration of hydrogencarbonate or acetate. The

TABLE 1

Recoveries of metal ions from mixtures at different pH values[a]

Mixture	pH	Mean recovery (%)	Mixture	pH	Mean recovery (%)
Cu	5.5	99.1 ± 1.5	Pb	5.5	97.9 ± 2.5
Pb		99.3 ± 1.1	Zn		98.2 ± 1.6
Ni		98.7 ± 1.8	Ni		99.0 ± 1.4
			Cd		99.1 ± 1.3
Cu	7.5	98.9 ± 1.7	Cu		98.9 ± 1.4
Zn		99.0 ± 2.0	Mn		98.4 ± 2.0
Pb		98.8 ± 1.2			
			Zn	7.5	98.3 ± 1.5
Cu	6.0	98.5 ± 1.3	Cd		98.0 ± 1.1
Pb		99.1 ± 1.5	Mn		97.5 ± 2.4
Cd		99.0 ± 1.1	Cu		98.9 ± 1.4
Zn		98.4 ± 3.0	Pb		99.9 ± 1.7

[a]Mixtures of metal ions (each at 0.1 mg l^{-1}) in 1 l of solution were passed through a column at 6 ml min^{-1}; retained metal ions were eluted with 25 ml of 1 M nitric acid. Each result is the mean of 5 runs with standard deviation.

TABLE 2

Recovery of metal ions from Cellex-P with different concentrations and volumes of nitric acid[a]

Nitric acid		Recovery (%)					
Molarity	Volume (ml)	Cu	Pb	Ni	Mn	Cd	Zn
1	5	95	81	89	94	96	96
	10	98	98	95	96	98	99
	15	99	99	98	98	99	99
2	5	97	87	90	97	97	97
	8	98	95	95	98	99	98
	10	99	99	98	98	99	99

[a]Solutions containing all the metal ions (each at 0.1 mg l^{-1}) at pH 5 were passed through the column. Elution was as specified.

TABLE 3

Influence of salts on the retention of metal ions[a]

Salt	Amount added (mg l^{-1})	Recovery (%)					
		Cu	Ni	Pb	Mn	Zn	Cd
NaCl	100	99	99	98	97	99	99
	500	99	98	98	99	98	99
	1000	99	97	99	99	99	98
Na_2SO_2	100	99	98	99	98	98	99
	500	95	99	99	98	98	97
$NaNO_3$	100	99	91	98	98	99	99
Na_2CO_3	100	99	94	97	98	99	98
$KHCO_3$	50	98	97	97	97	99	99
	200	96	96	82	99	97	96
Na acetate	10	99	98	96	98	99	99
	100	98	97	84	96	98	98
NaK tartrate	10	99	98	99	95	99	99
	100	99	99	98	94	99	98

[a]In each test, the salt was added to the mixture of metal ions (each at 0.1 mg l^{-1}) at pH 6. Elution was done with 25 ml of 1 M nitric acid.

TABLE 4

Influence of calcium nitrate on the retention of metal ions

Cellex-P[a] (g)	Calcium conc. (mg l^{-1})	Recovery (%)					
		Cu	Ni	Pb	Zn	Cd	Mn
0.2	5	60	21	99	43	51	52
	10	57	12	98	21	32	39
1.0	10	87	64	99	99	95	98
1.2	10	99	74	99	98	99	98
1.5	10	99	97	99	99	99	99
2.0	30	94	66	99	94	97	79

[a]Other conditions as for Table 3.

TABLE 5

Determination of metal ions in tap water by a.a.s. after preconcentration on Cellex-P[a]

Metal	Cu	Ni	Mn	Zn	Pb	Cd
Conc. ($\mu g\ l^{-1}$)	2.3 ± 0.20	0.78 ± 0.13	21.1 ± 2.2	67.6 ± 4.6	3.1 ± 0.34[b]	1.5 ± 0.30

[a]Results are the mean and range (95% confidence limit) of 5 separate determinations. [b]Determination of lead by anodic stripping voltammetry (6-min preconcentration at −0.8 V vs. SCE) gave a result of 3.2 ± 0.35 $\mu g\ l^{-1}$.

effect of calcium nitrate on the retention of metal ions on Cellex-P depended on the size of the resin bed (Table 4). Quantitative recovery of Cu, Pb, Zn and Cd required a bed height of 16.5 cm (2.0 g of Cellex-P) when the column diameter was 10.5 mm. To obtain quantitative retention of nickel and manganese, a longer column of Cellex-P was sometimes necessary. Although the presence of calcium ions in the sample can prevent quantitative recovery of these metal ions, calcium itself is not bound quantitatively by Cellex-P; with the sample containing 30 mg of calcium only 5% was retained. This behaviour of calcium is very convenient for the determination of metal ions by a.a.s. The amount of calcium present in the eluate with nitric acid does not cause spectral interferences.

In most of the experiments, metal ions were added at 0.1 mg l^{-1} concentrations. Quantitative recoveries were also possible when the concentration of each metal ion was 0.05 or 0.01 mg l^{-1}. Thus the method is applicable over a reasonably wide concentration range.

The method was adopted for the preconcentration and determination of Pb, Zn, Cd and Cu in tap water which was found to contain about 30 mg l^{-1} calcium. The recommended procedure is given under Experimental. The results are presented in Table 5. Without the preliminary preconcentration, the determination of these metal ions is impossible.

The efficiency of Cellex-P for the preconcentration of metal ions is not

only similar to that of other chelating resins recommended for such preconcentrations but is better in some respects. The kinetics of the ion-exchange processes is much better which means that high flow rates can be used to achieve rapid preconcentration of metal ions.

REFERENCES

1 M. C. Genaro, C. Balocchi, E. Campi, E. Mentasti and R. Argua, Anal. Chim. Acta, 151 (1983) 339.
2 S. J. De Mora and R. M. Harrison, Anal. Chim. Acta, 153 (1983) 307.
3 G. Reggers and R. Van Grieken, Fresenius Z. Anal. Chem., 317 (1984) 520.
4 L. M. Cabezon, Talanta, 31 (1984) 597.
5 K. Brajter and I. Miazek, Fresenius Z. Anal. Chem., 315 (1983) 121.

Analytica Chimica Acta, 185 (1986) 279—285
Elsevier Science Publishers B.V., Amsterdam — Printed in The Netherlands

SYNTHESE UND EXTRAKTIONSEIGENSCHAFTEN VON 2-(SYM-DIBENZO-14-KRONE-4-OXY)ESSIGSÄURE BZW. -n-HEXANSÄURE

E. UHLEMANN* und H. GEYER

Pädagogische Hochschule "Karl Liebknecht", DDR-1500 Potsdam (Deutsche Demokratische Republik)

K. GLOE und P. MÜHL

Akademie der Wissenschaften der DDR, Zentralinstitut für Festkörperphysik und Werkstofforschung, DDR-8027 Dresden (Deutsche Demokratische Republik)

(Eingegangen den 10. Oktober 1985)

SUMMARY

(*Synthesis and extraction behaviour of 2-(sym-dibenzo-14-crown-4-oxy)-acetic and -hexanoic acid*)

An improved synthesis for carboxylic acid derivatives of dibenzo-14-crown-4 using sodium amide is described. The reagents were studied for the extraction of alkali and alkaline earth metal ions. The dependence of the metal distribution on pH and ligand concentration is used to evaluate the composition of the extracted species. 2-(sym-Dibenzo-14-crown-4-oxy)hexanoic acid is a very good extractant for alkaline earth metal ions but is also of interest for lithium.

ZUSAMMENFASSUNG

Eine verbesserte Synthese für Carbonsäurederivate von Dibenzo-14-krone-4 unter Verwendung von Natriumamid wird beschrieben. Die Extraktion von Alkali- und Erdalkalionen mit diesen Substanzen wurde untersucht. Aus der Abhängigkeit der Metallverteilung von pH und Ligandkonzentration konnte die Zusammensetzung der extrahierten Spezies ermittelt werden. 2-(sym-Dibenzo-14-krone-4-oxy)hexansäure ist ein sehr gutes Extraktionsmittel für Erdalkali-ionen, ist aber auch für Lithium von Interesse.

Die hervorragende Eigenschaft von Kronenethern ist ihr Komplexbildungsvermögen für Alkali- und Erdalkali-ionen. Der Einsatz als Extraktionsmittel wird aber dadurch eingeschränkt, daß die Extraktion des Kronenether-Metall-Komplexes vom gleichzeitigen Übergang der Anionen in die organische Phase abhängig ist. Für die Anionen von Mineralsäuren wird dieser Phasenübergang wegen ihrer intensiven Hydratation stark behindert. Eine Möglichkeit, diese Schwierigkeit zu umgehen, bieten ionisierbare Kronenether, die das erforderliche Gegenion selbst enthalten. Zu dieser Gruppe von Liganden gehören die Kronenethercarbonsäuren.

Grundlegende Arbeiten zur Synthese, zum Extraktionsverhalten und zum Einsatz von Kronenethercarbonsäuren als carrier in Flüssigmembransystemen

0003-2670/86/$03.50

wurden von Bartsch und Mitarbeitern [1—11] hauptsächlich an Dibenzokronenetheroxycarbonsäuren unterschiedlicher Hohlraumgröße, Lipophilie und Substitution durchgeführt. Diese Verbindungen stellen Derivate entsprechender sym-Hydroxydibenzokronenether dar. Lipophile Dicarbonsäuren des Kronenethers 18-Krone-6 wurden hinsichtlich ihres Einsatzes als carrier untersucht [12—14]. Es liegt auch eine Strukturanalyse für den Lithiumkomplex mit 2-(sym-Dibenzo-14-krone-4-oxy)essigsäure vor [15]. Extraktionsuntersuchungen mit Dibenzo-14-krone-4-oxycarbonsäuren wurden bisher nur bei Vorliegen eines hohen Metall-ionen-Überschusses bzw. im komplexen Salzgemisch vorgenommen [4—9]. Deshalb verfolgte die vorliegende Untersuchung das Ziel, die Extraktionsparameter unter Bedingungen zu bestimmen, die neben Aussagen zur Extraktionseffektivität exakte Informationen über die Zusammensetzung der extrahierten Komplexe zulassen. Bei der Synthese von Kronenethercarbonsäuren wurde mit Erfolg Natriumamid als Kondensationsmittel eingesetzt.

EXPERIMENTELLES

Synthese von Kronenethercarbonsäuren

2-(sym-Dibenzo-14-krone-4-oxy)essigsäure. In einem 250-ml Dreihalskolben, ausgerüstet mit Rührer, Rückflußkühler, Trockenrohr, Tropftrichter und Gaseinleitungsrohr, werden unter Reinststickstoff 2,8 g (0,072 mol) feinpulverisiertes Natriumamid in 100 ml peroxid- und wasser-freiem Tetrahydrofuran suspendiert. Dazu gibt man innerhalb von 30 min 3,8 g (0,012 mol) des Hydroxykronenethers, gelöst in 30 ml Tetrahydrofuran. Dann ist noch für weitere 3 h zu rühren. Die Reaktionsmischung wird kurz auf Siedetemperatur erhitzt, dann auf Zimmertemperatur abgekühlt, und es werden in einer dreistündigen Periode 3,4 g (0,024 mol) Bromessigsäure, gelöst in 30 ml Tetrahydrofuran, zugegeben. Danach wird der Kolbeninhalt für weitere 4 h unter Stickstoff bei Zimmertemperatur kräftig gerührt. Nach Beendigung der Reaktion dampft man das Lösungsmittel im Vakuumrotationsverdampfer ab und versetzt den festen Rückstand vorsichtig mit Wasser, um überschüssiges Natriumamid zu zerstören. Zu der entstehenden stark basischen wäßrigen Lösung wird nun Dichlormethan gegeben. Dabei fällt an der Phasengrenze ein feinkristalliner, farbloser Niederschlag aus, der abgetrennt und mehrfach mit Wasser gewaschen wird. Die so gereinigten Kristalle schüttelt man mit einer Mischung von Chloroform und verdünnter Salzsäure. Dabei geht der Feststoff vollständig in die organische Phase. Die Chloroformphase wird abgetrennt, mit Wasser gewaschen und nach dem Trocknen über Magnesiumsulfat im Vakuum eingedampft. [Farbloses Pulver, Schmp. 138—140°C (Lit. 140—141°C [15]), Ausbeute 75%, MM = 374.]

2-(sym-Dibenzo-14-krone-4-oxy)-n-hexansäure. Die Synthese erfolgt wie oben beschrieben unter Verwendung von α-Brom-n-hexansäure. Nach Verdampfung des Lösungsmittels Tetrahydrofuran wird das Reaktionsprodukt unter Kühlung mit Wasser versetzt und die entstandene ölige Suspension zur

Beseitigung des unumgesetzten Kronenethers zweimal mit 50 ml Cyclohexan extrahiert. Anschließend versetzt man die wäßrige Suspension bis zur sauren Reaktion mit 2 M Salzsäure. Dabei entsteht ein brauner Feststoff, der abgetrennt, mehrmals mit Wasser gewaschen und schließlich in Dichlormethan gelöst wird. Diese Lösung ist nochmals mit Salzsäure zu schütteln und mit Wasser bis zur neutralen Reaktion zu waschen. Man trocknet über Magnesiumsulfat und dampft im Vakuum ein. Der Rückstand wird in Dichlormethan gelöst und fraktioniert mit Petrolether gefällt. Das Reaktionsprodukt schmilzt oberhalb 50°C ohne scharfen Schmelzpunkt. [Ausbeute 70%, MM = 430.]

Flüssig-Flüssig-Extraktion

Die pH-Abhängigkeit der Extraktion wurde unter den folgenden Bedingungen untersucht: (a) für Li^+, Mg^{2+}, Ca^{2+} und Ba^{2+}, $c_M^{n+} = 10^{-4}$ M, $c_L = 10^{-2}$ M; (b) für Na^+, K^+, Rb^+ und Sr^{2+}, $c_M^{n+} = 10^{-4}$ M, $c_L = 10^{-3}$ M.

Die Bedingungen für die Untersuchungen zur Abhängigkeit der Extraktion von der Ligandkonzentration waren für Li^+, Na^+, Rb^+, Mg^{2+}, Ca^{2+} und Sr^{2+}: (c) $c_M^{n+} = 10^{-4}$ M, $c_L = 5 \times 10^{-4}$—10^{-2} M, Gleichgewichts-pH-Wert = 8,1. Als Metallsalze kamen die entsprechenden Nitrate (a) bzw. Chloride (b, c) zum Einsatz. Als organische Phase diente Chloroform. Weiterhin galt $V_{org}:V_w$ = 1:1, Schüttelzeit t = 30 min und T = 20°C. Die Einstellung des pH-Wertes wurde bei (a) mit Tetramethylammoniumhydroxid, bei (b) und (c) mit Triethanolamin/Salzsäure vorgenommen.

Die Bestimmung des Metallgehaltes in der wäßrigen Phase erfolgte für Li flammenemmissionsspektralphotometrisch und für Mg, Ca, Ba flammenabsorptionsspektralphotometrisch. Zur Absicherung der Ergebnisse wurde bei allen Versuchsreihen stichpunktartig auch der Metallgehalt der organischen Phase nach Rückextraction mit 0,1 M Salzsäure bestimmt. Für Na, K, Rb und Sr erfolgte die Bestimmung der Verteilungsverhältnisse auf radiometrischem Wege.

ERGEBNISSE UND DISKUSSION

2-(sym-Dibenzo-14-krone-4-oxy)essigsäure

Für dieses Extraktionsmittel ist die pH-Abhängigkeit der Extraktion von Li^+, Mg^{2+} und Ca^{2+} in Abb. 1 dargestellt. Bemerkenswert ist die beachtliche Extraktion von Li^+ bei pH $\approx$ 7.

Die Abnahme der Konzentration des Lithiums in der organischen Phase bei höheren pH-Werten sollte eine Folge der bei ungenügend lipophilen, ionisierbaren Kronenethern beobachteten hohen Wasserlöslichkeit sowohl des entstehenden Metallkomplexes als auch des unter basischen Bedingungen ausschließlich vorliegenden Kronenethercarbonsäureanions sein [5]. Die Erdalkalimetalle werden von der Kronenetheressigsäure insbesondere bei hohen pH-Werten besser als Lithium extrahiert.

Besonders auffällig ist das Extraktionsverhalten des Liganden gegenüber

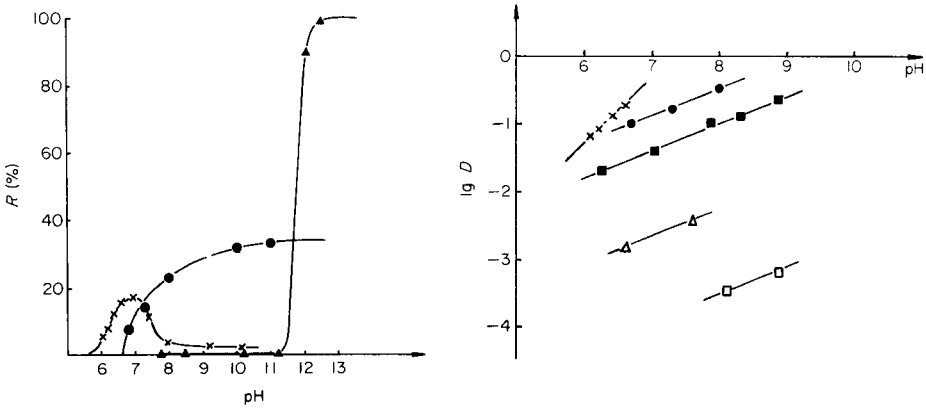

Abb. 1. pH-Abhängigkeit der Extraktion mit 2-(sym-Dibenzo-14-krone-4-oxy)essigsäure: (•) Ca^{2+}; (▲) Mg^{2+}; (X) Li^+. Exp. Bedingungen entsprechend (a).

Abb. 2. Lg D/pH-Darstellung der Extraktion mit 2-(sym-Dibenzo-14-krone-4-oxy)essigsäure: (•) Ca^{2+}; (▪) Sr^{2+}; (X) Li^+; (△) Na^+; (□) Rb^+. Exp. Bedingungen entsprechend (a) für Ca^{2+} und Li^+ bzw. (b) für Sr^{2+}, Na^+ und Rb^+.

Magnesium. Hier wurde bis zum pH-Wert 11,5 keine Veränderung der Magnesiumkonzentration in der Wäßrigen Phase gefunden. Erst bei einem pH-Wert von 12 sank der Magnesiumgehalt der wäßrigen Phase fast augenblicklich auf Null. Dieser sprunghafte Übergang des Magnesiums in die organische Phase wird auf die Bildung eines kolloiden Systems zwischen $Mg(OH)_2$ und dem Extraktionsmittel zurückgeführt [16].

In Abb. 2 ist das Verteilungsverhältnis D_M in Abhängigkeit vom Gleichgewichts-pH-Wert der wäßrigen Phase für Li^+, Na^+, Rb^+, Ca^{2+} und Sr^{2+} dargestellt. Der Anstieg der Geraden ist dabei für Li^+ ca. 1, für Ca^{2+}, Sr^{2+}, Rb^+ und Na^+ aber nur ca. 0,5. Dieses Ergebnis deutet im Falle von Li^+ auf die aufgrund der Größenverhältnisse (d_{Li^+} = 0,12 nm, $d_{14\text{-Krone-4}}$ = 0,12—0,15 nm) erwartete Komplexzusammensetzung von 1:1 hin. Die geringeren Werte für Ca^{2+}, Sr^{2+}, Rb^+ und Na^+ sind offensichtlich eine Folge der bereits diskutierten Löslichkeitsverhältnisse in wäßriger Lösung insbesondere bei pH-Werten $\geqslant 7$. Das bestätigen Ergebnisse von Extraktionsuntersuchungen für Ca^{2+}, Sr^{2+}, Rb^+, Na^+ und Li^+ bei konstantem pH-Wert und wechselnder Ligandkonzentration. Wie Abb. 3 zeigt, ergibt sich der Anstieg für Li^+ zu ≈ 1 und korreliert damit mit der pH-Abhängigkeit und der Röntgenstrukturanalyse des kristallinen Komplexes, über die Bartsch u.a. berichtet haben [15]. Für die größeren Metallionen Na^+, Rb^+, Ca^{2+} und Sr^{2+} beobachtet man demgegenüber einen Anstieg von ≈ 2, so daß entsprechend den Größenverhältnissen von Kationen- zu Hohlraumdurchmesser 2:1-Komplexe mit Sandwich-struktur gebildet werden.

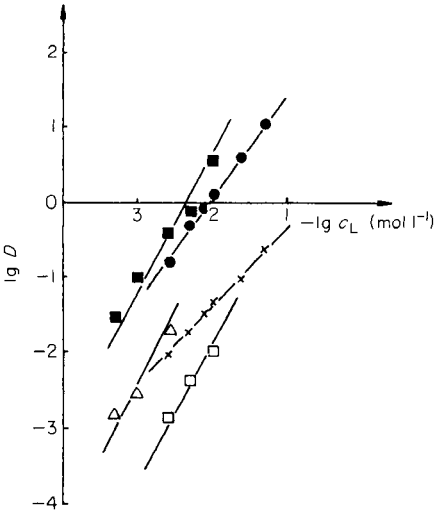

Abb. 3. Abhängigkeit des Verteilungsverhältnisses von der Ligandkonzentration für 2-(sym-Dibenzo-14-krone-4-oxy)essigsäure: (•) Ca^{2+}; (▪) Sr^{2+}; (×) Li^+; (△) Na^+; (□) Rb^+. Exp. Bedingungen entsprechend (c).

Extraktion mit 2-(sym-Dibenzo-14-krone-4-oxy)hexansäure

Die Abhängigkeit der Extraktion für Ba^{2+}, Ca^{2+}, Mg^{2+} und Li^+ vom pH-Wert ist in Abb. 4 wiedergegeben. Die lg D/pH-Darstellungen zeigen die Abb. 5 und 6. Im Vergleich zum Essigsäurederivat des Kronenethers zeigt die

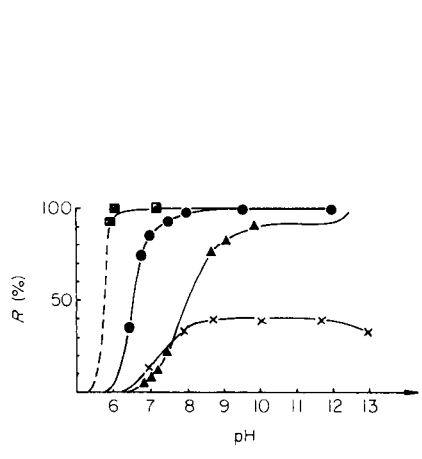

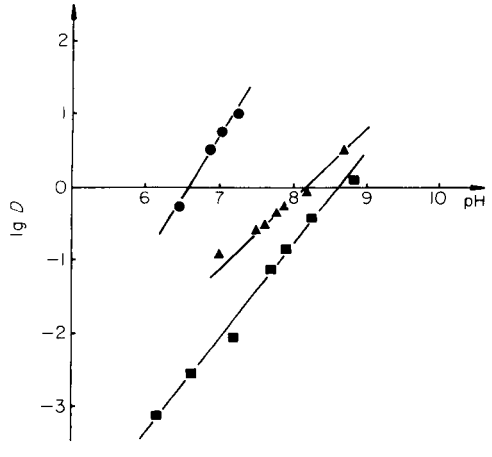

Abb. 4. pH-Abhängigkeit der Extraktion mit 2-(sym-Dibenzo-14-krone-4-oxy)hexansäure: (▲) Mg^{2+}; (•) Ca^{2+}; (▪) Ba^{2+}; (×) Li^+. Exp. Bedingungen entsprechend (a).

Abb. 5. Lg D/pH-Darstellung der Extraktion von Erdalkali-ionen mit 2-(sym-Dibenzo-14-krone-4-oxy)hexansäure: (▲) Mg^{2+}; (•) Ca^{2+}; (▪) Sr^{2+}. Exp. Bedingungen entsprechend (a) für Mg^{2+} und Ca^{2+} bzw. (b) für Sr^{2+}.

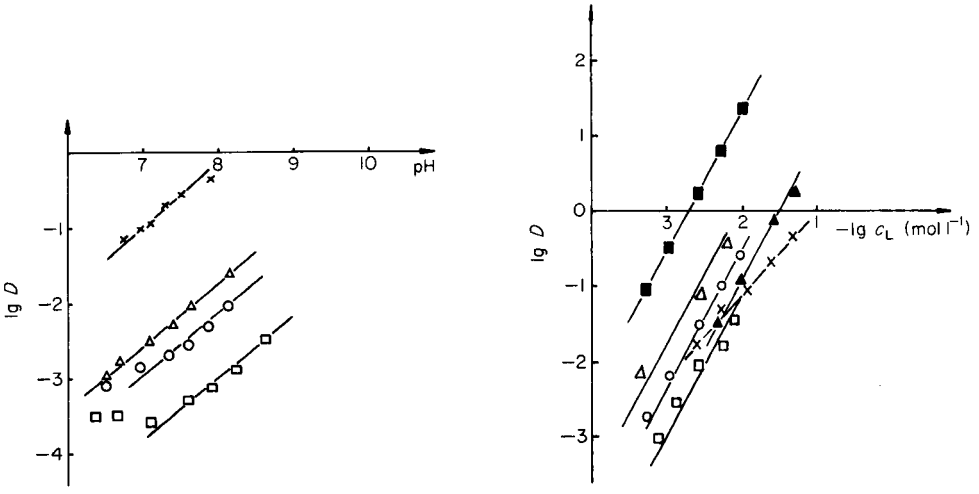

Abb. 6. Lg D/pH-Darstellung der Extraktion von Alkali-ionen mit 2-(sym-Dibenzo-14-krone-4-oxy)hexansäure: (×) Li^+; (△) Na^+; (○) K^+; (□) Rb^+. Exp. Bedingungen entsprechend (a) für Li^+ bzw. (b) für Na^+, K^+ und Rb^+.

Abb. 7. Abhängigkeit des Verteilungsverhältnisses von der Ligandkonzentration für 2-(sym-Dibenzo-14-krone-4-oxy)hexansäure: (×) Li^+; (△) Na^+; (○) K^+; (□) Rb^+; (▲) Mg^{2+}; (■) Sr^{2+}. Exp. Bedingungen entsprechend (c).

n-Hexansäureverbindung eine deutliche Erhöhung der Extraktionsfähigkeit. Dies ist in erster Linie durch die erheblich gesteigerte Lipophilie des Liganden sowohl in neutraler als auch ionisierter Form begründet. Auffällig ist weiterhin die deutliche Bevorzugung der Extraktion von Erdalkali-ionen im Vergleich zu den Alkali-ionen. Für erstere kann in allen Fällen bei entsprechender Wahl der Bedingungen eine quantitative Extraktion erreicht werden. Systeme, die den neutralen Kronenether bzw. eine langkettige Carbonsäure allein oder im Gemisch enthalten, zeigen unter analogen Bedingungen kein derartig gutes Extraktionsvermögen. Bemerkenswert ist auch die relativ hohe Extrahierbarkeit des Li^+ von ca. 40% bei pH $\geqslant 8$ ($c_L = 10^{-2}$ M).

Die graphische slope-Analyse der Kurven im lg D/pH-Diagramm (Abb. 5 und 6) zeigt, daß im Falle von Ca^{2+} und Sr^{2+} jeweils zwei Wasserstoffionen pro Metallion, bei Na^+, K^+ und Rb^+ aber jeweils eines ausgetauscht werden. Die Zusammensetzung der extrahierten Komplexe ergibt sich entsprechend Abb. 7 aus den Anstiegen der Geraden im lg D/lg c_L-Diagramm für alle untersuchten Metallionen mit Ausnahme von Li^+ zu 2:1 für das Verhältnis Ligand:Metallion. Die Ausbildung von 2:1-Komplexen ist eine allgemein beobachtete Erscheinung bei derartigen Komplexbildnern, wenn der Metallionendurchmesser größer als der Durchmesser des Kronenetherhohlraumes ist. Allerdings müssen im vorliegenden Fall die 2:1-Komplexe der Alkalimetallionen offensichtlich aus einem ionisierten und einem neutralen Kronenethermolekül aufgebaut sein, während im Falle der Erdalkaliionen zwei

Kronenethercarboxylatanionen im gebildeten Komplex vorliegen müssen (vgl. Abb. 6 und 7). Dabei führt die Bindung der Erdalkalimetallionen an zwei Carboxylationen zu einem wesentlichen Anwachsen der Komplexstabilität [18]. Damit dürften die strukturellen Unterschiede, die sich für Alkali- und Erdalkali-metallionen ergeben, die Ursache für die relativ großen Unterschiede in der Extrahierbarkeit sein.

Für Li^+ ergibt sich erwartungsgemäß die Bildung einer 1:1-Verbindung. Die Selektivitätsreihen $Ba^{2+} > Ca^{2+} > Sr^{2+} > Mg^{2+}$ und $Na^+ > K^+ \geqslant Li^+ > Rb^+$ stimmen mit den für ähnliche Verbindungen erhaltenen Ergebnisse überein [17]. Aufgrund der unterschiedlichen Komplexzusammensetzungen der extrahierten Metallkomplexe (1:1 bzw. 2:1) hängen die Selektivitätsunterschiede entscheidend von den gewählten experimentellen Bedingungen (pH-Wert, Konzentration des Extraktionsmittels) ab.

Herrn Dr. M. Raab, Akademie der Wissenschaften der DDR, Zentralinstitut für Ernährung, Potsdam-Rehbrücke danken wir für die Durchführung von AAS-Bestimmungen.

LITERATUR

1 R. A. Bartsch, U.S. Pat. 4,421,923 (1983).
2 R. A. Bartsch, Y. Liu, S. I. Kang, B. Son, G. S. Heo, P. G. Hipes und J. B. Bills, J. Org. Chem., 48 (1983) 4864.
3 R. A. Bartsch, G. S. Heo, S. I. Kang und J. Strzelbicki, J. Org. Chem., 47 (1982) 457.
4 J. Strzelbicki, G. S. Heo und R. A. Bartsch, Sep. Sci. Technol., 17 (1982) 635.
5 J. Strzelbicki und R. A. Bartsch, Anal. Chem., 53 (1981) 1894.
6 G. S. Heo, R. A. Bartsch, L. L. Schlobom und J. G. Lee, J. Org. Chem., 46 (1981) 3574.
7 W. A. Charewicz und R. A. Bartsch, Anal. Chem., 54 (1982) 2300.
8 J. Strzelbicki und R. A. Bartsch, Anal. Chem., 53 (1981) 2251.
9 W. A. Charewicz, G. S. Heo und R. A. Bartsch, Anal. Chem., 54 (1982) 2094.
10 B. Czech, B. Son und R. A. Bartsch, Tetrahedron Lett., 24 (1983) 2923.
11 B. Czech, A. Czech und R. A. Bartsch, Org. Prep. Proc. Int., 15 (1983) 349.
12 T. M. Fyles, C. A. McGawin und D. M. Whitfield, J. Org. Chem., 49 (1984) 753.
13 T. M. Fyles und D. M. Whitfield, Can. J. Chem., 62 (1984) 507.
14 L. M. Dulyea, T. M. Fyles und D. M. Whitfield, Can. J. Chem., 62 (1984) 498.
15 G. Shoham, D. W. Christianson, R. A. Bartsch, G. S. Heo, U. Olsher und W. N. Lipscomb, J. Am. Chem. Soc., 106 (1984) 1280.
16 J. Strzelbicki und R. A. Bartsch, Anal. Chem., 53 (1981) 2247.
17 R. A. Bartsch, W. A. Charewicz und S. J. Kang, Proceedings ISEC 83, Denver 1983, Paper No. 27d, S.369.
18 J. M. Lehn, Struct. Bonding, Berlin, 16 (1973) 15.

Analytica Chimica Acta, 185 (1986) 287—294
Elsevier Science Publishers B.V., Amsterdam — Printed in The Netherlands

DETERMINATION OF GLYCEROL, 1,2-PROPANEDIOL AND TRIGLYCERIDES BY HIGH-PERFORMANCE LIQUID CHROMATOGRAPHY AND A POST-COLUMN REACTOR CONTAINING IMMOBILIZED GLYCEROL DEHYDROGENASE

NOBUTOSHI KIBA*, KAZUYUKI GOTO[a] and MOTOHISA FURUSAWA

Department of Chemistry, Faculty of Engineering, Yamanashi University, Kofu 400 (Japan)

(Received 10th May 1985)

SUMMARY

A fluorimetric method is described for the determination of glycerol, 1,2-propanediol and triglycerides in serum by high-performance liquid chromatography with an on-line post-column reactor containing immobilized glycerol dehydrogenase. Before separation, triglycerides are cleaved with lipase and esterase. The polyhydric alcohols are separated from each other on a Finepak SIL C_{18} (10 μm) column with water as eluent. The NADH produced from the enzymatic reaction is monitored by fluorimetry. Calibration curves are linear between 0.01 mM and 1.0 mM for glycerol or 2.0 mM for 1,2-propanediol. The method gave satisfactory results for control sera.

Triglyceride determinations are important in clinical diagnosis, so that reliable, selctive and economic methods are in demand. Determinations have been based on enzymatic hydrolysis with lipase, followed by the enzymatic determination of glycerol with glycerol kinase, pyruvate kinase and lactate dehydrogenase, or glycerol kinase and glycerol-3-phosphate dehydrogenase [1—5]. The enzymes are expensive.

Although there are many methods that utilize glycerol dehydrogenase (E.C. 1.1.1.6) for glycerol determinations [6—10], the enzyme suffers from lack of selectivity; it oxidizes not only glycerol (1,2,3-propanetriol) but also 1,2-ethanediol, 1,2-propanediol and 1,2-butanediol. In practice, the plasma of patients receiving continual therapy contains large amounts of 1,2-propanediol, which is widely used in the pharmaceutical industry as a solvent for drugs in intravenous and oral dosages and as a stabilizer for vitamins. From a practical point of view, the polyhydric alcohols must be separated from each other prior to the enzymatic determinations.

Mixtures of polyhydric alcohols have been separated by high-performance liquid chromatography (h.p.l.c.) on ion-exchange or reversed-phase columns

[a]Present address: Department of Research and Development, Hakubakumai Co. Ltd., Masuho-cho 400-05, Japan.

0003-2670/86/$03.50

and detected by refractometry. Although a combination of h.p.l.c. and an immobilized enzyme reactor necessarily causes additional band broadening, the additional selectivity provided by the post-column reaction tends to offset the loss in resolution. Glycerol dehydrogenase has been immobilized onto the inner surface of nylon tubing and used as a reactor for triglyceride determinations in a continuous-flow system [11, 12]. Open-tubular reactors are, however, unsuitable for the post-column reactor [13], and packed-bed reactors are better for keeping the resolution as intact as possible.

In this paper, glycerol dehydrogenase is covalently bound to alkylamine on polystyrene beads by the glutaraldehyde immobilization method. The immobilized enzyme column is used for the on-line detection of chromatographically separated polyhydric alcohols. Nicotinamide adenine dinucleotide (NADH), which is generated in the enzymatic reaction, is monitored in a flow-through fluorimetric detector, which provides high sensitivity. The h.p.l.c. system is applied to the assays of glycerol, 1,2-propanediol and triglycerides in serum. Triglycerides were first hydrolysed with lipase and esterase.

EXPERIMENTAL

Chemicals

All chemicals were of analytical grade. Chloromethylated polystyrene beads (Bio-Beads S-X1, 200—400 mesh, 1.25 meq g^{-1}) were purchased from Bio-Rad Laboratories, Richmond, CA; 1,8-diamino-4-aminomethyloctane from Asahi Kasei, Osaka; NAD (grade I) from Boehringer Mannheim; glycerol dehydrogenase (52.8 U mg^{-1} of solid, *Cellulomonas sp.*) from Toyobo, Osaka; Lipase (2940 U mg^{-1} of protein) and esterase (160 U mg^{-1} of protein) from Sigma Chemical Co. Phosphate buffer (K_2HPO_4/NaH_2PO_4, 0.01 M, pH 7.0) and carbonate buffer ($NaHCO_3/K_2CO_3$, 0.1 M, pH 10.0) were prepared. The NAD solution (10 mM) was prepared daily in the phosphate buffer. Glycerol, 1,2-ethanediol, 1,2-propanediol, 1,2-butanediol, and Tween-20 were obtained from Nakarai Chemicals, Kyoto.

Preparation of the immobilized enzyme column reactor

Chloromethylated polystyrene beads (10 g) were left to swell in 200 ml of benzene and then 10 ml of 1,8-diamino-4-aminomethyloctane was added. After refluxing with stirring for 10 h, the beads were filtered on a Büchner funnel, and washed successively with 50 ml of benzene, 100 ml of methanol, 100 ml of (1 + 100) hydrochloric acid and 200 ml of water. A stainless-steel column (250 mm × 4.0 mm) was fitted with a stainless-steel filter (3 μm) at the bottom and a packing column at the top, and then filled with the phosphate buffer. The aminoalkylated beads were slurried for 10 min in an ultrasonic bath and poured into the packing column, which was connected to a pump. For 1 h, the phosphate buffer was pumped through the column, maintaining a pressure of 50 kg cm^{-2} and a temperature of 40°C. The packing

column was disconnected, fitted with a stainless-steel filter (10 μm) and connected to the h.p.l.c. pump. Glutaraldehyde (2.5%) in the phosphate buffer (60 ml) was pumped through the column for 2 h at a flow rate of 0.5 ml min^{-1} at 30°C, followed by water for 5 h at a flow rate of 1.0 ml min^{-1}. Enzyme solution (30 ml) which contained 10 mg of glycerol dehydrogenase in the phosphate buffer was circulated through the column at 20°C. The temperature of the enzyme solution in the reservoir was kept at 4°C throughout the immobilization procedure. The column was washed with the NAD solution.

Apparatus

The h.p.l.c. apparatus and the immobilized enzyme column reactor are shown in Fig. 1. The h.p.l.c. apparatus consisted of a reciprocating pump, BIP 1 (JASCO, Tokyo) and a sampling valve, KHP U1-130 (Kyowa Seimitsu, Tokyo) with a 100-μl loop. A 100-μl aliquot of the sample solution was injected onto a column (500 × 4.6 mm) of Finepak SIL C_{18} (10 μm; JASCO) with a guard column (30 × 4 mm) containing Shodex ODS (5 μm) with water as mobile phase (1.0 ml min^{-1}). The analytical column temperature was ambient. The detection system consisted of a four-way connector, a reactor and a Hitachi fluorescence spectrophotometer, 650-10S, fitted with a flow cell (volume 18 μl). The NAD solution and the carbonate buffer (pH 10.0) were added via a double-plunger pump, KHU-W-52 (Kyowa Seimitsu), both at flow rates of 0.5 ml min^{-1}. The reactor was thermostated at 40 ± 0.2°C. The fluorimeter was operated at λ_{ex} = 348 nm and λ_{em} = 465 nm. All tubing used was made of stainless-steel (0.25 mm i.d. × 1/16-in. o.d.).

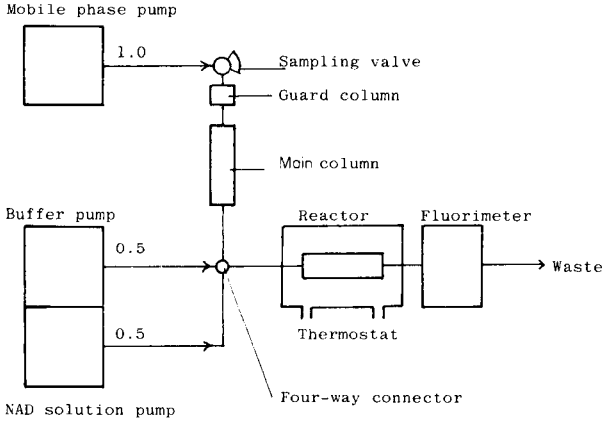

Fig. 1. Schematic diagram of the system. The numbers on the lines are flow rates in ml min^{-1}. Mobile phase, water; buffer, $NaHCO_3/K_2CO_3$, 0.1 M, pH 10.0; NAD solution, 10 mM in phosphate buffer (0.01 M, pH 7.0). See text for further detail.

Procedures

Determination of glycerol and 1,2-propanediol. Sample serum (1.0 ml) was diluted with the phosphate buffer (1.0 ml) and an aliquot was injected onto the column. Calibration graphs were obtained by plotting concentration of glycerol or 1,2-propanediol against peak height.

Determination of triglycerides. To 1.0 ml of sample serum were added 3.0 ml of the phosphate buffer, 1.0 ml of lipase, 0.2 g of esterase and 0.5 ml of Tween 20. The mixture was incubated for 15 min at 30°C. The supernatant liquid was withdrawn from the suspension with a syringe through a column guard (pore size 0.45 μm). An aliquot of the solution was injected onto the column. The concentration of triglycerides was calculated from the calibration graph for glycerol.

After all the measurements, the system was washed with the phosphate buffer and the column reactor was kept at room temperature.

RESULTS AND DISCUSSION

Characterization of the immobilized enzyme column reactor

The effect of pH on the enzymatic reaction for glycerol as substrate was studied in carbonate buffers in the range 9.0—11.0 for both free and immobilized enzymes. The free enzyme was examined by using an enzyme solution (10 U ml^{-1}), prepared by dissolving the enzyme in the NAD solution, and a reaction tube (PTFE, 50 cm × 1.0 mm i.d.) instead of the column reactor. Figure 2A shows the pH-dependence of the activity of the free and immobilized enzymes. The optimum pH for the free enzyme was 9.0 and immobilization shifted the maximum to pH 10.0. Carbonate buffers giving pH 10.0 were examined under similar conditions. The buffers which were prepared from only sodium salts or potassium salts did not give stable results and the activity of the immobilized enzyme was gradually reduced. Buffers containing $NaHCO_3/K_2CO_3$ or $Na_2CO_3/KHCO_3$ gave satisfactory

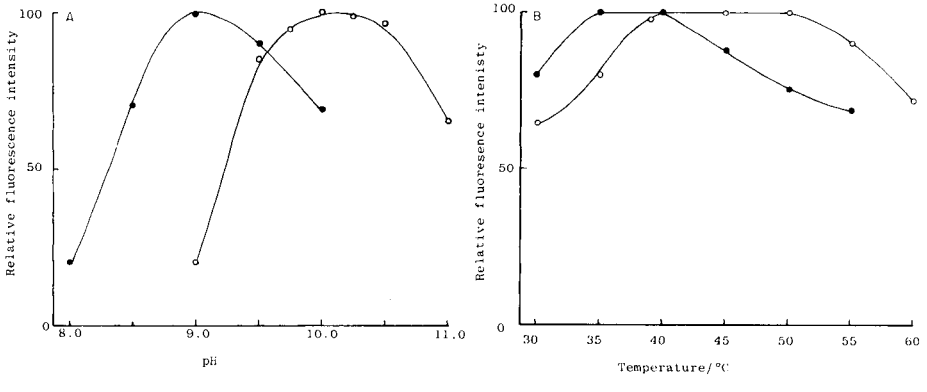

Fig. 2. Effect of pH (A) and temperature (B) on the apparent activity of free and immobilized glycerol dehydrogenase: (●) free enzyme; (○) immobilized enzyme.

results. These results may indicate that the activating effect of K^+ on the enzymatic reaction compensates for the inhibitory effect of Na^+ [14].

The effect of temperature was examined in a similar manner to the pH effect. The free and immobilized enzymes showed maximal activity at 35–40°C and 40–50°C, respectively (Fig. 2B).

The effect of flow rate was examined as follows. The eluent (water) was pumped at a flow rate of 1.0 ml min^{-1} and the flow rate of the carbonate buffer was varied together with that of the NAD solution. The results (Fig. 3) show that the maximum peak height (relative fluorescence intensity) was at a flow rate of 2.0 ml min^{-1}, while greater peak area was obtained at lower flow rates. The decrease in peak height at low flow rates can be explained by peak broadening.

The selectivity of the immobilized enzyme was examined over 60 days. The results are listed in Table 1. The enzyme showed slow reaction with 1,3-butanediol and 2,3-butanediol, and no reaction with 1,3-propanediol or 1,4-butanediol. Great variation in activity arose mainly during the first five days after the preparation of the immobilized enzyme column, and subsequently, the activity for glycerol decreased gradually. But 50% of the activity still remained even after 60 days. When stored at 4°C in the presence of phosphate buffer (K_2HPO_4/NaH_2PO_4, 0.1 M, pH 7.0) in column form, the immobilized enzyme was stable for at least 3 months.

A large excess of NAD favoured the oxidation reactions; 10 mM NAD was chosen because of its high price.

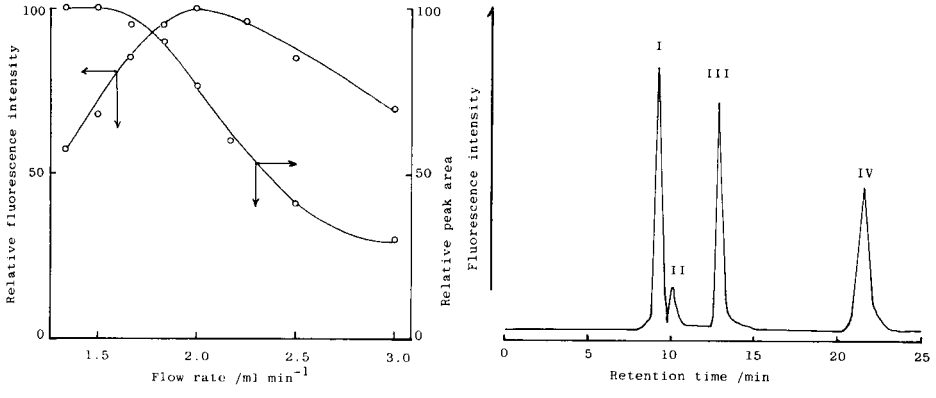

Fig. 3. Effect of flow rate on the peak height and peak area.

Fig. 4. Separation of a mixture of polyhydric alcohols. Sample, 100 µl; mobile phase, water at 1.0 ml min^{-1}; buffer, $NaHCO_3/K_2CO_3$ solution (0.1 M, pH 10.0) at 0.5 ml min^{-1}; NAD solution, 10 mM in phosphate buffer at 0.5 ml min^{-1}; separation column, 500 mm × 4.6 mm i.d., Finepak SIL C_{18}. Peaks: (I) glycerol; (II) 1,2-ethanediol; (III) 1,2-propanediol; (IV) 1,2-butanediol.

TABLE 1

Selectivity of the immobilized glycerol dehydrogenase

Day	Relative activity[a]			
	Glycerol	1,2-Propanediol	1,2-Butanediol	1,2-Ethanediol
1	100	91	83	15
2	100	93	86	15
3	85	100	91	14
4	78	100	93	10
5	75	100	97	9
6	73	100	100	9
10	70	100	100	9
20	65	100	100	9
30	63	100	100	9
40	60	100	100	9
50	53	96	100	9
60	52	94	100	9

[a]The peak based on the most active substrate in each day was taken as 100.

Separation

The h.p.l.c. separation of glycerol, 1,2-ethanediol, 1,2-propanediol and 1,2-butanediol was studied with the immobilized enzyme column reactor. Mixtures of polyhydric alcohols have been separated by h.p.l.c. on an aminopropyl column, with water/acetonitrile (1:5) as mobile phase [15]. The use of an organic solvent was unsuitable here because 10% acetonitrile destroyed the immobilized enzyme. Although high resolution was obtained with an ion-exchange column (Shodex Ionpak CH-801, 600 mm × 8.0 mm i.d.) with water at 1.0 ml min^{-1} as eluent, the retention times of the different compounds were affected by changes in the concentrations of ions in the sample. The mixture was well resolved on a Finepake SIL C_{18} (10 μm; 500 mm × 4.6 mm i.d.) column, as shown in Fig. 4. The separation parameters of the compounds are listed in Table 2.

TABLE 2

Separation parameters for polyhydric alochols

Polyhydric alochols	Retention time (min)	Capacity factor (k')	Resolution	Separation factor (α)
Glycerol	9.2	0.25		
1,2-Ethanediol	10.2	0.36	1.00	1.44
1,2-Propanediol	13.0	0.71	1.87	1.97
1,2-Butanediol	21.4	1.93	3.36	2.72

TABLE 3

Results for glycerol, 1,2-propanediol and triglycerides in control sera[a]

Compound	Mean found (mM)	Relative standard deviation (%)[b]		Certified value (mM)
		Within day	Day-to-day	
Glycerol	0.21	3.5	4.0	0.21
1,2-Propanediol[c]	4.0	2.3	2.4	4.0
Triglycerides	1.50	3.8	3.9	1.54

[a]Precinorm S, lot 21-611, for glycerol and Precilip, lot 1.375, for triglycerides. [b]$n = 10$. [c]1,2-Propanediol was added to the Precinorm S.

Calibration graphs were prepared for glycerol, 1,2-propanediol and 1,2-butanediol, covering the range 0.01– 5.0 mM. The upper limits were lowered with decreasing activity of the immobilized enzyme, owing to the downward curvature of the plots. The calibration graphs for glycerol, 1,2-propanediol and 1,2-butanediol were linear up to 1.0 mM, 2.0 mM and 2.0 mM, respectively. The plot of peak height against concentration of the compounds was linear and passed through the origin.

Application

Table 3 lists the results obtained by the h.p.l.c. analysis of a control serum for the determination of free glycerol and 1,2-propanediol. The serum used Precinorm S from Boehringer Mannheim. 1,2-Propanediol was added to the serum. Table 3 also includes results for the determination of triglycerides in a Precilip control serum from Boehringer Mannheim. All these results agree well with the certified values and are reproducible.

Conclusion

Glycerol dehydrogenase immobilized on polystyrene beads provides a highly active enzyme column reactor. The stability of the enzyme to changes in temperature and pH in storage is enhanced by the immobilization. Band broadening in the column reactor is minimized by the close packing of the beads in the stainless-steel column, which has excellent mechanical features. The use of the post-column reactor in h.p.l.c. provides a selective, reliable and fairly economic method for the determination of glycerol, 1,2-propanediol and triglycerides.

REFERENCES

1 G. Bucolc and H. David, Clin. Chem., 19 (1973) 476.
2 A. R. MacRae, Clin. Biochem., 10 (1977) 16.
3 G. Lehnus and L. Smith, Clin. Chem., 24 (1978) 27.
4 P. Schwandt, W. O. Richter and N. Kriegisch, Clin. Chem., 27 (1981) 512.
5 V. R. Lauderdale, U.S. Pat. 4309502, January 1982.
6 M. G. Gore, Anal. Biochem., 75 (1976) 604.

7 L. H. Boobis and R. J. Maughan, Clin. Chim. Acta, 132 (1982) 173.
8 A. K. Chen, J. A. Starzmann and C. C. Liu, Biotechnol. Bioeng., 24 (1982) 971.
9 A. S. Attiyat and G. D. Christian, Analyst (London), 105 (1980) 154.
10 T. A. Kelly and G. D. Christian, Analyst (London), 109 (1984) 453.
11 W. Hinsch and P. U. Sundaram, Clin. Chim. Acta, 104 (1980) 87.
12 W. Hinsch, W.-D. Ebersbach and P. V. Sundaram, Clin. Chim. Acta, 104 (1980) 95.
13 R. S. Deelder, A. T. J. M. Kuijpers and Van Den Berg, J. Chromatogr., 259 (1983) 545.
14 E. C. C. Lin and B. Magasanik, J. Biol. Chem., 285 (1960) 1820.
15 R. Schwarzenbach, J. Chromatogr., 117 (1976) 206.

Analytica Chimica Acta, 185 (1986) 295—306
Elsevier Science Publishers B.V., Amsterdam — Printed in The Netherlands

CHELATE AND INTRAMOLECULAR ION-PAIR FORMATION
A Guiding Concept for Structure/Selectivity Relationships in the Liquid-Liquid Extraction of Alkali and Alkaline Earth Metal Ions by Anionic Crown Ether Derivatives

YOSHIKI KATAYAMA, RYUJI FUKUDA and MAKOTO TAKAGI*

Department of Organic Synthesis, Faculty of Engineering, Kyushu University, Hakozaki, Higashi-ku, Fukuoka 812 (Japan)

(Received 31st December 1985)

SUMMARY

Crown ether dyes with pendent anionic side-arms were synthesized for extraction-spectrophotometry of alkali and alkaline earth metal ions. Dramatic changes in metal selectivity were obtained simply by changing the nature of the anionic side-arm on the same crown ether skeleton. A structure/metal selectivity relationship is discussed in detail in terms of "chelate" and "intramolecular ion-pair" formation. Small metal cations (high charge density) are preferred in the extraction by a crown ether reagent with a charge-localized anionic side-arm through the formation of a "chelate". Large metal cations (low charge density) are preferred in the extraction by reagents with a charge-delocalized anionic side-arm through the formation of an "intramolecular ion-pair". Steric restrictions imposed by the side-arm on the metal ion approaching the crown ether are also an important factor in controlling the selectivity of these reagents.

Numerous studies have been devoted to the understanding of complex stability and metal selectivity of crown ethers since their discovery in 1967 [1]. Recently, crown ether derivatives with extra coordination sites, typically ethereal or anionic groups, on the periphery of the macrocycles have been introduced in attempts to increase metal selectivity and/or complex stability in analytical and separation chemistry as well as in biological membrane-related research [2—9].

In the course of studies in the development of spectrophotometric reagents for alkali metals, various crown ethers substituted with anionic groups have been studied for the liquid-liquid extraction of alkali metal ions. Anionic groups were found to produce quite different effects on the metal selectivity depending on their chemical nature and the location of their introduction. The concepts of chelation and intramolecular ion-pairing have been suggested in order to explain some of the peculiar metal extraction selectivities exhibited by such crown ether derivatives [2—4].

However, the concepts of chelation and intramolecular ion-pairing, which concern the mode of interaction between the crown ether—bound metal cation and the anionic side-arm of the crown ether, have remained rather

0003-2670/86/$03.50

vague and have not been founded on an experimentally firm basis. Some authors have shown that introduction of anionic groups can lead not to enhancement but to diminution of the metal-complexing selectivity of crown ethers [5, 7]. This seems to oppose the idea that the selectivity of metal complexation (or extraction) can be improved by suitable positioning of the anionic side-arm on crown ethers.

In the present paper, several new crown ether derivatives are introduced in order to clarify and refine the above-mentioned concepts, which are extended to intramolecular "contact" and "solvent-separated" ion-pairs as well as to "normal" and "sterically rigid" chelates. It is shown that extraction-spectrophotometric reagents with dramatically different metal selectivity can be obtained simply by changing the nature of the anionic side-arm on the same crown-ether skeleton.

EXPERIMENTAL

Evaluation of acidity and metal extraction constants

The crown ether reagent (3—10 mg) was weighed and dissolved in 20 ml of dioxane. The solution was diluted to 100 ml with water containing a pH buffer. The final solution contained 4×10^{-3} M each of tartaric acid, 2-(morpholino)ethanesulfonic acid (MES), *N*-[tris(hydroxymethyl)methyl]glycine and boric acid in addition to 1×10^{-4} M crown ether reagent. Aqueous 0.2 M tetramethylammonium hydroxide (TMAH) was then added dropwise to the solution to obtain the required pH. The absorption spectrum of the solution was then measured.

To evaluate the metal extraction constants, equal volumes (10 ml) of a 1,2-dichloroethane solution of the crown ether reagent and an aqueous pH-buffered solution of the metal salt were equilibrated on a mechanical shaker for 20 min at 25°C. The aqueous solution contained either 0.1 M alkali metal chloride or 1×10^{-2} M alkaline earth metal nitrate. The pH was controlled with MES, boric acid and TMAH as outlined above for the measurement of acidity constants. After centrifugation for 10 min, the absorption spectrum of the organic phase was measured in a 1-cm standard quartz cell. Extraction constants were calculated conventionally as outlined previously [10].

Synthesis of crown ether reagent

o-Nitrobenzylbromide. o-Nitrotoluene (73 mmol) and *N*-bromosuccinimide (73 mmol) were refluxed for 12 h in carbon tetrachloride in the presence of a small amount of benzoyl peroxide as radical initiator. The reaction mixture was then concentrated under reduced pressure and passed through a silica-gel column. The fraction which eluted with hexane was collected. The product was a 1:1 mixture of *o*-nitrotoluene and the desired *o*-nitrobenzyl bromide, as revealed by n.m.r. spectra. [Yellow liquid; yield 50%. ^{1}H-n.m.r. ($CDCl_3$, chemical shift from internal TMS): δ(ppm) = 7.1—8.0 (m, Ar—H), 4.8 (s, Ar—CH_2), 2.6 (s, methyl H).]

N-*(2-Nitrobenzyl)-monoaza-15-crown-5.* Monoaza-15-crown-5 (4.56 mmol), *o*-nitrobenzyl bromide (4.56 mmol) and triethylamine (18.2 mmol) were mixed and stirred in 10 ml of tetrahydrofuran (THF) for 24 h at room temperature. After removal of THF and triethylamine under reduced pressure, the residue was taken up in chloroform and washed with aqueous tartaric acid solution. The organic phase was concentrated and subjected to silica-gel column chromatography. [Yellow viscous oil; yield 98%. ^{1}H-n.m.r. ($CDCl_3$): δ = 7.2—7.9 (4H, m, Ar—H), 3.9 (2H, s, Ar—CH_2), 3.5—3.8 (16H, m, CH_2O), 2.4—2.9 (4H, t, J = 6 Hz, CH_2N).]

N-*(2-Aminobenzyl)-monoaza-15-crown-5 [11].* *N*-(2-Nitrobenzyl)-monoaza-15-crown-5 (4.46 mmol), iron(III) chloride hexahydrate (100 mg) and activated charcoal were mixed and refluxed in methanol for 10 min under nitrogen. Hydrazine monohydrate (0.01 mol) was then added to the mixture over a period of 10 min. After refluxing for 6 h, the reaction mixture was filtered. The filtrate was concentrated under reduced pressure. [Yellow viscous oil; yield 95%. ^{1}H-n.m.r. ($CDCl_3$): δ = 6.5—8.0 (4H, m, Ar—H), 4.1 (2H, s, Ar—CH_2), 3.5—3.8 (16H, m, CH_2), 2.7—2.6 (4H, t, J = 6 Hz, NCH_2).]

N-*(2-picrylaminobenzyl)-monoaza-15-crown-5 (compound 1).* *N*-(2-Aminobenzyl)-monoaza-15-crown-5 (4.24 mmol) and picryl chloride (4.46 mmol) were mixed and stirred in 10 ml of methanol for 20 min at room temperature. Then, sodium hydrogencarbonate (1 g) was added in small portions, and stirring was continued for 2 h at room temperature [12]. The reaction mixture was then concentrated, and an aqueous tartaric acid solution was added to make the mixture slightly acidic (pH 5—4). The mixture was extracted with chloroform, and the desired product in the chloroform solution was purified by silica-gel column chromatography followed by recrystallization from cyclohexane. [Orange crystals; yield 48%. ^{1}N-n.m.r. ($CDCl_3$): δ = 9.0 (2H, s, picryl H), 6.5—7.5 (4H, m, Ar—H), 3.9 (2H, s, Ar—CH_2), 3.5—3.8 (16H, m, CH_2O), 2.8—3.1 (4H, t, J = 8 Hz, NCH_2). Found: 51.7% C, 5.55% H, 13.0% N. Calculated for $C_{23}H_{29}N_5O_{10}$: 51.6% C, 5.5% H, 13.1% N.]

N,N-*Bis(2-nitrobenzyl)-diaza-15-crown-5.* The compound was synthesized analogously to *N*-(2-nitrobenzyl)-monoaza-15-crown-5. [Yellow viscous oil; yield 74%. ^{1}H-n.m.r. ($CDCl_3$): δ = 7.1—7.9 (8H, m, Ar—H), 4.0 (4H, s, Ar—CH_2), 3.4—3.7 (16H, m, CH_2O), 2.7—3.0 (8H, t, J = 8 Hz, NCH_2).]

N,N-*Bis(2-aminobenzyl)-diaza-15-crown-5.* The compound was synthesized analogously to *N*-(2-aminobenzyl)-monoaza-15-crown-5. [White solid; yield 96%. ^{1}H-n.m.r. ($CDCl_3$): δ = 6.5—8.0 (8H, m, Ar—H), 4.1 (4H, s, $ArCH_2$), 3.5—4.0 (12H, m, CH_2O), 2.7—3.1 (8H, m, NCH_2).]

N,N-*Bis(2-picrylaminobenzyl)-diaza-15-crown-5 (compound 2).* The compound was synthesized analogously to reagent 1. [Orange crystals; yield 30%. ^{1}H-n.m.r. ($CDCl_3$): δ = 9.0 (4H, s, picryl H), 6.7—7.4 (8H, m, Ar—H), 4.0 (4H, s, Ar—CH_2), 3.6—3.9 (12H, m, CH_2O), 2.8—3.2 (8H, m, NCH_2). Found: 46.15% C, 4.1% H, 14.3% N. Calculated for $C_{36}H_{38}N_{10}O_{15} \cdot 0.9\ CHCl_3$: 14.26% C, 4.1% H, 14.6% N.]

N,N-*Bis(2-nitrobenzyl)-diaza-18-crown-6.* The compound was synthesized analogously to *N*-(2-nitrobenzyl)-monoaza-15-crown-5. [Yellow viscous oil; yield 96%. ^{1}H-n.m.r. ($CDCl_3$): δ = 7.1–7.9 (8H, m, Ar–H), 4.0 (4H, s, Ar–CH_2), 3.4–3.7 (16H, t, J = 6 Hz, CH_2O), 2.7–3.0 (8H, t, J = 8 Hz, NCH_2).]

N,N-*Bis(2-picrylaminobenzyl)-diaza-18-crown-6 (compound 3).* The compound was synthesized analogously to *N*-(2-picrylaminobenzyl)-monoaza-15-crown 5 (compound 1). [Orange crystals; m.p. 207–207.7°C; yield 32%. ^{1}H-n.m.r. ($CDCl_3$): δ = 9.0 (4H, s, picryl H), 6.7–7.4 (8H, m, Ar–H), 4.0 (4H, s, Ar–CH_2), 3.6–3.9 (16H, t, J = 6 Hz, CH_2O), 2.9–3.2 (8H, t, J = 8 Hz, NCH_2). Found: 48.5% C, 4.7% H, 14.5% N. Calculated for $C_{38}H_{42}N_{10}O_{16} \cdot 0.5\ CHCl_3$: 48.5% C, 4.5% H, 14.7% N.]

RESULTS AND DISCUSSION

Synthesis of crown ether reagents

The structural formulae of the crown ether derivatives (crown ether reagents) prepared here are shown below along with analogous compounds reported in the literature. The route for the synthesis of reagent 1 is as follows:

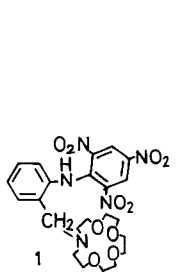

1

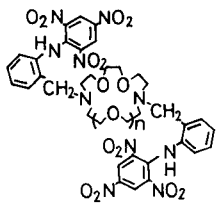

2 (n=1)
3 (n=2)

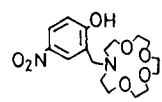

4

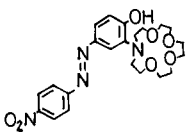

5

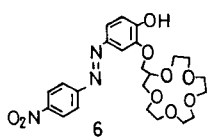

6

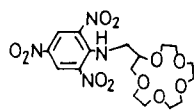

7

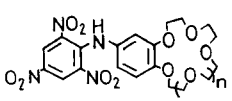

8

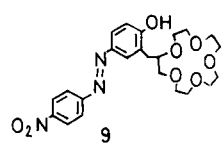

9

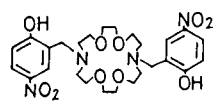

10

Monoaza-15-crown-5 was condensed with *o*-nitrobenzyl bromide to lead to *N*-(*o*-nitrobenzyl)monoaza-15-crown-5, which was then reduced to an aromatic primary amine. The reaction of the amine with picryl chloride gave reagent 1. Reagents 2 and 3 were synthesized via a similar synthetic route by

starting from diaza-crown ethers, i.e., diaza-crown ether [2.1] (Kryptofix 21; Merck) and diaza-crown ether [2.2].

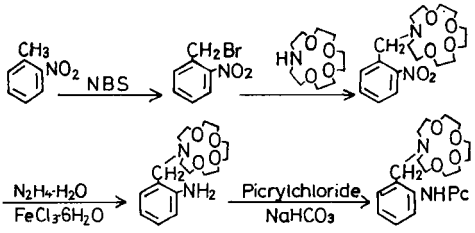

Extraction study and acidity constants

The extraction of alkali and alkaline earth metal ions was examined in a similar manner to that described before [3] in water/1,2-dichloroethane systems. The acidity constants were obtained in water containing 20% (v/v) dioxane at 25°C. The metal extraction and the acidity equilibrium constants are defined in Eqns. 1—3 for reagent 1 (HL stands for 1), and in Eqn. 4 for reagents 2 and 3 (H_2L' stands for 2 and 3). The subscripts a and o denote the aqueous and organic solutions, respectively.

$$H_2L^+ \rightleftharpoons H^+ + HL \quad : \quad K_{a1} = [H^+][HL]/[H_2L^+] \tag{1}$$

$$HL \rightleftharpoons H^+ + L^- \quad : \quad K_{a2} = [H^+][L^-]/[HL] \tag{2}$$

$$(HL)_o + (M^+)_a \rightleftharpoons (ML)_o + (H^+)_a \quad : \quad K_{ex} = [ML]_o[H^+]_a/[HL]_o[M^+]_a \tag{3}$$

$$(H_2L')_o + (M^{2+})_a \rightleftharpoons (ML')_o + 2(H^+)_a \quad : \quad K_{ex} = [ML']_o[H^+]_a^2/[H_2L']_o[M^{2+}]_a \tag{4}$$

The acidity constants for reagents 1, 4, 5, 6 and 7 are listed in Table 1. The acidity constants of reagents 2 and 3 were not obtained because of the limited solubility of these reagents in aqueous dioxane. Because the crown

TABLE 1

Acidity[a] and alkali-metal extraction constants[b] of crown ether reagents (25°C)

Crown ether	$-\log K_{a1}$	$-\log K_{a2}$	$-\log K_{ex}$			Selectivity[c]		
			Li	Na	K	Li/K	Li/Na	Na/K
1	5.55	10.2	11.80	8.90	10.10	0.020	0.0013	16
4[d]	5.79	9.69	9.15	9.76	10.4[e]	13	4.0	3.3
5[d]	8.97	11.37	8.99	9.30	10.99	100	2.0	50
6[d]		7.51	9.80	8.40	9.20	0.25	0.04	6.3
7[d]			7.1	7.41	6.1	0.1	2.0	0.05

[a]In 20% (v/v) dioxane-water. [b]Water/1,2-dichloroethane. For typical experimental conditions, see Fig. 1. [c]Ratio of extraction constants. [d]Quoted from the literature for compound 4 [13], compound 5 [4], compound 6 [14] and compound 7 [9]. [e]re-examined.

ethers reported here showed a distinct color change on dissociation of protons, the constants were readily obtained by standard spectrophotometric measurements.

The distribution of the reagent between water and 1,2-dichloroethane strongly favors the organic solution. Figure 1 shows typical spectra of the organic phase when an alkali metal ion was extracted with crown ether reagent 1 in organic solution.

Table 1 summarizes the equilibrium constants obtained in this work for the extraction of alkali metal ions by compound 1. Some related constants are quoted from the literature for other crown ether derivatives. The averaged extraction constants K_{ex} (in $-\log$ unit) for Li^+, Na^+, and K^+ extractions are about the same among reagents 1 (10.3), 4 (9.6), and 5 (9.8). The corresponding averaged constants for reagents 6 (9.1) and 7 (6.9) are lower, indicating that the extraction of metal ion takes place at lower pH. This reflects the fact that reagents 1, 4, and 5 contain a basic amino nitrogen in the crown ether ring, and the ammonium proton must be dissociated for the metal ions to bind with the crown ether [3].

"Chelate" formation and alkali metal selectivity

With regard to the metal selectivity of these crown ethers, reagent 4 shows poor extraction selectivity between the alkali metal ions. The structure of the reagent, as revealed by inspection of CPK space-filling models, allows the formation of a six-membered chelate ring which comprises an amino nitrogen, a methylene carbon, two aromatic carbons, a phenolate oxygen and the metal ion in the crown ether. The anionic side-arm, the *o*-hydroxybenzyl group, is rather flexible and provides no appreciable size-limiting effect (cf.

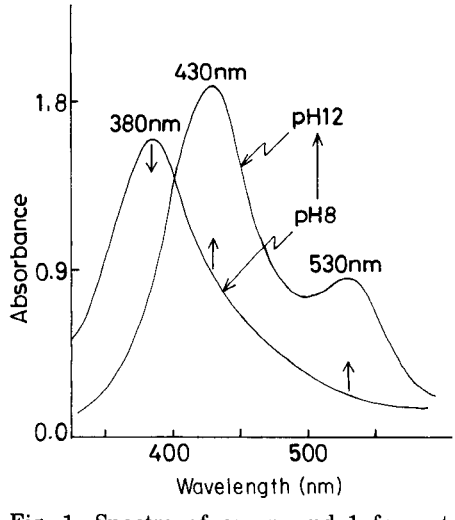

Fig. 1. Spectra of compound 1 for extraction of sodium ion at pH 8 and pH 12. 1,2-Dichloroethane (10 ml) containing 1×10^{-4} M compound 1 was equilibrated at various pH with 10 ml of aqueous solution containing 0.01 M NaCl at 25°C.

reagent 5) on the metal ions coming into the crown ether ring. Thus, the situation is similar to the case of classical metal chelates of aliphatic ligands ("normal chelate"); the metal-complexing selectivity is governed by the stability of the coordinate bond between the phenolate oxygen and the metal ion (as well as by the stability of the bond between the amino nitrogen and the metal). This factor favors the extraction of lithium. The extractability, however, is also governed by the ease of dehydration of the metal ion and by the size-selectivity of crown ethers. This factor favors the extraction of K^+ over Li^+. The metal-extraction selectivity exhibited by reagent 4 in Table 1 obviously reflects a compromise between these two factors.

Reagent 6 also provides rather poor metal-extraction selectivity. The difference between the highest extraction constant (for Na^+) and the lowest (for Li^+) is 1.40 (log unit), compared with the corresponding differences of 0.7 for reagents 4 and 1.3 for reagent 7. Formally, reagent 6 forms an eight-membered ring chelate when the phenolate oxygen on the side-arm coordinates to the metal ion in the crown ether ring. In the classical concept of chelates, eight-membered rings are unstable, and it is probable that the structure of the extracted metal complex assumes the character of an intramolecular ion-pair [14]. Some water molecules may remain in the coordination sphere of the metal and assist (or mediate) the interaction of phenolate oxygen and metal. Therefore, the metal complexes formed in the extraction by reagent 6 could be described as "loose" chelates or intramolecular ion-pairs with some intervention from water molecules. It has been mentioned before [3, 14] that a subtle change in the nature of such "loose chelate" complexes can lead to a considerable alteration of metal-extraction selectivity.

In contrast to compound 6, reagent 5 forms a five-membered metal chelate from the phenolate side-arm and the metal in the crown ether. Inspection of molecular models indicates that this chelate ring is very rigid and sterically much more confined than is the case for the six-membered metal chelates from reagent 4. The size-selectivity of the crown ether (15-crown-5) seems to also be enhanced by the presence of a capping phenolate oxygen which protrudes close to the center of the cavity of the crown ether [4]. This situation defines "rigid chelate" formation in the extracted alkali metal complexes. The extraction of potassium by compound 5 is considerably depressed, as exemplified by the Na/K selectivity of 50 as compared with the corresponding value of 1.3 for reagent 4; both reagents have the same crown ether skeleton (monoaza-15-crown-5) with a cavity size which fits the size of sodium ion. However, the extraction of both Li^+ and Na^+ is promoted. The enhancement of the lithium extraction is due to the favorable coordination interaction (i.e., stable chelate formation), while the enhanced extraction of sodium is due to both favorable coordination interaction and favorable cavity size of the crown ether ring.

The consideration of metal-extraction selectivity according to the classical concept of chelate ion is summarized in Fig. 2, which is obviously a very simplified model. A detailed comparison of the metal-extraction constants

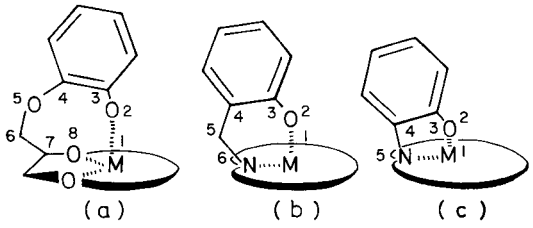

Fig. 2. Schematic representation of the structure of the extracted alkali metal complexes: (a) loose chelate (reagent 6); (b) normal chelate (reagent 4); (c) sterically-confined, rigid chelate (reagent 5).

would have to take into consideration such factors as the detailed conformation of the anionic side-arm and the basicity of the chelate-forming functional groups [3].

Intramolecular "ion-pair" complex and selectivity for alkali metals

Reagent 7 favors the extraction of potassium because the delocalized anionic charge on the picryl group stabilizes the extracted complex as an ion-pair structure rather than a chelate [9]. However, the picrylamino group in reagent 7 is quite flexible and can assume various configurations around the crown ether. Also, the anionic dipole of the *o*-nitro group can come close to the metal ion, providing some coordination interaction to the Li^+ or Na^+ held in the crown ether ring; this might account for the decreased selectivity for potassium (against Na^+ and Li^+) exhibited by reagent 7 compared with picrylamino-substituted benzo-crown-ethers [10]. The crown ether reagent 8 forms intramolecular ion-pair complexes [10, 15, 16] showing a K/Na selectivity (ratio of extraction constants) of more than 10^2 (for a benzo-18-crown-6 derivative with $n = 2$ in structure 8) and a Li/K selectivity of more than 10^4 (for a benzo-15-crown-5 derivative with $n = 1$ in structure 8). Therefore, the structures of the alkali metal complexes formed with compound 7 are considered to be somewhere between the two extreme structural possibilities of intramolecular ion-pair complex, i.e., a "solvent-separated" ion-pair and a "contact" ion-pair. An example of the former is obviously the extraction of metals by reagent 8. The latter is discussed below for reagent 1.

The extraction behavior of reagent 1 towards alkali metal ions is characterized by a relatively high selectivity for sodium ion and low selectivity for lithium ion. The Na/K selectivity of 16 is very unusual, and is unprecedented in picrylamino-substituted crown ether extractants. The pK_{a1} value, corresponding to the dissociation of picrylamino-proton, is also unusual. The acidity constant (pK_a) of this type of diarylamine (arylpicrylamine) is usually 10—11 in aqueous solution (and in aqueous solution containing 5—10% dioxane), as has been reported for reagent 8 [10, 15, 16]. The observed value of 5.55 for compound 1 is unusually low. There are no electronic factors conceivable for producing such an effect and the factor must be stereochemical.

A CPK space-filling model of compound 1 in the H_2L^+ form indicated that the molecule is extremely congested around those two nitrogen atoms unrelated to nitro groups. Proton dissociation from the picryl group somewhat releases the strain, but the conformational freedom of the side-arm is still very limited. If the crown ether-bound metal ion is to interact effectively with the anionic picrylamino group, the aromatic nucleus of the picryl group must stack in parallel with the crown ether ring (in its planar conformation). The metal complex in this conformation may be defined as an intramolecular "contact ion pair", because the metal ion in the crown ether is forced to interact directly with the delocalized anionic charge in the side-arm if the structural picture presented above is followed rigorously. The abnormalities surrounding the acidity constants and metal extractions for reagent 1 might be attributed to the steric congestion associated with the introduction of the picrylamino group; the rigid capping of the 15-crown-5 ring by the planar picrylamino group could be a major factor contributing to the high selectivity for sodium ion; there may be no room for the potassium ion to nest in the 15-crown-5 ring.

Figure 3 outlines the schematic structures of the intramolecular ion-pair complexes that can exist in organic solution. These pictures are simplified and are only qualitative, as is the case for Fig. 2. The term "chelate" means implicitly that there is a σ-bond type of interaction between the metal and a particular coordinating atom of the anionic side-arm. The exact nature of this σ-bond interaction, whether electrostatic or covalent, is not of major concern at present. Similarly, the term "ion-pair" means that there is only electrostatic interaction between the positive bulk charge (of the crown ether-bound metal ion) and the negative bulk charge of the functional group in the side-arm; no specific atom—atom interaction is implicated. In this sense, the concept of chelate applies mainly to anionic groups of relatively high basicity (localized anionic charge with low acidity constant of the conjugate acid). In contrast, the concept of intramolecular ion-pair applies to complexes in which anionic groups have low basicity (high acidity constant of the conjugate acids) or an inherently delocalized charge. The two concepts do not contradict or exclude each other; they may overlap or even cross over in some cases. For example, reagent 9, because of the peculiar orientation of its phenolic side-arm, shows a Na/K selectivity of 0.59 [3]; the metal complex of 9, therefore, may be described either as an intramolecular ion-pair (partly solvent-separated ion-pair; type b, Fig. 3) [3] or as a chelate (loose chelate; type a, Fig. 2).

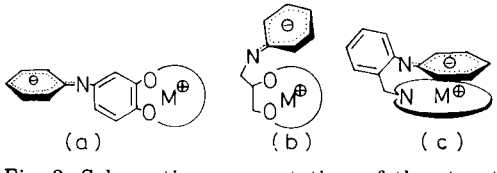

Fig. 3. Schematic representation of the structure of extracted alkali metal complexes as "intramolecular ion-pair" complexes: (a) "solvent-separated" (reagent 9); (b) "partly solvent-separated (or partly contact)" (reagent 7); (c) "contact" (reagent 1).

It is noteworthy that the difference in lithium selectivity is quite striking between reagents 1 and 5. While reagent 5 favors the extraction of lithium by a factor of 100 over the least extractable potassium, reagent 1 extracts lithium least, with a factor of only 0.0013 compared to the most favored sodium ion. Both reagents are based on the same monoaza-15-crown-5 skeleton. Therefore, this extraordinary difference in metal selectivity can only be due to the difference in the nature of the anionic side-arm.

Extraction of alkaline-earth metal ions

Another example of the dramatic effect of the anionic side-arm on extraction selectivity is found in the extraction of alkaline earth metals by reagent 3. Table 2 summarizes the extraction constants. Calcium is three hundred times more extractable than barium when reagent 10 is used as extractant [19]. When reagent 3 is used, calcium is 10^5 times less extractable than barium. Therefore, the selectivity ratio between the two reagents is more than 3×10^7 for the extraction of Ca^{2+} and Ba^{2+}. This enormous difference in metal selectivity is again caused solely by the difference in the nature of the side-arm, because the crown ether macrocycles are the same in both reagents.

The phenolic side-arm in reagent 10 most probably forms a six-membered chelate with the crown ether-bound metal ion in a similar manner to that depicted in Fig. 2b. This type of interaction helps to stabilize the calcium complex, because coordination is most effective with calcium which has the highest charge density among the three alkaline earth metals discussed. Reagent 3 would formally form a similar six-membered chelate if the anionic picrylamino group could coordinate to metal ions through its amino nitrogen. However, as has been shown with reagent 1, the charge in the picrylamino group is delocalized over the entire aromatic nucleus and the three nitro groups, and steric congestion strongly inhibits direct interaction (or coordination) of the nitrogen with metal ions. Steric hindrance on coordination of the anionic amino nitrogen has been documented with structurally-related, but even less hindered, sulfonamide ligands in their complexation and extraction of metal ions [15, 16]. These effects lead to stabilization of the ion-pair

TABLE 2

Extraction of alkaline earth metal ions by crown ether reagents (25°C)[a]

Crown ether	$-\log K_{ex}$			
	Mg	Ca	Sr	Ba
2	20	20	19.4	19.6
3	20	20	20	15.0
10[b]	16	12.5	13.5	15.1

[a]Water/1,2-dichloroethane. Experimental conditions are similar to those for Fig. 1.
[b]Cited from [19].

rather than the chelate in organic solution. Barium ion has a lower charge density than calcium ion, and therefore is more favorable for ion-pair complex formation. Moreover, its ionic diameter fits the size of diaza-18-crown-6 macrocycle. Both factors contribute to the enhanced extractability of barium by reagent 3.

Interestingly, neither reagent 2 nor 3 showed any ability to extract transition and post-transition metal ions such as Cu^{2+} and Zn^{2+}. This is in distinct contrast with the behavior of reagent 10 or its smaller-crown ether analog, both of which possess rather high extraction ability for these metal ions [17]. Obviously, the anionic picrylamino group cannot interact effectively with these metal ions which are stabilized only by forming strong coordinate bonds in spatially defined configurations.

Conclusion

The complex chemistry of alkali metal ions in solution has recently been largely concerned with the use of crown ethers as ligands. Much information has been derived from measurements of complex stability in homogeneous solution as well as metal extraction in a liquid-liquid heterogeneous system. Most of these studies have been limited to only standard or neutral crown ethers. There have been few systematic physicochemical studies on the alkali metal complexes formed from anionic ligands, especially as related to liquid-liquid extraction. The present study shows that the concepts of "chelate" and "intramolecular ion-pair" are useful in understanding the structure/metal selectivity relationship exhibited by crown ether-based anionic (proton-dissociable) extraction reagents. An immediate outcome of this approach is that it gives some guiding principles for the development of extraction-spectrophotometric reagents specific to each of the alkali and alkaline earth metal ions. These concepts, though not yet rigorous from a physicochemical point of view, are also expected to help in giving a basic picture for describing the structures of alkali and alkaline earth metal complexes in organic solution.

REFERENCES

1 R. M. Izatt and I. J. Christensen (Eds.), Synthetic Multidentate Macrocyclic Compounds, Academic Press, New York, 1978.
2 M. Takagi and K. Ueno, in F. Vögtle and E. Weber (Eds.), Topics in Current Chemistry, Host Guest Complex Chemistry III, Vol. 121, Springer-Verlag, Berlin, 1984, p. 39.
3 Y. Katayama, K. Nita, M. Ueda, H. Nakamura and M. Takagi, Anal. Chim. Acta, 173 (1985) 193.
4 Y. Katayama, H. Nakamura and M. Takagi, Anal. Sci., 1 (1985) 393.
5 A. Kaifer, D. A. Gustowski, L. Echegoyen, V. J. Gatto, R. A. Schultz, T. P. Cleary, C. R. Morgan, D. M. Goil, A. M. Rios and G. W. Gokel, J. Am. Chem. Soc., 107 (1985) 1958.
6 K. Kimura, M. Tanaka, S. Kitazawa and T. Shono, Chem. Lett., (1985) 1239.
7 R. A. Bartch, B. P. Czech, S. I. Kang, L. E. Stewart, W. Walkowiak, W. A. Charewicz, G. Heo and B. Son, J. Am. Chem. Soc., 107 (1985) 4997 and references therein.

8 K. Nakashima, Y. Yamawaki, S. Nakatsuji, S. Akiyama, T. Kaneda and S. Misumi, Chem. Lett., (1983) 1415.
9 B. P. Bubnis and G. E. Pacey, Tetrahedron Lett., 25 (1984) 1107.
10 H. Nakamura, M. Takagi and K. Ueno, Anal. Chim. Acta, 52 (1980) 1668.
11 T. Hirashima and O. Manabe, Chem. Lett., (1975) 259.
12 T. Yamashita, H. Nakamura, M. Takagi and K. Ueno, Bull. Chem. Soc. Jpn., 53 (1980) 1550.
13 H. Nakamura, H. Sakka, M. Takagi and K. Ueno, Chem. Lett., (1981) 1305.
14 H. Nakamura, H. Nishida, M. Takagi and K. Ueno, Anal. Chim. Acta, 139 (1982) 219.
15 M. Takagi, H. Nakamura and K. Ueno, Anal. Lett., 10 (1977) 1115.
16 H. Nakamura, M. Takagi and K. Ueno, Talanta, 26 (1979) 921.
17 H. Nakamura, T. Yoshida, M. Todoko, K. Ueno and M. Takagi, Bull. Chem. Soc. Jpn., 57 (1984) 2839.
18 S. Ide, T. Yoshida, S. Matsuno, M. Takagi and K. Ueno, Anal. Chim. Acta, 149 (1980) 235.
19 M. Shiga, H. Nishida, H. Nakamura, M. Takagi and K. Ueno, Bunseki Kagaku, 32 (1983) E293.

Analytica Chimica Acta, 185 (1986) 307—313
Elsevier Science Publishers B.V., Amsterdam — Printed in The Netherlands

DETERMINATION OF CADMIUM IN ENVIRONMENTAL MATERIALS BY FAST NEUTRON ACTIVATION ANALYSIS

M. ESPRIT, C. VANDECASTEELE and J. HOSTE

Institute for Nuclear Sciences, Rijksuniversiteit Gent, Proeftuinstraat 86, B-9000 Gent (Belgium)

(Received 16th December 1985)

SUMMARY

Cadmium is determined by activation analysis with fast neutrons, obtained by irradiation of a thick beryllium target with 14.5-MeV deuterons. Cadmium-111m, formed via the $^{112}Cd(n, 2n)^{111m}Cd$ and $^{111}Cd(n, n')^{111m}Cd$ reactions, is separated by liquid—liquid extraction with zinc diethyldithiocarbamate in chloroform and measured with a Ge(Li) γ-spectrometer. For low concentrations, cadmium is precipitated as cadmium ammonium phosphate after the extraction. NBS and BCR reference materials were analyzed: for concentrations between 3 and 500 $\mu g\ g^{-1}$, the relative standard deviation ranges from 5 to 3%. The results obtained for sewage sludge are compared with those obtained by reactor neutron activation analysis.

As cadmium is a very toxic pollutant, its determination in environmental samples (e.g., airborne particulate matter) is of great practical interest. This holds also for materials such as sewage sludges, where the cadmium concentration must be known in order to estimate the risk of soil and water pollution when these materials are used as fertilizers.

Atomic absorption spectrometry, inductively-coupled plasma/atomic emission spectrometry (i.c.p./a.e.s.), isotope-dilution mass spectrometry, emission spectrometry, anodic stripping voltammetry, photon activation and reactor neutron activation analysis are currently used for the determination of cadmium in environmental materials. In a recent round-robin organized by BCR, results for cadmium in the ash from a city waste incineration plant ranged from 410 to 570 $\mu g\ g^{-1}$, illustrating that, even at high concentrations, the determination of cadmium is a difficult task.

The determination of cadmium by activation analysis with fast neutrons, produced by irradiation of a thick beryllium target with 14.5-MeV deuterons, is described. The $^{112}Cd(n, 2n)^{111m}Cd$ (threshold energy, 9.5 MeV) and $^{111}Cd(n, n')^{111m}Cd$ ($Q = 0$) reactions are free from nuclear interferences under these conditions [1]. Cadmium-111m has a 48.6-min half-life and emits 245-keV γ-rays. Reactor neutron activation analysis uses the $^{114}Cd(n, \gamma)^{115}Cd$ reaction ($t_{1/2}$ = 2.224 d) [2—4].

0003-2670/86/$03.50

EXPERIMENTAL

Samples, standards and irradiation

Four types of materials were analyzed: urban particulate matter (NBS/SRM 1648), Moroccan phosphate rock (BCR/CRM 32), city waste incineration ash (BCR/CRM 176) and sewage sludge (BCR/CRM 144). For each analysis, about 0.2 g of urban particulate matter, 1 g of phosphate rock, 0.5 g of city waste incineration ash and 0.8 g of sewage sludge were used. The powders were packed in aluminium foil and compacted at the bottom of a cylindrical polyethylene container (12-mm internal diameter).

As a standard, 0.2 g of cadmium oxide (U.C.B., pro analysi) was used.

The irradiation set-up has been described by Esprit et al. [1]. The 1-mm thick beryllium target was irradiated with a 20—40-μA beam of 14.5-MeV deuterons. The samples and the standards were irradiated separately, placed directly behind the target holder. The irradiations lasted 5 min for the standards and between 20 and 60 min for the samples, depending on the cadmium concentration.

Aluminium foils (50 μm thick, 12-mm diameter) were placed on both sides of the samples and the standards. The total ^{24}Na activity ($t_{1/2}$ = 15.03 h; E_γ = 1.369 MeV) from ^{27}Al(n, α)^{24}Na, corrected for decay and for the different irradiation times and weights of the aluminium foils, was used to normalize to the same neutron flux. Because the standard is thinner than the sample, this is only accurate if the neutron flux varies linearly over the sample height. Figure 1 shows the ^{24}Na activity in 12-mm diameter aluminium foils placed at different distances from the target in a polyethylene container. Up to 10 mm from the target holder, the activity varies linearly with the distance; so, if the sample is less than 9 mm thick, the normalization procedure is accurate. The thickness of the samples ranged from 2—3 mm for urban particulate matter to 8 mm for the sludges.

Radiochemical separation

The main γ-ray peaks in a Ge(Li) γ-ray spectrum of an irradiated sample (sludge) are from ^{24}Na ($t_{1/2}$ = 15.03 h) produced by ^{27}Al(n, α)^{24}Na, ^{56}Mn ($t_{1/2}$ = 2.576 h) produced by ^{56}Fe(n, p)^{56}Mn, ^{27}Mg ($t_{1/2}$ = 9.46 min) produced by ^{27}Al(n, p)^{27}Mg, ^{29}Al ($t_{1/2}$ = 6.6 min) produced by ^{29}Si(n, p)^{29}Al and ^{41}Ar ($t_{1/2}$ = 1.83 h) from ^{41}K(n, p)^{41}Ar. The high matrix activity masks the ^{111m}Cd peaks, so that a chemical separation of ^{111m}Cd is required.

The radiochemical separation is adapted from the procedure of Wyttenbach and Bajo [5]. Cadmium is separated from acidic solution by liquid—liquid extraction with zinc diethyldithiocarbamate [Zn(DDC)$_2$] in chloroform, and back-extracted into 2 M hydrochloric acid. For concentrations below 30 μg g^{-1}, cadmium is precipitated as cadmium ammonium phosphate monohydrate after the extraction, to increase the detection efficiency.

The Zn(DDC)$_2$ is prepared by mixing aqueous equinormal solutions of sodium diethyldithiocarbamate and zinc nitrate. The Zn(DDC)$_2$ precipitate

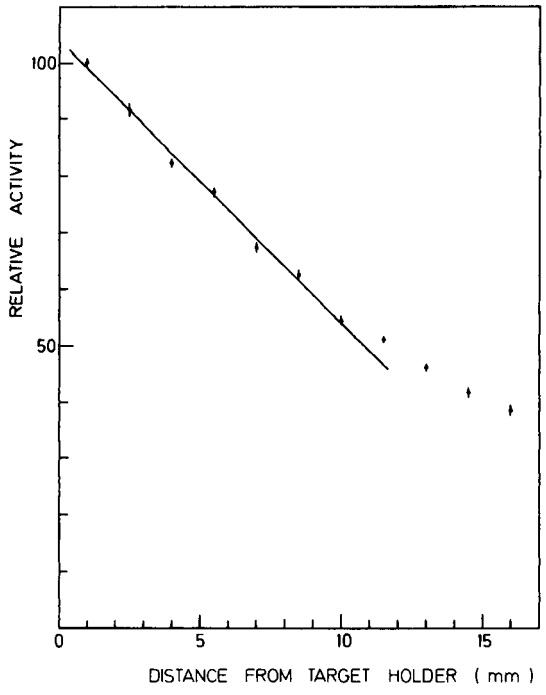

Fig. 1. Neutron flux as a function of the distance from the target holder.

is dissolved in chloroform and recrystallized by addition of ethanol and evaporation of the chloroform [5].

The procedure for the chemical separation is as follows. After irradiation, transfer the sample to a nickel crucible and mix with 5.5 g of sodium carbonate, 2.5 g of sodium hydroxide and 2 g of sodium nitrate. Heat over a Bunsen burner until fusion is complete. Dissolve the melt in 30 ml of 14 M nitric acid and wash the crucible with water. Add 0.5 mg of cadmium nitrate. Filter off the silicic acid formed. Dilute the filtrate to 150 ml and adjust the pH to 1.5—2 with ammonia. Extract twice successively by shaking the solution mechanically for 3 min with 30 ml of 0.005 M $Zn(DDC)_2$ in chloroform and collect the organic phases. Back-extract cadmium twice into 20 ml of 2 M hydrochloric acid (2 min each). Transfer the total aqueous phase to a polyethylene vial for counting.

For low concentrations, dissolve 200 mg of cadmium oxide in the hydrochloric acid solution, neutralize and heat to 80°C. Add 20 ml of 1 M diammonium hydrogenphosphate and filter off the cadmium ammonium phosphate on a glass filter covered with a membrane filter (0.8 μm pore size). Figure 2 shows a Ge(Li) γ-ray spectrum of the cadmium ammonium phosphate for phosphate rock.

For the sludge, after the liquid—liquid extraction, the 245-keV peak of ^{111m}Cd is superimposed on a high Compton-continuum, mainly from ^{56}Mn ($t_{1/2}$ = 2.576 h; E_γ = 847 keV) and ^{24}Na ($t_{1/2}$ = 15.03 h; E_γ = 1369 keV)

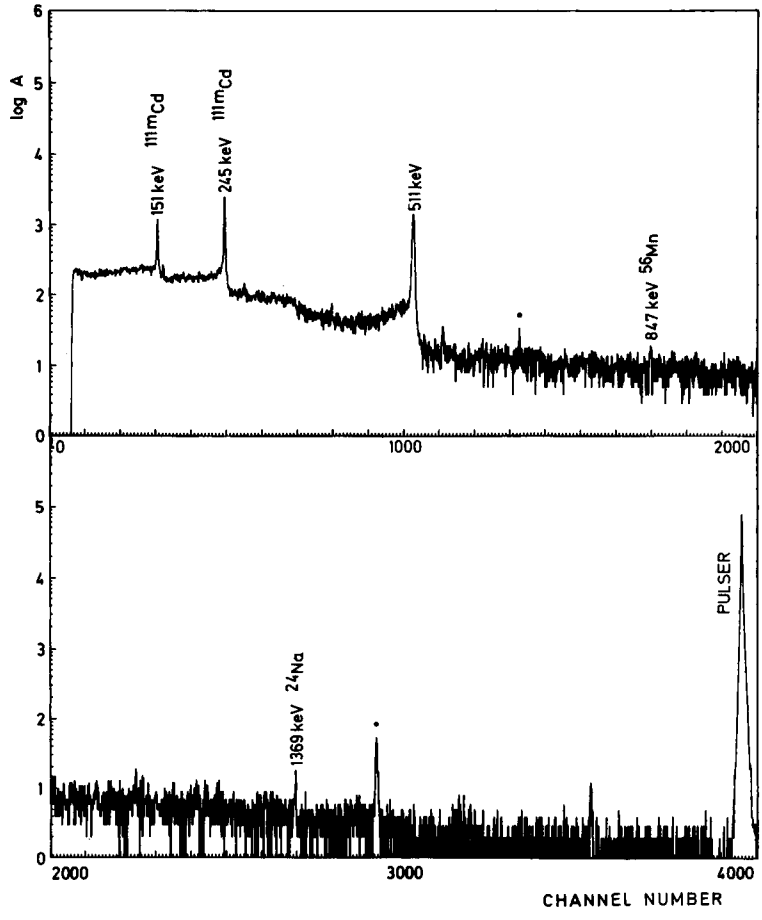

Fig. 2. The Ge(Li) γ-ray spectrum of the precipitated cadmium ammonium phosphate for phosphate rock, BCR 32. Irradiation time 60 min; beam intensity 20 μA; waiting time 65 min; measuring time 100 min.

formed from iron and aluminium, respectively. Adding sodium carbonate carrier avoids coprecipitation of ^{24}Na with the cadmium ammonium phosphate. In order to avoid precipitation of manganese as its ammonium phosphate, manganese is separated as manganese dioxide [6]: add 200 mg of cadmium oxide, 30 mg of manganese nitrate and 10 ml of 0.1 M ammonium peroxodisulphate, neutralize, heat to oxidize manganese(II) and filter off the manganese dioxide. Precipitate and filter off cadmium ammonium phosphate.

Yield of the chemical separation

The conditions for quantitative extraction of cadmium were studied by tracer experiments with ^{115}Cd ($t_{1/2}$ = 2.224 d; E_γ = 528 keV), produced by irradiation of cadmium nitrate in a nuclear reactor. For solutions containing

up to 1 mg of cadmium, one extraction at pH 2 yielded more than 97% extraction, when the solutions were shaken for at least 1 min.

The total yield of the chemical separation was evaluated by adding ^{115}Cd to an inactive sample before the separation. The yield calculated from the ^{115}Cd activity before and after the separation was 100.2% with a standard deviation of 1.3% (5 experiments) for a typical fly ash, and 99.8% with a standard deviation of 0.6% (2 experiments) for the sludge, indicating quantitative recovery.

Measurements

The Ge(Li) detector used had a relative detection efficiency of 20% and an energy resolution of 2.1 keV FWHM at 1.332 MeV. A 50-Hz pulser was used to correct for dead-time losses and pulse pile-up. The detector was coupled to a Canberra S40 multichannel analyzer, interfaced to a VAX 11/780 VMS computer. The samples were measured in polyethylene bottles or in glass filter crucibles, centred in a polyethylene ring.

Measurements of the samples started 40—70 min after the end of the irradiation, with measuring times ranging from 20 to 100 min. The standards were measured for 10 min, three hours after the irradiation, after dissolution in 40 ml of 2 M hydrochloric acid or in a glass filter crucible after precipitation of cadmium ammonium phosphate. The 245-keV peak of ^{111m}Cd in the standards and the samples and the 1369-keV peak of ^{24}Na in the flux monitors were measured.

A correction factor was applied for differences between the glass filter crucibles. The factor was established by irradiating a cadmium foil (100 μm thick) and measuring it in all the crucibles. The correction factors were evaluated with a precision better than 1% and varied from 0.936 to 1.000 for the 245-keV peak.

RESULTS AND DISCUSSION

Table 1 gives the results for the certified reference materials tested. For concentrations between 3 and 500 $\mu g\ g^{-1}$, the experimental standard deviation ranges from 5 to 3%. For the NBS urban particulate matter, the results agree with the certified value and with the 70 $\mu g\ g^{-1}$ (standard deviation 6 $\mu g\ g^{-1}$) obtained by Greenberg [7] using thermal neutron activation analysis. For the BCR Moroccan phosphate rock, the extraction was followed by precipitation; the result is again in good agreement with the certified value.

Figure 3 summarizes the results of a round-robin organized by BCR for the certification of cadmium in city waste incineration ash. Each result is the mean of 4 or 5 determinations, the error bars corresponding to two standard deviations. The present result is in excellent agreement with the certified value (Table 1).

Reactor neutron activation analysis was also used for the sewage sludge (BCR/CRM 144). ^{115}Cd was separated by the procedure described; ^{64}Cu

TABLE 1

Results for certified reference materials

Sample	Cadmium content ($\mu g\ g^{-1}$)				
	Found[a]	s	$s\%$	n	Certified
NBS/SRM 1648[b]	70.5	2.5	3.5	3	75 ± 7
BCR/CRM 32[c]	21.39	0.62	2.9	4	20.8 ± 0.7
BCR/CRM 176[d]	475	14	3.0	4	470 ± 9
BCR/CRM 144[e]	2.89	0.15	5.2	5	3.41 ± 0.25

[a]Mean value found, with standard deviation, relative standard deviation and number of determinations. [b]Urban particulate matter. [c]Moroccan phosphate rock. [d]City waste incineration ash. [e]Sewage sludge.

($t_{1/2}$ = 12.7 h, β^+) was afterwards extracted with antimony(III) diethyldithiocarbamate in chloroform and the aqueous phase was measured with a Ge(Li) γ-ray spectrometer. Tracer experiments showed that this chemical separation of cadmium was quantitative. The result obtained, 2.72 $\mu g\ g^{-1}$ with a standard deviation of 0.11 $\mu g\ g^{-1}$ (5 determinations), is in excellent agreement with the result obtained by fast neutron activation analysis (Table 1). These results are somewhat lower than the certified value which was derived from the results obtained by atomic absorption spectrometry, d.c.p. and i.c.p./a.e.s., isotope-dilution mass spectrometry, differential-pulse anodic stripping voltammetry, and thermal and fast neutron activation analysis. The results described in this paper were included in the calculation of the certified value. A possible explanation of the low results obtained by activation analysis with fast and thermal neutrons is that activation analysis is free from reagent blanks. Analysis in this laboratory by i.c.p./a.e.s. with particular attention to avoiding systematic errors from blanks and contamination [8] yielded

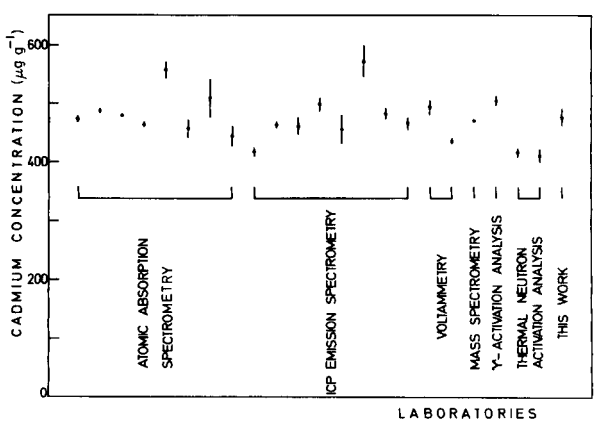

Fig. 3. Results of the BCR round-robin for cadmium in the city waste incineration ash.

2.62 μg g^{-1} with a standard deviation of 0.07 μg g^{-1} (5 determinations), in good agreement with our activation results.

Under the conditions mentioned, with a 1-h irradiation at 40 μA, a 1-h waiting time and a 100-min measuring time, the detection limit L_D, calculated as described by Currie [9] was 0.12 μg g^{-1}.

Conclusion

The method permits an accurate and relatively rapid determination of cadmium. The chemical separation of ^{111m}Cd is applicable to different kinds of materials. Although the method is less sensitive than thermal neutron activation analysis, it has the advantage of being much faster.

We acknowledge Dr. K. Strijckmans for interesting discussions, and the NFWO and IIKW for financial support. C. Vandecasteele is a senior research associate of the National Fund for Scientific Research.

REFERENCES

1 M. Esprit, C. Vandecasteele and J. Hoste, J. Radioanal. Nucl. Chem., Artic., 88 (1985) 31.
2 M. Gallorini, R. R. Greenberg and T. E. Gills, Anal. Chem., 50 (1978) 1479.
3 M. T. G. Valentini, N. Genova and R. Stella, Radiochem. Radioanal. Lett., 44 (1980) 359.
4 M. Gallorini, E. Orvini, A. Rolla and M. Burdisso, Analyst, 106 (1981) 328.
5 A. Wyttenbach and S. Bajo, Anal. Chem., 47 (1975) 1813.
6 F. P. Treadwell, Analytical Chemistry, Vol. II, 9th edn., Wiley, New York, 1935, p. 564.
7 R. Greenberg, Anal. Chem., 51 (1979) 2004.
8 P. D. I. Taylor, B. Desmet and R. Dams, Bull. Soc. Chim. Belg., 95 (1986) 295.
9 L. A. Currie, Anal. Chem., 40 (1968) 586.

Analytica Chimica Acta, 185 (1986) 315—319
Elsevier Science Publishers B.V., Amsterdam — Printed in The Netherlands

Short Communication

DESCRIPTION OF AN AXIALLY-DISPERSED PLUG FLOW MODEL FOR THE FLOW PATTERN IN ELEMENTS OF FLUID SYSTEMS

SPAS D. KOLEV and ERNÓ PUNGOR*

Institute of General and Analytical Chemistry, Technical University of Budapest, Gellért tér 4, H-1502 Budapest XI (Hungary)

(Received 31st December 1985)

Summary. The Laplace transforms of the output signals from a three-sectional system (i.e., fore-section, investigated vessel and after-section), in which the sections have different diameters, are described for δ-function, rectangular and arbitrary input signals by using the axially-dispersed plug flow model. Equations for the mean residence time and the variance of the response of the system are reported. The results could be used to evaluate the axial dispersion coefficient in flow analysis or process systems, for system modelling and optimization.

The rapid development of flow techniques requires a better understanding of the transport processes in different apparatus so that mathematical modelling and optimization can be improved. Among the concepts of chemical engineering which are applied to such problems, three types of hydraulic model are important for describing flow patterns in fluid systems; these are the tanks-in-series, combined, and dispersion models [1]. The last type appears to be closer to the real physical nature of fluid flow, in systems which consist mainly of tubular elements, than the first two types. The most widely applicable of the dispersion models is the axially-dispersed plug flow model, which is mathematically simple in comparison with other representatives of this group. The only parameter included in this model is the axial dispersion coefficient which is analogous to the molecular dispersion coefficient from Fick's laws:

$$\partial c/\partial t = (D_L\, \partial^2 c/\partial x^2) - u\, \partial c/\partial x + S \qquad (1)$$

(Symbols are defined in Table 1.) Generally there are no theoretical expressions for the calculation of the axial dispersion coefficient and the stimulus/response technique [1] developed for engineering purposes remains the only method for its determination. In this technique, the coefficient is calculated from a mathematical description of the stimulus (i.e., the input signal, which is simply a tracer introduced into the fluid system) and the response (i.e., the output signal recorded as the tracer leaves the vessel investigated). This can be done either by curve fitting or by using previously found relationships between the moments of the tracer response curve and the unknown parameter.

0003-2670/86/$03.50

TABLE 1

Symbols and definitions[a]

c	Tracer concentration (kmol m^{-3})
c_M	$= [\int_0^\infty vc\ dt]/V_t$. Integral average tracer concentration in the test section (kmol m^{-3})
C	$= c/c_M$. Dimensionless concentration
$\bar{C}$	Laplace transform of C
d	Diameter of test section (m)
D_L	Axial dispersion coefficient ($m^2\ s^{-1}$)
L	$= x_m - x_o$. Length of the test section (m)
p	Laplace complex variable
P	$= uL/D_L$. Peclet number
Q	$= [p/(\gamma P) + 0.25]^{1/2}$
S	Source term (kmol $m^{-3}\ s^{-1}$)
t	Time (s)
u	Linear flow rate ($m\ s^{-1}$)
v	Volumetric flow rate ($m^3\ s^{-1}$)
V_t	$= (\pi/4)[(x_m - x_e)d_b^2 + x_e d_r^2 - x_o d_a^2]$. Volume of the test section (m^3)
V	$= (\pi/4)Ld^2$. Volume of the test section if the diameter is constant (m^3)
x	Axial position (m)
X	$= x/L$. Dimensionless axial position
γ	$= V_t/V$
$\delta(\theta)$	Dimensionless Dirac delta function
θ	$= tv/V_t$. Dimensionless time
$\mu^{(n)}$	nth moment of the tracer curve about the origin
$\mu^{(1)}$	$= \int_0^\infty C\theta\, d\theta$. Mean of the tracer curve
σ^2	$= \int_0^\infty C(\theta - \mu^{(1)})^2 d\theta$. Variance of the tracer curve
$\Delta\mu^{(1)}$	Difference in means of the tracer curve at the two measurement points
$\Delta\sigma^2$	Difference in variance of the tracer curve at the two measurement points
$\psi(\theta)$	Input signal at point X_o
$\overline{\psi(p)}$	Laplace transform of $\psi(\theta)$

[a]Subscripts a and b refer to the fore-section and after-section, respectively (Fig. 1); subscript e refers to the end of the investigated vessel; subscripts o and m refer to the beginning and end of the test section, respectively; subscript r refers to the investigated vessel.

Usually, analytical solutions of the model are impossible because their Laplace transforms are too complicated; curve fitting can thus be achieved only by numerical methods. The second option of determining the unknown parameter is more easily done because the moments of the tracer response curve can be calculated directly from the Laplace transform of the solution of the model, as was shown by van der Laan [2]:

$$\mu^{(n)} = \lim_{p \to 0} (-1)^n\, d^n \bar{C}_m / dp^n \qquad (2)$$

Levenspiel and Smith [3] derived such equations for the case of a perfect δ-function input of the tracer and a doubly infinite system. Van der Laan [2] extended this treatment for finite vessels by introducing fore- and after-sections with their own dispersion characteristics (Fig. 1) and using the

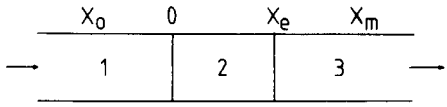

Fig. 1. Scheme of a three-sectional flow system: (1) fore-section; (2) investigated vessel; (3) after-section.

boundary conditions of Wehner and Wilhelm [4]. Aris [5], corrected by Bischoff [6], generalized this approach for the case in which the mathematical description of the input signal or its Laplace transform is unknown, by introducing two measurement points, one before the investigated vessel and the other inside or after it. Later, this idea was developed by Levenspiel and Bischoff [1, 7].

The equations derived in the above-mentioned papers are limited to three-sectional systems, all three with equal diameters. This fact considerably decreases their applicability in both chemical engineering and flow analysis because the investigated vessels often have diameters different from those of the other two sections (e.g., connecting tubes or special reactors). This more general case is covered by the equations described below.

Theoretical equations

A three-sectional system with the measurement point situated in the after-section and the injection point in the fore-section will be considered (Fig. 1). Its mathematical description consists of the following set of partial differential equations in dimensionless quantities and variables:

$$\frac{\partial C_a}{\partial \theta} + \gamma_a \frac{\partial C_a}{\partial X} - \frac{\gamma_a}{P_a} \frac{\partial^2 C_a}{\partial X^2} = \gamma_a \psi(\theta)\delta(X - X_o) \qquad (X \leqslant 0) \tag{3}$$

$$\frac{\partial C_r}{\partial \theta} + \gamma_r \frac{\partial C_r}{\partial X} - \frac{\gamma_r}{P_r} \frac{\partial^2 C_r}{\partial X^2} = 0 \qquad (0 \leqslant X \leqslant X_e) \tag{4}$$

$$\frac{\partial C_b}{\partial \theta} + \gamma_b \frac{\partial C_b}{\partial X} - \frac{\gamma_b}{P_b} \frac{\partial^2 C_b}{\partial X^2} = 0 \qquad (X_e \leqslant X) \tag{5}$$

The corresponding initial and boundary conditions are

$$C_a(X, 0) = C_r(X, 0) = C_b(X, 0) = 0$$

$$C_a(0^-, \theta) = C_r(0^+, \theta)$$

$$C_a(0^-, \theta) - \frac{1}{P_a} \frac{\partial C_a(0^-, \theta)}{\partial X} = C_r(0^+, \theta) - \frac{1}{P_r} \frac{\partial C_r(0^+, \theta)}{\partial X}$$

$$C_r(X_e^-, \theta) = C_b(X_e^+, \theta)$$

$$C_r(X_e^-, \theta) - \frac{1}{P_r} \frac{\partial C_r(X_e^-, \theta)}{\partial X} = C_b(X_e^+, \theta) - \frac{1}{P_b} \frac{\partial C_b(X_e^+, \theta)}{\partial X}$$

and $C_a(-\infty, \theta)$ and $C_b(\infty, \theta)$ must be finite.

The solution of Eqns. 3—5 in the Laplace domain for $X = X_m$ is

$$\overline{C_b(X_m)} = \overline{C_m} = \overline{\psi(p)}\{2Q_r \exp[-P_a(1/2 - Q_a)X_o + P_b(1/2 - Q_b)(X_m - X_e) + P_r(1/2 - Q_r)X_e]\}/B \tag{6}$$

where

$$B = (Q_a + Q_r)(Q_r + Q_b) - (Q_r - Q_a)(Q_r - Q_b)\exp(-2P_rQ_rX_e)$$

Usually $\psi(\theta)$ is considered to be a δ-function or a rectangular function, and the corresponding Laplace transforms are

$$\psi(\theta) = \delta(\theta); \quad \overline{\psi(p)} = 1 \tag{7}$$

$$\psi(\theta) = \begin{cases} 1 & (0 < \theta < k) \\ 0 & (\theta > k) \end{cases}; \quad \overline{\psi(p)} = [1 - \exp(-p)]/p \tag{8}$$

The equations obtained for the mean residence time and the variance of the output signal are as follows.

For the δ-function input (Eqn. 7):

$$\mu_m^{(1)} = \frac{X_e}{\gamma_r} + \frac{X_m - X_e}{\gamma_b} - \frac{X_o}{\gamma_a} + \frac{1}{\gamma_a P_a} + \frac{1}{\gamma_b P_b} \tag{9}$$

$$\sigma_m^2 = 2\frac{X_e}{\gamma_r^2 P_r} + 2\frac{X_m - X_e}{\gamma_b^2 P_b} - 2\frac{X_o}{\gamma_a^2 P_a} + \frac{3}{\gamma_a^2 P_a^2} + \frac{3}{\gamma_b^2 P_b^2} - \frac{2}{\gamma_r^2 P_r^2} + \frac{2}{\gamma_a P_a \gamma_r P_r} + \frac{2}{\gamma_b P_b \gamma_r P_r} + 2\frac{(1-a)(1-b)}{\gamma_r^2 P_r^2}\exp(-P_rX_e) \tag{10}$$

where $a = \gamma_r P_r/\gamma_a P_a$ and $b = \gamma_r P_r/\gamma_b P_b$.

For the rectangular input (Eqn. 8):

$$\mu_m^{(1)} = \frac{X_e}{\gamma_r} + \frac{X_m - X_e}{\gamma_b} - \frac{X_o}{\gamma_a} + \frac{1}{\gamma_a P_a} + \frac{1}{\gamma_b P_b} + \frac{k}{2} \tag{11}$$

$$\sigma_m^2 = 2\frac{X_e}{\gamma_r^2 P_r} + 2\frac{X_m - X_e}{\gamma_b^2 P_b} - 2\frac{X_o}{\gamma_a^2 P_a} + \frac{3}{\gamma_a^2 P_a^2} + \frac{3}{\gamma_b^2 P_b^2} - \frac{2}{\gamma_r^2 P_r^2} + \frac{2}{\gamma_a P_a \gamma_r P_r} + \frac{2}{\gamma_b P_b \gamma_r P_r} + 2\frac{(1-a)(1-b)}{\gamma_r^2 P_r^2}\exp(-P_rX_e) + k^2/12 \tag{12}$$

Quite often either the input signal or its Laplace transform is not known. In this case, the system should include two measurement points [1, 5—7]. This can be done if the injection is done upstream of the point $X = X_o$, which becomes the first measurement point. The second point is at $X = X_m$ as in the above derivations. Such a system will be described by Eqns. 3—5, but in Eqn. 3, the right-hand side will become zero because no tracer is introduced there. Also, the boundary condition that $C_a(-\infty, \theta)$ be finite must be changed to $C_a(X_o, \theta) = C_o(\theta)$, where $C_o(\theta)$ is the tracer curve recorded at $X = X_o$.

The Laplace domain solution of these equations at $X = X_m$ will be

$$\overline{C_m} = \overline{C_o}\, 4Q_a Q_r \exp\left[P_b(1/2 - Q_b)(X_m - X_e)\right]/D \tag{13}$$

where

$$D = (Q_r + Q_a)\{(Q_r - Q_b)\exp\left[P_a(1/2 + Q_a)X_o - P_r(1/2 + Q_r)X_e\right]$$
$$+ (Q_r + Q_b)\exp\left[P_a(1/2 - Q_a)X_o - P_r(1/2 - Q_r)X_e\right]\}$$
$$- (Q_r - Q_a)\{(Q_r - Q_b)\exp\left[P_a(1/2 - Q_a)X_o - P_r(1/2 + Q_r)X_e\right]$$
$$+ (Q_r + Q_b)\exp\left[P_a(1/2 + Q_a)X_o - P_r(1/2 - Q_r)X_e\right]\}$$

The differences in the mean and in the variance of the tracer response curve at the two measurement points are

$$\Delta\mu^{(1)} = \mu_m^{(1)} - \mu_o^{(1)} = \frac{X_m}{\gamma_b} - \frac{X_o}{\gamma_a} + \frac{1-a}{\gamma_r P_r}\left[1 - \exp(P_a X_o)\right] - \frac{1-b}{\gamma_r P_r}$$
$$\left[1 - \exp(P_a X_o - P_r X_e)\right] \tag{14}$$

$$\Delta\sigma^2 = \sigma_m^2 - \sigma_o^2 = \frac{2}{\gamma_r P_r} + \frac{1}{\gamma_r^2 P_r^2}\{-2 + 2a - 5a^2 + 2b + 3b^2$$
$$+ 2(1-b)\gamma_r P_r\left[(X_e/\gamma_r) - (X_m/\gamma_b)\right] + 2(1-a)(\gamma_r P_r X_o/\gamma_a)$$
$$+ 4(1-a)\left[(\gamma_r P_r X_o/\gamma_a) - 1 - a\right)\exp(P_a X_o) + 4(1-b)\{1 + b$$
$$- \gamma_r P_r\left[(X_o/\gamma_a) - (X_e/\gamma_r)\right]\}\exp(P_a X_o - P_r X_e) + (1-b)^2\exp\left[2(P_a X_o$$
$$- P_r X_e)\right] + (1-a)^2\exp(2P_a X_o) + 2(1-a)(1-b)\left[1 - \exp(2P_a X_o)\right]$$
$$\exp(-P_r X_e)\} \tag{15}$$

It can be seen that systems which have sections with equal diameters are a special case of the models proposed above; the coefficients γ_a, γ_b and γ_r become equal to unity.

REFERENCES

1 O. Levenspiel and K. B. Bischoff, Adv. Chem. Eng., 4 (1963) 95.
2 E. Th. van der Laan, Chem. Eng. Sci., 7 (1958) 187.
3 O. Levenspiel and W. K. Smith, Chem. Eng. Sci., 6 (1957) 227.
4 J. F. Wehner and R. H. Wilhelm, Chem. Eng. Sci., 6 (1956) 89.
5 R. Aris, Chem. Eng. Sci., 9 (1959) 266.
6 K. B. Bischoff, Chem. Eng. Sci., 12 (1960) 69.
7 K. B. Bischoff and O. Levenspiel, Chem. Eng. Sci., 17 (1962) 245.

Analytica Chimica Acta, 185 (1986) 321—327
Elsevier Science Publishers B.V., Amsterdam — Printed in The Netherlands

Short Communication

FIBRE-OPTIC FLUORESCING SENSOR FOR AMMONIA

OTTO S. WOLFBEIS* and HERMANN E. POSCH
Institut für Organische Chemie, Karl-Franzens-Universität, A-8010 Graz (Austria)
(Received 16th December 1985)

Summary. The fluorescing sensor is based on the change in fluorescence intensity of a buffered pH indicator solution entrapped in silicone rubber. Exposure to ammonia increases the pH of the trapped solution; this increases the fluorescence intensity, which is monitored via an optical fibre bundle. Ammonium chloride in 0.001 M sodium hydroxide, or the indicators themselves, can serve as buffers. Effects of sensor preparation and buffer composition on response time, reversibility and sensitivity are discussed.

Continuous determination of ammonia in gaseous or liquid samples is nowadays done almost exclusively with the help of potentiometric ammonia electrodes. In view of the increasing concern for environmental quality, but also for the purpose of continuous sensing in bioreactors and biological samples, ammonia electrodes have found widespread application. Although the principle of such ammonia sensors is well known and various types are commercially available, their design and performance have been improved in recent years, mainly as a result of contributions by Mascini and Cremisini [1] as well as Meyerhoff and co-workers [2, 3]. Both the response time and the reversibility have been improved considerably. Ammonia electrodes have also been applied in combination with flow-injection systems [4]. Apart from direct sensing of ammonia, the electrodes have also been used as transducers for monitoring enzymatic reactions during which ammonia is released or consumed. The determination of urea which, by catalytic action of urease, is hydrolyzed to give ammonia and carbon dioxide is a representative example [4]. Finally, ammonia electrodes can also be exploited for monitoring the binding of antigens to antibodies [5]. Despite the utility of present-day electrochemical ammonia sensors, they have some disadvantages: (a) they do not lend themselves to miniaturization; (b) it is not easy to sterilize them; (c) their performance can be affected by surface potentials, resulting in drifting signals; and (d) as in other potentiometric methods, a reference electrode is required along with its troublesome liquid—liquid junction.

Some of these disadvantages can be avoided by using optical methods, ideally in combination with fibre optics. Fibre-optic methods for the determination of ammonia have already been reported. Thus, David et al. [6] described a probe consisting of a fibre light guide covered with a solution of

0003-2670/86/$03.50

ninhydrin in polyvinylpyrrolidone, which becomes violet on contact with ammonia and so attenuates the light transversing the fibre. Because the ninhydrin reaction is irreversible, the sensor is also irreversible. Moreover, it is suitable only for gaseous samples because the cover is water-soluble. A related working principle has been described by Smock et al. [7]. A reversible ammonia sensor has been reported [8] that exploits the spectral changes of an ammonia-sensitive oxazine dye deposited on the surface of an optical fibre. Colour changes from red to blue (and reverse) are monitored via the attenuation of the evanescent wave [9], i.e., the fraction of the electromagnetic wave that evanesces into the optically less dense phase at the moment of total reflection at the interface between fibre and dye.

In continuation of earlier work on fluorescing sensors [10, 11], a new sensor is described here for ammonia. It is based on the pH changes of a polymer-entrapped buffer system attached to the distal end of a fibre and in contact with an ammonia-containing sample. Changes in pH are followed with an added pH indicator via an optical fibre. In contrast to former types of sensor, it is applicable to both gaseous and liquid samples.

Experimental

Chemicals. A stock 0.01 M solution of ammonium chloride was prepared in distilled water and diluted to the appropriate molarity with water and 0.1 M sodium hydroxide (to release free ammonia). The solutions were stored in well-stoppered flasks to prevent vapourization of ammonia. Fresh solutions were prepared weekly.

The indicators used were acridine orange (excitation and emission maxima at 480 and 540 nm, respectively), 1-hydroxypyren-3,6,8-trisulphonate (HPTS, 460/520 nm), and 1-naphthol-4-sulphonate (360/440 nm). They were obtained from Fluka or Eastman-Kodak and used as received.

The following aqueous solutions were used for preparation of the suspensions in silicone rubber that served as sensing layers: (a) 1 mM acridine orange hydrochloride in 0.01 M ammonium chloride; (b) a 0.1% (w/v) solution of 1-hydroxynaphthalene-4-sulphonic acid sodium salt in water, adjusted to pH 8.2—8.4 with 0.01 M sodium hydroxide; (c) 0.1% and 1% (w/v) solutions of HPTS in water, adjusted to pH 7.1 with 0.01 M sodium hydroxide.

Preparation of the sensing membranes. A portion (27.0 g) of a vinyl-terminated polydimethylsiloxane (silicone polymer PS-443; Petrarch Systems, Bristol, PA 19007) and 0.0195 g of chloroplatinic acid (PC-075; Petrarch) were carefully mixed. A second mixture, consisting of 0.1 g of PS-925 (polyvinylmethylsiloxane) and 9.9 g of PS-443 (as above) was also prepared. Then 19.95 g of the first mixture, 0.05 g of the second mixture, and 4.0 ml of the aqueous indicator solution were emulsified for 5 min in a mechanical emulsifying machine (Turrax).

A portion (0.9 g) of the white emulsion and 0.1 g of product PS-123 (a hydrogen-donating dimethylsiloxane polymer that causes polymerization) were intimately mixed and rapidly smeared onto a glass platelet to give a

film 50 ± 10 μm thick. Polymerization occurs within 10 min at room temperature. The resulting layers were tested for their sensing properties. They were either directly irradiated with the excitation beam of the fluorimeter, or attached to the distal end of the fibre. All experiments were done and all samples were stored in a room thermostatted to 23 ± 1°C.

A second type of silicone rubber membrane was obtained from Silgel 601A and 601B (two silicone prepolymers which can be cured thermally; Wacker Chemie, Burghausen, W. Germany). A mixture of 9.0 g of 601A and 1.0 g of 601B was emulsified with 2 ml of a 0.1% solution of 1-naphthol-4-sulphonate in water/glycerol (9:1, v/v), the pH of which was adjusted to 8.4. It is essential not to allow the mixture to become warm in the Turrax emulsifier; once thermal curing has started, it is difficult to detach the mixture. A ca. 100-μm thick film was then produced on several glass slides. Curing was achieved by immersing the slides in water at 50—55°C for 30 min. Milky-white sensor spots were obtained that were attached, within the fluorimeter, to the flow-through cell.

Optical arrangement. This is shown schematically in Fig. 1. Light from a 250-W xenon light source (LS) was passed through a monochromator (M_1) to isolate the 460-nm line for HPTS, or the 360-nm line for the naphtholsulphonate. The radiation was then focussed with lens L_1 onto the sensing layer within the fluorimeter or into a bifurcated fibre-optic light guide (F) made of poly(methyl methacrylate) or quartz (both from Moritex Corp., Tokyo). Both consisted of ca. 70 fibre strands per bundle, with an internal diameter of ca. 6 mm at the common end. The plastic fibres (1.5 m long) were used for excitation of the acridine orange and HPTS-based sensors, and the quartz fibres for the naphtholsulphonate-based sensors. Because of the shortness of the quartz fibres, light attenuation in the ultraviolet range was negligible. The end of the fibre was covered with a sensing membrane (S), prepared as described above. The sensor head was inserted into a flow-through chamber through which sample solutions containing definite amounts of ammonia were pumped at a rate of ca. 15 ml min^{-1}, using a peristaltic pump.

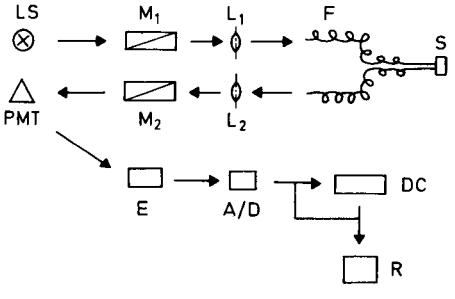

Fig. 1. Schematic diagram of the experimental arrangement of the ammonia fluorescence sensor. See text for detail.

Fluorescence was collected by the second fibre bundle and guided to a photomultiplier tube (PMT) after passing the emission monochromator (M_2) and lens L_2. The signal was amplified in an electronic circuit (E), digitized in A/D, stored in a desk computer (DC; HP 9815A) and/or sent to an X-Y recorder (R; HP 7225A). Most of the optical components were parts of an Aminco SPF-500 spectrofluorimeter.

In some experiments, the flow-through cell covered with the sensing layer was placed within the fluorimeter so that there was no need for fibres. The sensing layers were placed in the focus of the excitation beam. The data obtained were practically the same.

Results

Choice of buffer composition and indicator. Initial experiments were done with ammonium chloride as the internal buffer system. When 1 mM acridine orange in 0.01 M ammonium chloride was used without added sodium hydroxide, the sensor responded rapidly to ammonia, but the changes were not reversible, probably because of the low pH (ca. 5.80). The strong fluorescence intensity of the sensing layer after exposure to ammonia could be reduced only by treatment with 0.01 M hydrochloric acid for 30 min.

However, when the pH of the solution was increased to 8.23 by applying a more alkaline filling solution (10 mM naphtholsulphonate in 0.01 M NH_4Cl plus 0.001 M NaOH), a slow but reversible change in fluorescence intensity was observed. Curve 1 in Fig. 2 shows how the fluorescence changes as the ammonia concentration of the sample is varied.

Instead of ammonium chloride, the indicator itself may serve as a buffer. 1-Hydroxypyren-3,6,8-trisulphonate (HPTS) and the naphtholsulphonate were chosen because they are readily soluble in water, with pK_a values of 7.3 and 8.3, respectively. Solutions (0.3%) were prepared and adjusted to various

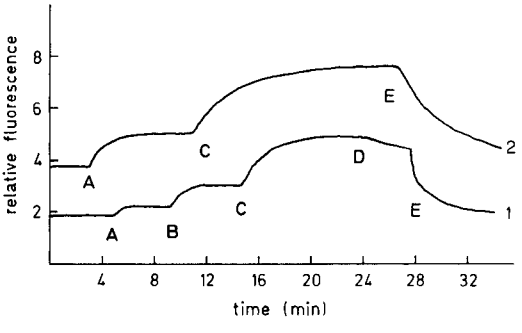

Fig. 2. Typical response of the ammonia sensors based on silicone rubber-entrapped indicator solutions. Curves: (1) 1-naphthol-4-sulphonate in ammonia buffer (0.01 M NH_4Cl in 1 mM NaOH); (2) 0.3% naphtholsulphonate in water, adjusted to pH 8.2. Starting with water, the sensing membranes were exposed to the following ammonia solutions: (A) 0.1 mM; (B) 0.5 mM; (C) 1 mM. Washing was done with pure water (D) and 0.1 M hydrochloric acid (E).

pH values between 7.1 and 8.7. While the HPTS-based sensors showed either poor reversibility (at pH < 8), or poor signal changes (at pH > 8), the naphtholsulphonate-based sensor displayed promising properties. Curve 2 in Fig. 2 shows the response of this kind of sensing layer to various concentrations of ammonia in water. The relative signal change is smaller than that shown in curve 1 and the response time is distinctly slower.

Response. Response times were typically 2—5 min. They are affected by various factors. The first is the size of the water droplets in the silicone sensing layer; experience is needed to produce identically responding membranes. Qualitatively, the response time became slower as the size of the water droplets increased, i.e., the shorter the prepolymer was mechanically emulsified. Hand-mixed polymer membranes gave extremely slow responses. Another factor that influences the response time is the thickness of the sensing layer. A 100-μm membrane was found to respond at about a third of the rate for a 50-μm membrane. Finally, an increase in buffer concentration decreased the response times.

No differences were found in the relative signal changes of the sensors prepared from the Petrarch and Silgel polymers. Because the former material allowed a much finer emulsion to be produced, its response time was much faster than that of the Silgel polymer.

Reversibility. Sensors with indicator filling solutions at pH values below 7.0 were found not to be reversible. Even when the sensor was exposed to 0.01 M hydrochloric acid, the low signal that was observed initially was never reached again. Good reversibility was observed at pH values above 8.0. But, though it would seem that even higher pH would improve reversibility, the increasing interference from carbon dioxide (which lowers the pH) sets a limit. Thus, the choice of pH will always be a compromise between ideal reversibility and interference by acidic gases. Again, the sensing layers prepared from the Petrarch silicone rubber had distinctly quicker response times than the Silgel membranes.

Under water, the membranes recovered more slowly than they responded to ammonia-containing solutions. Recoveries usually took 2—5 times longer than responses. This could be significantly accelerated by washing with 0.01 M hydrochloric acid and water (Fig. 2, curve 1).

Sensitivity and detection limits. Sensors with an ammonium chloride buffer of pH 5 as a filling solution showed high sensitivity, with detection limits of 10^{-6} M ammonia and less, but were not reversible. At the present stage of development, a detection limit of 10^{-5} M ammonia seems to be a reasonable value for fully reversible sensors. The signal-to-noise ratio is ca. 30 at 10^{-5} M ammonia.

Sensitivity is governed to some extent by the buffer capacity. The higher the capacity, the lower the relative changes in pH and so the wider the dynamic response range. Sensitivity will, of course, also be governed by the pK_a of the indicator. Ideally, the pK_a should be in the range of the pH of the filling solution after exposure to ammonia.

Interferences. Acidic gases known [1, 12, 13] to interfere with gas-sensing electrodes were found to interfere here as well. The strongest effects were observed with sulphur dioxide and nitrous oxide. The influence of carbon dioxide increases with the pH of the filling solution. A change from nitrogen-saturated water to air-saturated water did not affect the signal from sensors with internal buffers at pH 8.2—8.4. Thus, the effect of 0.2 Torr CO_2 remains negligible, and oxygen does not act as a dynamic quencher. Acetic acid (0.1% in water) interferes strongly with all kinds of sensors having filling solutions at $\geqslant$pH 6.

Discussion

The ammonia sensor described above is based on the changes of fluorescence intensity of a buffer system entrapped in a polymer. Silicone rubber was selected as the polymer because its permeability for ammonia is excellent. Unlike the gas-sensing electrodes and the optical CO_2 sensor [14], in which the buffer solutions are separated from the sample solution by a gas-permeable membrane (e.g., PTFE), the buffered indicator solution is trapped as a fine emulsion in an ammonia-permeable polymer. This is possible because there is no need for direct contact between the fibre optic and filling solution, which is in striking contrast to electrochemical sensors.

Two types of silicone polymer were tested. Sensors prepared from the Petrarch material showed faster responses in both directions. The Silgel polymer is unsuitable for the preparation of very fine emulsions because it tends to cure on prolonged vortexing; and it does not form even films on glass.

Two kinds of buffer were used. The 0.01 M ammonium chloride/0.001 M sodium hydroxide is the buffer normally used with the potentiometric sensors [1—4]. The indicator itself at high concentration can also serve as a buffer. The indicators were chosen to have pK_a values slightly below the pK_a of ammonia (9.3) and to be highly fluorescent, with good water solubility and spectral data suitable for use with plastic fibre optics which are unsuitable for near-u.v. radiation.

Acridine orange has good spectral properties (the excitation and emission maxima are in the visible range) but it is not very soluble in water and so cannot serve as the buffer. The relatively poor solubility in water also causes rather poor signal intensities from the ca. 50-μm sensing layers. Glycerol (or polyethylene glycol) was added to prevent water from evaporating from the sensing layer; this produced a more concentrated filling solution and so an increase in signal intensity. HPTS has good spectral properties, but its pK_a value (7.3) is too low compared to the pH values of the filling solution after exposure to ammonia; the relative signal changes remain poor. The naphtholsulphonate buffer system showed the best results; its pK_a of 8.3 makes it suitable as both indicator and buffer. The only disadvantage is that u.v. excitation is needed. More suitable indicators are being sought.

The response time of the sensor (2—6 min) is comparable to that of most electrochemical sensors. A much smaller sensor layer, e.g., attached to the

tip of a single fibre, might improve the response times. The layers used in this work had an area of ca. 20 mm^2. An interesting idea is to use an air gap between the sample and filling solution [4, 15]; this prevents any contact between sample and the inner solution and gives improved response times.

REFERENCES

1 M. Mascini and C. Cremisini, Anal. Chim. Acta, 92 (1977) 277.
2 W. N. Opdycke, S. J. Parks and M. E. Meyerhoff, Anal. Chim. Acta, 155 (1983) 11 and references therein.
3 Y. Fraticelli and M. E. Meyerhoff, Anal. Chem., 53 (1981) 992.
4 J. D. Joseph, Anal. Chim. Acta, 169 (1985) 249, and references therein.
5 S. B. Brontman and M. E. Meyerhoff, Anal. Chim. Acta, 162 (1984) 363.
6 D. C. David, M. C. Willson and D. S. Ruffin, Anal. Lett., 9 (1976) 389.
7 P. L. Smock, T. A. Orofino, G. M. Wooten and W. S. Spencer, Anal. Chem., 51 (1979) 505.
8 J. F. Giuliani, H. Woltjen and N. L. Jarvis, Opt. Lett., 8 (1983) 54.
9 G. J. Müller, Am. Chem. Soc. Symp. Ser., 102 (1979) 505.
10 See, e.g., O. S. Wolfbeis, H. E. Posch and H. W. Kroneis, Anal. Chem., 57 (1985) 2556.
11 O. S. Wolfbeis, Trends Anal. Chem., 4 (1985) 184.
12 M. E. Lopez, Anal. Chem., 56 (1984) 2360.
13 W. E. Morf, I. A. Mostert and W. Simon, Anal. Chem., 57 (1985) 1122.
14 D. W. Lübbers and N. Opitz, Z. Naturforsch., Teil C, 30 (1975) 532.
15 J. Růžička and E. H. Hansen, Anal. Chim. Acta, 69 (1974) 129.

Analytica Chimica Acta, 185 (1986) 329—333
Elsevier Science Publishers B.V., Amsterdam — Printed in The Netherlands

Short Communication

CHEMILUMINESCENCE DETERMINATION OF BUPRENORPHINE HYDROCHLORIDE BY FLOW INJECTION ANALYSIS

ABDUL A. ALWARTHAN and ALAN TOWNSHEND*
Chemistry Department, University of Hull, Hull HU6 7RX (Great Britain)
(Received 15th December 1985)

Summary. A direct, simple and rapid flow-injection method is described for determining buprenorphine hydrochloride (10^{-8}—10^{-4} M) based on its chemiluminescent oxidation with potassium permanganate in polyphosphoric acid. The limit of detection is 1×10^{-8} M (0.5 pmol per injection) and the log-log calibration is linear up to 1×10^{-4} M; the r.s.d. is 0.7% for a 10 μg ml^{-1} solution (n = 10). The method is directly applicable to aqueous solutions of tablets containing the drug (0.2 mg/tablet).

Buprenorphine [I; 5α, 7α(s)-17-(cyclopropylmethyl)-α-(1,1-dimethylethyl)-4,5-epoxy-18,19-dihydro-3-hydroxy-6-methoxy-α-methyl-6,14-ethenemorphinan-7-methanol] is an oripavine derived from the opium alkaloid thebaine [1]. It is a potent, long-acting drug and has both narcotic antagonist and

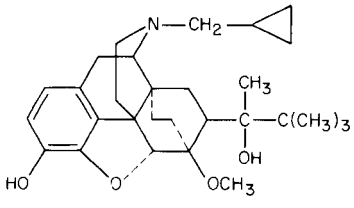

(I)

partial agonist properties. It produces typical morphine-like subjective effects and meiosis but these effects are of slower onset and longer duration than those of morphine. Therefore, it has been suggested as a maintenance drug in the treatment of opiate addiction [2].

Methods for determining drugs such as morphine and morphine-like derivatives in biological fluids are very important in forensic science and clinical chemistry. Conventional methods for their determination in biological samples include thin-layer and gas-liquid chromatography, u.v.-visible spectrophotometry, spectrofluorimetry and radioimmunoassay [3].

Abbott and co-workers [4, 5] found that down to 1 fmol of morphine could be determined by oxidation with potassium permanganate in an acidic medium to give chemiluminescence, which was monitored in a flow-injection system. A similar method has been developed for buprenorphine, and is described in this communication.

0003-2670/86/$03.50

Experimental

Reagents. Polyphosphoric acid (essentially tetraphosphoric acid; general-purpose reagent) and AnalaR potassium permanganate were supplied by BDH Chemicals. Buprenorphine hydrochloride was donated by Reckitt and Colman, Pharmaceutical Division, Hull. Deionized water was used throughout. A stock solution of 0.5 M polyphosphoric acid was prepared by dissolving 8.6585 g of the concentrated acid in 100 ml of water.

Flow system and apparatus. The flow-injection manifold for chemiluminescence detection is shown in Fig. 1. An aqueous solution of polyphosphoric acid acting as a carrier stream for buprenorphine was supplied through R_1, and the potassium permanganate solution through R_2. The sample was injected into the acidic stream from a 52-μl teflon rotary valve injector (Rheodyne RH-5020). The streams were propelled by an Ismatec Mini-S-840 peristaltic pump and mixed at a perspex T-piece. All tubing was 0.9 mm i.d. The flow cell was a coil made of glass tubing (2.3 mm i.d., 34 cm long), spiralled to a diameter of 25 mm and backed by a mirror for maximum light reflection to the photomultiplier tube (PMT) [6, 7]. The PMT was a semi-transparent end-window type (EMI No. 9844B) powered by a stabilized EHT power supply (up to 1500 V) [6, 7]. The signal from the PMT was fed to a chart recorder, and the peak height was measured.

Optimization of conditions. The polyphosphoric acid and potassium permanganate concentrations, the total flow rate and the effect of the tube length between the injection port and the T-piece, all of which affect the intensity of the chemiluminescence signal, were investigated. The effect of different polyphosphoric acid concentrations is shown in Fig. 2; the greatest response was obtained in ca. 0.05 M polyphosphoric acid, compared to 0.1 M for morphine [4]. The potassium permanganate concentration must be controlled carefully, because too much oxidant causes excessive oxidation of such narcotic agents [8], while too little produces smaller chemiluminescent signals. The greatest peak height was obtained with

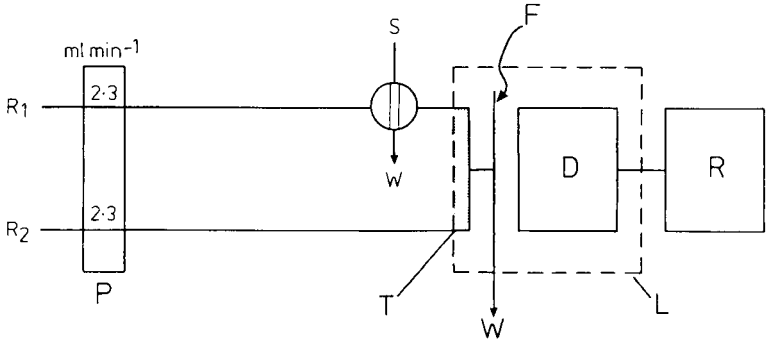

Fig. 1. Flow-injection manifold for buprenorphine determination: R_1, carrier stream; R_2, oxidant stream; P, pump; S, injection valve; W, waste; T, perspex T-piece; F, coiled flow cell; D, detector; R, chart recorder; L, light-tight box.

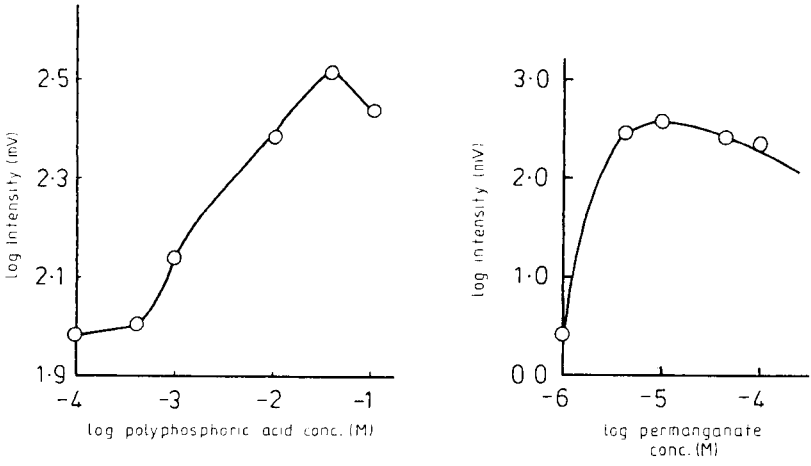

Fig. 2. Effect of polyphosphoric acid concentration on the peak height for 1×10^{-5} M buprenorphine hydrochloride, with 1×10^{-5} M permanganate as oxidant.

Fig. 3. Effect of potassium permanganate concentration on the signal from 1×10^{-5} M buprenorphine hydrochloride, with 0.05 M polyphosphoric acid as carrier.

1×10^{-5} M permanganate, but 1×10^{-4} M gave only slightly less sensitivity for 1×10^{-5} M drug (Fig. 3).

The intensity increased with increasing flow rate. As the total flow rate (the flow rate was the same in both channels) was increased from 1 to 10 ml min^{-1}, the peak height increased almost linearly (Fig. 4A). To establish the effect of sample dispersion on the buprenorphine signal, the distance between the injection valve and T-piece was varied. As shown in Fig. 4B, the longer the distance, the smaller the peak height, but the peak became wider, as would be expected from the increased dispersion. Therefore, the best distance, as used in this work, was 24 cm, the smallest practical distance. At a flow rate of 10.0 ml min^{-1} with a 24-cm distance, however, the r.s.d. (n = 5) for the determination of 5.2 μg ml^{-1} buprenorphine was 3.1%, compared to 2.0% at 5 ml min^{-1}, and 1.8% at 4.6 ml min^{-1}; a flow rate of 4.6 ml min^{-1} (2.3 ml min^{-1} in each channel) is recommended because of the greater precision and economy in the use of reagents. The recommended conditions for the determination of buprenorphine hydrochloride are, therefore, 0.05 M polyphosphoric acid, 1×10^{-5} M permanganate, a total flow rate of 4.6 ml min^{-1} and a tube length of 24 cm between the injection valve and the detector.

Results and discussion

A log-log calibration graph obtained under the above conditions was linear over the range 1×10^{-8}—1×10^{-4} M buprenorphine with a slope of 0.80, compared with a slope of 0.67 for morphine [4]. Above 1×10^{-4} M, the slope decreased, because the permanganate concentration became a

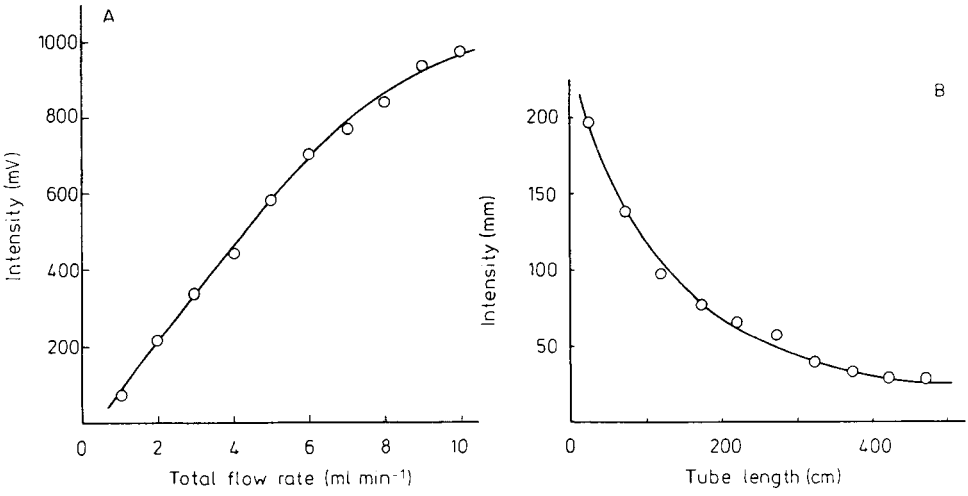

Fig. 4. Effects of total flow rate and tube length on the signal from 1×10^{-5} M buprenorphine. HCl, with 1×10^{-5} M permanganate as oxidant and 0.05 M polyphosphoric acid as carrier: (A) flow rate with a tube length of 24 cm; (B) tube length with a flow rate of 5 ml min^{-1}.

limiting factor. The mean relative standard deviation was 1.5% for 1—5 μg ml^{-1} buprenorphine hydrochloride, and for ten replicate injections of 10 μg ml^{-1}, was 0.7%, as shown in Table 1. The limit of detection (twice the blank noise) was 1×10^{-8} M (5 ng ml^{-1}). This corresponds to 5×10^{-13} mol (0.25 ng) per injection. The time needed for triplicate measurements of 5.0 μg ml^{-1} was less than 1 min.

The chemiluminescent oxidation of buprenorphine, like that of morphine, is very rapid, reaching maximum intensity in less than 1 s. This is confirmed by the effect of flow rate on the signal. The signal increases as the flow rate increases up to a total flow rate of 10 m min^{-1}, at which rate the sample takes 8.4 s to pass from the T-piece to the exit of the coiled cell. Thus more

TABLE 1

Short-range calibration results for buprenorphine hydrochloride

Conc. (μg ml^{-1})	Signal height (mV)	S.d. (mV)[a]	R.s.d. (%)[a]
1	128	2.9	2.3
2	233	2.9	1.2
3	327	2.9	0.9
4	397	6.0	1.5
5	493	7.0	1.4
10	1500	11[b]	0.7[b]

[a]For 3 replicate injections. [b]For 10 replicate injections.

of the initial emission is monitored than at lower flow rates. Even at the maximum flow rate investigated, most of the chemiluminescence had ceased by the time the sample reached the exit of the flow cell.

The method was evaluated by determining buprenorphine hydrochloride in a sample of Temgesic Sublingual tablets (Reckitt and Colman), which contained ca. 0.2 mg of buprenorphine hydrochloride per 60-mg tablet. Standard addition and direct calibration methods were used. Standards of 0.0, 2.0, 4.0 and 6.0 $\mu g\ ml^{-1}$ in 25-ml solutions were prepared from pure buprenorphine hydrochloride. A similar set of standards was also prepared, which each contained 5.0 ml of a tablet solution containing ca. 2 $\mu g\ ml^{-1}$ buprenorphine hydrochloride. Direct calibration gave a mean result of 3.9 $\mu g\ ml^{-1}$ for triplicate injections of a solution prepared from a tablet dissolved in 50 ml of water, amounting to 0.195 mg of buprenorphine hydrochloride in a tablet. The standard addition graph was parallel to the normal linear calibration graph, and gave a value of 0.22 mg per tablet.

The method can therefore be applied directly to solutions prepared from tablets containing buprenorphine without further treatment. Undoubtedly, it is also sufficiently sensitive to be used for post-column detection of buprenorphine after h.p.l.c. separation, as has been done for morphine [5] and could thus be applied to the detection of traces of buprenorphine in body fluids.

REFERENCES

1 S. N. Steen, R. L. Smith, S. Jeretin, M. Petrun, M. S. Mok and M. Lippmann, IRCS Med. Sci. Libr. Compend., 7 (1979) 597.
2 D. R. Jasinski, J. S. Pevnick, J. D. Griffith, C. W. Gorodetzky and E. J. Cone, Probl. Drug Dependence, (1976) 112.
3 I. Jane and J. F. Taylor, J. Chromatogr., 109 (1975) 37.
4 R. W. Abbott, A. Townshend and R. Gill, Analyst (London), 111 (1986) 635.
5 R. W. Abbott and A. Townshend, Anal. Proc., 23 (1986) 25.
6 A. T. Faizullah and A. Townshend, Anal. Proc., 22 (1985) 15.
7 A. Wheatley, Ph.D. Thesis, University of Hull, 1983.
8 H. J. Kupferberg, A. Burkhalter and E. L. Way, J. Chromatogr., 16 (1964) 558.

Analytica Chimica Acta, 185 (1986) 335—339
Elsevier Science Publishers B.V., Amsterdam — Printed in The Netherlands

Short Communication

GAS-CHROMATOGRAPHIC DETERMINATION OF 1-(2-CHLOROETHYL)-3-(*TRANS*-4-METHYLCYCLOHEXYL)-1-NITROSOUREA IN PLASMA AFTER REACTION WITH TRIFLUOROACETIC ANHYDRIDE

B. CADDY and O. R. IDOWU*[a]

Forensic Science Unit, Department of Pharmaceutical Chemistry, University of Strathclyde, Royal College Building, 204, George Street, Glasgow G1 1XW (Great Britain)

(Received 24th October 1985)

Summary. The reaction of 1-(2-chloroethyl)-3-(*trans*-4-methylcyclohexyl)-1-nitrosourea (methyl-CCNU) with trifluoroacetic anhydride is reported. Gas-liquid chromatography of the resulting trifluoroacetyl derivative is applied to determine methyl-CCNU in plasma with a limit of detection of 1.5 $\mu g\ ml^{-1}$.

Several approaches to the determination of the anti-cancer drug methyl-CCNU (I) have been reported and the problems have been discussed [1—3]. One of the methods was based on the denitrosation of methyl-CCNU with peroxyacetic acid and subsequent gas-liquid chromatographic determination of the resulting urea (II) as the trifluoroacetyl derivative (III). As discussed

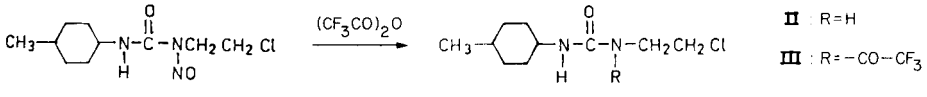

I

earlier, a drawback of this method is that it lacks selectivity for the intact drug because acidic denitrosation of methyl-CCNU may occur in the gastric medium.

During an investigation into the possible presence of the denitrosated derivative of methyl-CCNU (II) in the urine of a patient treated with the drug, an attempt was made to determine methyl-CCNU in urine both before and after treatment of the urine with peroxyacetic acid; the difference between the results should account for any intact methyl-CCNU present in the urine. However, no measurable difference was found between the two determinations, which indicated either the absence of the intact drug in the urine sample or that methyl-CCNU reacted with trifluoroacetic anhydride to yield 1-(β-chloroethyl)-1-trifluoroacetyl-3(*trans*-4-methylcyclohexyl)urea (III), the

[a]Present address: Department of Chemistry, University of Ibadan, Ibadan, Nigeria.

0003-2670/86/$03.50

same derivative as obtained on reaction of denitrosated methyl-CCNU with trifluoroacetic anhydride [2]. Methyl-CCNU was therefore treated with trifluoroacetic anhydride to examine the latter possibility. This report describes a simple gas-liquid chromatographic method for methyl-CCNU in plasma, based on the finding that methyl-CCNU reacts with trifluoroacetic anhydride to give the same derivative as described earlier for denitrosated methyl-CCNU [2].

Experimental

Reagents and equipment. The methyl-CCNU was provided by Ciba-Geigy. *N,N*-Dimethylaniline (reagent grade; BDH Chemicals) was used as received.

The Perkin-Elmer F11 gas chromatograph used was fitted with a flame ionisation detector and a glass column (2 m long, 2 mm i.d.) packed with 20% (w/w) Apiezon-L on Gas-Chrom W (80—100 mesh) and operated at an oven temperature of 185°C and injector temperature of 224°C, with a nitrogen carrier gas flow rate of 31 ml min^{-1}.

Reaction of methyl-CCNU with trifluoroacetic anhydride. Methyl-CCNU (100 mg) was dissolved in 2 ml of trifluoroacetic anhydride and the mixture was kept at room temperature for 1 h and then in a water bath at 45°C for 5 min. A yellow semi-solid was obtained on evaporation of excess of trifluoroacetic anhydride under dry nitrogen. A first attempt to recrystallise the product was unsuccessful. The reaction procedure was repeated and the yellow semi-solid was examined directly by high-resolution mass spectrometry.

Preparation of calibration graphs for methyl-CCNU in plasma. A solution of methyl-CCNU in methanol (500 μg ml^{-1}) was prepared by dissolving 50 mg of the drug in methanol in a 10-ml volumetric flask. A capillary pipette was used to transfer 0.01 to 0.1-ml aliquots of this solution to five glass-stoppered test tubes. Drug-free, ice-cooled blood plasma (2 ml) was added to each test tube to give concentrations of the drug in plasma equivalent to 2.5—25 μg ml^{-1}. After addition of 4 ml of redistilled ether, the plasma solutions were extracted by agitating on a vortex mixer for 2 min, the aqueous layers were removed and a little anhydrous sodium sulphate was added to the ether extracts to dry them. The extracts were decanted into a series of narrow-ended test tubes and evaporated to dryness under a stream of dry nitrogen.

Trifluoroacetic anhydride (0.2 ml) was added to the residue in each test tube, and the mixtures were kept at room temperature for 1 h and heated for 5 min in a water bath at 45°C. Excess of reagent was removed under dry nitrogen and the residues were reconstituted in 20—30 μl of dichloromethane. The dichloromethane solutions were allowed to evaporate to dryness in a water bath at 45°C and the residues were redissolved in 5 μl of a 25 μg ml^{-1} solution of *N,N*-dimethylaniline in dichloromethane. A 3-μl aliquot of each solution was injected into the chromatograph in turn, with the chromatographic conditions as stated above. A graph of the peak height ratio of the

trifluoroacetyl derivative to dimethylaniline vs. concentration of methyl-CCNU was constructed.

Preparation of calibration graphs for methyl-CCNU in ether. A 500 μg ml^{-1} solution of methyl-CCNU was prepared by dissolving 50 mg of the drug in ether in a 10-ml volumetric flask. Aliquots (0.01—0.1 ml) of the solution were placed in narrow-ended test tubes and 4.0 ml of ether was added to each. The solutions were evaporated to dryness, and the trifluoroacetate derivative was isolated and injected for chromatography as described above.

Results and discussion

Determination of methyl-CCNU by direct reaction with trifluoroacetic anhydride. A yellow semi-solid was obtained on evaporation of a solution of methyl-CCNU in trifluoroacetic anhydride. Examination of the product by gas chromatography revealed the presence of a compound which had the same retention time as the trifluoroacetyl derivative of denitrosated methyl-CCNU, as reported earlier [2]. The product was also examined by high-resolution mass spectrometry, which revealed the presence of both unchanged methyl-CCNU and the trifluoroacetyl derivative of methyl-CCNU (III).

Although there has been no previous report of the reaction of nitrosoureas with trifluoroacetic anhydride, the closely related *N*-nitrosamines have been reacted with fluorinated anhydrides in the presence of pyridine as catalyst, and the structure of the products identified [4—6]. The structures reported for these derivatives show no evidence for denitrosation of the nitrosamines by the anhydrides. Cleavage of the *N*-nitroso bond by trifluoroacetic anhydride, as reported here, may be peculiar to a nitrosourea as distinct from nitrosamines.

The yield of the reaction between methyl-CCNU and trifluoroacetic anhydride was calculated to be 14.5 ± 3.0%, by comparison of the peak-height ratios obtained for ethereal solutions of the drug (Table 1) and those obtained when the pure denitrosated urea was treated with the reagent as reported earlier [2], because the latter reaction was quantitative. An attempt to improve this low yield by conducting the reaction in a chloroform solution of trifluoroacetic anhydride and heating the mixture on a water bath (60°C for 30 min) was not successful, the methyl-CCNU being recovered unchanged. No attempt was made to use pyridine to catalyze the reaction because of the known extreme instability of methyl-CCNU to base.

Gas chromatography of the trifluoroacetyl derivative was found to be applicable to the determination of methyl-CCNU after its extraction from plasma and subsequent reaction with trifluoroacetic anhydride. A typical chromatogram obtained by treatment of a plasma extract is shown in Fig. 1.

Linear calibration graphs were obtained when standard solutions of the drug extracted from plasma and made up in ether were examined (Table 1). A comparison of the regression equation for plasma and ether standards shows the recovery of the drug from plasma to be 83%, a result which is consistent with earlier reports [2, 3].

TABLE 1

Calibration results for methyl-CCNU extracted from plasma and dissolved directly in ether

Methyl-CCNU taken (μg ml^{-1})	Peak-height ratio of derivative to dimethylaniline[a]	
	Plasma[b]	Ether[c]
2.5	0.22(27)	0.16
5.0	0.42(21)	0.40
10.0	0.82(18)	0.66
15.0	0.97(8)	1.12
20.0	1.20(9)	1.76
25.0	2.23(5)	2.16

[a]Each value is the mean of 4 separate determinations for plasma, and 2 for ether. The relative standard deviations (%) are shown in parentheses. [b]Regression equation: $y = 0.079(\pm 0.010)x - 0.033(\pm 0.153)$ where y is the peak-height ratio and x is the concentration of methyl-CCNU in μg ml^{-1}. Standard error = 0.231. [c]Regression equation: $y = 0.095x - 0.162$.

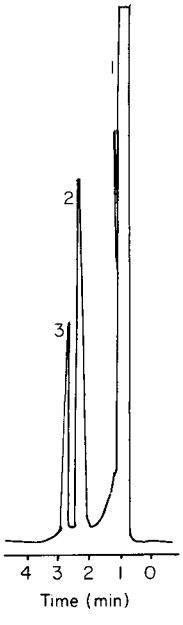

Fig. 1. Gas chromatogram of 1-(β-chloroethyl)-1-*N*-trifluoroacetyl-3-(4-methylcyclohexyl)-urea from the reaction of a plasma extract of methyl-CCNU with trifluoroacetic anhydride: (1) solvent front; (2) 1-(β-chloroethyl)-1-*N*-trifluoroacetyl-3-(4-methylcyclohexyl)urea; (3) *N*,*N*-dimethylaniline (standard).

A detection limit (2σ) of 1.5 $\mu g\ ml^{-1}$ was found for the complete method, a relatively high value which may be accounted for by the low yield of the derivatisation reaction. The method is, however, simple and moderately fast; it will be of use when, for example, toxic levels of methyl-CCNU have to be measured and simplicity and speed become paramount requirements. Greater sensitivity may also be achieved if an electron-capture detector is used.

REFERENCES

1 B. Caddy and O. R. Idowu, Analyst (London), 107 (1982) 301, 556.
2 B Caddy and O. R. Idowu, Analyst (London), 107 (1982) 556.
3 B. Caddy and O. R. Idowu, Anal. Chim. Acta, 160 (1984) 249.
4 J. B. Brooks, C. C. Alley and R. S. Jones, Anal. Chem., 47 (1972) 1881.
5 T. A. Gough, K. Sugden and K. S. Webb, Anal. Chem., 47 (1975) 509.
6 T. A. Gough, M. A. Pringuer, K. Sugden, K. S. Webb and C. F. Simpson, Anal. Chem., 48 (1976) 583.

Analytica Chimica Acta, 185 (1986) 341—346
Elsevier Science Publishers B.V., Amsterdam — Printed in The Netherlands

Short Communication

SPECTROPHOTOMETRIC DETERMINATION OF OXALIC ACID IN PRESENCE OF GLYOXYLIC ACID AND CHLORIDE

G. PIERRE*, M. EL KORDI and G. CAUQUIS

Laboratoire de Chimie Organique Analytique (UA CNRS 321), Université Scientifique et Médicale de Grenoble, B.P. 68, 38402 Saint Martin d'Hères Cedex (France)

(Received 8th October 1985)

Summary. Glyoxylic acid gives a yellow 1:1 complex, $[Fe—CHOCOO]^{2+}$ with iron(III). The dissociation constant, measured by two spectrophotometric methods, is $K = 9.7 \pm 1$ mol l^{-1}. Oxalic acid gives two complexes with iron(III) which absorb in the same range around 400 nm. With appropriate precautions and corrections, oxalic acid concentrations of about 10^{-1}—10^{-2} M can be determined in the presence of glyoxylic acid and chloride.

In the course of an investigation of the synthesis of glyoxylic acid by electrochemical oxidation of glyoxal, it was observed that oxalic acid is always present, resulting from a further oxidation of glyoxylic acid [1]. The reactions can be written:

$$CHOCHO - 2e^- + H_2O \rightarrow CHOCOOH + 2H^+ \quad (1)$$

$$CHOCOOH - 2e^- + H_2O \rightarrow COOHCOOH + 2H^+ \quad (2)$$

$$COOHCOOH - 2e^- \rightarrow 2CO_2 + 2H^+ \quad (3)$$

As the glyoxal is incompletely oxidized at the end of electrolysis, which could result from a Kolbe reaction on glyoxylic acid, the solution contains frequently three or more products (residual glyoxal, glyoxylic acid, oxalic acid and sometimes formic acid) in addition to the supporting electrolyte. These by-products are formed because none of them is oxidized at a well defined potential in an aqueous medium on different anode materials [1].

In order to follow the progress of the reaction, it is necessary to determine the concentrations of each of the constituents with good precision several times during the electrolysis. The concentrations of glyoxal and glyoxylic acid can be measured by polarography [1], which needs only a small volume of solution (50—500 μl). The determination of oxalic acid causes a particular problem. The pure acid is easy to titrate with a strong base, but the method is not useful here because other acidic species present have pK_a values close to those of the oxalic acid, and because free protons are formed during the electrolysis (reactions 1—3): oxalic acid (pK_a = 1.23 and 4.19) glyoxylic acid (pK_a = 3.32) and sometimes formic acid (pK_a = 3.75) which can be obtained

0003-2670/86/$03.50

in some conditions from the reaction:

$$CHOCHO - 2e^- + 2H_2O \rightarrow 2HCOOH + 2H^+ \quad (4)$$

The precipitation of calcium oxalate, whether followed by gravimetry or another procedure is complicated here by the presence of glyoxylic acid giving also poorly soluble calcium salt. All these methods are time-consuming and need samples of 10—20 ml to obtain reproducible results.

Some years ago, Szetey et al. [2] proposed an interesting spectrophotometric determination of oxalic acid based on the formation of the iron(III) complex $[Fe—C_2O_4]^+$. This method would be simple if oxalate were the only species giving a complex with iron, but some experiments showed that there were interferences. The purpose of this communication is to show the existence of a complex between glyoxylic acid and iron(III), and to describe how this spectrophotometric technique can be used to determine oxalic acid in presence of glyoxylic acid. The method is designed for use with chloride solutions which are frequently used as the supporting electrolyte [1].

Experimental

Spectra were recorded on a Beckman Acta III-C spectrophotometer with cells of 1-cm pathlength. Stock solutions of oxalic acid (Prolabo) and of iron(III) perchlorate (Fluka) were standardized, respectively, with sodium hydroxide and by atomic absorption spectrometry. All the dilutions were made with 1 M perchloric acid in deionized/twice-distilled water.

Procedure. The sample solution (100 μl) and 5 ml of 5×10^{-2} M iron(III) perchlorate in 1 M perchloric acid are placed in a 10-ml flask. The volume is adjusted to 10 ml with the acid solution. The spectrum is quickly recorded against a solution of 2.5×10^{-2} M iron(III) perchlorate in the reference cell. Absorbances at 400 nm are used routinely.

Results and discussion

Although formic acid gives no complex with iron(III), glyoxylic acid interferes in the determination of oxalic acid by spectrophotometry. The errors are positive or negative, depending on the experimental conditions, by comparison with prepared solutions of the two acids. Several attempts to find the reasons for these errors led to the following conclusions. In aqueous 1 M perchloric acid, the yellow complex obtained by adding iron(III) perchlorate to a solution of oxalic acid shows only a continuum increasing from 480 nm to 360 mm (Fig. 1, curve 4); the latter wavelength corresponds to the absorption of iron(III) perchlorate itself (curve 2). The complex is stable for several hours only in absolute darkness. Exposed to daylight, its colour vanishes within a few hours, depending on the lighting of the room. Thus in all cases, the measurements must be made as soon as the complex is prepared. Although there is some absorption by iron(III) at 420 nm, measurements are possible even at slightly lower wavelengths if the reference cell contains iron perchlorate at the same concentration as the sample cell. The addition of

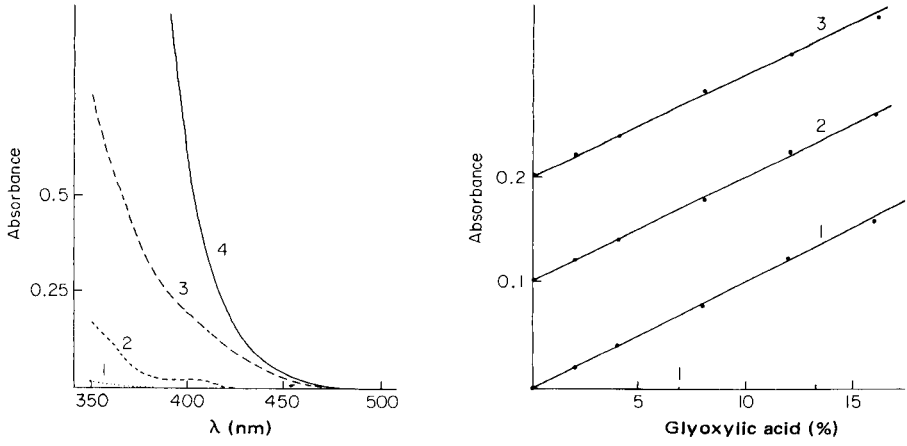

Fig. 1. Absorption of the different species and complexes in 1 M perchloric acid (1-cm cells; 1 N $HClO_4$ reference): (1) 10^{-1} M CHOCOOH; (2) 5×10^{-2} M iron(III) perchlorate; (3) 5×10^{-2} M CHOCOOH/5×10^{-2} M iron(III) perchlorate; (4) 5×10^{-3} M COOHCOOH/5×10^{-2} M iron(III) perchlorate.

Fig. 2. Influence of the concentration of glyoxylic acid on the absorption of solutions containing different concentrations of oxalic acid: (1) 0; (2) 6.6×10^{-2} M; (3) 1.32×10^{-1}. Conditions: 5×10^{-2} M iron(III) perchlorate, 400 nm, 1-cm cells.

glyoxal does not alter the colour of the complex, when the dilution factor is considered [2]. No change in absorbance is observed when pure glyoxal is mixed with an iron(III) solution, so it can be concluded that no complex is formed. However, the colour of the yellow solution increases when glyoxylic acid is added to a solution of the iron(III)/oxalic acid complex (Fig. 2, curves 2, 3) or to an iron(III) solution alone (Fig. 2, curve 1). This new complex absorbs in the same range as the oxalic acid complex (Fig. 1, curve 3), which causes large errors in the determination of oxalic acid, as oxalic acid is 6—10 times less concentrated than glyoxylic acid in the solution obtained from electrolysis of glyoxal [1].

The iron(III)/glyoxylic acid complex. The increased absorbance is not caused by traces of oxalic acid in glyoxylic acid; this was confirmed by liquid chromatography with an Aminex ion-exclusion column (HPX-87H, Bio-Rad). Moreover, the behaviour of the two complexes is different (Fig. 3) when their absorptions are compared by the continuous variations method [3]. For oxalic acid, the shape of the curve, indicates a 2:1 complex [4, 5] but the composition at the maximum and the inflection suggest rather a mixture of 1:1 and 1:2 complexes. In contrast, curves 1, 2 and 3 related to glyoxylic acid indicate the formation of only a 1:1 complex; the maximum is obtained for equimolar concentrations of the two constituents and there is no change in slope on either side of the maximum [4, 5]. The reaction is therefore

$$CHOCOOH + Fe^{3+} \rightarrow [Fe{-}CHOCOO]^{2+} + H^+$$

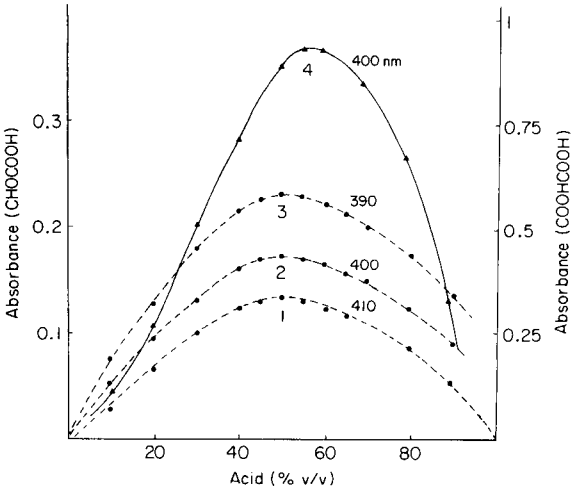

Fig. 3. Application of the continuous variations method to the different complexes of iron with oxalic and glyoxylic acid. Initial concentrations: (1—3) [Fe(III)] = [COOHCHO] = 10^{-1} M; (4) [Fe(III)] = [COOHCOOH] = 1.5×10^{-2} M. Wavelength: (1) 410 nm; (2) 400 nm; (3) 390 nm; (4) 400 nm (1-cm cells).

For this complex, the molar absorptivities (in l mol^{-1} cm^{-1}) measured at different wavelengths are 4.60 at 390 nm, 3.44 at 400 nm, and 2.72 at 410 nm.

Dissociation constant of the [Fe—CHOCOO]$^{2+}$ complex in 1 M perchloric acid. The dissociation constant, defined by $K = [Fe^{3+}][CHOCOOH]/[Fe—CHOCOO]^{2+}$ was evaluated from the continuous-variations plots using different concentrations of both constituents [3]. However, the low absorbances and the broad peaks do not allow very precise values of K to be achieved. Accordingly, K was also calculated by the method of dilution [6], i.e., measurement of the concentration of the complex (by spectrophotometry) at different concentrations of its constituents. If a substance disociates, and C_1 and C_2 are its concentrations in two solutions with $C_2 < C_1$ and $V = C_1/C_2$ (dilution factor), it is easy to demonstrate [6] that $K = C_1(1 - F)^2/F$, where F is the undissociated fraction of the substance in the undiluted solution C_1 and can be expressed as

$$F = r/[V(r-1)]\{(V-1) - [(V-1)^2 - (r-1)(V^2r^{-1} - 1)]\}^{1/2}$$

where r is the ratio of the undissociated substance, here the complex, in the more concentrated solution to that in the less concentrated solution. This ratio is measured by spectrophotometry and corresponds to the ratio of the absorbances of the two solutions because glyoxylic acid is transparent and the small absorbance of iron(III) is cancelled by using an iron(III) solution in the reference cell.

The two methods are not precise. The average of all the measurements (Tables 1 and 2) gives a value of $K = 9.7 \pm 1$, all the concentrations being

TABLE 1

Determination of K by the continuous variations method (20° C)

λ (nm)	Fe^{3+} (M)	CHOCOOH (M)	x	K (mol l^{-1})
400	0.101	0.05	0.440	11.1
390	0.101	0.05	0.447	9.8

TABLE 2

Determination of K by the dilution method (20° C)

λ (nm)	V	Absorbance	K (mol l^{-1})	λ (nm)	V	Absorbance	K (mol l^{-1})
400	1	0.233	—	390	1	0.296	—
	1.33	0.147	9.3		1.33	0.180	8.6
	2	0.075	10.3		2	0.094	9.3

expressed in mol l^{-1}. Like the oxalic acid complex, this complex is not stable. On exposure to daylight, its absorbance decreases by about 30% of its initial value within 4 h. Thus the absorption curves have to be recorded within a few minutes after preparation of the complexes.

Influence of the chloride ion. The yields of the electrosyntheses of glyoxylic acid are improved when the medium contains chloride as the anion in the supporting electrolyte [1]. Thus, another difficulty is caused by the yellow chloroferrate(III) complex. As the system becomes even more complicated if glyoxylic acid and chloride are present simultaneously, two series of experiments were conducted in a 1 M perchloric acid medium with different concentrations of oxalic acid; the evolution of the absorbance was monitored during the addition of known amounts of chloride or glyoxylic acid. The concentration ranges studied were those normally present during the electrolyses, i.e., 0.3—1% (w/w) oxalic acid, 2—10% glyoxylic acid and 1—4% chloride. The solutions were diluted ten times before the spectra were recorded. Iron(III) was always in large excess and the absorbance of oxalic acid at 400 nm increased linearly with the concentration of chloride and glyoxylic acid, following the equation Absorbance (corrected) = Absorbance (measured) $- 0.34x - 0.01y$, where x and y are respectively the amounts (by weight) of chloride and glyoxylic acid in the solution. This corrected absorbance value is then compared with a calibration curve obtained for oxalic acid alone in the iron(III) solution. Under such conditions, 100 μl suffices for the determination of the oxalic acid and the results are precise within 4% by comparison with standard solutions.

Under the experimental conditions used, oxalic acid cannot be determined by liquid chromatography on an Aminex HPX-87H column with 10^{-2} M sulphuric acid as eluent. Chloride must be avoided in the column, and the

retention times of nitric and perchloric acids, which are possible electrolytes in the oxidation of glyoxal, are the same as that of oxalic acid.

We thank la Société Française Hoechst for financial support.

REFERENCES

1 G. Pierre, M. El Kordi, G. Cauquis, G. Mattioda and Y. Christidis, J. Electroanal. Chem., 186 (1985) 167.
2 E. Szetey, G. Inzelt and G. Horanyi, Acta Chim. Acad. Sci. Hung., 98 (1978) 367.
3 P. Job, C.R. Acad. Sci. Paris, 180 (1925) 928; Ann. Chim., Paris, 9 (1928) 113.
4 K. S. Klausen and F. J. Langmyhr, Anal. Chim. Acta, 28 (1963) 335; 40 (1968) 167.
5 E. Asmus, Z. Anal. Chem., 183 (1961) 321.
6 L. I. Katzin and E. Gebert, J. Am. Chem. Soc., 76 (1954) 2049.

Analytica Chimica Acta, 185 (1986) 347—349
Elsevier Science Publishers B.V., Amsterdam — Printed in The Netherlands

Short Communication

ION-SELECTIVITY OF PLASTICIZERS IN POLY(VINYL CHLORIDE) MEMBRANE ELECTRODES

SOLFRID BUØEN, JOHANNES DALE and WALTER LUND*
Department of Chemistry, University of Oslo, Box 1033, 0315 Oslo (Norway)
(Received 4th December 1985)

Summary. Electrode membranes were prepared which contained only PVC and a plasticizer. The plasticizers studied were tris(2-ethylhexyl)phosphate, 2-nitrophenyl octyl ether and bis(1-butylpentyl)adipate. The response and selectivity of these ligand-free PVC electrodes towards alkali and alkaline earth cations are reported.

During an investigation of the possible use of various crown ethers as ionophores in poly(vinyl chloride) (PVC) membrane electrodes, the predominating effect of the plasticizer became apparent. It was found that the PVC-plasticized membranes exhibited a near-Nernstian response to alkali metals, even in the absence of any specific ionophore. The response and selectivity of the membranes were governed by the plasticizer used.

Relatively little has been reported concerning the behaviour of ligand-free PVC membranes. In connection with the evaluation of various ionophores, Simon and co-workers have evaluated the selectivity coefficients log $K^{\mathrm{Pot}}_{\mathrm{Ca,X}}$ and log $K^{\mathrm{Pot}}_{\mathrm{Mg,X}}$ for ligand-free membranes plasticized with 2-nitrophenyl octyl ether [1, 2], and log $K^{\mathrm{Pot}}_{\mathrm{PbA,X}}$ for a membrane plasticized with bis(1-butylpentyl)adipate [3]. Further, a Nernstian response to hydrophobic organic cations has been noted for a membrane plasticized with dioctylphthalate [4]. In this communication, the response of ligand-free PVC membranes towards alkali and alkaline earth metal ions is reported. Three of the commonly used plasticizers were studied; these were tris(2-ethylhexyl)phosphate (TEHP), 2-nitrophenyl octyl ether (NPOE) and bis(1-butylpentyl)adipate (BBPA).

Experimental

Electrodes. The composition of the membranes was 33% PVC and 67% plasticizer (TEHP, NPOE or BBPA). The membranes were prepared by dissolving 180 mg of PVC and 360 mg of the plasticizer in 3 ml of tetrahydrofuran. Only ISE-reagents from Fluka were used. The solution was poured into a Petri dish (diameter 4 cm), and the solvent was evaporated at room temperature.

A disk (8-mm diameter) was cut from the PVC membrane and incorporated into a home-made electrode. The electrode body was made from a 1-ml dis-

0003-2670/86/$03.50

posable syringe (Gillette), which was equipped with a teflon ring to fasten the membrane. The diameter of the exposed part of the membrane was 2 mm. The syringe piston was replaced by a shielded wire, with a tip of silver. This served as the inner reference electrode, in combination with an inner filling solution of 0.01 M of the appropriate alkali metal chloride. The electrodes were conditioned by soaking in a 1 M alkali metal chloride solution for 24 h. The external reference electrode was of the sleeve type, Orion 9001 (Ag/AgCl), with 900001 filling solution. A salt bridge, consisting of 0.1 M ammonium nitrate in agar gel was used in conjunction with this electrode.

Measurements. The e.m.f. measurements were made at 25.0° C, with an Orion Research model 811 pH meter. Calibration plots were obtained by dilution of 0.1 M solutions of the appropriate alkali metal chlorides. The selectivity coefficients were determined by the separate solutions method.

Results and discussion

From Fig. 1, it can be seen that the PVC membranes respond in a Nernstian fashion to alkali metal ions. The TEHP-plasticized membrane, when used as a lithium electrode, exhibited a slope of 54 mV/pC_M, for concentrations between 10^{-1} and 10^{-3} M of lithium chloride. When the NPOE-plasticized membrane was used as a potassium electrode, a slope of 43 mV/pC_M was observed in the same concentration region. A 45 mV/pC_M slope was obtained for the BBPA-plasticized membrane used as a sodium electrode, but only for concentrations between 10^{-1} and 10^{-2} M.

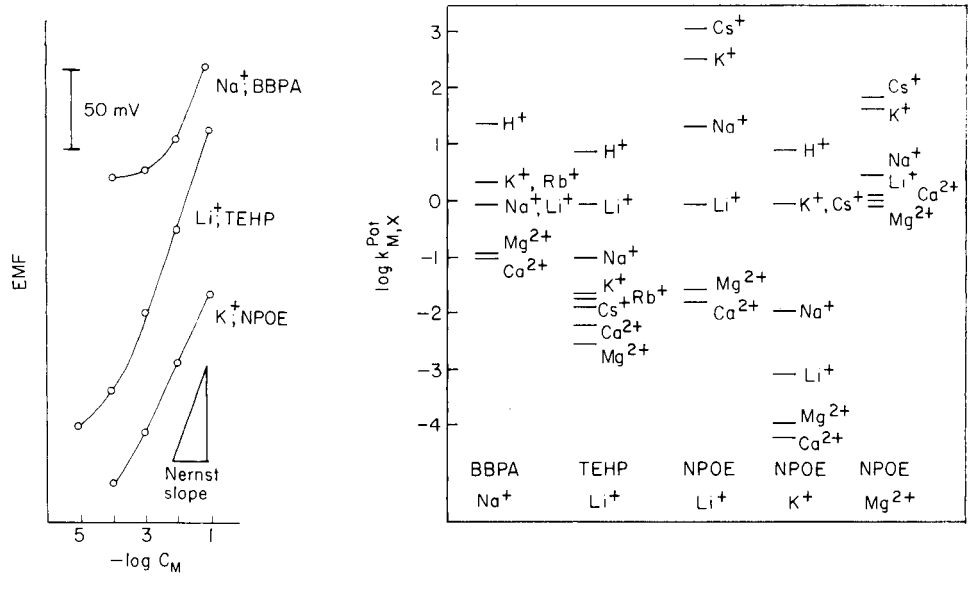

Fig. 1. E.m.f. response of the ligand-free PVC membranes to alkali metals in solution. The metal ion and plasticizer are indicated on each curve.

Fig. 2. Selectivity coefficients of the ligand-free PVC membranes. The plasticizer and the reference cation are indicated at the bottom of the figure.

The selectivity coefficients obtained with these membranes are shown in Fig. 2. The reference cations are indicated at the bottom of the figure. Thus, the values in the first column refer to the coefficient log $K^{Pot}_{Na,X}$, those in the second column to log $K^{Pot}_{Li,X}$, and so on. Accordingly, the BBPA and TEHP membranes were conditioned with sodium and lithium chloride, respectively, whereas the NPOE membrane was examined in the lithium, potassium and magnesium modes. The log $K^{Pot}_{Mg,X}$ values obtained for the NPOE-plasticized membrane compare reasonably well with the results of Erne et al. [2].

The above results illustrate that the plasticizer, in addition to its proper function, also partly behaves as an ionophore, and thus competes with the ionophore which is usually added to such membranes. Although the behaviour of these ligand-free membranes differs from that expected of a good electrode, the same will be true for many new ionophores that are examined. Hence, to assess the effect of a new ionophore, the response and selectivity of the plasticizer must always be considered carefully. Of course, the advantages of using a good ionophore in addition to the plasticizer are easily recognized. Such an ionophore improves both the Nernstian response and the selectivity of the membrane very significantly. Further, the ligand-free membranes show a poorer reproducibility and a more marked drift than more conventional electrodes.

REFERENCES

1 R. Bissig, E. Pretsch, W. E. Morf and W. Simon, Helv. Chim. Acta, 61 (1978) 1520.
2 D. Erne, N. Stojanac, D. Ammann, P. Hofstetter, E. Pretsch and W. Simon, Helv. Chim. Acta, 63 (1980) 2271.
3 E. Lindner, K. Toth, E. Pungor, F. Behm, P. Oggenfuss, D. H. Welti, D. Ammann, W. E. Morf, E. Pretsch and W. Simon, Anal. Chem., 56 (1984) 1127.
4 J. R. Luch, T. Higuchi and L. A. Sternson, Anal. Chem., 54 (1982) 1583.

Analytica Chimica Acta, 185 (1986) 351—354
Elsevier Science Publishers B.V., Amsterdam — Printed in The Netherlands

Short Communication

COATED-WIRE ION-SELECTIVE ELECTRODE FOR THE DETERMINATION OF GOLD(III)

J. A. ORTUÑO, T. PÉREZ RUIZ and C. SÁNCHEZ-PEDREÑO*
Department of Analytical Chemistry, University of Murcia, 30071-Murcia (Spain)
(Received 7th October 1985)

Summary. A coated-wire gold(III)-selective electrode based on the 1,2,4,6-tetraphenylpyridinium tetrachloroaurate(III) ion-pair is described. The response is Nernstian in the gold concentration range 10^{-2}—3×10^{-6} (slope 59.0 mV/pAu). Of the 22 ions tested, only the interference of thallium(III) is important. The electrode is applied to the determination of gold in an Ag-Pd-Au alloy with satisfactory results.

Coated-wire electrodes containing, as electroactive materials, negatively charged halide and pseudohalide complexes of the metal ions to be determined have been reported. Iron [1], copper [2], mercury [3], zinc [4] and bismuth [5] have been measured as their chloro complexes, and cobalt [6] as its tetrathiocyanatocobaltate(II) complex. The ion-pair complexes formed by these complex anions with Aliquat-336S [1—5] and benzalkonium [6] were incorporated into a poly(vinyl chloride) (PVC) matrix for coating a metal wire electrode.

The formation and extraction of an ion-pair of tetrachloroaurate(III) with 1,2,4,6-tetraphenylpyridinium has been reported recently [7]. The high extractability and good selectivity of this ion-pair suggested its application as an electroactive material in coated-wire electrodes. The selectivity of these sensors depends on the extractability of the ion-pair involved. In this communication, an electrode for the selective determination of gold(III) is reported.

Experimental

Reagents and apparatus. Wherever possible, analytical-reagent grade chemicals were used. Synthesis of 1,2,4,6-tetraphenylpyridinium perchlorate (TPPP) was as before [7]. A gold(III) standard solution (0.01 M) was prepared by dissolving tetrachloroauric acid in 0.1 M hydrochloric acid and standardized by the iodimetric method with thiosulphate [8].

Potentials were measured at room temperature with a Philips PW9415 ion-selective meter against a Philips R-44/2-SD/1 calomel double-junction reference electrode. Magnetic stirring was used.

Electrode preparation and use. The electroactive material was prepared by

0003-2670/86/$03.50

adding 0.0968 g of TPPP dissolved in 3 ml of acetone to 80 ml of 2.5×10^{-3} M gold(III) solution in 1.4 M hydrochloric acid. The mixture was stirred for 1 h; then the precipitate was filtered off, washed with distilled water and dried at 105°C.

Two different electrodes were made by varying the composition of coatings on the electrode in the following manner. For electrode A, PVC (0.1 g), dibutyl phthalate (0.2 g) and electroactive material (0.01 g) were dissolved in 3 ml of tetrahydrofuran. A platinum wire (about 2 cm long, 1.0-mm diameter) sealed into the end of a glass tube and soldered on to a shielded cable, was dipped in this solution fifteen times and the solvent was evaporated with an air drier after each immersion. A membrane film was formed on the platinum surface and the electrode was allowed to set overnight. For electrode B, PVC (0.1 g), dibutyl phthalate (0.1 g) and electroactive material (0.01 g) were dissolved in 3 ml of tetrahydrofuran and the process was completed as described for electrode A.

The electrodes were immersed in a hydrochloric acid solution of the same concentration as the standards, with constant stirring, until they gave a constant potential value (about 1 h). The responses of the electrodes to 10^{-2}—10^{-7} M gold(III) were studied for solutions with hydrochloric acid concentrations varying from 0.1 to 1.0 M.

The electrodes were stored dry and immersed in hydrochloric acid solution as above, before each series of measurements.

Results and discussion

Response range and effect of hydrochloric acid concentration. Figure 1 shows the response characteristics of electrodes A and B to gold(III) concentrations of 10^{-2}—10^{-7} M at various hydrochloric acid concentrations. The electrode was transferred from low to high gold(III) concentrations. The length of the linear portion of the calibration curve was found to depend on the hydrochloric acid concentration. The linear portion was shorter for 1 M hydrochloric acid for both electrodes. In 0.1 M hydrochloric acid, electrode A gave a linear relationship between potential and the logarithmic gold(III) concentration in the range 3×10^{-3}—10^{-6} M (slope = —58.8 mV/log [Au], correlation coefficient = 0.9999), and electrode B behaved similarly in the range 10^{-2}—3×10^{-6} M (slope = —59.0 mV/log [Au], correlation coefficient = 0.9999). All subsequent solutions were prepared in 0.1 M hydrochloric acid.

Response time and reproducibility. Uemasu and Umezawa [9] suggested that response times of ion-selective electrodes be defined as the time necessary to achieve a specified rate of potential change. This definition was discussed in a recent review [10]. According to these authors, it is possible to find a time t (Δt, ΔE) when the size of the potential change becomes at most ΔE during time Δt. Response times for electrode A and B are shown in Table 1. As reported by Catrall et al. [11], the response time increased with a decrease in the amount of plasticizer.

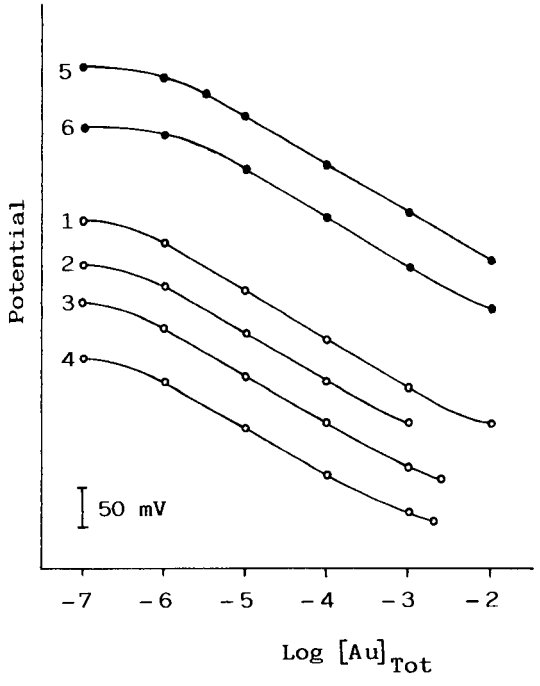

Fig. 1. Calibration curves for electrode A (curves 1–4) and electrode B (curves 5 and 6) in solutions containing different concentrations of hydrochloric acid: (1) 0.1 M; (2) 0.25 M; (3) 0.6 M; (4) 1 M; (5) 0.1 M; (6) 1 M.

TABLE 1

Response times of gold(III) electrodes prepared by the two methods

Au(III) concentration step	t (1, 0.1)[a] (min)	
	Electrode A	Electrode B
$10^{-7} \rightarrow 10^{-6}$ M	1	2.5
$10^{-6} \rightarrow 10^{-5}$ M	0.5	1.5
$10^{-5} \rightarrow 10^{-4}$ M	0.5	1.5
$10^{-4} \rightarrow 10^{-3}$ M	0.25	0.25
$10^{-3} \rightarrow 10^{-2}$ M	0.25	0.25

[a] t (Δt, ΔE): Δt, min; ΔE, mV.

Potential drifts have often been observed in coated-wire electrodes; they depend on the proportion of plasticizer in the coating. Reducing the plasticizer level from about 65% (electrode A) to about 50% (electrode B) significantly reduced the potential drifts. A compromise must be reached between reproducibility and response time. The advantage of increased reproducibility found for electrode B offsets the disadvantage of its longer response at low concentrations, and therefore electrode B was selected.

TABLE 2

Selectivity coefficients for different ions

$K^{pot}_{Au,j}$	Ion
10^{-5}	NO_3^-, Cl^-
5×10^{-5}	SO_4^{2-}, Ag^+, Mn^{2+}, Ni^{2+}, Pb^{2+}, Cu^{2+}, Zn^{2+}, Cd^{2+}, Cr^{3+}, In^{3+}, Ga^{3+}, As(V)
2×10^{-4}	ClO_4^-, Hg^{2+}, Fe^{3+}
5×10^{-4}	Pd^{2+}
2×10^{-3}	Bi^{3+}
5×10^{-3}	Pt(IV)
10^{-2}	Sb(V)
0.80	Tl^{3+}

The potential for an individual standard gold(III) solution could be reproduced, for consecutive measurements, to within ±0.1 mV. The slope of the calibration graph remained practically the same for a period of two weeks, and then began to decrease slowly. The detection limit of the electrode [12] was 9×10^{-7} M.

Interferences. The effect of interferences of other ions was evaluated by measuring selectivity coefficients, $K^{pot}_{Au,j}$, by the mixed solution technique. The results presented in Table 2 show good selectivity. Thallium(III) causes the largest interference.

Analytical applications. The utility of the new gold(III)-selective electrode was checked by using it for the determination of gold in a silver-palladium-gold alloy for dental prosthesis. The sample was dissolved in aqua regia; the solution was evaporated almost to dryness, transferred with water to a calibrated flask of appropriate volume, and diluted to the mark with a hydrochloric acid solution to give a final concentration of 0.1 M. The gold(III) concentration was evaluated by direct potentiometry, from a calibration graph prepared with gold(III) standard solutions. The average value of three determinations was 3.05% gold (standard deviation 0.05), in agreement with the 3.0% gold certified by Sociedad Española de Metales Preciosos, S.A.

REFERENCES

1 R. W. Catrall and Chin-Poh Pui, Anal. Chem., 47 (1975) 93.
2 R. W. Catrall and Chin-Poh Pui, Anal. Chim. Acta, 83 (1976) 355.
3 R. W. Catrall and Chin-Poh Pui, Anal. Chem., 48 (1976) 552.
4 R. W. Catrall and Chin-Poh Pui, Anal. Chim. Acta, 87 (1976) 419.
5 P. W. Alexander and J. P. Joseph, Talanta, 28 (1981) 931.
6 K. Burger and G. Pethö, Anal. Chim. Acta, 107 (1979) 113.
7 J. A. Ortuño, T. Pérez Ruiz, C. Sánchez-Pedreño and P. Molina Buendía, Microchem. J., 30 (1984) 71.
8 F. E. Beamish, The Analytical Chemistry of the Noble Metals, Pergamon, Oxford, 1966.
9 I. Uemasu and Y. Umezawa, Anal. Chem., 54 (1982) 1198.
10 M. A. Arnold and M. E. Meyerhoff, Anal. Chem., 56 (1984) 20R.
11 R. W. Catrall, S. Tribuzio and H. Freiser, Anal. Chem., 46 (1974) 2223.
12 I. U. P. A. C., Pure Appl. Chem., 48 (1976) 127.

Analytica Chimica Acta, 185 (1986) 355—358
Elsevier Science Publishers B.V., Amsterdam — Printed in The Netherlands

Short Communication

DIFFERENTIAL-PULSE ANODIC VOLTAMMETRIC DETERMINATION OF DISSOLVED AND ADSORBED PHOSPHATE IN TURBID NATURAL WATERS

K. MATSUNAGA*, I. KUDO and M. YANADA

Department of Chemistry, Faculty of Fisheries, Hokkaido University, Hakodate 041 (Japan)

K. HASEBE

Department of Chemistry, Faculty of Science, Hokkaido University, Sapporo 060 (Japan)

(Received 31st July 1985)

Summary. Orthophosphate in turbid natural waters exists in dissolved and adsorbed forms. Phosphate adsorbed on suspended matter in turbid waters is difficult to determine spectrophotometrically. In the voltammetric method, the peak current is related to the reoxidation of the molybdophosphate complex at a glassy-carbon electrode. This allows the determination of dissolved and adsorbed phosphate at micromolar levels in natural waters, especially turbid waters, with good precision and accuracy.

Spectrophotometric methods for the determination of phosphate in natural waters have been widely used (see, e.g., [1, 2]). High sensitivity and good precision are possible for natural waters containing small amounts of suspended matters. In natural waters with high turbidity, however, the absorbance of the suspended matter (i.e., turbidity) must be measured and a correction applied for the turbidity. It is very difficult to measure accurately the absorbance of turbidity because the values can be scattered. Although the amount of suspended matter can be decreased by filtration, the phosphate concentration in the filtrate also decreases considerably. Thus it is difficult to measure phosphate concentrations accurately in very turbid waters. No method seems to have been reported for the determination of both dissolved and adsorbed phosphate in natural waters.

Fogg et al. [3] and Fogg and Bsebsu [4] showed that the molybdophosphate complex is reduced on a stationary glassy-carbon electrode and that the reoxidation current of the reduced complex can be used to determine phosphate in an aqueous solution. Here the applicability of this method to natural waters is examined and adsorbed phosphate is also determined. The results by the voltammetric method are compared with those obtained by spectrophotometry [2].

0003-2670/86/$03.50

Experimental

Mixed reagent. Dissolve 1.5 g of sodium molybdate and 1.5 g of tartaric acid in 45 ml of water and add 5 ml of concentrated hydrochloric acid. The mixed solution is discarded after three days when it becomes brown.

All other reagents were of analytical-reagent grade.

A Yanako Voltammetric Analyzer P-1000 was used with a glassy-carbon electrode (GC-P2, 3-mm diameter), a platinum wire as counter electrode and a saturated calomel electrode as reference electrode. Sweep rate, pulse amplitude and pulse interval were 5 mV s^{-1}, 50 mV and 0.1 s, respectively. The glassy-carbon electrode was cleaned by ultrasonic treatment in methanolic 1 M sodium hydroxide before use.

Procedure. The sample solution (20 ml), 27 ml of acetone and 3 ml of the mixed reagent were poured into a 50-ml volumetric flask, and the mixture was diluted to the mark with water. The solution was transferred to a voltammetric cell and stirred for 10 min. A differential-pulse voltammogram was recorded between 0 and +0.5 V. The concentration of phosphate was determined by a standard addition method.

Results and discussion

Optimum conditions. The phosphate solution for initial tests was 2.5 μM in distilled water. The effect of acetone was first examined. Although the peak current decreased with increasing amounts of acetone, constant values were obtained with more than 25 ml of acetone. When the amount of mixed reagent added was varied from 1 ml to 10 ml, the peak current remained constant at about 48 nA. Although Fogg et al. [3] used 10 ml of the reagent, 3 ml of the reagent was found to be enough to prevent the interference of silicate, even when 750 μM silicate was present in the waters. A certain standing time is needed after the reagent has been added. For standing times of $\geqslant$9 min, the peak currents of the molybdophosphate complex remained constant.

The reproducibility of the method was tested for river and sea waters. The relative standard deviations for five determinations were 4.2% for 2.5 μM phosphate in sea water, and 5.1% for 1 μM phosphate in river water.

Comparison with the spectrophotometric method. Marine sediment, which had been soaked in 1 M sulfuric acid to remove phosphate, was added to a CSK standard solution (1 and 2 μM phosphate). The known phosphate concentration in the solution including a large amount of sediment was determined by both the spectrophotometric and voltammetric methods. The absorbances of the blue complexes including turbidity and those of only the turbidity without color development were measured as described by Strickland and Parsons [2]. Table 1 shows that all the absorbances were considerably scattered; the phosphate concentrations found spectrophotometrically were 0.46 and 1.49 μM for 1.00 and 2.00 μM phosphate actually present, respectively. In contrast, the voltammetric method gave good accuracy and precision (Table 1).

TABLE 1

Measurement of phosphate in a CSK standard solution containing a large amount of sediment[a]

Phosphate present (μM)	Absorbance	Phosphate found (μM)
Spectrophotometry		
0[b]	0.216 ± 0.052	—
1	0.258 ± 0.038	0.46 ± 0.70
2	0.351 ± 0.036	1.49 ± 0.71
Voltammetry		
1	—	0.97 ± 0.05
2	—	1.93 ± 0.27

[a]The values were calculated from 6 determinations at the 95% confidence limit. [b]Turbidity only was measured.

Phosphate concentrations in waters containing various amounts of suspended matter, were determined by both methods (Fig. 1). When the absorbance of the suspended matter was below 0.01, all values were almost on a 1:1 line. When the absorbance of the suspended matter was above 0.01, the values obtained spectrophotometrically were significantly lower than those obtained by the voltammetric method (cf. Table 1).

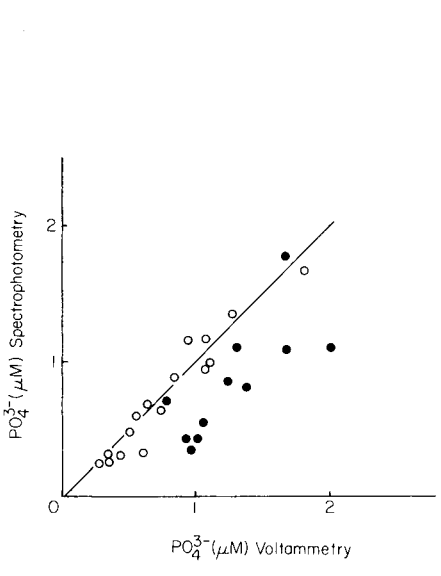

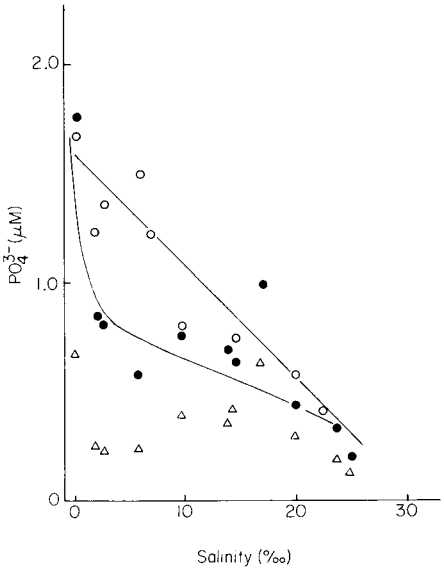

Fig. 1. Comparison of the voltammetric and spectrophotometric methods. The solid line shows the 1:1 relationship. Absorbance of turbidity: (○) < 0.01; (●) > 0.01.

Fig. 2. Phosphate measured vs. salinity: (○) voltammetry; (●) spectrophotometry; (△) phosphate in the filtrate (spectrophotometry).

Measurement of phosphate in an estuary. The phosphate concentrations measured by both methods were plotted against salinity (Fig. 2). The values obtained by the voltammetric method are on a dilution line, whereas those obtained by the spectrophotometric method are below that line, especially at low salinity. When phosphate in filtrates (0.45-μm pore size) was determined spectrophotometrically, the values were significantly lower. The most plausible reason is that a major portion of the phosphate in water containing large amounts of suspended matter is adsorbed on the suspended matter and is then removed when the water is filtered. The curve correspondong to the spectrophotometric data (Fig. 2) is considered to show adsorption of phosphate on marine sediment or assimilation of phosphate by phytoplankton. While phosphate in a red tide outbreak estuary is completely assimilated by phytoplankton [5], phosphate in an estuary having normal primary production is only adsorbed on the suspended matter. Figure 2 indicates that phosphate measured by the spectrophotometric method is in dissolved and adsorbed forms.

We thank Prof. T. R. Parsons of University of British Columbia for reading the manuscript.

REFERENCES

1 J. Murphy and J. P. Riley, Anal. Chim. Acta, 27 (1972) 31.
2 J. D. H. Strickland and T. R. Parsons, A Manual of Seawater Analysis, 2nd edn., Fish. Res. Board Can., Report no. 167 (1972) 49.
3 A. G. Fogg, N. K. Bsebsu and B. J. Birch, Talanta, 28 (1981) 473.
4 A. G. Fogg and N. K. Bsebsu, Analyst (London), 107 (1982) 566.
5 K. Matsunaga, K. Igarishi, S. Fukase and H. Tsubota, Estuarine Coastal Shelf Sci., 18 (1984) 615.

Analytica Chimica Acta, 185 (1986) 359—362
Elsevier Science Publishers B.V., Amsterdam — Printed in The Netherlands

Short Communication

VOLTAMMETRIC DETERMINATION OF NITRATE, PERCHLORATE AND IODIDE AT A HANGING ELECTROLYTE DROP ELECTRODE

V. MAREČEK*, H. JÄNCHENOVÁ, Z. SAMEC and M. BŘEZINA

J. Heyrovský Institute of Physical Chemistry and Electrochemistry, Czechoslovak Academy of Sciences, U. továren 254, 102 00 Prague 10 (Czechoslovakia)

(Received 3rd October 1985)

Summary. The use of a hanging electrolyte drop electrode is examined for the determination of nitrate, perchlorate and iodide. A three-electrode system was used with a polarographic analyzer. Crystal violet dicarbollylcobaltate(III) electrolyte in the nitrobenzene phase and magnesium sulphate in the aqueous phase with a $Pb/PbSO_4$ reference electrode made it possible to increase the viable potential range. For nitrate, the peak current/concentration relation was linear over the range 0—5 × 10^{-5} M, and nitrate in potable water was easily determined.

Electrolysis at the interface between two immiscible electrolyte solutions has been exploited for analytical purposes [1] and a simple three-electrode system with a hanging electrolyte drop electrode (HEDE) has been described [2]; the reference electrode in the aqueous phase also functioned as the counter electrode. Micromolar concentrations of some cations were determined by differential-pulse stripping voltammetry (d.p.s.v.). For the determination of anions, it was necessary to find suitable electrolytes for increasing the potential range.

Experimental

In the assembly of the HEDE [2], an electromagnetic valve was used instead of a calibrated microsyringe; this made it possible to control the drop volume and drop fall in a better defined way. The latter was achieved with an electromagnet-driven scythe-shaped knife across the tip of capillary. The whole system works similarly to a static mercury electrode. This three-electrode system was connected to a PA-3 polarographic analyzer (Laboratorní přístroje, Prague), which was modified by positive feedback for automatic IR-drop compensation. Differential pulse voltammetry (d.p.v.) was done with a pulse amplitude of 50 mV 100 ms^{-1} and a polarization rate of 10 mV s^{-1}.

Analytical-grade chemicals (Fluka) were used for the preparation of the electrolyte solutions in distilled nitrobenzene. Tetraphenylarsonium dicarbollylcobaltate(III) (TPAsDCC) [DCC = 3,3-*commo-bis*(undecahydro-1,2-dicarba-3-cobalta-*closo*-dodecarborate)] or crystal violet-DCC (CVDCC) were precipitated from a solution of DCC^-, which was prepared by K. Baše

0003-2670/86/$03.50

(Institute of Inorganic Chemistry, ČSAV, Prague). The electrolyte solutions were prepared in twice-distilled water from analytical-grade magnesium chloride or sulphate (Lachema, Brno).

The reference electrodes were Ag/AgCl or $Pb/PbSO_4$; the latter will be described in a later paper.

Results and discussion

Figure 1 shows the d.p. voltammograms of perchlorate in the aqueous phase for two electrochemical systems with different base electrolytes. The first system (curve a, Fig. 1) is

Ag/AgCl RE 1, CE 1	2.5 mM $MgCl_2$ (water)	5 mM TPAsDCC I (nitrobenzene) CE 2 ↑	5 mM TPAsCl (water)	AgCl/Ag RE 2 (I)

where reference electrode RE 1 also acts as counter electrode CE 1 (CE 2 is the counter electrode in the nitrobenzene phase). The potential difference of this system is defined by

$$E_1 = \varphi_{RE1}(Ag) - \varphi_{RE2}(Ag) = \Delta_w^{Ag}\varphi_{RE1} + \Delta_n^w\varphi - \Delta_n^w\varphi^0_{TPAs^+} - \Delta_w^{Ag}\varphi_{RE2} + I(R_w + R_n) \quad (1)$$

where $\Delta_n^w\varphi = \varphi(w) - \varphi(n)$ is the potential difference between the aqueous test solution and the formal potential for the tetraphenylarsonium cation in the reference electrode for the nitrobenzene phase; the potential difference in this system is well established because $TPAs^+$ cation is dissolved in both phases. In the second system (curve b, Fig. 1),

$Pb/PbSO_4$ RE 1, CE 1	5 mM $MgSO_4$ water	5 mM CVDCC nitrobenzene CE 2 ↑	2.5 mM $MgCl_2$ water	AgCl/Ag RE 2 (II)

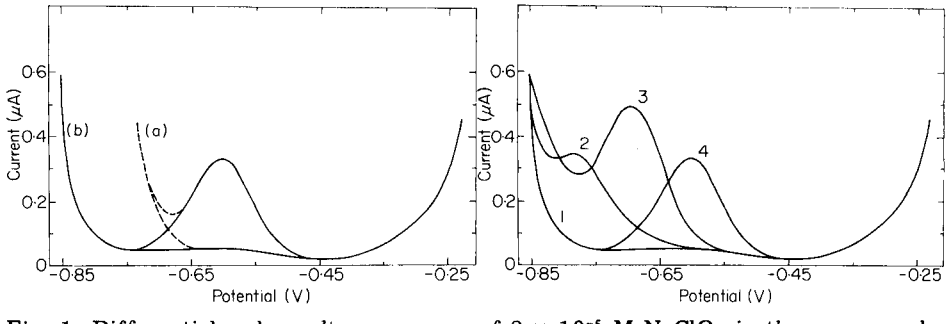

Fig. 1. Differential pulse voltammograms of 2×10^{-5} M $NaClO_4$ in the aqueous phase: (a) in cell I; (b) in cell II.

Fig. 2. Differential pulse voltammograms: (1) base electrolyte; (2) 2×10^{-5} M sodium nitrate; (3) 2×10^{-5} M lithium iodide; (4) 2×10^{-5} M sodium perchlorate in water. The base electrolytes were 5 mM CVDCC in nitrobenzene and 5 mM $MgSO_4$ in water. Starting potential, —0.23 V.

there is no common ion at this reference interface. Nevertheless, because the current flowing through the reference electrode is negligible, the equilibrium conditions are maintained and the potential difference is constant. The potential difference, E_2, is now

$$E_2 = \varphi_{RE1}(Pb) - \varphi_{RE2}(Ag) = \Delta_w^{Pb}\varphi_{RE1} + \Delta_n^w\varphi - \Delta_n^w\varphi_{RE2} - \Delta_w^{Ag}\varphi_{RE2} + I(R_w + R_n) \quad (2)$$

Comparison of both potential values in Fig. 1 indicates that the value of $\Delta_n^w\varphi_{RE2}$ is −89 mV, which is a mixed potential difference for CV^+ and Mg^{2+}, and DCC^- and Cl^-, partitioned between the aqueous and nitrobenzene phases in the reference electrode RE2. The final term in Eqns. 1 and 2 represents the contribution of the electrolyte resistance in the aqueous (R_w) and nitrobenzene (R_n) phases.

Figure 2 shows the d.p.v. peaks for nitrate, iodide and perchlorate. The difference in potentials of the nitrate and perchlorate peaks is −180 mV and that of the iodide and perchlorate peaks is −92 mV; these values are in reasonable agreement with the published values −173 mV [3] and 110 mV [4], which were obtained at a stationary interface. The d.p.v. peaks for nitrate in the range 2×10^{-6}—5×10^{-5} M are shown in Fig. 3. The dependence of the peak current on concentration is linear over this range. The determination of nitrite is more difficult at the HEDE because the free energy of transfer of

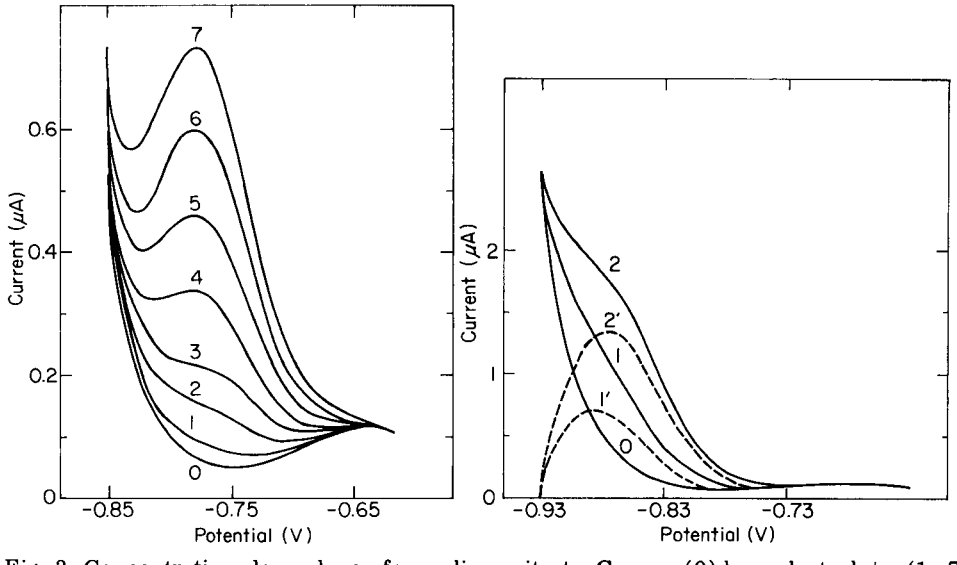

Fig. 3. Concentration dependence for sodium nitrate. Curves: (0) base electrolyte; (1—7) 2, 6, 10, 20, 30, 40 and 50×10^{-6} M, respectively. Base electrolytes as for Fig. 2; starting potential, −0.62 V.

Fig. 4. Voltammograms: (0) base electrolyte; (1) 5×10^{-5} M sodium nitrite; (2) 1×10^{-4} M sodium nitrite in water. Base electrolytes as for Fig. 2. Dashed curves 1′ and 2′ have been corrected for the base electrolyte current.

nitrite from water to nitrobenzene is high. Voltammograms for 5×10^{-5} and 1×10^{-4} M nitrite in water are shown in Fig. 4. Because the peak is close to the transfer of the base electrolyte ions CV^+ and sulphate, subtraction of the base electrolyte current is difficult and the peak potential shifts with concentration.

As an example of the use of HEDE in the analysis of a real sample, the determination of nitrate in potable water was tested. The voltammogram was recorded for the base electrolyte (cf. curve 0, Fig. 3). Addition of 0.2 ml of potable water to the 5 ml of aqueous electrolyte produced a voltammogram very similar to curve 4 (Fig. 3), and a standard addition of 0.2 ml of 5×10^{-4} M nitrate produced a voltammogram the same as curve 6. From these data, and the linear relationship between peak current and concentration, the nitrate content in the sample of potable water was 5×10^{-4} M (ca. 9.5 mg l^{-1}). The advantage of this procedure is that it retains the features of voltammetric methods without requiring deaeration of samples.

REFERENCES

1 J. Koryta, Electrochim. Acta, 24 (1979) 293.
2 V. Mareček and Z. Samec, Anal. Chim. Acta, 141 (1982) 65.
3 B. Hundhammer, T. Solomon and H. Alemer, J. Electroanal. Chem., 149 (1983) 179.
4 B. Hundhammer and T. Solomon, J. Electroanal. Chem., 157 (1983) 19.

Analytica Chimica Acta, 185 (1986) 363—368
Elsevier Science Publishers B.V., Amsterdam — Printed in The Netherlands

Short Communication

SIMULTANEOUS DETERMINATION OF TIN AND LEAD BY ANODIC STRIPPING VOLTAMMETRY WITH ADDITION OF SURFACTANT

J. GEORGES and M. MERMET*

Laboratoire de Chimie Analytique III (CNRS, UA 04-435), Université Claude Bernard, 43 Boulevard du 11 Novembre 1918, 69622 Villeurbanne Cedex (France)

(Received 13th December 1985)

Summary. The influence of various surfactants on the simultaneous determination of tin(IV) and lead(II) by differential-pulse stripping voltammetry at a hanging mercury drop electrode in an acidic medium is reported. With addition of Pluronic-F68 or Brij-78, the tin wave disappears, while the lead wave is not affected. With a deposition time of 1 min at —0.8 V vs. Ag/AgCl, 10^{-7} M concentrations of each ion can be determined if the Sn/Pb ratio is $\leqslant 3$.

Anodic stripping voltammetry (a.s.v.) is well suited to the trace determination of certain metal ions but interferences often occur, which can hamper the simultaneous determination of these elements. In particular, the separation of tin and lead is difficult. Indeed, tin(IV) shows a great tendency towards hydrolysis and polymerization. In acidic media, hydrolysis can be suppressed but the lead and tin peaks then overlap [1, 2]. This problem has been solved by introducing a separation step prior to the a.s.v. [3, 4], by selective complexation of one of the metals [5, 6], by separation of the peaks with a suitable supporting electrolyte such as 1 M ammonium iodide/0.5 M hydrochloric acid [7], or more recently, by the addition of acetyltrimethylammonium bromide [8].

The aim of the present work was to study the inhibitory effects of several surfactants in order to establish the best working conditions for the simultaneous determination of tin and lead in acidic media, by masking the tin wave with a surface-active species.

Experimental

A Princeton Applied Research (PAR) model 174A polarographic analyzer was coupled with a Sefram TRP XY recorder. The reference was an Ag/AgCl/saturated potassium chloride electrode, to which all potentials mentioned are referred. The working electrodes were a dropping mercury electrode (DME PAR model 303) for current/potential curves, and a hanging mercury drop electrode (HMDE; Metrohm E-410) with a drop size corresponding to 7 divisions of the micrometer for a.s.v. The auxiliary electrode was a platinum wire. For the differential pulse stripping mode, the pulse modulation was

0003-2670/86/$03.50

25 mV, the scan rate 2 mV s^{-1} and the pulse repetition time 0.5 s. Solutions were stirred during the deposition period and the stirrer was switched off 30 s before the stripping step.

The stock tin(IV) solution was tin(IV) chloride in hydrochloric acid solution (Merck). Further dilution was done just before use with 1.2 M hydrochloric acid. Standard lead(II) solutions were prepared from lead nitrate (analytical grade).

The following polyoxyethylene surfactants were used: Brij-35 [$C_{12}H_{25}(OCH_2CH_2)_{23}OH$], Brij-72 [$C_{12}H_{25}(OCH_2CH_2)_4OH$], Brij-78 [$C_{18}H_{37}(OCH_2CH_2)_2OH$], and Pluronic-F68 [$OH(OCH_2CH_2)_a(OCHCH_2)_b(OCH_2CH_2)_aOH$].

Water was deionized and distilled in glass.

Results and discussion

Surface-active properties of surfactants. Surface-active compounds are known to adsorb at the electrode/solution interface and this can modify the behaviour of electroactive species in polarography and in anodic stripping voltammetry (a.s.v.). A common method of obtaining information about surfactant adsorption at electrodes is to record electrocapillary curves; the interfacial tension of any mercury/solution interface varies with the electrode potential and presents a maximum at the zero charge point [2, 9]. Generally, surfactants decrease the interfacial tension and so lower the electrocapillary curve in the potential range where they adsorb [10]. Anionic surfactants adsorb preferentially at positive potentials, cationic surfactants at negative potentials and non-ionic surfactants over almost the whole potential range. Non-ionic surfactants such as Pluronic-F68, under the conditions of a.c. polarography, show between the positive and negative tensammetric peaks a depression of surface tension over a wide range of potentials (0.1—1.8 V) [11], which corresponds to the potential range of adsorption. Uncharged surfactants were examined here because the potential range where their adsorption is the strongest corresponds to the reduction of tin and lead. Moreover, ionic surfactants are often unsuitable because they may cause precipitation with the medium and, even if they are adsorbed, their influence on electrode processes is generally less important [12].

A polyoxypropylene—polyoxyethylene copolymer (Pluronic-F68) and a series of polyoxyethylene ethers (Brij) were examined in this work.

Effects of various surfactants on the tin and lead reduction processes. A typical d.c. polarogram obtained at a DME in a solution containing 5×10^{-4} M tin(IV) is shown in Fig. 1A. The first wave is ill-defined around —0.40 V, which corresponds to the reduction of tin(IV) to tin(II); the second wave, at —0.52 V, corresponds to the reduction of tin(II) to tin amalgam. Under exactly the same conditions lead(II) behaves as expected (Fig. 1B); the half-wave potential for its reduction to the amalgam is —0.52 V. Because the two waves evolve at the same potential (—0.52 V), peak overlap is observed in a.s.v. when both metal ions are present.

When a surfactant (Pluronic) is added to the same solution, its adsorption

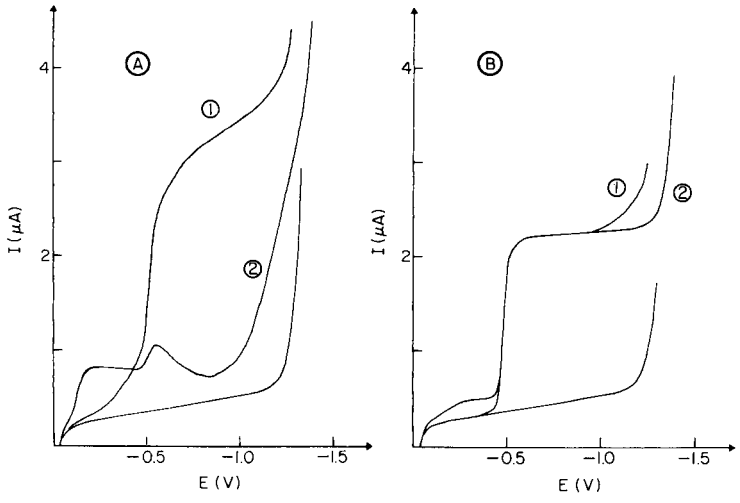

Fig. 1. D.c. polarographic waves in 1.2 M HCl/0.5 M Na_2SO_4: (A) 5×10^{-4} M Sn(IV); (B) 5×10^{-4} M Pb(II). Curves: (1) without Pluronic-F68; (2) with 5×10^{-5} M Pluronic-F68.

has different effects on the electrochemical reduction of the two ions. Pluronic-F68 has practically no influence on the shape and potential of the Pb(II)/Pb(Hg) wave. In contrast, the effect on tin is great; the first wave seems to be better defined but adsorption becomes important when the current corresponding to the second wave begins to increase. When the surfactant concentration is large enough, the current decreases quite sharply, with a minimal value at —0.8 V. The current increases again from —1.0 V but it is difficult to say if this corresponds to the Sn(II)/Sn(Hg) step, with a potential shift, because the wave is overlapped by the cathodic limit. The minimum observed on tin voltammetric curves, in the presence of surfactant, suggests that there is some inhibition in a.s.v.

In differential-pulse (d.p.) a.s.v., the tin and lead stripping peaks occur at essentially the same potential (Fig. 2), but the tin signal can be completely suppressed by addition of a surfactant (Table 1) and proper selection of the deposition potential. The potential chosen corresponds to the minimum observed on the diffusion current plateau, i.e., —0.8 V. However, the stripping peaks were practically unaffected by the electrolysis potential, within the range —0.65 V to —0.85 V.

Pluronic-F68 and Brij-78 give the same effect (Table 1), whereas tin inhibition is less distinct with Brij-35; Brij-72 and Brij-30 were not sufficiently soluble to be effective. The inhibitory effect is maximal when the concentration of added surfactant is large enough (5×10^{-4} M for Pluronic-F68 or 2×10^{-4} M for Brij-78). According to Koryta [13], that corresponds to full coverage of the mercury by the adsorbate. It has been observed with Pluronic-F68 [11] and sodium dodecylsulfate [14] that the optimum concentration corresponds approximately to the critical micelle concentration [15].

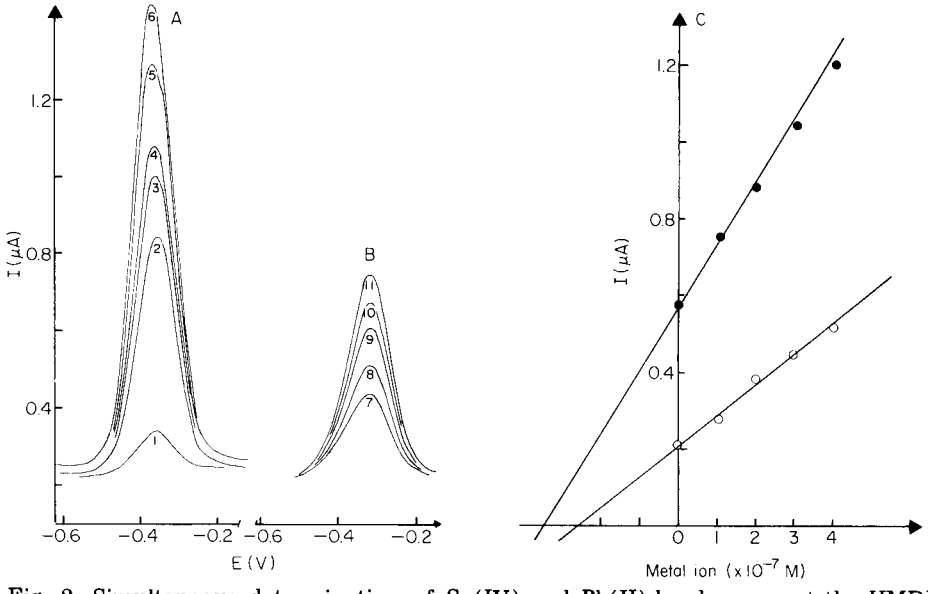

Fig. 2. Simultaneous determination of Sn(IV) and Pb(II) by d.p.a.s.v. at the HMDE in 1.2 M HCl/0.5 M Na_2SO_4 (deposition potential −0.8 V; scan rate 2 mV s^{-1}; pulse height 25 mV). (A) Curves obtained without Pluronic: (1) blank; (2) unknown solution containing Sn(IV) and Pb(II); (3)—(6) increasing added amounts of Sn(IV) to obtain 1, 2, 3 and 4 × 10^{-7} M. (B) Curves obtained with Pluronic (5 × 10^{-5} M): (7) same as (6) with Pluronic added; (8)—(11) increasing added amounts of Pb(II) to obtain 1, 2, 3 and 4 × 10^{-7} M. (C) Corresponding regression lines for standard additions of Sn (•) and Pb (○).

TABLE 1

Influence of various surfactants on the stripping peaks for 5 × 10^{-7} M tin or lead in 1.2 M HCl/0.5 M Na_2SO_4[a]

Surfactant	Amount added (M)	Peak height (μA)	
		Sn	Pb
Pluronic-F68	—	1.22	2.36
	5 × 10^{-4}	0	1.26
Brij-78	—	1.22	2
	2 × 10^{-4}	0	1.26
Brij-35	—	1.4	2.1
	2 × 10^{-4}	0.4	1.7

[a]Electrolysis time 1 min, pulse amplitude 25 mV, deposition potential −0.8 V. Residual currents are subtracted.

The influence of the surface-active species also depended on the nature of the supporting electrolyte. The best results were obtained with sodium sulfate [11]. In the concentration range studied ($1-7 \times 10^{-7}$ M Sn(IV) or Pb(II)), the relationship between the peak current and the concentration was linear whether or not surfactant was present. The average ratio between the slopes of the plots with and without surfactant vs. concentration was about 0.05 for tin and 0.30 for lead. In the case of tin(IV), the peak was not completely removed, because the blank originated principally from traces of lead contained in the water. For this reason, improvement in the detection limit was difficult to attain. The linearity of the plots means that the extent of inhibition is independent of the metal ion concentration within reasonable ranges.

Analytical procedures for tin(IV) and lead(II) by a.s.v. Acidified solutions containing both metal ions were pre-electrolyzed at −0.8 V for 1 min prior to the recording of the stripping curve. Standard aliquots of tin(IV) solution were added and the cycle was repeated. The heights of the stripping peaks were measured, representing the total concentration of tin and lead. Surfactant was then added in order to suppress the tin signal. The lead concentration was evaluated by standard additions of lead(II) and the appropriate calculated peak height was subtracted from the total peak height to obtain the tin concentration. Three standard additions were sufficient and satisfactory regression lines were obtained. Such an experiment is shown in Fig. 2. Several experiments were done with different lead/tin ratios. The results are summarized in Table 2. At higher tin/lead ratios (e.g., 3:1) measurement of the lead peak height was significantly less accurate because the tin peak was incompletely masked.

The sensitivity of the proposed method is poorer than that available with conventional stripping methods because of the surfactant adsorption. In conclusion, the inhibitory effect of a well chosen surfactant can be useful for simultaneous determinations of low concentrations of the two elements, without preliminary separation.

TABLE 2

Results for simultaneous determination of lead and tin in various mixtures[a]

Solution	Found[b]			
	Pb ($\times 10^{-7}$ M)		Sn ($\times 10^{-7}$ M)	
	$\bar{x}$	R.s.d.	$\bar{x}$	R.s.d.
Pb (1×10^{-7} M)/Sn (1×10^{-7} M)	0.96	0.10	1.16	0.19
Pb (2×10^{-7} M)/Sn (1×10^{-7} M)	2.15	0.09	0.96	0.20
Pb (3×10^{-7} M)/Sn (3×10^{-7} M)	2.9	0.13	2.86	0.21
Pb (2×10^{-7} M)/Sn (6×10^{-7} M)	2.6	0.23	4.9	0.32

[a]Operating conditions as for Table 1. [b]Mean ($\bar{x}$) and relative standard deviation for 5 separate determinations.

REFERENCES

1 A. M. Bond, Anal. Chem., 42 (1970) 1165.
2 I. M. Kolthoff and J. J. Lingane, Polarography, Interscience, New York, 1952.
3 T. V. Nghi and F. Vydra, J. Electroanal. Chem., 71 (1976) 333.
4 T. M. Florence and Y. J. Farrar, J. Electroanal. Chem., 51 (1974) 191.
5 S. Glodowski and Z. Kublik, Anal. Chim. Acta, 104 (1979) 55.
6 E. Desimoni, F. Palsimano and L. Sabbatini, Anal. Chem., 52 (1980) 1889.
7 A. M. Shafiqul Alam. O. Vittori, H. Tersigni and G. Courtois, Anal. Chim. Acta, 91 (1977) 325.
8 J. Hernandez, Mendez, R. Carabias Martinez and M. E. Gonzales Lopez, Anal. Chim. Acta, 138 (1982) 47.
9 D. M. Mohilner, in A. J. Bard (Ed.), Electroanalytical Chemistry, Vol. 1, M. Dekker, New York, 1966.
10 B. Breyer and H. H. Bader, Alternating Current Polarography and Tensammetry, Interscience-Wiley, New York, 1963.
11 J. Georges, Anal. Chim. Acta, 121 (1980) 29.
12 J. Nader, DEA, University of Lyon I, 1981.
13 J. Koryta, Collect. Czech. Chem. Commun., 18 (1953) 206.
14 J. W. Chen, DEA, University of Lyon I, 1984.
15 K. Shinoda, T. Nakagawa, B. Tamamushi and T. Isemura, Colloid Surfactants, Academic Press, New York, 1963.

Analytica Chimica Acta, 185 (1986) 369—375
Elsevier Science Publishers B.V., Amsterdam — Printed in The Netherlands

Short Communication

POROUS GLASS AS AN EFFICIENT ADSORBENT FOR VOLATILE ATMOSPHERIC POLYCHLORINATED BIPHENYL CONGENERS

F. BOUCHERTALL and J. C. DUINKER*

Institute for Marine Research, Marine Chemistry Department, Düsternbrooker Weg 20, 2300 Kiel (Federal Republic of Germany)

(Received 31st December 1985)

Summary. Porous glass is a more efficient adsorbent than Amberlite XAD-2 resin for volatile polychlorobiphenyls (PCB) in the atmospheric vapour phase. The adsorption efficiencies for individual PCB congeners are compared by analysis of the extracts by capillary gas chromatography (electron-capture detection); individual congeners are used as reference compounds. Efficiencies for some di-, tri- and tetra-chloro congeners are between 1.7 and 7 times higher for porous glass than for XAD-2 resin; values for penta-, hexa- and hepta-chloro congeners are very similar. The calculated "total" PCB (as the sum of individual congeners) was about four times higher for porous glass, because of the contribution from congeners with low chlorine numbers. Commercial mixtures may not reflect the real composition of PCB mixtures in the atmosphere.

It is generally accepted that the atmosphere provides an important route for the transport of polychlorinated biphenyls (PCB) from the continents to the oceans [1—3]. In remote areas, atmospheric deposition may even be the main source [4, 5]. Accurate knowledge of concentrations in the atmosphere are required for estimations of fluxes, mass balances and residence times [6, 7]. Reported values for total PCB are in the low ng m^{-3} range. Thus, large volumes of air (of the order of tens to hundreds of m^3) have to be processed to obtain sufficient material for the analyses.

In the most commonly applied collection methods, air is pumped through a glass-fiber filter to retain particles; the filter is backed up by a solid adsorbent to extract the fraction present in the (operationally defined) vapour phase. There is at present no generally accepted method of analysis for atmospheric PCB because of the following technical and analytical problems [8]. It is uncertain, for each compound, to what extent the phase separation defined above reflects the actual vapour/particulate partitioning in the atmosphere. The vapour phase is commonly considered to be the dominant phase. This conclusion is based on experimental data [1—3, 8, 9] as well as on theoretical considerations [10]. Small particles passing through the filter may be trapped by the adsorbent; this uncertainty will remain until better methods have been developed. The second problem relates to the variable collection efficiency of the common solid adsorbents; several authors have

0003-2670/86/$03.50

observed that, particularly, the most volatile PCB fraction is not collected efficiently by polyurethane foam plugs [2, 11, 12] or XAD-2 resin [8, 13] in high-volume sampling systems.

The third problem is the lack of uniformity in the methods of analysis and reporting format for PCB, in both the qualitative and quantitative sense. This is caused by the complexity of the PCB mixtures in environmental samples, the inadequacy of existing methods to unravel these compositions in all their detail, and the diversity of the various attempts to solve the problem by simplifying assumptions. In all cases, quantitative estimates of PCB in atmospheric samples have been presented in terms of commercial mixture equivalents, usually on the basis of packed column chromatography, but in some recent cases on the basis of capillary column chromatography. This approach obviously produces inaccurate results if the compositions of the sample and reference materials are different, as is usually the case [14—16].

Several low-molecular weight (di- and tri-chloro) PCB congeners have been detected in sea water at appreciable concentrations [15, 16]. In order to be able to relate these findings with data on atmospheric concentration and deposition, an adsorbent with better adsorption characteristics for these compounds in atmospheric samples than the materials currently available [8] was sought. Porous glass was found to be a good choice. Its efficiency was compared with that of XAD-2 resin by application of the individual PCB congener approach. In this way, ambiguities associated with the use of commercial mixtures as reference materials were minimized. Also, this approach was studied to see how much it could help to improve understanding of the behaviour of specific PCB congeners in the atmosphere.

Experimental

Porous glass was obtained from Serva (Heidelberg, F.R.G.). It has the following characteristics: mesh size 20/80; mean pore diameter 19×10^{-9} cm; pore volume 0.71 $cm^3\ g^{-1}$; surface area 9.2 $m^2\ g^{-1}$. It was pre-extracted with dichloromethane and baked at 250°C in a muffle furnace for 36 h. Amberlite XAD-2 was successively extracted with methanol, acetonitrile, acetone and dichloromethane. Each extraction was continued for 12 h in a Soxhlet extractor. The material was not allowed to get dry. Glass-fiber filters (7-cm diameter, Whatman GF/F) were pre-extracted with dichloromethane and baked at 400°C in a muffle furnace for 36 h. Filters were mounted in stainless steel (SS) holders with SS rain shelters and were backed up by the respective adsorbent, packed into a 2.2×20 cm SS column.

Air was pulled through the system in several experiments for 1—5 days (15—75 m^3 at 10 $dm^3\ min^{-1}$). Samples were collected on top of Kiel lighthouse, which is located in Kiel Bight (Western Baltic), some 25 km north of the city of Kiel. For each sample collected, a blank collection, without pump, was conducted at the same time with an identical system placed at a distance of 50 cm. This resulted in the appearance of some peaks, which were absent in the system prior to this procedure (Fig. 1b, A).

The penetration of PCB vapours and the adsorption capacity of porous

glass was tested by drawing 100 m^3 of filtered air through two columns in series. The front column was filled with porous glass; the second column was filled with porous glass or XAD-2, in parallel experiments. In another experiment, XAD-2 was used without the back-up trap, for comparison with various recent experiments with XAD-2 [8, 13]. After sampling, the columns were extracted with 100 cm^3 of dichloromethane pumped into the column from below, in order to prevent the formation of air bubbles in the column. The extracts were concentrated under vacuum at low temperature (<3°C) to ca. 100 μl, and then separated by silica-gel column chromatography into three fractions of increasing polarity. The first fraction (eluted with n-hexane) contained the PCBs. The fractions were analyzed by fused silica capillary gas chromatography (g.c.) with an electron-capture detector. Peaks were identified and quantified by using individual PCB congeners as reference compounds [17].

The suitability of solvents was checked by the g.c. method after concentration from 250 ml to 100 μl until a proper batch was obtained. Otherwise, n-hexane was distilled in a 1.5-m still, after treatment with concentrated sulfuric acid and chromatography on an alumina column, and then checked by the g.c. method after concentration.

Results and discussion

The chromatograms from the front porous-glass traps used in the different experiments were indistinguishable. One is represented together with the blank of porous glass in Fig. 1(a). The back-up columns in these experiments (i.e., porous glass or XAD-2) did not contain any component at concentration levels above the respective blank levels; and the levels remained below ca. 5% of the levels for the front trap. Thus, porous glass is an efficient adsorbent for the components collected almost completely on the front trap.

A chromatogram from the XAD-2 trap, used without the back-up trap, is also shown in Fig. 1. It has been demonstrated that XAD-2 resin is an efficient adsorbent for PCB fractions with relatively high degrees of chlorination [13, 19]. If it is assumed that these results obtained with packed columns can be extrapolated to a model involving individual congeners with relatively high chlorine numbers, then congener no. 138 (which is a hexachlorobiphenyl present to a significant extent in both commercial mixtures and in environmental samples [16, 17]) can be taken as a reference compound to estimate the collection efficiency of other congeners.

Duinker and Hillebrand [17] identified and quantified those PCB congeners in the chromatograms which were well separated from other compounds on a SE-54 fused silica capillary column and which were also available in sufficiently pure form for qualitative and quantitative reference purposes. For these congeners, the relative concentrations with respect to congener no. 138 were calculated for both porous glass and XAD-2 (Table 1). The adsorption efficiencies for the dichloro- and trichloro-biphenyls are between 3 and 7, and for three tetrachloro congeners (nos. 41, 44 and 61) between

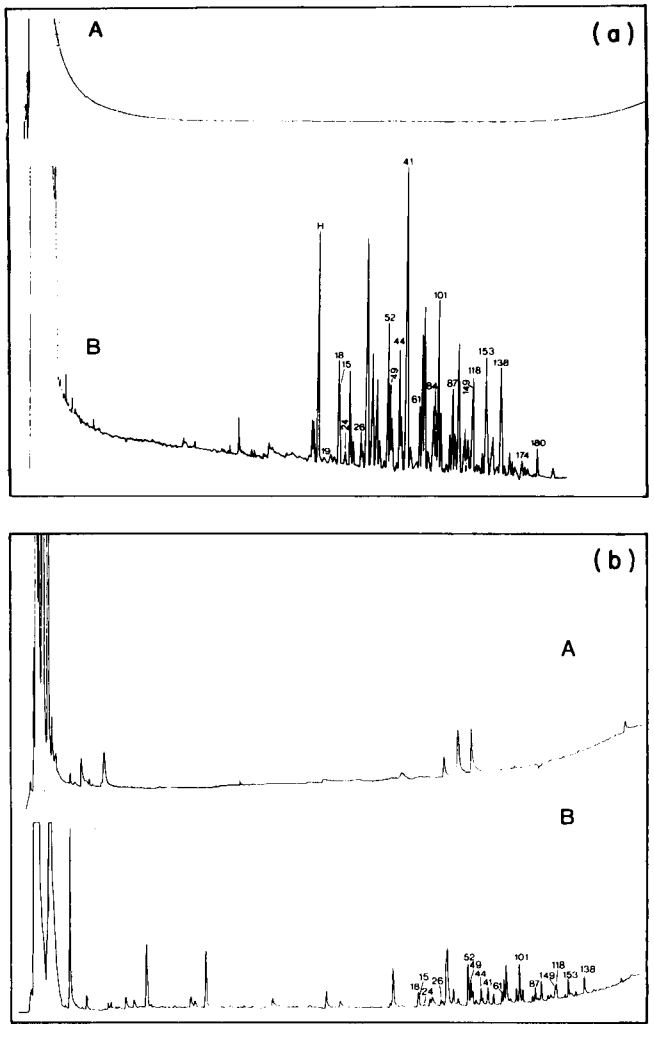

Fig. 1. Temperature-programmed gas chromatograms with an electron-capture detector on a fused silica (0.15-μm) SE-54 capillary column (0.20 mm i.d.) for atmospheric vapour-phase PCB fractions. (a) Adsorption on porous glass (B); (b) adsorption on XAD-2 resin (B). Chromatograms A are the relevant blank determinations (see Experimental section). Peaks are identified by numbers representing individual congeners according to IUPAC rules [18]. Chromatographic conditions as reported earlier [17]. H is a hexachlorobenzene.

1.7 and 7, times higher for porous glass than for XAD-2. For one tetrachloro congener (no. 52), the two pentachloro, the two hexachloro and the two heptachloro congeners, the efficiencies for the two adsorbents were found to be very similar. Thus, porous glass is a considerably more efficient adsorbent material for several volatile PCB congeners than XAD-2.

Doskey and Andren [13] introduced XAD-2 as an adsorbent for atmos-

TABLE 1

Ratio (F_i) of the concentrations (C) of PCB congener (i) and congener no. 138 in the vapour phase (pg m^{-3}), determined by adsorption on porous glass and on XAD-2 in a high-volume sampling system[a]

PCB congener, i	Structure	$F_i = C_i/C_{138}$	
		Porous glass	XAD-2
18	2, 2', 5	1.9	0.6
15	4, 4'	1.4	0.5
24	2, 3, 6	0.7	0.1
26	2, 3', 5	1.4	0.3
52	2, 2', 5, 5'	2.2	2.1
44	2, 2', 3, 5'	1.7	1.0
41	2, 2', 3, 4	3.3	0.5
61	2, 3, 4, 5,	2.3	0.6
101	2, 2', 4, 5, 5'	2.3	1.9
118	2, 3', 4, 4', 5	1.0	0.7
153	2, 2', 4, 4', 5, 5'	0.8	0.8
138	2, 2', 3, 4, 4', 5	1	1
187	2, 2', 3, 4', 5, 5', 6	0.2	0.2
180	2, 2', 3, 4, 4', 5, 5'	0.4	0.2

[a]The congeners are identified by their systematic IUPAC numbering system [18] and the position of the chlorine atoms in the biphenyl molecular framework.

pheric PCBs. They tested the efficiency for congener no. 52. The present results suggest that their results can be used as a model for congeners with chlorine number >4, but lower efficiencies than for congener no. 52 were found for several other tetrachloro- and for all trichloro- and dichloro-biphenyls in the atmospheric samples.

The individual congener approach thus shows considerable differences in trapping efficiencies for the various congeners. These differences may be less clear when commercial mixtures are used as reference materials to evaluate sample chromatograms. This can explain, at least partly, the qualitative and quantitative variations reported in the literature, which are caused by the usually different peak patterns of the chromatograms obtained for samples and commercial mixtures. These differences are more obvious in capillary column than in packed column chromatograms, in which several peaks merge. For example, although practically all the peaks in the chromatogram of the vapour phase shown in Fig. 1 have a corresponding peak in Clophen-A30 (or in the equivalent Aroclor mixture of similar overall chlorine content), this mixture has a different composition [17]. Thus, it is a less suitable reference material for evaluating the PCB mixture in samples. Depending on the peak (or combination of peaks) selected for comparison, various quantitative results, differing by several 100%, could have been obtained. This aspect will be considered in more detail in a later paper.

The occurrence of commercial mixtures with a lower degree of chlorination (i.e., Aroclor 1242) than corresponds to the usually reported commercial mixtures with a medium or high degree of chlorination (Aroclor 1248 and 1254) in the atmosphere has been reported before [3, 9, 19, 20]. The present findings suggest that even more volatile PCB fractions than those corresponding to the composition of Aroclor 1242 are important in the atmosphere. Unless their contributions are taken into account, the total PCB in the atmosphere will be seriously underestimated. For instance, for the sample used to produce Fig. 1, the summed contribution of the individual congeners, corresponding to the chromatographic region where the peaks of Clophen-A30 elute, was 200 pg m^{-3}, whereas the summed contribution of the congeners corresponding to Clophen-A60 was 50 pg m^{-3}. The underestimation can be avoided by determining individual congeners in combination with efficient adsorbent material for these volatile compounds. Information on individual congeners is also important for evaluating air/water exchange and other processes more accurately than has been possible with commercial mixtures as reference materials [8, 21, 22]. The assignment of g.c. peaks to individual PCB congeners has been made on the basis of detailed analyses of commercial mixtures by g.c. with electron-capture detection and by g.c./m.s. [17], with the aid of 102 individual congeners as reference compounds. It is not impossible that some details will have to be modified in the future, in the light of the chromatographic data for all 209 congeners made available recently [23]. Considerable experimental work is needed in this respect, however.

Porous glass seems to be an appropriate material for use in parallel with other materials like Florisil [24], polyurethane foam plugs [2, 11], XAD-2 resin [13] and Tenax [20] for extracting PCB present in the vapour phase in high-volume sampling systems. No carry-over between samplings was found with porous glass. It is chemically and thermally stable and ideal blanks (for g.c. of an eluate after concentration from 500 ml to 100 μl) are easily obtainable, in contrast to present findings for XAD-2, despite many consecutive extractions with various pure solvents, of various polarities, over longer time periods (Fig. 1). Such problems were also reported by Hollod and Eisenreich [19] despite earlier reports [13].

REFERENCES

1 G. R. Harvey and W. G. Steinhauer, Atmos. Environ., 8 (1974) 777.
2 T. F. Bidleman and C. E. Olney, Bull. Environ. Contam. Toxicol., 11 (1974) 442.
3 E. Atlas and C. S. Giam, Science, 211 (1981) 163.
4 D. A. Peel, Nature, 254 (1975) 325.
5 S. Tanabe, H. Hidaka and R. Tatsukawa, Chemosphere, 12 (1983) 277.
6 L. P. Burkhard, D. E. Armstrong and A. W. Andren, Environ. Sci. Technol., 19 (1985) 590.
7 C. S. Giam, E. Atlas, H. S. Chan and G. Neff, Atmos. Environ., 14 (1980) 65.
8 P. V. Doskey and A. W. Andren, Environ. Sci. Technol., 15 (1981) 705.

9 T. J. Murphy and C. P. Rzeszutko, J. Great Lakes Res., 3 (1977) 305.
10 C. E. Junge, in I. H. Suffet (Ed.), Fate of Pollutants in the Air and Water Environment, Wiley-Interscience, New York, 1977, p. 7.
11 R. G. Lewis, A. R. Brown and M. D. Jackson, Anal. Chem., 49 (1977) 1680.
12 C. G. Simon and T. F. Bidleman, Anal. Chem., 51 (1979) 1110.
13 P. V. Doskey and A. W. Andren, Anal. Chim. Acta, 110 (1979) 129.
14 J. C. Duinker, M. T. J. Hillebrand and J. P. Boon, Neth. J. Sea Res., 17 (1983) 19.
15 IOC (UNESCO), Paris, Technical Report No. 26, 1983.
16 J. C. Duinker and M. T. J. Hillebrand, Bull. Environ. Contam. Toxicol., 31 (1983) 25.
17 J. C. Duinker and M. T. J. Hillebrand, Environ. Sci. Technol., 17 (1983) 449.
18 K. Ballschmiter and M. Zell, Fresenius Z. Anal. Chem., 302 (1980) 302.
19 G. J. Hollod and S. J. Eisenreich, Anal. Chim. Acta, 124 (1981) 31.
20 W. N. Billings and T. F. Bidleman, Environ. Sci. Technol., 14 (1980) 679.
21 V. E. McClure, Environ. Sci. Technol., 10 (1976) 1223.
22 S. J. Eisenrech, B. B. Looney and J. D. Thornton, Environ. Sci. Technol., 15 (1981) 30.
23 M. D. Mullin, C. M. Pochini, S. McCrindle, M. Romkes, S. H. Safe, Environ. Sci. Technol., 18 (1984) 468.
24 C. S. Giam, H. S. Chan and G. S. Neff, Anal. Chem., 49 (1977) 1671.

Analytica Chimica Acta, 185 (1986) 377—380
Elsevier Science Publishers, B.V., Amsterdam — Printed in The Netherlands

Short Communication

DETECTION AND DETERMINATION OF FORMALDEHYDE DIMETHYLHYDRAZONE IN MIXTURES WITH 1,1-DIMETHYLHYDRAZINE

K. N. NINAN*, V. P. BALAGANGADHARAN and T. S. RAMASUBRAMANIAN

Analytical and Spectroscopy Division, Vikram Sarabhai Space Centre, Trivandrium 695022 (India)

(Received 10th December 1985)

Summary. Small amounts of formaldehyde dimethylhydrazone (FDMH) present as impurity in unsymmetrical dimethylhydrazine (UDMH) give a yellow color (λ_{max} = 456 nm) on heating with excess of sulphuric acid; the detection limit is 50 μg ml^{-1} FDMH. Differences in the basicity of the two compounds in anhydrous acetic acid and in methanol are used to determine the two compounds in mixtures containing $\geqslant$5% (w/w) FDMH.

1,1-Dimethylhydrazine, $(CH_3)_2NNH_2$, more commonly known as unsymmetrical dimethylhydrazine (UDMH), is primarily used as a liquid propellant in rockets. Its purity requirement is above 98.0% (w/w) [1]. Commercially, it is prepared by chloramination of ammonia or by Hofmann degradation of 1,1-dimethylurea [2, 3]. Unsymmetrical DMH is easily oxidized by various reagents, including those used in the above processes. Methylene dimethylhydrazine $(CH_3)_2NN{:}CH_2$, usually known as FDMH (formaldehyde dimethylhydrazone), is the major product of oxidation [4,5]. Various methods have been suggested for the removal of FDMH to obtain UDMH of the required purity [6]. It is, therefore, necessary to have methods for the detection of FDMH at frequent intervals, during the process of its removal.

Quantitative methods for determining UDMH include redox titration with potassium iodate and acid-base titration with perchloric acid in anhydrous acetic acid [7—9]. However, these methods cannot distinguish between UDMH and FDMH. Gas chromatography is the recommended method of determining UDMH because it can effectively separate FDMH and other impurities such as water, ammonia and dimethylamine [1]. But the process liquor cannot be injected directly into a gas chromatograph because it contains large quantities of dissolved alkali and water. In this communication, a simple qualitative colour test is presented for the detection of FDMH as well as a simple chemical method for determining FDMH in UDMH/FDMH mixtures.

Experimental

Procedure for colour development. To 10 ml of a process solution of UDMH (ca. 3%), add diluted (1 + 9) sulphuric acid slowly to neutralize

and then 5 ml in excess. Cover the beaker with a watch glass and heat over a boiling water bath, or in an air oven kept at 100—105°C, for 20 min. A yellow colour indicates the presence of FDMH in the sample.

Quantitative procedure. Weigh accurately about 2 g of UDMH/FDMH mixture into a 100-ml volumetric flask containing 50 ml of cold anhydrous acetic acid and dilute to volume with anhydrous acetic acid. Titrate a suitable aliquot (20 ml) with 0.1 M perchloric acid in anhydrous acetic acid using methyl violet (1% solution) as indicator [8]. The volume of acid needed is a measure of total hydrazines because of the levelling effect of acetic acid. (The potassium iodate method [7, 9] can also be used to determine the total hydrazines.) In the second step, weigh accurately about 2 g of the UDMH/FDMH mixture into a 100-ml volumetric flask containing methanol and dilute to volume with methanol. Titrate a suitable aliquot (20 ml) with methanolic 0.1 M hydrochloric acid using bromocresol green (1% solution) as indicator. This titration gives a measure of the UDMH alone.

Results and discussion

Colour test for FDMH. Both FDMH and UDMH are colourless liquids. When heated with excess of acid, pure UDMH does not give any colour; but UDMH containing FDMH as impurity gives a yellow colour, the intensity of which decreases with decreasing FDMH concentration. The development of colour is independent of the quantity of acid. However, an excess of about 5 ml of diluted (1 + 9) acid for 10 ml of process liquid was found to be satisfactory.

The spectrum of the coloured solution showed a broad absorption band around 450 nm; from the derivative spectrum, the wavelength of maximum absorption was 456 nm. In order to optimize the heating time and the acid to be used, the colour was developed with mineral acids or acetic acid for different intervals of time. The results obtained are summarized in Table 1, which shows that sulphuric acid gives the best colour at around 100°C; below 100°C, the colour development was slow. Initially, the value of this absorbance depends on the heating time upto about 20 min. Once developed, the colour is stable for hours.

TABLE 1

Effect of acid and heating time on colour development from 1.6 mg ml^{-1} FDMH

Acid used[a]	Absorbance at 456 nm for different heating times (min)			
	5	10	20	30
Sulphuric	0.362	0.381	0.390	0.390
Hydrochloric	0.341	0.352	0.360	0.360
Nitric	0.331	0.340	0.345	0.345
Acetic	0.340	0.356	0.360	0.361

[a]A 5-ml excess of diluted (1 + 9) acid was used.

TABLE 2

Effect of concentration of FDMH on absorbance

FDMH conc. (mg ml^{-1})	0.30	0.50	1.00	2.00	3.00
Absorbance (456 nm)	0.12	0.15	0.20	0.54	0.98

In order to establish the linearity of the absorbance versus concentration relationship, the colour was developed with solutions containing different concentrations of FDMH; the other ingredients were in approximately the same concentrations as in the process liquor. The results (Table 2) indicate that the absorbance is not linear with concentration and, therefore, this colour test cannot be proposed as a quantitative method at this stage. The method is an excellent means of detecting FDMH in concentrations as low as 50 $\mu g\ ml^{-1}$, which gives a clear yellow solution with an absorbance of about 0.004. The coloured species is not extractable in common solvents. Under an inert atmosphere (nitrogen blanket), a process liquor containing as much as 3.0 mg ml^{-1} FDMH did not produce a colour which implies that the colour is due to oxidation products of FDMH. Efforts are in progress to establish the nature of the species.

Determination of FDMH in UDMH/FDMH mixtures. In non-aqueous titrations with perchloric acid in anhydrous acetic acid, both UDMH and FDMH have the same basicity because of the levelling effect of acetic acid [7, 8]. The titration with iodate [7, 9] also gives the total hydrazines only. In methanolic medium, only UDMH is a strong enough base to be titrated with methanolic hydrochloric acid; FDMH is too weak. The difference, in terms of equivalents, between the two titration methods gives the concentration of FDMH alone because both of them react as monovalent bases.

To establish the validity of the above procedure, two field samples as well as one synthetic standard were analysed for FDMH and UDMH by the proposed method and by gas chromatography (g.c.) [1]. The results are given in Table 3. The suggested method has a precision and accuracy com-

TABLE 3

Comparison of chemical and g.c. results for FDMH/UDMH mixtures

	Field sample				Synthetic mixture (90:10)	
	1		2			
	UDMH	FDMH	UDMH	FDMH	UDMH	FDMH
Chemical method	94.4	5.7	88.9	10.8	98.9	9.7
	94.3	5.7	88.8	10.9	90.1	9.5
	94.4	5.8	88.9	10.9	90.1	9.7
G.c.	94.0	5.5	88.9	10.6	89.5	10.2
	94.0	5.5	88.6	10.9	89.4	10.1
	94.0	5.4	88.8	10.8	89.5	10.1

parable with those of g.c. and can be recommended for pure UDMH/FDMH mixtures containing not less than 5% (w/w) FDMH. The method must, however, be checked against g.c. for non-specific impurities in field samples of uncertain composition.

We thank Mr. M. R. Kurup and Dr. K. V. C. Rao for their encouragement.

REFERENCES

1 U.S. Military Specification MIL-P-25604 D, April, 1978.
2 H. H. Sisler, F. Neth, R. Drago and D. R. Yancy, J. Am. Chem. Soc., 76 (1954) 3906.
3 V. R. Ohme and H. Preuschhof, J. Prakt. Chem., 312 (1970) 349.
4 J. B. Class, J. H. Aston and T. S. Oakwood, J. Am. Chem. Soc., 75 (1953) 2937.
4 H. H. Sisler, M. A. Mathur, S. R. Jain and R. Greengard, Ind. Eng. Chem. Prod. Res. Dev., 20 (1981) 181.
6 U.S. Patent 4,154,658, May, 1979.
7 H. E. Malone, The Analysis of Rocket Propellants, Academic Press, London, 1976, p. 44.
8 N. M. Serencha, J. G. Hanna and E. J. Kuchar, Anal. Chem., 37 (1965) 1116.
9 R. A. Penneman and L. F. Audrieth, Anal. Chem., 37 (1965) 1116.

ANALYTICA CHIMICA ACTA, VOL. 185 (1986)

AUTHOR INDEX

Optimization of Chromatographic Selectivity

A Guide to Method Development

by **P. Schoenmakers,** *Philips Research Laboratories, Eindhoven, The Netherlands*

(Journal of Chromatography Library, 35)

This is the first detailed description of method development in chromatography – the overall process of which may be summarized as: method selection, phase selection, selectivity optimization, and system optimization. All four aspects receive attention in this book.

Chapter 1 gives a short introduction, describes chromatographic theory and nomenclature, and outlines the method development process. Chapter 2 describes guidelines for method selection, and quantitative concepts for characterizing and classifying chromatographic phases. Selective separation methods, from both gas and liquid chromatography are given in Chapter 3; the main parameters of each method are identified and simple, quantitative relations are sought to describe their effects. Criteria by which to judge the quality of separation are discussed in Chapter 4 with clear recommendations for different situations. The specific problems involved in the optimization of chromatographic selectivity are explained in Chapter 5. Optimization procedures, illustrated by examples, are extensively described and compared on the basis of a number of criteria. Suggestions are made both for the application of different procedures and for further research. The optimization of programmed analysis receives special attention in Chapter 6, and the last chapter summarizes the optimization of the chromatographic system, including the optimization of the efficiency, sensitivity and instrumentation.

Those involved in developing chromatographic methods or wishing to improve existing methods will value the detailed, structured way in which the subject is presented. Because optimization procedures and criteria are described as elements of a complete optimization package, the book will help the reader to understand, evaluate and select current and future commercial systems.

1986 362 pages
US $ 84.00 / Dfl. 210.00
ISBN 0-444-42681-7

ELSEVIER SCIENCE PUBLISHERS

P.O. Box 211, 1000 AE Amsterdam, The Netherlands
52 Vanderbilt Avenue, New York, NY 10017, USA

7366

SCIENTIFIC COMPUTING AND AUTOMATION (EUROPE)

Conference (and Exhibition)
13-15 May, 1987
Amsterdam, The Netherlands

Europe's first conference on Scientific Computing and Automation - devoted to the latest advances in this area as applied to **chemistry** (pharmaceutical, analytical, environmental, synthesis), **the life sciences** (clinical, microbiological), and **engineering and technology** (biotechnology, chemical engineering) - offers the international scientific community opportunities to share and build upon their experiences in:

COMPUTING
AUTOMATION
ROBOTICS
ARTIFICIAL INTELLIGENCE AND EXPERT SYSTEMS

The program will include sessions on:

LIMS/LAN
Intelligent Instruments
Impact of New Hardware on the Laboratory
Expert Systems in Clinical Laboratories and Medicine
New Techniques in Medical Computing
Computer Aided Organic Synthesis / Computer Aided Molecular Modelling
Off-the-Shelf Software and Chemometrics
Laboratory Robotics
Expert systems
Data Handling and Automation in Instrumental Analysis
Data Handling and Automation in Pharmaceutical Laboratories
Computer Applications in Biotechnology

PLEASE SEND YOUR ABSTRACTS BEFORE 1 DECEMBER 1986 to the Conference Chairman:

Prof. D. L. Massart
Farmaceutisch Instituut
Vrije Universiteit Brussel
Laarbeeklaan 103
1090 Brussels
Belgium

Enquiries for participation to:
Keith Foley
Scientific Computing and Automation
P. O. Box 330
1000 AH Amsterdam
The Netherlands

CLEOPATRA

Chemometrics Library: an Extendable Set of Programs as an Aid in Teaching, Research and Applications

Authors: G. Kateman, P.F.A. van der Wiel, T.A.H.M. Janse and B.G.M. Vandeginste

- a package of programs for
  - (post) graduate education
  - (industrial) training courses
- provides quick insight on how to solve your problems around:
  - sampling of lots
  - monitoring
  - reconstruction
  - autocorrelation
  - curve fitting
  - Fourier filtering
- highly interactive
- high quality graphics
- runs on IBM-PC and HP-9845
- clear, fully descriptive manual with tutorial
- easy to use
- no prior knowledge of any specific computer jargon necessary
- US $ 820.00 (IBM-PC), US $ 735.00 (HP-9845-B)
- CLEOPATRA, extension I
  Three New Modules: Modules Sequential Analysis, Kalman Filtering, Simplex Optimization
- US $ 375.00

AVAILABLE FROM:

Elsevier Scientific Software (JIC)
52 Vanderbilt Avenue
New York, NY 10017 USA
Phone: (212) 916 1250
Telex: 420643

or
Elsevier Scientific Software
P.O. Box 330
1000 AH Amsterdam
THE NETHERLANDS
Phone: (020) 5862 828
Telex: 18582

Write to us for further information on our other programs

No shipping charge if paid in advance

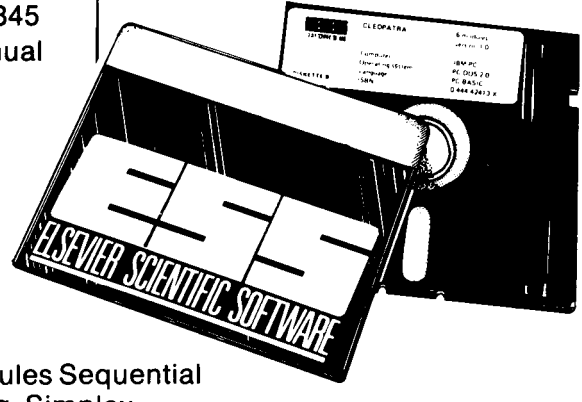

ELSEVIER SCIENTIFIC SOFTWARE

IBM-PC is a registered trademark of IBM

(continued from outside back cover)

CONTENTS

(Abstracted, Indexed in: Anal. Abstr.; Biol. Abstr.; Chem. Abstr.; Curr. Contents Phys. Chem. Earth Sci.; Life Sci.; Index Med.; Mass Spectrom. Bull.; Sci. Citation Index; Excerpta Med.)

(continued on inside back cover)